TECTONIC EVOLUTION OF THE PALAEOTETHYS OCEAN IN NW TURKEY

ELIZABETH ANNE PICKETT

THESIS SUBMITTED FOR THE DEGREE OF
DOCTOR OF PHILOSOPHY
UNIVERSITY OF EDINBURGH

1994

Abstract

NW Turkey displays a series of pre-Jurassic tectonostratigraphic units which are critical to our understanding of the western portion of the sutured Palaeotethys Ocean and the processes involved in its tectonic evolution. During this study, sedimentological, structural and lithological data were collected from NW Turkey, with the aim of elucidating the Late Palaeozoic-Early Mesozoic history of the Palaeotethys Ocean. These units are: (a) ultrabasic slabs with metamorphic soles (Denizgören/Lesbos Ophiolites) emplaced onto Upper Permian carbonate platform units (e.g. Karadag Unit), (b) amphibolites and gneisses (Kazdag Massif), (c) Permo-Triassic volcanosedimentary units (Karakaya Complex) with an Upper Triassic-Jurassic sedimentary cover (Bayirköy/Halilar Formations and Bilecik Limestone), (d) thick Triassic carbonate platforms overlying mélange units (Chios and Karaburun sequences).

A major focus of this study is the Karakaya Complex, a deformed, low-grade metamorphic assemblage of oceanic origin which comprises a SE-dipping stack of distinct tectonostratigraphic units (Nilüfer, Ortaoba, Kalabak and Çal Units), here interpreted as a Palaeotethyan accretionary complex. The Nilüfer Unit comprises spilites, volcaniclastics and limestone. The spilites have within-plate geochemical signatures and this, together with the absence of terrigenous material, leads to an interpretation as a seamount sequence. The tectonically overlying Ortaoba Unit comprises basalt-chert-turbidite sequences. The coarsening-upward nature of the turbidites and the MORB-type geochemistry of the basalts suggests a subduction-related trench setting. The Kalabak Unit consists of sheared phyllites and is tentatively interpreted as an abyssal sequence. The Çal Unit lies at the top of the structural pile and comprises Permian carbonate platform units on terrigenous basements, together with volcanic- and limestone-rich debris flows. The Çal Unit is interpreted as a rifted carbonate platform. Perched basins composed of siliciclastic and condensed carbonate sequences also developed during subduction-accretion (Bayirköy/Halilar Formations). In the western Biga Peninsula and Lesbos, ultrabasic slabs and metamorphic soles are emplaced onto Permian carbonate platform units (e.g. Karadag Unit and Lesbos platform carbonates). Geochemical studies indicate that the ultrabasics were probably formed above a subduction zone. The Karadag Unit displays structures consistent with ophiolite emplacement towards the north. The Karaburun Peninsula and Chios are composed of mélanges, containing Silurian-Carboniferous limestone blocks, overlain by thick Triassic-Cretaceous carbonate platform units. The two sequences are tentatively interpreted as rift-related sequences overlain by passive margin carbonate build-ups. The Karakaya Complex in NW Turkey verges NW, a trend also recorded by the Denizgören Ophiolite and the Chios/Karaburun mélanges. A palaeomagnetic study of the Jurassic Bilecik Limestone shows an anticlockwise rotation of 47° in the Biga Peninsula since the Jurassic, thus restoring the Karakaya structures to an approximately E-W position with northward vergence. Restored structural trends therefore imply the presence of a south-dipping Palaeotethyan subduction zone during the Late Permian-Triassic.

Regionally, there is evidence of subduction, arc volcanism and marginal basin formation along the Eurasian continental margin during the Palaeozoic. This was followed in the study area (NW Turkey) by south-dipping, intra-oceanic subduction, which generated the Karakaya Complex. The Denizgören/Lesbos Ophiolites appear to have originated from a spreading event within this evolving accretionary setting. With further convergence, the ophiolitic crust was emplaced northwards onto a carbonate platform. Finally, in Tertiary times, the Kazdag Massif formed as a metamorphic core complex, resulting from regional extension.

Öz

KB Türkiye, kenetlenmis Paleotetis okyanusunun bati kesimini ve tektonik evriminde rol alan islevleri anlamamizda kritik öneme sahip, bir dizi geç Jura öncesi tektonostratigrafik birim kapsar. Bu çalisma sirasinda, Paleotetis okyanusunun Geç Paleozoyik-Erken Mesozoyik tarihini ortaya koymak amaciyla, KB Türkiye'den sedimentolojik, yapisal ve litolojik veriler toplanmistir. Bu birimler: (a) Ust Permiyen karbonat platform birimleri (Karadag Birimi) üzerine yerlesmis metamorfik tabanli ultrabazik kütleler (Denizgören/Lesbos Ofiyolitleri), (b) amfibolitler ve gnaysler (Kazdag Masifi), (c) Ust Triyas-Jura sedimentleriyle örtülü (Bayirköy/Halilar Formasiyonlari ve Bilecik Kireçtasi) Permo-Triyas volkanosedimanter birimler (Karakaya Karmasigi), (d) melanj birimlerini (Chios ve Karaburun istifleri) üzerleyen kalin Triyas karbonat platformlaridirlar.

Bu Çalismanin odak noktasi, burada Paleotetis yigisim karmasigi olarak yorumlanan, GD'ya egimli farkli tektonostratigrafik birimlerden (Nilüfer, Ortaoba, Kalabak ve Çal Birimleri) olusan, deforme, okyanusal kökenli düsük dereçeli metamorfik birim, Karakaya Karmasigidir. Nilüfer Birimi spilitler, volkaniklastikler ve kireçtaslarindan olusaur. Spilitlerin levha-içi jeokimyasal karakteri ile birlikte terijen malzemenin yoklugu, bir denizalti tepesi yorumuna yol açmistir. Tektonik olarak üzerleyen Ortaoba Birimi bazalt-çört-türbidit istiflerini kapsar. Türbiditlerin üste dogru kabalasan niteligi ve bazaltlarin MORB-tipi jeokimyasi, yitim ile iliskili, hendek ortamina isaret eder. Kalabak Birimi makaslanmis fillitlerden olusur ve tercihen abisal bir istif olarak yorumlanmistir. Çal Birimi yapisal istifin en üstünde yer alir ve volkanik ve kireçtasi bakindan zengin moloz akintilarinin da bulundugu terijen bir temel üzerine gelen Permiyen karbonat platformu birimlerinden olusar. Çal Birimi riftlesmis karbonat platformu olarak yorumlanmistir. Silisiklastik ve kondanse karbonat istiflerini içeren (Bayirköy/Halilar Formasyonlari) tünek havzalarda yitim-yigisim sirasinda gelismislerdir. Bati Biga Yarimadasinda ve Lesbos'da, ultrabazik kütleler ve metamorfik tabanlar, Permiyen karbonat platformlari (Karadag Birimi ve Lesbos karbonat platformlari) üzerine yerlesmislerdir. Jeokimyasal çalismalar, ultrabaziklerin olasilikla bir yitim zonunun üzerinde olduguna isaret etmektedir. Karadag Birimi, ofiyolit yerlesiminin kuzeye dogru olmasi ile uyumlu yapilar gösterir. Karaburun Yarimadasi ve Chios, Silüriyen-Karbonifer kireçtasi bloklari içeren melanj ve bunlari örten kalin Triyas-Kretase karbonat platform birimlerinden olusar. Bu iki istif, pasif kenar karbonat yigimi ile örtülen, riftlesme ile ilgili istifler olarak yorumlanmislardir. KB Türkiyedeki Karakaya Karmasigi KB verjanslidir; bu trend Denizgören Ofiyoliti ve Chios/Karaburun melanjlarinda da gözlenmistir. Jura Bilecik Kireçtasinin paleomanyetik çalismasi, Biga Yarimadasinin Juradan bu yana 47 derece saatin aksi yönünde döndügünü gosterir, böylece Karakaya yapilarini kuzeye verjansli yaklasik D-B pozisyonuna getirir. Bu nedenle restore yapisal trendler, Geç Permiyen-Triyas sirasinda güneye egimli Paleotetis yitiim zonunun varligini gösterir.

Bölgesel olarak, Paleozoyik sirasinda, Avrasya kita kenari boyunca yitim, yay volkanizmasi ve kenar havza olusumunun delilleri vardir. Bunu çalisma alaninda (KB Türkiye), Karakaya Karmasigini üreten güneye egimli, okyanus içi yitim izledi. Denizgören/Lesbos Ofiyolitleri, bu olgunlasan yigisim ortamindaki bir yayilma olayi ile iliskili gözükmektedir. Dahada ilerleyen konverjans ile ofiyolitik kabuk kuzeye dogru bir karbonat platformu üzerine yerlesti. Nihayet Tersiyer döneminde bölgesel gerilme neticesinde Kazdag Masifi metamorfik çekirdek kompleksi olarak olustu.

ACKNOWLEDGEMENTS

I would like to thank my supervisors, Alastair Robertson and John Dixon at Edinburgh University, and Aral Okay at Istanbul Technical University, for all their time and help, both in Edinburgh and in the field. My project was funded by NERC and they are thanked for fieldwork and conference funding. My project has greatly benefitted from discussions with Timur Ustaömer, Peter Clift and Ian Sharp. The ERASMUS scheme allowed me to visit the Université de Paris Sud at Orsay for three months and I thank Olivier Monod for his friendliness and help.

I thank Dodie James, Geoff Angel, Diana Baty, Stuart Kearns and Pete Hill for teaching me laboratory techniques and for their help and advice throughout my thesis. Mike Hall and Jane Foster are thanked for making numerous thin-sections as is Shane Voss who helped me with computer problems on many occasions.

I thank all my field assistants, especially Ruth Jones and Hamide Kayaci, with whom I first ventured, bewildered, into the Kazdag Mountains. Thanks also to Serdar Akyüz and Koray Özgül for their friendship during my first trip to Turkey. Fieldwork logistics and the recurring nightmare of sending rock samples back to Britain were eased by Seref Tonbul, Ismet Özgenç and Cenk Yaltirak.

My palaeomagnetic study was made possible by Ellen Platzman from Oxford University who took me as a drilling assistant to Turkey and spent a lot of time showing me the ropes. I am very grateful for all her time and effort. Buffy McClelland kindly allowed me to use the equipment in Oxford and Brian Daniels helped me when I got stuck. I am grateful to Sara Vickery and Halcyon Martin for all their hospitality in Oxford. Many friends have made my time as a PhD student enjoyable. I would especially like to thank Jonathan Wilson, Anne Payne, Pauline Thompson, Clare Glover, Ruth Jones, Rachel Flecker, Sara Vickery, Julie Hardiman, Jerry Lloyd, Peter Clift and Marianne Broadgate, for lots of reasons but mostly for being good friends. Many thanks to Rachel Flecker for our adventures in the Taurus Mountains, and without whose help I would never have made the dreaded 1st of September 1994!

And to my family, who were probably wondering when I'd finally finish the "great work of fiction", thanks for their support and recuperative weekends in Yorkshire. I'd like to show them the beauty of Turkey one day.

CONTENTS

CHAPTER 1
INTRODUCTION

CHAPTER 2
THE NILÜFER UNIT: ACCRETED SEAMOUNT SEQUENCES

CHAPTER 3
THE ORTAOBA AND KALABAK UNITS: ACCRETED TRENCH AND DEEP-SEA SEQUENCES

CHAPTER 4
THE ÇAL UNIT: DISRUPTED PERMIAN CARBONATE PLATFORMS AND DEBRIS FLOWS

CHAPTER 5
UPPER TRIASSIC-JURASSIC SEDIMENTARY COVER: A PERCHED ACCRETIONARY PRISM-TOP BASIN

CHAPTER 6
THE KAZDAG MASSIF: A METAMORPHIC CORE COMPLEX

CHAPTER 7
THE DENIZGÖREN AND LESBOS OPHIOLITES, THEIR METAMORPHIC SOLES AND THE UNDERLYING CARBONATE PLATFORMS

CHAPTER 8
CHIOS AND THE KARABURUN PENINSULA: RIFT AND PASSIVE MARGIN SEQUENCES

CHAPTER 9
PALAEOMAGNETIC STUDY OF THE BILECIK LIMESTONE

CHAPTER 1

INTRODUCTION

1.1 Introduction

Turkey is a segment of the Alpine-Himalayan mountain belt which stretches from the Betics to Tibet, between the stable cratons of Eurasia in the north and Gondwana in the south (Figure 1.1). Within this vast suture zone can be found the remnants of oceanic basins known collectively as the Tethys Ocean. The Mediterranean Sea is the last surviving remnant of this ocean and is itself currently being consumed along the Aegean-Cyprus arc. Tethys is a very general term which applies to all the components which make up this complex collage of oceanic fragments, accretionary complexes, ophiolites and rifted blocks (Figure 1.2). There is a general consensus that a large, essentially Palaeozoic ocean ("Palaeotethys") was succeeded by smaller, Mesozoic ocean basins ("Neotethys") which formed as a result of rifting along the northern Gondwanan margin. Whereas the evolution of the Neotethys has been widely investigated, that of the older Palaeotethys remains poorly understood, due in most part to the deformed and fragmentary nature of Palaeotethyan terranes. The Karakaya Complex of northern Turkey represents one such Palaeotethyan fragment and the study of its constituent tectonostratigraphic units comprises a large part of this thesis.

The section below gives a general introduction to the history of Tethyan research and outlines the various models put forward for the evolution of the Palaeotethys. The reader is referred to Robertson & Dixon (1984), Sengör *et al.* (1984) and Ustaömer (1993) and references therein, for further detail. This is followed by a discussion of the tectonic belts of Turkey and their significance in terms of Tethyan evolution. The Karakaya Complex is an important element of the Pontide belt in the north and a summary of previous research on the complex as a whole is given in Section 1.4. A general introduction to my field area in the Biga Peninsula and surrounding regions of NW Turkey is then followed by a summary of previous work in these areas. The previous research carried out on individual tectonic units and formations is discussed more fully in the relevant chapters. An outline of the objectives and approach of my work is followed by a brief summary of the units studied. Finally, the broad layout of the thesis is described.

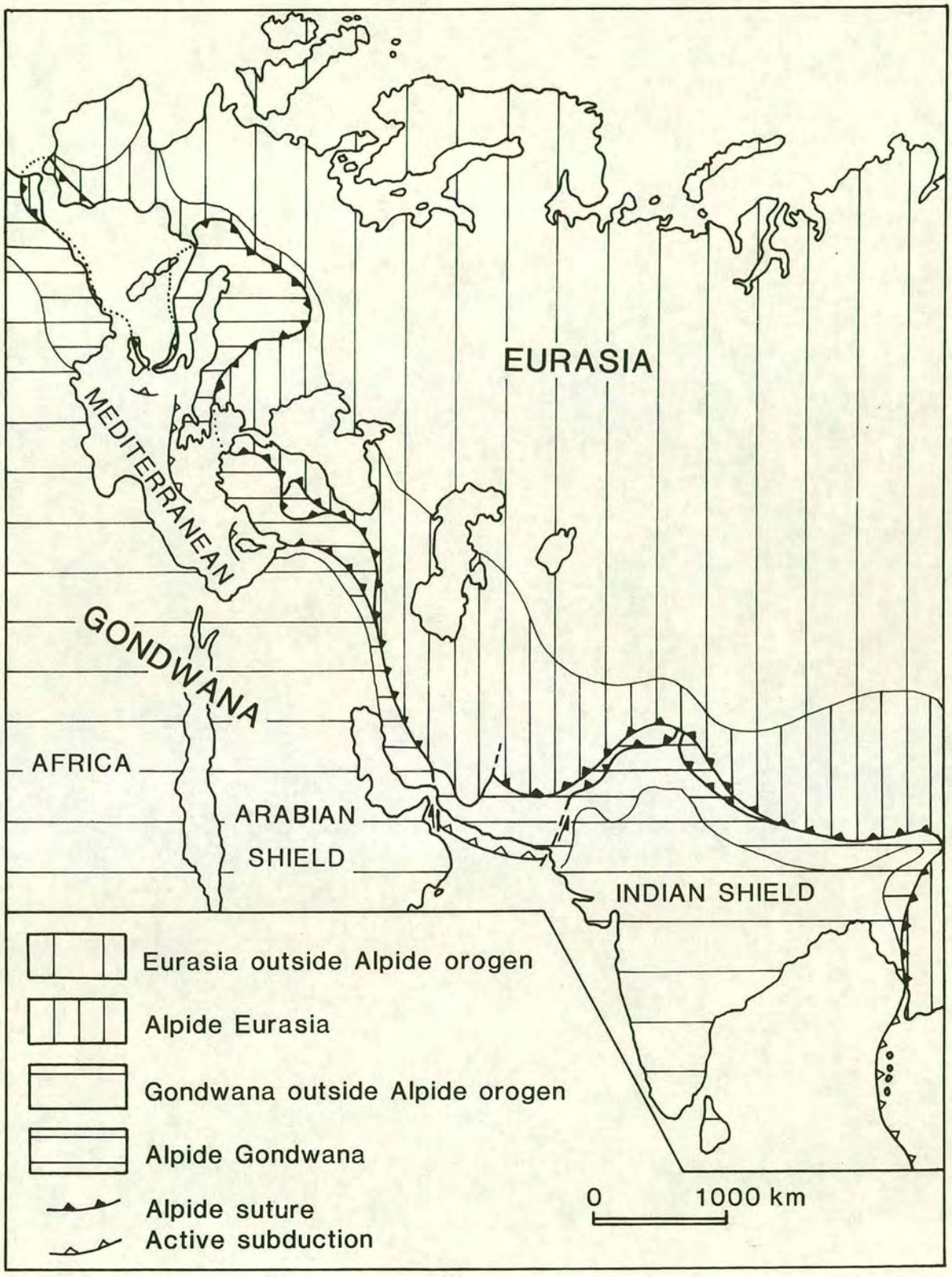

Figure 1.1 Tectonic map of the Alpine-Himalayan orogenic belt, showing the major Alpide sutures (after Okay, 1989).

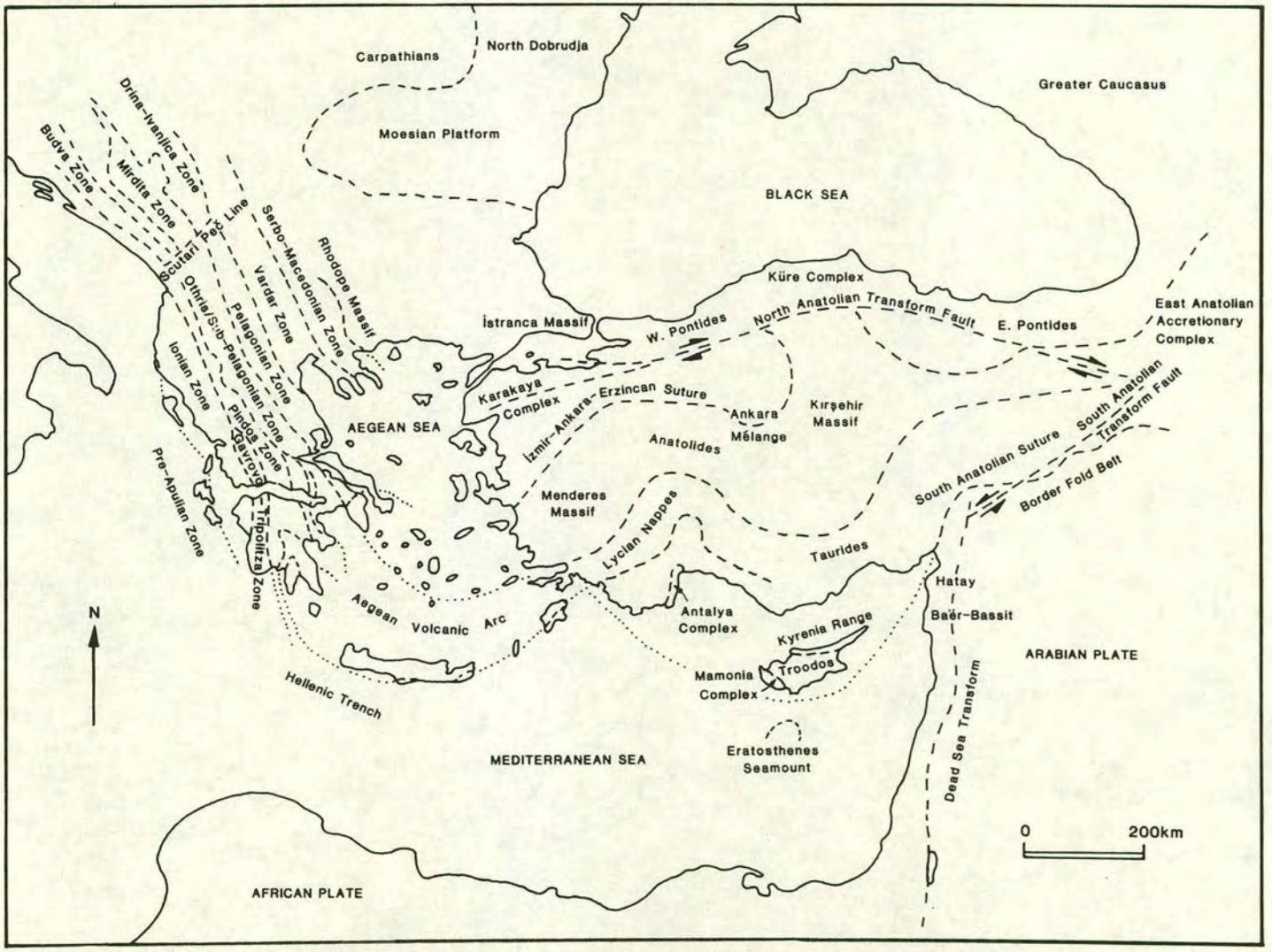

Figure 1.2 The principal tectonic units and sutures of the Eastern Mediterranean region (modified after Robertson & Dixon, 1984).

1.2 The Tethys Ocean

It has long been recognized that a wide ocean, of which the Mediterranean is but a small relic, once separated the Eurasian and Gondwanan landmasses. The idea was first postulated by Neumayr (1885) whose work on Jurassic faunas led him to propose that an ancient equatorial seaway extended from India to Central America, separating Eurasia from Africa and South America. Suess (1893) gave this ocean the name "Tethys" and suggested that the Alpine-Himalayan mountain belt had formed by its closure. Research by Wegener (1929), Carey (1958) and Wilson (1963) suggested that the Tethys did not extend around the equator; rather, it originated as a westward-narrowing, wedge-shaped gulf into the supercontinent Pangaea during Late Palaeozoic times. This oceanic embayment is commonly referred to as Palaeotethys (or Palaeo-Tethys) (Laubscher & Bernoulli, 1977; Hsü, 1977; Stöcklin, 1974; Sengör, 1979) and is presumed to have closed by subduction during post-Triassic times (e.g. Smith, 1971; Dewey *et al.*, 1973; Hsü, 1977). Smaller Tethyan ocean basins that opened during and after the Triassic are collectively known as the Neotethys (Laubscher & Bernoulli, 1977; Sengör, 1979). How Palaeotethys closed is a matter of conjecture and the subject has led to radically different published models which can be divided into "southward subduction" and "northward subduction" models (Figures 1.3 & 1.4 respectively).

a) Southward subduction model

Sengör (1979) and Sengör *et al.* (1980, 1984) postulated that the formation of the Neotethys was coeval with the disappearance of the Palaeotethys. In their model a strip of continental landmass called the Cimmerian continent detached itself from northern Gondwana in the Permo-Triassic, migrated northwards across the Palaeotethys and collided with the Eurasian margin from the Late Triassic to the Early Jurassic. The Palaeotethys was destroyed by southward-dipping subduction under the Cimmerian continent, accompanied by the formation of back-arc basins (e.g. the Karakaya "basin") and the opening of a strand of the Neotethys further south (Figure 1.3a). The northward migration of the Cimmerian continent left the newly created Neotethys in its wake, as well as other continental fragments which which would follow this northward motion during later times (e.g. the Tauride-Anatolide platform, the Kirsehir Massif and the Sakarya microcontinent). In this model the position of the Karakaya Complex to the south of the Palaeotethyan suture and its apparent northward-vergence led to the postulation that the Karakaya suture represented a Palaeotethyan back-arc basin which closed by southward subduction

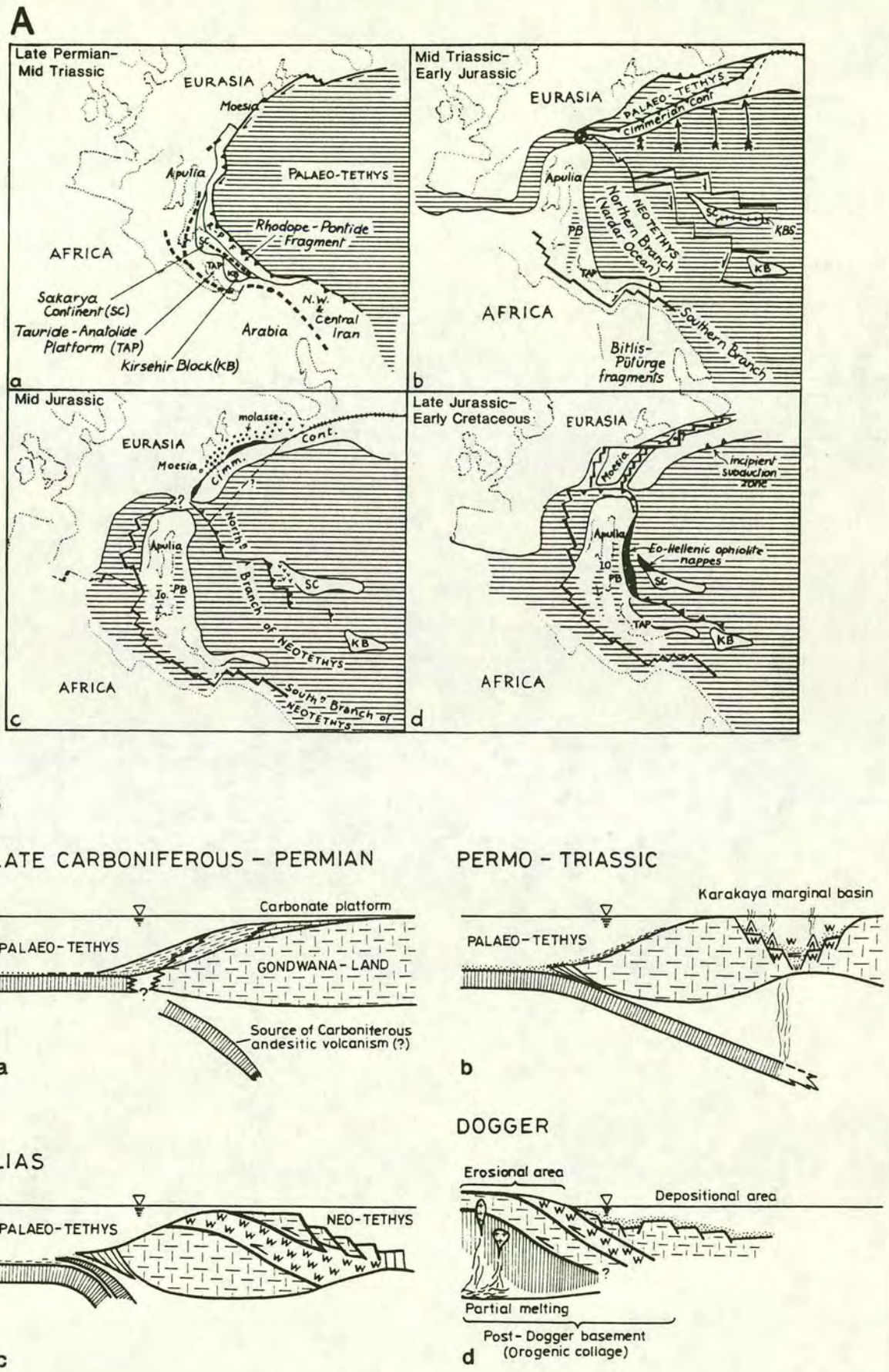

Figure 1.3 Southward subduction of the Palaeotethys according to (a) Şengör *et al.* (1984) (redrawn by Robertson & Dixon, 1984), and (b) Tüysüz (1990).

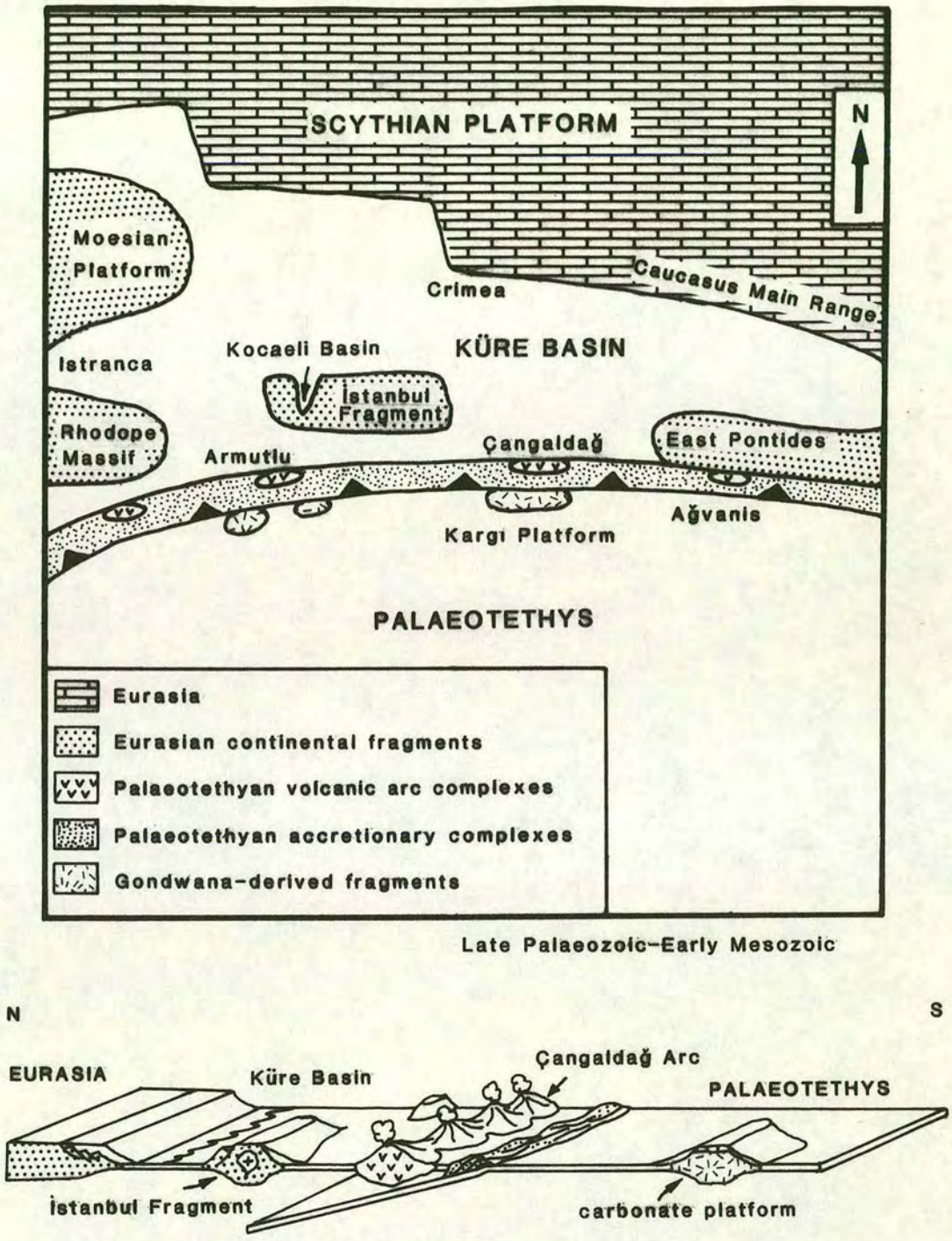

Figure 1.4 Closure of the Palaeotethys by northward subduction, according to Ustaömer & Robertson (1993).

before the Late Triassic. More recent variations on this theme have been put forward by Okay *et al.* (1991) and Tüysüz (1990). Figure 1.3b shows the Carboniferous-Jurassic evolution of the Palaeotethys according to Tüysüz (1990) and clearly illustrates the concept of the Karakaya Complex as a back-arc basin, in agreement with the models of Sengör (1979) and Sengör *et al.* (1980).

b) Northward subduction model

Adamia *et al.* (1981) and Adamia & Belov (1989) developed a very different model based on their work in the Caucasus and applied by them to the Eastern Mediterranean region. Their model involved long-lived northward subduction which was active throughout Palaeozoic, Mesozoic and Tertiary time. Robertson & Dixon (1984) and Ustaömer & Robertson (1993, 1994) have also argued that the distinction between the Palaeotethys and Neotethys is not as definite as postulated by Sengör *et al.* (1984). Their models involved the more gradual disappearance of the Palaeotethys during the Mesozoic and into the Tertiary, by both intra-oceanic subduction and northward subduction under the Eurasian margin. The destruction of the Palaeotethys was accompanied by rifting of the north margin of Gondwana and the formation of Neotethyan basins such as the Pindos Ocean. As with the model of Sengör *et al.* (1984), the model of Robertson & Dixon (1984) involves northward-drifting continental fragments (e.g. the Sakarya microcontinent and the Kirsehir, Menderes and Tauride blocks). In this scenario the Karakaya Complex, in the southern part of the Pontides, represents a subduction-accretion complex formed from Palaeotethyan oceanic material, although the northward-vergence of the complex is not in accordance with northward subduction and needs to be explained. Figure 1.4 illustrates the fate of the Palaeotethys according to Ustaömer & Robertson (1993), based on their work in the central Pontides (see position of Küre Complex in Figure 1.2). Northward subduction under an active Eurasian margin led to the formation of a back-arc basin (Küre Basin) and an intra-oceanic arc (Çangaldag arc). Cessation of the main Palaeotethyan subduction was followed by southward underthrusting of the Küre Basin prior to the Late Jurassic (Ustaömer & Robertson, 1994).

The Neotethyan tectonic framework of the Tethyan region is better understood than that of the Palaeotethys (see Robertson & Dixon, 1984; Sengör *et al.,* 1984, Dercourt *et al.,* 1986 and references therein for a fuller description of the Neotethys). There is a general consensus that the Eastern Mediterranean Neotethys was in existence from the Late Triassic to Late Cretaceous and that it opened as a result of rifting along the

north margin of Gondwana from Late Palaeozoic time onwards. Closure of the Neotethys was largely controlled by the convergence and collision of Gondwana and Eurasia in Late Cretaceous-Tertiary time.

1.3 Tectonic divisions of Turkey

Turkey has traditionally been divided into four major tectonic belts which trend approximately east-west and are, from north to south (Figure 1.2):

1. Pontides
2. Anatolides
3. Taurides
4. Border Fold Belt (in SE Turkey only)

Further subdivisions have been made within the basic framework of these belts as shown in Figure 1.2. These belts are essentially a Mesozoic "Neotethyan" feature, and are separated by sutures comprising Late Mesozoic to Tertiary ophiolites and ophiolitic mélanges. The most prominent of these sutures is the Izmir-Ankara-Erzincan Suture Zone which separates the Pontides from the Anatolides and Taurides. The Pontide tectonic belt is believed to be of Eurasian origin, whilst the Anatolides and Taurides are Gondwanan (Robertson & Dixon, 1984; Sengör *et al.,* 1988; Adamia *et al.,* 1987).

The Pontides, constituting a North Tethyan domain, acted as an active margin at the southern edge of the Eurasian continent during the Mesozoic. The Taurides, or South Tethyan domain, acted as a passive margin at the northern edge of the African-Arabian continent until the Late Cretaceous Arabian obduction. The Anatolides are essentially the metamorphic equivalent of the Taurides and thus may be considered part of the South Tethyan passive margin. The Menderes Massif, which makes up much of the Anatolides in western Turkey is as yet poorly understood.

The area studied in this thesis lies at the western end of the Pontides and preserves units which reflect the evolution and subsequent destruction of the older Palaeotethys. This area of NW Turkey contains pre-Jurassic tectonic units (e.g. Karakaya Complex, Kazdag Massif, Denizgören Ophiolite) which have hitherto been studied as separate entities and which, when considered together provide us

with a great deal of insight into the tectonic and sedimentary evolution of NW Turkey, and the Palaeotethys ocean system in general.

1.4 The Karakaya Complex

The Karakaya Complex is an east-west trending belt of low-grade metamorphic deep-sea sedimentary and volcanic rocks which stretches across Turkey from the Biga Peninsula in the west as far as Erzincan in the east (Figure 1.5). It was first described from the Kazdag area of the Biga Peninsula by Bingöl (1968) and Bingöl *et al.* (1973). The predominantly Permo-Triassic ages obtained from the Karakaya Complex are consistent with a Palaeotethyan origin and have led to several interpretations regarding its formation and evolution within the Palaeotethyan tectonic framework. The hypotheses divide into two main categories, which involve either sedimentary, relatively *in situ*, basinal processes, or tectonic juxtaposition and imbrication of deep-sea sequences. The first option was initiated by Bingöl *et al.* (1973) with their model of gravity sliding in Early Triassic extensional basins, and subsequently developed by Kaya *et al.* (1986, 1989) who postulated purely lithological repetition of olistostromes in a layer-cake sequence.

Interpretations such as these contrast strongly with tectonically orientated hypotheses in which tectonostratigraphy, rather than stratigraphy, is emphasized. Tekeli (1981) described the Karakaya Complex (part of his "North Anatolian Mélange") as a subduction-accretion complex which formed in the fore-arc region of an active margin. Üsümezsoy (1987) also placed the Karakaya Complex within an accretionary complex, this time above a north-dipping subduction zone. Okay *et al.* (1991) postulated formation of a Late Permian Karakaya rift basin above a south-dipping Palaeotethyan subduction zone. In their model an entire active margin tectonostratigraphy, including rift, intra-arc, fore-arc and accretionary units, is represented by the Karakaya units. Their model is broadly in agreement with the plate reconstructions of Sengör *et al.* (1980) and Sengör & Yilmaz (1981) in which the Karakaya Complex formed as a back-arc basin behind a south-dipping Palaeotethyan subduction zone. Closure of the Karakaya basin is relatively well constrained in the west of Turkey by the Upper Triassic age of the oldest unconformable sediments (Tekeli, 1981). Further east the oldest unconformable cover sequences are late Liassic, possibly indicating diachronous closure from west to east (Tekeli, 1981).

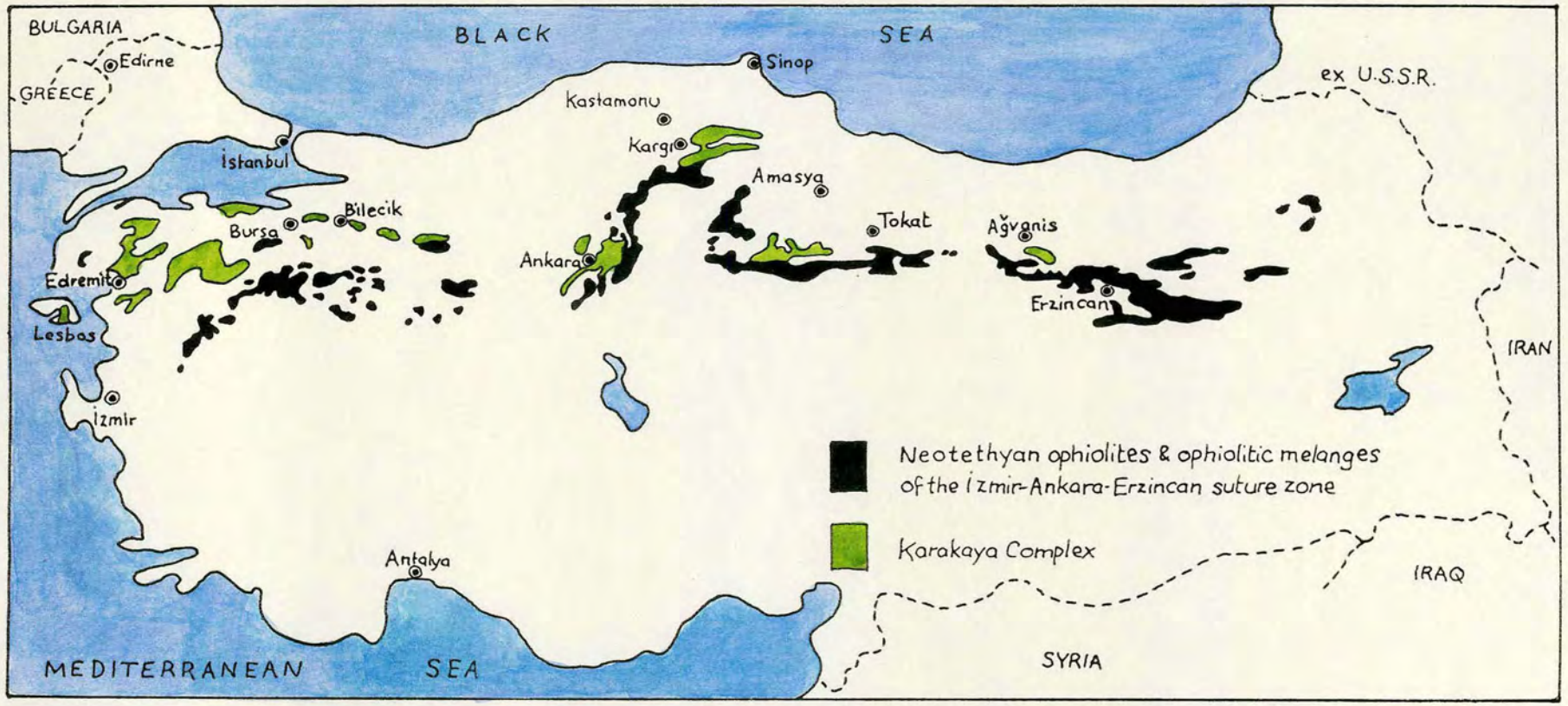

Figure 1.5 Distribution of the Karakaya Complex and the Neotethyan ophiolites of the Izmir-Ankara-Erzincan Suture Zone (after an unpublished map by Cin, 1991).

1.5 Introduction to the Biga Peninsula and surrounding regions

The main area considered in this study is the Biga Peninsula and regions to the south (Figure 1.6). The field area is bounded to the north by the Marmara Sea and the straits of Gelibolu at Çanakkale (also known as the Dardanelles and the ancient Hellespont), and to the east by the Aegean Sea. The Greek islands of Lesbos and Chios just off the Turkish coast were also studied. The southern boundary of the studied area is marked by the Neotethyan ophiolites and mélanges of the Izmir-Ankara-Erzincan Suture Zone. Reconnaissance work was also carried out further east, along the southern shores of the Sea of Marmara as far as the mountain of Uludag near Bursa.

The Biga Peninsula is the ancient Troad and is the setting for the Iliad. This Greek epic poem describing the siege of Troy is attributed to Homer and was composed before 700 B.C. Many of the mountains, rivers and cities described in the Iliad can be recognized in the present-day Biga Peninsula and surrounding regions. The southern part of the Biga Peninsula is dominated by the Kazdag Massif (Mount Ida in the Iliad) with its peaks of Sarikiz and Babadag (meaning respectively "yellow girl" and "father mountain" in Turkish), which rise to 1774m above the surrounding coastal plains. Deep gorges cut through the densely forested slopes to the white marbles and grey gneisses of the Kazdag metamorphic rocks. The high forests and crags are home to brown bears, wild boar, wolves and eagles. The bare summit plateau rises above dense pine forests and supports an Alpine-type flora. The mountains slope down to steep rolling hills of scrub and olive groves which support small mountain villages and isolated farms. Access is by rough village and forestry tracks and, away from the main villages, by goat tracks. Near the Aegean coast, around Edremit Bay, flat plains of olive trees surround the market towns of Edremit (the ancient Adramyttium), Havran and the coastal resort of Akçay. The villages and hills of this region are shown on Figure 1.7. The enclosed boxes are mapped regions referred to in the following chapters.

The central Biga Peninsula region, around the town of Çan (Figure 1.6) is a dry area of low rolling hills. To the west, between Çanakkale and Ezine, lie the ruins of Troy on a flat windswept plain which stretches to the Aegean Sea. Eastwards, low country with large lakes gives way to the massif of Uludag ("great mountain" in Turkish, and the ancient Mount Olympos of Asia Minor) whose 2350m peak dominates the southern shore of the Marmara Sea and towers over the city of Bursa. South of the

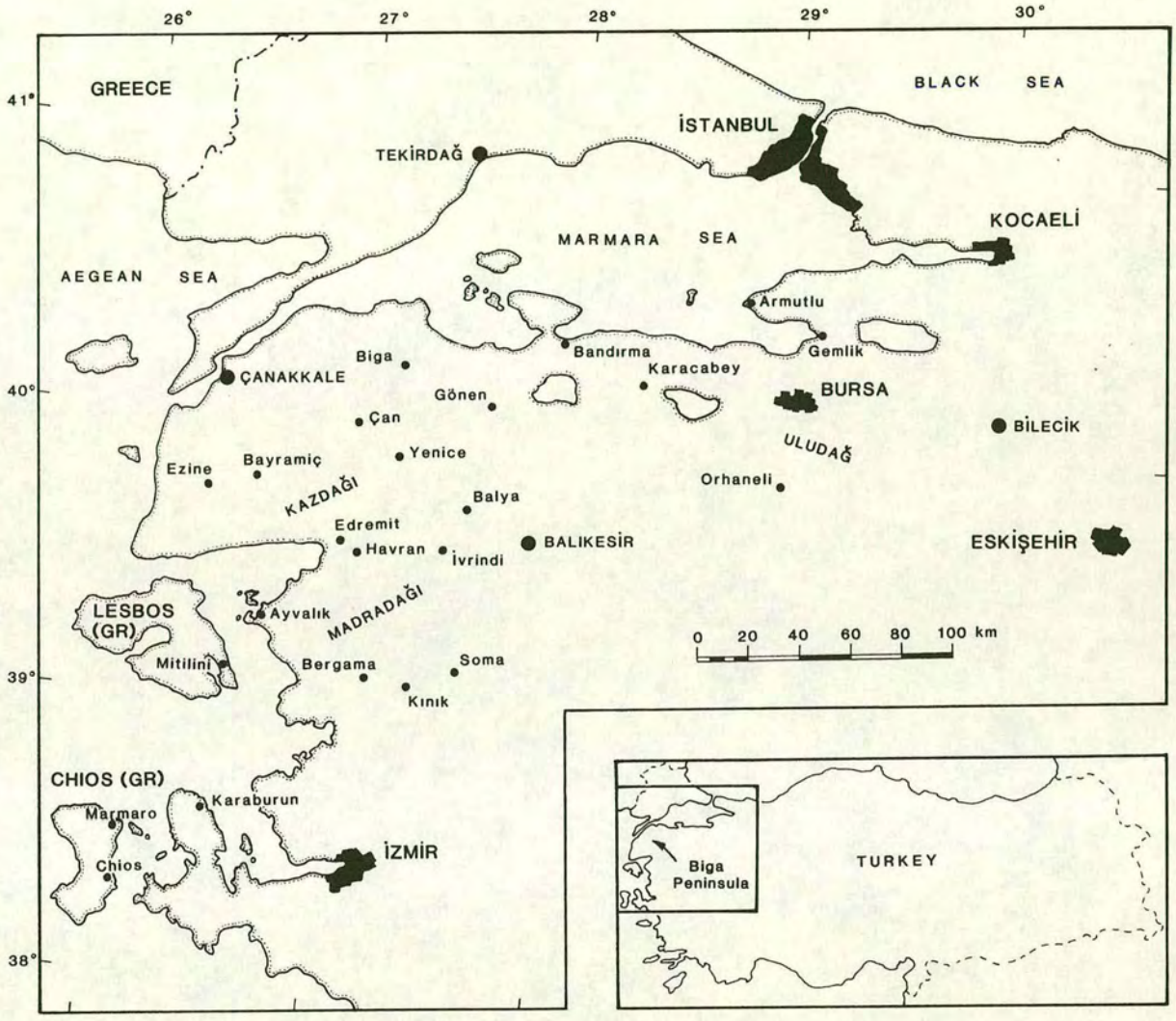

Figure 1.6 Location map of NW Turkey showing the towns and mountains mentioned in the text.

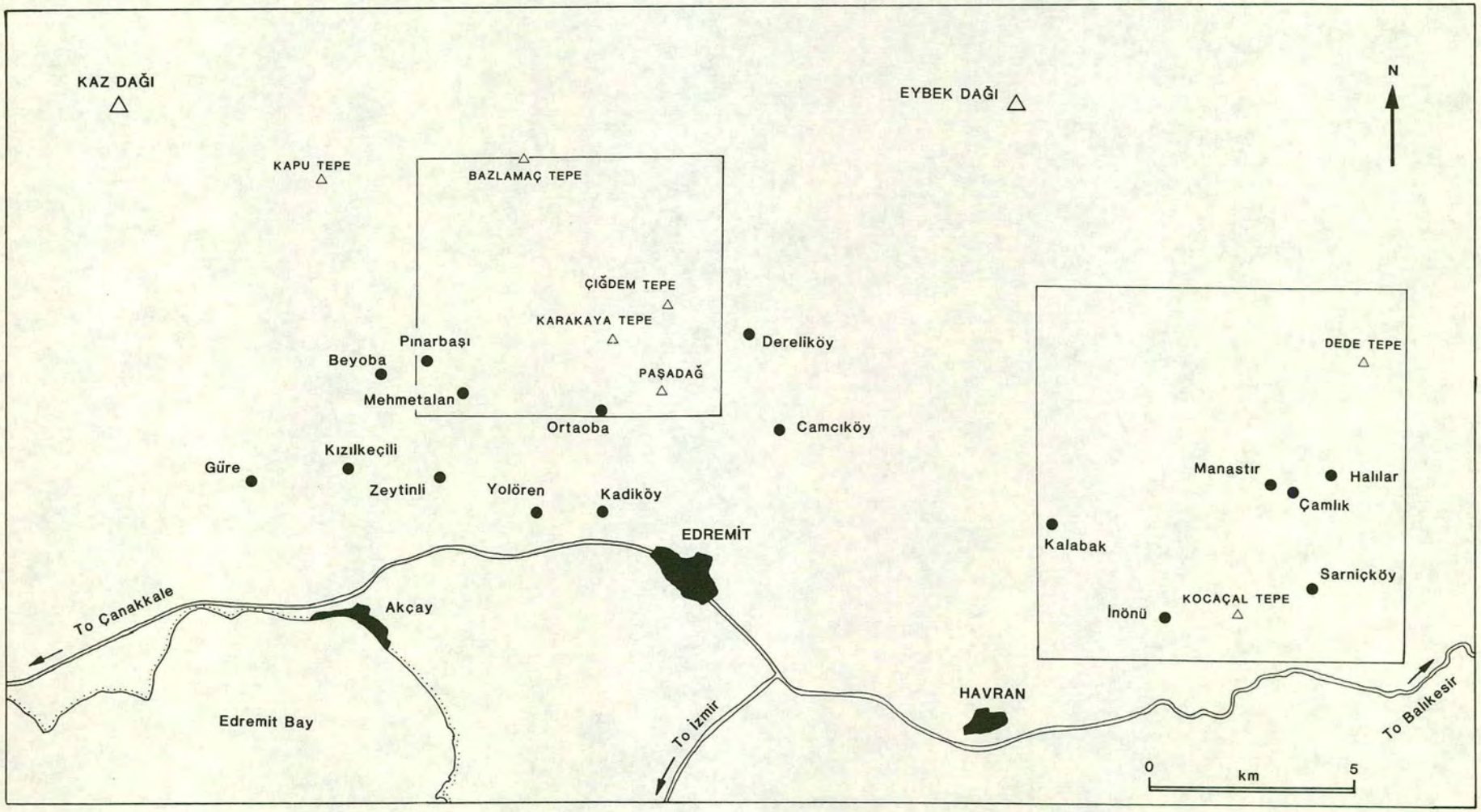

Figure 1.7 Location map of the Edremit-Havran region. Boxes show outlines of mapped areas.

Biga Peninsula is the beautiful Kozak forest with its huge round granite boulders, and the ancient citadel of Pergamon, which once housed one of the greatest libraries of the ancient world, perched high on a crag at Bergama.

The people of this region of northern Turkey are mainly farmers who rear goats, sheep and cattle on the scrubby hillsides and grow olive and fig trees on the least stony slopes. In the less mountainous central and northern Biga Peninsula, crops such as sunflowers and melons are common. Mules, donkeys and horses are a major source of transport and labour. Edremit and Havran are busy market towns which support all the hill villages and are themselves the focus of extensive olive farming on the surrounding coastal plains. Akçay on the coast near Edremit is a growing resort for Turks living in the cities of Istanbul, Izmir and Ankara.

1.6 Geological setting of the field area

The southern part of the Biga Peninsula is dominated by the elongate dome of the Kazdag Massif which trends NE-SW from the Bay of Edremit (Figure 1.8). The mountain range is flanked by smaller hills which comprise the deformed volcanic and sedimentary rocks of the Karakaya Complex and, at the western extent of the Kazdag range, by a sliver of Neotethyan mélange (Çetmi Ophiolitic Mélange). The Kazdag trend is reflected by the NE-SW orientation of the Karakaya units to the southeast of the massif. In this area the Karakaya Complex forms a SE-dipping stack of distinct tectonostratigraphic units which are now juxtaposed against the Kazdag Massif by major extensional detachment faults. In the southeast part of the Biga Peninsula, the disrupted limestone platforms and debris flows around Balya and Ivrindi form the northern end of a belt of relatively undeformed clastics and Permian limestones which extends southwestwards towards Kozak and Bergama.

West of the Kazdag Massif, in the region around Ezine, the structural trend is predominantly N-S to NNE-SSW and is defined by an elongate sliver of harzburgite (the Denizgören Ophiolite) which has an along-strike equivalent on the Greek island of Lesbos just off the Turkish coast. However, elements of the NE-SW trend of Kazdag are present in the Çamlica Micaschists which are juxtaposed against the ultrabasic slab and have a strong SE-dipping foliation.

Further south, on the Greek island of Chios and the Karaburun Peninsula near Izmir the structural trend is N-S. Thick Triassic platform sequences are exposed in both

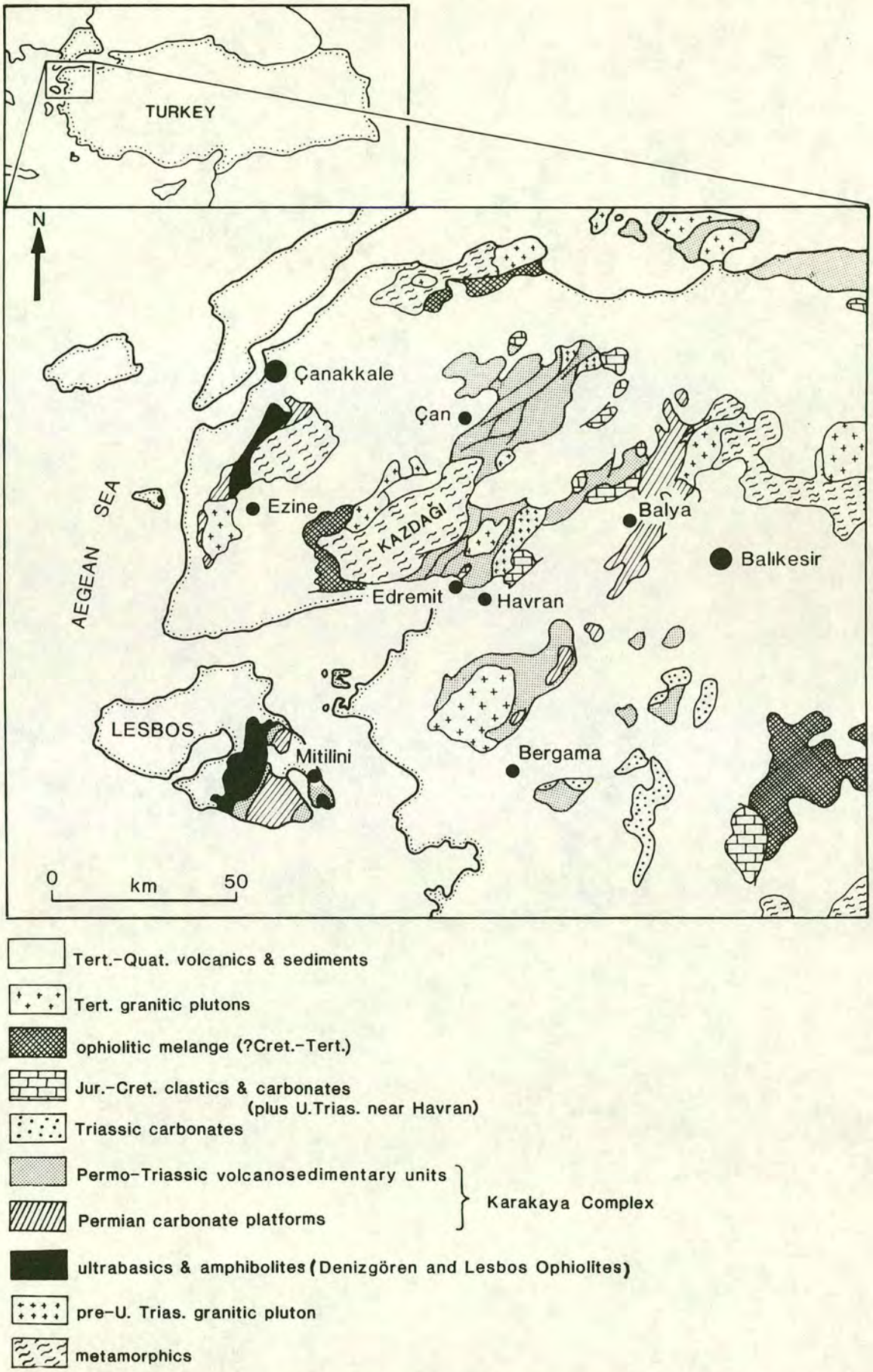

Figure 1.8 Geological map of the Biga Peninsula and surrounding regions. Compiled from maps by Bingöl (1989), Katsikatsos *et al.*, (Lesbos) 1982 and Okay *et al.* (1991).

regions and overlie mélange sequences containing blocks of volcanics and Palaeozoic limestone.

Tertiary to Recent tectonics have played a large role in the structural arrangement of the Biga Peninsula and surrounding regions. The "escape" of Anatolia towards the west as a result of movement along the North and East Anatolian Faults produced N-S extension in western Turkey (e.g. Sengör *et al.,* 1985) (Figure 1.9). A series of E-W trending grabens which testify to this extension can be recognized along the Aegean coast from Edremit to Izmir. Many small structures mirror the major, north- and south-dipping graben-bounding faults, and form a distinct feature of the Aegean coast region. Tertiary tectonics may also be partly responsible for the NE-SW trending normal faults which are particularly common in the Biga Peninsula area and may be related to the strands of the North Anatolian Fault which splay across the north and central part of the Biga Peninsula. These normal faults have a very similar trend to that of the Kazdag and Karakaya units, implying that the Tertiary activity may have reactivated older lineaments.

1.7 Previous research in the field area

Several early travellers and geologists made geological observations in the Biga Peninsula and surrounding regions (e.g. Diller, 1883; Chaput, 1932). Since then many regional studies of small areas have been made in the Biga Peninsula and surrounding areas. Nonetheless, there are no comprehensive, detailed published geological maps of the whole region and thus the geology remains poorly known in many areas. Studies made in the southern Biga Peninsula region include work on the metamorphic rocks of the Kazdag Massif by van der Kaaden (1959), Bingöl (1968, 1971), Bingöl *et al.* (1973) and Schuiling (1959). Broad-based regional investigations were carried out in the Edremit-Havran area by Gümüs (1964), Aslaner (1965) and Krushensky *et al.* (1980). Blanc (1965) described the limestone-rich debris flows and their Liassic cover in the Çan region. Mesozoic clastic and carbonate rocks to the east of Kazdag were the subject of detailed palaeontological and sedimentological studies by Aygen (1956) and Altiner *et al.* (1991). The ultrabasic rocks of the Denizgören Ophiolite and the underlying Permian platform in the western part of the Biga Peninsula were described by Kalafatçioglu (1973). More recently, Okay *et al.* (1991) described the broad geology of the Biga Peninsula and put forward tectonic models for its formation. The spilites and Permian limestone of the Bergama region south of the Biga Peninsula have been studied by Akyürek & Soysal (1983), Kaya *et al.* (1986),

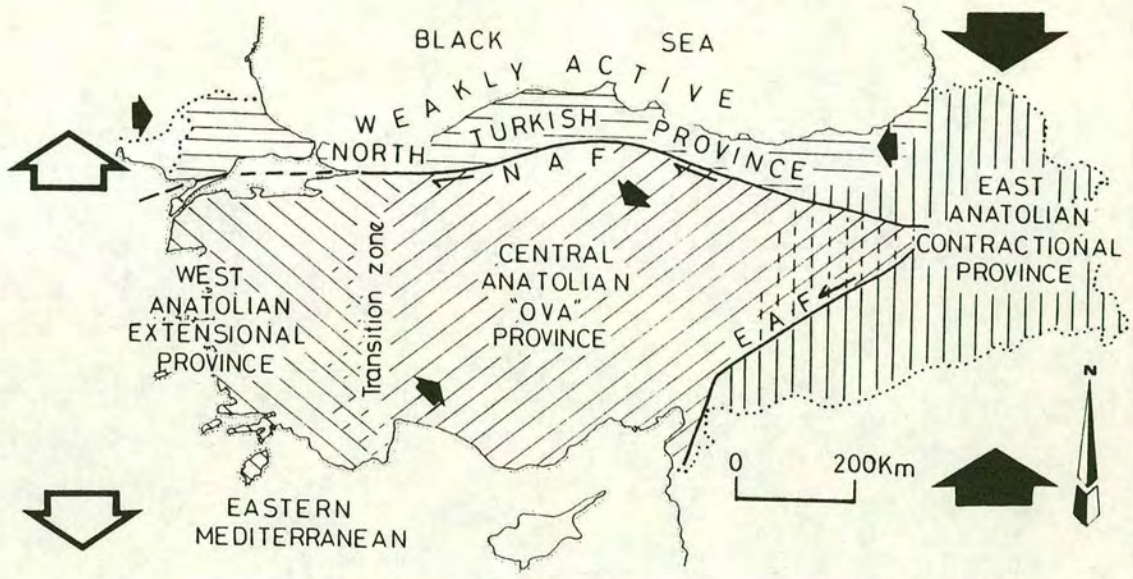

Figure 1.9 The four main neotectonic provinces of Turkey, produced by post-Mid Miocene westward escape of Anatolia along the dextral North Anatolian Fault (NAF) and the sinistral East Anatolian Fault (EAF) (from Şengör *et al.*, 1985). The four regimes are (a) East Anatolian contractional province of N-S shortening, (b) the weakly active North Turkish province with limited E-W shortening, (c) the West Anatolian extensional province characterized by strongly active N-S extension, and (d) the Central Anatolian province whose NE-SW shortening and NW-SE extension has produced complex basins or "ovas". The arrows show shortening (black) and extension (white) and are approximately proportional to the magnitude of the total strain.

Kaya *et al.* (1989) and Kaya & Mostler (1992). Recent work in this region by Okay *et al.* (1993) has related units in the Bergama region with those present near Edremit in the Biga Peninsula. Table 1.1 shows the previous stratigraphic and tectono-stratigraphic schemes for the units of the Karakaya Complex in NW Turkey and their relation to the tectonostratigraphy presented here.

The Tertiary to Recent geology of the Biga Peninsula has received somewhat more attention than the Palaeozoic to Mesozoic, owing to its good exposure and economic value. Siyako *et al.* (1989) summarized the Tertiary sedimentary and volcanic sequences of the Biga and Gelibolu Peninsulae, and described the predominantly NE-SW trending neotectonic fault systems. The extensive Tertiary volcanics and their associated plutons have long been the focus of mineral exploration. Gold and manganese within hydrothermally-formed veins associated with the thick volcanic piles have been extracted since Roman times (Maynard, pers. comm., 1991). The volcanics have also been the focus of several palaeomagnetic studies (e.g. Kissel & Laj, 1988; Platzman *et al.*, in press) to determine tectonic rotations caused by the North Anatolian Fault. The tectonic "escape" of Anatolia towards the west has been investigated by the study of the fault patterns and grabens along the Aegean coast. This region of Turkey is still tectonically active to the present day and various seismic studies have been carried out on earthquakes and subsurface hydrothermal systems (Schindler, 1993).

1.8 Objectives and approach of the thesis

This study has concentrated on the collection of new sedimentological, geochemical and structural data from NW Turkey with the aim of further elucidating the Late Palaeozoic to Early Mesozoic tectonic evolution of the western portion of the Palaeotethys ocean. Fieldwork was carried out over a wide area of NW Turkey, involving data collection from many critical areas rather than the detailed mapping of one small area. This approach has allowed the building up of a broad picture and will hopefully pave the way for future, more specific studies, in this crucial but relatively poorly understood area.

Reconnaissance over a much wider area, including areas to the east and the Greek islands of Lesbos and Chios has allowed comparison and correlation with the areas which were studied in more detail. Palaeotethyan regions in central and eastern Anatolia were not visited but recent detailed investigations in the Central Pontides

Table 1.1 Previous stratigraphic and tectonostratigraphic schemes for the Karakaya Complex in NW Turkey and their correlation with the tectonostratigraphy presented in this thesis. Thick black lines represent tectonic contacts.

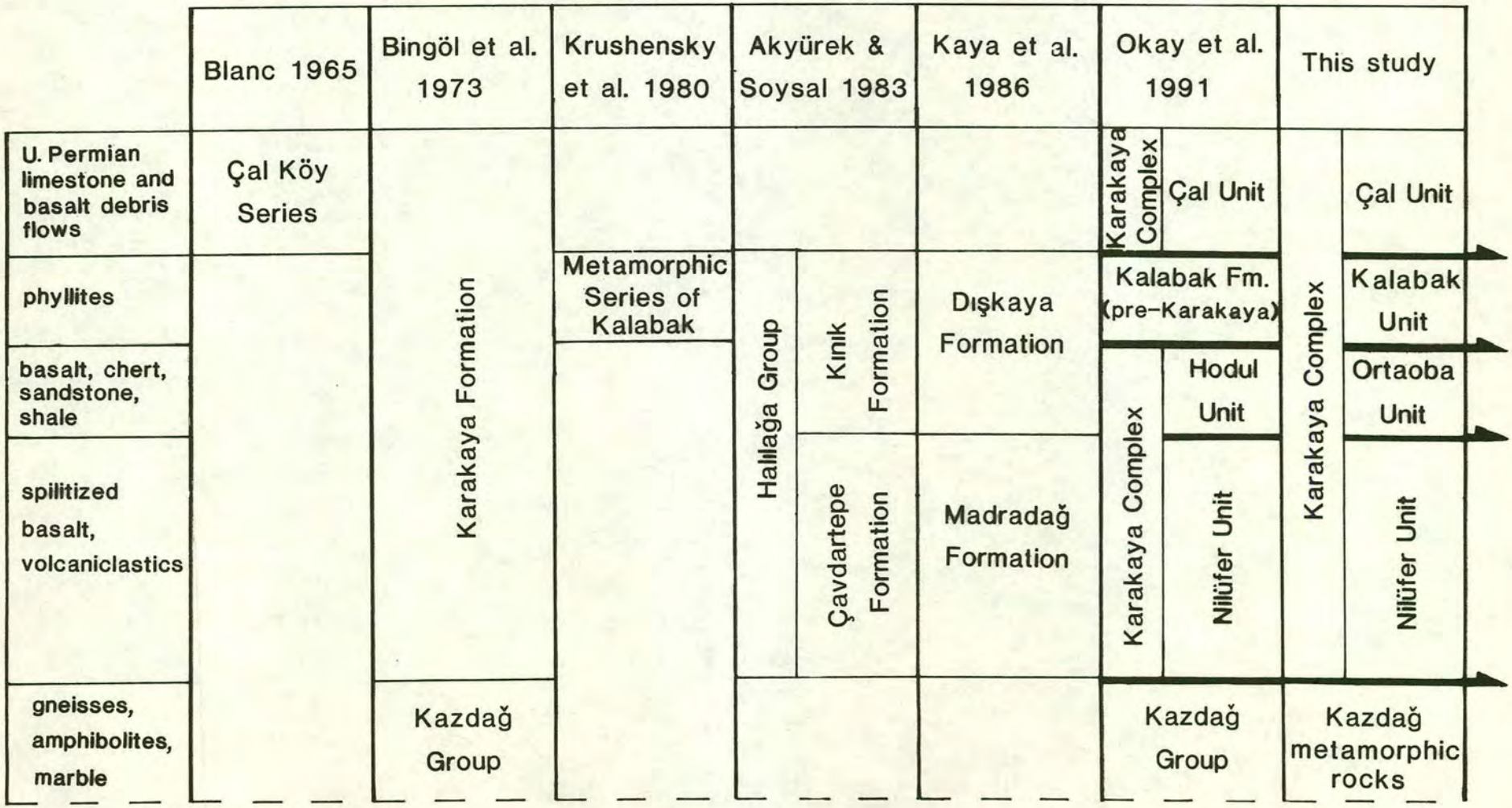

(Ustaömer, 1993) have allowed direct comparison with the region studied in this thesis.

The main objectives of this work were originally to gain a detailed understanding of the Karakaya Complex and to integrate the data into a general model for the evolution and subsequent destruction of the Palaeotethys Ocean in NW Turkey. This approach has necessarily involved the investigation of many Palaeotethyan elements other than the Karakaya Complex. The aims of this thesis can be summarized as follows:

The first main objective was to establish the lithological and structural nature of the Karakaya Complex and to interpret its tectonic setting. The Karakaya Complex was divided into several distinct tectonostratigraphic units on the basis of rock types and inferred tectonic boundaries between them. Owing to the patchy nature of the exposure and the intense shearing of many outcrops, data were collected from many individual sites and then correlated on the basis of lithology and with reference to key localities. These units, as described in this thesis, are not constrained geographically and include all the outcrops of a particular lithological association occurring within the field area. For example, the term "Nilüfer Unit" has been used to describe all the outcrops of the volcaniclastic association from Uludag in the north to the Bergama region in the south, regardless of local names in the literature. Field observations were followed up with laboratory-based studies such as thin-section petrographic work and geochemical analysis.

A large part of the laboratory-based studies involved the collection and geochemical analysis of volcanic rocks. Established methods of tectonic discrimination (e.g. Pearce & Cann, 1973) were then used to distinguish between the volcanic rocks and to define likely tectonic settings for their eruption, thus going some way to filling the large gap which exists in the literature with respect to igneous geochemistry.

A major aim of the study was to place the Karakaya Complex within the wider setting of the Palaeotethyan active margin. Field- and laboratory-based techniques have allowed the detailed interpretation of the components of the Karakaya Complex as elements of a Palaeotethyan accretionary complex. Many other tectonic units were investigated, both to establish their relationship with the Karakaya Complex and to deduce their tectonic settings in order to better understand the Palaeotethyan system as a whole.

An important aspect of the study has been the direct comparison of the studied units with those recognized in both ancient and modern active margin settings. Comparison with similar units reported from well-constrained and well-preserved active margin complexes around the world has provided invaluable information about the evolution of this relatively poorly understood active margin. The investigation of processes operating at present-day active margins, such as those in the SW Pacific, has allowed detailed interpretations of the Palaeotethyan units, particularly those of the Karakaya Complex.

A subsidiary part of the project has been a palaeomagnetic analysis of Mid Jurassic limestones (the Bilecik Limestone) of the Biga Peninsula, in an attempt to determine palaeolatitudes and to constrain the extent and timing of tectonic rotations which may have occurred in this region since the Mid Jurassic.

Fieldwork was carried out over three seasons during the summers and autumns of 1990, 1991 and 1992. The first field season was spent in the Edremit area and work focused on the Karakaya tectonostratigraphic units to the southeast of the Kazdag Massif. In particular, many samples of basalt were collected for geochemical analysis. During the following season, fieldwork was extended to adjacent areas. Karakaya units in the central Biga Peninsula area were studied, as was the ophiolitic fragment in the west and the Mesozoic cover in the Havran area. The final field season involved an extensive programme of reconnaissance work in areas adjacent to the original field area. In particular, the area around Bergama yielded invaluable information on Permian carbonate platforms and provided an almost intact section through one of the volcanic sequences of the Karakaya Complex. Following a field excursion to the islands of Lesbos and Chios during the spring of 1992, Chios was revisited along with its Turkish mainland equivalent, the Karaburun Peninsula.

There are very few detailed geological maps of the studied regions and most fieldwork was done using very generalized large-scale geological maps, topographic maps and published reports by various authors. In particular, maps from a report by Okay *et al.* (1991) were used in the Çan, Altinoluk, Balya and Ezine areas and a map by Bingöl (1971) was used in the Kazdag Massif. A few relatively detailed geological maps have been produced by the Turkish Institute of Mineral Exploration (M.T.A.) for the Bergama and Bandirma regions and were used in the study of these areas.

In Edinburgh several laboratory-based techniques have been used in conjunction with data collected in the field. These include microscope work on thin-sections, X-ray fluorescence spectroscopy (XRF), X-ray diffraction (XRD) and electron microprobe analysis. A palaeomagnetic study of Jurassic limestones was also carried out at the Department of Earth Sciences, Oxford University. Descriptions of the techniques are given in Appendices 1 and 5.

The aim of the project therefore has been to use a variety of methods to describe the Late Palaeozoic to Early Mesozoic sedimentary, volcanic and tectonic history of the Palaeotethys in NW Turkey. This integrated approach has led to a better understanding of the Karakaya Complex, and Palaeotethyan evolution as a whole.

1.9 Tectonostratigraphy

NW Turkey displays several major pre-Jurassic tectonic units (Figure 1.8), whose significance and relationships are poorly understood. Extensive Tertiary volcanics cover much of NW Turkey and separate many of the units, making their contacts and relationships difficult to establish. The units can be divided into several major tectonic entities which are (approximately from NW to SE):

1. Ultrabasic slab with metamorphic sole (Denizgören and Lesbos Ophiolites) emplaced onto a Permian platform (Karadag Unit).
2. Amphibolite gneisses and marbles of the Kazdag Massif (Kazdag "metamorphics").
3. Permo-Triassic sedimentary and volcanic rocks of the Karakaya Complex (Nilüfer, Ortaoba, Kalabak and Çal Units) with Upper Triassic-Jurassic sedimentary cover (Halilar and Bayirköy Formations and Bilecik Limestone).
4. Disrupted Permian platforms on clastic basement (here interpreted as part of Çal Unit).

The main focus of this study is the Karakaya Complex, a deformed, low-grade metamorphic assemblage of oceanic, or at least deep sea origin. The Karakaya Complex comprises a stack of distinct tectonostratigraphic units which can be distinguished primarily on the basis of their lithologies and the geochemistry of their constituent volcanic rocks. Figure 1.10 shows shows generalized sections through the three most distinctive Karakaya units (Nilüfer, Ortaoba and Çal Units), on the basis of sections studied in the Bergama, Edremit and Çan regions. The various units of the

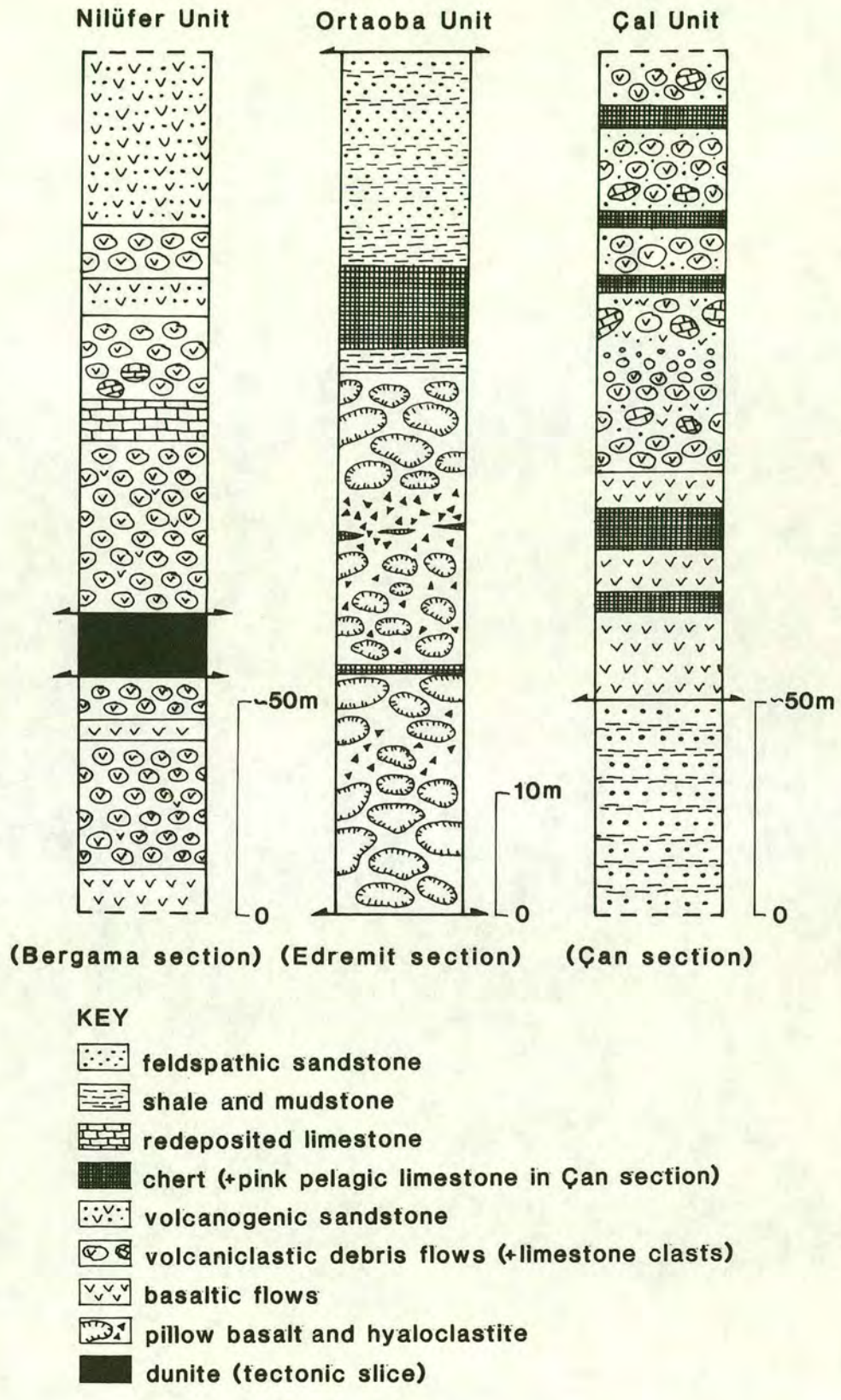

Figure 1.10 Generalized successions through the Nilüfer, Ortaoba and Çal Units, based on sections studied in the Bergama, Edremit and Çan regions respectively.

Karakaya Complex and their relationships with each other are particularly well exposed in the Edremit region. A schematic cross-section for this region is shown in Figure 1.11. The line of section marked X is shown in more detail in Figure 1.12.

The Karakaya Complex is probably the single most critical pre-Jurassic unit in the Biga Peninsula as its components clearly represent Palaeotethyan sea floor and reflect the processes involved in their incorporation into an accretionary complex. However, the Karakaya Complex cannot be considered in isolation from the other pre-Jurassic units outlined above. The relationship between the complex and the other units outlined above provides perhaps our best opportunity to consider Palaeotethyan evolution in this area as a whole.

1.10 Thesis organization

Chapters 2, 3 and 4 focus on the major Karakaya units which have been recognized within the field area. In Chapter 5 the Upper Triassic to Mid Jurassic sedimentary rocks which lie directly above the Karakaya Complex are discussed.

Chapters 6, 7 and 8 are concerned with related tectonic units which are significant in terms of Palaeotethyan evolution but which were studied in less detail than the Karakaya Complex. The Kazdag metamorphic rocks are discussed in Chapter 6 and the Denizgören and Lesbos Ophiolites in Chapter 7. Chapter 8 deals with the Palaeozoic-Mesozoic geology of Chios and the Karaburun Peninsula.

Chapter 9 is a palaeomagnetic study of the Jurassic Bilecik Limestone. The palaeomagnetic work has produced inconclusive palaeolatitudes but shows that tectonic rotations have taken place in the Biga Peninsula since the Jurassic. Finally, Chapter 10 outlines the pre-Jurassic tectonic and sedimentary evolution of this part of Turkey in the light of the data presented throughout the thesis.

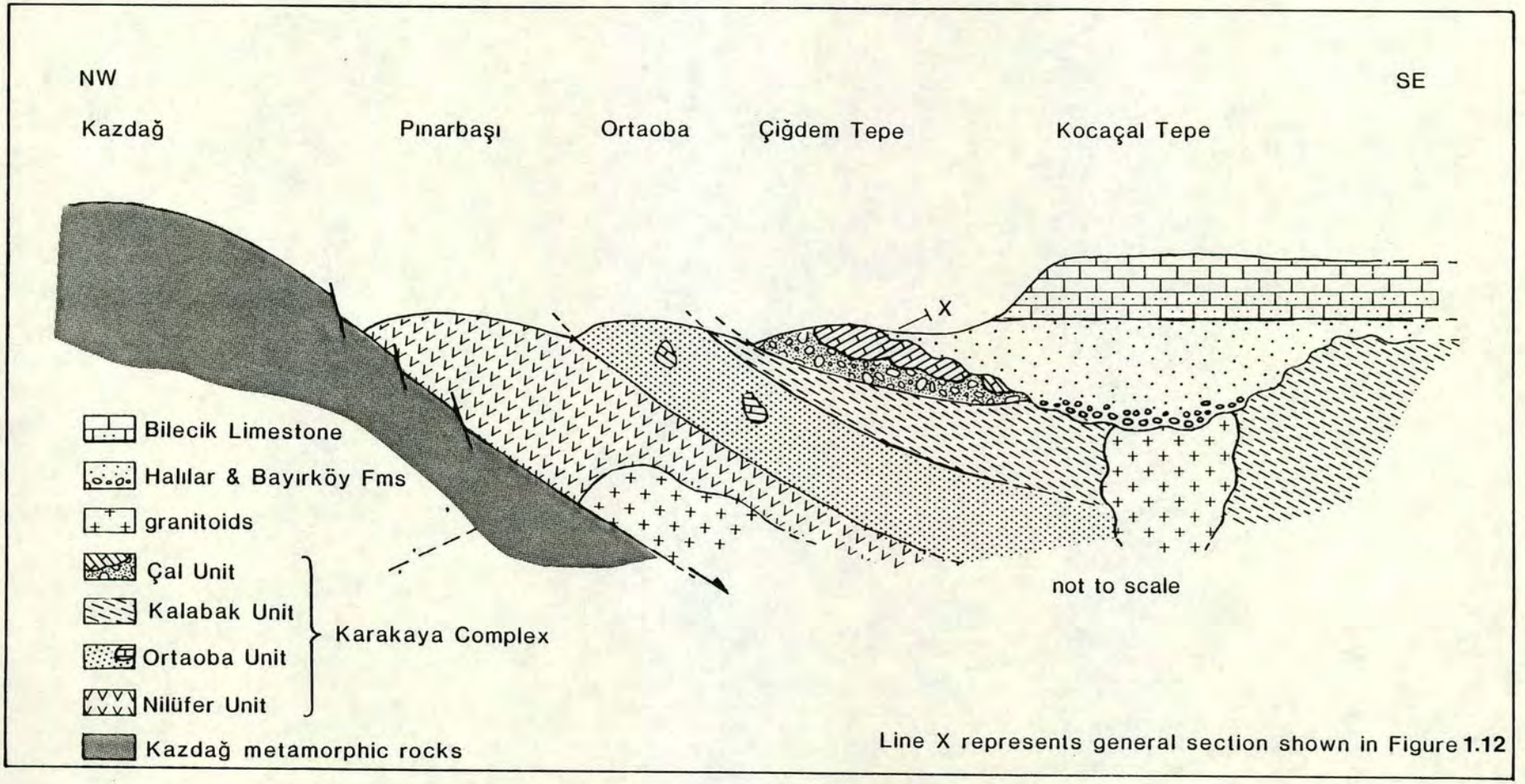

Figure 1.11 Schematic cross-section of the Edremit region, showing juxtaposition of the Karakaya units and their relationship with the Kazdağ Massif and the overlying Upper Triassic-Jurassic sedimentary sequence.

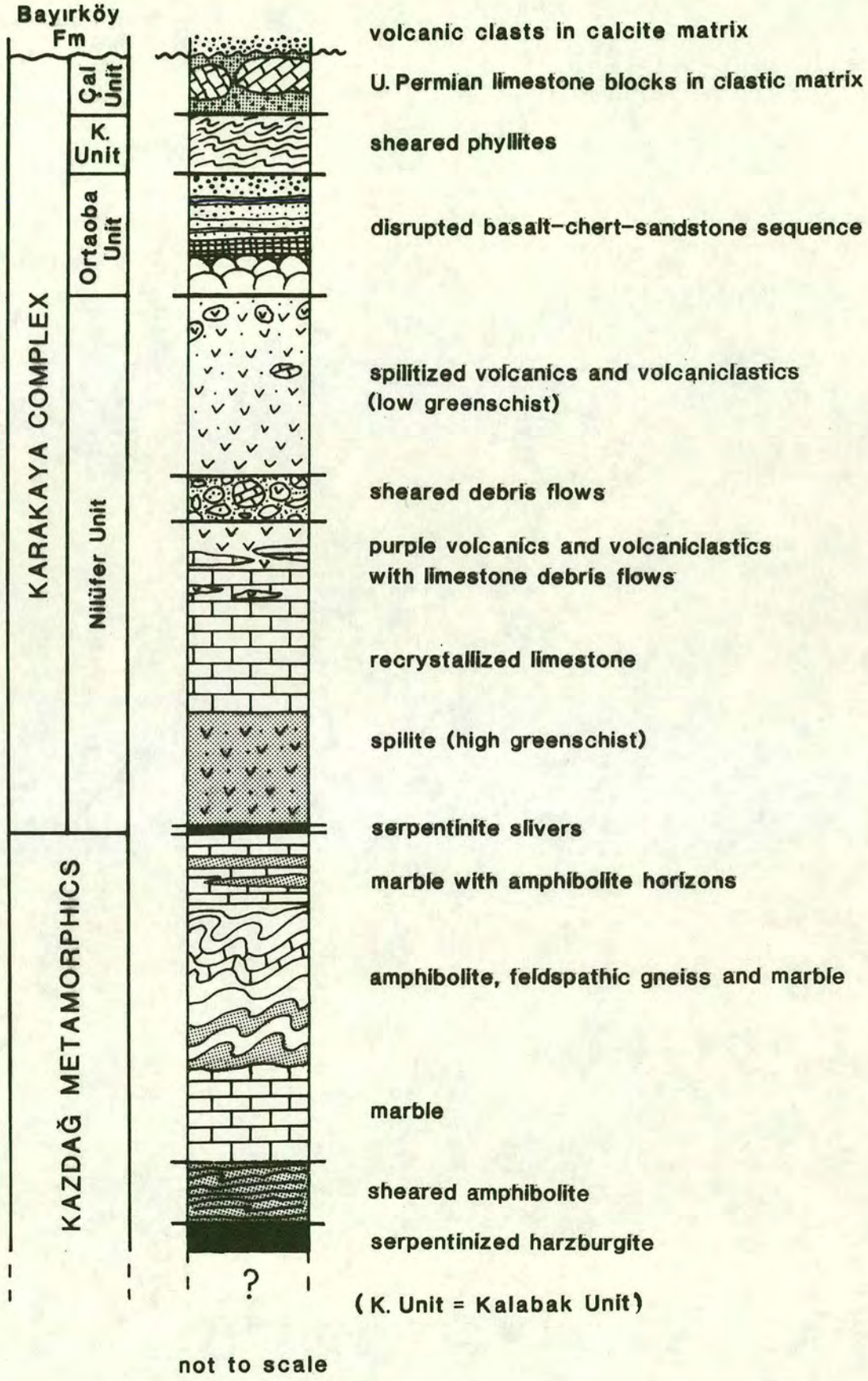

Figure 1.12 Schematic section through the Kazdag Massif and Karakaya Complex in the Edremit region.

1.11 Note on placenames and their pronunciation

a) Placenames

Throughout this thesis, most of the features of the field area are referred to by their full Turkish names, thus necessitating a brief explanation of their meanings. The words listed below are typically found as endings after the names of hills, villages and rivers.

çay	stream
dag	mountain
dere	valley or stream
köy	village
tepe	hill

Many Turkish placenames have direct meanings which can be readily translated. For example, Ortaoba means middle nomad camp, Kozak means fir cone and Karakaya Tepe means black rock hill.

b) Spelling and pronunciation

The Turkish alphabet was introduced by Kemal Atatürk in 1928. It uses the Latin alphabet with some additions. The letters are pronounced as in English except that u is as in 'put' not as in 'cup', and c is pronounced j. In addition, Turkish uses the following letters:

ç	like ch in church
g	lengthens the preceeding vowel but is not sounded
i	(without a dot) is like i in cousin
s	like sh in shoe
ö	same as the German ö
ü	same as the German ü

CHAPTER 2

THE NILÜFER UNIT: ACCRETED SEAMOUNT SEQUENCES

2.1 Introduction

The Nilüfer Unit is predominantly composed of volcanic and volcaniclastic rocks. It forms the lowest exposed tectonostratigraphic unit of the Karakaya Complex in NW Turkey and takes its name from the Nilüfer River, between Bursa and Orhaneli (Figure 1.6). The Nilüfer Unit has a very wide distribution over NW Turkey and, in this study, is described mainly from the Edremit and Bergama regions (Figure 2.1). Reconnaissance in the Bursa and Bandirma areas has revealed the presence of very similar rocks which also display similar lithologies and geochemistry to those in the Edremit and Bergama areas. As discussed in Chapter 1 this unit has various names in the literature (see Table 1.1). For the sake of clarity and consistency this sequence is hereafter called the Nilüfer Unit. The bulk of the unit consists of green spilitized basalts and volcaniclastic rocks with minor intercalations of marble and bedded volcanogenic sandstones and siltstones.

The aim of the work presented in this chapter was to determine the origin of the Nilüfer Unit, especially the tectonic setting of its voluminous volcanics. Only when this was achieved could the unit be interpreted in terms of its relationship with the other Karakaya units, thus shedding light on the evolution of the accretionary complex as a whole. Most of this chapter is concerned with the various lithologies of the Nilüfer Unit and the geochemistry of the basaltic rocks.

2.2 Previous work

The Nilüfer Unit, as defined in this thesis, has been previously studied in both the Edremit and Bergama regions. On the published M.T.A. maps of the Bergama region, this volcanic unit is called the Çavdartepe Formation (after Akyürek & Soysal, 1983). The Çavdartepe Formation is part of their Halilaga Group, which also includes the clastic Kinik Formation, and corresponds closely to the Karakaya Complex of the Biga Peninsula. Kaya *et al.* (1986) also studied the geology of the Bergama area and named the volcanic sequence the Madradag Formation. The Çavdartepe and Madradag Formations are essentially the same unit. Kaya & Mostler (1992)

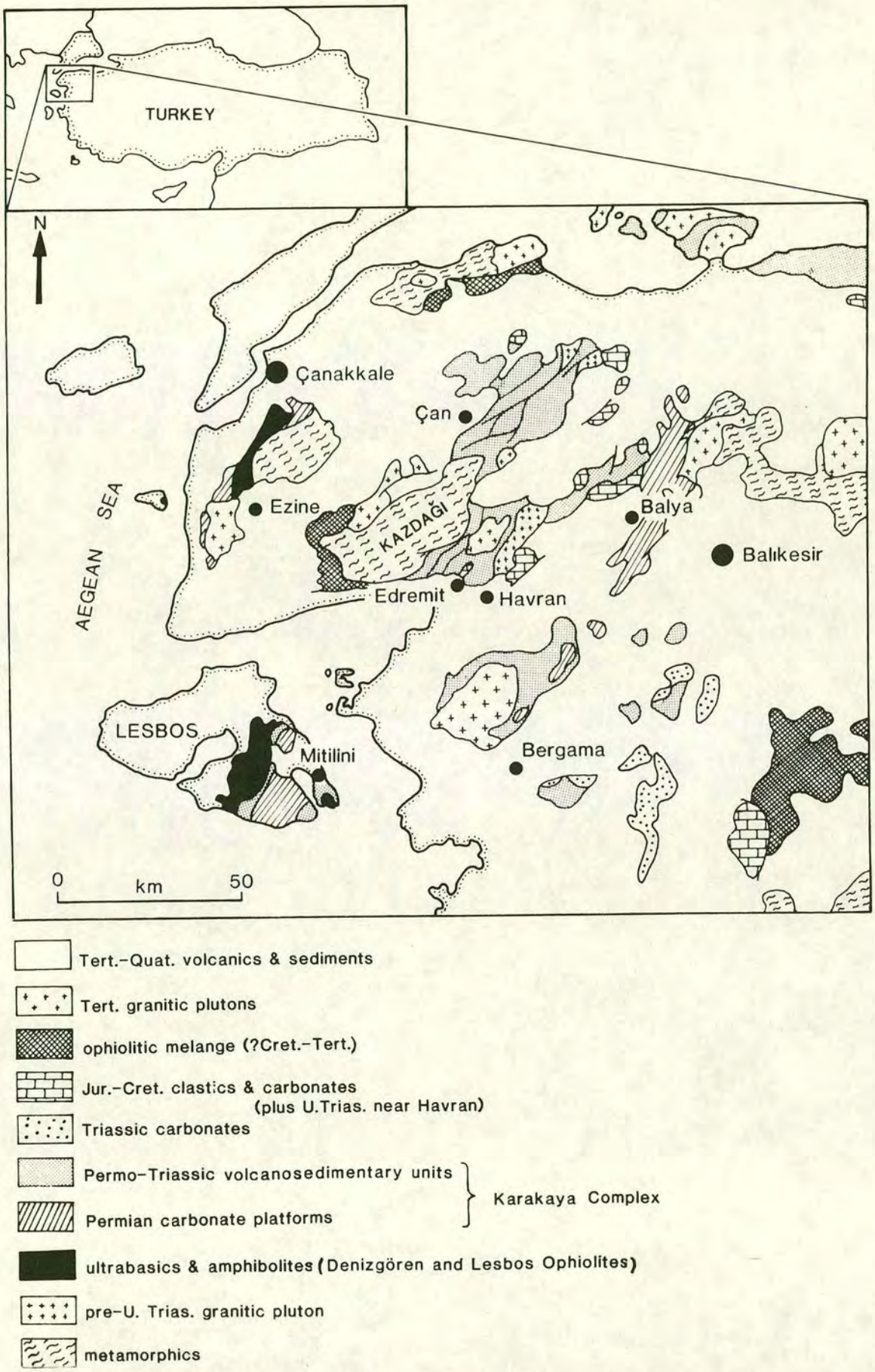

Figure 2.1 Generalized geological map of the Biga Peninsula and surrounding areas.

discovered Middle Triassic conodonts in redeposited limestone at the top of their Madradag Formation in the Bergama region.

The Nilüfer Unit has been recognized in the Bursa region and was named by Okay *et al.* (1991) after the Nilüfer River which runs southwards from the city. Okay *et al.* (1991, 1993) also named the volcanic sequences near Edremit and Bergama the Nilüfer Unit, a usage which is adopted here. Table 1.1 shows the various names of the Nilüfer Unit and their correlation with this study.

2.3 Lithologies of the Nilüfer Unit

In the Nilüfer Unit a wide spectrum of lithologies exists between the end-members of massive basalt and volcanogenic sandstone and mudstone. Volcaniclastic rocks make up at least 80% of the Nilüfer Unit in most localities and comprise both pyroclastic and epiclastic rocks (whose definitions are outlined below). Several distinct facies of the Nilüfer Unit were recognized during fieldwork in the Edremit and Bergama regions and are listed below. A continuous spectrum of facies exists between the six end-members.

a) Massive lava flow with primary basaltic textures.
b) Massive welded ignimbrite flow.
c) Purple streaky ash/ignimbrite.
d) Clast-supported volcanogenic conglomerate.
e) Bedded volcanogenic mudstone and fine-grained sandstone.
f) Limestone turbidite intercalated with volcanogenic sedimentary rock.

2.3.1 Terminology of volcaniclastic rocks

"Volcaniclastic" is a non-genetic term for any fragmental aggregate of volcanic parentage, irrespective of origin (Cas & Wright, 1987). "Volcaniclastic" includes the origin-specific terms "pyroclastic" and "epiclastic". "Pyroclastic" refers to aggregates formed by explosive volcanic activity and deposited by purely volcanic transport processes. Examples of pyroclastic rocks are tuffs and ignimbrites. "Epiclastic" is used to describe deposits that were produced by normal surface fragmentation processes (e.g. weathering, erosion), or were finally deposited by normal surface transport processes (e.g. mass flow, turbidity currents, suspension etc.). Epiclastic rocks include conglomerates, sandstones and mudstones.

Deciding whether massive volcaniclastic flows are pyroclastic or epiclastic can be very difficult (Wright & Mutti, 1981) and the Nilüfer Unit is no exception. Although it is tempting to interpret many of the Nilüfer volcaniclastics as primary eruptive products, it is also possible that they represent remobilized pyroclastic debris. Both pyroclastic and epiclastic rocks have been positively identified in the Nilüfer Unit, but these examples tend to represent end-member types. Where identifiable, volcaniclastic rocks from the Nilüfer Unit fall into the following categories:

Pyroclastic
- *a) Green, welded fine-grained ignimbrite*
- *b) Purple ash-flow tuff and/or fine-grained ignimbrite*

Epiclastic
- *a) Green volcanogenic sandstone*
- *b) Green and purple volcanogenic siltstone/mudstone*
- *c) Green volcanogenic breccia (± limestone clasts)*

2.4 Edremit area

Northwest of Edremit the Nilüfer Unit crops out between the metamorphic rocks of the upper parts of the Kazdag Massif and the predominantly clastic Ortaoba Unit which is discussed in the next chapter (Figures 2.2 and 2.3). The Nilüfer Unit, as defined in this thesis, can be broadly divided into four horizons in the Edremit area. These are, from base to top: high-greenschist facies volcanics, recrystallized limestone, purple volcanics, sheared debris flows and low-greenschist facies volcanics (Figure 2.4). The contacts which form the top and base of the Nilüfer Unit are undoubtedly tectonic. The divisions between the units within the Nilüfer Unit are less clear but are probably also tectonic. The two lower horizons are in the high-greenschist facies and are highly recrystallized and relatively featureless. The higher horizons are in the lower greenschist facies and, as a result, contain much better preserved sedimentary and igneous internal features. This chapter concentrates on the lithologies of this upper part of the Nilüfer Unit.

The best exposure is along the valley which runs due north of Ügü tasi (Figure 2.5). The road cutting along the east side of the valley displays a varied assemblage of facies which were extensively sampled for geochemical analysis. A small steep-sided valley, running approximately NE-SW, joins the main valley near its north end (enclosed by box A in Figure 2.5) and provides an excellent site for the observation of facies of the Nilüfer Unit in this area.

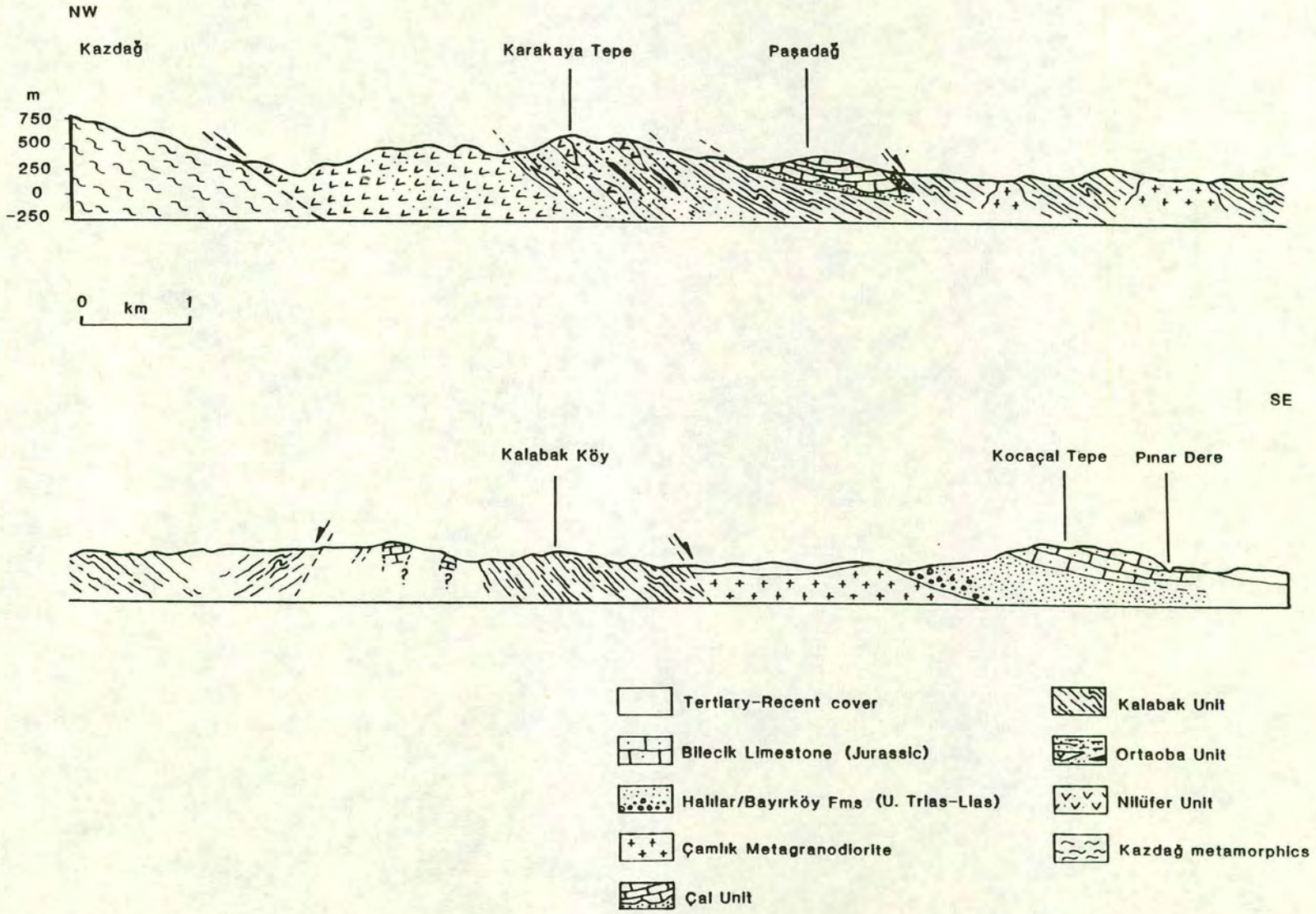

Figure 2.2 Cross-section through the Karakaya Complex in the Edremit area (modified after Aslaner, 1965).

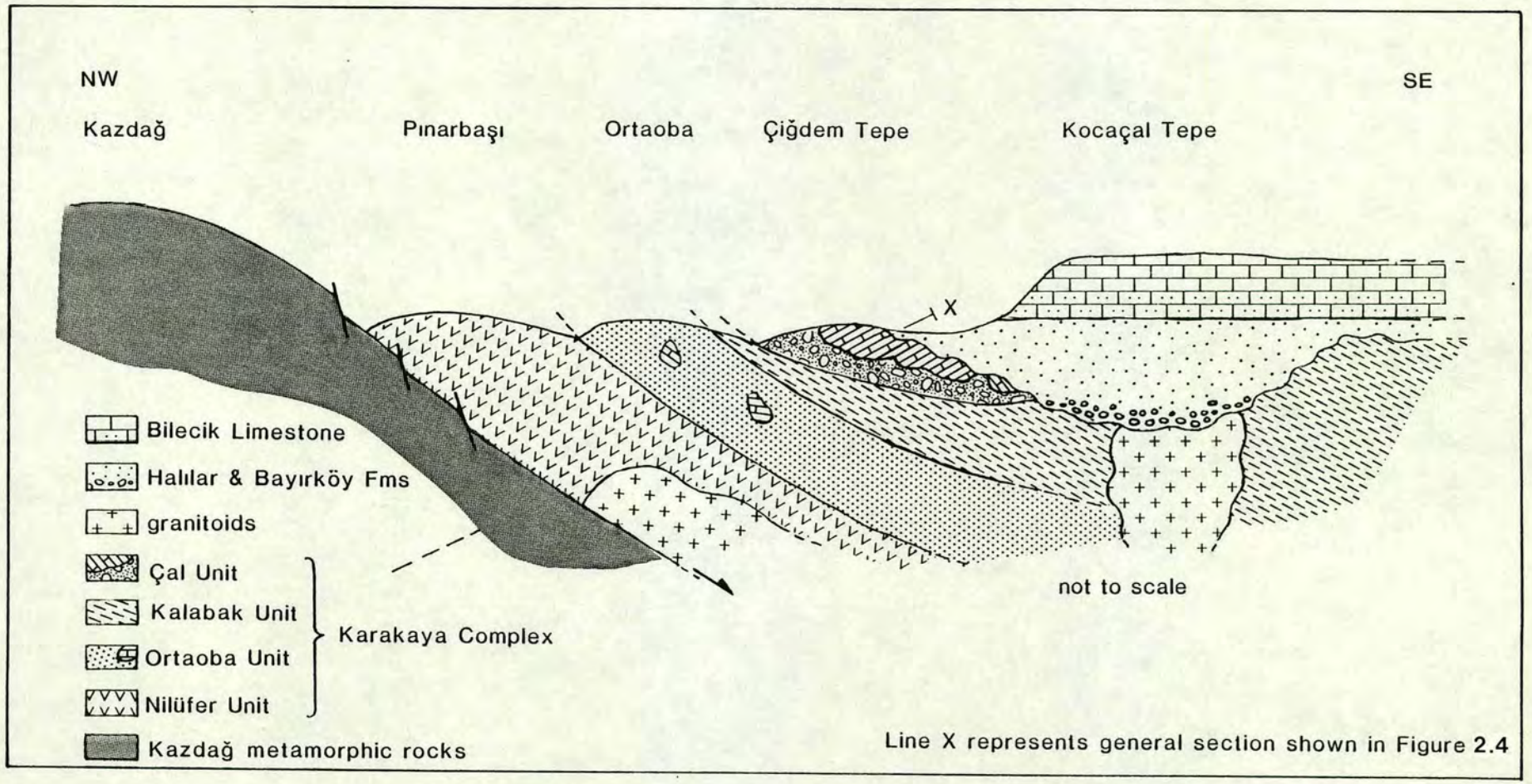

Figure 2.3 Schematic cross-section through the Karakaya Complex in the Edremit-Havran region.

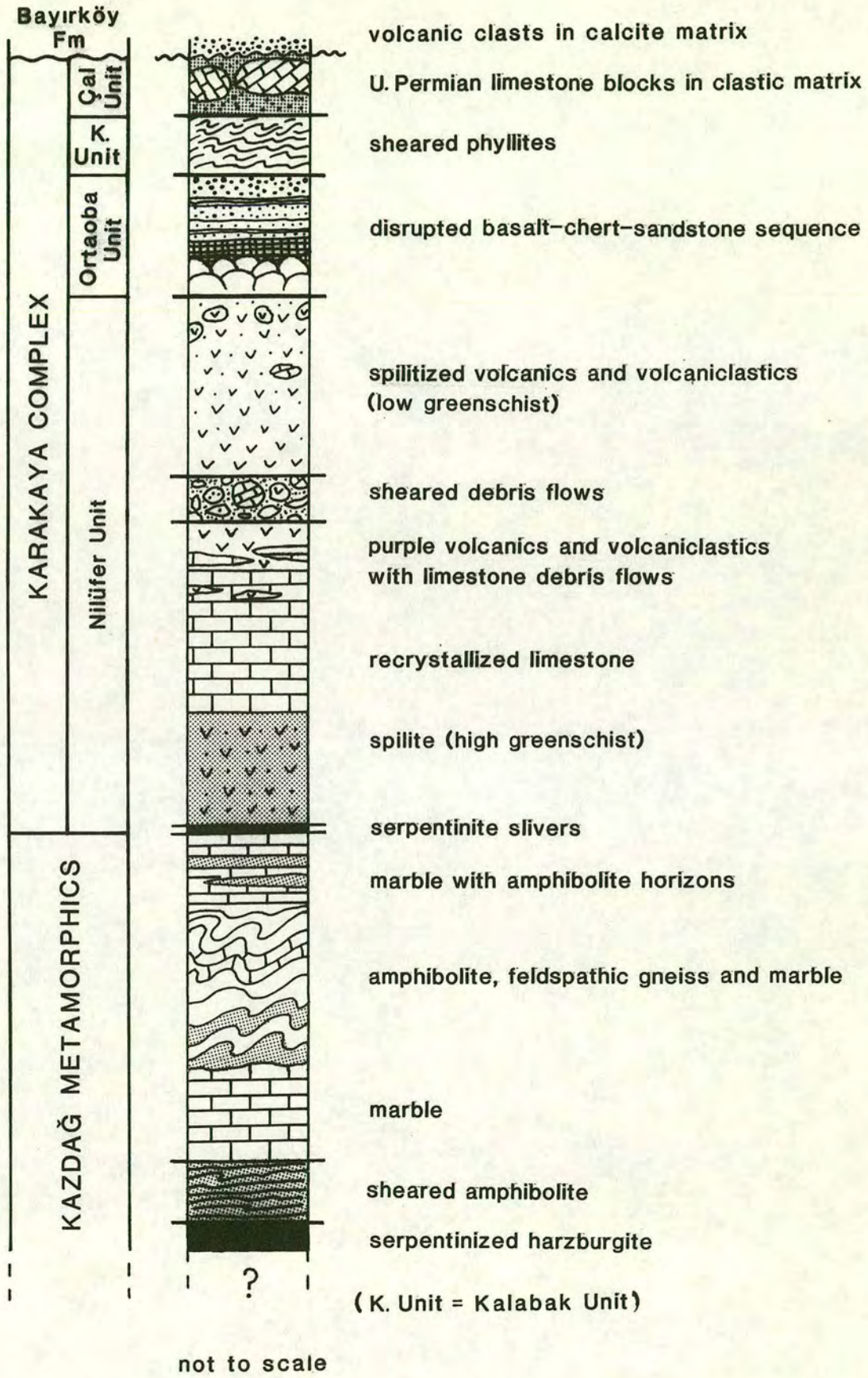

Figure 2.4 Schematic section through the Karakaya Complex in the Edremit region.

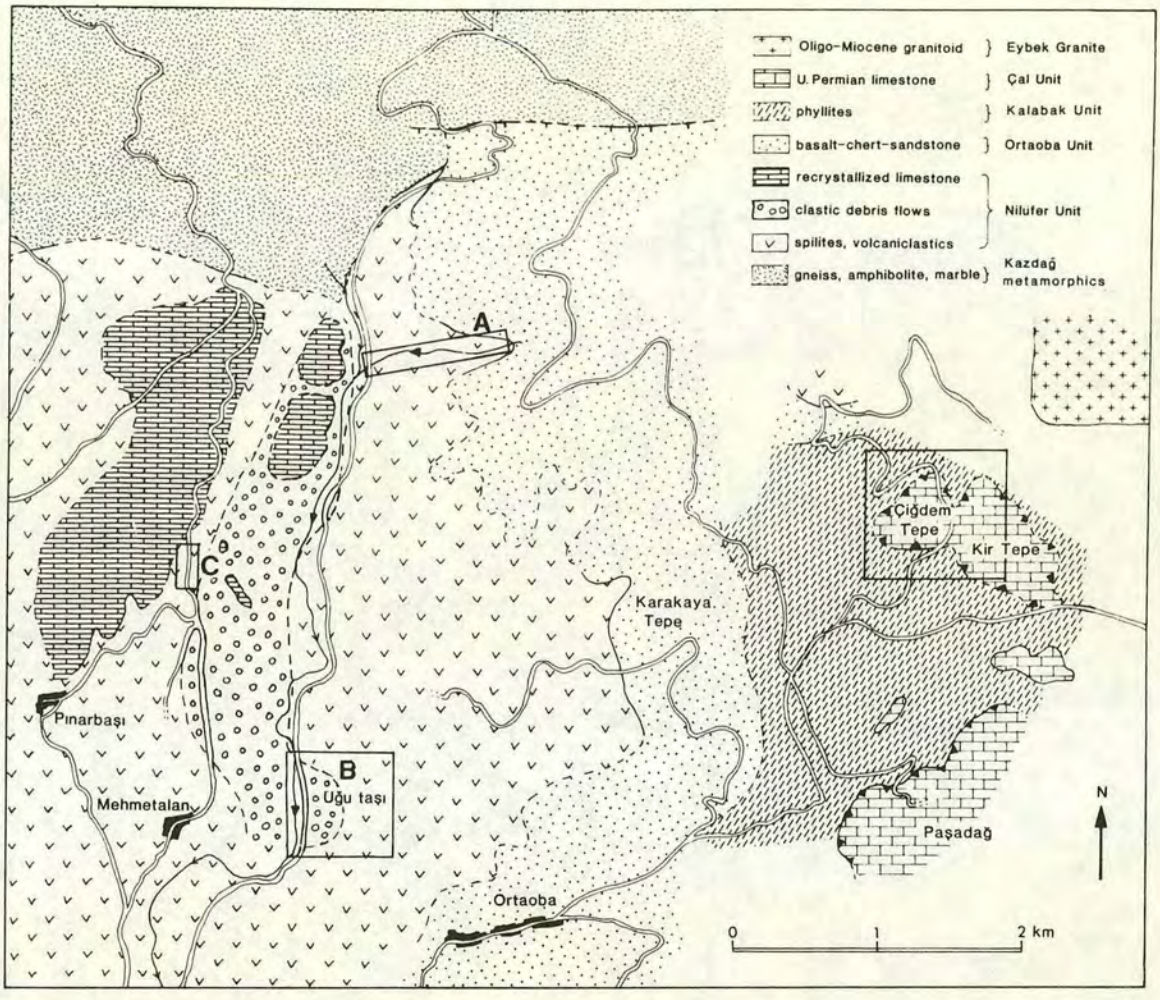

Figure 2.5 Geological map of the region north of Edremit (from an unpublished map by Okay and my fieldwork). The areas enclosed by boxes A, B and C are referred to in the text.

2.4.1 Main lithological associations

Massive lavas and volcaniclastic debris flows form most of the outcrop along the main valley north of Zeytinli, whereas volcaniclastic conglomerates and volcanogenic sedimentary rocks predominate in the smaller, subsidiary valley which trends NE-SW. The main lithologies are described below.

a) Massive lava flow with primary basaltic textures

Massive flows of primary volcanic rocks are exposed along the main N-S trending valley north of Ügü tasi. Their boundaries are impossible to trace as they appear to grade both laterally and vertically into volcaniclastic flows of sedimentary origin. The two types of massive flow are difficult to distinguish in the field, as they are both green and largely structureless. In thin-section, however, a variety of textures were observed, which allow the distinction between primary lavas and volcaniclastic rocks. The most common primary basaltic textures include subophitic, intergranular, amygdaloidal and porphyritic textures. A combined subophitic and porphyritic texture in which clinopyroxene phenocrysts are set in a fine-grained subophitic groundmass is particularly common. The clinopyroxene is slightly pink indicating possible Ti enrichment. Most of the lavas are considerably altered and display plagioclase albitization, alteration of clinopyroxene to chlorite and devitrification of glass. Vesicles are infilled with chlorite and calcite and are commonly rimmed with epidote crystals. In places alteration has proceeded to such an extent that the entire rock has been replaced by chlorite and actinolite.

Basalts become progressively more altered and metamorphosed towards the Kazdag Massif. Along the road towards the summit of Kazdag basalts are very sheared and display almost complete replacement by actinolite, chlorite, epidote and quartz. The strong fabric and the presence of replacement quartz is absent from the basalts in the valleys north of Zeytinli.

b) Massive welded ignimbrite flow

Massive pyroclastic flows are very similar in appearance to primary volcanic lava flows and are closely associated in outcrop. They are exposed along with primary lava flows in the main valley north of Zeytinli. In hand specimen the pyroclastic rocks have a streaky appearance and small clasts up to a few millimetres across can be discerned. Well-preserved ignimbritic textures are revealed in thin section. Glass-rich examples contain chlorite-filled vesicles and small clasts of fine-grained basalt

(Figure 2.6). The basalt clasts are draped by the glassy material and have diffuse edges, implying a degree of fusion with the original hot glassy matrix. Other examples are much less glassy and comprise isolated glass fiamme in a chloritic matrix. The fiamme shapes were clearly produced when in a semi-lithified state, by deformation within a hot flow.

c) Sheared purple volcanics

Fine-grained purple volcanics are exposed near the village of Pinarbasi and along the road running north from Mehmetalan (Figure 2.5). They are sheared, friable and streaky and associated with large white recrystallized limestone blocks (Figure 2.7). An outcrop of this lithology near the junction of the two roads contains pale lath-like plagioclase crystals with slight preferred orientation. Further along the Mehmetalan road, purple partings are present within recrystallized limestone and may represent a reworked version of the primary volcanic rock described above. Thin-section study shows that the purple shale is rich in small grains of hematite and contains reworked clasts of the same material.

d) Clast-supported volcanogenic conglomerate

This facies is very common in the small valley marked A in Figure 2.5. Clasts are up to 20cm in size and are predominantly volcanic or volcaniclastic (Figure 2.8a and 2.8b). The conglomerates range in colour from green to brown, depending on the degree of alteration of the particular outcrop. The freshest outcrops are a clear greenish-blue colour. A large proportion of the clasts have a distinctive texture of rounded black blebs (up to 5mm across) in a finer grained groundmass. Owing to considerable chloritization, the original nature of elements such as these blebs is often unclear. However, it seems likely that they are relict clinopyroxene phenocrysts or, in some cases, glassy shards. Other clasts consist of recrystallized white limestone, amygdaloidal basalt, purple shale, fine-grained volcanogenic sandstone and pale green volcanic shale. Several of the volcanogenic sandstone clasts contain calcite veins which clearly predate formation of the volcaniclastic conglomerate and may reflect hydrothermal activity. The matrix consists of fine- to medium-grained volcaniclastic debris and is identical to many of the finer grained clasts. The limestone clasts are invariably white and very recrystallized, although grey, kinked banding was observed in one large clast (Figure 2.8b). Two clasts of crimson-red vitreous jasper were also observed. In one locality the conglomerates contain contorted veins of bright green epidote.

Figure 2.6 Photomicrographs of typical pyroclastic textures in the Nilüfer Unit north of Edremit.

(a) Glassy material with vesicles in the matrix of an ignimbritic flow north of Ügü tasi (sample 54a/90, PPL, field of view: 5.5mm)

(b) Basaltic clasts and glassy fiammé in same the sample as above. Fusing of the contacts between the clasts and the glassy blebs is evidence for a pyroclastic, rather than epiclastic, origin (sample 54a/90, PPL, field of view: 8.5mm).

(c) Basaltic clasts and glass shards in ignimbritic flow north of Mehmetalan (sample 102b/90, PPL, field of view: 11mm)

a

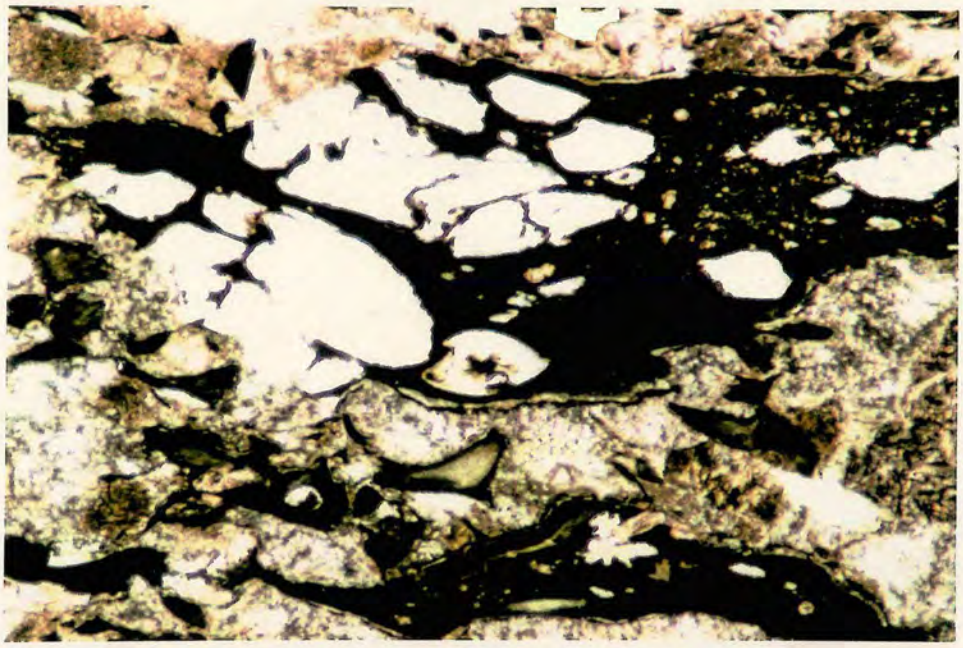

b

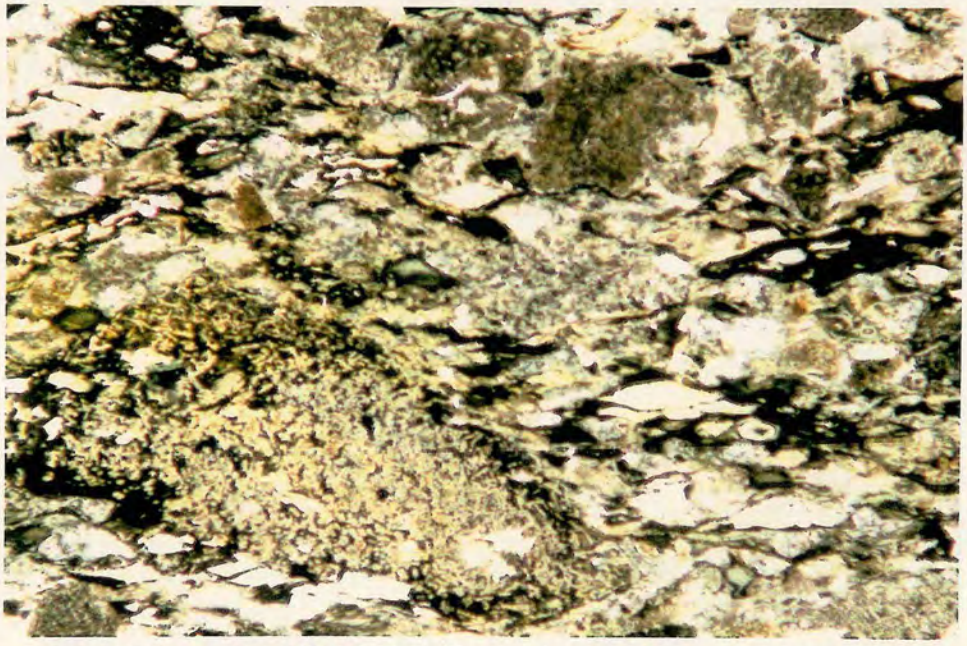

c

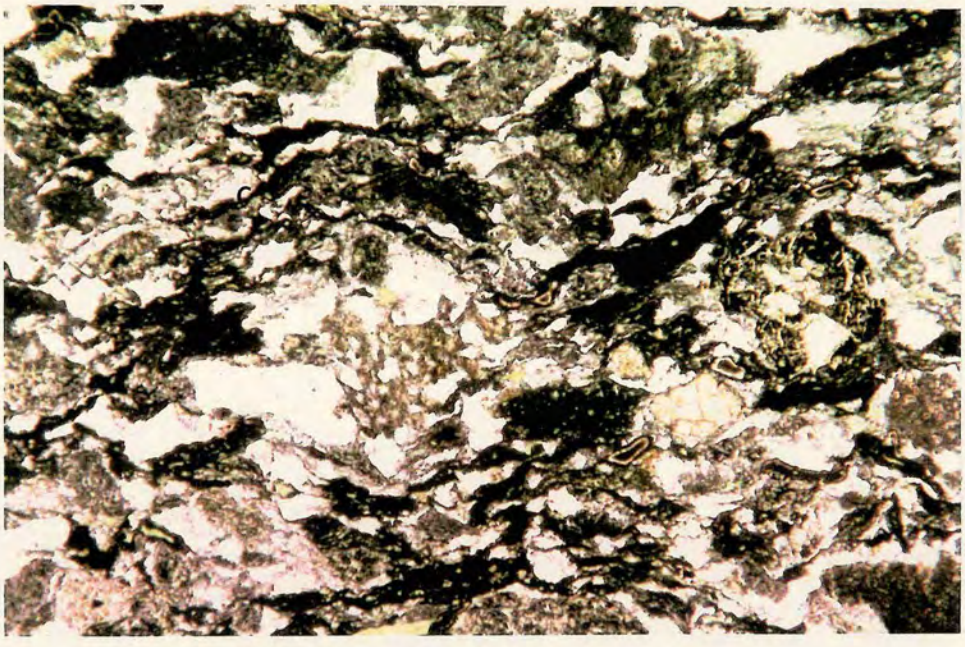

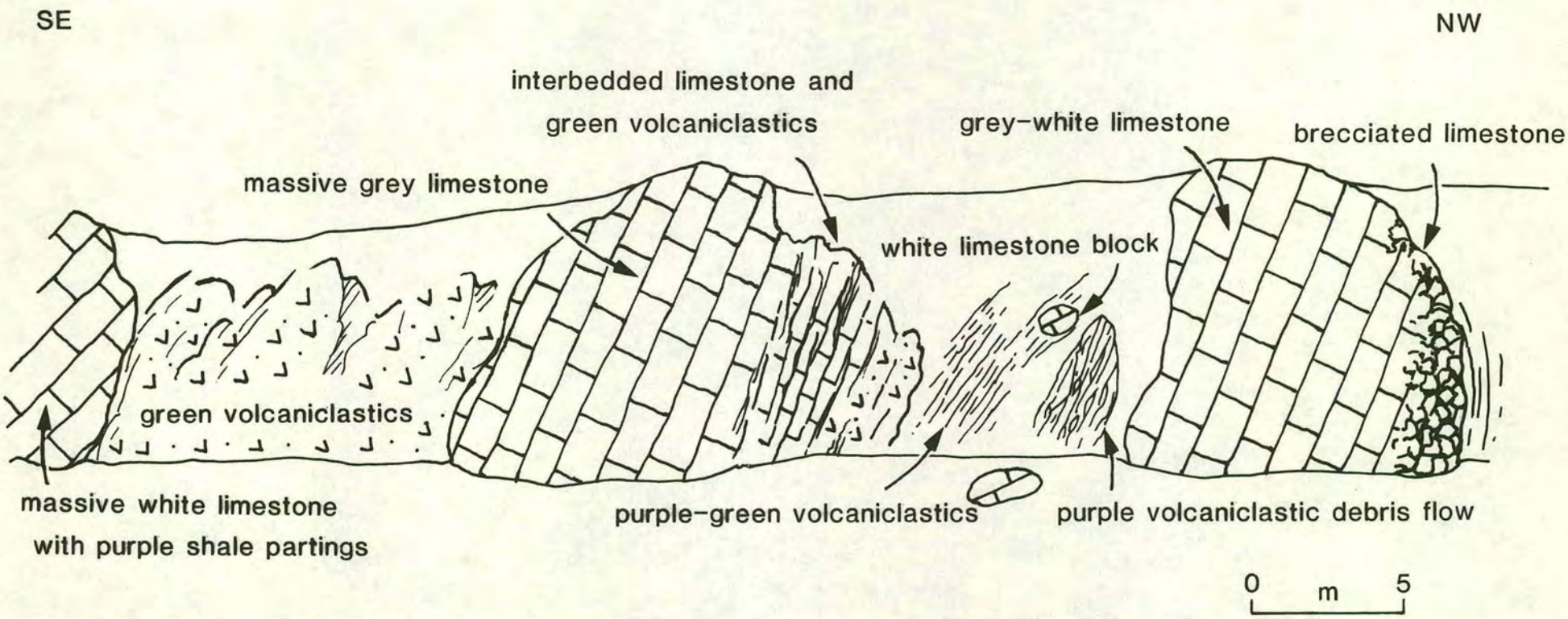

Figure 2.7 Field sketch of road section (box C in Figure 2.5) showing limestone blocks and intervening volcanics.

Figure 2.8 Lithologies observed in the valley marked C in Figure 2.5.

(a) Clast-supported conglomerate of predominantly basaltic clasts.

(b) Volcanogenic conglomerate which contains basaltic, volcanogenic sedimentary rocks and recrystallized white limestone clasts. Note the relict laminations in the limestone clast in the centre of the picture.

(c) Fine-grained green volcanogenic sandstone interlaminated with purple siltstone, below the logged sequence in Figure 2.9.

a

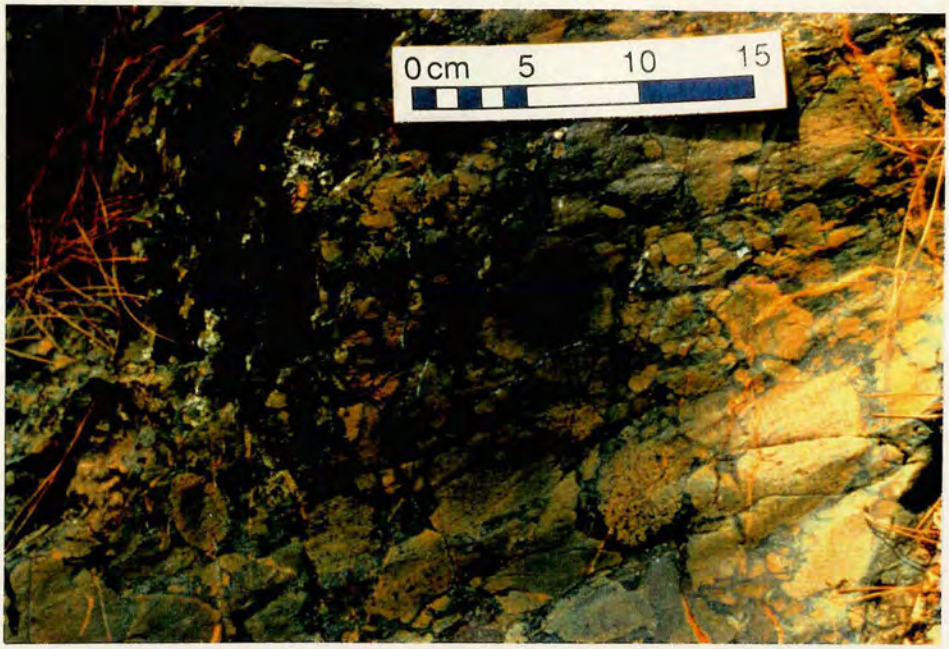

b

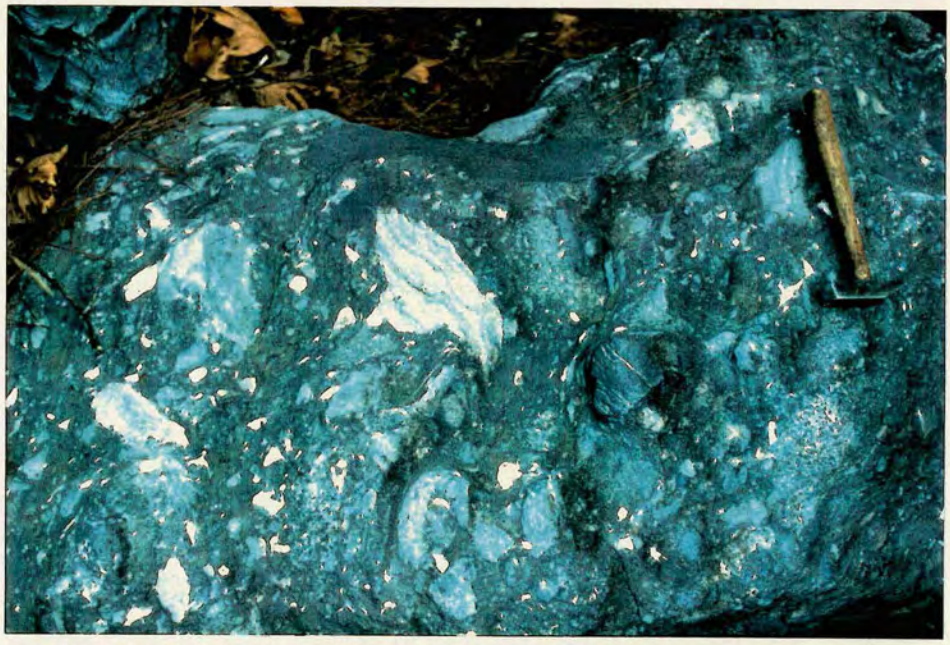

c

e) Bedded volcanogenic mudstones and fine-grained sandstones

Bedded volcanogenic siltstones and sandstones form a relatively minor part of the Nilüfer Unit in the Edremit region, but are common in the small valley described above. A particularly good outcrop lies at the intersection of the valley with the road running north from Zeytinli. The outcrop displays a sequence of interbedded green volcanogenic siltstones and sandstones (Figure 2.9). The finer grained beds are pale green and cherty, while the sandstones are a slightly darker green and contain rare clasts of a similar lithology up to 3cm in size. Further up the valley green and purple mudstones and siltstones are intercalated with limestone turbidites, as described below.

f) Limestone turbidites intercalated with volcanogenic sedimentary rocks

In the lower part of the valley there is an excellently exposed redeposited limestone layer 2m thick (Figure 2.9). The limestone is pale grey and partially recrystallized with a sugary texture. The limestone horizon has sharp contacts with the overlying and underlying volcanogenic sedimentary rocks and, despite its recrystallization, has retained many of its original sedimentary features. The base of the limestone bed is marked by a conglomerate of flattened limestone, green spilite and fine-grained black clasts, which fines upwards into medium-grained calcarenite. The limestone intercalation overlies fine-grained volcanogenic sandstone and siltstone which display fine laminations and soft sedimentary deformation. The sedimentary structures appear to have been tectonically enhanced to create small recumbent isoclinal folds (Figure 2.8c). A similar facies of limestone and volcanogenic sedimentary rocks also occur north of the village of Pinarbasi (Figures 2.5 and 2.10).

2.4.2 Debris flow unit

a) East of Mehmetalan

A coarse debris flow unit is closely associated with the Nilüfer Unit in the Edremit area. Although not mapped in detail, it appears that the debris flow constitutes one or more tectonic "slices" of limited lateral extent, which are interleaved with spilites of the Nilüfer Unit and, to a lesser extent, clastic rocks of the Ortaoba Unit. The debris flow unit is best exposed along the river bed just east of Mehmetalan (Figure 2.11). The *in situ* outcrop is poor, but the lithologies are excellently exposed in loose boulders along the river bed (Figure 2.12a). A matrix of coarse-grained sandstone and dark grey and green mudstone contains ellipsoidal clasts 0.5cm-20cm in length. The average clast size is 3-8cm. Clasts consist of green volcanic rocks, fine-, medium-

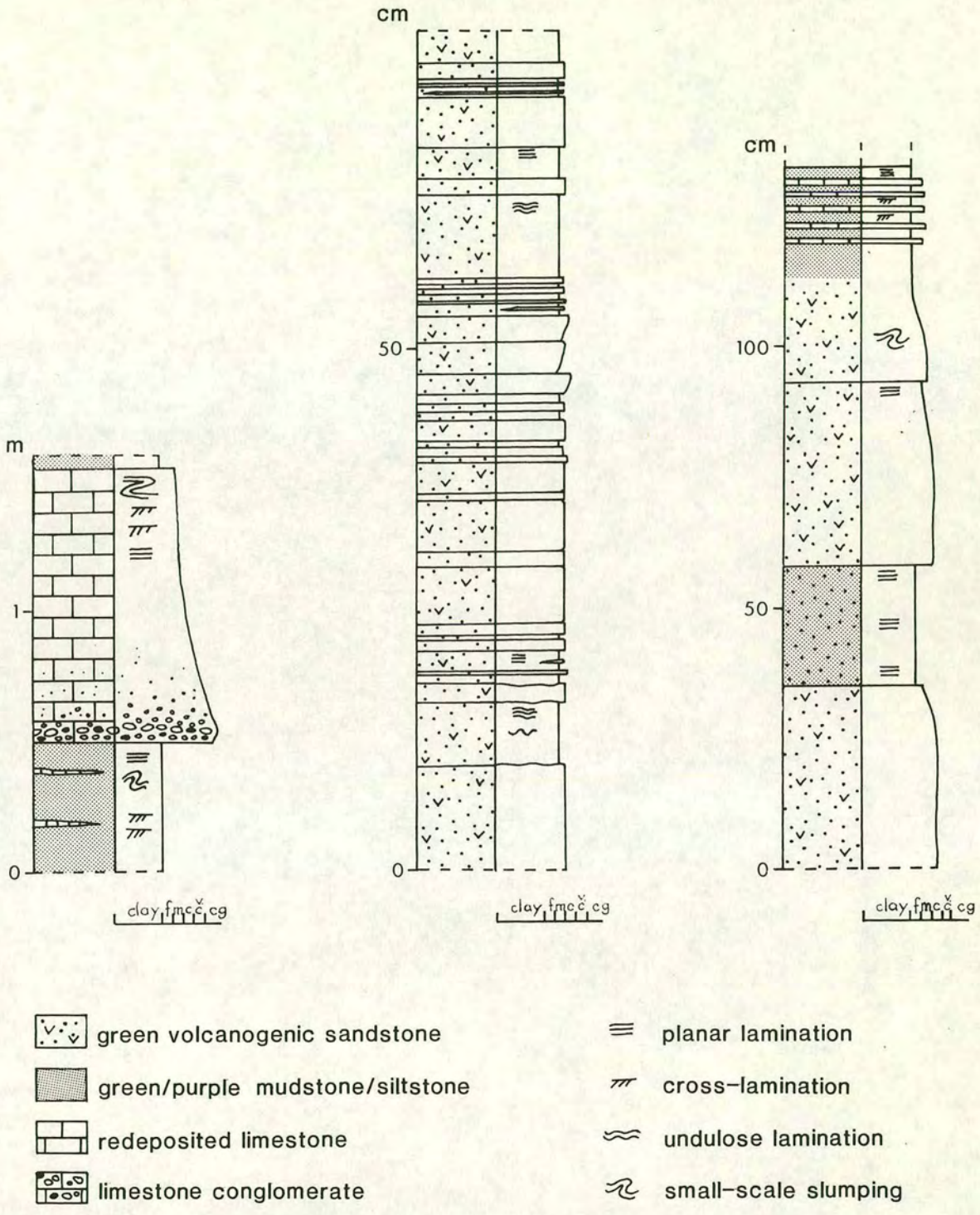

Figure 2.9 Representative logs through the sedimentary facies of the Nilüfer Unit in the valley marked by box A in Figure 2.5.

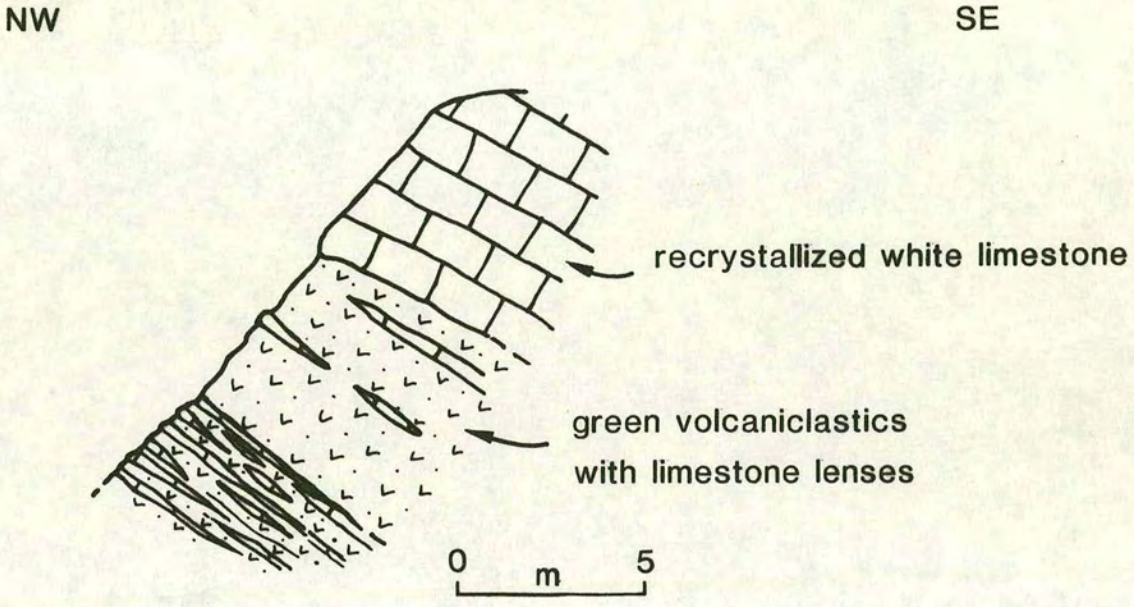

Figure 2.10 Field sketch of volcanogenic shale interbedded with recrystallized limestone, approximately 1km north of Pınarbaşı.

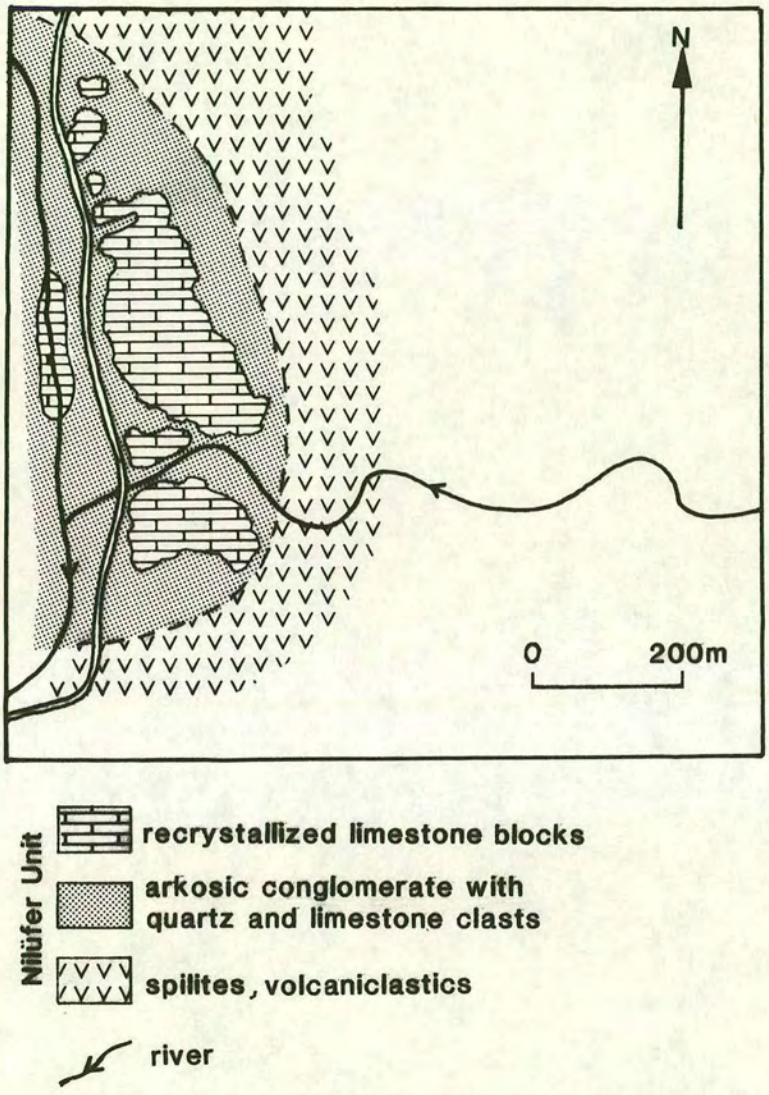

Figure 2.11 Map of region known as Üğü taşı, east of Mehmetalan, (box B in Figure 2.5). The debris flow unit is well exposed along the bed of the south-flowing river.

Figure 2.12

(a) Poorly sorted conglomerate, interpreted as a debris flow, exposed as boulders in the river west of Ügü tasi.

(b) Photomicrograph of the debris flow unit showing sheared carbonate and quartz clasts in a fine-grained, foliated matrix. The veined carbonate clast on the right of the picture represents the margin of a limestone block over 5m across (XPL, field of view: 21mm).

(c) Limestone blocks in a matrix of feldspathic sandstone north of Mehmetalan.

a

b

c

and coarse-grained reddish sandstone, pink quartzite, white quartz, grey quartz and rare granite. The volcanic clasts consist of porphyritic lava, green mudstone and volcaniclastic rocks. Volcanic and sandstone clasts are the most predominant. All the clasts are angular with the exception of the granite and felsic volcanic clasts which are well-rounded. In addition to the clast types described above, other boulders observed in the river bed contain clasts of dark grey limestone, grey fissile mudstone and streaky grey recrystallized limestone. The grey recrystallized limestone forms clasts from a few centimetres up to several metres in size. Figure 2.12b shows a thin-section photomicrograph through the margin of one of these blocks. A buff nodular texture is common in the limestone. Similar debris flow exposures also occur along the mountain road running north from Mehmetalan and along the road running north of Pasadag through the Ortaoba Unit.

b) North of Mehemetalan

The outcrops north of Mehmetalan are located between massive spilites of the Nilüfer Unit, as shown in Figure 2.4. There, debris flows are associated with deformed, interbedded feldspathic sandstone and shale sequences (Figure 2.13). These debris flows are much finer grained than those east of Mehmetalan and commonly comprise clast-supported conglomerates with clasts up to only a few centimetres in size. They also display a smaller range of clasts, consisting predominantly of siltstone, grey mudstone, fine-grained sandstone and quartz grains. Rare, rounded granitic clasts were observed. The clasts are considerably compressed and draped by wispy dark laminae. Limestone blocks were observed in a few horizons. One exposure contains abundant rounded, dark grey limestone blocks up 2-30cm across (Figure 2.12c), together with grey micaceous mudstone clasts (2-4cm across). Large dark grey limestone blocks (up to 2m across) also occur sporadically within the sandstone-shale sequences. One limestone block is mantled by a coarse limestone breccia which confirms a sedimentary rather than tectonic origin for these blocks.

The contacts of the debris flow outcrops with the surrounding spilitic rocks are not clearly exposed. The debris flow unit is inferred to be a tectonic slice on the basis of the intense shearing of the debris flows and the massive pyroclastic, rather than epiclastic, nature of the surrounding Nilüfer rocks.

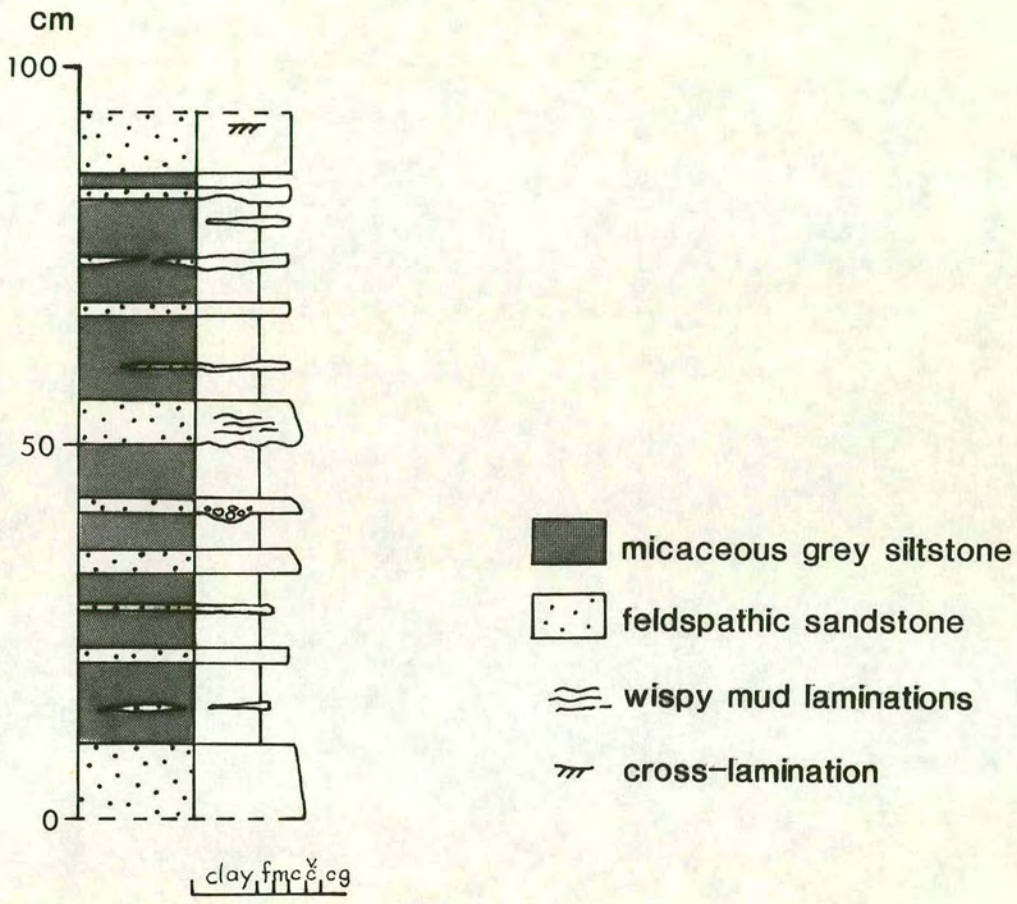

Figure 2.13 Representative log through sandstones and shales associated with the debris flow unit north of Mehmetalan.

2.5 Bergama area

The Bergama region (Figure 2.14) displays the most complete succession through the Nilüfer Unit in NW Turkey. The succession is more complete than that observed near Edremit and displays an almost intact sequence from massive lava flows to bedded volcanogenic turbidites and cherty sediments, with an intervening sequence of volcaniclastic flows. The entire sequence is at least 1km thick. Kaya & Mostler (1992) have described Middle Triassic conodonts from limestone interbedded with phyllites at the top of the unit.

2.5.1 Main lithological associations

A distinctive feature is the presence of intercalated redeposited limestone debris flows and discrete limestone lenses. Near the base of the sequence there is a significant change in structural style from relatively undeformed spilites to highly foliated and schistose grey-green phyllites. This occurs over 100-200m and may imply that a relatively thick sequence has been tectonically removed. The lowest unfoliated rocks of the Nilüfer Unit comprise lava flows intercalated with volcaniclastic flows. A sliver of weathered dunite 30m wide was observed near the village of Koyyeri. It may represent a slice of the basement to the Nilüfer Unit which was tectonically emplaced into higher levels of oceanic crust during accretion processes. The main lithological assemblages observed in the Bergama region are described below.

a) Massive lava flow with primary basaltic textures.

A good outcrop of primary extrusive rocks can be found along the road between Köyyeri and Hacilar (Figure 2.14) and is shown in the field sketch in Figure 2.15. The lava is pale green and homogeneous on a small scale. It is extremely hard and almost vitreous in places. Round features within the lava were identified as degassing structures, although superficially they resemble small pillows. The structures are isolated from each other within a massive lava "matrix" and do not possess the characteristic dark glassy rinds of most pillow lavas. Vesicles up to 2mm in diameter increase in concentration towards the boundaries of the structures. The vesicles are infilled with pale yellow-green chloritic and epidotitic material. The massive lava passes abruptly but gradationally into the ubiquitous ignimbrites and volcaniclastic debris flows of the Nilüfer Unit.

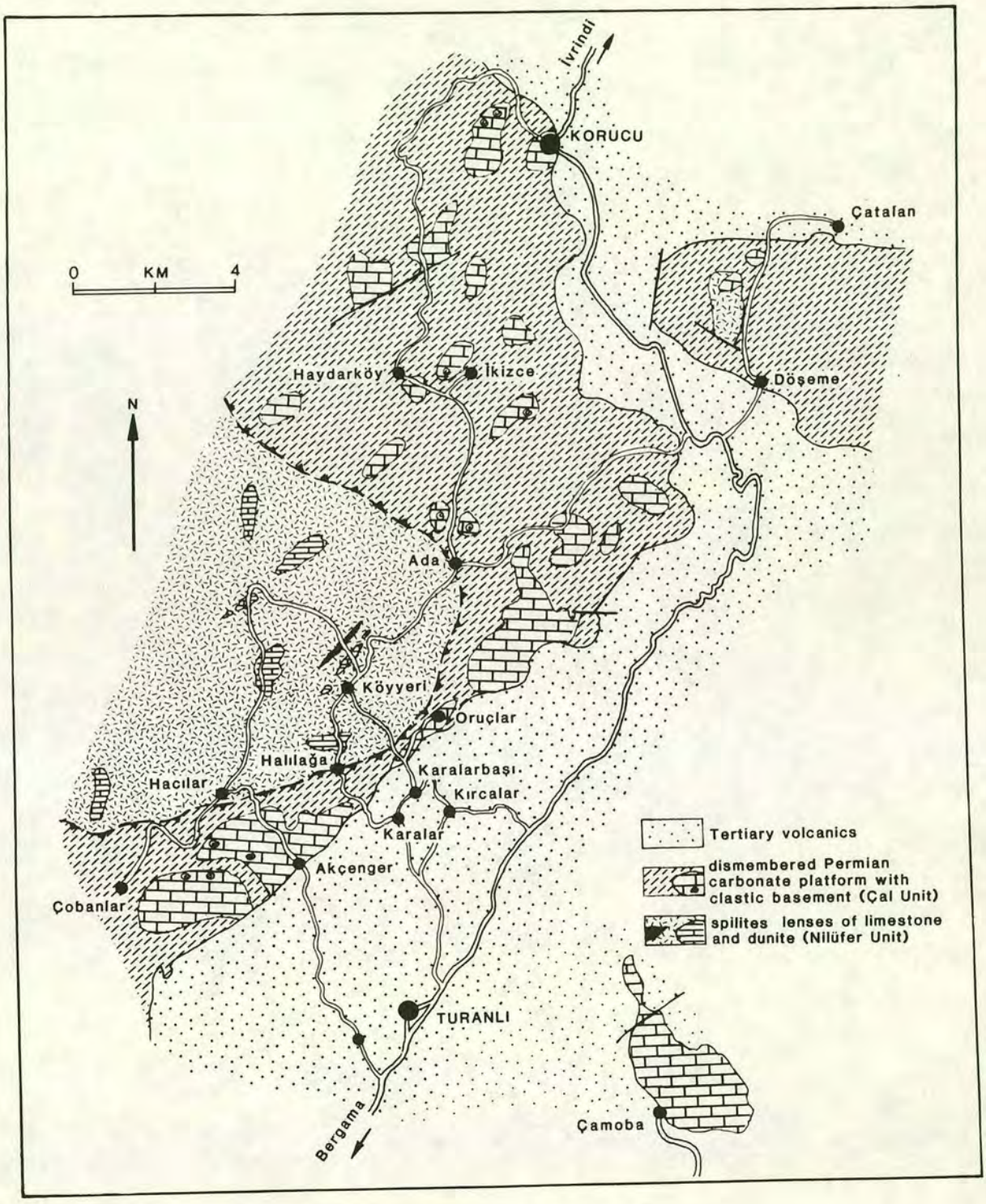

Figure 2.14 Geological map of the region north of Bergama (after the M.T.A. mapsheet Balıkesir G 4 and my own fieldwork).

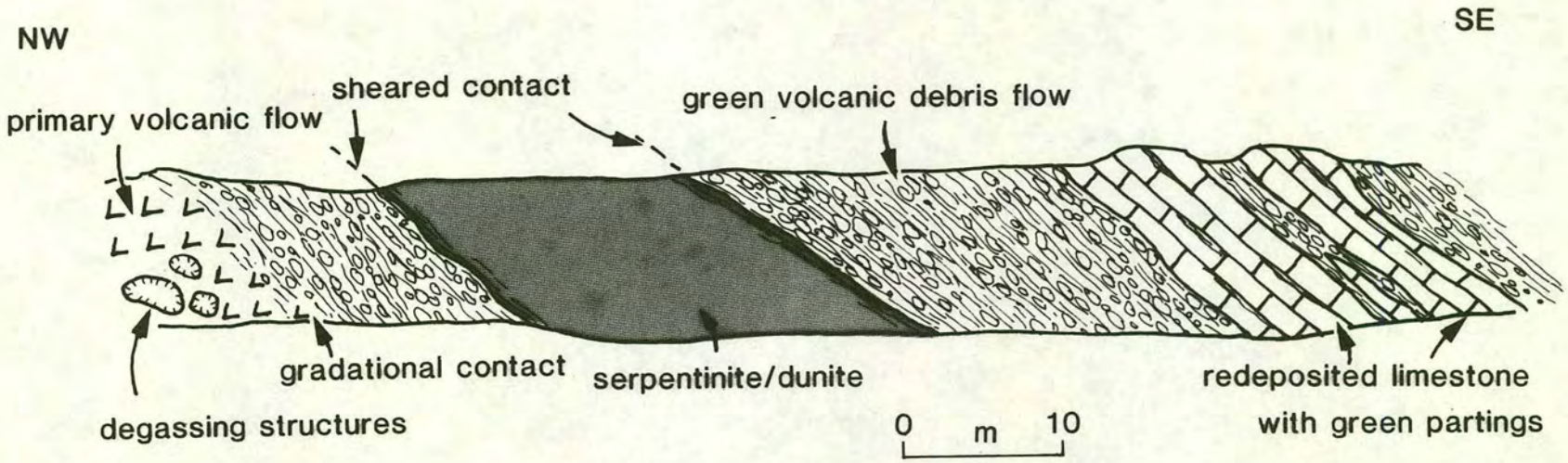

Figure 2.15 Field sketch near Köyyeri showing a section through the basaltic and volcaniclastic sequence. Note the tectonically intercalated dunite slice.

In thin-section the lava displays intergranular, seriate (e.g. Figure 2.16a) and subophitic textures despite being almost wholly chloritized in many samples.

b) Massive welded ignimbrite flow.

The distinction between finer grained volcaniclastic debris flows and primary ignimbrite flows is not clear owing to extensive chloritization. However, several exposures do have distinct igneous textures with fused glass shards and a characteristically streaky, fluid-like appearance (Figure 2.16b). In thin-section, black flame-like glassy shards are aligned with the overall flow direction producing a primary volcanic texture.

c) Clast-supported volcanogenic conglomerate.

Epiclastic volcanogenic debris flows are exposed above the massive lava flows and ignimbrites, and are identical to those observed in the Edremit region. Basaltic and ignimbritic clasts, as well as fine-grained green clasts which may be epiclastic or pyroclastic, make up the bulk of the rock. The matrix is fine-grained and green.

d) Bedded volcanogenic mudstone and fine-grained sandstone.

The highest levels of the Nilüfer unit in the Bergama region are characterized by a thick succession of volcanically-derived turbidites with thin partings of volcanogenic mudstones (Figure 2.16c). The volcanogenic sandstones are siliceous and pale green in colour. They are well-bedded with beds ranging from 3cm-20cm. The grain-size ranges from fine- to medium-grained. Slight fining-upward grading can be observed in some beds, indicating that they are the right way up. Between the beds are thin partings (2mm-2cm) of dark siliceous mudstone.

An outcrop of fine-grained cherty green sandstone interbedded with green and grey mudstone (Figure 2.17a) may represent more distal parts of the volcanogenic sedimentary pile described above. The sandstone is laminated on a millimetre scale and grading indicates that it is the right way up. This small sequence passes up into siliceous grey-green mudstone.

e) Limestone turbidite intercalated with volcanogenic sedimentary rock.

Redeposited limestone bands are a common feature of the Nilüfer Unit in the Bergama region and the thicker bands can be traced laterally over distances of up to 1km. The limestone beds range in thickness from 2cm to 3-4m and commonly contain partings of green or purple shale. Figure 2.17b shows limestone interbedded

Figure 2.16

(a) Photomicrograph of seriate basalt from Köyyeri, along the road section shown in Figure 2.15. The sample displays clinopyroxene phenocrysts and a range of sizes of plagioclase laths in a fine-grained glassy groundmass. Rounded vesicles are infilled with epidote and chlorite (sample 21/9/92-19c, PPL, field of view: 4mm).

(b) Deformed volcaniclastic rock from Köyyeri showing a basaltic clast in a chloritized matrix which contains relict glass shards. It is difficult to decide whether rocks such as this are pyroclastic or epiclastic (sample 25/9/92-7, PPL, field of view: 6mm).

(c) Volcanogenic sandstones exposed between Köyyeri and Karalarbasi.

a

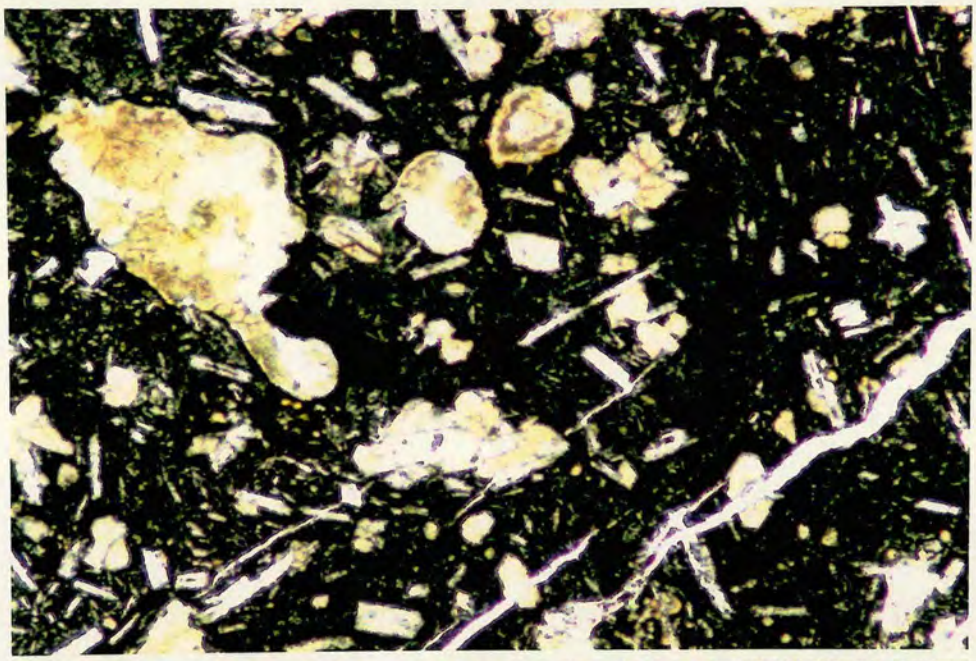

b

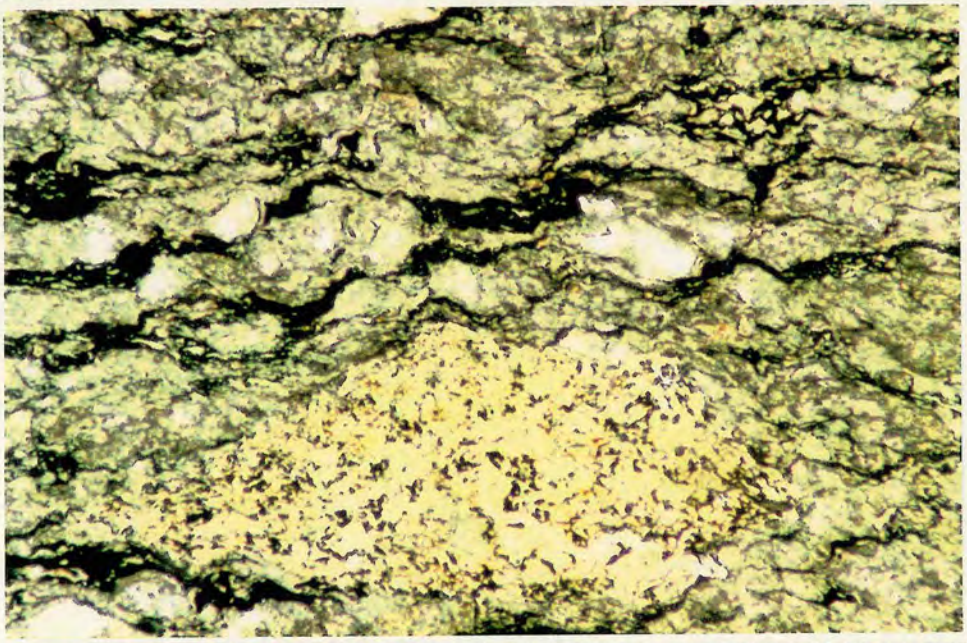

c

Figure 2.17

(a) Fine-grained cherty sandstone interbedded with green and grey mudstone, possibly representing the more distal equivalent of the volcanogenic sandstones shown in Figure 2.16c.

(b) Lenses of recrystallized limestone in foliated purple shale near Hacilar.

(c) Large-scale intercalations of redeposited limestone and green volcanogenic shale near Köyyeri.

a

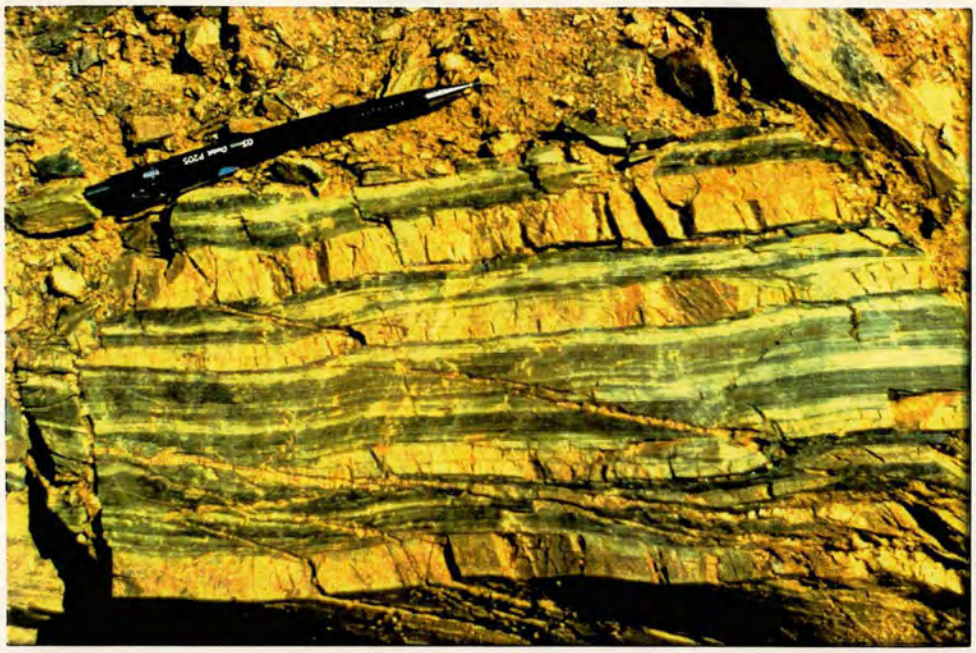

b

c

with foliated purple-green volcanogenic shale. Despite extensive recrystallization it is clear that the limestone was originally composed of clasts. The clasts are now present as flattened and fused lenses which can be distinguished from each other by the sutured, stylolitic seams which outline them. In places the sutured clast boudaries are defined by thin seams of fine-grained green material. Limestone and volcanogenic shale are also intercalated on a larger scale as shown in Figure 2.17c. An intercalated volcaniclastic-limestone sequence is well-exposed NW of Köyyeri and is shown in Figure 2.18.

Towards the hill of Madradag, in the lower levels of the sequence, fine-grained green and blue-grey schists are intercalated with lenses of recrystallized limestone which become less common down sequence. Owing to their distinct blue-grey colours and very fine grain-size two samples of schist were analyzed by X-ray diffraction to check for the existence of glaucophane. However, no blueschist minerals were found. The minerals detected, in likely order of abundance, were:

Sample 22/9/92-10: albite, ripidolite (a chlorite), quartz, hematite.
Sample 22/9/92-7: tremolite, clinochlore (a chlorite), albite, ?hematite.

f) White fine-grained ash

Outside the village of Ada (Figure 2.14) the ubiquitous green volcaniclastic rocks pass into very pale beige/white shale with feldspathic sandstone lenses (Figure 2.19). The contact between the two is very sheared and may represent a tectonic contact between underlying spilitic rocks and a unit containing terrigenous as well as volcanic components (e.g. the Çal Unit; see Chapter 4). The feldspathic sandstone passes into massive and thick-bedded conglomerates along the road out of the village towards Haydarköy.

2.6 The Nilüfer Unit in other regions

Nilüfer-type sequences are also present in several other regions of NW Turkey and are briefly described below. In the case of the Bursa area (the type locality of the Nilüfer unit of Okay *et al.,* 1991) the volcanic lithologies are clearly equivalent to those in the Edremit and Bergama regions. However, in other areas, such as Çan, Kinik and Soma, correlation with the Nilüfer Unit is more tentative.

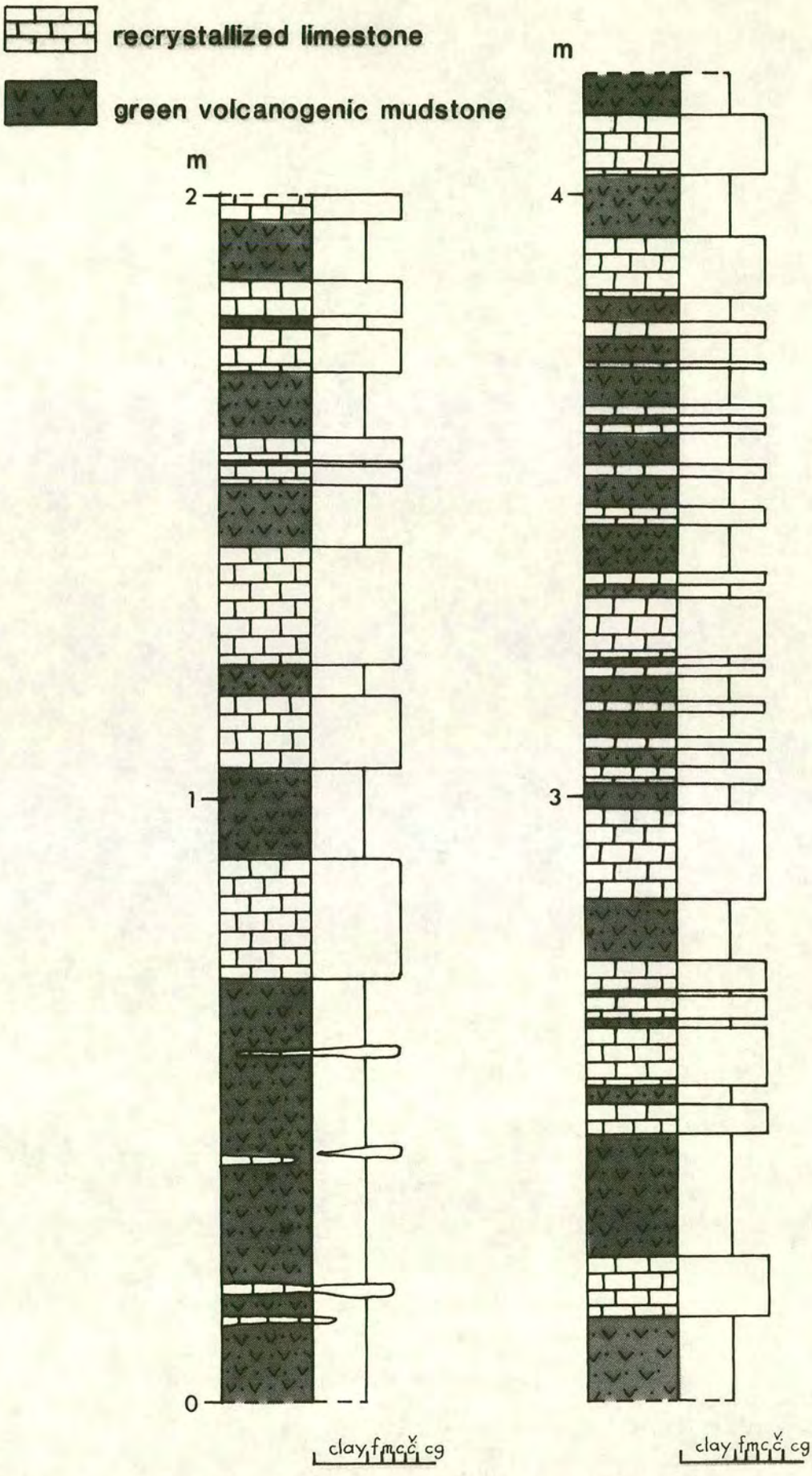

Figure 2.18 Representative log through interbedded volcanogenic shale and limestone NW of Köyyeri.

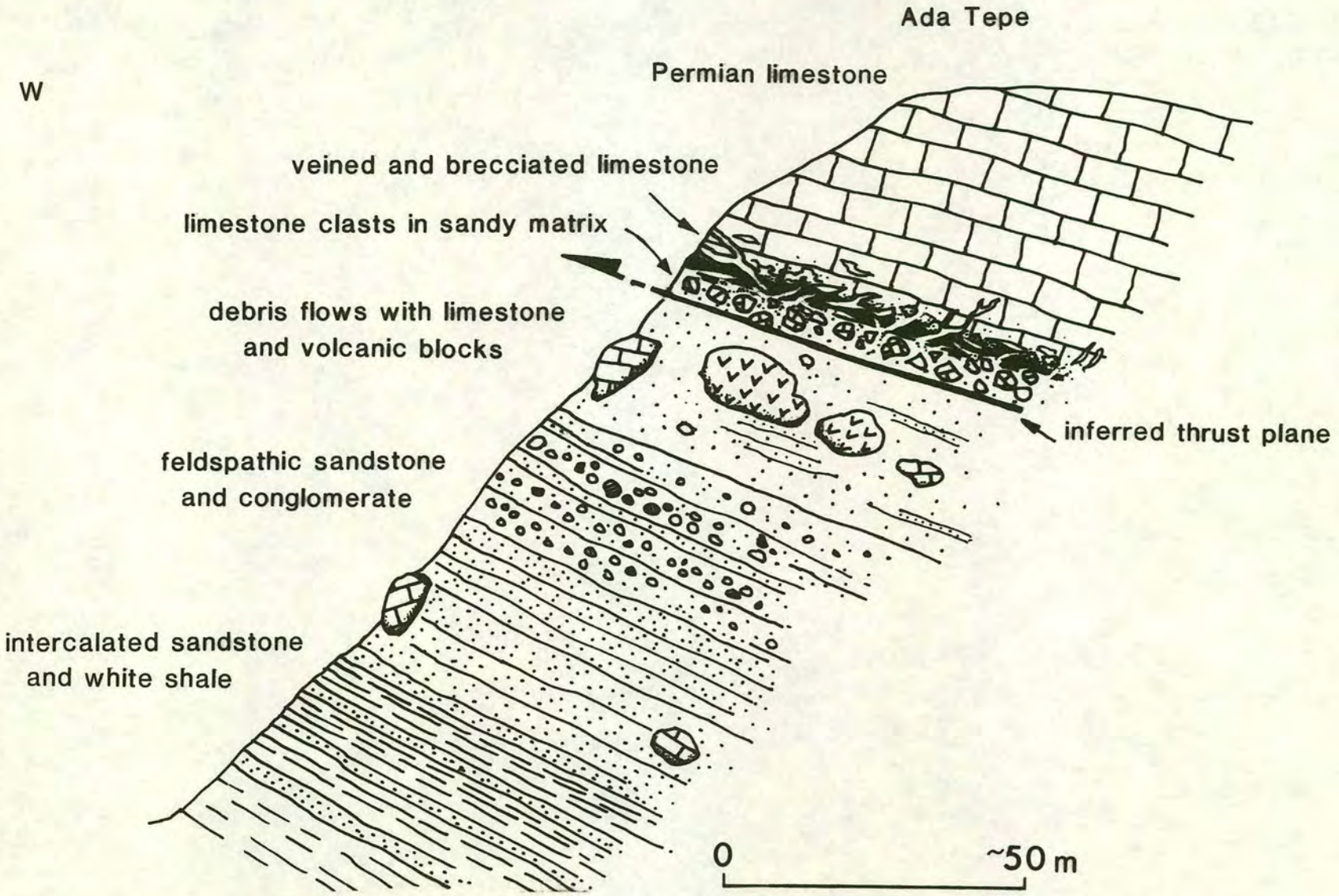

Figure 2.19 Field sketch of Ada Tepe showing the upward succession from white shale to coarse clastics and debris flows. The sequence is tectonically overlain by Permian limestone of the Çal Unit.

2.6.1 Bursa area

Around the massif of Uludag, south of the city of Bursa, Karakaya-type rocks are exposed. Among these is a thick sequence of green metabasites whose constituent lithologies and geochemistry compare well with the spilites around Edremit and Bergama. These are particularly well exposed around the Nilüfer dam and along the main roads from Bursa to Orhaneli.

In the most part the volcanic rocks comprise a monotonous dark green sequence containing few internal features. The rocks have a slight foliation and a sheen which is almost vitreous in places. Along the road to Orhaneli volcaniclastic rocks containing well-preserved "blebby" clasts are exposed although they are at a slightly higher metamorphic grade than their equivalents near Edremit and Bergama. This may have been caused by emplacement of the plutonic rocks which make up the core of the Uludag mountain. The presence of pink Ti-augite and kaersutite (Okay *et al.*, 1991) indicate an alkaline affinity. Okay *et al.* (1991) also observed incipient blue sodic amphibole replacing the kaersutite. Features within the volcanics are much less well preserved in the Bursa region owing to the higher grade of metamorphism, making an individual study more difficult, but allowing comparison with the better preserved western examples.

Despite metamorphism to high greenschist/amphibolite facies (and locally blueschist facies; Okay *et al.*, 1991), volcaniclastic rocks from the Bursa area retain good volcanic textures. A finely laminated appearance in hand specimen is revealed in thin-section as a primary ignimbritic texture. Well-preserved clinopyroxene crystals within a streaky chlorite and amphibole groundmass probably represent relict phenocrysts. The crystals are poorly sorted, implying that it may have been deposited from an ignimbrite rather than a tuff.

2.6.2 Bandirma area

The Nilüfer Unit crops out on the Kapidag Peninsula (which juts into the Marmara Sea, west of Bandirma; see location map in Figure 1.6) and along the shores of the Marmara Sea to the east. However, like the spilites near Bursa, they are more metamorphosed and their constituent lithologies are less well preserved than in the Edremit and Bergama regions. They comprise green, foliated meta-volcanics with very few original structures or lithological features. On the Kapidag Peninsula, the

spilites are intercalated with marble bands. The sequence is highly foliated and folded. Folds are small, tight and asymmetrical and are probably parasitic to folds on a much larger structure.

South and east of Bandirma the Nilüfer Unit forms poorly exposed outcrops of weathered green volcanics and volcanogenic sedimentary rocks with a SE-dipping foliation. East of Bandirma tectonic lenses of sodic amphibole-bearing eclogites up to 100m long have been found within this unit (Okay *et al.*, 1991), but were not observed during this study

2.6.3 Çan area

In the Çan region of the central Biga Peninsula (Figure 2.1) the Nilüfer Unit crops out as foliated meta-tuffs known as the Sazak Metatuffs, after a village in this region (see also Figure 4.8. The rocks have a rather difference appearance in the field from the other rocks of the Nilüfer Unit. They are foliated and silvery grey to beige, rather than the massive green volcanics of other areas but are clearly of volcanic origin, having tuffaceous textures. Okay *et al.* (1991) noted the presence of Ti augite in these rocks.

Middle Triassic limestone to the southeast of the town of Biga, east of Çan, was named the Camialan Limestone by Okay *et al.* (1991) after a village in this region. Okay *et al.* (1991) interpreted the Camialan Limestone as tectonic blocks within the Çal Unit and tentatively suggested that the limestone originally represented the upper parts of the Çal Unit.

The Camialan Limestone is exposed along a valley which follows the Biga-Hosoba road, SE of Biga. A steep-sided gorge has been cut through the limestone which is mostly white or grey and highly recrystallized. A good example of the limestone is shown in the sketch in Figure 2.20. The limestone in this outcrop displays an overall shallowing upward sequence. Foliated green shale forms a horizon at the base of the outcrop. It is overlain by thin-bedded limestone with replacement chert nodules and lenses along bedding planes. Higher in the sequence the chert dies out and the bases of beds become pink. The pink colour gradually fades to grey away from the bases of the beds. The bedded limestone passes up into thicker bedded and massive white limestone which contains pink patches and rare chert. Massive white limestone forms the top of the section. Despite their recrystallization the massive limestones at the top

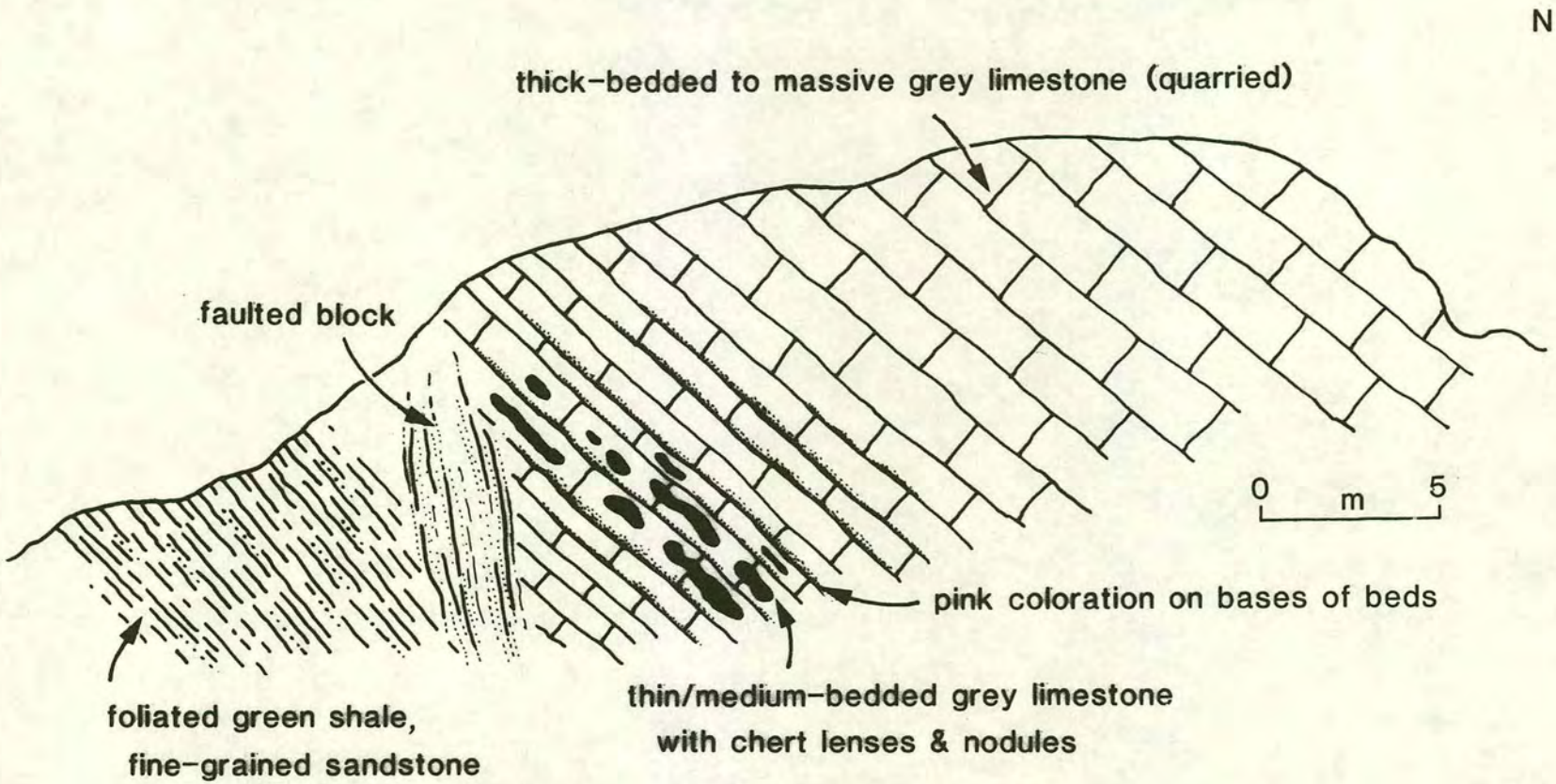

Figure 2.20 Field sketch of an exposure of the Camialan Limestone, approximately 10km SE of Biga. The foliated green shale is at the base of the sequence.

of the sequence in Figure 2.20 have yielded molluscs, algae, echinoderms and foraminifera (Okay *et al.*, 1991). An Anisian age has been proposed on the basis of determinations by D. Altiner (in Okay *et al.*, 1991). He identified *Meandrospira dinarica*, *Glomospirella grandis*, *Glomospira densa*, *Ammobaculites*, Duartaminadae and *Endothyra* or *Endothyrella* sp.. The contacts of the limestone with the surrounding Çal Unit were not observed.

Owing to the green, possibly volcanogenic, shale at the base of the section described above and the Middle Triassic age of the limestone, I have tentatively correlated the Camialan Limestone with the Nilüfer Unit which, in the Bergama region, also displays Middle Triassic limestone interbedded with phyllites and volcanogenic sedimentary rocks.

2.6.4 Armutlu area

The Armutlu Peninsula juts out into the Sea of Marmara due north of Bursa (see location map in Figure 1.6). It is bounded to north and south by depressions caused by strands of the North Anatolian Fault. Fieldwork was not carried out on the Armutlu Peninsula as part of this study. However, published literature describes the presence of meta-volcanics of pre-Late Cretaceous age in the "Iznik Metamorphics" (Akartuna, 1968; Goncuoglu *et al.*, 1987) and it is possible that these are Nilüfer Unit equivalents. However, further fieldwork and geochemical studies are needed before the Armutlu section can be definitely correlated with the Edremit and Bergama sequences.

2.6.5 Kinik and Soma area

Two large exposures of white Triassic limestone dominate the small valley near the village of Kapikaya, southwest of Kinik (location map; Figure 1.6). The limestone is partially recrystallized, but is locally fossiliferous and oolitic. Fossils are micritic and set in a sparry matrix. They include foraminifera, shell fragments, echinoderm debris, bryozoa and algae. Green-grey quartzose sandstone, limestone breccia and weathered vesicular basalt crop out at the base of the limestone crags, but their contacts with each other and the Triassic limestone are not exposed. The sandstone contains clasts of limestone and is undeformed. The basalt also contains rare limestone clasts. The limestone crags and their associated lithologies are surrounded by sheared and foliated dark phyllites which cover an extensive area. The contact is not exposed but the sharp

contrast in deformation between the sandstone and the underlying phyllites suggests that it may be unconformable.

Undeformed sandstone, breccia and vesicular basalt are also found along the road which runs due south from Kinik. A particularly good outcrop of breccia is exposed near the col, approximately 4km south of Kinik. The outcrop is 5-6m wide and may represent a channel deposit within a predominantly sandy sequence. Clast lithologies include black chert, rare green chert, cream limestone, red laminated limestone, fine- to medium-grained sandstone, light grey limestone and translucent quartz/quartzite. The clasts are very angular (except the quartz) and poorly sorted and are set in a micaceous, sandy to muddy matrix. The clasts are generally 0.5-8cm in size, although one red limestone clast is 30cm long. Basaltic blocks crop out above the breccia.

The region around the quarrying town of Soma is characterized by imposing crags of white Triassic and Cretaceous limestone. The most accessible exposures of Triassic limestone are near the village of Darkale (called Altinli on the M.T.A. map Balikesir-G5), 3km south of Soma. Darkale is perched high on a crag and is surrounded by high rugged peaks of both Triassic and Cretaceous limestone. The village itself is built on dark green volcaniclastic sandstones and conglomerates which are rich in limestone clasts up to 2m in size. Red ribbon chert crops out on the hillsides immediately west of Darkale, above the level of the green volcaniclastics. The chert forms large coherent rafts within limestone-rich debris flows. A block of dark chert was also observed. Redeposited limestone with replacement chert overlies the ribbon chert horizon. It is likely that an original volcaniclastic-chert-limestone sequence was incorporated into mega-debris flows. The original sequence is preserved within debris flows as a quasi-stratigraphy up the hillside.

The steep-sided valley below the east margin of the village displays a sequence which passes up from calcturbidites to sandstone turbidites and, at the top, more coarse debris flow horizons. The calcturbidites contain dark replacement chert similar to that on the hillside west of the village. The debris flows contain very rounded cobbles of silicic green volcanics up to 1m in size and limestone clasts up to 2m across. One limestone clast contains disarticulated megalodonts.

Although the nature of these Triassic sequences is not very clear, it appears that massive Triassic limestone overlies a clastic basement which itself unconformably overlies deformed phyllites of the Kinik Formation (interpreted as part of the

Karakaya Complex, possibly equivalent to the Kalabak Unit of the Edremit area). The coarse material within the conglomerates was derived from proximal chert, limestone and sandstone sources, possibly in part from the underlying Karakaya Complex. The basaltic outcrops associated with the clastics are difficult to interpret owing to their poorly exposed contacts with the surrounding sandstones and conglomerates. They may be large reworked blocks within the clastic sequence or, alternatively, represent localized lava flows. The Triassic sequence at Soma, although disrupted by incorporation into debris flows, appears to record massive limestone build-up above a volcaniclastic basement, with an intervening horizon of ribbon chert and redeposited limestone. The lack of terrigenous material within the volcaniclastics and the presence of abundant limestone clasts suggests a close affinity with the Nilüfer Unit. The coarse, epiclastic nature of the volcanic material implies deposition on the flanks of a volcanic edifice where mass wasting, debris flows and turbidity currents would have been the major depositional processes.

2.7 Summary of the lithologies of the Nilüfer Unit in NW Turkey

When considered as a whole, the Nilüfer Unit in NW Turkey can be divided into the five main lithological associations listed below:

1. *Massive basic lava flows*
2. *Massive basic ignimbrite flows.*
3. *Epiclastic volcanic breccias (± limestone clasts)*
4. *Volcanogenic sedimentary rocks*
5. *Limestone turbidites and debris flows*

Association 2 is unusual as ignimbrites are generally felsic rather than basic. However, analyses show them to be definitely basaltic and many of the textures observed in thin-section are clearly ignimbritic. All the observed lithologies of the Nilüfer Unit can be described under one of these five headings. The relative proportions of each facies type vary according to locality. The unit is relatively complete and best exposed in the Bergama region. Thus a generalized stratigraphy can be compiled on the basis of the Bergama sequence and applied to less complete sequences of the Nilüfer Unit elsewhere in the Biga Peninsula region.

2.8 Correlation of the Nilüfer Unit across northern Turkey

The Nilüfer Unit, as defined and described in this thesis, is restricted to the greenschist volcanic sequences exposed in the regions of Edremit, Bergama, Bandirma and Bursa. However, similar sequences are scattered throughout the Pontide belt of northern Turkey and extend as far east as the Agvanis Group which is exposed southwest of Trabzon in eastern Turkey. The Agvanis Group shows a remarkable similarity to the Nilüfer Unit and is described below for comparison.

2.8.1 The Agvanis Group

The Agvanis Group is exposed in northeastern Turkey, southwest of the major Black Sea port of Trabzon. The Agvanis Group is a 4.5km thick sequence consisting mainly of metabasites with intercalated metadacite, marble, calcschist and phyllite. The following descriptions are all based on studies in the Agvanis region by Okay (1984). The meta-basites, which make up the bulk of the Agvanis Group, are all metamorphosed to greenschist facies and comprise meta-lavas and meta-tuffs. The meta-lavas are commonly interbedded with marbles and green phyllites (up to 20m thick) and locally include marble fragments. Black, banded meta-lavas with pillow shapes in places are present in the lower parts of the sequence. The meta-tuffs are laminated and contain alternations of epidote-rich and chlorite-rich bands. Like the meta-lavas they are commonly interbedded with white marble bands up to 5m thick. Except for the dacites, this sequence is very similar to the Nilüfer Unit, especially the succession exposed near Bergama. The Nilüfer and Agvanis sequences also display a similar degree of metamorphism in that they both contain typical greenschist facies mineral assemblages.

2.9 Metamorphism of the Nilüfer Unit

The Nilüfer Unit as a whole has undergone at least three main stages of metamorphism.

a) spilitization (low to intermediate temperature greenschist metamorphism)
b) high temperature greenschist metamorphism
c) blueschist/eclogite metamorphism

Yardley (1989) defined the the lower temperature zone of metabasic greenschist facies as being characterized by the mineral assemblage: actinolite, epidote, albite, chlorite and stilpnomelane. The higher temperature zone is characterized by: hornblende, actinolite, albite, chlorite, epidote and garnet.

High greenschist and blueschist/eclogite facies metamorphism are prevalent in the Bursa area, whereas spilitization alone appears to have affected the Bergama area. The Edremit area displays spilitization, with high greenschist metamorphism in the lower levels of the Nilüfer Unit. I assume that *all* the volcanic rocks of the Nilüfer Unit originally underwent early spilitization, regardless of their present grade. Overprinting by later, higher grades of metamorphism then occurred preferentially in the Bursa area.

2.9.1 Spilitization

Spilites are metabasalts in which the plagioclase has been largely albitized and which contain secondary hydrous phases replacing glass or primary igneous minerals. They commonly contain epidote layers and veins. In the field, spilites commonly have a distinctive turquoise-green colour and epidote is a bright apple-green. Minerals reported from spilites include actinolite, tremolite, hornblende, albite, chlorite, talc, epidote, nontronite, quartz, sphene and magnetite (Humphris & Thompson, 1978).

Despite being almost ubiquitous in preserved fragments of oceanic crust, spilites are not restricted to ancient volcanic sequences. Samples dredged from modern oceans display a range from fresh to metamorphosed greenschist facies basalt (e.g. Carlsberg Ridge in the Indian Ocean; Cann, 1969). This is now widely believed to result from metasomatism accompanying hydrothermal metamorphism near the sea-floor (Yardley, 1989 and references therein). In modern ocean crust, heat flow measurements indicate that open circulation of seawater continues until the upper crust becomes sealed by a thick sedimentary cover, or by precipitation of seconday minerals in voids (Anderson & Hobart, 1976). Studies in the lavas and sheeted dykes of the Troodos ophiolite, Cyprus, by Gillis & Robinson (1990), showed that magmatic intrusion at depth drove hydrothermal cells within Troodos oceanic crust. The flow of cold seawater through the extrusive sequence maintained low temperatures (<50°C) and low levels of alteration. As the crust moved away from the spreading-axis, progressive seawater/rock interaction eventually restricted the access of the water to the lavas. Similar precipitation sequences to those observed in Troodos have been

documented by Alt *et al.* (1985) from DSDP hole 504B in the eastern Pacific. Alt *et al.* (1985) found that the lava/sheeted dyke boundary marks an abrupt change in alteration conditions from low to high temperatures and high to low water/rock interaction. They showed that alteration is generally pervasive in the upper few tens of metres of crust, whereas underlying rocks display a variation of degrees of alteration.

Rocks of the Nilüfer Unit contain a mineral assemblage which includes actinolite, hornblende, albite, epidote, chlorite and opaques. By analogy with spilites dredged from modern oceans it is likely that this assemblage is largely the result of long-lived sea-floor metamorphism at temperatures of up to 250°C (and possibly much lower, by comparison with the Troodos lavas; Gillis & Robinson, 1990). Nevertheless, subsequent higher temperature metamorphism undoubtedly took place within parts of the Nilüfer Unit, as evidenced by the development of amphiboles in the Nilüfer Unit near Bursa and in the lower levels of the sequence near Edremit. Blue sodic amphiboles in the Bursa area and sodic amphibole-bearing eclogites east of Bandirma (Okay *et al.,* 1991) also imply that parts of the Nilüfer Unit underwent a very high pressure metamorphic event.

By contrast, spilites which have undergone little further metamorphism are found in the Bergama and Edremit regions. The basalts and volcaniclastic rocks are in the low greenschist facies and have a very "fresh", albeit green, appearance in the field. The internal structures of all the lithologies are well-preserved in the field but when observed in thin-section, the original minerals are almost completely replaced. These rocks lack the development of amphiboles which characterizes the higher grade rocks from the Bursa area and those from the lower levels of the Edremit sequence. A radiometric dating study carried out by British Petroleum on Turkish samples, including several from the Biga Peninsula, involved deducing the temperature of metamorphism from their mineralogy. A temperature range of 250-300°C was given for the spilite samples 53c/90 and 80a/90 (Worden, 1993), which were collected from the valley north of Zeytinli. This temperature range is consistent with spilitization caused by sea-floor hydrothermal metmorphism.

2.9.2 High-greenschist metamorphism

In metabasic rocks the higher temperature zone of the greenschist facies includes hornblende, actinolite, albite, chlorite, epidote and garnet. Near Bursa the volcanic

rocks of the Nilüfer Unit are foliated and metamorphosed to high-greenschist facies as indicated by the development of amorphous green amphibole. Quartz is also present as polycrystalline lenses within the foliated and chloritic groundmass. The lower levels of the Nilüfer Unit in the Edremit region, which are exposed on the eastern slopes of the Kazdag Massif, also display amphiboles. In the field these rocks are very dark green to almost black, and vitreous or schisty in places.

2.9.3 Blueschist/eclogite metamorphism

Okay *et al.* (1991) found incipient blue sodic amphibole replacing kaersutite in the Nilüfer Unit of the Bursa region, although I did not observe this. They also reported the presence of tectonic lenses (<100m in size) of sodic amphibole-bearing eclogites in the Nilüfer Unit east of Bandirma.

At the southwestern end of the Kazdag Massif, in the Upper Cretaceous Çetmi Ophiolitic Mélange of Okay *et al.* (1991) there are tectonic lenses of blueschist-bearing eclogites up to 3km long. These tectonic blocks were collectively named the Elliayak Eclogite by Okay *et al.* (1991) and described by them as garnet micaschists and metabasic rocks metamorphosed in the eclogite facies; the schists consisting of quartz, white mica, garnet and calcite, and the blue-green eclogites comprising garnet, omphacite, glaucophane, epidote and white mica. Their presence within the virtually unmetamorphosed Çetmi Ophiolitic Mélange suggests that these eclogite and blueschist slivers may represent deeply buried portions of either the Nilüfer Unit or the Kazdag metamorphic rocks. Further work on their geochemistry and structural relations needs to be done before their affinity can be determined.

2.10 Metamorphic gradients across accretionary complexes

Studies of various accretionary complexes indicate that the earliest accreted (i.e. structurally highest) slivers of oceanic material appear to have undergone the deepest burial (e.g. the Franciscan Complex, Central European Alps and the Sanbagawa belt of Japan; Ernst, 1971, 1988). An illite crystallinity survey in the Adheres Peninsula of Greece (Clift, 1990) also showed that palaeotemperatures (i.e. depth of burial) increase on moving *up* the structural sequence of the low-grade accretionary Ermioni Complex. The data imply that the eastern part of the Ermioni Complex were buried to greater depths than the western portion. The schematic cross-section through an accretionary prism in Figure 2.21 shows how the highest structural levels of the

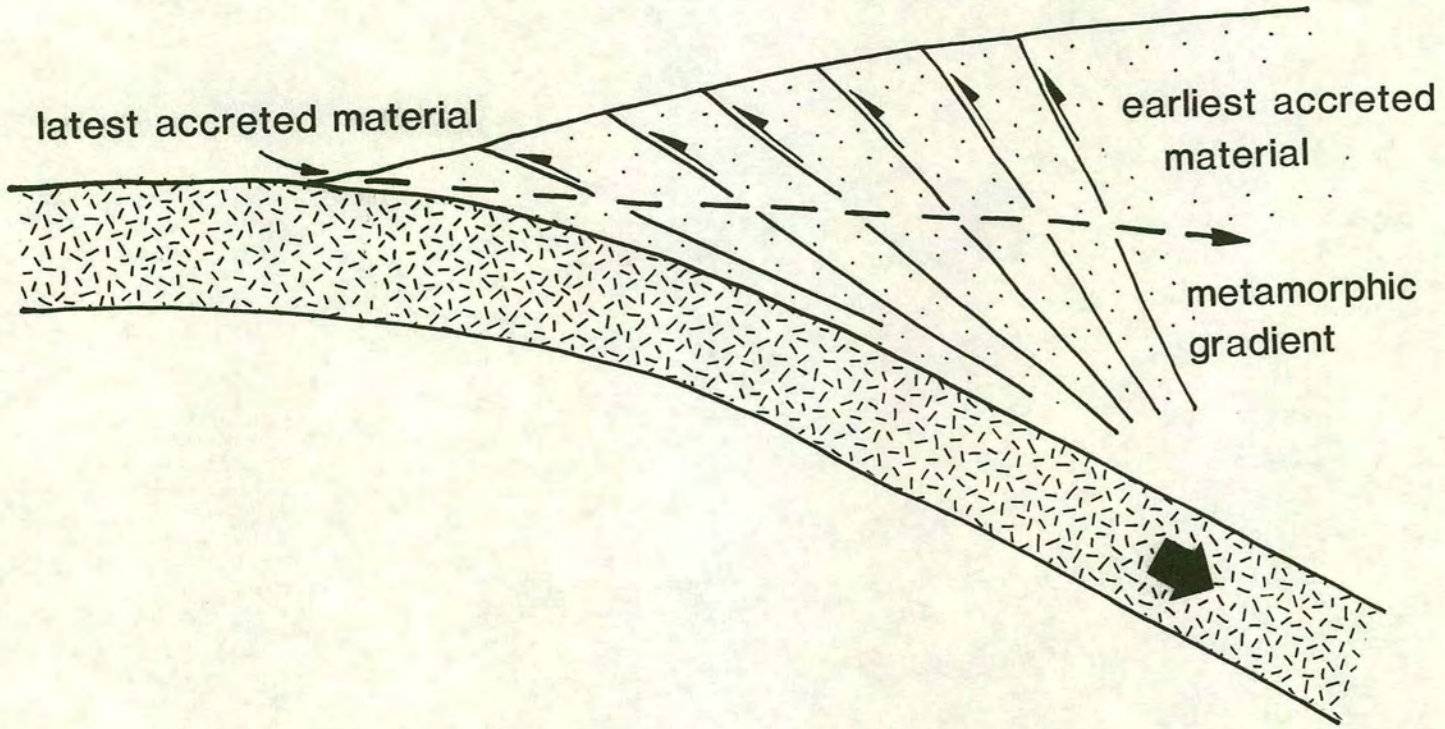

Figure 2.21 Highly simplified sketch of an accretionary complex showing the progressive accretion of oceanic material and the increase in metamorphic gradient through the stack.

complex, as exposed today, were buried to the greatest depths. A similar situation may also apply to the Nilüfer Unit in NW Turkey, as discussed below.

2.11 Metamorphic gradients within the Nilüfer Unit

Owing to the scattered distribution of the Nilüfer Unit and the laterally changing structural trends of the Karakaya Complex as a whole, it is very difficult to ascertain the direction and nature of any metamorphic gradients. Nonetheless, it is clear that they exist, as the difference between the metamorphic grades of the Nilüfer Unit in the Bursa and Edremit/Bergama areas is marked. The presence of blueschists and eclogites in the Bursa, Bandirma and Kazdag areas is also significant.

If the blueschists near Kazdag are slices of Nilüfer Unit which subsequently became incorporated into a younger mélange they may correlate with the blueschists reported from the Bursa and Bandirma areas. If this is the case the metamorphic gradient increases from south to north. By analogy with other accretionary complexes this would imply that the earliest accreted (i.e. structurally highest) parts of the Nilüfer Unit lie towards the north. This places a possible constraint on the subduction polarity. However, this is by no means certain as any definite lateral correlation between the various Nilüfer exposures is impossible. Moreover, the present-day south-dipping nature of the Karakaya Complex in the Biga Peninsula does not agree with a northward-dipping subduction zone (unless later modification has occurred) if a typical accretionary complex is envisaged. In typical accretionary complexes such as those of the SW Pacific and the western USA the internal structures mirror the dip of the subduction zone.

2.12 Structure of the Nilüfer Unit

The Nilüfer Unit is the structurally lowest observed unit of the Karakaya Complex in NW Turkey. In the Edremit region it forms a SE/E-dipping, tectonically bounded, slice between the Kazdag Massif and higher units of the Karakaya Complex. To the south, in the Bergama region, the Nilüfer Unit forms a similar, northward-vergent slice up to 1000m thick. In the Bursa and Bandirma regions the overall structure of the unit is unclear and was little studied in this project. Small-scale structures in all these regions were measured and are discussed below. Unfortunately, owing to the scarcity of structures in the predominantly massive spilites and the lack of way-up structures, relatively few conclusions can be drawn from the measurements.

2.12.1 Edremit area

a) Spilites and volcaniclastics

Apart from shearing and flattening of the clasts in many of the clast-supported rocks very few structures are present in the spilites and volcaniclastics. The shalier parts of the epiclastic volcaniclastic sequences display rare small-scale folds which have very few consistent directions (Figure 2.22). However, folds west of Karakaya Tepe (site B in Figure 2.22) show a general dip in axial planes towards the NE quadrant and fold axes which dip N or E/SE. One outcrop of volcanogenic mudstone exposed up the E-W trending valley north of Zeytinli (box A in Figure 2.22) displays well-developed folding, veining and the development of incipient cleavage along the attenuated limbs of folds.

b) Terrigenous sedimentary rocks within the Nilüfer Unit

Buff schists which crop out south of Mehemetalan are interpreted to be part of the Nilüfer Unit. They have both N and S dipping axial planes and fold axes which plunge shallowly NE and SW (Figure 2.22). Feldspathic sandstones north of Mehmetalan tend to have NW-dipping axial planes and fold axes which plunge in a range of directions including N and S. Rod-like structures with a wavelength of 0.5-1m are a distinct feature of these sandstones. The trend and plunge of the rods is consistently N or S, reflecting the orientation of many of the fold axes.

2.12.2 Bergama area

Apart from a general southward dip very few structures were observed within the spilitic part of the Bergama sequence. Flattening of clasts occurs parallel to a crude foliation, as shown in the field sketch in Figure 2.15. Folds were observed in the phyllitic sequence east of Bergama but are regarded as part of the Ortaoba Unit and are discussed in Chapter 3.

2.12.3 Bursa area

The Nilüfer Unit is strongly foliated and folded in the Bursa area. Although no structural studies were undertaken as part of this thesis, Okay *et al.* (1991) reported isoclinal and tight folds with steep, predominantly north-dipping, axial planes.

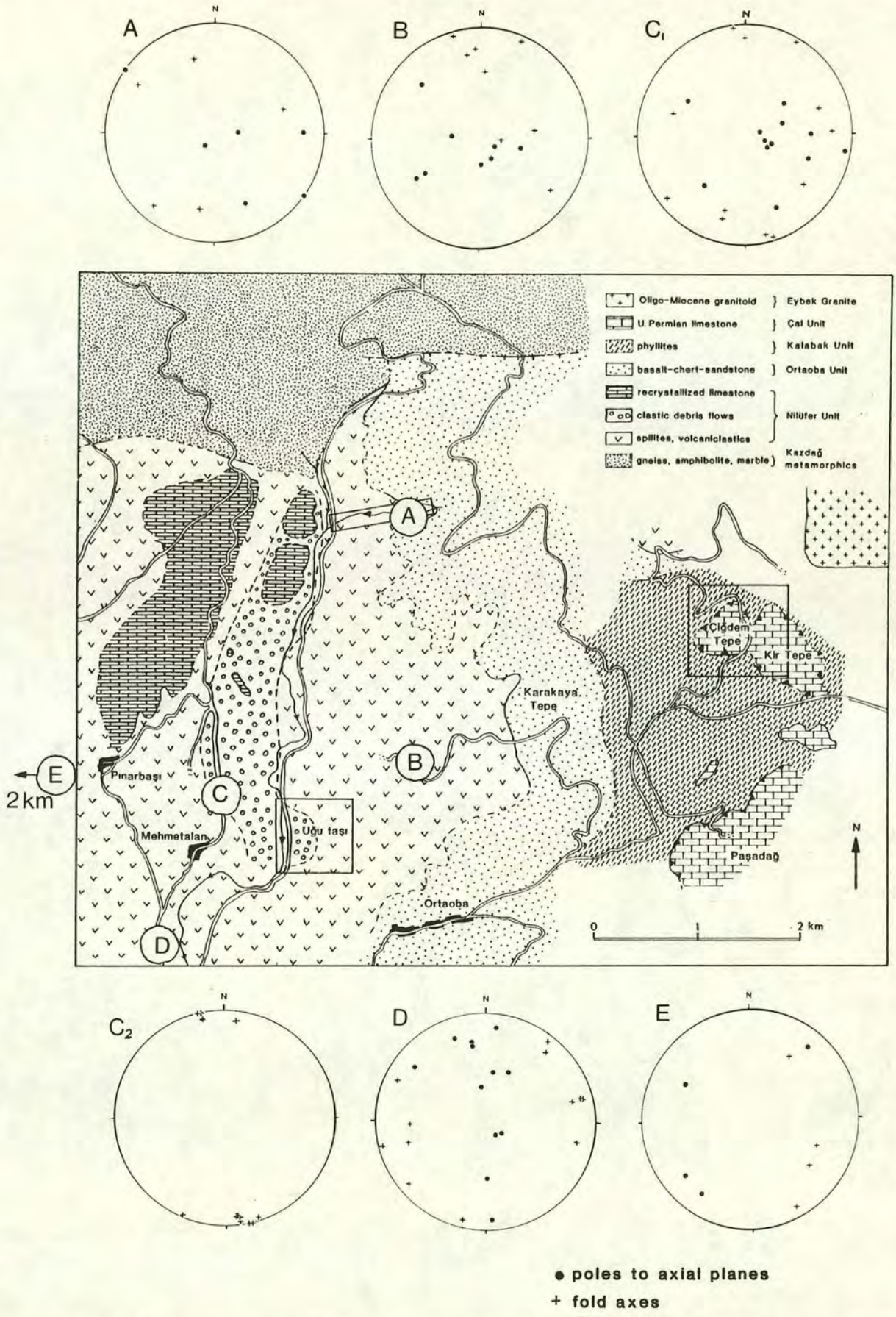

Figure 2.22 Stereoplots for folds in the Nilüfer Unit north of Edremit. The letters on the stereoplots correspond to the sites on the map.

2.12.4 Bandirma area

The Nilüfer spilites on the western coast of the Kapidag Peninsula, are highly sheared and folded. The folds are tight and asymmetrical towards the south, but owing to the absence of way-up structures, facing directions could not be determined. The axial planes dip NNE and the fold axes generally plunge ESE, implying tectonic transport towards the SSW (assuming the sequence is not overturned).

2.13 Basalt geochemistry

Correlation between the geochemical characteristics of modern volcanic rocks and their tectonic setting provides a powerful tool for the discrimination of ancient meta-volcanic sequences from poorly understood settings (for a good summary see Rollinson, 1993 and references therein). With this in mind, volcanic rocks from the Karakaya Complex were sampled and analyzed by X-ray fluorescence (XRF) and electron microprobe techniques. XRF was used to determine the bulk rock geochemistry of the lavas, while microprobe analyses were carried out on individual clinopyroxene phenocrysts. In order to make interpretations regarding the tectonic settings of the volcanics, the data were then plotted on established tectonomagmatic discrimination diagrams and normalized trace element diagrams. Results from the spilites of the Nilüfer Unit are discussed below, after a brief introduction to the application of bulk rock XRF analysis and clinopyroxene analysis. Results from the other Karakaya units are discussed in the appropriate chapters.

a) Application of bulk rock XRF data

The XRF technique is used to determine the major and trace element chemistry of prepared rock samples and has particularly strong applications to the study of basaltic rocks. The geochemical data obtained by this method, when plotted on geochemical variation and discrimination diagrams, can provide invaluable information on the origin and evolution of magmatic rocks as well as their tectonic setting. Studies carried out on basaltic rocks from known tectonic settings have led to the development of "tectonomagmatic discrimination diagrams" which may be used to elucidate the tectonic setting of ancient volcanic sequences (e.g. Pearce & Cann, 1973; Floyd & Winchester, 1975; Pearce, 1982; Meschede, 1986). These diagrams use both major and trace elements, although on the whole immobile trace element geochemistry is most useful for tectonomagmatic discrimination.

Normalized multi-element diagrams or "spider diagrams" are also a very useful way of depicting basalt geochemistry (e.g. Wood *et al.*, 1979; Sun, 1980; Pearce, 1983; Saunders & Tarney, 1984). They are based on a grouping of incompatible trace elements, normalized to their abundances in either typical MORB, chondrite, or primordial mantle (depending on most likely parental source).

b) Application of electron microprobe data from clinopyroxenes

The composition of clinopyroxenes varies according to the chemistry of their host lavas. As a result of this property the geochemical characteristics of clinopyroxenes preserved in spilites and metabasites may be used to identify the original magmatic setting (e.g. Nisbet & Pearce, 1977; Leterrier *et al.*, 1982). Leterrier *et al.* (1982) devised a set of discrimination diagrams based on a study of clinopyroxene phenocrysts from recent volcanic rocks from known tectonic settings. They found that groundmass clinopyroxenes show the same tendencies as phenocrysts, but tend to show a larger spread. Leterrier *et al.* (1987) also demonstrated the application of this method to palaeovolcanic rocks belonging to the zeolite or greenschist metamorphic facies. Owing to its applicability to ancient, meta-volcanic sequences, this method was applied to the spilites and metabasites of the Karakaya Complex in conjunction with XRF analysis of their bulk rock chemistry.

2.14 Whole-rock analysis of basalts

Samples of spilite were collected from the Nilüfer Unit in the Bergama, Edremit, Bursa and Bandirma regions for geochemical analysis by X-ray fluorescence. The largest suites were collected from Bergama and Edremit where the freshest spilites are exposed. They are predominantly green and highly chloritic but nevertheless retain good relict igneous textures and produce XRF analyses in which the immobile elements at least have been little affected by spilitization.

2.14.1 Edremit area

Basalts from the Nilüfer Unit were collected from the road cutting in the river valley east of Mehmetalan, and also from the mountain road running due north of Mehmetalan (Figure 2.5). Two distinct types of basalt were found in this region and their geochemistry is described below. One basalt type is green and spilitic and typical of the Nilüfer Unit as a whole. The other type is fine-grained and purple. The two suites are referred to in this section as the "purple" and "green" suites and their

geochemistry is described separately. The purple volcanics are tectonically below the green spilites and are thus described first. (As shown on Figure 2.4 higher grade green spilites also occur *below* the purple volcanics and crop out further west in the Kazdag Massif. Only one sample (123a/90) was analyzed from this unit. Its geochemistry is very similar to that of the higher spilite sequence. Thus these spilites are tentatively assigned to the Nilüfer Unit, possibly representing deeper levels of the same sequence).

a) "Purple suite"

The "purple suite" is very localized in extent compared to the green spilites. It forms outcrops along a short stretch of the road north of Mehmetalan, marked C in Figure 2.5. The purple volcanics are highly sheared and possess a strong fissility in places. Large flattened plagioclase crystals, exposed on some surfaces, confirms their igneous rather than sedimentary origin. Despite a highly sheared nature many of these rocks have a distinct streaky appearance and the presence of abundant feldspar crystals suggests an origin as a crystal tuff, or ignimbrite. Data for this suite are shown on the discrimination diagrams as triangles. The samples plot in the within-plate field of the Zr/Y-Ti/Y plot (Figure 2.23a) and close to the alkali-tholeiitic boundary in the P_2O_5-Zr plot (Figure 2.23b). On the Ti/Y-Nb/Y diagram they plot predominantly within the alkali basalt field (Figure 2.25a). Their within-plate characteristics are clearly shown by the Zr/Y-Zr, Ti-Zr, Ti/Y-Nb/Y and Cr-Y diagrams (Figures 2.24 and 2.25).

MORB-normalized plots for these volcanics show the "humped" patterns characteristic of within-plate basalts with very strong enrichment in the LIL elements (except Sr) and the HFS elements Nb, P, Zr and Ti (Figure 2.26). Th is considered to be one of the few LIL elements which is relatively immobile during alteration (Saunders & Tarney, 1984) and its high degree of enrichment implies that the general LIL enrichment is a primary feature. The low value of Sr relative to the other LIL elements may reflect the recrystallization and removal of plagioclase. Nb enrichment and the enrichment of Ti relative to Y are characteristic features of within-plate patterns and are clearly shown in Figure 2.26. The trace-element patterns for alkaline within-plate basalts from the Azores (Pearce, 1982) are very similar to those from this suite.

b) "Green suite"

The "green suite" comprises blocky spilites, typical of the Nilüfer Unit, which form continuous exposure along the valley road east of Mehmetalan and crop out

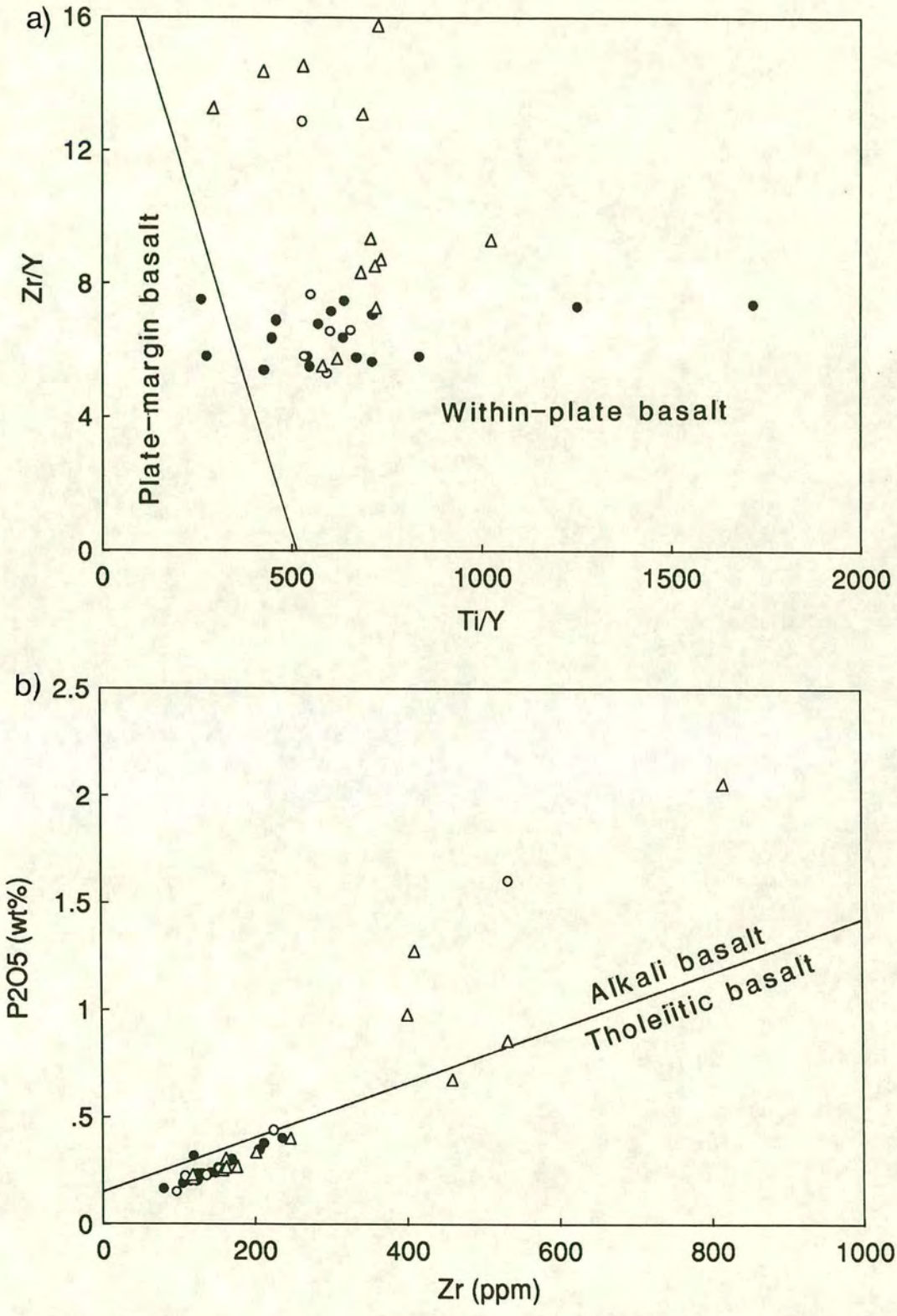

Figure 2.23 Tectonic discrimination diagrams for the Nilüfer Unit in the Edremit region. (a) Zr/Y-Ti/Y plot (fields from Pearce & Gale, 1977), (b) P_2O_5-Zr plot (fields from Winchester & Floyd, 1976). The "purple suite" is represented by triangles and the "green suite" by closed circles (from the road east of Mehmetalan) and open circles (road north of Mehmetalan).

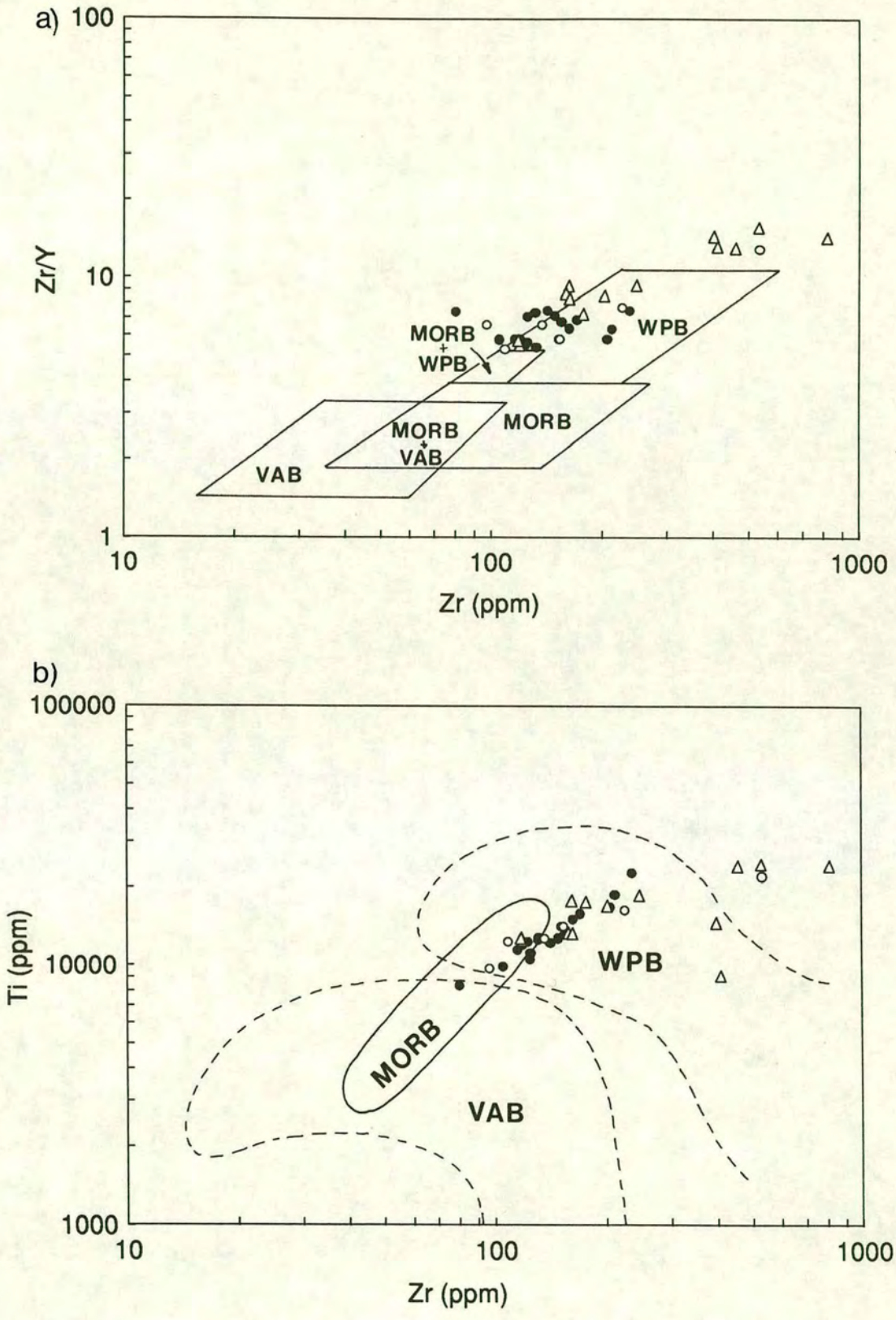

Figure 2.24 Tectonic discrimination diagrams for the Nilüfer Unit in the Edremit region. (a) Zr/Y-Zr plot (fields from Pearce & Norry, 1979), (b) Ti-Zr plot (fields from Pearce, 1982). The "purple suite" is represented by triangles and the "green suite" by closed circles (from the road east of Mehmetalan) and open circles (road north of Mehmetalan).
(MORB: mid-ocean ridge basalt, WPB: within-plate basalt, VAB: volcanic-arc basalt)

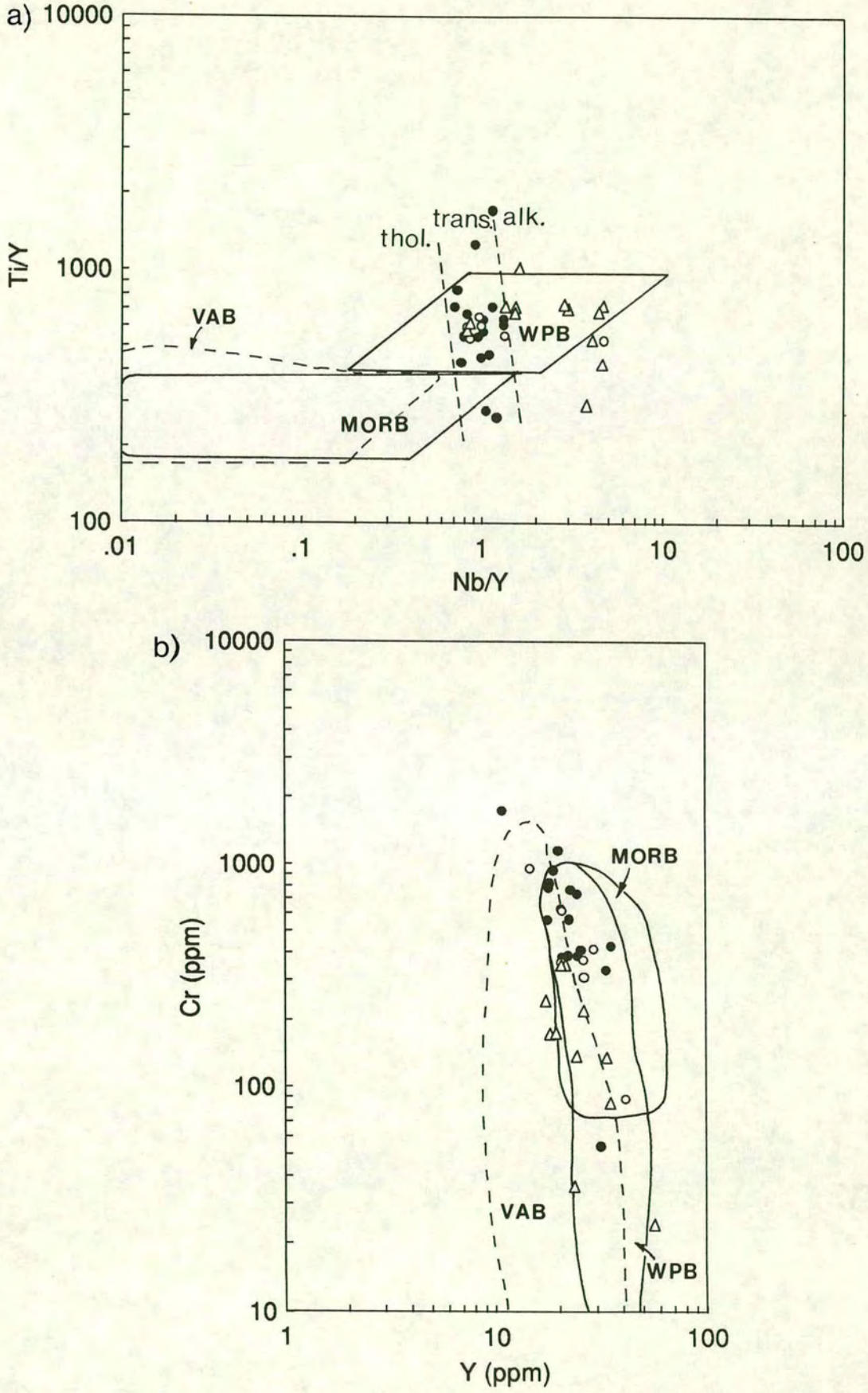

Figure 2.25 Tectonic discrimination diagrams for the Nilüfer Unit in the Edremit region. (a) Ti/Y-Nb/Y plot (fields from Pearce, 1982), (b) Cr-Y plot (fields from Pearce, 1982). The "purple suite" is represented by triangles and the "green suite" by black circles (from the road east of Mehmetalan) and white circles (road north of Mehmetalan).

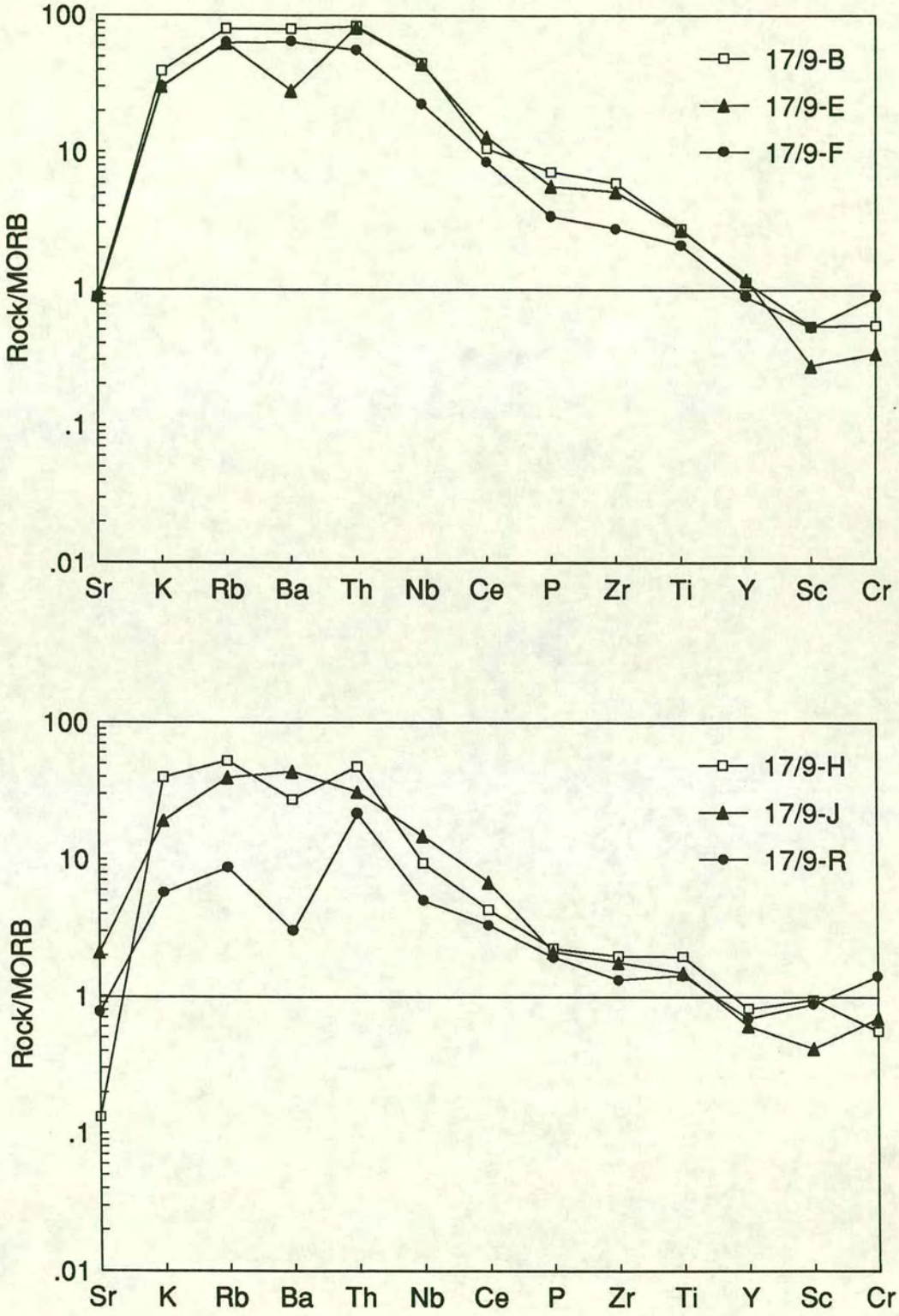

Figure 2.26 MORB-normalized multi-element plots for the "purple suite" of the Nilüfer Unit (normalizing values from Pearce, 1983; Sc and Cr from Pearce, 1982).

sporadically along the road north of Mehmetalan. The XRF data from basalts along these two roads were plotted on discrimination diagrams (Figures 2.23-2.25) as closed circles (road east of Mehmetalan) and open circles (road north of Mehmetalan). The P_2O_5 -Zr diagram (Figure 2.23b) separates alkali basalts from tholeiitic basalts and indicates that the green spilites are slightly more tholeiitic than alkalic, although they plot very close to the boundary. More detailed discrimination, using the Ti/Y-Nb/Y plot, shows them to be transitional between alkalic and tholeiitic (Figure 2.25a). The Zr/Y-Ti/Y diagram indicates a within-plate rather than plate-margin origin, a setting confirmed by the more detailed Zr/Y-Zr, Ti-Zr, Ti/Y-Nb/Y and Cr-Y discrimination diagrams. On all these diagrams the basalts of the "green suite" form a well-defined cluster in and around the within-plate basalt (WPB) field. On the Ti-Zr diagram they form a clear Ti-Zr fractionational crystallization trend.

The WPB affinity of this suite of basalts is reflected by the MORB-normalized plots, examples of which are shown in Figures 2.27 and 2.28. The plots display characteristic WPB "humped" patterns which have similar patterns to those of the "purple suite", although they generally display much less enrichment. The three traces in Figure 2.27a show the range of degrees of enrichment measured in these samples. In several cases the more mobile LIL elements are depleted relative to Th (e.g. Figure 2.27b), indicating some kind of alteration which did not affect the relatively immobile Th.

2.14.2 Bergama area

A suite of spilites was collected from road cuttings around the villages of Köyyeri and Ada in the Bergama region. Most of the samples were taken along the road cutting shown in the field sketch in Figure 2.15, owing to the fresh, massive nature of the volcanics. The spilites are identical, both in the field and in thin-section, to the "green suite" near Edremit. On basalt discrimination diagrams the Bergama spilites plot in very similar positions to those from the Edremit region, i.e. almost entirely within the WPB fields (Figures 2.29 and 2.30).

MORB-normalized plots for these samples also display WPB patterns with enrichment of Nb, P, Zr, Ti and the LIL elements (Figures 2.31 and 2.32). Figure 2.32 shows the various degrees of enrichment measured in the Bergama spilites. The different amounts of enrichment are probably primary features as the Th values are significantly different. The samples in Figure 2.32a were collected from the same

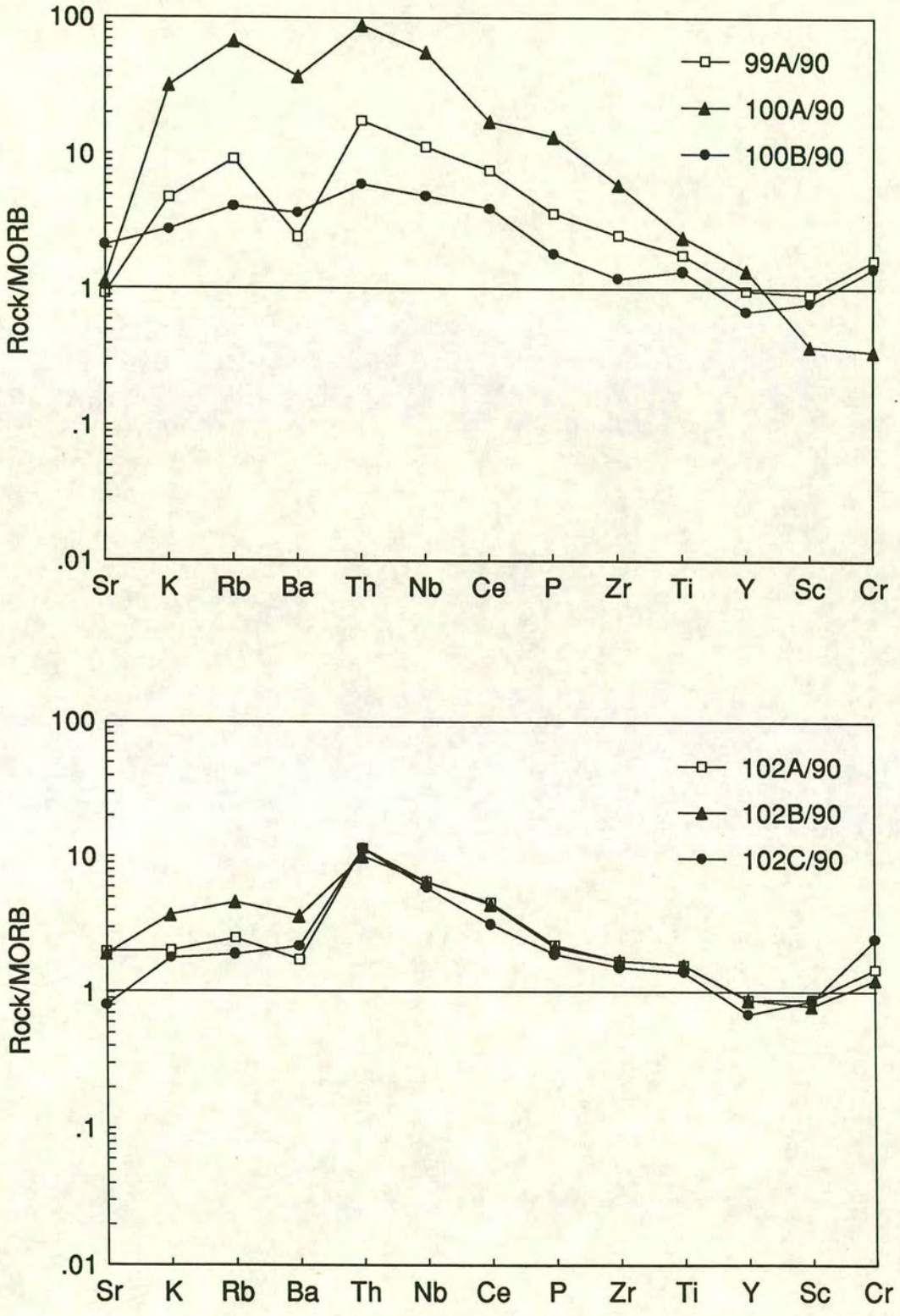

Figure 2.27 MORB-normalized multi-element plots for the "green suite" of the Nilüfer Unit (sampled from the road north of Mehmetalan). Normalized as for Figure 2.26.

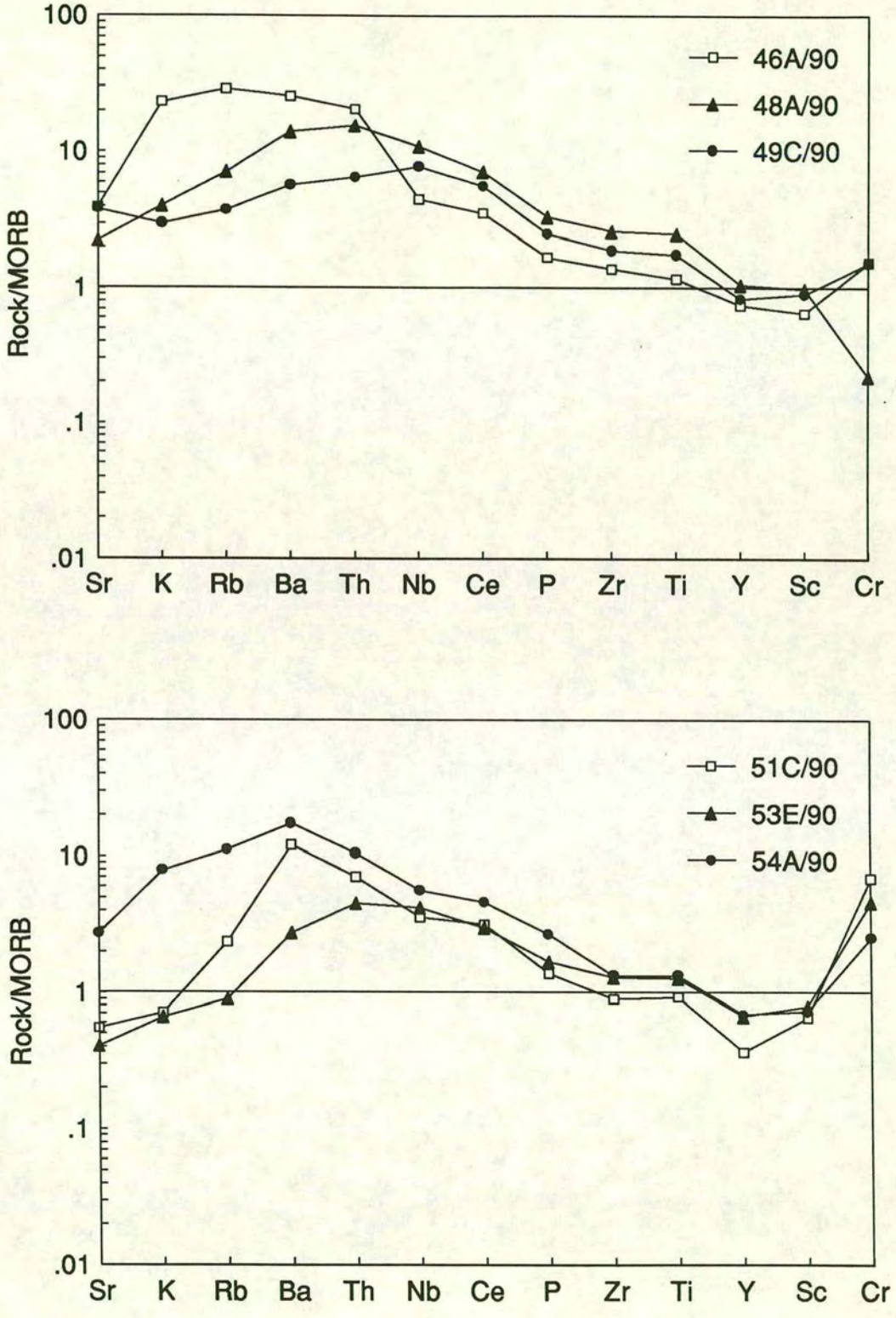

Figure 2.28 MORB-normalized multi-element plots for the "green suite" of the Nilüfer Unit (sampled from the road east of Mehmetalan). Normalized as for Figure 2.26.

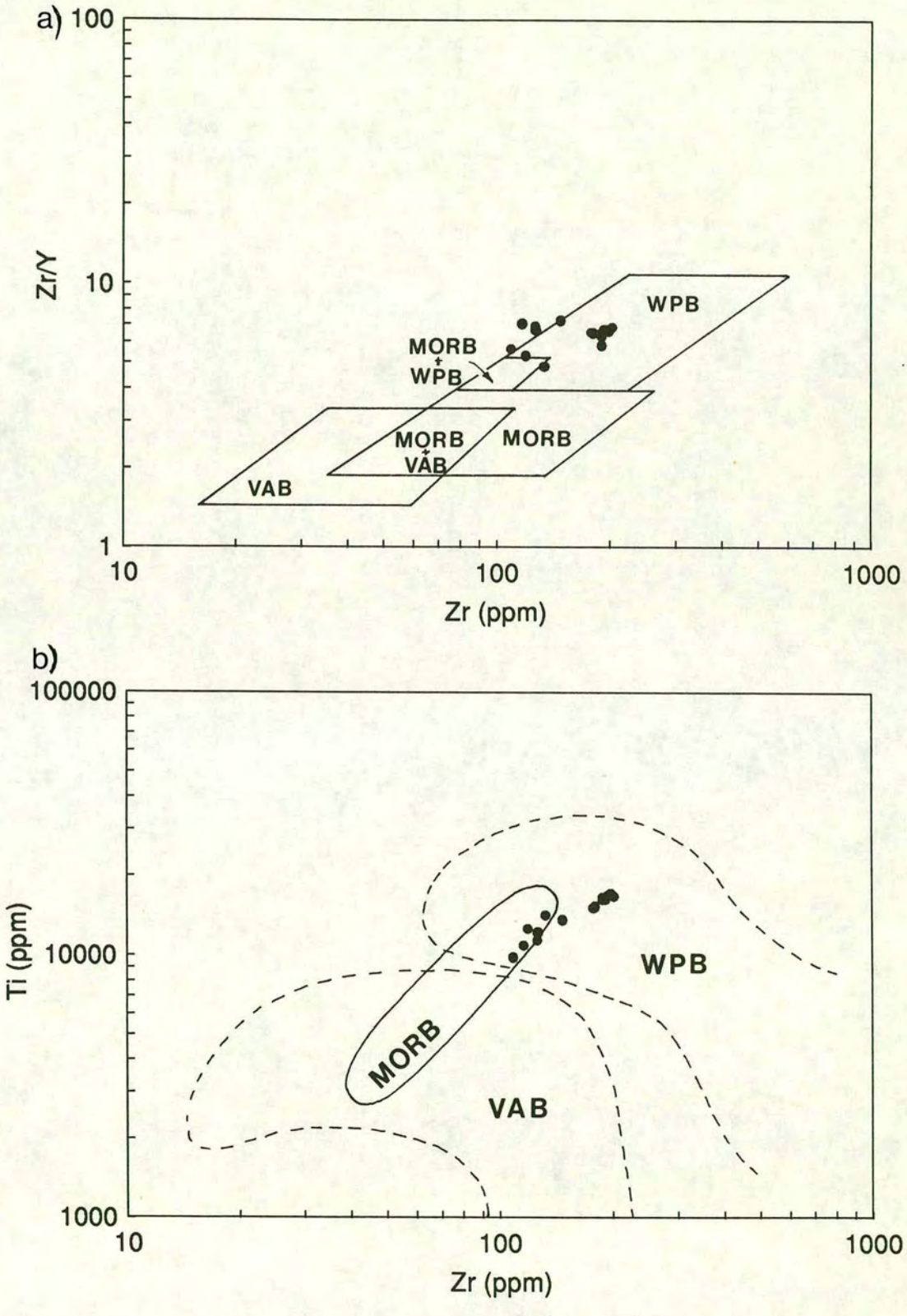

Figure 2.29 Tectonic discrimination diagrams for the Nilüfer Unit in the Bergama region. (a) Zr/Y-Zr plot (fields from Pearce & Norry, 1979), (b) Ti-Zr plot (fields from Pearce, 1982).

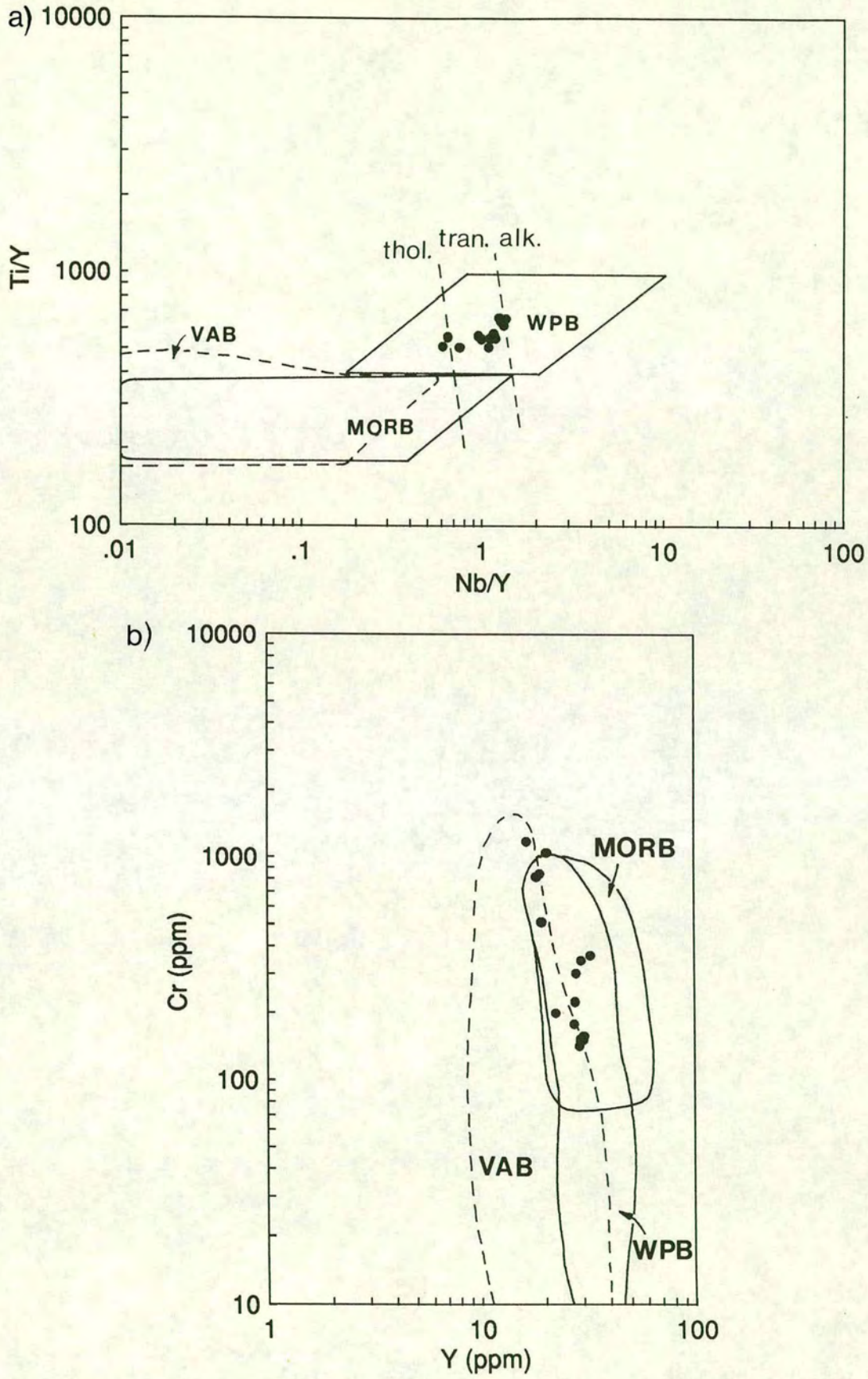

Figure 2.30 Tectonic discrimination diagrams for the Nilüfer Unit in the Bergama region. (a) Ti/Y-Nb/Y plot (fields from Pearce, 1982), (b) Cr-Y plot (fields from Pearce, 1982).

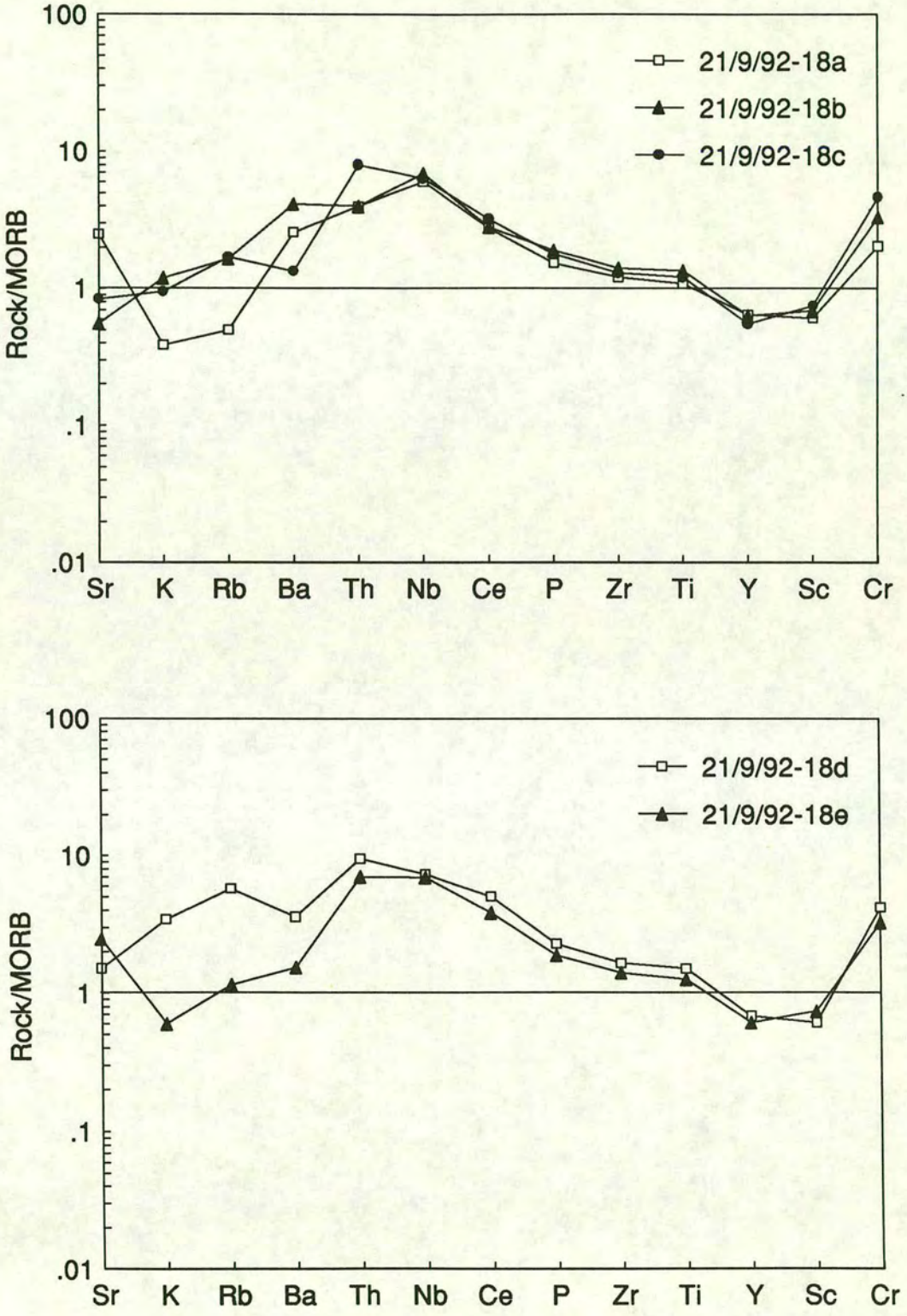

Figure 2.31 MORB-normalized multi-element plots for the Nilüfer Unit in the Bergama region. Normalized as for Figure 2.26.

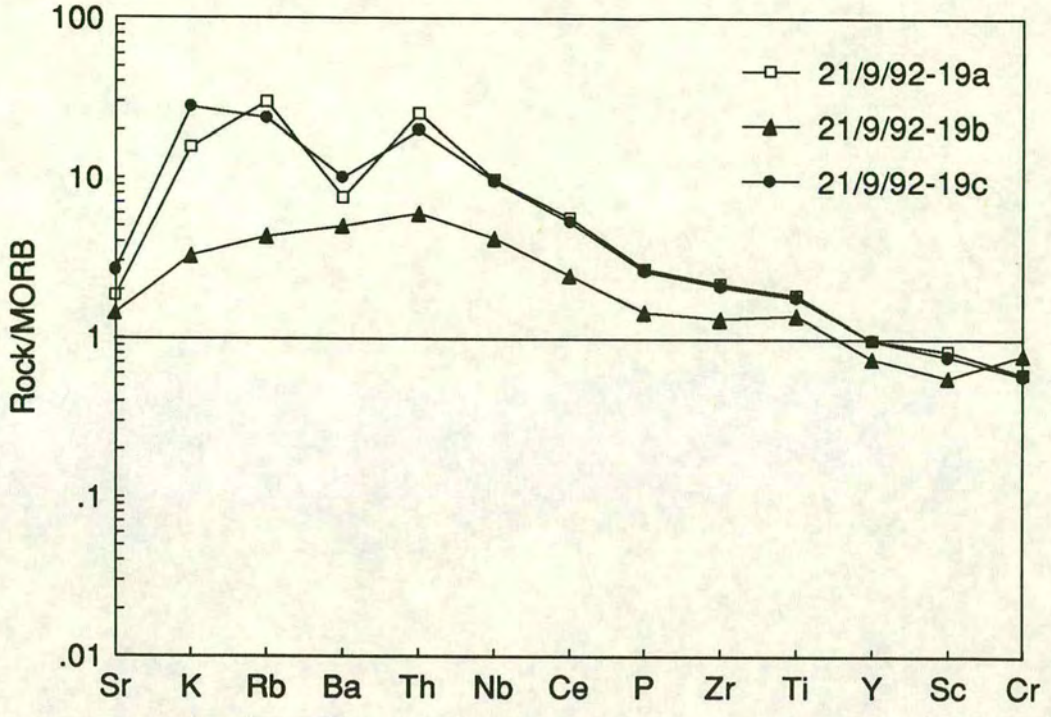

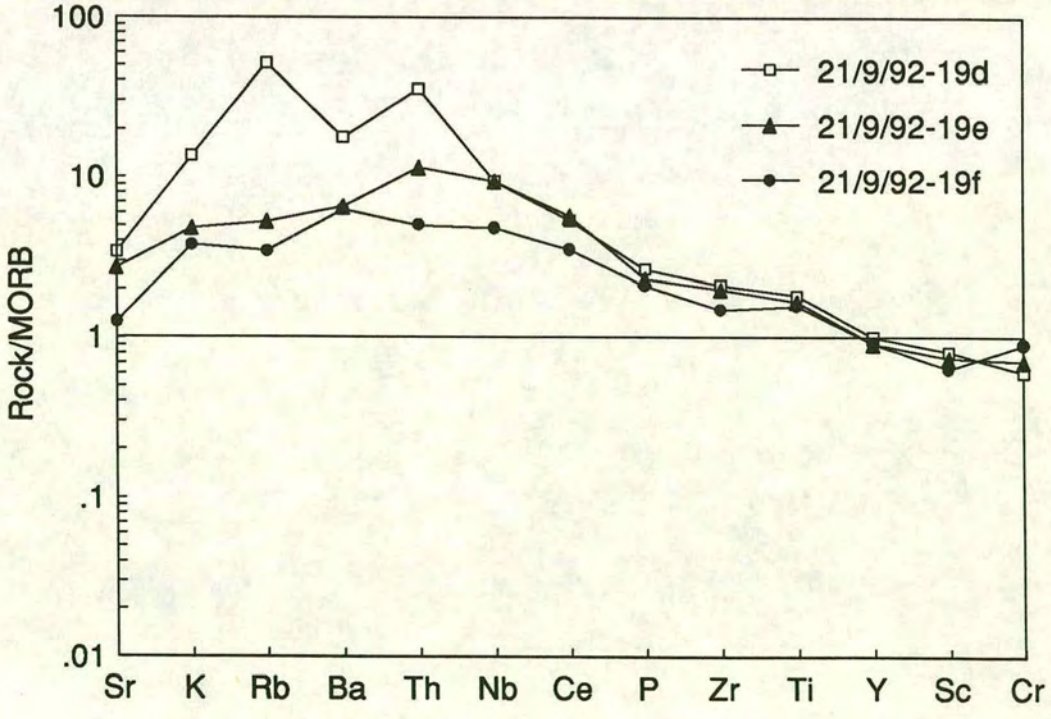

Figure 2.32 MORB-normalized multi-element plots for the Nilufer Unit in the Bergama region. Normalized as for Figure 2.26.

outcrop and display a wide variation in enrichment for such closely related basalts. Sample 21/9/92-19b displays relatively low enrichment compared with the other two samples and its trace closely resembles those of enriched MORBs. However, the sample displys distinct enrichment of Ti relative to Y, a characteristic feature of the Nilüfer basalts and WPB in general.

2.14.3 Bursa and Bandirma areas

Although the spilites in these areas were not studied in any detail, several samples were collected with the aim of making tentative comparisons with those from the Edremit and Bergama regions. A few spilites were collected from beside the dam in the Nilüfer River, south of Bursa and from a sheared outcrop several kilometres north of Karacabey, east of the Marmara Sea port of Bandirma. The spilites have a very close geochemical affinity with those from Edremit and Bergama, plotting in the WPB fields of basalt discrimination diagrams (Figures 2.33 and 2.34) and displaying characteristic "humped" WPB MORB-normalized patterns (the depletion of K, Rb and Ba relative to Th is probably a secondary feature caused by their mobility) (Figure 2.35). The MORB-normalized patterns for the samples from the two localities are similar to each other and also to the patterns displayed by the Edremit and Bergama samples.

2.15 Microprobe analysis of clinopyroxenes

Clinopyroxene crystals in Nilüfer spilites from the Edremit area were analyzed by electron microprobe. The crystals chosen for analysis were mainly small phenocrysts, although a few may represent interstitial groundmass material. Despite their dark brown and dusty appearance the clinopyroxenes are relatively fresh and, when analyzed, gave good totals between 99 and 101. Where possible, both cores and rims of phenocrysts were analyzed and plotted as circles (cores) and triangles (rims) on Figure 2.36. The results for both cores and rims plot predominantly in the non-alkali and non-orogenic fields respectively. These clinopyroxenes are thus closely related to transitional or tholeiitic basalts and, more precisely, to non-orogenic tholeiites. This characterization is in good agreement with the whole-rock geochemistry of the spilites.

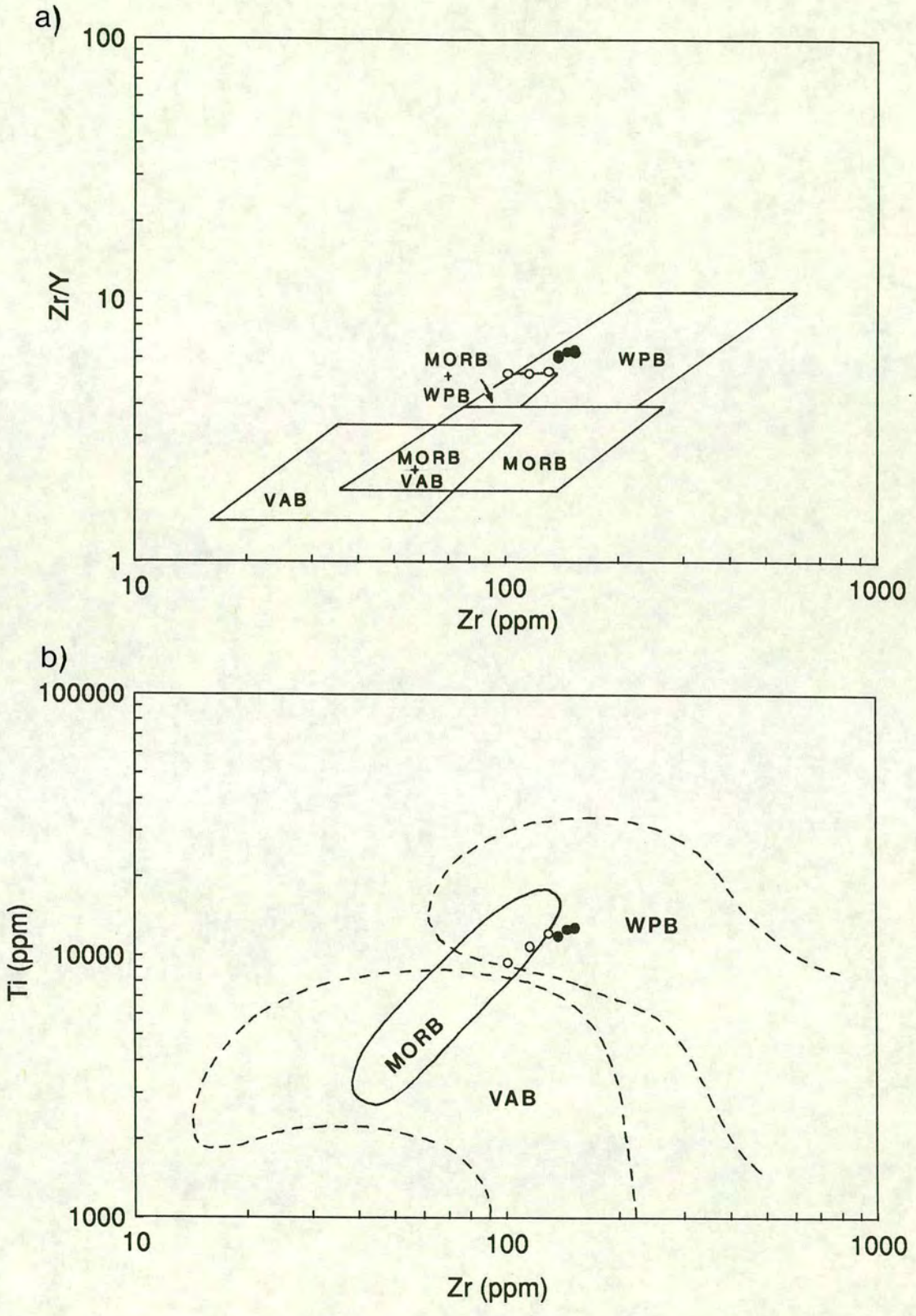

Figure 2.33 Tectonic discrimination diagrams for the Nilüfer Unit in the Bursa (closed circles) and Bandırma (open circles) regions. (a) Zr/Y-Zr plot (fields from Pearce & Norry, 1979), (b) Ti-Zr plot (fields from Pearce, 1982).

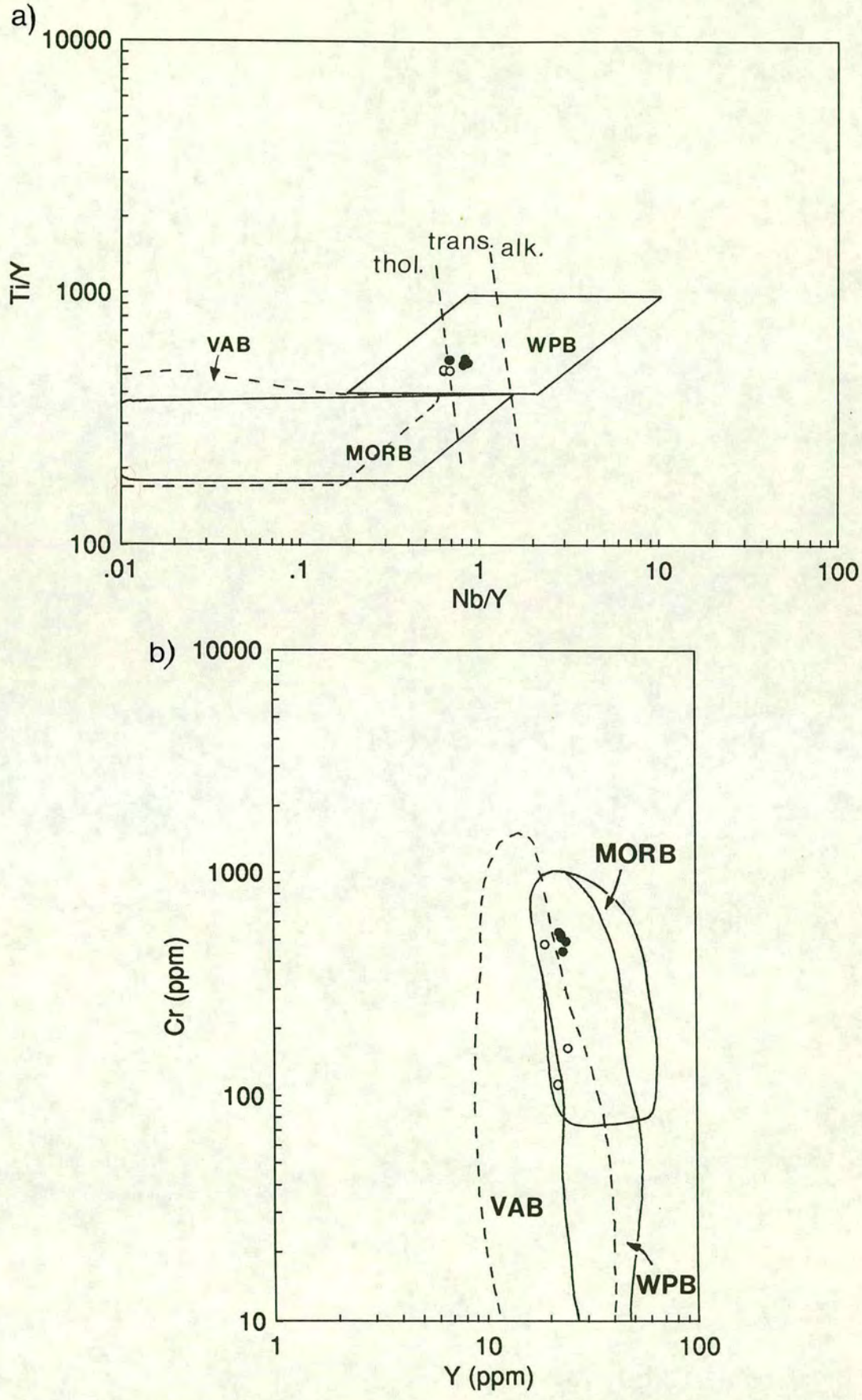

Figure 2.34 Tectonic discrimination diagrams for the Nilüfer Unit in the Bursa (closed circles) and Bandırma (open circles) region. (a) Ti/Y-Nb/Y plot (fields from Pearce, 1982), (b) Cr-Y plot (fields from Pearce, 1982).

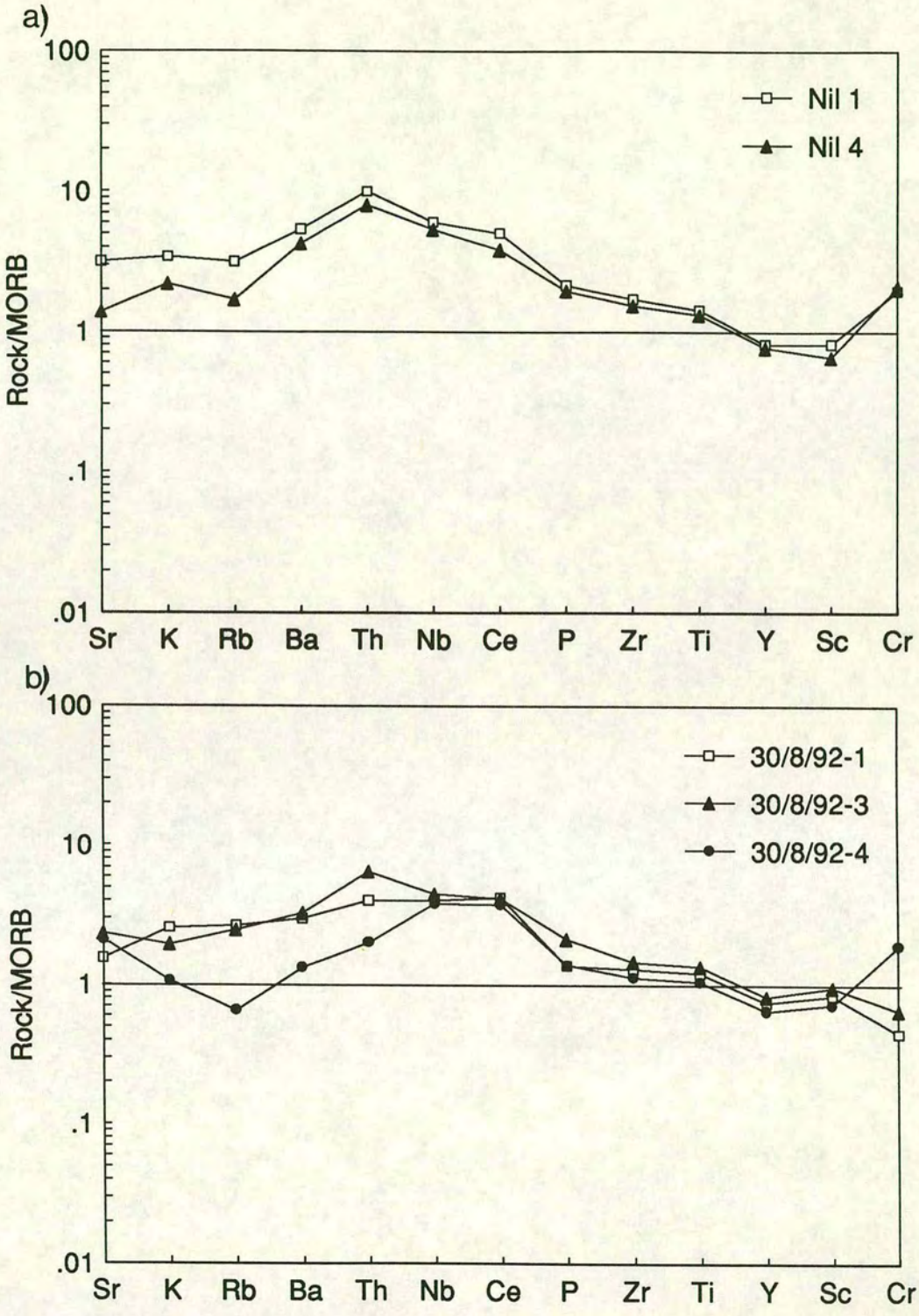

Figure 2.35 MORB-normalized multi-element plots for the Nilüfer Unit in (a) the Bursa region and (b) the Bandırma region. Normalized as for Figure 2.26.

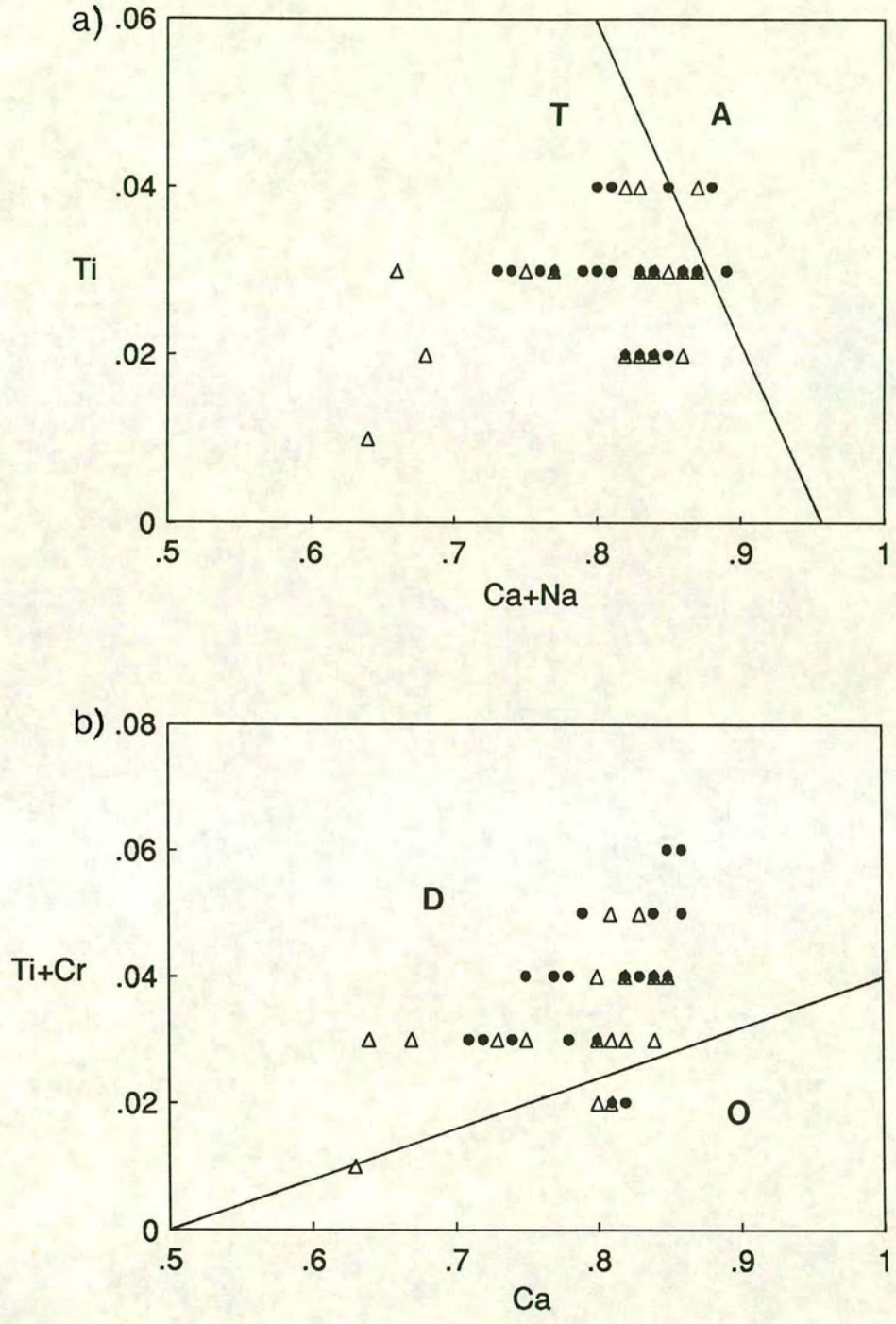

Figure 2.36 Tectonic discrimination diagrams for clinopyroxenes in basalts from the "green suite" of the Edremit region. (a) Ti vs (Ca+Na) plot showing the fields for alkali basalts (A) and tholeiitic and calc-alkali basalts (T), (b) (Ti+Cr) vs Ca plot showing the fields for MORB and other tholeiites from spreading zones (D) and volcanic-arc basalts (O) (fields from Leterrier *et al.*, 1982). Clinopyroxene compositions are expressed in cations per six oxygens. Circles represent phenocryst cores and triangles represent rims.

2.16 Interpretation of geochemistry

The basaltic rocks of the Nilüfer Unit have remarkably consistent geochemical characteristics which can be recognized in spilites from many regions of NW Turkey including the Edremit, Bergama, Bandirma and Bursa regions. Basalt discrimination diagrams and multi-element plots clearly indicate a within-plate setting for all the volcanic sequences. Spilites from the Edremit area were divided into two suites on the basis of field observations and, subsequently, their geochemistries. An alkalic suite ("purple suite") and a much more voluminous transitional/tholeiitic suite ("green suite") were identified. Equivalents of the alkalic suite were not observed elsewhere in the Biga Peninsula or Bergama regions. Despite their differences both these suites plot in the within-plate fields of discrimination diagrams. Analysis of clinopyroxenes from the transitional suite in the Edremit region confirms the non-alkalic, non-orogenic nature of these rocks.

Taken on its own, a within-plate geochemical signature is not particularly diagnostic and can signify either continental rift *or* oceanic island settings. Interpretation of within-plate basalts therefore requires a more integrated approach, involving study of the sequence as a whole. In particular, associated sedimentary rocks can help to distinguish between the two possibilities. For example, Upper Triassic within-plate basalts of the Antalya region, SW Turkey, have been interpreted as rift basalts on the basis of their association with proximal terrigenous sedimentary rocks (Robertson & Waldron, 1990; Robertson *et al.,* 1991). An alternative, open ocean seamount origin for the Antalya basalts was considered unlikely, in view of the associated terrigenous clastics. The compositions of the Antalaya basalts are very similar to the Triassic basalts within the Mamonia Complex, SW Cyprus (Malpas *et al.,* 1987). However, the Mamonia basalts were interpreted by Robertson *et al.,* (1991) as seamounts or basement highs, rather than rift basalts, owing to the distal, deep-water nature of the sediments which locally overlie them.

Although feldspathic sandstones, shales and debris flows occur as slices within the Nilüfer Unit, terrigenous material is noticeably absent from the spilitic and volcaniclastic sequences, thereby confirming an origin far from land. Thus, the within-plate geochemistry, together with the associated carbonates, suggests an intra-oceanic, rather than rift, setting. The abundance of volcaniclastic debris flows implies a slope setting sourced by lava flows and volcanic detritus. An environment which would fit all these characteristics is that of a volcanic ocean island or seamount.

2.17 Interpretation of the Nilüfer Unit

Comparisons of the lithologies and geochemistry of the Nilüfer Unit with volcanic rocks from modern and ancient settings has led to its interpretation as an intra-oceanic seamount sequence which was subsequently accreted at a trench. In this section I briefly outline the main characteristics of seamounts and their accretion before discussing the features of the Nilüfer Unit within a seamount framework and within the framework of the accretionary Karakaya Complex as a whole. Finally, several modern and ancient analogues are suggested for the Nilüfer Unit.

2.17.1 Seamount development

Seamounts are volcanic edifices (generally <10km-25km in diameter; Cas & Wright, 1987) that build upwards from oceanic abyssal planes, either near or far away from spreading ridges. They range from individual edifices with basal diameters as small as 1km, up to structures such as Hawaii which has become a major subaerial shield system of many volcanoes.

The growth of oceanic seamounts was first investigated in detail by Jones (1966) whose model is shown in Figure 2.37. In this model pillow lavas form the basal levels of the seamount. When the lava pile gets close to sea level, the reduced hydrostatic pressure may produce explosive eruptions which mantle the pillows with pyroclastic deposits. Emergence above sea level may produce passive lava eruptions with the formation of a lava cap over the volcaniclastics. Rapid quenching at the edges of these eruptions produces hyaloclastites and flow-foot breccias. This is a very simplified model and more recent studies have highlighted the complex interaction of intrusive, pyroclastic and epiclastic processes that contribute to volcanic island and seamount build-up. In their work on the Pliocene seamount series of La Palma in the Canary Islands, Staudigel & Schminke (1984) found that intrusive processes (e.g. sills and small plutons) at depth contribute significantly to the growth of seamounts. They also recognized two main stages in the evolution of the extrusive sequence:

1. an early "deep-water stage" of sill emplacement and pillow extrusion onto the sea floor.

2. a later "shoaling stage" as the seamount reaches a critical depth for exlosive volcanism and clastic processes become more important.

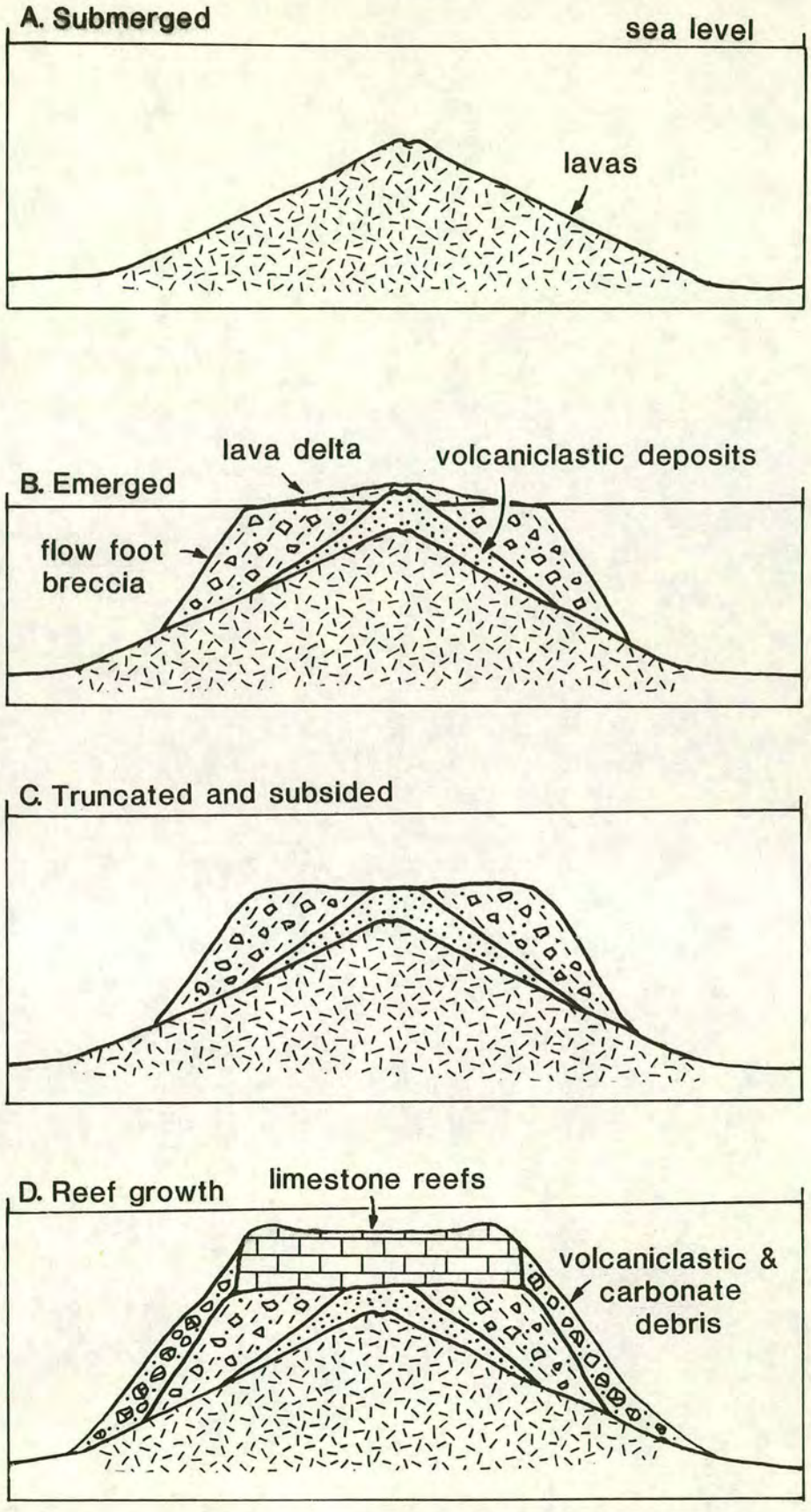

Figure 2.37 Model for the construction of a carbonate-capped seamount (stages A, B and C after Jones, 1966).

This later stage produces the thick volcaniclastic aprons that characterize seamounts and volcanic islands. Detailed studies have been carried out on the morphology of volcaniclastic aprons and the processes involved in their formation by Busby-Spera (1987, 1988). Her studies have focused on the Gran Cañon Formation in Baja California, Mexico, which is interpreted as a deep-marine volcaniclastic apron that prograded across a back-arc basin, during growth of an island arc in the Mid Jurassic. A thick sequence of lava flows, tuffs and graded tuff breccias was blanketed by epiclastic volcanic muds, silts and sands, that record abrupt cessation of volcanism and erosion of the arc. Although not strictly from a seamount setting, the Gran Cañon Formation nevertheless provides an excellent example of the type of sequence generated by an oceanic volcanic island.

Older seamounts may become colonized by reef-building organisms which contribute clastic carbonate debris to the seamount flanks (Figure 2.37). Establishment of fringing reefs could produce a thick apron of coarse volcaniclastic and carbonate detritus. These facies would grade laterally into the background pelagic facies of the abyssal planes. The carbonate blocks and calcturbidites within the Nilüfer Unit were probably derived from reefal material which capped the edifice and thus represent the flanks of a seamount. Distal to abyssal facies are represented by the fine-grained volcanogenic silts and cherty horizons that were observed in both the Edremit and Bergama regions.

2.17.2 Accretion of seamounts

Geophysical studies of modern active margins have shown that when ocean islands arrive at trenches, they undergo a certain amount of "tectonic erosion", but are often absorbed into the accretionary complex as relatively intact sequences (Lallemand & Le Pichon, 1987; Ballance *et al.*, 1989). This may explain why seamount material is so abundant in many ancient accretionary complexes. Current examples of seamount subduction were studied during the French-Japanese KAIKO project using Seabeam mapping, seismic profiling and submersible diving (e.g. Cadet *et al.*, 1987). Several dives focused on the Daiichi-Kashima seamount, which is currently being subducted at the Japan Trench (Figure 2.38). The seamount is cut in two by normal faulting (with vertical displacement up to 1600m) and the trenchward block is subsiding into the trench. Limestone breccia was observed between the seamount and the inner trench wall. The inner trench wall is composed of hemipelagic mudstones. Seamount material (limestone) was observed in the landward slope of the trench, above the level

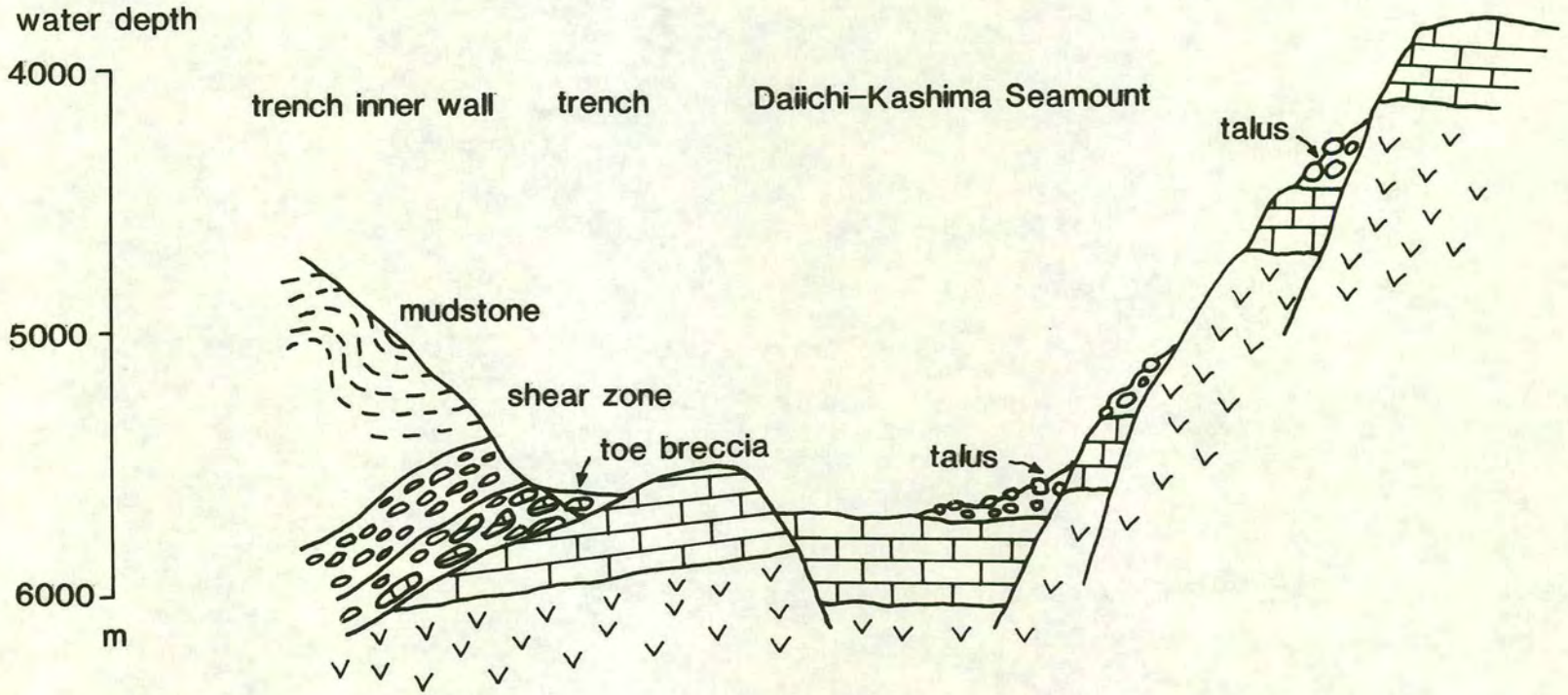

Figure 2.38 Interpreted section across the Japan Trench at the point where the Daiichi-Kashima Seamount is being dismembered and subducted (after Cadet *et al.*, 1987).

of the down-faulted seamount block. This may be evidence that tectonic mixing is taking place between seamount materials and trench wall material, as shown in Figure 2.38. Further evidence is provided by the morphology of the landward slope of the trench which is characterized by several scarps. These may be an expression of thrusts in the lower part of the slope, hence suggesting accretionary processes at the toe of the landward wall (Kobayashi *et al.*, 1987). Another subducting seamount has also been recognized at the intersection of the Kyushu-Palau Ridge at the Nankai Trough (Le Pichon *et al.*, 1987). Seismic profiles show a subducting seamount which is half covered by the accretionary wedge.

Using these modern examples from Japan, Taira *et al.* (1989) developed a model for seamount accretion in which initial breakup by normal faulting and toe brecciation are followed by progressive burial under an accretionary wedge (Figure 2.39). Slicing of the seamount occurs beneath the accretionary wedge. The upper levels are incorporated into the accretionary wedge while the lower parts may be underplated at greater depths. It is likely that similar processes occurred during incorporation of the Nilüfer Unit into the Karakaya accretionary complex. The upper levels (presumably limestone) were scraped off within the accretionary prism, leaving the volcanic pile intact. This has been remarkably well preserved, implying that it was probably accreted towards the end of subduction activity and thus was not subducted to any great depth.

2.17.3 Discussion

The Nilüfer Unit is interpreted as the middle to upper levels of a seamount which became incorporated into an accretionary complex during subduction, in a setting similar to that of the present-day Japan and Kuril Trenches (Figure 2.40). The seamount formed in an open ocean environment far from any terrigenous clastic supply and became capped with limestone reefs which built up on the volcanic basement. Steep flanks led to the formation of extensive debris flows which incorporated volcanic and limestone clasts in a volcanogenic matrix. More distal deposits are represented by fine-grained volcanogenic sandstones and mudstones. Cherty interbeds reflect the background deep-water sedimentation present in oceans. The lower part of the spilite unit comprises massive lava and probably represents the basal levels of the seamount, produced during its initial eruptive activity and growth. The sliver of serpentinized dunite observed near Bergama may be a fragment of even deeper oceanic crust, incorporated into the accretionary complex during subduction.

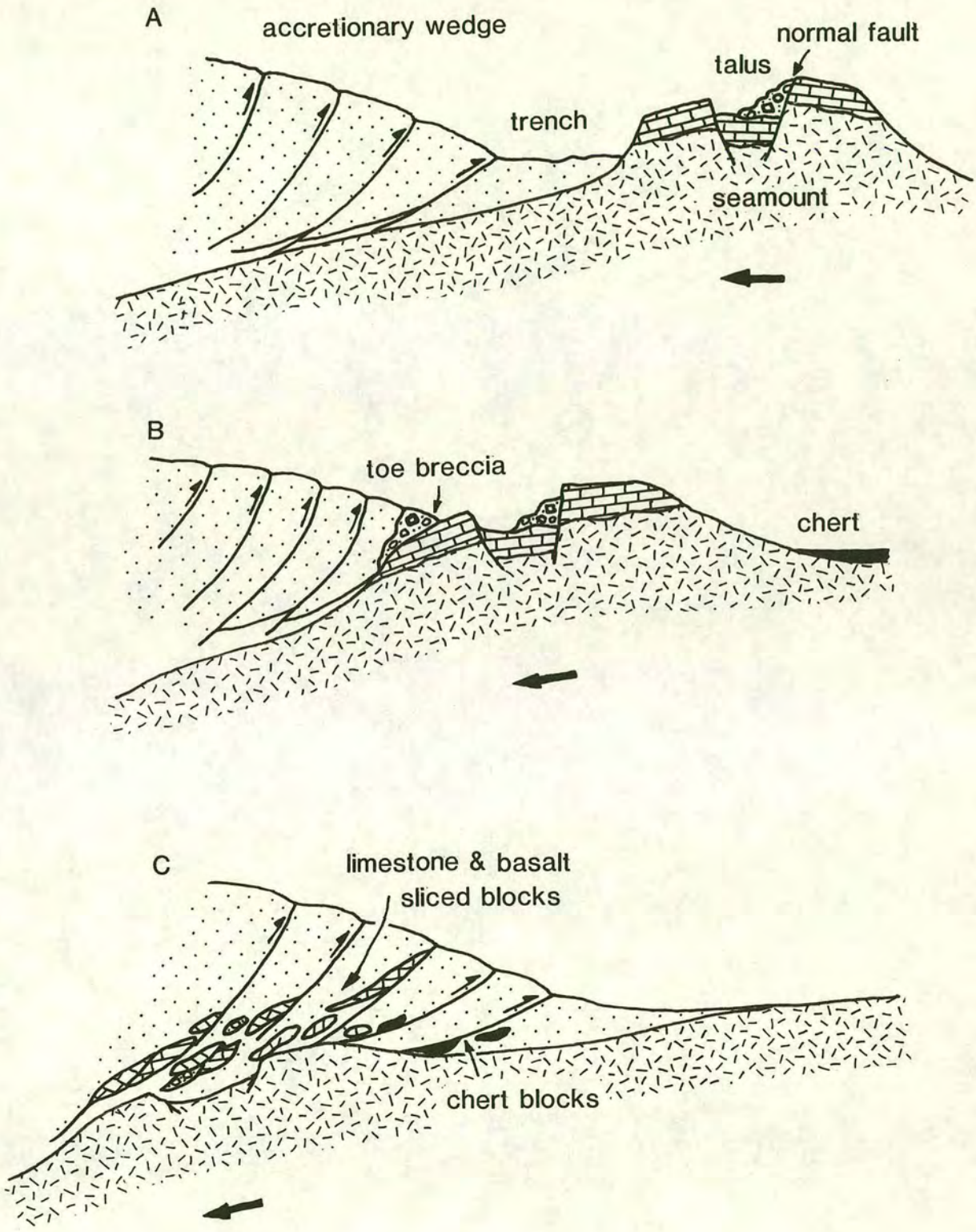

Figure 2.39 Model for the arrival of a seamount at a trench and its incorporation into an accretionary prism (after Taira *et al.*, 1989).

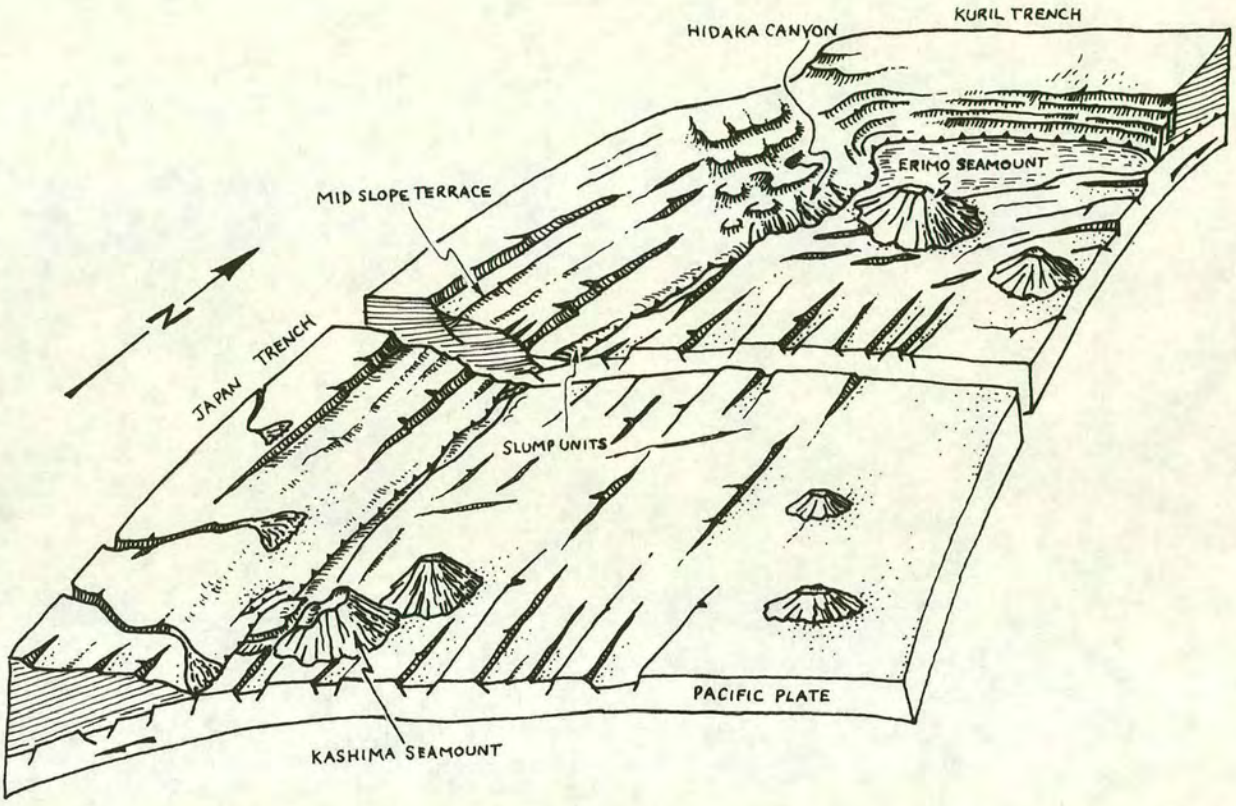

Figure 2.40 Idealized morphology of the Japan and Kuril Trenches based on Sunbeam mapping, seismic profiling and submersible dives (after Cadet *et al.*, 1987).

Modern seamounts have basal diameters up to 25km, although they are usually less than 10km across (Cas & Wright, 1987). Their heights range from hundreds of metres to several kilometres. Examples of seamount slivers within the on-land accretionary complexes of Japan range in size from 8km x 6km to 20km x 15km as illustrated by Taira *et al.* (1989). The Nilüfer Unit by comparison is distributed over much of NW Turkey and also further east (e.g. the Agvanis Massif; Okay *et al.,* 1984). The area studied in this thesis alone covers over 160km by 100km and displays scattered exposures of the Nilüfer Unit along its length and width. The Nilüfer Unit is thus most likely to represent several relatively small seamounts. This scenario could imply several individual edifices; the Bergama, Edremit, Bandirma and Bursa "seamounts".

2.18 Other examples of inferred seamounts

Inferred dismembered seamounts have been recognized in many ancient accretionary complexes. Some of the best known examples occur in Japan, where Palaeozoic-Mesozoic accretionary complexes preserve inferred seamount associations (e.g. Sano, 1988; Sano & Kanmera, 1988; Sano *et al.,* 1992). For example, the Okumino Group of the Mino terrane, SW Japan, comprises basalt, limestone and chert and has been interpreted as a Permian seamount complex, preserved with fragments of deep oceanic crust and cover (e.g. Sano, 1988; Jones *et al.,* 1993). The mélanges of the Franciscan Complex of California also contain abundant mafic rocks, interpreted as dismembered seamounts within an accretionary prism (e.g. near San Simeon; Davidsen & Cloos, 1985).

The Tethyan complexes of the Eastern Mediterranean region, especially from the Neotethys, also contain many examples of seamount-type associations. In central Greece, the Pagondas Complex below the Euboea ophiolite contains WPB lavas, deep-marine sedimentary rocks and detached coralline limestone blocks. This association was interpreted as a disrupted seamount within an accretionary complex by Robertson (1991). Similar associations are also present within the accretionary complexes below the Pindos and Vourinos ophiolites of northern Greece, and have been interpreted as ocean margin and/or fully oceanic seamounts (e.g. the Avdella Complex, Pindos; Jones & Robertson, 1991). The Late Triassic Oman Exotic limestones and underlying Haybi Volcanic Group, were interpreted as ocean island seamounts, based on basalt geochemistry (Searle *et al.,* 1980). The Mamonia Complex in Cyprus also includes elements interpreted as seamounts. The Triassic reefal limestone blocks within the complex are interpreted as carbonate build-ups on

oceanic islands (Clube & Robertson, 1986; Malpas *et al.*, 1987, 1992). Abundant blocks of basalt in the Ankara Mélange, central Turkey, also display within-plate geochemistries. Their association with deep-marine sediments has led Floyd (1993) to suggest formation adjacent to the flanks of a seamount, which subsequently became dismembered during subduction and accretion.

Older, possibly Palaeoethyan, seamounts have also been documented in the Eastern Mediterranean region. For example, in the central Pontides of northern Turkey, the Kargi Complex has been interpreted as a Permian seamount by Ustaömer (1993). He also interpreted blocks within the overlying Domuzdag-Saraycikdag Complex as seamount fragments within a Palaeotethayn accretionary complex.

CHAPTER 3

THE ORTAOBA AND KALABAK UNITS: ACCRETED TRENCH AND DEEP-SEA SEQUENCES

3.1 Introduction

Deformed sequences of clastic rocks are a common component of the Karakaya Complex in NW Turkey. These sequences are well exposed near Edremit, where a deformed clastic sequence stratigraphically overlies a basement of chert and pillow basalt. This association of lithologies occurs within fault-bounded slivers and is named as the Ortaoba Unit after a village in the Edremit region. Structurally above the Ortaoba Unit lies a thick phyllitic unit which contains rare marble blocks and beds and is here referred to as the Kalabak Unit. The contact between the two units is not sharp, but appears to be an imbricated zone which contains elements of both sequences. The Kalabak Unit is also exposed near Havran, where it is intruded by a granodiorite pluton (the Çamlik Metagranodiorite) and is overlain by Upper Triassic clastics of the Halilar Formation.

Phyllitic sequences, very similar to those of the Kalabak Unit, also occur near the town of Kinik in the Bergama region. On the basis of their constituent lithologies, metamorphic grade and position below Triassic sediments, the Kinik phyllites are here regarded as being equivalent to the Kalabak Unit.

In the field the sheared shales within the Ortaoba Unit are very similar to the phyllites of the Kalabak Unit. However, thin-section observations have shown the Kalabak phyllites to be considerably more metamorphosed than those of the Ortaoba Unit. For this reason, the two units are described and interpreted separately in this chapter. Work on the deformed clastic sequences of NW Turkey has focused largely on the Ortaoba Unit, owing to its well-preserved basalt-chert-sandstone sequences. The Kalabak Unit, by contrast, retains no coherent sedimentary sequences and yields little information regarding depositional environments or tectonic settings. In this chapter I describe the Ortaoba Unit and discuss possible settings for its formation, before briefly describing the Kalabak Unit and the pre-Upper Triassic granite which intrudes it.

3.2 Previous work

a) Ortaoba Unit

The Ortaoba Unit was recognized in the Edremit area by Bingöl *et al.*, (1973) who described sandstones and volcanics to the southeast of Kazdag. More recently, Okay *et al.* (1991) named this unit the Hodul Unit after a hill in the central Biga Peninsula area. However, their Hodul Unit is a much broader classification than the one adopted here as it also includes undeformed clastics of the Upper Triassic cover in the Havran region and limestone-rich debris flows near Balya. This is erroneous, as the Havran clastics unconformably overlie deformed sedimentary rocks of the Karakaya Complex and thus should be treated as a completely different rock unit. For this reason the name "Hodul Unit" is confusing and is therefore dropped. In this thesis the deformed sandstone sequences are regarded as part of the Ortaoba Unit (along with the underlying basalt and chert), and the relatively undeformed clastic cover is called the Halilar Formation.

b) Kalabak Unit

The Kalabak Unit was first described in detail by Krushensky *et al.* (1980) and named the Kalabak Metamorphic Series after the village of Kalabak in the Havran region. Okay *et al.* (1991) renamed the unit the Kalabak Formation and regarded it as of pre-Karakaya age owing to their misinterpretation of the Upper Triassic clastics near Havran as being part of the Karakaya Complex. As with the other tectonostratigraphic units of the Karakaya Complex, the Kalabak phyllites are described in this thesis as a unit rather than a formation. In the Bergama region, deformed, low-grade metamorphic sedimentary rocks were described as the Kinik Formation in published M.T.A. reports (Akyürek & Soysal, 1983). In this thesis these rocks have been assigned to the Kalabak Unit.

3.3 Lithologies of the Ortaoba Unit

The Ortaoba Unit, as defined in this thesis, crops out in both the Edremit and Bergama regions and is best preserved north of Edremit (Figures 3.1 and 3.2). In this region, a disrupted clastic sequence lies stratigraphically above a pillow lava basement, with an intervening bedded chert horizon. The clastic part of the sequence is dominated by interbedded quartzo-feldspathic sandstone and dark shale. Conglomerate horizons, interpreted as debris flows, form a minor part of the sequence. The main lithologies

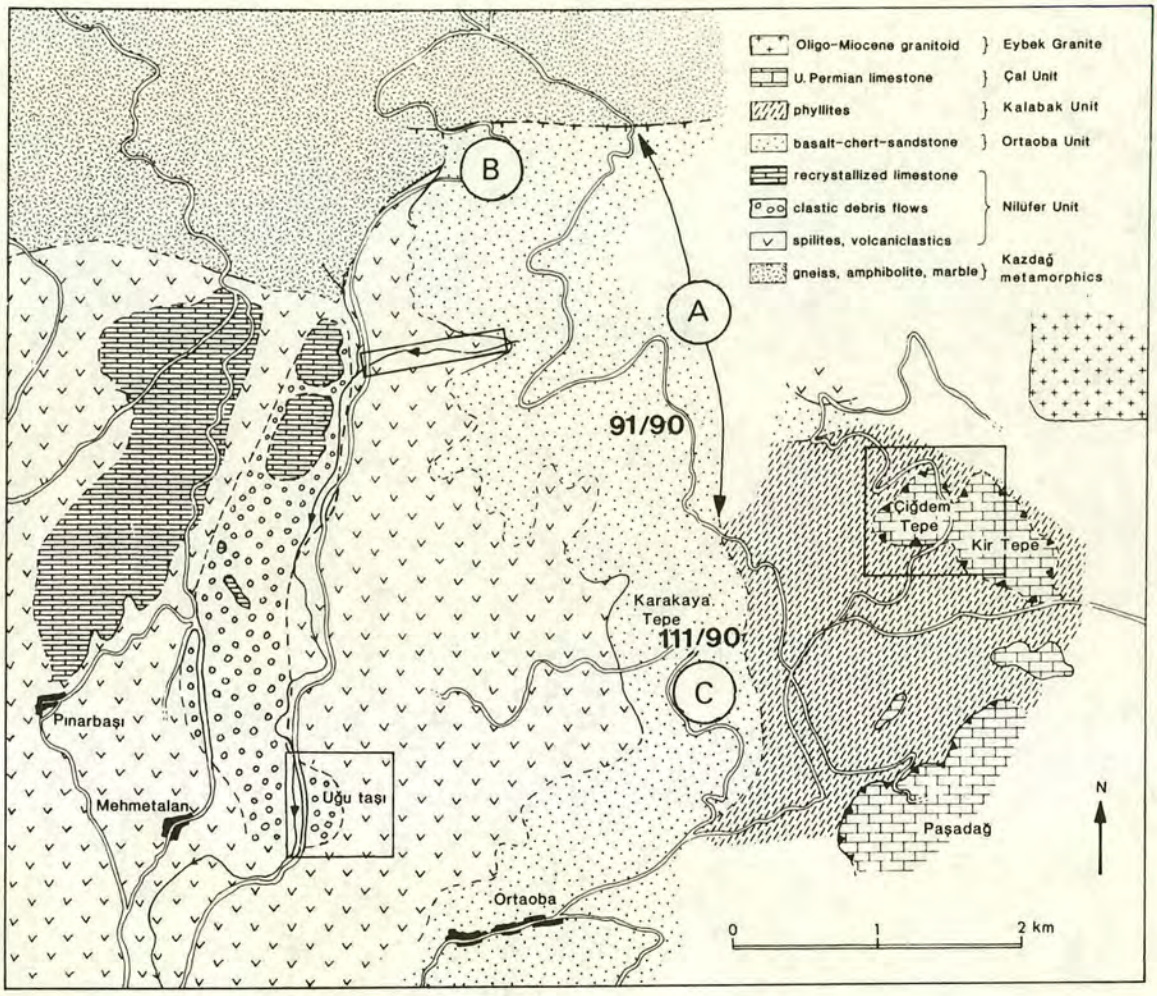

Figure 3.1 Geological map of the region north of Edremit (after an unpublished map by Okay and my own fieldwork). A, B and C represent the main study areas and are referred to in the text and later figures. Sites 91/90 and 111/90 display the best exposed sequences through the Ortaoba Unit and were the sites of more detailed studies.

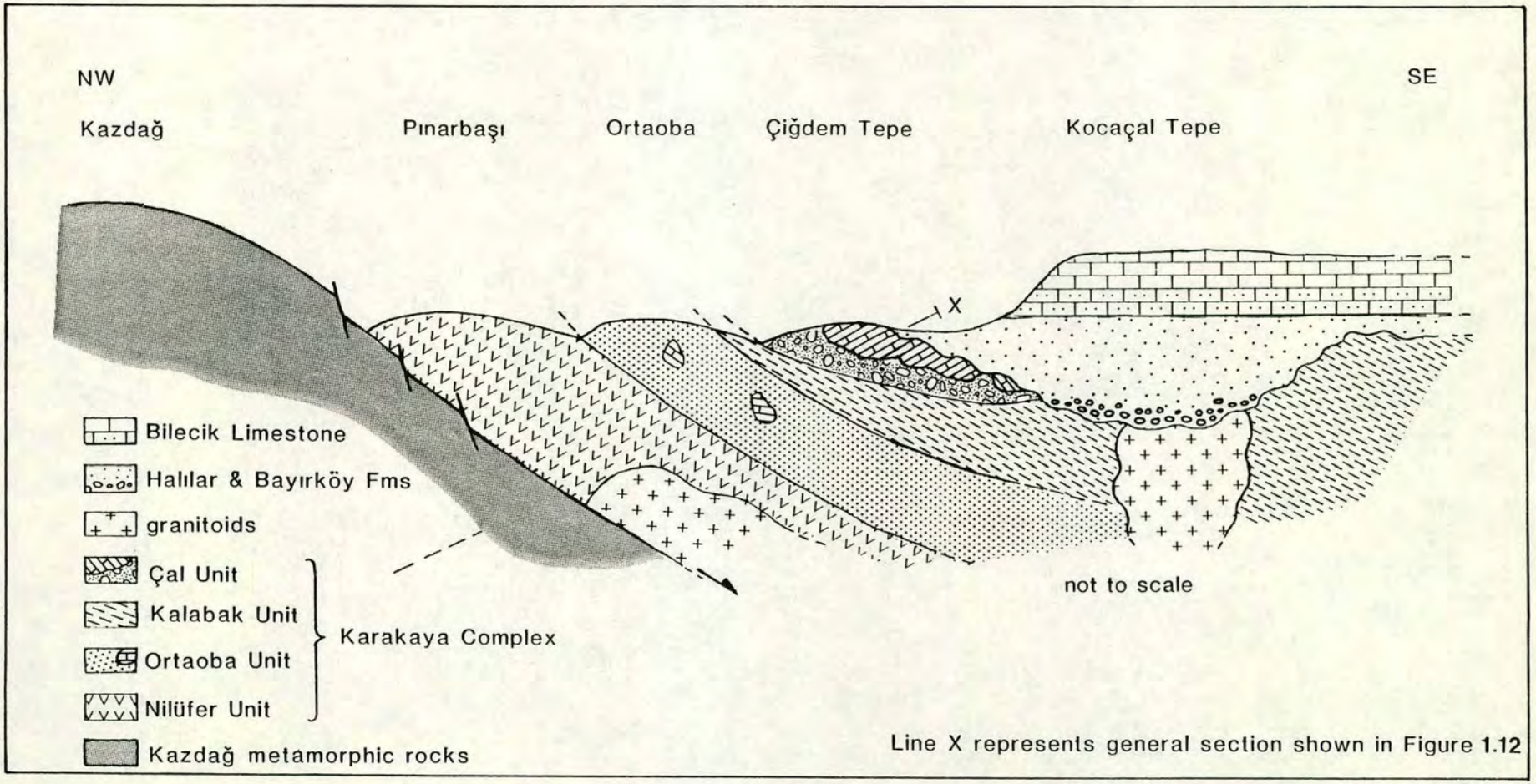

Figure 3.2 Schematic cross-section of the Edremit region, showing the position of the Ortaoba Unit in relation to the other Karakaya units.

which make up the Ortaoba Unit in both the Edremit and Bergama areas are described below.

3.3.1 Edremit area

The Ortaoba Unit crops out in a north-south trending belt, bounded to the west by the spilitic unit and to the east by the phyllites of the Kalabak Unit (Figure 3.1). Both boundaries are tectonic as evidenced by shearing and the imbrication of the unit with the adjacent units. The unit is particularly well exposed along the mountain road north of the village of Ortaoba and also the road which runs south of Karakaya Tepe. The exposures along both these roads display a deformed sandstone-shale sequence. Rare tectonic slices preserve the lower contact of the clastics with the underlying pillow lavas (Figure 3.3). Approximately 10m of bedded grey chert separates the clastics from the lava. Along the road which runs north from Ortaoba the basalt-chert-sandstone sequence is repeated at least three times as fault-bounded slivers.

a) Volcanics

Volcanic rocks are exposed along the road running north of Ortaoba and also along the road past Karakaya Tepe. Pillow lavas were observed at a few localities along the Ortaoba road (marked A on Figure 3.1) and in one locality along the Karakaya Tepe road (site C on Figure 3.1). These lavas display well-preserved elongate pillows ranging from 15cm by 5cm to 1-2m by 0.5m in size, surrounded by dark rims of devitrified glass (Figure 3.4a). The smaller "pillows" probably represent minor lobes "budding" off the larger ones. Inter-pillow material consists of hyaloclastite and breccias of broken pillow fragments and glassy material. Between some pillows small pockets of grey chert were observed. Silicification has produced a vitreous, almost translucent appearance in some pillows. Such pillows commonly contain pyrite cubes, disseminated throughout the basalt. Small infilled vesicles up to 0.5mm in diameter form a ring around the pillow perimeters while the central parts of the pillows are massive. By analogy with vesicles studied in the Coast Range Ophiolite, California (Hopson *et al.*, 1981), the vesicles in the Ortaoba pillow basalts indicate a deep water origin at typical mid-ocean ridge depths (i.e. 2-3km). The curvature of the pillows clearly indicates that they are the right way up, albeit slightly tilted. In thin-section a variety of igneous textures were observed (e.g. Figure 3.4b and 3.4c). The most common textures are intergranular, intersertal and subophitic textures comprising albitized plagioclase, brown devitrified glass and chloritized

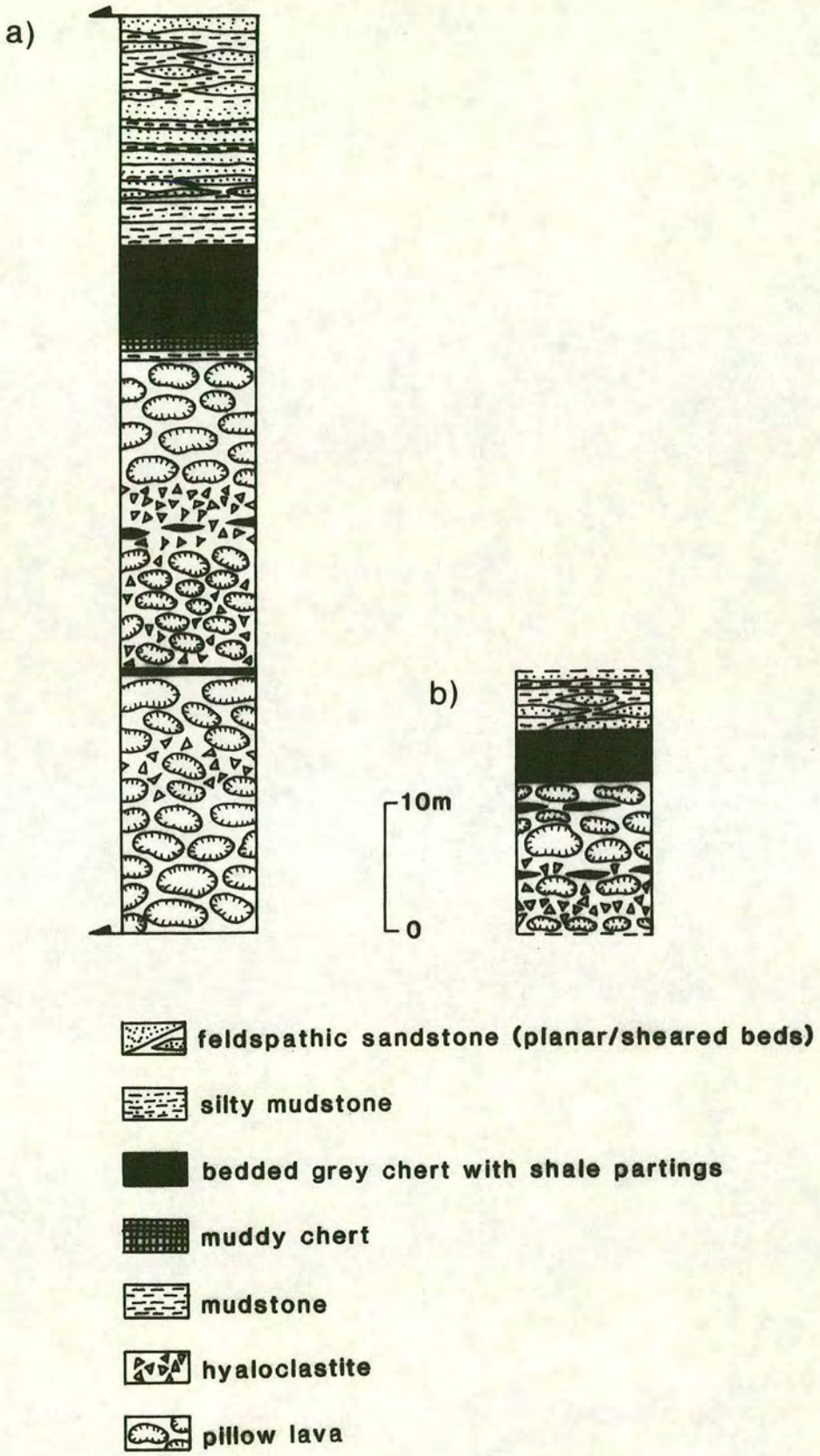

Figure 3.3 Logs through the lower levels of the Ortaoba Unit, showing the stratigraphic succession from pillow basalt to chert to turbiditic sandstones and shales at (a) site 91/90 and (b) site 111/90 (sites are marked on map in Figure 3.1).

Figure 3.4

(a) Pillow basalts at the base of the logged sequence at site 91/90. The pillows are clearly defined by their glassy rims and young towards the top left of the picture.

(b) Intersertal and subophitic textures in Ortaoba pillow basalt. Albitized laths of plagioclase are enclosed in a groundmass of chloritized clinopyroxene and dark devitrified glass (sample 22/10/91-3 from site 91/90, PPL, field of view: 2mm).

(c) Glassy quench textures in pillow basalt. The glass is devitrified and predominantly altered to chlorite (sample 91e/90 from site 91/90, PPL, field of view: 5mm).

a

b

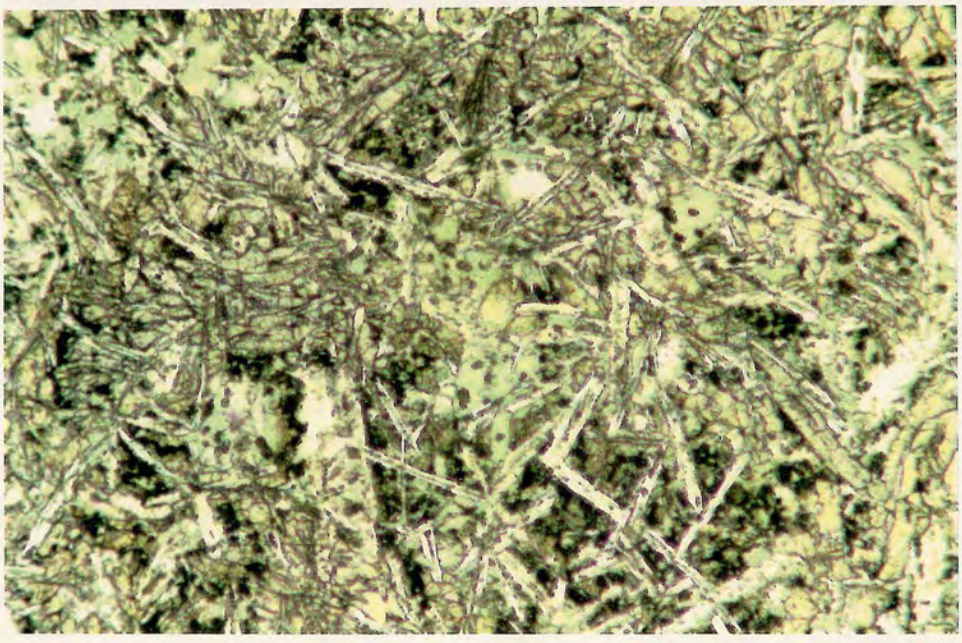

c

clinopyroxene. The fine-grained material from pillow margins displays textures indicative of rapid cooling.

Along the road beyond Ortaoba, the basalt lying immediately below the chert interval is stained dark red and orange, probably as a result of sulphide mineralization (Figure 3.5a). It is brittle and crumbly and has a strong sulphurous smell when struck with a hammer. Near Karakaya Tepe the basalt is less altered, indicating that the mineralization is localized. Elsewhere along the road north of Ortaoba the lavas are unpillowed, massive and dark green. These outcrops are shear-bounded and have no primary contacts with the bedded chert as described above. Hyaloclastite is common within these outcrops and is usually associated with secondary calcite veining and calcite rinds on small basalt fragments. Many of these outcrops have been silicified to some degree and have a semi-vitreous appearance. It appears, therefore, that most of the basalt of the Ortaoba Unit is massive and unpillowed, with pillows only appearing near the top of the pile, immediately beneath the sedimentary cover. Ballard *et al.* (1979) considered unpillowed sheet flows to be analogous to modern subaerial unchannelled pahoehoe flows erupted at high discharge rates, and pillow basalts to be analogous to tube-fed pahoehoe lavas erupted at much lower discharge rates. Thus, the transition from massive flows to pillows in the Ortaoba Unit could reflect a decrease in extrusion rate.

b) Chert

The chert overlying the pillow lava is medium-bedded and green-grey to dark grey in colour. Grey chert forms the bulk of the chert horizons north of Edremit and excellent exposures are found at sites 91/90 and 111/90 (sites marked on the map in Figure 3.1). Figure 3.5a and 3.5b show the chert intervals at sites 91/90 and 111/90 respectively. It forms well bedded horizons between 5 and 10m thick. The chert beds are generally semi-continuous to continuous on an outcrop scale, but lensing out is common. The individual beds are 4-20cm thick and intercalated with mudstone. The mudstone is of two main types which are black and light buff, respectively. The light buff mudstone is more common near the base of the chert horizon. Near the top of the chert interval the interbeds contain increasing amounts of small clastic grains, heralding arrival of the coarser grained input, which forms the thick clastic sequence above. In hand specimen, the chert has a dark homogeneous appearance and breaks easily into sharp fragments along planar fractures. The chert weathers to a buff grey, or reddish orange. In thin-section, the chert consists entirely of microcrystalline and cryptocrystalline quartz, with scattered quartz grains. A few highly recrystallized

Figure 3.5

(a) Field photograph of logged section at site 91/90 (looking NNE). The basalt (on the right of the picture) forms the top of the pillow basalt pile and is stained red, probably as a result of sulphide mineralization. The hammer marks a horizon of metalliferous, muddy chert directly overlying the basalt, which passes up into the grey chert visible on the left of the picture.

(b) Bedded chert at site 111/90 (as logged in Figure 3.3b). The sequence youngs to the left of the picture (west).

(c) Thin-bedded cherty sandstone and shale sequence, 2km north of site 91/90 (looking E). Note the listric normal fault dipping south directly above the hammer.

a

b

c

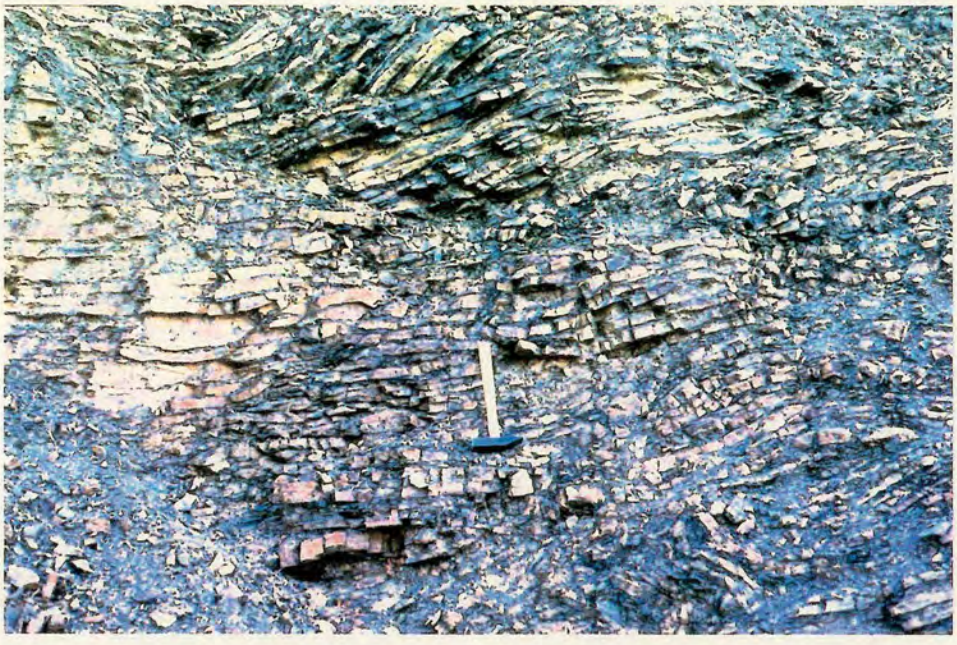

relics of radiolarian tests were observed in one specimen but were too recrystallized to extract and identify. Laminations on a millimetre-scale in some chert beds are defined by slight concentrations of mica, chlorite and clays.

Slivers of bedded chert can be observed elsewhere in the Edremit region, but they are invariably shear-bounded and have no primary contacts. These chert slivers, like the more intact sequences described above, consist of thin- to medium-bedded grey chert intercalated with black mudstone. The light buff intercalations were only observed within the chert sequence on the Ortaoba road.

Thin layers of metalliferous, muddy chert occur between the basalt and bedded grey chert which crop out north of Edremit (Figure 3.5a). The chert has a weak fissility and is dark orange-brown. The mudstone which occurs as thin partings between the chert beds is also slightly siliceous, as indicated by its hardness and brittle fracture.

c) Clastic sequence

The lowermost clastics are fine- to medium-grained and, at the very base of the sequence, slightly cherty (Figure 3.5c). Up sequence, the clastics become coarser and thicker-bedded with the appearance of discontinuous, massive sandstones and conglomeratic horizons. The sandstones are interbedded with shales which pass from being black and light buff in the chert sequence to being dark grey throughout most of the sandstone sequence. A representative section through interbedded sandstones and shales is shown in Figure 3.6.

Rare conglomerate horizons, interpreted as debris flows, are present within the Ortaoba Unit north of Pasadag. These horizons are very similar to the inferred debris flows whic occur tectonically within the Nilüfer Unit. One conglomerate along the road running north from the village of Ortaoba is rich in dark grey limestone clasts up to 30cm in size (Figure 3.7). Also present are clasts of coarse-grained quartzitic sandstone up to 30cm, beige mudstone, grey quartz and white feldspar. The sandy matrix contains dark wispy seams of mudstone parallel to bedding. Further north along the same road a thick conglomerate horizon can again be observed. Clast lithologies include mudstone, opaque white quartz, translucent grey quartz, green mudstone, fine-grained to coarse-grained sandstone and dark grey micritic limestone. The clast-types common to both conglomerates are therefore dark grey limestone, mudstone, sandstone and quartz.

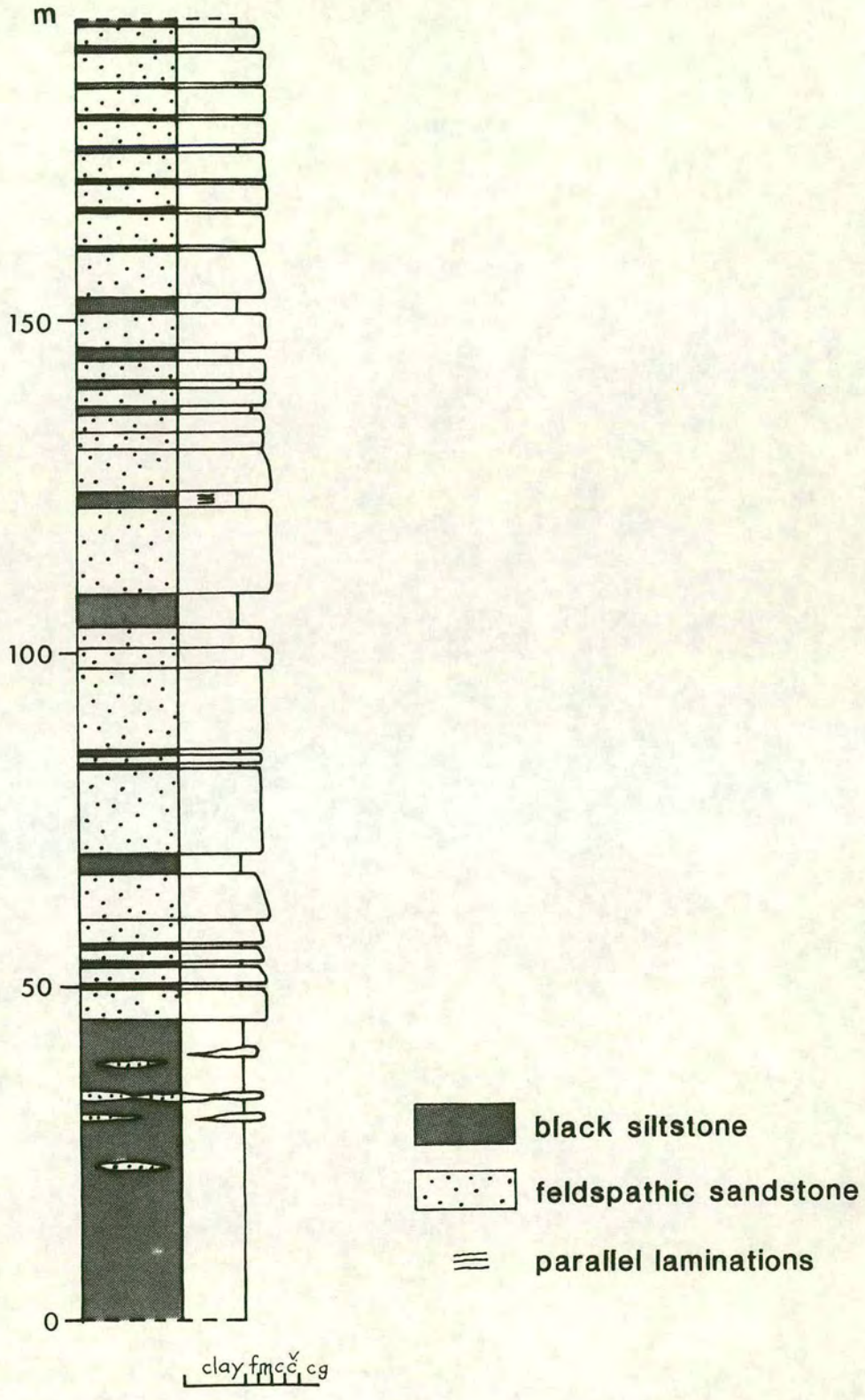

Figure 3.6 Representative log through the interbedded sandstones and shales of the Ortaoba Unit, 1.5km north of site 91/90.

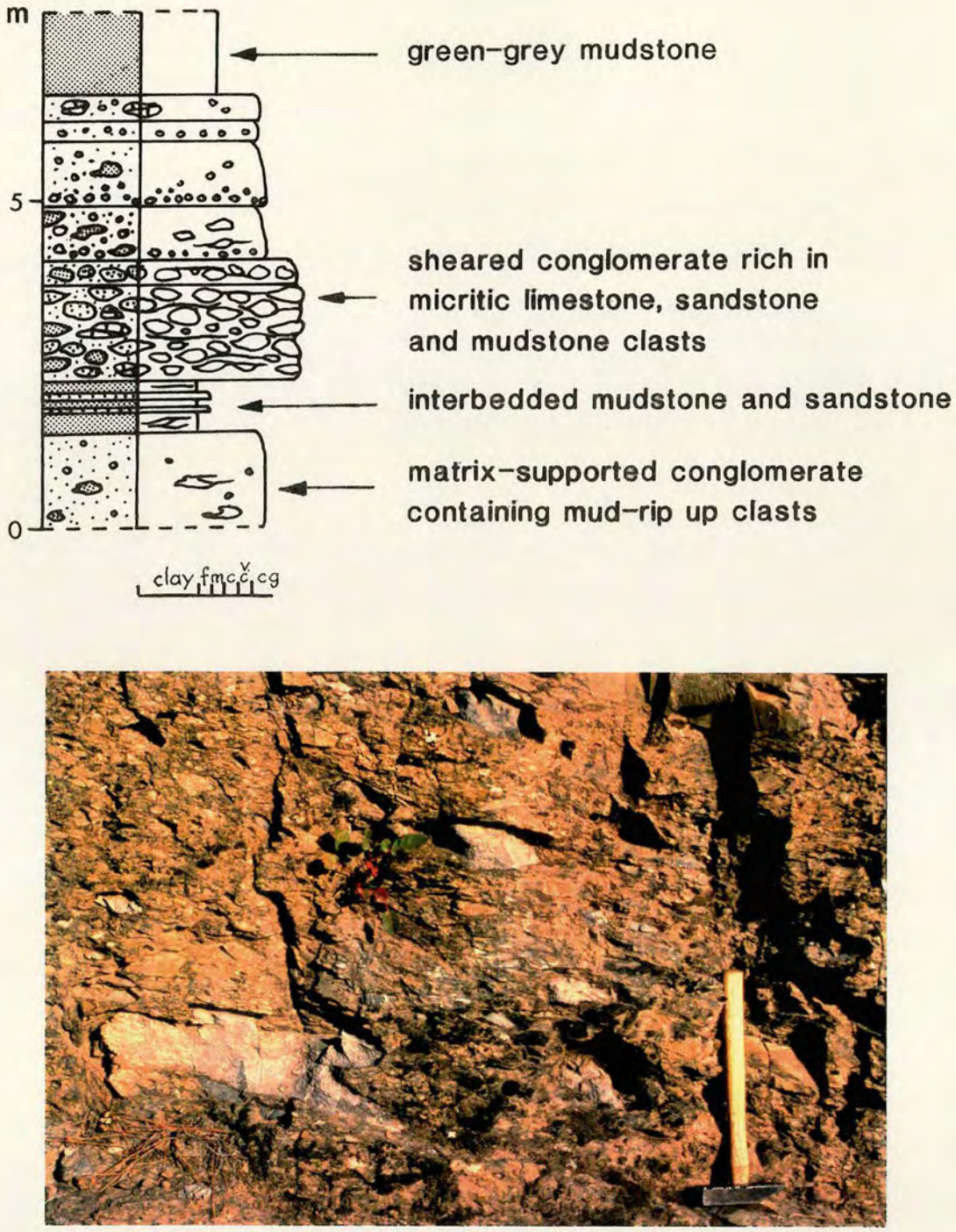

Figure 3.7 Log of a limestone-rich conglomeratic horizon, interpreted as a debris flow, north of site 91/90. The central part of the logged section displays sheared limestone, mudstone and sandstone clasts and is shown in the photograph.

Sandstone is the predominant lithology of the Ortaoba Unit in the Edremit region and is invariably interbedded with black shale. It forms a highly disrupted sequence above the lava and chert described in the previous sections. The original thickness of the sandstone preserved in this region is estimated at several hundred metres. The sandstone in the lower levels of the sequence (i.e. directly overlying the chert interval) is cherty, medium-grained and thin- to medium-bedded. Up sequence the sandstone becomes thicker bedded and generally coarser grained. The sandstone consists of quartz, plagioclase, alkali feldspar (including perthite and microcline) and abundant dark grey microcrystalline clasts (Figure 3.8a). The quartz grains display a range of recrystallization textures from straight extinction to polycrystalline textures, although those with straight extinction are rare.

Some of the grey microcrystalline clasts display faint relict phenocrysts and are thus interpreted as devitrified volcanics. However, many of the clasts have no igneous textures and are very similar to the recrystallized chert from lower in the sequence. Several of these grains in sample 76b/90 were qualitatively analyzed by electron microprobe and were found to comprise both quartz and albite. On the basis of the analyses and the relict igneous textures present in other clasts, the majority of the grains are interpreted as devitrified acidic volcanics. A small proportion of the microcrystalline clasts may, however, comprise recrystallized chert. Grey microcrystalline clasts very similar to those described above have also been observed in the sandstones in the Küre Complex, northern Turkey (Ustaömer & Robertson, 1994). These clasts were also interpreted as being predominantly devitrified acidic volcanics.

Minor amounts of white mica, clays, opaque oxides and sericite are also present around the clasts and within the fine-grained quartzose matrix. The clasts are flattened and recrystallized and commonly have fused contacts. A well-preserved basaltic clast with albitized plagioclase laths in a dark matrix was observed in one sample (46a/91). Rare schist, rutile and deformed sandstone clasts are also present.

Sedimentary structures within the sandstones are rare, having largely been obliterated by deformation and recrystallization. However, flame structures, normal grading and wispy dark laminations were locally observed. The sandstones are particularly well-preserved on the road to Karakaya Tepe. There, channelized conglomeratic horizons grade up into coarse-grained feldspathic sandstone. Load structures were observed at

a

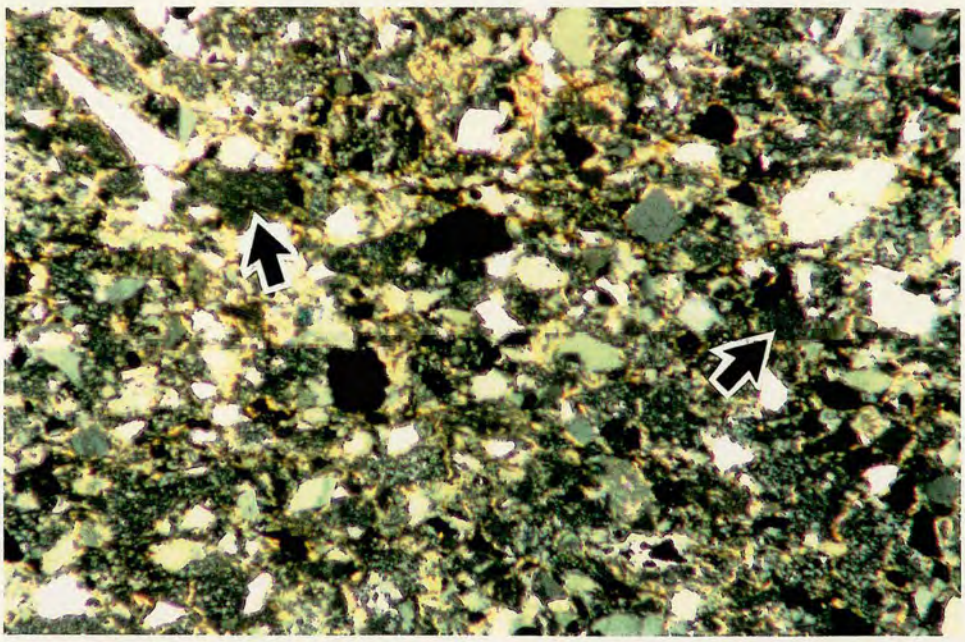

b

Figure 3.8

(a) Photomicrograph of a typical sandstone from the Ortaoba Unit, showing quartz and feldspar grains surrounded by sericite. The arrows point to the grey, microcrystalline grains which are abundant in the Ortaoba Unit and are interpreted as being predominantly devitrified volcanics (XPL, field of view: 12.5mm).

(b) Slump in sandstone and shale sequence south of Karakaya Tepe, in region marked C in Figure 3.1.

the base of the conglomerate. A well-preserved slump fold was also observed along this road, implying synsedimentary deformation on a slope (Figure 3.8b).

3.3.2 Bergama area

a) Volcanics

Rare outcrops of volcanics are present within the sandstones and phyllites in the Bergama region, east of Ayvalik (see location map; Figure 1.6). They comprise massive, dark green basalt which has no stratigraphic contacts with the surrounding sedimentary rocks. The lava is fragmental and brecciated in places and has a very similar appearance to the massive lavas which occur north of Ortaoba.

b) Chert

An isolated outcrop of thin-bedded chert was observed near Kinik. Although no contacts are exposed the chert is surrounded by sheared dark phyllites (the Kinik Formation of Akyürek & Soysal, 1983). The chert is pale green to pale pinkish in colour and highly recrystallized. This lithology may be the equivalent of the cherts near Edremit, while the dark phyllites may represent the Kalabak Unit). Thin-bedded black cherts were also observed which may, like the green chert, be equivalent to the cherts within the Ortaoba Unit near Edremit.

c) Clastic rocks

In the Kozak area, east of Ayvalik, an outcrop of coarse-grained to conglomeratic sandstones are exposed. They are highly recrystallized, probably as a result of the intrusion of the nearby Kozak pluton in Oligo-Miocene times. Thin-section study reveals the presence of abundant volcanic clasts. Many of the clasts are highly devitrified, but retain relict porphyritic and subophitic textures. The subophitic clasts are dark, whereas the porphyritic ones are almost clear in plane-polarized light. This may reflect the presence of both basic and acidic components. One of the volcanic clasts is cross-cut by veins which predate incorporation of the clasts into the conglomerate. Also observed were abundant metamorphic quartz clasts in various stages of recrystallization and a clast of fine-grained quartzose sandstone. The devitrified porphyritic clasts closely resemble the abundant dark grey, microcrystalline clasts which occur in the Ortaoba Unit near Edremit. They do, however, display much better-preserved igneous textures and have thus helped to confirm an igneous origin for many of the Edremit examples.

3.4. Sedimentary blocks within the Ortaoba unit

a) Limestone

Two main types of limestone are found as blocks within the clastics of the Ortaoba Unit in the Edremit area. These are:

i) dark grey limestone blocks up to 1m in size.
ii) white to light grey recrystallized limestone blocks up to 10m in size.

The dark grey limestone (i) is generally less sugary and more micritic than the white limestone. It tends to form relatively small clasts in debris flows within both the Ortaoba and Nilufer Units. Dark grey limestone blocks are common in debris flows and occur along with clasts of sandstone, mudstone, quartz and feldspar. They are generally small (maximum size of 1m in this area) and rounded to lensoid in shape. The lenses are found in the more deformed outcrops and were clearly formed by flattening of clasts rather than by layer-parallel extension of limestone beds. Many of the less recrystallized limestone blocks are fossiliferous and Carboniferous-Upper Permian fossils have been reported by Okay *et al.* (1991). On the road north of Mehmetalan dark grey limestone blocks up to 1m in size lie within a feldspathic sandstone and shale sequence. One block is mantled by a coarse limestone breccia derived from the block itself. Further north along the same road is an outcrop of feldspathic sandstone which contains abundant dark grey limestone blocks up to 20cm across. The blocks are undeformed and rounded unlike those north of Ortaoba which are generally flattened and lensoid in shape.

The white limestone (ii) forms much larger blocks such as those which crop out on the road from Kadiköy to Ortaoba (see location map; Figure 1.7). The limestone is heavily stylolitized and although internal structures are rare, vestigial laminations were observed in a block on the road mentioned above. Faint blue-grey bands 2mm to 2cm apart give the limestone a banded appearance and in one place there is evidence of syn-sedimentary deformation. Despite the high degree of recrystallization, relict beds (0.5-2cm thick) with grey shaly partings can still be recognized in places. The limestone is heavily stylolitized.

b) Quartzite

A large quartzite block up to 10m in diameter lies within sheared shale just north of Ortaoba village. In the field the block has a highly crystalline, blue-grey appearance.

In thin-section the rock is entirely made of interlocking quartz grains which have the characteristic intergranular appearance of fully developed sub-grains. Although the contacts of the block with the surrounding shales are not well exposed there is no evidence of faulting.

3.5 Serpentinite slivers

On the road from Kadiköy to Ortaoba there is a large exposure (approximately 100m in length) of serpentinite in which the dominant foliation dips east. Large "fish structures" are common and appear to indicate normal shearing towards the south (Figure 3.9). The entire outcrop consists of polished serpentinite phacoids in a less coherent serpentinitic matrix. Weathered basalt and phyllites are found above and below the serpentinite. Further up the road a slice of weathered basalt 6m thick is bounded by two slices of serpentinite approximately 0.5m thick which contain duplex structures.

3.6 Structure

The Ortaoba Unit is disrupted by a dense network of shear zones and faults. Faulting has cut out most of the basal pillow basalts except for a few slivers which are preserved north of Ortaoba and along the road to Karakaya Tepe (sites 91/90 and 111/90 respectively). In one locality two of these slivers are tectonically juxtaposed indicating tectonic repetition. Each slice contains a sequence which passes up from basalt to chert to sandstone. The contact between the two is a shallow fault which dips shallowly to the SE and has slickensides which indicate normal slip movement.

A strong penetrative cleavage is developed parallel to bedding within the shales of the Ortaoba Unit. The more competent sandstone beds display a range of degrees of deformation. Locally sandstones are undeformed but more commonly display shearing and layer-parallel extension as shown in Figure 3.10. Depending on the degree of shear the sandstone beds are semi-continuous and display necking, or may have been fully extended to form a block-in-matrix fabric. In the latter case the "blocks" are actually lenses within a shaly matrix which typically has a scaly foliation. Near Karakaya Tepe, debris flow horizons have been strongly sheared to produce the textures shown in Figure 3.10c. Some sandstone beds have been brittly deformed and are cut by faults. South-dipping normal faults such as that shown in Figure 3.11 occur along the road section marked A in Figure 3.1. The cherts are less deformed than the

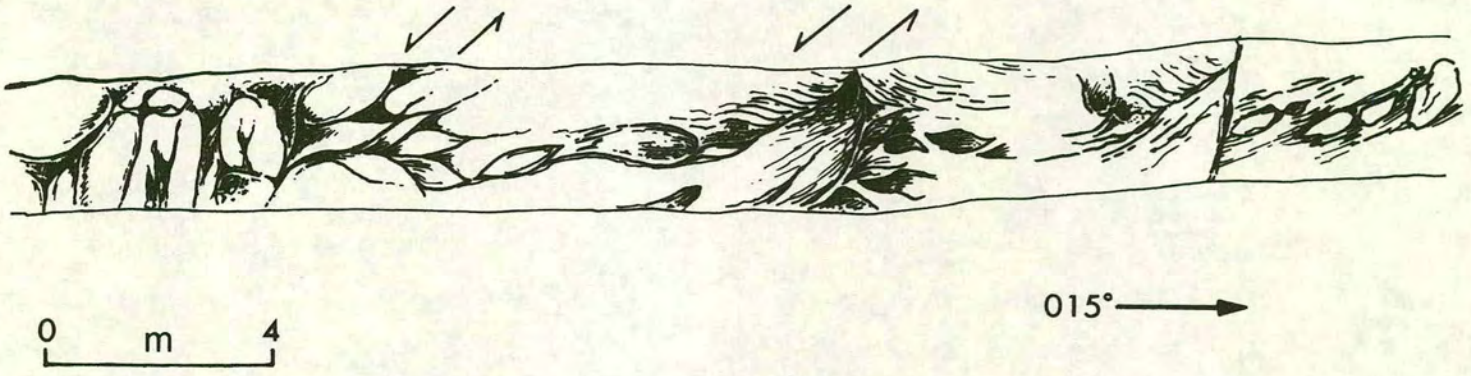

Figure 3.9 Field sketch showing the internal structures of a serpentinite slice along the road between Kadiköy and Ortaoba. Shear zones and phacoids suggest normal motion to the south.

Figure 3.10 Field photographs of typical structures observed in the Ortaoba Unit in the Edremit region.

(a) Shearing and boudinage within medium- to thick-bedded sandstones along road section marked A in Figure 3.1. The thick sandstone bed on the right of the picture displays attenuation and boudinage with quartz-filled extensional fractures perpendicular to the direction of extension.

(b) Layer-parallel extension in region marked B in Figure 3.1. The sandstone lenses are enclosed within a sheared, shaly matrix and probably represent originally continuous beds in an interbedded sandstone-shale sequence.

(c) Small-scale shearing and layer-parallel extension near Karakaya Tepe. In this case the sandstone lenses may record deformation of the clasts within a debris flow rather than continuous beds.

a

b

c

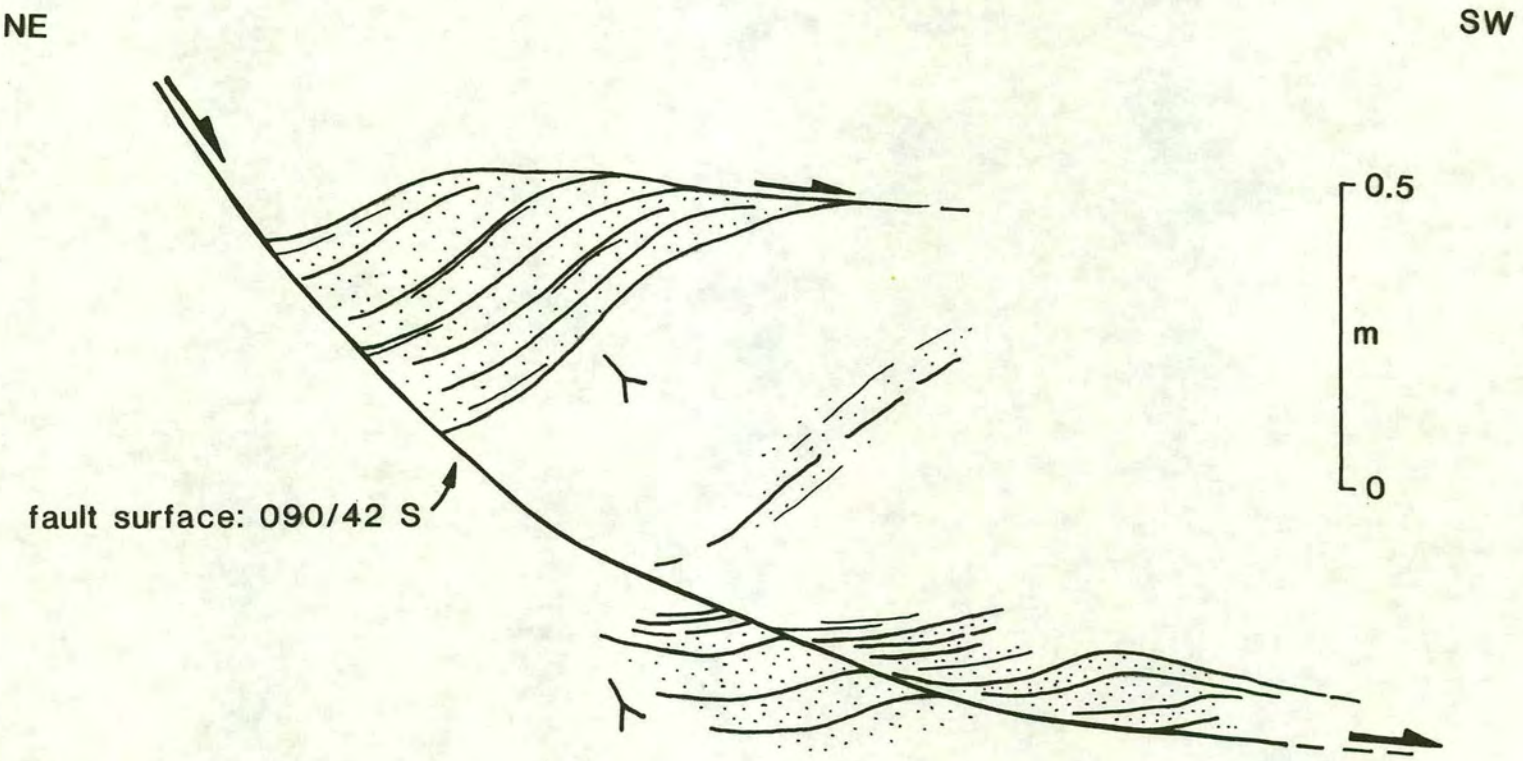

Figure 3.11 Sketch of a listric, south-dipping normal fault in sandstones and shales at the locality in Figure 3.5c.

sandstone-dominated part of the sequence although they do display some degree of layer-parallel extension especially in the upper levels. The layer-parallel extension is expressed as discontinuous layers and lenses of chert separated by thin partings of sheared mudstone. The basalt at the base of the sequence is undeformed and displays excellently preserved pillow shapes.

Within the clastic part of the Ortaoba Unit zones of intense disruption can be observed. They occur every few metres in some places and separate more coherent sections up to 100m thick. The sandstones of the Ortaoba Unit are folded on a scale of metres and display a wide range of fold types. Chevron folds and more rounded open folds are both common. Vergence directions of asymmetrical folds are difficult to determine as sedimentary way-up criteria such as grading are very rarely preserved. Fold data from the sandstones north of Ortaoba are shown in Figure 3.12. Axial planes predominantly dip E and SE and fold axes plunge in all directions, particularly SE and NE. Where grading is discernible it implies that the folds face north to the NW, indicating general northward tectonic transport.

3.6.1 Microstructure

In thin-section the sandstones of this unit display intense recrystallization and suturing of grain boundaries. Grains are commonly elongate and orientated with their long axes parallel to cleavage. The quartz grains invariably display highly developed undulose extinction and, in many cases, sub-grain formation. Feldspar grains are also highly strained as indicated by the deformed multiple twinning in plagioclase clasts. Mica, sericite and clay minerals are aligned along the cleavage and drape around the diffuse clast boundaries. The photomicrograph of a typical sandstone from the Ortaoba Unit in Figure 3.8a shows the diffuse boundaries of many clasts and interstitial sericite. The original matrix to the clasts is not apparent owing to the intense recrystallization and suturing of grain contacts. All these factors indicate that the sandstones underwent a high degree of small-scale penetrative deformation.

3.7 Geochemistry of the Ortaoba Unit

3.7.1 Basalt geochemistry

A suite of basalt samples was collected for geochemical analysis. The samples were collected from massive flows and pillow lavas in the Edremit region, along the roads

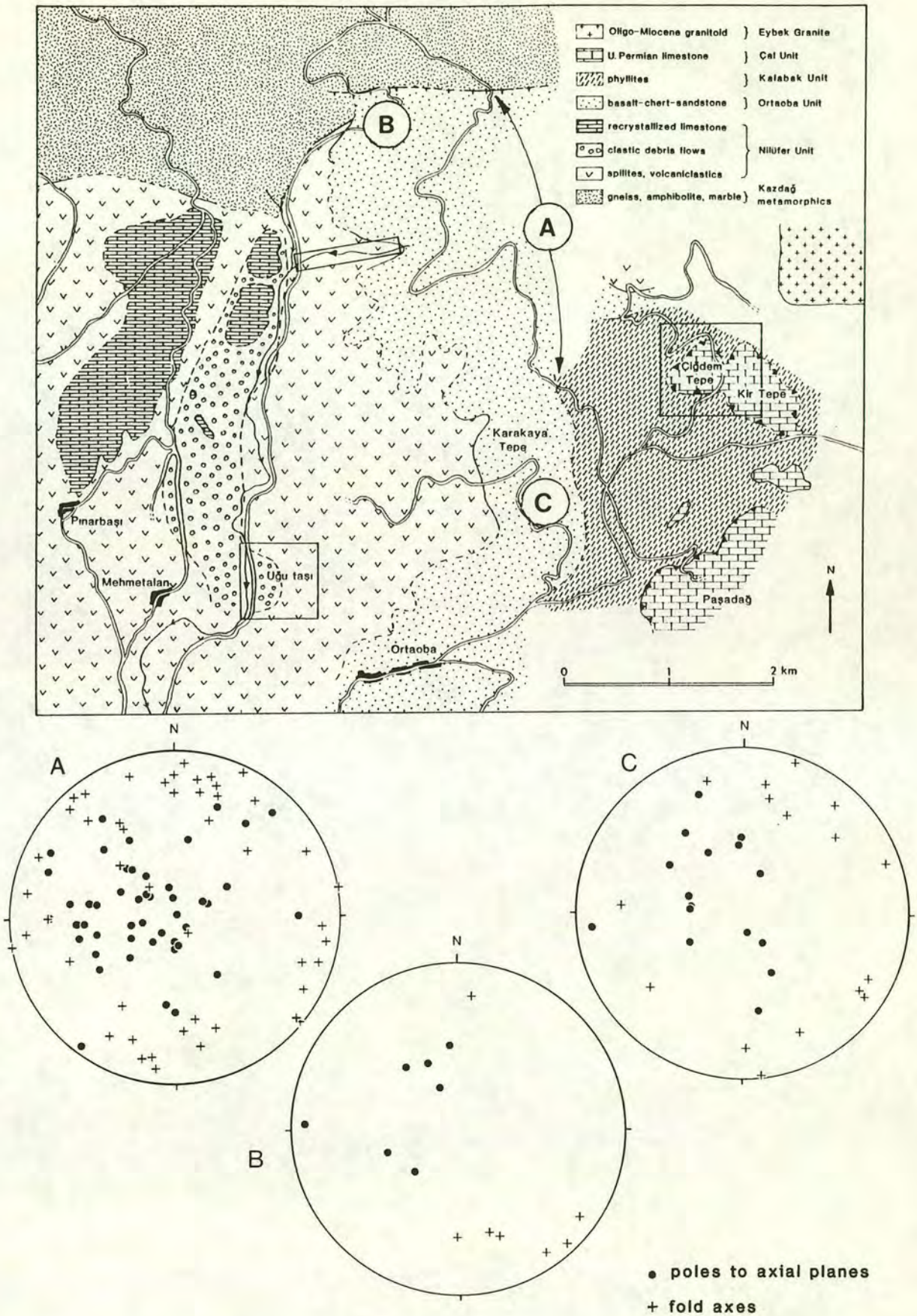

Figure 3.12 Stereoplots of fold data from the Ortaoba Unit in the Edremit region. The labels on the plots refer to the sites marked on the map.

running north of Ortaoba and to Karakaya Tepe. The results were plotted on discrimination diagrams and MORB-normalized plots. The Zr/Y-Ti/Y plot implies that the basalts are from a plate margin, rather than within-plate setting (Figure 3.13a) and the P_2O_5-Zr plot indicates a tholeiitic character (Figure 3.13b). The Zr/Y-Zr and Ti-Zr diagrams provide further discrimination and show the basalts to be dominantly of MORB type (Figure 3.14). The basalts follow a fractionation trend in the Ti-Zr diagram and are reasonably well-confined to the MORB field. The Ti/Y-Nb/Y plot (Figure 3.15a) confirms the predominantly tholeiitic nature of the Ortaoba basalts and implies either a volcanic arc or mid-ocean ridge setting. The Cr-Y diagram indicates a within-plate or mid-ocean ridge setting (Figure 3.15b).

The relatively flat patterns of the MORB-normalized plots also indicate a MORB origin (e.g. Figures 3.16a and 3.17a). The large ion lithophile (LIL) values are very variable and probably do not reflect the original composition of the rock. The Th enrichment in many of the samples, however, may be original and indicates that the rocks were probably slightly LIL enriched. The high field strength (HFS) elements are close to the MORB line, although slight variations occur in the Nb and Ce values. In Figures 3.16a and 3.17a the HFS elements exhibit a flat pattern with slight depletion in Nb relative to the other HFS elements and MORB. By contrast, two traces in Figures 3.16b and all the traces in 3.17b, display enrichment of Nb relative to the other HFS elements and MORB.

The patterns in Figures 3.16b and 3.17b show a variation of patterns which probably reflect the fact that they were taken from tectonic basalt slivers within the Ortaoba sequence, rather than from basalts which were observed to be stratigraphically within the sequence. The traces of samples 22/10/91-1 and 22/10/91-2 in Figure 3.16b display a significant Nb trough relative to Ce and considerable LIL enrichment. Zr, Ti, Y and Sc are depleted relative to MORB. Samples 22/10/91-3 and 22/10/91-4 do not display a Nb depletion and show HFS values relatively close to MORB. Th and Sr are enriched relative to MORB and imply that the strong depletions in K and Rb are secondary features. Samples 18/10/91-15a, 18/10/91-15b, 18/10/91-16 and 124a/90 (Figure 3.17b) show a concave curved pattern from Nb to Sc and have a slightly "humped" pattern, characteristic of within-plate basalts.

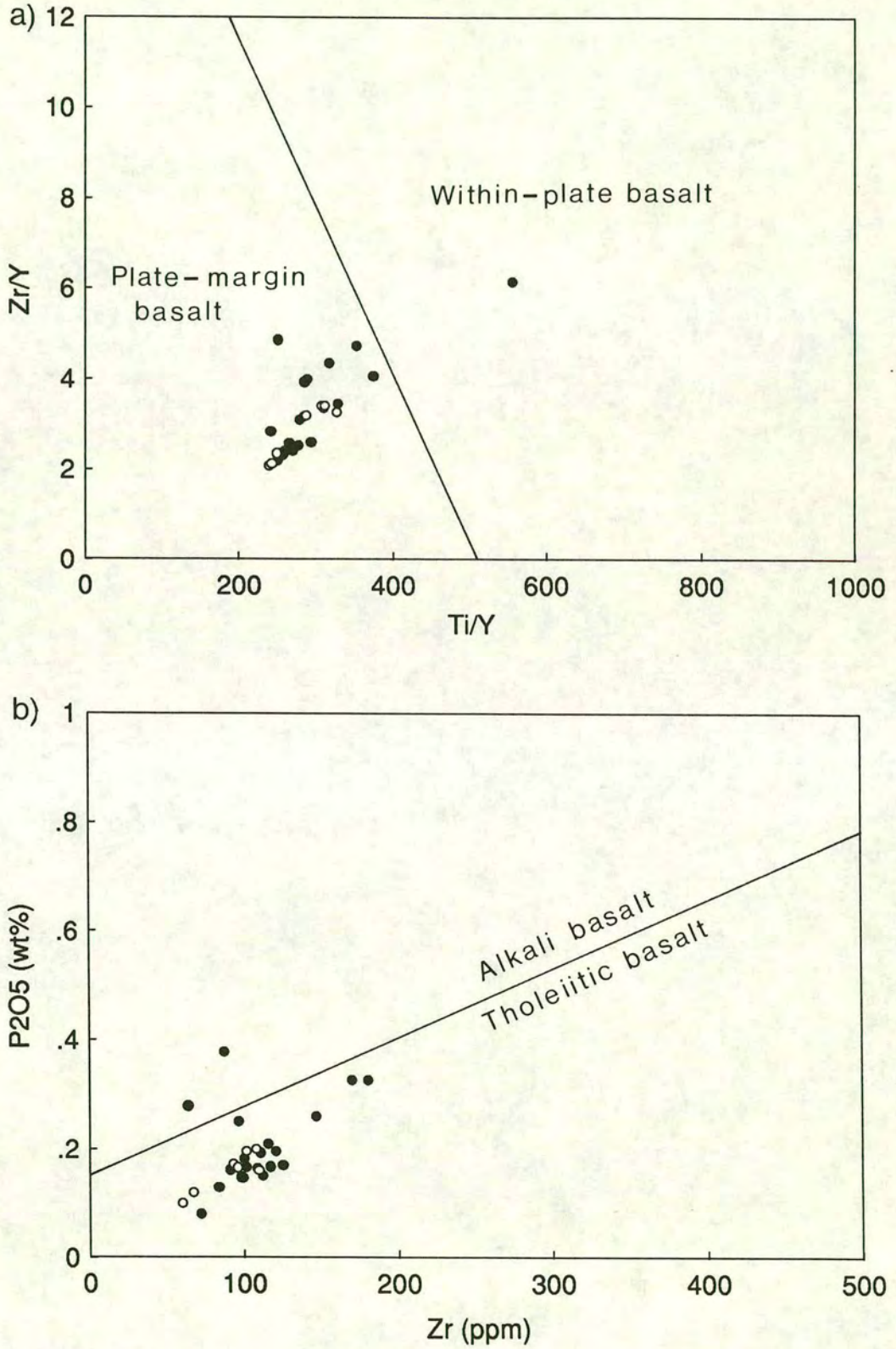

Figure 3.13 Tectonic discrimination diagrams for basalts of the Ortaoba Unit in the Edremit region. (a) Zr/Y-Ti/Y plot (fields from Pearce & Gale, 1977), (b) P_2O_5-Zr plot (fields from Winchester & Floyd, 1976). Samples are from areas A (solid circles) and C (open circles) as marked on Figures 3.1 and 3.12.

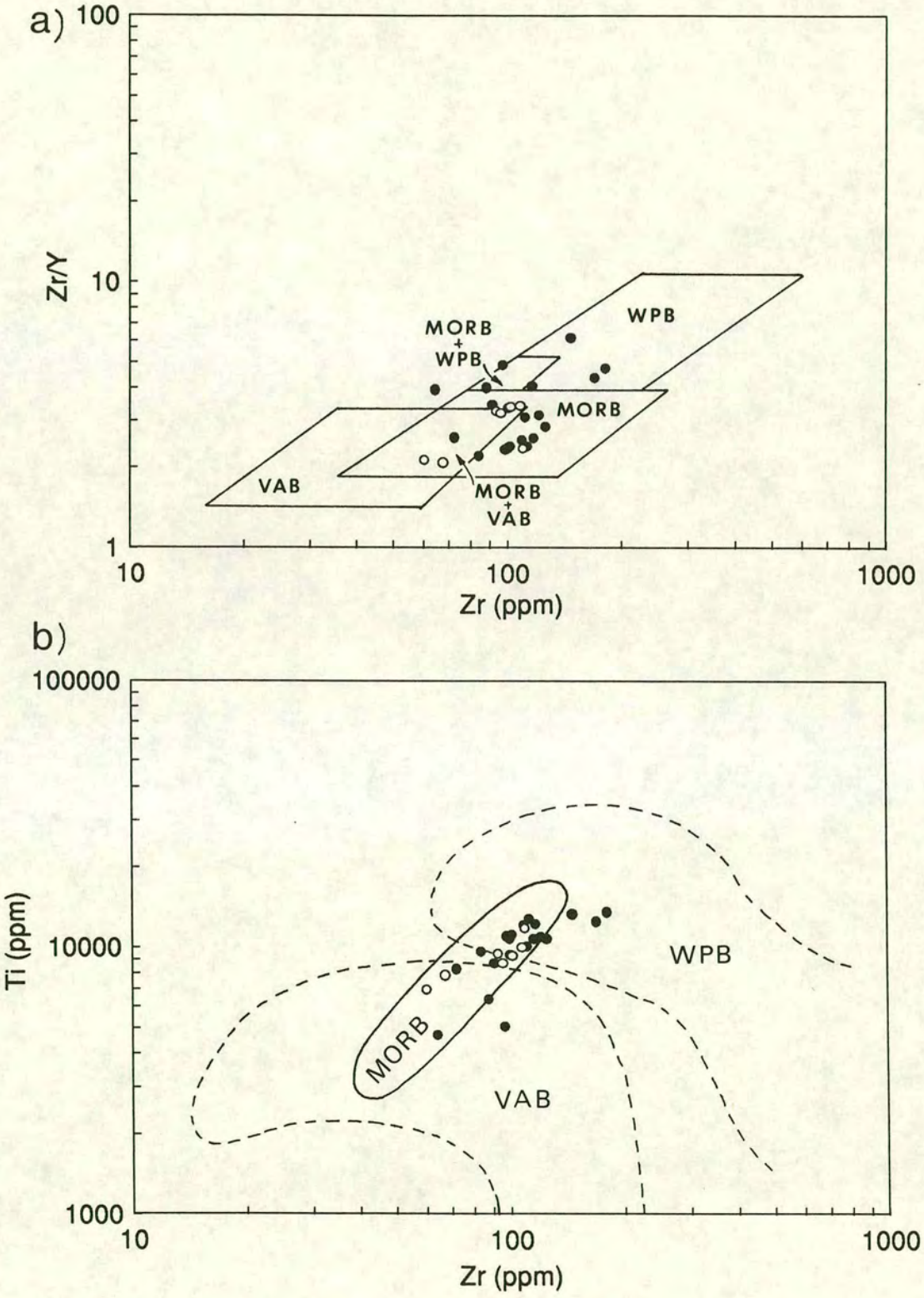

Figure 3.14 Tectonic discrimination diagrams for basalts of the Ortaoba Unit. (a) Zr/Y-Zr plot (fields from Pearce & Norry, 1979), (b) Ti-Zr plot (fields from Pearce, 1982). Samples are from areas A (solid circles) and C (open circles) as marked on Figures 3.1 and 3.12.
(MORB: mid-ocean ridge basalt, WPB: within-plate basalt, VAB: volcanic-arc basalt)

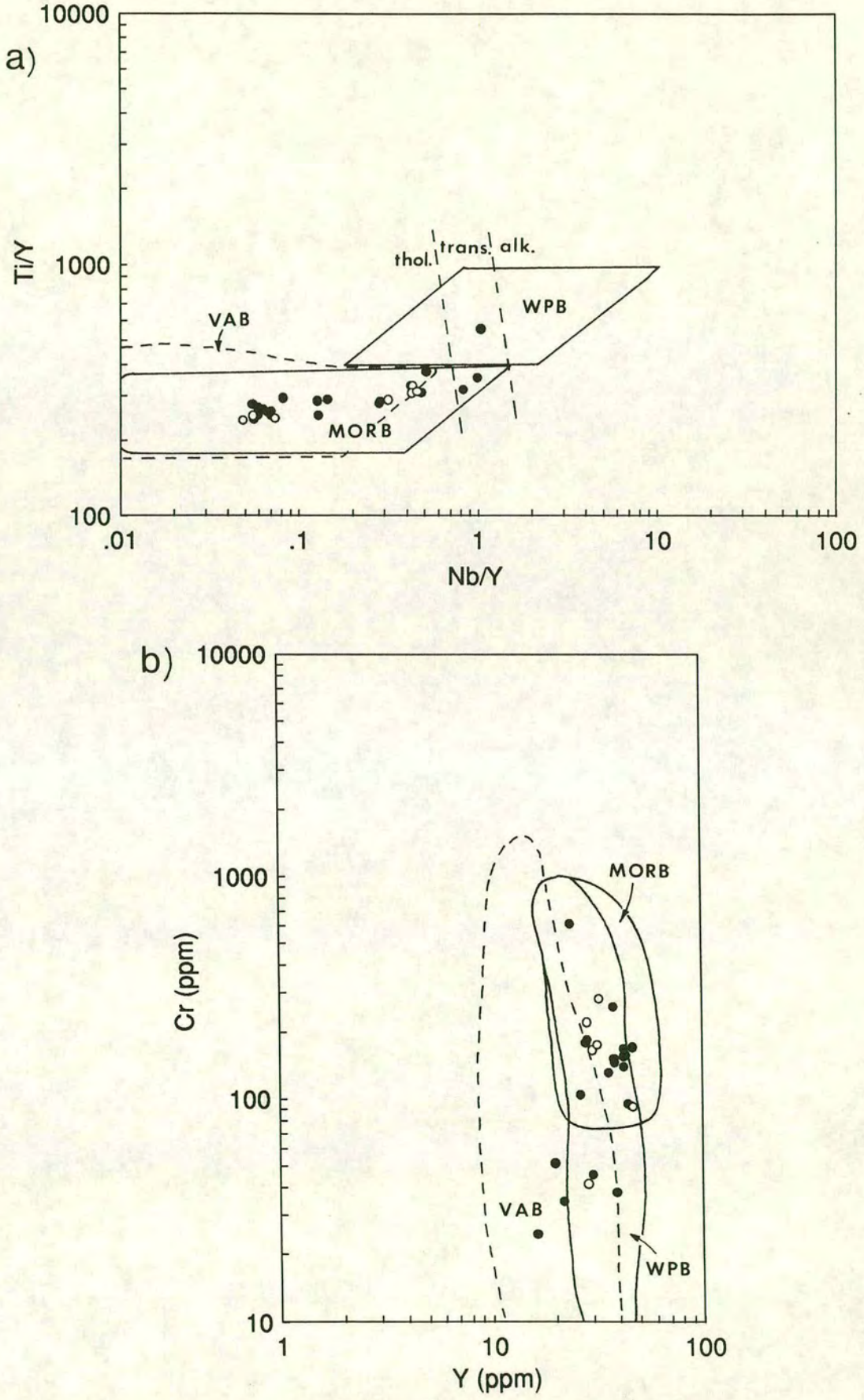

Figure 3.15 Tectonic discrimination diagrams for basalts of the Ortaoba Unit. (a) Ti/Y-Nb/Y plot (fields from Pearce 1982), (b) Cr-Y plot (fields from Pearce, 1982). Samples are from areas A (solid circles) and C (open circles) as marked on Figures 3.1 and 3.12.

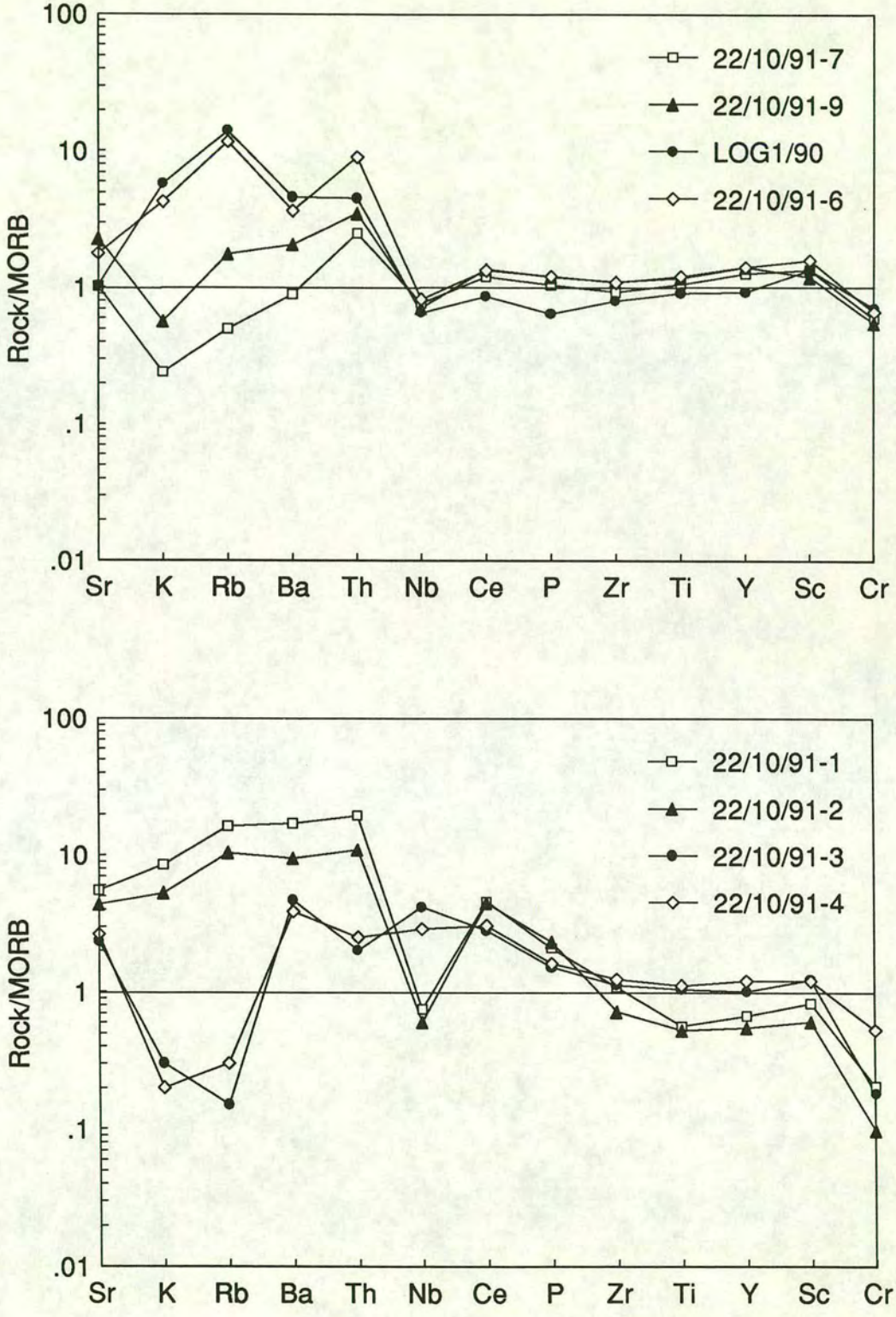

Figure 3.16 MORB-normalized multi-element plots for basalts from the road section A, north of Karakaya Tepe. Normalizing values from Pearce (1982 & 1983) (Appendix **4**).

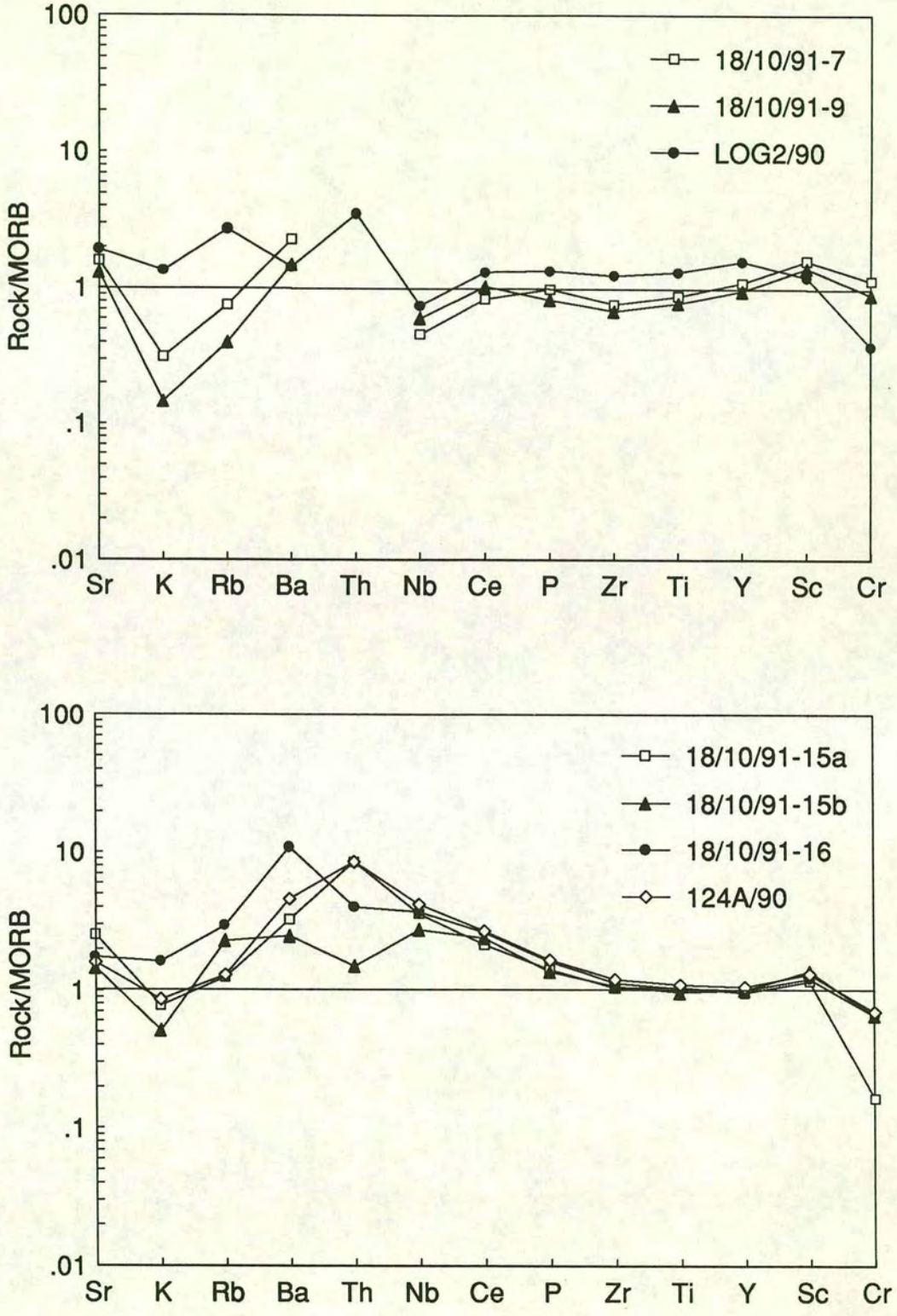

Figure 3.17 MORB-normalized multi-element plots for basalts from the road section C, south of Karakaya Tepe. Normalized as for Figure 3.16.

3.7.2 Microprobe analysis of clinopyroxenes

As outlined in more detail in Chapter 2, clinopyroxene geochemistry is a useful discriminant for basalts from different tectonic settings. Clinopyroxene crystals in four samples of pillow lava from the Ortaoba Unit in the Edremit area were analyzed by electron microprobe. The crystals chosen for analysis were mainly small phenocrysts, although owing to the fine-grained nature of the lavas several may in fact be groundmass material. Despite their dark brown and dusty appearance the clinopyroxenes are relatively fresh and when analyzed gave good totals between 99 and 101. Both cores and rims of larger phenocrysts were analyzed and plotted as circles (cores) and triangles (rims) on Figure 3.18. Many of the crystals, however, were too small to merit rim analyses. The results for both cores and rims clearly plot in the non-alkali and non-orogenic fields. These clinopyroxenes are thus closely related to tholeiitic basalts and, more precisely, to non-orogenic tholeiites. This characterization is in good agreement with the trace-element geochemistry of the basalts.

3.7.3 Sediment geochemistry

The trace element compositions of sedimentary rocks can be investigated using normalizing diagrams similar to those used for basalts. Various normalizing constants, representing average Phanerozoic values, are employed for different types of sediment. In this study the trace-element compositions of shales and fine-grained sandstones were studied using the North American shale composite (NASC), representing "average crustal material" (Gromet *et al.*, 1984).

Six inter-chert mudstones (91A/90-91F/90) were sampled at site 91/90. Sample 91a/90 was taken from immediately above pillow basalt and the other samples were taken progressively up sequence over a distance of approximately 10m. The NASC-normalized plots for 91A/90-91C/90 (Figure 3.19) show strong relative depletions in Ti, V, Cr and Sr. Samples 91D/90-91F/90 show a basic pattern which is not far removed from NASC but with depletions in Cr, Ni and Sr. The marked trough in Sr may reflect a lack of calcite or variations in plagioclase content relative to NASC. The concentrations of Ni and Cr are similar to or lower than NASC values, indicating little or no input from mafic or ultramafic sources. Three samples of inter-chert mudstone from locality 111/90 were also analyzed and plotted as NASC-normalized traces (Figure 3.20). The NASC-normalized patterns for these samples show strong

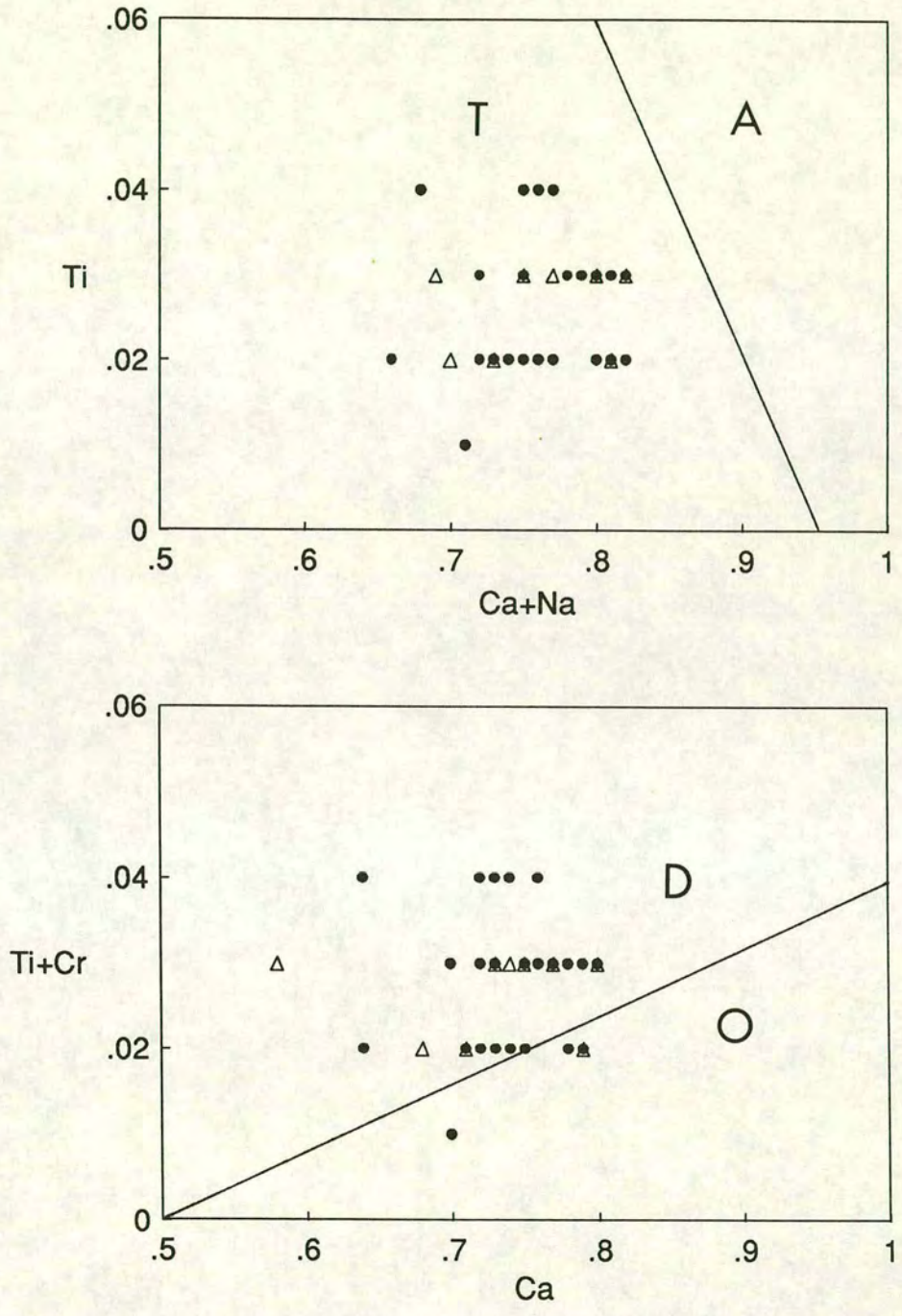

Figure 3.18 Tectonic discrimination diagrams for clinopyroxenes from basalts of the Ortaoba Unit. (a) Ti vs (Ca+Na) plot showing the fields for alkali basalts (A) and tholeiitic and calc-alkali basalts (T), (b) (Ti+Cr) vs Ca plot showing the fields for MORB and other tholeiites from spreading zones (D) and volcanic-arc basalts (O) (fields from Leterrier *et al.,* 1982). Clinopyroxene compositions are expressed in cations per six oxygens. Circles represent phenocryst cores and triangles represent rims.

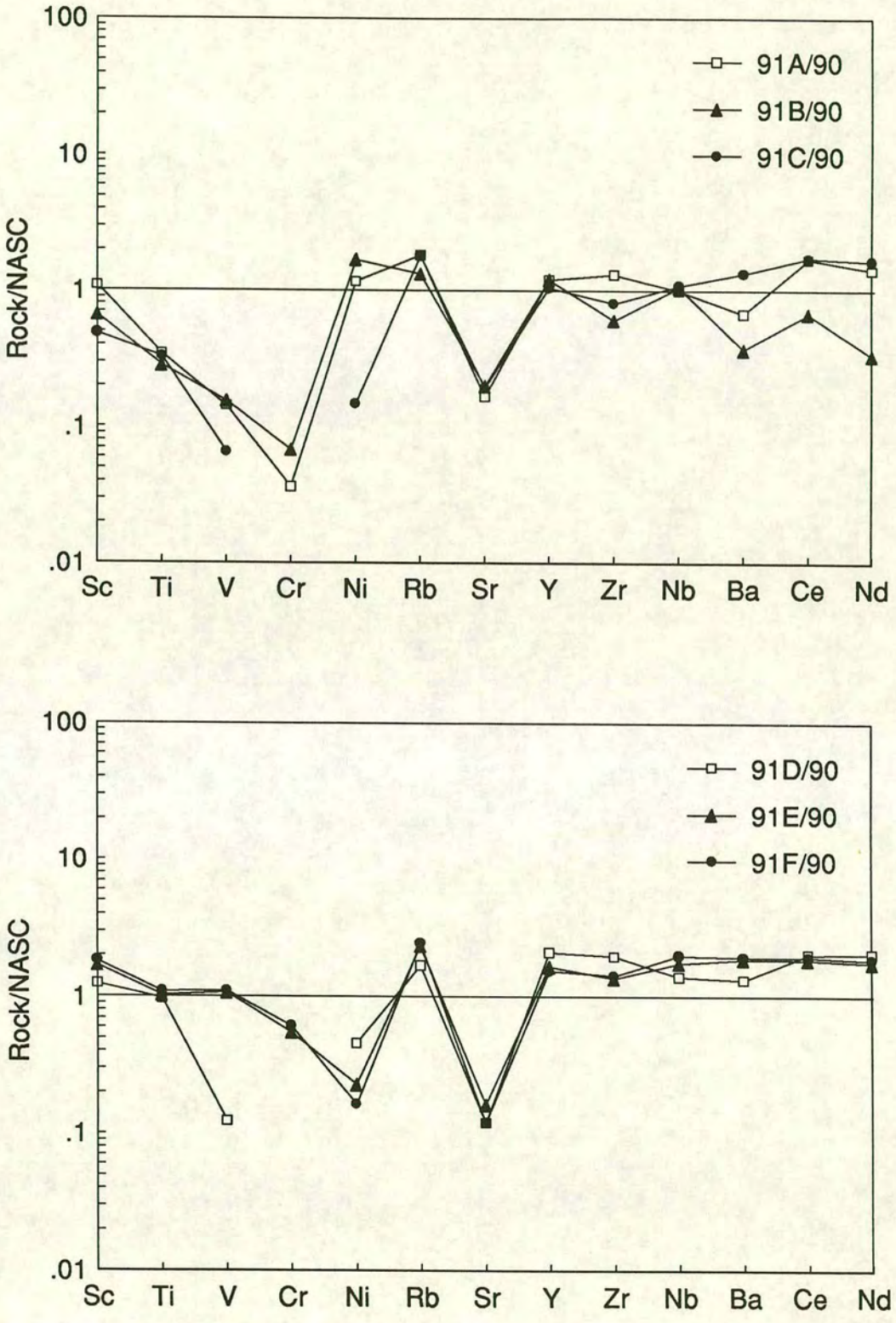

Figure 3.19 NASC-normalized multi-element plots for mudstone intercalations from site 91/90. The samples were taken at intervals up the chert sequence (from 91A to 91F). Normalizing values from Gromet *et al.* (1984) (Appendix 4).

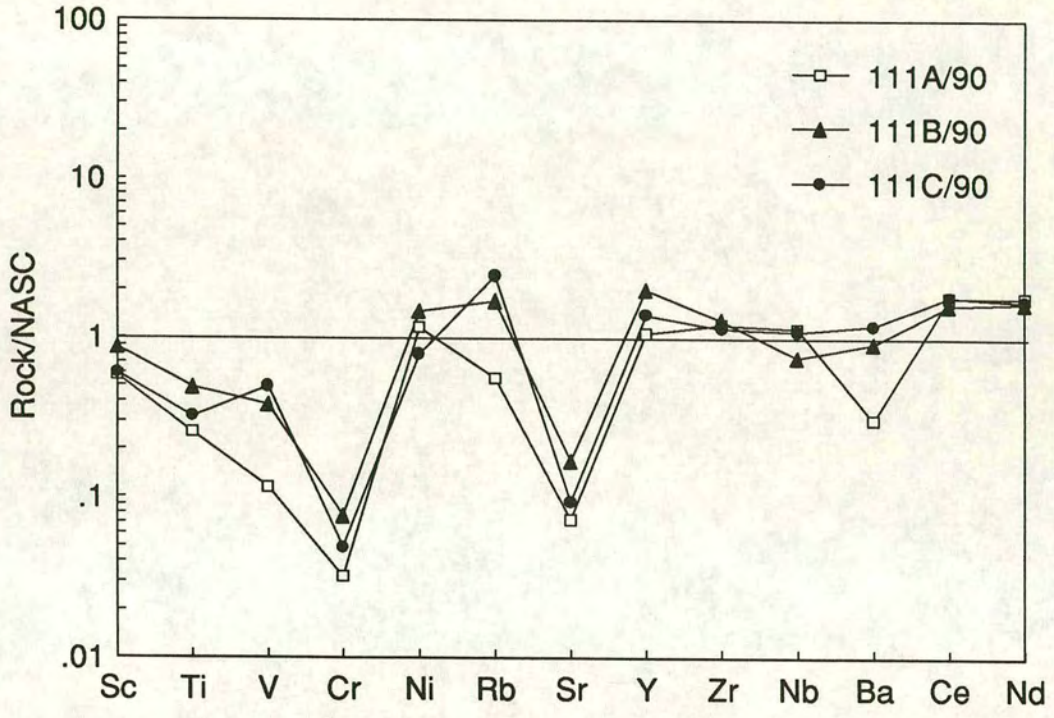

Figure 3.20 NASC-normalized multi-element plots for mudstone intercalations from site 111/90. The samples were taken at intervals up the chert sequence (from 111A to111F). Normalized as for Figure 3.19.

depletions in Cr and Sr and are very similar to those from the lower part of the sequence at locality 91/90. By normalizing an average deep sea clay against the average shale of Turekian & Wedepohl (1961), Robertson & Henderson (1984) illustrated the relative enrichment of Ni, Y, Ba, Ce and Nd in deep sea clays. Figure 3.19 also displays a similar, albeit slight enrichment in these elements, with the exception of samples 91C-91F which are significantly depleted in Ni.

Geochemical data for the mudstones from sites 91/90 and 111/90 were also plotted on La-Th-Sc and Th-Sc-Zr/100 discrimination diagrams devised for clastic rocks by Bhatia & Crook (1986). As shown in Figure 3.21 the mudstones plot predominantly in the active continental margin and continental island arc fields.

3.7.4 Interpretation of geochemistry

The basalt and clinopyroxene discrimination diagrams indicate that the Ortaoba basalts are tholeiitic and from plate margin settings. Basalt discrimination diagrams and MORB-normalized plots indicate that the Ortaoba basalts are predominantly MORB in character. The similarity of the HFS elements to the MORB trace implies a normal MORB (N-MORB), rather than an enriched MORB (E-MORB) source. Tectonic slivers of basalt within the sheared sandstones and shales of the Ortaoba Unit have very different geochemistries to the "*in situ*" Ortaoba basalts and may reflect tectonic interslicing with basalts from different tectonic settings (e.g volcanic-arc and within-plate).

The fine-grained sediments from the sequence directly above the pillow basalts display terrigenous signatures when normalized against NASC. Discrimination diagrams suggest an active margin source, although as yet is is impossible to say whether of Eurasian or Gondwana origin. The absence of fresh volcanic material implies that arc volcanism was not contemporaneous with deposition of the Ortaoba sedimentary rocks.

3.8 Interpretation of the Ortaoba Unit

The disrupted basalt-chert-sandstone sequence of the Ortaoba Unit near Edremit clearly indicates a relatively deep sea-floor setting. The basalts contain sparse, small vesicules, similar to those found in deep water lavas erupted at spreading ridges (i.e. at water depths of 2-3km). The 10m-thick chert interval implies a quiet abyssal

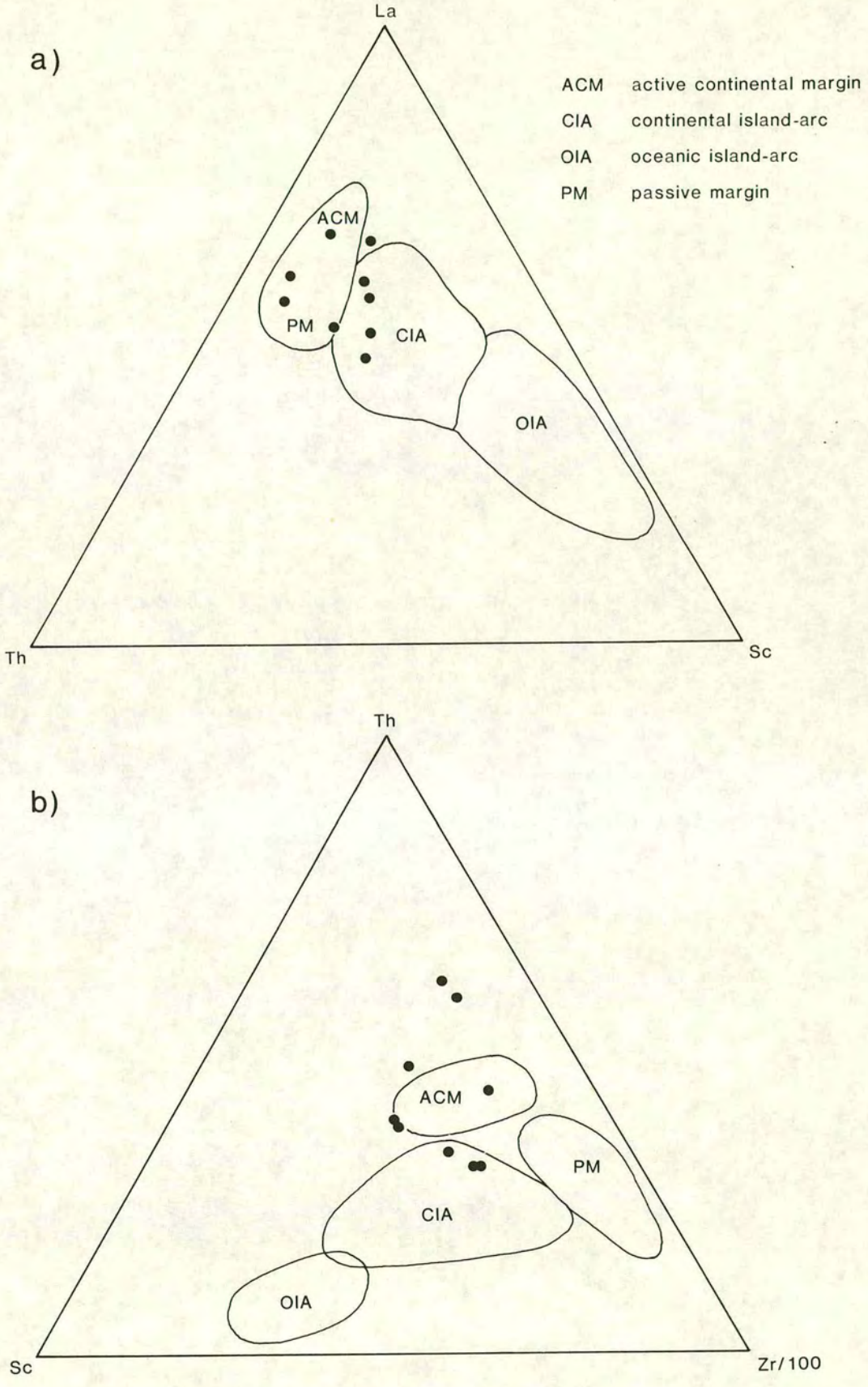

Figure 3.21 Tectonic discrimination diagrams for mudstone intercalations from sites 91/90 and 111/90. (a) La-Th-Sc plot and (b) Th-Sc-Zr/100 plot (fields from Bhatia & Crook, 1986).

environment where chert and muds accumulated on oceanic pillow basalts. Using rates of accumulation of siliceous ooze in the modern oceans (Berger & Winterer, 1974) it was calculated that the 10m of chert observed above the basalt would have taken approximately 2-5Ma years to form. The sulphide mineralization at the top of the pillow basalt pile was probably formed by black smokers similar to those active today near ocean ridges. The layer of reddish cherty mud between the basalt and the bedded chert probably represents the fall-out from these smoking chimneys and, if better developed, would constitute an ochre or umber similar to those described from Cyprus (Robertson & Hudson, 1972). The chert is interbedded with variously coloured mudstones. The pale buff mudstone may represent ash-rich layers. Up-sequence the chert gives way to turbiditic sandstones which become progressively coarser grained and more massively bedded upward. This may reflect the approach of a deep-sea basalt-chert sequence to a trench and the subsequent influx of progressively coarser grained terrigenous material. Within the trench region terrigenous material would be relatively coarse and would contain debris flows derived from the toe of the accretionary prism or from along the trench axis. Limestone blocks within the debris flows may have been derived from seamount material incorporated within the accretionary prism during an earlier phase of accretion.

Alternatively, the chert-clastic sequence could be interpreted in terms of a pelagic environment which received a clastic influx in response to a relative fall in sea level. For example, in the Mamonia Complex of SW Cyprus, Lower Cretaceous quartzose sandstones which overlie Jurassic radiolarian cherts are interpreted as a clastic influx related to relative sea level change on a continental margin (Robertson *et al.,* 1991). However, in this case, the sequence clearly forms part of a Neotethyan passive margin succession and is not associated with basal MORB-type basalts and adjacent accreted open-ocean units (e.g. the Nilüfer Unit). A simple sea level change is thus unlikely to have produced the coarsening upward sequence observed in the Ortaoba Unit. Tectonic processes, such as the approach of an oceanic plate to a trench and its incorporation into an accretionary complex (as outlined above) provide a much more likely explanation and allow all the features of the unit, as well as its position within the Karakaya Complex, to be explained. This model is therefore adopted here.

The Ortaoba basalts show geochemistries which indicate predominantly N-type MORB. The fact that the MORB-normalized traces are closely parallel to the normalizing line implies that the slight Nb depletions observed in a few of the "*in*

situ" basalts are unlikely to reflect a distinct arc signature. Tectonic slices of basalt within the Ortaoba Unit display both within-plate and arc-related characteristics and were probably sliced into the unit in an accretionary setting.

The occurrence of basalt-chert-sandstone sequences in the Ortaoba Unit may imply a relatively sediment-starved trench environment. The accretionary prisms associated with such trenches are slow to build up and have slowly prograding deformation fronts. Thrust faults within the accretionary prism may propagate along weak zones in the upper oceanic crust, producing slivers of basaltic crust, pelagic sediments and trench fill. Basaltic slivers are common within the Ortaoba Unit and, in a few cases, retain their original cover of bedded chert and coarsening-up turbidites. By contrast, trenches with large sediment supply develop thicker accretionary wedges which tend to shear off along décollements within the young trench fill. The resulting accretionary wedges are built up entirely of trench sediments.

3.9 Sedimentation in modern trenches

Subduction zone trench sediments may be derived from three main source areas which were reviewed by Pickering *et al.* (1989):

a) Oceanic-plate sediments passively conveyed by plate motion into a trench.
b) Lateral sediment input from the fore-arc.
c) Axial transport of sediments along the trench, possibly from distant areas.

a) Ocean-plate sediments
Oceanic-plate sediments can occur as a thin veneer above basaltic basement and may include chert, manganiferous sediments, pelagites and fine-grained turbidites. Sediment accumulation rates of such sequences tend to be slow (e.g. 2-5mm/1000years on the Cocos and Pacific plates), and below the carbonate compensation depth (CCD) (Schweller & Kulm, 1978). Other oceanic plates, by contrast, accumulate great thicknesses of terrigenous turbidites. On the Indian Plate, for example, the oceanic plate is covered by thousands of metres of turbidites (Moore *et al.*, 1982). The Lesser Antilles trench is likewise characterized by a thick clastic succession (Brown & Westbrook, 1987; Moore *et al.*, 1988).

b) Lateral sediment input

Lateral input from the fore-arc region of an active margin can produce significant thicknesses of trench sediment, including a variety of debris flows, turbidites and fine-grained deposits. Sediment may be derived locally, from the inner trench slope and lower slope regions, and also from more distal areas such as the upper slope and fore-arc ridge. Sediments are supplied to the trench via a system of canyons and slope channels and build up trench fans and sheet deposits. The fine-grained fraction of turbidity currents forms fine-grained deposits which mantle the topography and onlap slopes. Another example of lateral sediment supply to the trench includes volcanic and carbonate material derived from the flanks of subducting seamounts and fed in to the trench as debris flows and turbidites.

c) Axial sediment transport

Sediments carried along channels which develop parallel to the trench may also contribute significantly to the trench fill. Such channels may develop in topographic lows along the inner trench wall or on the outer side of the trench, depending on whether the trench is starved or well-supplied. Sediments deposited by lateral transport processes tend to comprise mainly coarse- to fine-grained turbidites. Axial channels have been observed in the Chile Trench (Thornburg & Kulm, 1987) and along the Nankai Trench (Taira & Niitsuma, 1986; Le Pichon *et al.,* 1987a & b). Axial channels may be diverted oceanwards by large lateral systems such as trench fans, as observed in the Nankai trench by Le Pichon *et al.* (1987b).

3.10 Preservation of trench fill and application to the Ortaoba Unit

The preservation of trench sequences depends to a large degree on the site of the decollement zone at the point of subduction. Thornburg & Kulm (1987) discussed the importance of the nature of trench-fill deposits in determining the location of successive decollement fronts and hence the nature of stratigraphic duplication within the accretionary prism. They suggested that sediment-starved trenches tend to decouple within the upper layer of the oceanic basaltic layer, whereas in thick trench successions little or no oceanic crust is accreted. Thus, the accretionary prisms of starved trenches comprise slices of basalt, pelagic sediments and trench-fill whereas the accretionary prisms of oversupplied trenches will consist entirely of trench sediments. Seismic evidence from many modern trenches suggests that oceanic crust and the overlying pelagites and hemipelagites generally tend to be subducted, whereas the trench turbidites are off-scraped and accreted (Pickering *et al.,* 1989). Seamount

subduction may also allow the preservation of trench stratigraphies. Partial accretion of a seamount leads to the incorporation of seamount material, as well as oceanic-plate sediments, into the accretionary prism. This process has been used to explain the origin of some melanges in the Shimanto Belt (Ogawa, 1985) and may be occurring at the present day in the Japan Trench where the Daiichi-Kashima seamount is being partially subducted and accreted.

The Ortaoba Unit consists of a variety of sedimentary facies which may reflect the nature of the trench-fill and also give us some insight into the accretion processes. North of Edremit the Ortaoba Unit comprises predominantly quartzo-feldpsathic clastics ranging from thin-bedded sandstones to massive sandstones and conglomerates. However, well-preserved slivers of pillow basalt overlain by bedded chert do occur, suggesting that the trench may have had a relatively low sediment supply and that decollement occurred in the upper levels of oceanic crust. In all cases bedded sandstones are observed to lie stratigraphically above the chert sequences. Slivers of serpentinized dunite within sheared shales north of Kadiköy confirm that fragments of ocean floor were incorporated within the accretionary prism. Despite considerable disruption by faulting and shearing, the clastics clearly display coarsening- and thickening-up sequences. Laterally discontinuous massive sandstones up to 1-2m thick with pebbly bases were observed along the road to Karakaya Tepe.

3.11 Ancient analogues

Numerous ocean floor and trench-fill sequences have been recognized throughout the geological record, many of which provide excellent analogues for the Ortaoba and Kalabak Units. Several of these sequences, including examples from accretionary complexes in the Eastern Mediterranean, Alaska, Scotland, California, Antarctica and Japan, are briefly discussed below.

a) Eastern Mediterranean region

In the Late Palaeozoic-Early Mesozoic Küre Complex of the central Pontides of northern Turkey, supra-subduction oceanic crust is overlain by hemipelagic muds and hundreds of metres of deep-sea terrigenous turbidites (Ustaömer & Robertson, 1994). Ustaömer & Robertson (1994) interpreted the Küre Complex as an accretionary complex containing thrust-bounded slices of deep-sea basalts and sediments. The Küre sequence has been interpreted as the remnants a Palaeotethyan back-arc basin

rather than a major oceanic suture by Ustaömer & Robertson(1994), owing to the absence of blueschists, MORB basalts and open-ocean sediments such as radiolarian chert. In this respect the Küre sequence differs from the Ortaoba Unit which contains MORB basalts and a significant chert component. The components of the Kure turbidites are very similar to those of the Ortaoba Unit. Both types of sandstone contain a large proportion of strained quartz, feldspar and devitrified acidic volcanic grains.

The Ermioni Complex on the Argolis Peninsula, Greece, comprises Early Tertiary terrigenous flysch intersliced with basic lavas and metalliferous and pelagic sediments (Clift & Robertson, 1989). The basalts have MORB/IAT characteristics and are commonly preserved along with their sedimentary cover of pink, micritic limestone and locally, massive sulphides. The Ermioni Complex as a whole is dominated by siliciclastic turbidites with locally pronounced layer-parallel extension. Clift & Robertson (1989) envisaged that the the basalt and pelagic slivers were detached from Late Cretaceous oceanic lithosphere during subduction and accretion of terrigenous trench sediments at a north-dipping subduction zone.

Fragments of oceanic crust and sedimentary cover occur within the Upper Triassic-Upper Jurassic Avdella Melange of the Pindos Mountains in northern Greece (Jones & Robertson, 1991). MORB basalts overlain by pelagic carbonates and radiolarites form intact successions within the melange. The melange also contains thrust-bound slices of terrigenous turbidites. The Avdella Melange represents Triassic and Jurassic Neotethyan oceanic crust and associated sediments which were generated and accreted in the Pindos Ocean.

Many other examples of ocean floor sequences have been described from the Eastern Mediterranean region (e.g. Hawasina Complex of Oman; Bechennec *et al.*, 1990; Mamonia Complex; Robertson *et al.*, 1991).

b) Other regions

The Chugach flysch terrane in southern Alaska has been interpreted as a Late Cretaceous trench-fill deposit (Nilsen & Zuffa, 1982) and provides an excellent analogue for the Ortaoba Unit. This unit consists predominantly of interbedded greywacke and shale with local conglomerate, limestone and volcanics (Nilsen & Zuffa, 1982). Locally, pillow lava and chert are in depositional contact with the turbidites, a feature observed within the Ortaoba Unit. Nilsen & Zuffa (1982)

estimated a stratigraphic thickness of 5000m for the turbidite succession. The Chugach flysch terrane is highly folded and faulted with bedding, axial planes and faults dipping northwards (i.e. landward) and striking parallel to the regional trend of the belt. Granitic batholiths intrude the Chugach flysch terrane in many areas and have been dated as Late Tertiary. These batholiths have been interpreted as products of anatectic melting of the accretionary complex rather than arc magmatism (Hudson & Plafker, 1979). The Nilüfer and Kalabak Units are similarly intruded by small granitic plutons which definitely predate the oldest overlying sediments of Upper Triassic age. Geochemical analysis indicates a volcanic-arc affinity for the granitoids in the Biga Peninsula but, owing to the ambiguity of granite discrimination, a post-collisional, anatectic origin is also a possibility.

The Southern Uplands of Scotland also preserves rocks interpreted as tectonic slices of ocean floor and trench sequences (Leggett *et al.*, 1984). Massive basalt and pillow lavas form the lowest part of the disrupted sequence. They are non-vesicular or sparsely vesicular, suggesting extrusion at several kilometres depth. The lavas are overlain by Fe-rich mudstones, radiolarian chert and siliceous mudstones. The chert is overlain by black shales and, further up-section, by a thick succession of greywacke turbidites with rare debris flow deposits. These associations are interpreted as slivers of ocean floor and trench sediment, offscraped above the northwards subducting Iapetus ocean crust during the Ordovician and Silurian.

Oceanic crust and trench sequences have also been recognized in the Franciscan Complex of California (Wahrhaftig, 1984; Karl, 1984). In the Marin Headlands area pillow basalt is stratigraphically overlain by approximately 80m of Lower Jurassic radiolarian chert and intercalated red shale. The chert and mudstone interval is overlain by dark shale and massive arkosic sandstone.

Many inferred trench-fill sequences have also been observed in the accretionary complexes of Japan. For example, in the Mino terrane of SW Japan, coarsening- and thickening-upward sandstone sequences and debris flow units overlie siliceous shale and chert, and have been interpreted as deposits laid down in trench-slope to trench-floor settings (Sano *et al.*, 1992).

In Antarctica, the Mesozoic LeMay Group of Alexander Island contains thrust-bounded slices of accreted ocean floor and trench-fill sedimentary rocks (e.g. Doubleday *et al.*, 1994). Oceanic basalts of MORB affinity are overlain by chert and

minor arkosic sandstones. Doubleday *et al.* (1994) described sequences from the NW LeMay Range which are remarkably similar to those of the Ortaoba Unit. There, thrust-bound slivers of basalt, chert and siliceous mudstone are interleaved with arkosic trench-fill sandstones. As with the Ortaoba Unit, primary stratigraphic contacts can be observed between the basalt and the chert and between the chert and sandstone.

3.12 Lithologies of the Kalabak Unit

The Kalabak Unit is well exposed NE of the village of Ortaoba (Figure 3.1) and at its type locality near the village of Kalabak, north of Havran (Figure 1.7). In both areas the unit comprises a sheared, folded sequence of dark phyllites and schists, with rare marble and metabasite horizons. The Kalabak Unit is also exposed near the town of Kinik in the Bergama region.

3.12.1 Edremit-Havran area

a) North of Edremit

In the Edremit region the Kalabak Unit crops out north of the prominent hill of Pasadag, and is tectonically bounded to the west by sandstones and shales of the Ortaoba Unit (Figures 3.1 and 3.2). The Kalabak Unit is tectonically overlain by klippen of the Çal Unit, which form the hills of Pasadag, Kir Tepe and Çigdem Tepe (Figure 4.17). The unit is best exposed along the roads which run over Çigdem Tepe and past Kir Tepe. Both these roads display a continuous succession of intensely sheared and foliated black phyllites (Figure 3.22a). The phyllites comprise quartz, albite, muscovite, biotite and chlorite. Massive, dark green metabasites also occur sporadically within the sequence. They consist of actinolite, epidote, chlorite and albite and, unlike the Ortaoba basalts, do not retain good igneous textures. The phyllites also contain rare recrystallized white and light grey marble blocks up to 2-3m in size. One such block lies just below the contact of the phyllites with the Çal Unit on the slopes of Çigdem Tepe. The block is very similar to those observed in the Ortaoba Unit near Kadiköy, being grey, very recrystallized, finely laminated and highly stylolitized. The phyllitic foliation drapes around the block which is slightly flattened in the plane of the foliation.

Serpentinite occurs at the contact between the Kalabak and Çal Units. A sliver of streaky serpentinitic material separates Kalabak phyllites from the overlying,

a

b

Figure 3.22

(a) Photomicrograph of a fold hinge in phyllite from the Kalabak Unit, 1km SW of Çiğdem Tepe, showing fine quartz- and clay/opaque-rich laminations (XPL, field of view: 15mm)

(b) Folded phyllites of the Kalabak Unit outside Kalabak village in the Havran area. The folds verge to the left of the picture (i.e. NW).

undeformed mudstones and sandstones of the Çal Unit which crop out on Çigdem Tepe. The serpentinitic plane dips shallowly south and cuts across the steep structures which characterize the underlying phyllites. A corresponding serpentinitic outcrop is also present near the village of Karadag on the slopes of Pasadag.

b) North of Havran

Near the village of Kalabak, the Kalabak Unit comprises a higher proportion of quartzo-feldspathic schists than in the Edremit area. Lithologies include dark phyllites, quartzo-feldspathic schists, banded marble and metabasites. Detailed petrographic work was carried out on the Kalabak Unit in the Havran region by Krushensky *et al.* (1980). They described the presence of actinolite-chlorite schist, quartz-rich phyllite, conglomeratic quartz-rich phyllite, banded marble, actinolitic quartz-rich phyllite, actinolitic and chloritic metaquartzite, metaclaystone and tremolitic schist. The rocks in this region are highly foliated, lineated and folded and a typical outcrop is shown in Figure 3.22b. The protoliths of these rocks were, in decreasing order of abundance, shales, quartz-rich clastics, volcanics and carbonates.

In the Havran region, the Kalabak Unit is intruded by the Çamlik Metagranodiorite and unconformably overlain by Upper Triassic conglomerates of the Halilar Formation. The contact between the Kalabak Unit and the Halilar Formation was not observed, although the unconformity between the Çamlik Metagranodiorite and the Halilar Formation is well exposed near the village of Manastir. No fossils have been found in the Kalabak Unit and its age is therefore constrained to the pre-Late Triassic only. The unmetamorphosed and relatively undeformed nature of the overlying Halilar Formation indicates that the intense shearing and greenschist metamorphism of the Kalabak Unit occurred in pre-Late Triassic times. Fragments of phyllite and schist have been observed within the Halilar clastics.

3.12.2 Kinik area

The Kalabak Unit in the Kinik region (Figure 1.6) is very similar to the exposures north of Edremit. A particularly good section through the thick sequence of dark phyllites is exposed 6km SW of Kinik. The phyllites are characterized by a steeply dipping foliation which dips consistently to the SE. Duplexes parallel to the foliation indicate motion to the NW. The sheared phyllites are overlain by undeformed clastics and Triassic limestone, thus indicating their age to be at least Triassic and confirming their early deformation and metamorphism.

3.13 Structure of the Kalabak Unit

a) Edremit-Havran region

In the southern part of the Biga Peninsula the Kalabak Unit forms a broad belt, approximately 15km wide, which trends NNE-SSW and mirrors the trends of the other Karakaya units and the Kazdag Massif. The Kalabak Unit dips towards the SE and is characterized by a consistent lineation and foliation. Figure 3.23 shows the predominantly SE-dipping foliation in the phyllites from the Edremit-Havran region (measured over an area approximately 10km by 5km). The lineation consistently trends NE-SW to NNE-SSW as shown in Figure 3.23c (measurements taken along the road to Çigdem Tepe).

Moderate to steep SE-dipping shear zones (Figure 3.23b) are common features of the Kalabak Unit. The shear zones bound duplexes which indicate thrusting towards the north, a direction which is confirmed by the common presence of small north-vergent asymmetrical folds and kinks (Figure 3.23d and 3.23e). Serpentinite within the Kalabak Unit outside Kalabak village contains "fish" structures also suggesting motion towards the north.

b) Kinik region

The Kalabak Unit in the Kinik region displays a strong foliation which dips steeply to both the SE and NW. The NW-dipping foliation planes have probably been slightly overturned from an originally SE-dipping position, as duplexes and shear zones consistently indicate transport towards the NW.

3.14 Interpretation of the Kalabak Unit

Study of the Karakaya Complex has focused primarily on the Nilüfer, Ortaoba and Çal Units, owing to their relatively good exposure and distinctive lithological assemblages. The Kalabak Unit, by contrast, is a monotonous sequence of poorly exposed, sheared phyllites and has been little studied during this project. Nevertheless, a few tentative interpretations can be made about the unit on the basis of field observations. The predominance of dark phyllites and their association with meta-basites suggests a deep-sea setting, possibly similar to that of the Ortaoba Unit. The Kalabak Unit may essentially be a finer grained equivalent of the Ortaoba sandstones, which was deposited in a setting further from the trench. Blocks and slivers of marble and basalt within the Kalabak Unit may have been incorporated into

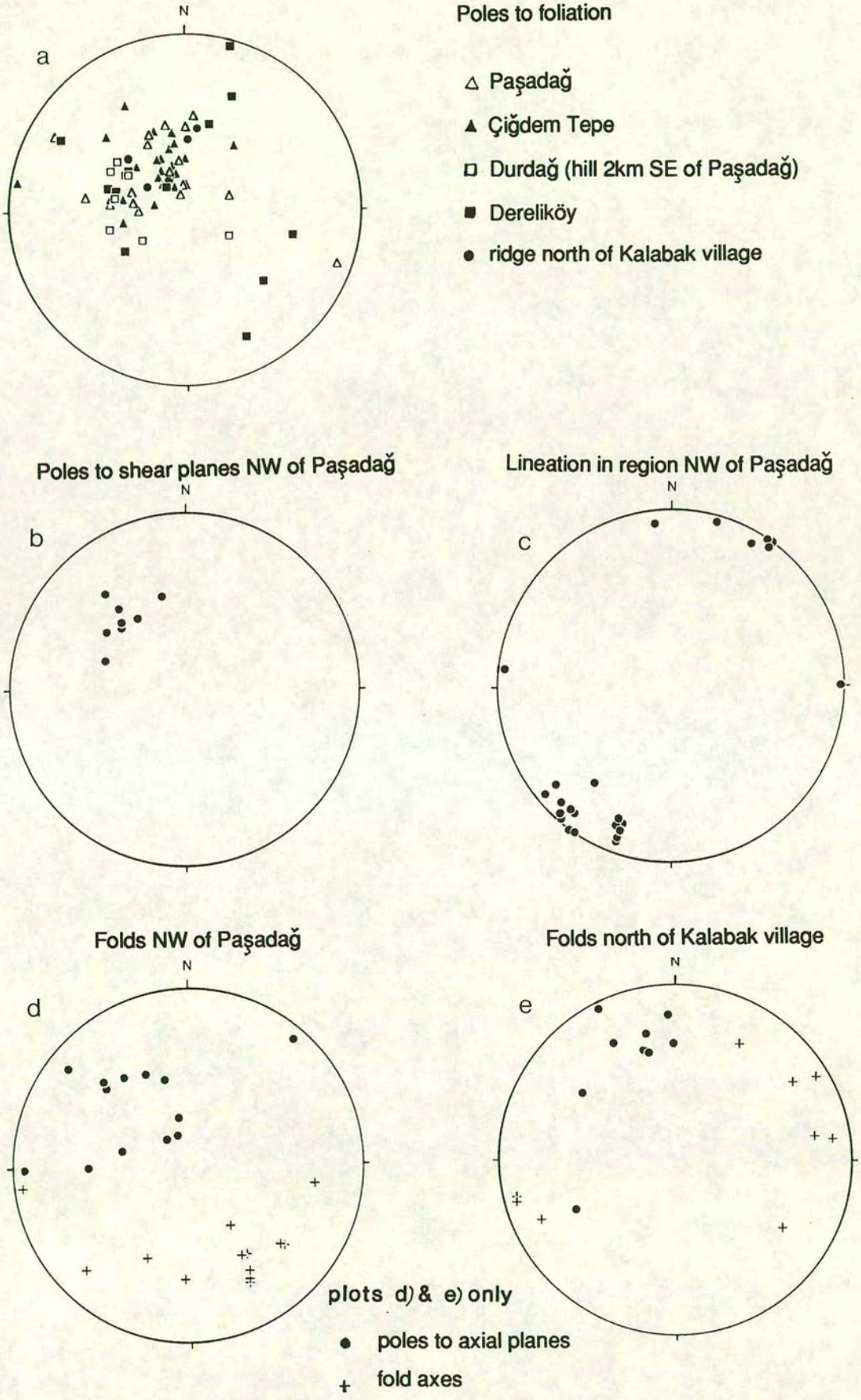

Figure 3.23 Stereoplots of structures in the Kalabak Unit in the Edremit-Havran area.

the unit by accretionary processes. The higher grade of metamorphism and general lack of sedimentological or igneous structures indicate that the Kalabak Unit was probably accreted at greater depths than the Ortaoba Unit

3.15 Granitic intrusions

The Kalabak Unit north of Havran is intruded by a granodiorite pluton, the Çamlik Metagranodiorite of Okay *et al.* (1991). The granodiorite is highly weathered and good intrusive contacts are not observed. North of the village of Çamlik a small enclave of phyllite 15m across is entirely surrounded by granodiorite and is thus assumed to represent a surviving fragment of the phyllitic country rock. The sub-circular nature of the outcrop argues against the possibility of its being a faulted block. Abundant clasts of the granodiorite are found within the overlying Upper Triassic sedimentary rocks of the Halilar Formation.

The granodiorite consists of feldspar, quartz and mica. In thin-section the feldspars are highly altered and range from being dusty in appearance to being totally sericitized. Aplitic veins cross-cut the main body of the granodiorite. A similar granodioritic pluton intrudes spilites of the Nilüfer Unit, on the eastern flanks of Kazdag, and forms the hanging wall of the shallow detachment fault which bounds the Kazdag Massif near the village of Beyoba (Figure 6.4). Around Beyoba, spilites have been considerably baked by the granodiorites and are darker and harder than those further away from the intrusion. Near Çamlik there is less evidence of contact metamorphism as the phyllites were clearly foliated and metamorphosed to greenschist facies before intrusion of the granodiorite.

The Oligo-Miocene Eybek Granodiorite also covers a large area to the north of Havran. It can be distinguished from the pre-Upper Triassic pluton discussed above by its much fresher appearance in the field. The Eybek pluton forms the peaked mountain of Eybek Dag whereas the older intrusives are not associated with any raised topography.

3.16 Geochemistry of the granitoids

a) Discrimination diagrams

Pearce *et al.* (1984) subdivided granites according to their intrusive settings into four main groups: ocean ridge granites (ORG), volcanic arc granites (VAG), within-plate

granites (WPG) and collision granites (COLG). They demonstrated, using ORG-normalized geochemical patterns, that the granites of these tectonic groups exhibit distinctive trace-element characteristics. Using analyses of granites from known settings they devised a set of discrimination diagrams to distinguish between granites from these broad tectonic settings.

Granodiorites from Çamlik and Beyoba were analyzed by X-ray fluorescence and plotted on the Nb-Y and Rb vs (Y+Nb) discrimination diagrams of Pearce *et al.* (1984) (Figure 3.24). In plot (a) the analyses cluster in the VAG and syn-COLG field. One analysis from the Oligo-Miocene Eybek pluton was also plotted for comparison. Plot (b) was used to distinguish between syn-collisional and volcanic-arc granites. The analyses clearly cluster in the VAG field. The Eybek Granodiorite plots very close to the Çamlik-Beyoba granodiorite, despite their widely varying ages (Oligo-Miocene and pre-Upper Triassic respectively). This is not surprising as both intrusions were probably formed by melting of the same material at depth and were both intruded through the same sequence of rocks (i.e. the Karakaya Complex). Pearce *et al.* (1984) pointed out that unusual degrees of crustal contamination (e.g. in areas near intrusion margins or near enclaves) may lead to problems with tectonic discrimination. In these cases the composition of the contaminant is likely to lie in the VAG or syn-COLG fields and may cause misclassification.

b) ORG-normalized geochemical patterns

Figure 3.25 shows ORG-normalized geochemical patterns for the Çamlik, Beyoba and Eybek granodiorites. Although the full range of elements used by Pearce *et al.* (1984) were not analyzed in this study, the patterns in Figure 3.25 may still be usefully compared with the typical examples given in their paper. The distinctively "humped" traces compare well with those from volcanic-arc and syn-collisional settings. The granodiorites are enriched in K, Rb, Ba, Th, and Ce relative to Nb, Zr and Y; typical features of volcanic-arc granites. A further feature of volcanic-arc granites is the low position of Y relative to ORG and this is also apparent in Figure 3.25. Many patterns for collisional granites possess very similar shapes to those of volcanic-arc granites, making clear-cut tectonic interpretations impossible. However, some of the distinctive characteristics of collisional granites, such as very high Rb concentrations and very low Ce contents are not shown by the samples in Figure 3.25.

In summary, the discrimination diagrams suggest that the granodiorites which intrude the Kalabak Unit are volcanic-arc granites, while ORG-normalized plots imply

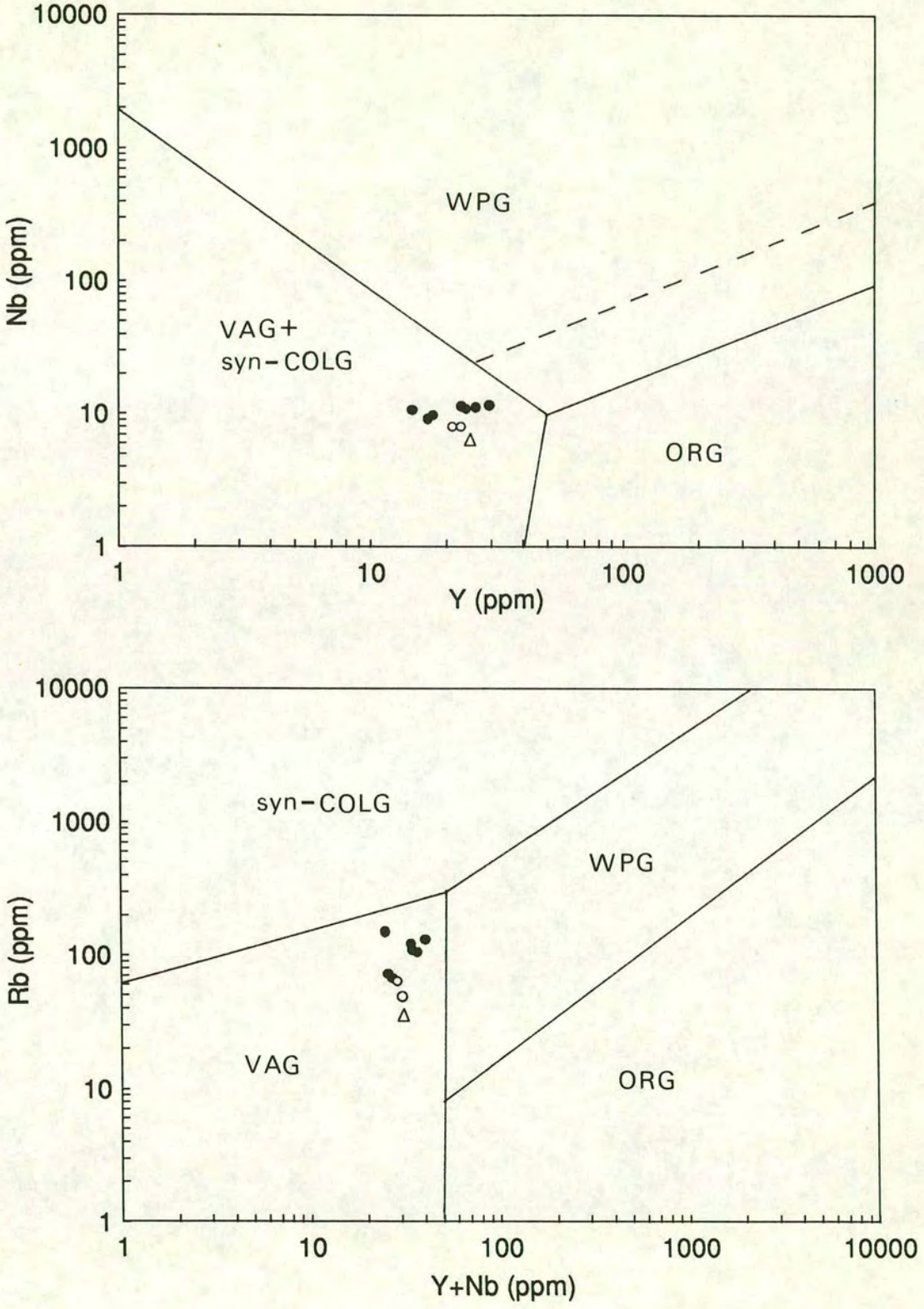

Figure 3.24 Tectonic discrimination diagrams for granodiorites in the Edremit-Havran region. (a) Nb-Y plot and (b) Rb-(Y+Nb) plot (fields from Pearce *et al.*, 1984). Samples are from the Çamlık Metagranodiorite (closed circles), the Beyoba granodiorite (open circles) and the Oligo-Miocene Eybek pluton (triangle).

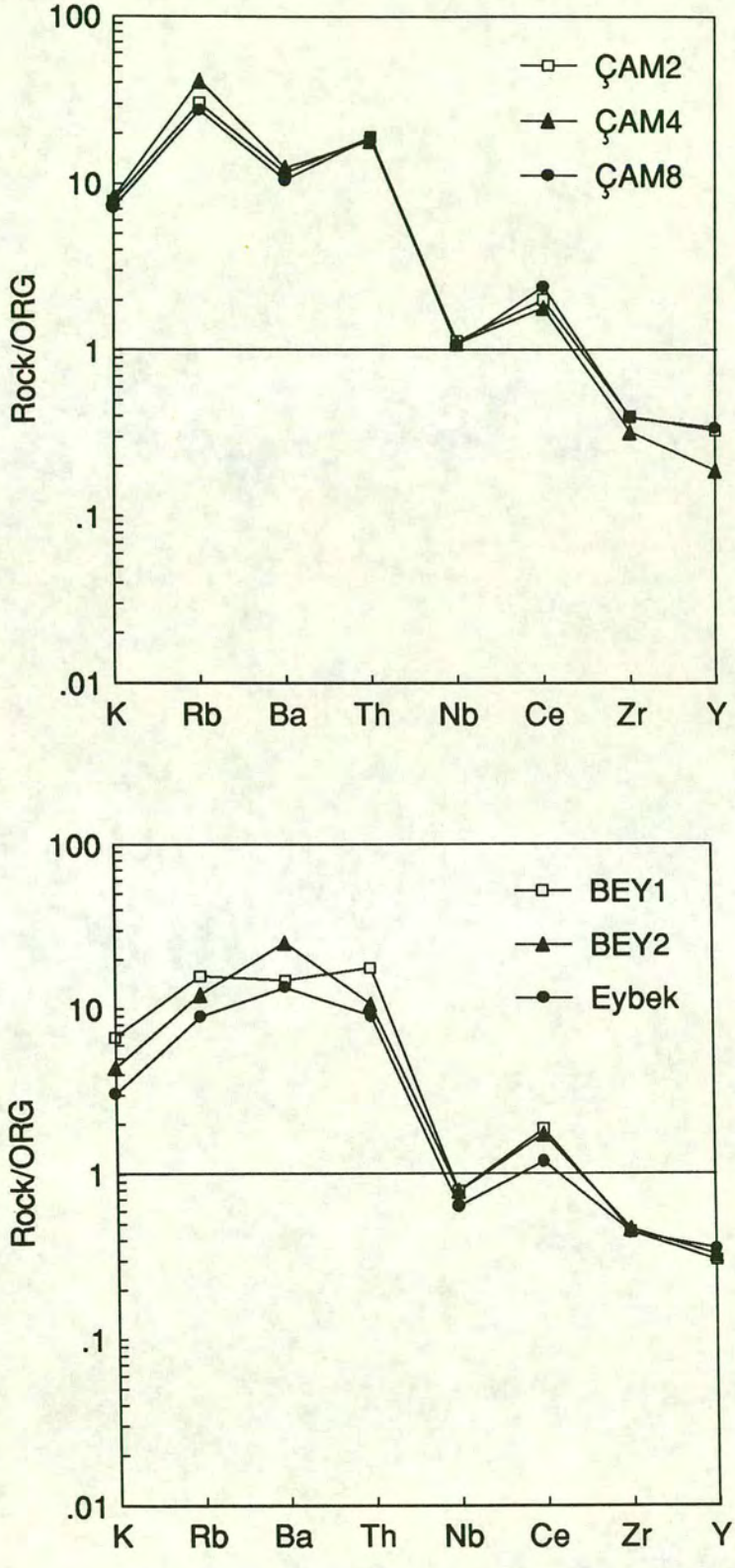

Figure 3.25 ORG-normalized multi-element plots for the Çamlık (ÇAM2, 4, 8), Beyoba (BEY1, 2) and Eybek plutons. Normalizing values from Pearce *et al.* (1984) (Appendix **4**).

volcanic-arc or possibly collisional settings. However, discrimination results for granites should be treated with caution for, as pointed out by Pearce *et al.* (1984), the fields on the discriminant diagrams strictly reflect source regions (and melting and crystallization histories) rather than tectonic regimes. For syn-collisional, volcanic-arc, ocean-ridge and within-plate granites, source regions and tectonic regimes are closely correlated. However, post-collisional granites can plot within the volcanic-arc, within-plate or syn-collisional fields depending on the relative proportions of mantle- and crust-derived magmas and on the enrichment history of the mantle concerned (Pearce *et al.*, 1984).

CHAPTER 4

THE ÇAL UNIT: DISRUPTED PERMIAN CARBONATE PLATFORMS AND DEBRIS FLOWS

4.1 Introduction

The Çal Unit is the structurally highest and least deformed unit in the Karakaya thrust stack. The lithologies which make up this unit form distinctive lithological assemblages which have been recognized in the southern and central parts of the Biga Peninsula and also in the Bergama area. The name "Çal Unit" has hitherto been used in a restricted sense, specifically to describe debris flows, rich in volcanic and Upper Permian limestone blocks, in the Çan and Edremit regions (Okay *et al.*, 1991). In this thesis, however, the usage of the name is broadened to include disrupted Upper Permian platform sequences in the Bergama and Balya regions.

The Çal Unit consists of disrupted Permian limestone platform sequences with a clastic basement, limestone- and volcanic-rich debris flows, red mudstones, pelagic limestone, thin lava flows and sandstone-shale sequences. Upper Permian limestone blocks up to many metres in size are a ubiquitous feature of this unit. Upper Permian limestone platform sequences on a clastic basement are beautifully exposed in the Bergama region. An Upper Permian carbonate platform on a clastic basement is also exposed near Ezine and is tectonically overlain by the Denizgören Ophiolite. This fragment of carbonate platform, although strictly belonging to the Çal Unit as defined in this chapter, is discussed in Chapter 7 owing to its bearing on the emplacement of the ophiolite. The volcanic- and limestone-rich debris flows of the Çal Unit are best exposed near the villages of Çalköy, Asagikaraasik and Yukarikaraasik in the Çan region of the central Biga Peninsula. At the top of the Çal Unit in this region a shallowly-dipping unconformity marks the base of the overlying clastics of the Lower Jurassic Bayirköy Formation. Facies within the Upper Permian limestone blocks were also studied near Pasadag, a hill north of Edremit in the southern Biga Peninsula region. In this region a shallow serpentinitic boundary separates the Çal Unit from the underlying sheared phyllites of the Kalabak Unit.

This chapter presents descriptions and interpretations of the main lithologies of this unit, based largely on fieldwork carried out in the regions of Çan, Edremit, Bergama and, to a lesser extent, Balya. Work in the Bergama, Balya and Edremit regions

mainly involved investigation of carbonate platform facies and associated clastics. In the Çan region the debris flows were investigated and basaltic clasts were collected for geochemical analysis and tectonic discrimination.

4.2 Previous work

The Çal Unit was first described as the Çal Köy Series by Blanc (1965), after the village of Çalköy along the road between Yenice and Çan. There was very little subsequent work on this unit until a recent study of the Biga Peninsula by Okay *et al.* (1991). They renamed the unit the Çal Unit and also recognized it in the Pasadag area of the Edremit region (Okay *et al.*, 1991). They assigned the unit to their Karakaya Complex. Similar units have been described from the Ankara region and are briefly outlined in Okay *et al.* (1991) and references therein. During fieldwork for this study small exposures of lithologies very similar to those near Çan were observed in the Bergama region near the town of Korucu. On the published M.T.A. maps these rocks are described as part of the Kinik Formation of Akyürek & Soysal (1983).

The disrupted Permian platform in the Bergama region was mapped and described by the M.T.A. (map sheet Balikesir-G4 and report, 1989), based largely on work by Akyürek & Soysal (1983). Okay & Siyako (1993) also mapped this region and interpreted the disrupted platform as limestone blocks within an olistostrome (their Hodul Unit). Many studies have been carried out on the Permian limestone in the Balya region since the original study by Neumayr (1887). One of the most extensive was that by Aygen (1956) who carried out a study of Permian limestone as part of his investigation of the Balya region. He made a detailed palaeontological study of the limestone and identified it as Upper Permian. The limestone forms part of his "nappe de Balya" which he interpreted as having been emplaced over Triassic clastic rocks by gravity sliding.

4.3 Disrupted platform near Bergama

In the Bergama region the Çal Unit is represented by a disrupted Upper Permian carbonate sequence which overlies the spilites and volcaniclastic sediments of the Nilüfer Unit (Figure 4.1). The contact between the two units is poorly exposed but appears to be highly sheared (e.g. near the villages of Halilaga and Hacilar), suggesting thrusting of the Çal Unit over the Nilüfer Unit. The lithologies observed in the Bergama region are described below.

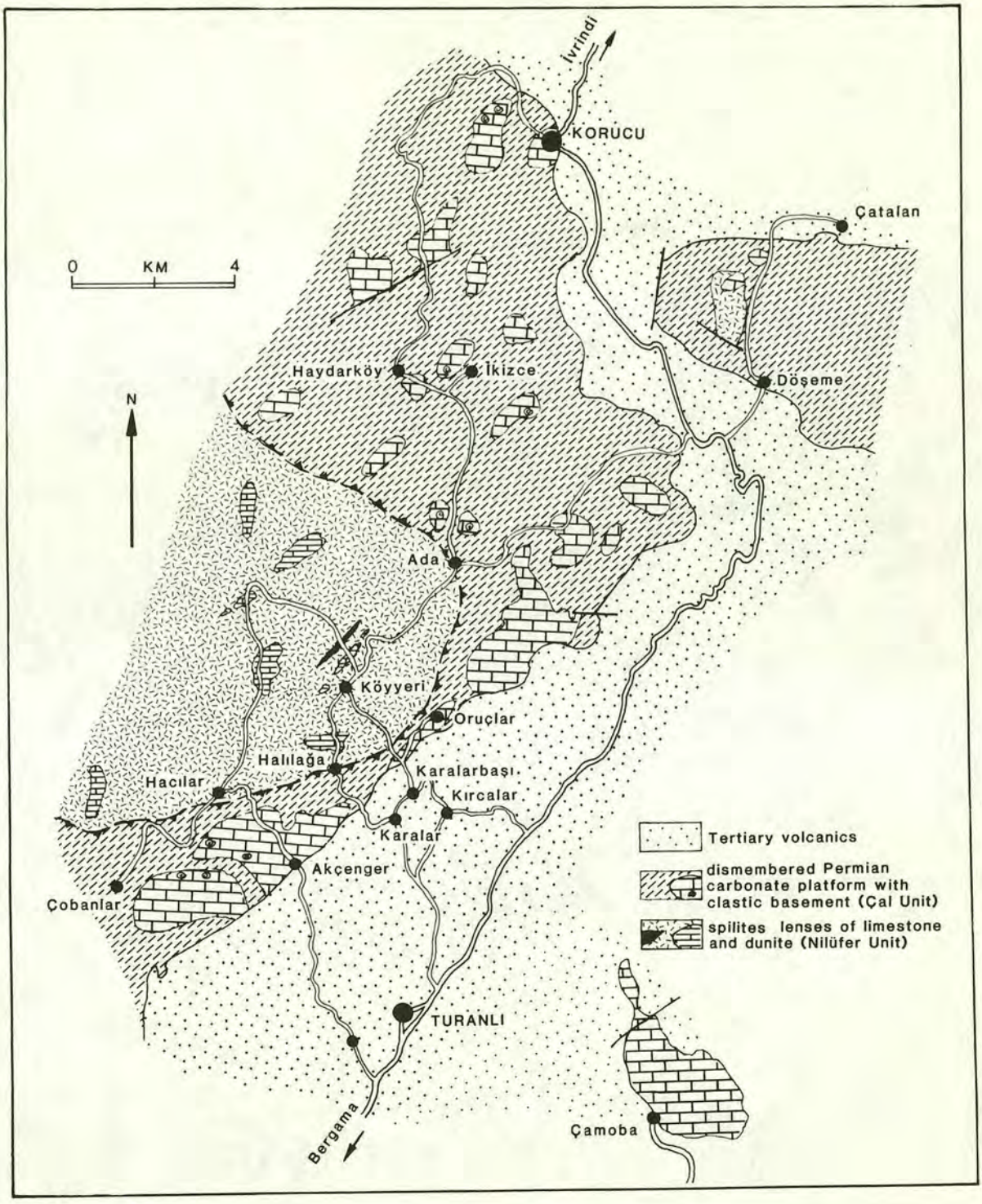

Figure 4.1 Geological map showing the disrupted carbonate platforms which make up the Çal Unit in the region north of Bergama (modified after M.T.A. map sheet Balıkesir-G4).

4.3.1 Lithologies

a) West of Korucu

Along the road running NW from Korucu partly recrystallized limestone blocks have sheared contacts with arkosic sandstone and conglomerate which may represent interbeds towards the base of the platform. It is not clear from the outcrops whether the limestone blocks were originally beds or blocks within a debris flow. Thick-bedded limestone is exposed further along the same road. The bedded limestone contains abundant fusulinids which are found in densely packed lenticular bands. Between the fusulinid packstone layers grey-buff micrite contains echinoderm spines, red algae, thin-shelled bivalves and micrite-coated brachiopod shells. Oolitic, semi-recrystallized limestone overlies the fusulinid-rich sequence. The bedded limestone gives way to sheared and folded black shale and sandstone lenses which contain partly recrystallized limestone blocks with sheared margins. One block displays vague oolitic shapes. Most of the blocks are 2-10m in size so it is possible that the bedded sequence described above is itself a block. The larger size of this block may have buffered its abundant fossils against recrystallization.

b) Gorge near Akçenger

The limestone gorge near the village of Akçenger (Figure 4.1) contains the best exposures of lithologies from the Permian carbonate sequence in this region. Light grey limestone with a buff nodular texture contains fusulinids up to 1.5cm long in densely packed horizons (Figure 4.2a). It is overlain by thin- to medium-bedded limestone containing fusulinids and ooids. Beds are 4-12cm thick with fossiliferous bases and micritic tops which indicate that the sequence is the right way up. The tops of beds are marked by stylolites. The limestone is overlain by coarse-grained feldspathic sandstone.

One limestone block (6m by 6m in size) within the gorge displays excellently preserved coralline, bryozoan (e.g. Figure 4.2b) and algal structures. Fossils are perfectly preserved in a grey micritic matrix. Grey micrite and buff siltstone infill cracks and crevices. Two generations of infills were recognized:

1. *An earlier micritic infill which occurs in reefal interstices*
2. *A later buff silty deposit which infills cracks due to breakup of the block*

Figure 4.2

(a) Photomicrograph of fusulinid-rich packstone from bedded sequence near the village of Akçenger (PPL, field of view: 22mm).

(b) Photomicrograph of a large, reef-building bryozoan in a limestone block near Akçenger (PPL, field of view: 27mm).

(c) Buff siltstone infilling cracks within coralline/algal limestone block near Akçenger. The homogeneous grey patches represent an earlier, micritic infilling of reefal interstices.

a

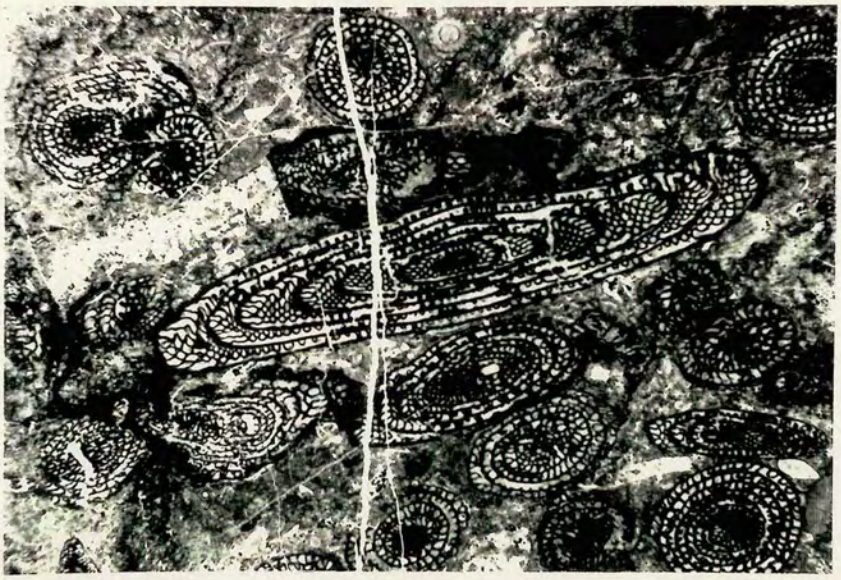

b

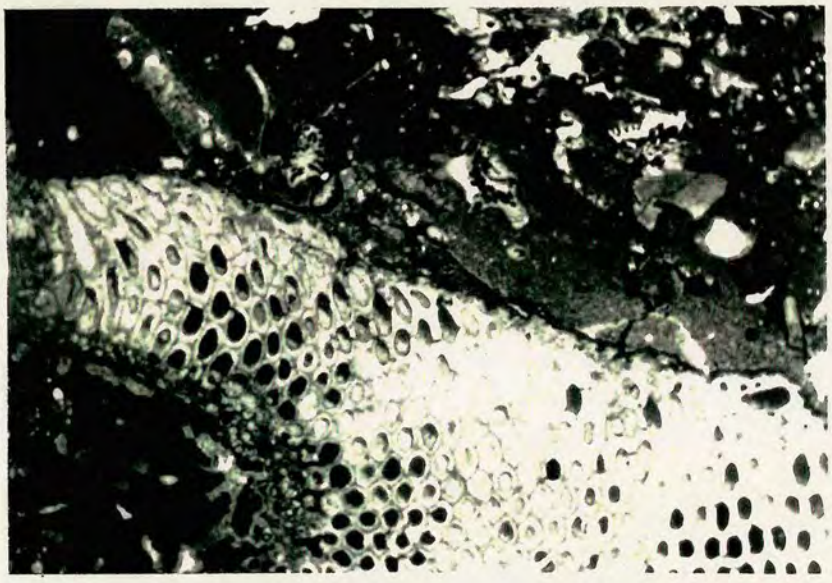

c

The second generation of buff silty material is shown in Figure 4.2c. The siltstone contains abundant small quartz grains, probably derived from the surrounding sandstones. Near Karalarbasi, limestone with a buff nodular texture, fusulinids and ooids is underlain by feldspathic sandstone. The limestone is thin-bedded in places and associated with sandstone and mudstone. On the road above Karalarbasi calcarenite packstones are interbedded with shales and beds (up to 2m thick) of crinoidal sandstone also rich in bryozoa and shell fragments.

c) Adaköy

The Permian platform also crops out on the top of the ridge (Ada Tepe) to the NE of the village of Adaköy (Figure 4.3). The sketch shows Permian limestone thrust over debris flows and feldspathic sandstones. The clastics are probably part of the basement to the platform, although they could also represent localized debris flows associated with the Nilüfer Unit (c.f. debris flows in the Nilüfer Unit near Edremit; Chapter 2). The base of the limestone is marked by a 5m thick breccia which contains angular limestone fragments (80-90%), sandstone, quartz and chert clasts in a coarse-grained quartz-rich sandy matrix. The clasts range in length from 1 to 5cm. The limestone clasts vary from being pale and recrystallized to being grey and fossiliferous. The sandstone matrix contains carbonate debris including small carbonate clasts and isolated, well-preserved fusulinids.

Coarse-grained sandstones, conglomerates and breccias are also exposed along the road which runs north of Adaköy towards Haydarköy. The most common lithology is structureless, massive, coarse-grained sandstone containing rounded quartz clasts in varying abundances. This rock has a distinctive blocky appearance and orange weathering in the field. Further along the road similar sandstone forms the matrix to numerous limestone blocks up to many tens of metres across. The matrix to these blocks also includes pale shaly material and green/beige mudstones. The limestone blocks appear to form a single horizon within the clastics.

Approximately 1km from Haydarköy, near the turnoff to Ikizce, one of these limestone blocks is particularly well exposed in the road cutting. Interbedded calcarenite and sandstone form the matrix at the edge of the block and pass into massive yellow sandstone away from the block. The outer edges of the limestone block are brecciated with a buff marly siltstone infilling spaces and fractures (Figure 4.4). The main body of the block contains ooids with isopachous cements, crinoids, filamentous algae, coralline structures and rare fusulinids. Loose fusulinids and

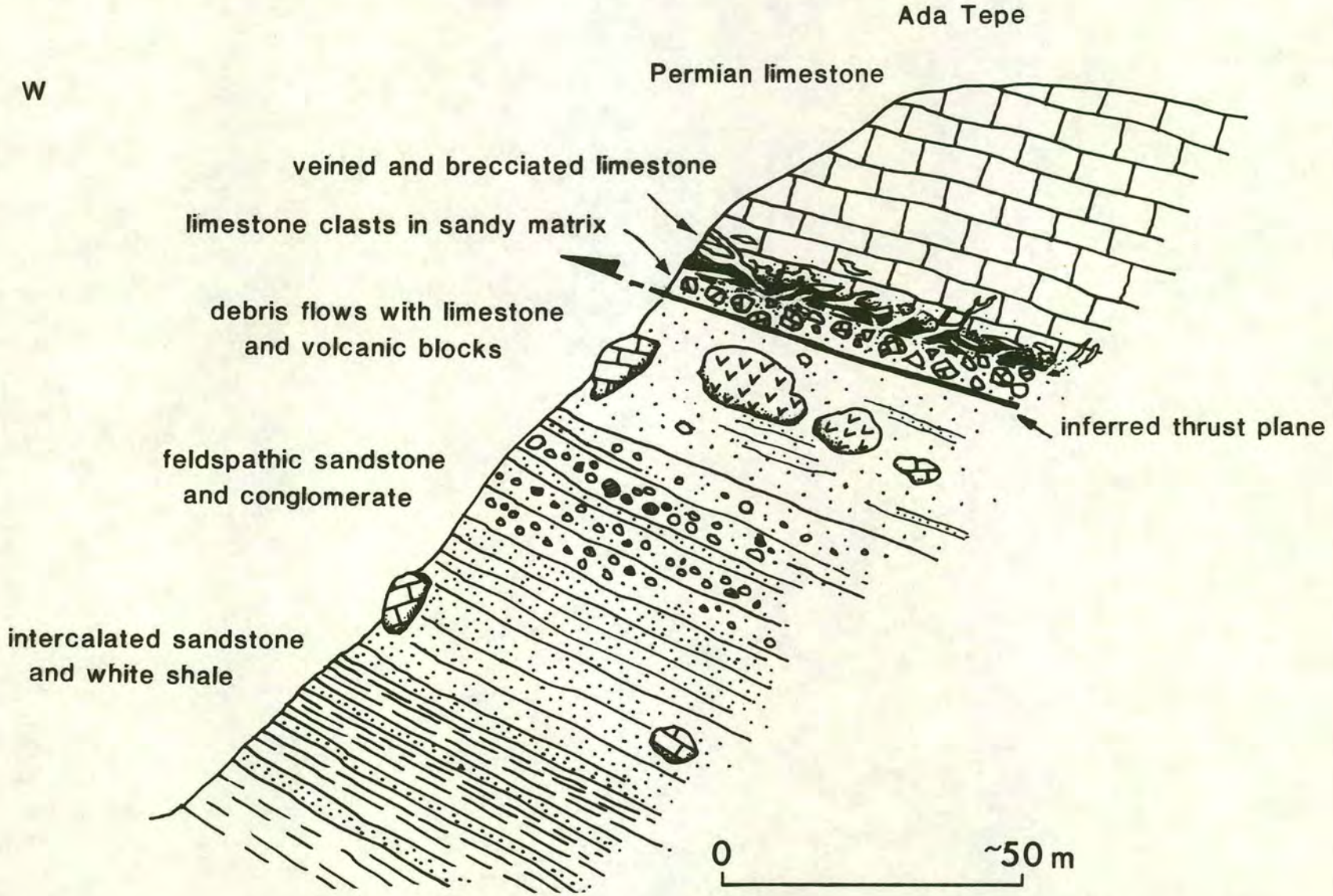

Figure 4.3 Field sketch of Ada Tepe near Adaköy, showing Permian limestone of the Çal Unit thrust over debris flows and clastics (which may either represent a slice of the platform basement or the upper levels of the Nilüfer Unit).

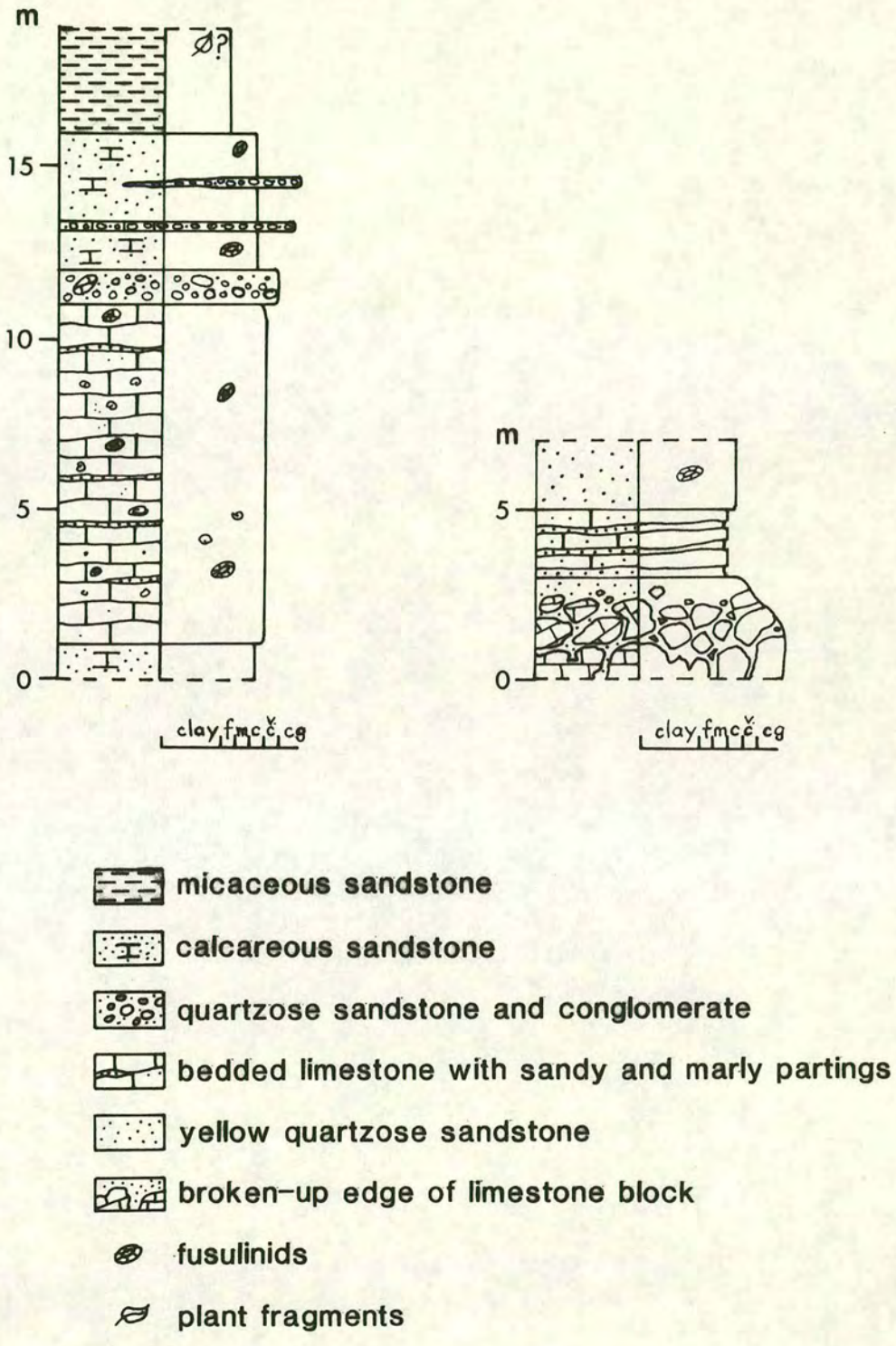

Figure 4.4 Representative logs through the bedded limestone and sandstone sequences between Haydarköy and İkizce. The log on the right represents a short section through the contact between a limestone block and the surrounding matrix of calcareous sandstone and bedded limestone. Note the presence of loose fusulinids within the sandstone.

broken fusulinid fragments are also present within the sandstone which surrounds the block. The sandstone contains fractured quartz grains with strongly undulose extinction, rare alkali feldspars and clasts of fine-grained sandstone.

Calcarenites and conglomerates are well exposed along the road to Ikizce. The conglomerates contain white, grey and dark grey quartz clasts up to 3cm in size and are interbedded with calcareous sandstones. Grading indicates that the sequences is the right way up. Beds become more massive up sequence. One conglomerate layer contains angular black chert clasts and pink and grey quartz clasts in a very coarse-grained matrix. A little further along the road is a conglomerate which contains clasts of limestone (up to 7cm), rare black chert, green volcanics, black mudstone and laminated calcarenite. The limestone and mudstone clasts are rectangular whereas the chert and volcanics are rounded. A nearby outcrop of massive limestone is approximately 50m high and stratigraphically underlain by 6m of bedded calcareous fusulinid/shelly packstones. The beds are 5-30cm thick and interbedded with dark shaly partings. Oysters were observed on the tops of some beds. The massive limestone is inaccessible but may represent a reefal buildup on a shallow-water carbonate-shale substrate.

d) Çamoba

A hill of Permian limestone (Çaltepe), surrounded by Tertiary volcanic flows, lies immediately east of the village of Çamoba (Figures 4.1 and 4.5). The hill was mapped by the M.T.A. and its limestone divided into several types as shown in Figure 4.5. A section through the limestone on the western side of the hill was logged as part of this study (Figure 4.6). The main lithologies are buff marly limestone, dark grey shale and fossiliferous packstone. The fossiliferous part of the sequence contains fusulinids, high-spiral gastropods, ammonoids, corals, thin shell fragments and shelly coquinas. Six main facies were identified on the basis of their field appearance. These facies are indicated on the log in Figure 4.6 and are described below.

Facies 1: Packstone containing abundant bioclastic debris in a slightly marly micritic matrix. Fossils include foraminifera, thin shell fragments,bryozoa, algae and oyster fragments. The shell fragments are aligned sub-parallel to bedding.

Facies 2: Similar to facies 1 but is coarser grained and rich in fusulinids, algae and oyster fragments. Foraminfera were identified as *Pachyphloia* sp., *Colaniella* sp., *Hemigordius* sp. and *Hemigordiopsis* sp..

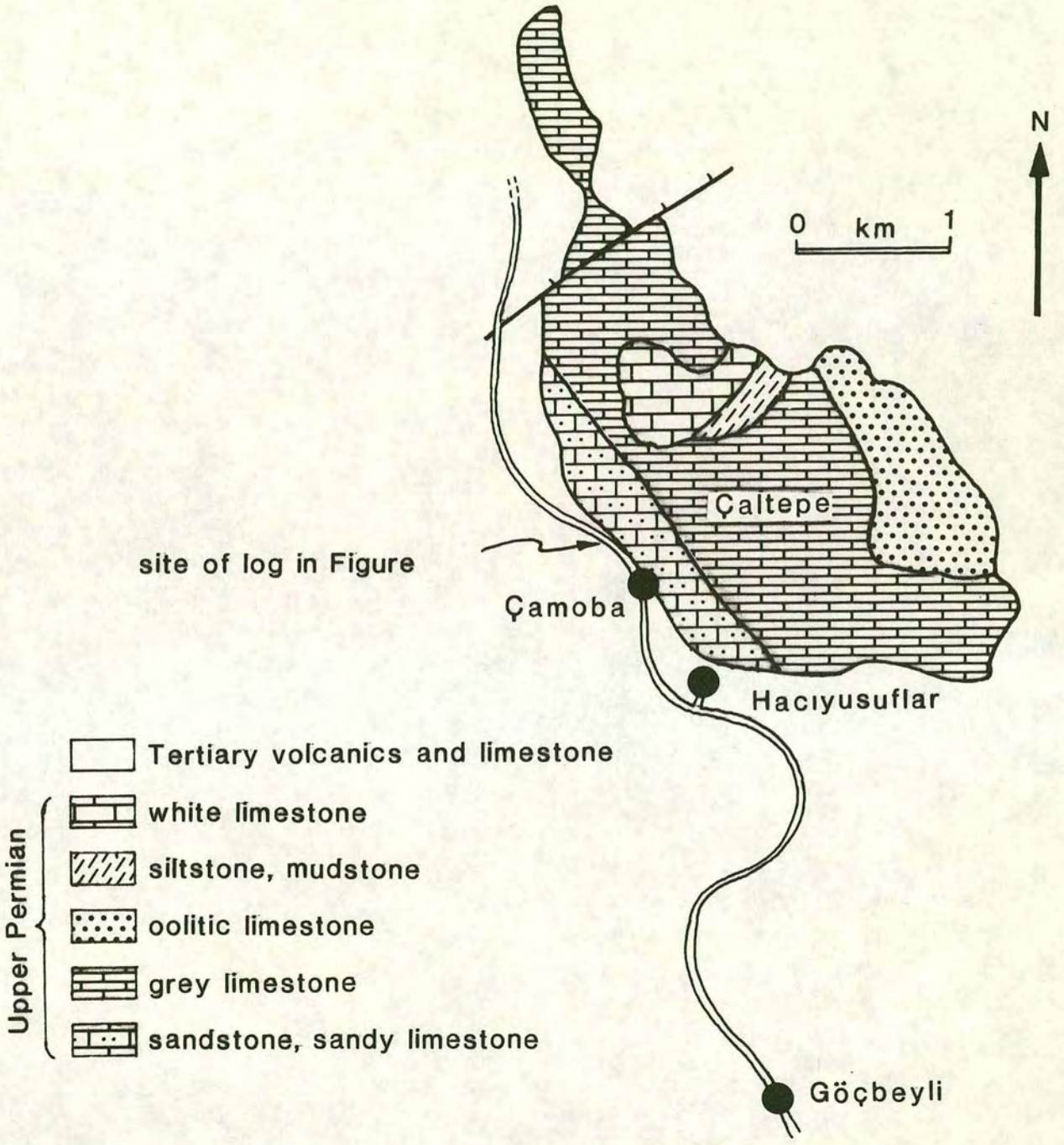

Figure 4.5 Map of Çaltepe hill near Çamoba village, east of Turanlı, showing a variety of Upper Permian limestone facies (after the M.T.A. map sheet Balıkesir-G4).

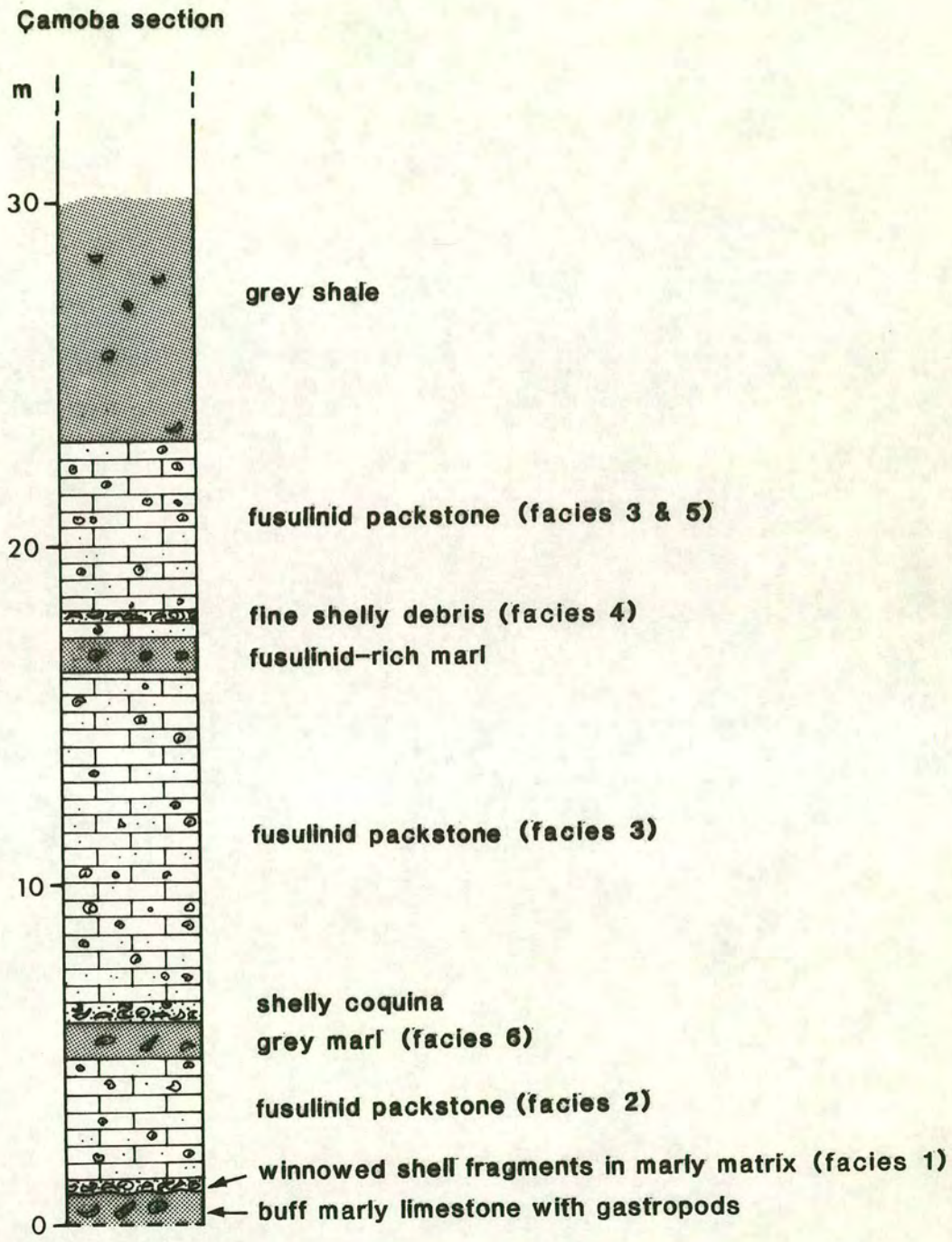

Figure 4.6 Log through the limestone of Çaltepe at the site indicated in Figure 4.5. The various facies are described more fully in the text.

Facies 3: This facies is even richer in fusulinids than facies 2. It also contains oysters, crinoids, bryozoa, algae, gastropods and the foraminifera *Pachyphloia* Schwageri (Figure 4.7a).

Facies 4: Buff micrite with wispy calcite shell fragments and rare recrystallized foraminfera. The matrix is microcrystalline calcite and coloured brown by ?organic material (Figure 4.7b).

Facies 5: Fine-grained brown micrite with alternating radiolarian-rich and radiolarian-poor layers. Other fossils include very thin shells (probably ostracods) (Figure 4.7c).

Facies 6: Grey marl with some interlayers of foraminiferal packstone.

4.4 Disrupted platform near Balya

A disrupted Permian carbonate platform similar to that in the Bergama region forms a belt stretching NE through Ivrindi and Balya, east of the Biga Peninsula. The region around Balya was visited during fieldwork, although detailed studies were not carried out. Outcrop in this region is restricted to a few roads around Balya and basal contacts with the underlying, presumably Karakaya, units are not observed.

4.4.1 Lithologies

a) Ivrindi-Balya road

Fragments of a Permian carbonate platform are exposed in the region of Balya. Interbedded limestone, sandstone and shale crop out along the road from Ivrindi to Balya, just outside Balya. The limestones at this locality are thin- to medium-bedded, micritic and fossiliferous. Thin, crenulated shells concentrated in shelly lags are common. Also present are small foraminfera (including *Colaniella*), red algae, bryozoa, ?coral fragments and pisoids. Pale beige shale is the most common intercalation. The sandstone intercalations consist mainly of quartz and feldspar and contain traces of cross bedding. A limestone "block" within this sequence displays coralline structures (corals replaced by sparry calcite) and laminated micritic infills. The block appears to be underlain by the sandstones, shales and thin-bedded limestones described above. Its upper boundary is unclear.

Figure 4.7 Photomicrographs of limestone facies 3, 4 and 5 from Çaltepe.

(a) Facies 3: packstone containing gastropods, pelagic bivalve fragments and neritic foraminifera (e.g. below large gastropod on right of picture) (PPL, field of view: 13mm)

(b) Facies 4: shell fragments of pelagic bivalves (PPL, field of view: 17.5mm).

(c) Facies 5: laminated micrite with abundant recrystallized radiolaria and pelagic bivalve shells (PPL, field of view: 6mm).

a

b

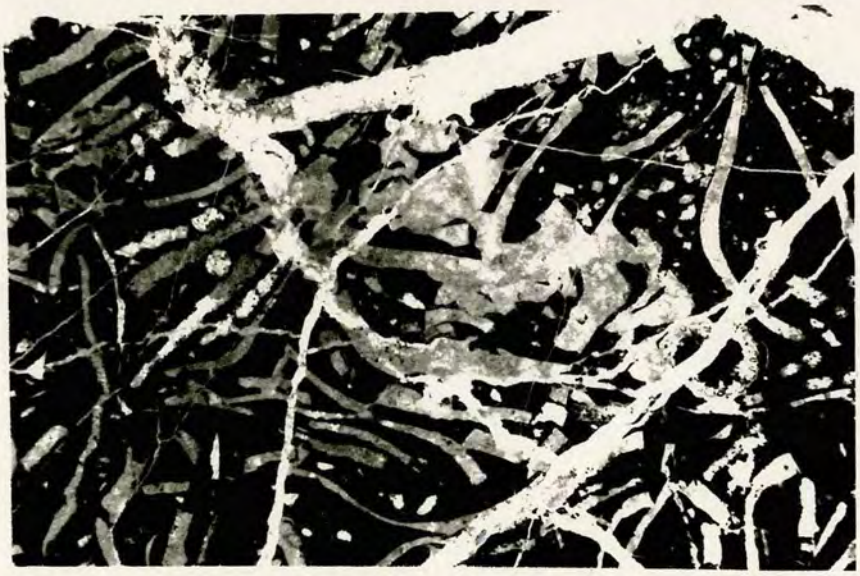

c

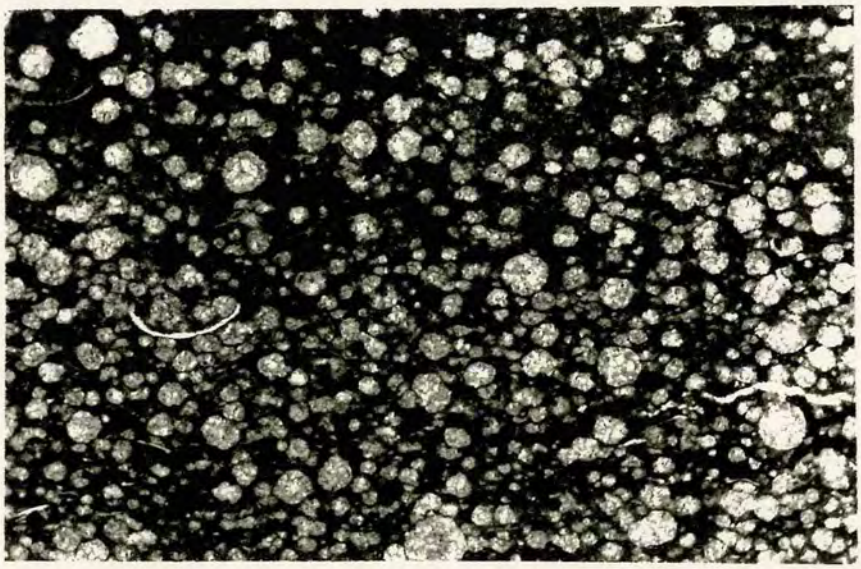

b) NE of Balya (Ilica-Samli road)

Limestone blocks and clastics can also be observed a few kilometres NE of Balya. Just by the turnoff from the main road out of Balya is a large outcrop of limestone breccia which contains clasts of fusulinid-rich limestone, pink limestone, fine- and medium-grained sandstone and algal limestone. The matrix is sandy and calcareous and contains loose fusulinids. Close to this outcrop are green sandstones and siltstones whose relationship with the limestone breccia is unclear owing to poor exposure.

Near the base of one limestone block is an intraformational conglomerate of angular limestone clasts. The clasts vary in colour and some are fusulinid-rich. Others contain gastropods, echinoderm debris and quartz grains. The matrix comprises quartz grains, alkali feldspars (including microcline and perthite) and fusulinid fragments set in sparry calcite. Cherty sandstones and mudstones form a nearby outcrop.

A large outcrop of conglomerate lies along the rough track which heads east from the Ilica-Samli road. The conglomerate contains well-rounded cobbles of basalt, pale green felsic volcanics with quartz phenocrysts and crinoidal limestone. This sequence is interpreted to be equivalent to the sandstones, shales and conglomerates near Bahçelerköy which have been dated as Upper Triassic (Aygen, 1956) and is thus discussed further in the chapter on the Upper Triassic-Jurassic sedimentary cover (Chapter 5).

4.4.2 Ages of limestone blocks in the Balya region

The fossiliferous limestone blocks in the Balya region have been the subject of detailed palaeontological investigations by various workers including Aygen (1956) and Okay *et al.* (1991). Okay *et al.* (1991) observed that Upper Permian limestone constituted 90% of the blocks. Other blocks yielded Early Carboniferous, Middle-Late Carboniferous and Late Carboniferous-Early Permian ages. The Upper Permian limestone is particularly abundant in endothyracids, fusulinids and algae, including *Glomospira* sp., *Pseudoglomospira* sp., *Tuberitina* sp., *Pachyphloia* sp., *Palaeotextularia* sp., *Climacammina* sp., *Cribrogenerina* sp., *Globivalvulina* sp., *Lasiodiscus* cf. *tenuis*, *Reichelina* sp., *Stafella* sp., *Codonofusiella* sp., *Verbeekina* sp., *Neoschwagerina* sp., *Hemogordius* sp., *Gymnacodium* sp., *Mizzia* sp. and *Girvanella* cf. *media*.

4.5 Discussion

a) Bergama region

The Upper Permian limestone in the Bergama region occurs as large blocks with a matrix of bedded clastics and calcarenites. The limestone blocks are found at more or less the same level at the top of the clastic sequence and are here interpreted as the disrupted remains of a platform which built up on a clastic basement. The fauna within the limestone blocks implies a shallow water carbonate environment, with coralline, algal and bryozoan build-ups on the platform edge. The abundant fusulinids reflect an inner platform environment and their presence within calcareous clastics implies reworking and redeposition in a shallow marine setting. In the Çamoba section (Figure 4.6), the grey foraminiferal marls may represent lagoonal settings, while the radiolarian- and pelagic bivalve-rich facies reflect deeper conditions in the outer platform or basinal regions.

The Upper Permian limestone blocks and associated clastics overlie the Mid Triassic Nilüfer Unit with a sheared contact and are therefore interpreted as a thrust sheet. Disruption of the platform clearly occurred during its emplacement as evidenced by considerable brecciation of the limestone along thrust contacts (Figure 4.3). However, the blocky nature of the limestone and the infilled cracks at the edges of blocks may also testify to break-up of the platform before its final emplacement.

b) Balya region

The Balya platform is interpreted as an along-strike extension of the Bergama platform. It comprises reefal constructions and displays evidence for a proximal clastic source which produced intermittent influxes of mudstone and quartzo-feldspathic sandstone. Like the Bergama platform it has a poorly exposed, sheared contact with underlying Triassic rocks and was probably also emplaced as a thrust sheet. The limestone is more broken up than in the Bergama region and forms blocks within debris flows, as described by Okay *et al.* (1991). Relatively rare Carboniferous blocks are also present within the clastic matrix (Aygen, 1956; Okay *et al.,* 1991).

4.6 Lithologies of the Çal Unit in the Çan area

Debris flows of the Çal Unit are best exposed in the Çan region of the central Biga Peninsula. In particular, the lithologies which make up the unit are exposed along the road to the village of Çalköy and along the road between the neighbouring villages of

Asagikaraasik and Yukarikaraasik (henceforth referred to as the Çalköy and Karaasik sections) (Figure 4.8). These two localities were briefly described by Okay *et al.* (1991) and remain the best exposed sections through the Çal Unit debris flows. Owing to the generally poor exposure no other easily accessible localities for the Çal Unit have been found in this region. The Çalköy and Karaasik sections display a wide range of lithologies and have allowed the reconstruction of a relatively complete sequence for the Çal Unit in this region (Figure 4.9). The sequences at the two localities will be described separately and then correlated to give an overall succession for the unit in this part of the Biga Peninsula.

4.6.1 Çalköy section

The village of Çalköy is perched on a hill just to the north of the main road between Yenice and Çan. The winding track up to the village provides a good section through the lithologies of the upper parts of the Çal Unit. Just outside the village a transgressive unconformity between the Çal Unit and Jurassic cover rocks has been observed (Blanc, 1965; Okay *et al.*, 1991).

The Çalköy section comprises a sequence of debris flows which can be divided into four main types on the basis of clast and matrix lithology. Shearing and faulting has disrupted the sequence, especially in the upper and lower parts, making primary contacts between individual flows difficult to establish. However, good grading and stratigraphic contacts can be observed in the central part of the section where the flows are least deformed. The four main types of debris flow are described below.

a) Limestone-rich debris flow

This lithological association comprises a clast-supported conglomerate predominantly consisting of limestone blocks up to 1m in size, with fine-grained dark purple/black interstitial mudstone. The limestone blocks are clast-supported, limestone-dominated conglomerates. They consist of creamy white, pink and dark pink limestone clasts in a matrix of fine-grained dark material similar to that which encloses the larger blocks. Rare clasts of the matrix material are also present, and are probably volcanogenic mudstone. Fractures within the limestone clasts are filled with the same fine-grained, dark purple matrix.

Limestone-rich debris flows are found in the middle part of the Çal section as a layer several metres thick which contains several fining-upward sequences (Figures 4.10

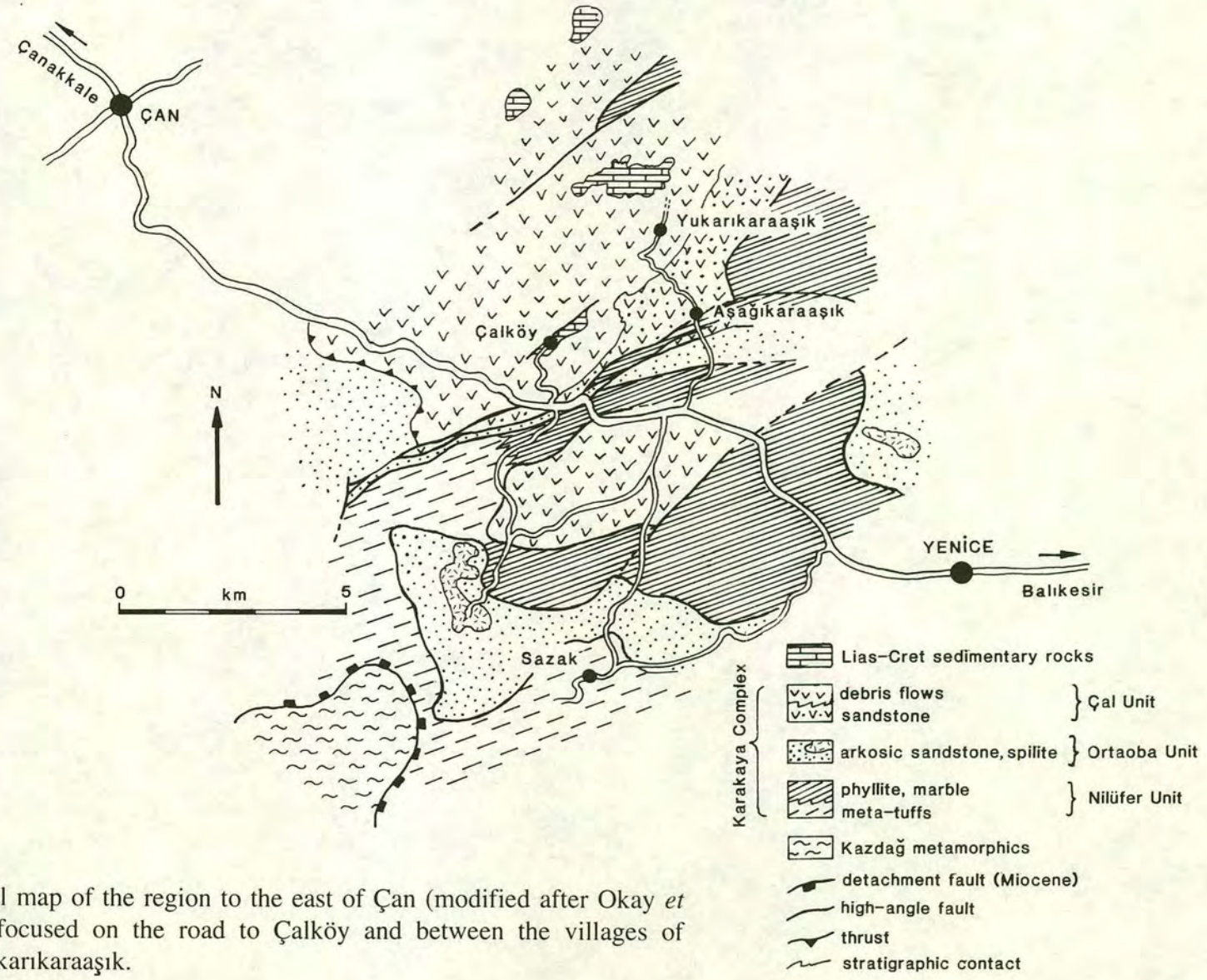

Figure 4.8 Geological map of the region to the east of Çan (modified after Okay *et al.*, 1991). Studies focused on the road to Çalköy and between the villages of Aşagıkaraaşık and Yukarıkaraaşık.

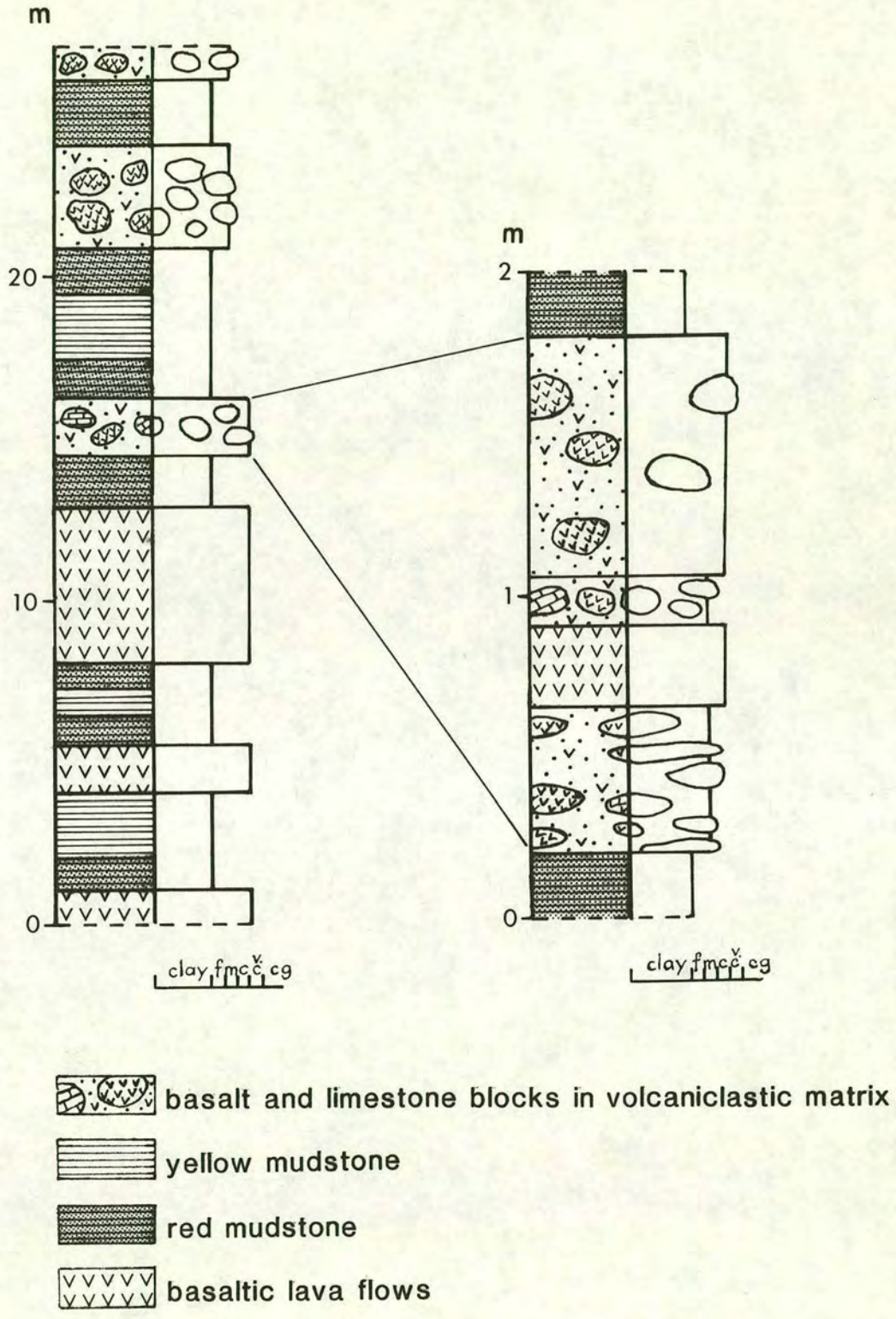

Figure 4.9 Generalized log of the Çal Unit in the area around Çalköy and the Karaaşik villages, with an expanded view of the central part of the sequence.

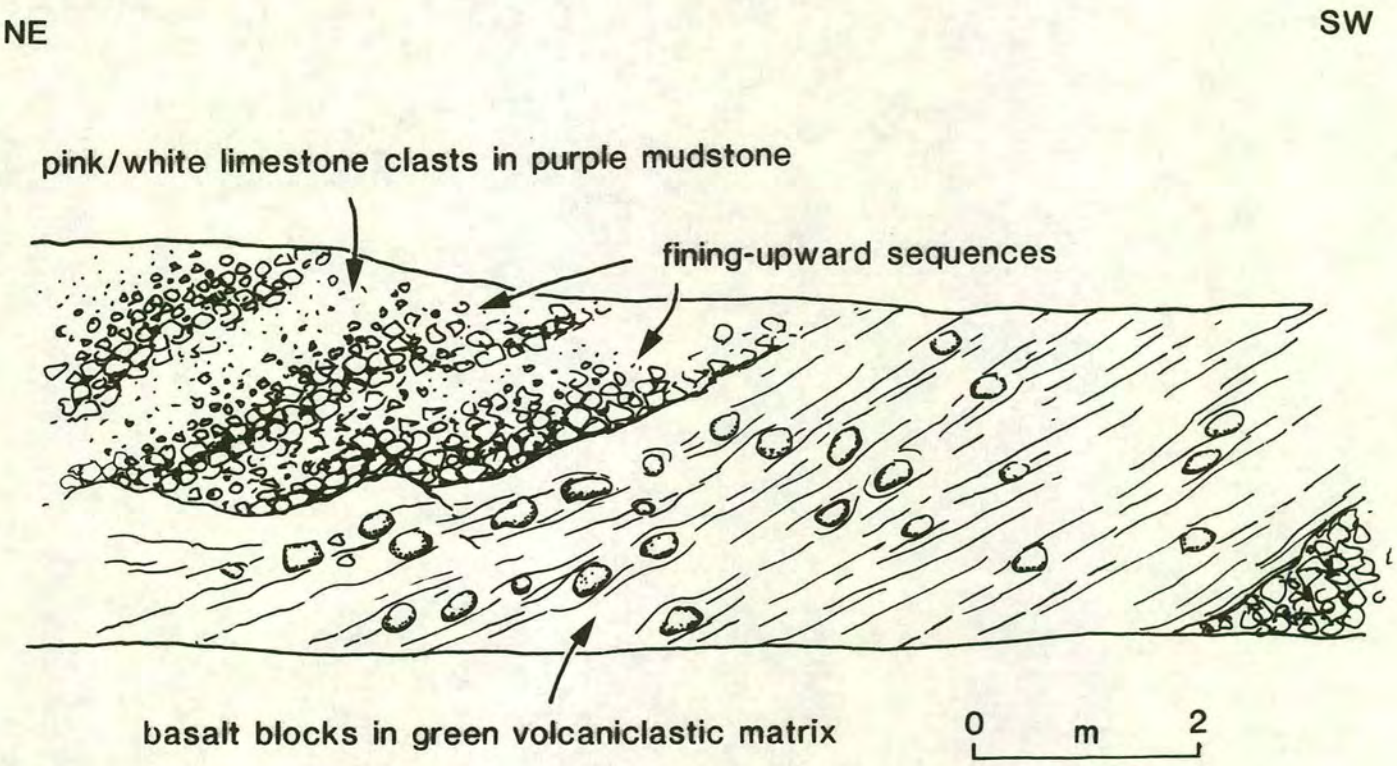

Figure 4.10 Field sketch along the road to Çalköy, showing the fining-upward sequences in the limestone-rich debris flow and the underlying, predominantly volcanogenic debris flow.

and 4.11a). It has a sharp base and overlies a volcanic-rich debris flow, with a 2cm-thick intervening layer of fine-grained pink mudstone. The clast-size and thickness of the debris flow varies laterally and contains a limestone block which is approximately 10m by 20m in size. This block is juxtaposed against volcanics with a primary contact. Brecciation at the edges of the block occurs to a depth of 5cm. The brecciated zone is very similar to the conglomerates described above, implying that much of the debris flow was derived from the break-up of similar large limestone blocks. The volcanic material adjacent to the limestone block comprises dark brown pillows (15cm-1m in diameter) surrounded by green-yellow interpillow material. The pillows appear to be *in situ* and may represent a primary volcanic flow intercalated with the debris flow. Another possibility is that the pillows were transported a short distance as intact clasts within a volcanogenic debris flow.

This association is the only observed example, within the Çal Unit as a whole, of a debris flow which displays two distinct phases of conglomerate formation. Small limestone clasts from slightly different sources (as indicated by their different colours of white, pink and dark pink) were incorporated into a conglomerate, which subsequently became disrupted. As a result of this disruption a second conglomerate was formed. An example of this lithology is shown in Figure 4.11b, where it can be observed that the limestone clasts within the dark, fine-grained matrix are themselves made up of sutured limestone clasts.

Thin-section study shows that the limestone clasts are very recrystallized and are fused along their edges. The interstitial material is thus found along sutures and pressure solution seams. Figure 4.11c is a photomicrograph of a sample from the limestone-rich debris flow shown in Figure 4.11a and 4.11b. A mixture of volcanic and limestone components are present. The limestone clasts are micritic and contain fragments of bryozoa, echinoids, foraminifera, shells, algae and a stromatolite/oncoid. Sparry calcite forms a matrix to the carbonate fragments and replaces them in places. The volcanic clasts are fine-grained and purple, green and brown-black in colour. They include fine-grained basalt, glass and green chloritized material. The basaltic clasts display volcanic textures, such as aligned albitized plagioclase laths and relict pyroxene phenocrysts. The boundaries around all the clasts are stylolitic and defined by irregular seams of fine-grained dark material and opaques. Calcite fragments are commonly incorporated within these zones. Rare quartz clasts with undulose extinction were also observed.

Figure 4.11

(a) A view of the contact between the limestone-rich debris flows (upper part of photograph) and the underlying volcaniclastic debris flow (as sketched in Figure 4.10).

(b) A closer view of the limestone-rich debris flow shown in (a). Note the suturing around the limestone clasts and the interstitial, fine-grained, purple volcanogenic mudstone.

(c) Photomicrograph of the lithology shown in (b). Fine-grained green volcanic material can be clearly seen around sutured clasts of bioclastic limestone (PPL, field of view: 20mm)

a

b

c

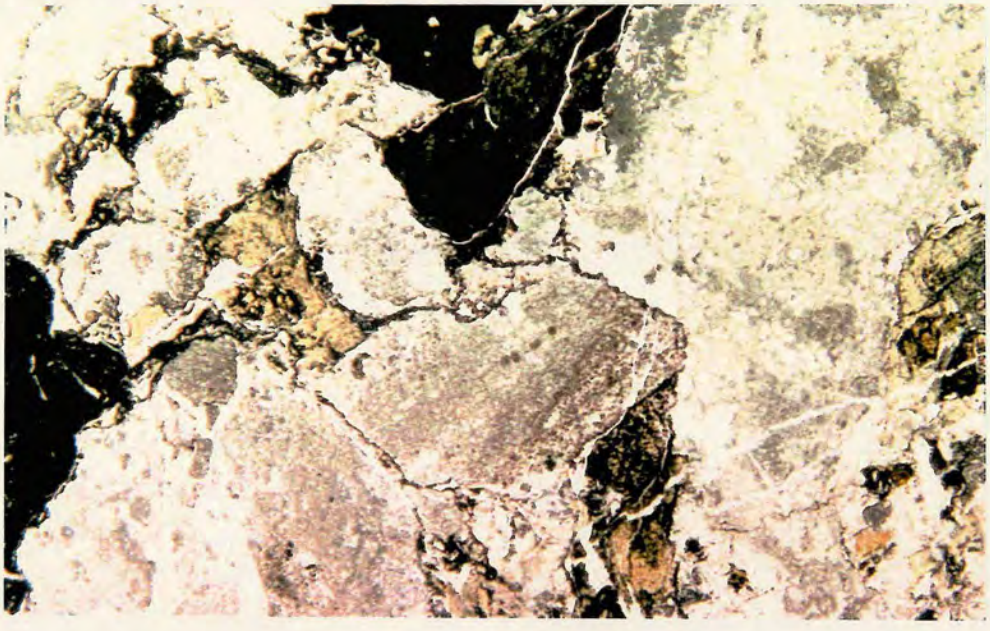

b) Volcanic-rich debris flow

An example of this lithology is the debris flow which is found immediately beneath the limestone debris flow described above (see lower part of photograph in Figure 4.11a). It is yellowish-green and has a very rubbly appearance. Unlike the flow above it is matrix-supported and contains clasts of volcanic origin, including fragments of pillow lava. Most of the clasts are highly weathered dark purple basalt and green spilitized basalt up to 30cm by 15cm in size. The matrix is volcanogenic siltstone to coarse-grained sandstone and reworked volcanic detritus. The flow has a sharp top which is overlain by 2cm of pink mudstone. The base of the flow was not clearly exposed.

The basaltic clasts are predominantly porphyritic and contain abundant phenocrysts and glomerophenocrysts of clinopyroxene (olivine was also observed in sample 21/10/91-2), together with round amygdales, in fine-grained and devitrified glass groundmasses. The clinopyroxenes are euhedral and are in various stages of replacement by calcite (e.g. Figure 4.13a). Sample 22/8/92-34 is spherulitic and porphyritic. Chloritized spherulites and clinopyroxene crystals are set in a groundmass which displays intersertal, intergranular and subophitic textures.

c) Limestone and volcanic debris flow

A facies containing almost equal proportions of limestone and volcanic clasts is the most common type of debris flow in the unit as a whole. This facies is present above and below the two associations outlined above and is invariably matrix-supported with clasts of vesicular basalt and recrystallized grey limestone. Limestone is present as blocks up to several metres in size, although the average size is 10-30cm. The volcanic clasts are generally smaller and have an average size of 10cm. The matrix is sheared brown and red volcanogenic mudstone. Sedimentary structures such as grading were not observed.

In the upper part of the Çal Unit near the village of Çalköy, thin beds of red shale and pink pelagic limestone occur as an intercalation within the debris flows of this association. The beds are up to 15cm thick and are laterally discontinuous over several metres. Deformed calcturbidites are present within the debris flows of this association. They are exposed as poorly-defined regions within the debris flows and were probably distinct blocks which became disrupted during deposition of the debris flow. Two blocks of calciturbidites were observed along the road to Çalköy. They

consist of thin-bedded grey and pink limestone respectively and are both considerably folded.

4.6.2 Summary

The Çal Unit in its type locality can thus be divided into a series of debris flows of which three are clearly exposed. Two of the debris flows: the volcanic-rich and limestone-rich flows (Figures 4.10 and 4.11a) are separated by a sharp stratigraphic contact. The limestone-rich debris flow differs from the others in being clast-supported. It contains a series of fining-upward layers, indicating that the sequence is the right way up. An interesting feature of this debris flow is the two phases of conglomerate development. The origin of this is well illustrated by a large limestone block which displays fracturing and conglomerate formation around its margins. A lower debris flow contains both limestone and basalt clasts in a sheared shaly matrix.

4.6.3 Karaasik section

The road which connects the villages of Asagikaraasik (Lower Karaasik) and Yukarikaraasik (Upper Karaasik) is a good reference section for the lower levels of the Çal Unit (Figure 4.8). These two villages lie off the main Yenice-Çan road close to the village of Çalköy. The main lithological associations along this road are described below.

a) Limestone breccia

Limestone breccia crops out near the top of the Karaasik section and consists of blocks of limestone up to 0.5m in size in a matrix of volcanic debris. Some of the volcanic material may be weathered primary lava flows interbedded with the blocky material. The limestone blocks in this association commonly display coralline and algal associations. A very similar lithological association is exposed along the main Yenice-Çan road, at the base of the Çal section, and is here taken to be part of the same horizon, thus allowing correlation between the two sections.

b) Volcanic flows with red mudstone

An intact bedded sequence occurs below the limestone breccia described above. Thin lava flows are intercalated with red and yellow mudstones (Figures 4.12 and 4.13b). The lava flows are approximately 6-25cm thick and highly silicified, a feature which led to their erroneous interpretation as bedded chert by Okay *et al.* (1991). Rare

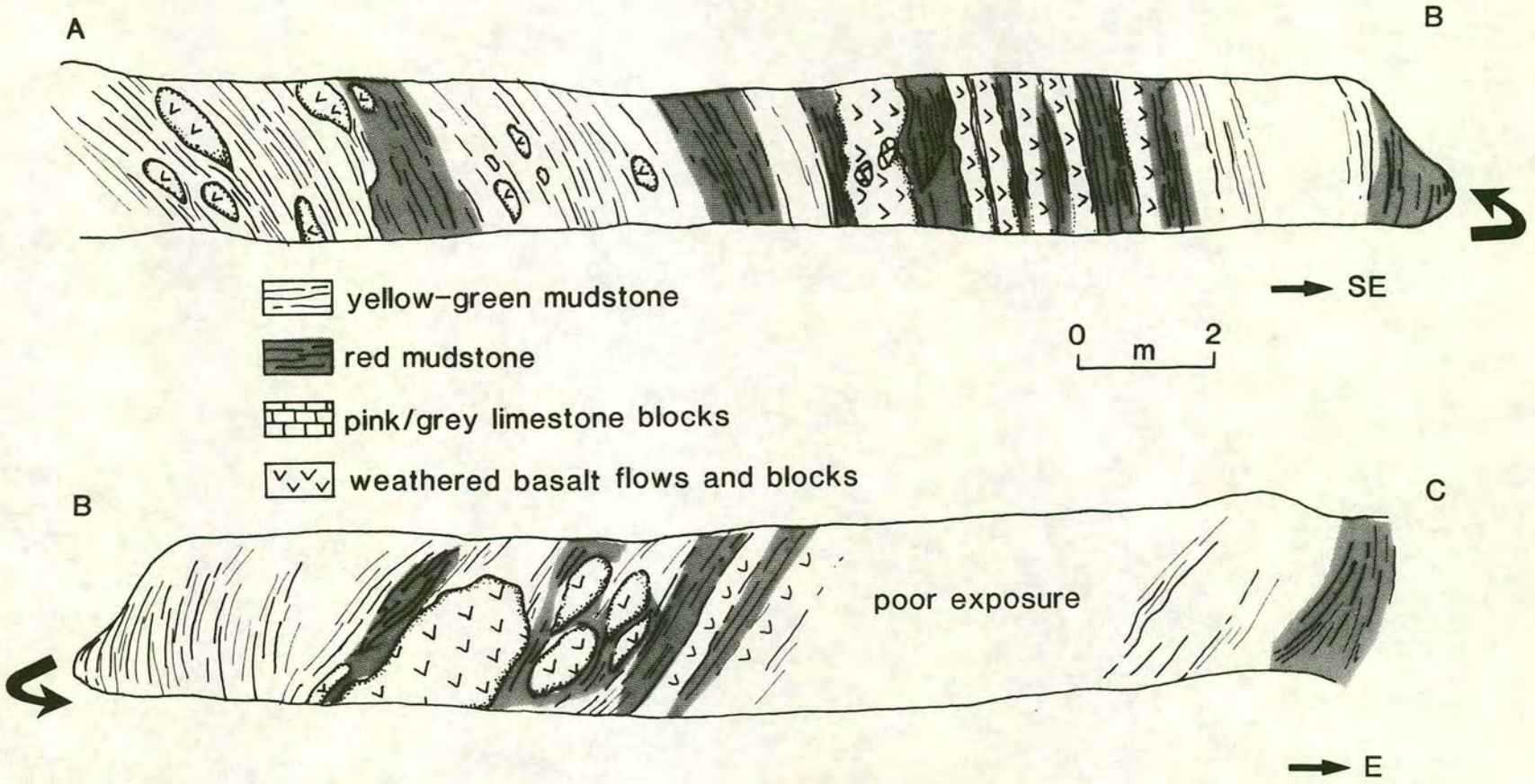

Figure 4.12 Field sketch along the road between Aşagıkaraaşık and Yukarıkaraaşık, showing the alternating horizons of red and yellow-green mudstone, debris flows and thin lava flows.

Figure 4.13

(a) Photomicrograph of porphyritic basalt from a block in the Çalköy section (sample 21/10/92-2). The basalt displays glomerophenocrysts of clinopyroxene altered to calcite (PPL, field of view: 8.5mm).

(b) Field photograph of steeply dipping, thin basaltic lava flows along the Karaasik road. The lava flows stand out in relief against the interbedded red mudstone.

(c) Rounded blocks of basalt in a matrix of red mudstone along the Karaasik road.

a

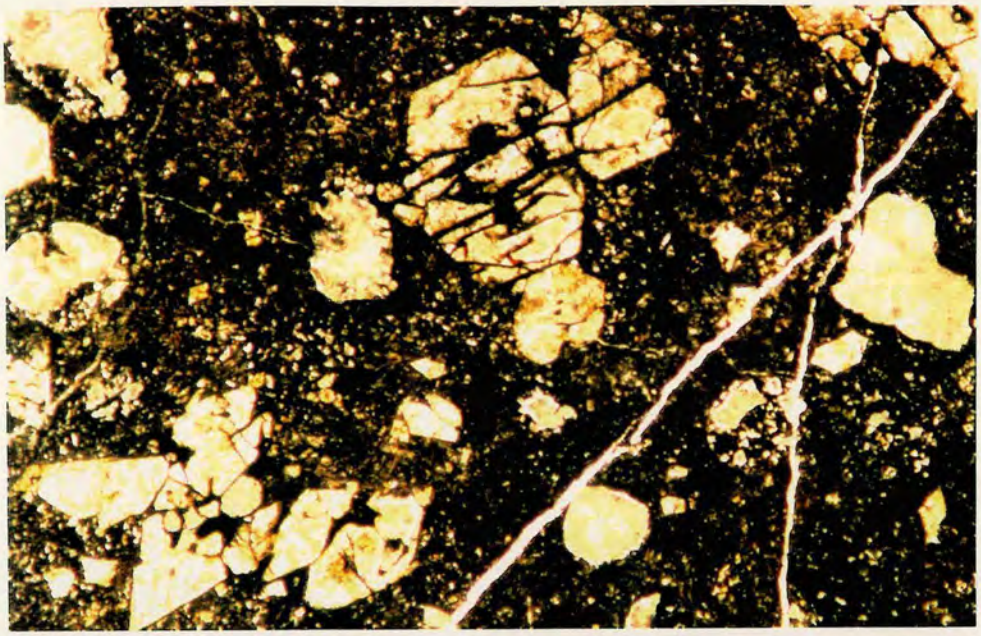

b

c

limestone clasts are found within the flows. The flows are overlain and underlain with primary stratigraphic contacts by mudstones and thin debris flows. The mudstones are generally red to red-brown in colour and contain green-yellow bands whose colour may be due to leaching or an increased ash content. The debris flows contain basalt and limestone clasts in a muddy and volcanogenic matrix (Figure 4.13c). Thin grey bands within the mudstones may represent ash layers. Several metres below the lava flows is an outcrop of thin-bedded pink cherty limestone.

c) Interbedded sandstone and shale

A sequence of interbedded sandstone and shale occurs at the base of the Karaasik section. The sandstone is grey, medium- to coarse-grained and rich in mica and feldspar. It is intercalated with thin beds of pale green siltstone and fine-grained sandstone. There is a fault contact between the clastics and the overlying debris flow/mudstone/lava assemblage. A sliver of the same sandstone occurs higher in the sequence, implying that the clastics were deposited elsewhere and subsequently faulted into the debris flow sequence.

4.7 Lithologies of the Çal Unit in the Edremit area

The Çal Unit is also exposed, although to a lesser extent, in the region of Edremit in the southern part of the Biga Peninsula. Figure 4.14 schematically shows the relationship of the Çal Unit with the other units in this region. The unit occurs as klippen on the tops of hills north of Edremit, namely Pasadag, Kir Tepe and Çigdem Tepe (Figure 4.15). In the Edremit region the range of lithologies of the Çal Unit is much less than in the Çan area. Limestone is the predominant lithology in the Edremit area and debris flows are not observed. Although no deductions about the sequence of the Çal Unit can be made from the lithologies in this area, the large size of the limestone blocks compared to those in the Çan area allows a more detailed interpretation of the setting of the Çal Unit as a whole.

The predominant lithology of the Çal Unit in the Edremit area is limestone. Limestone forms prominent caps on the hills of Pasadag, Kir Tepe and Çigdem Tepe and is either made up of several large discrete blocks, each 10s of metres across, or a disrupted section of a carbonate platform. It is impossible to distinguish between these two alternatives on the basis of the exposed limestone. Matrix is locally exposed near the base of the klippe on Çigdem Tepe and comprises red mudstone and micaceous sandstone. Volcanic rocks were observed only as loose blocks and as a

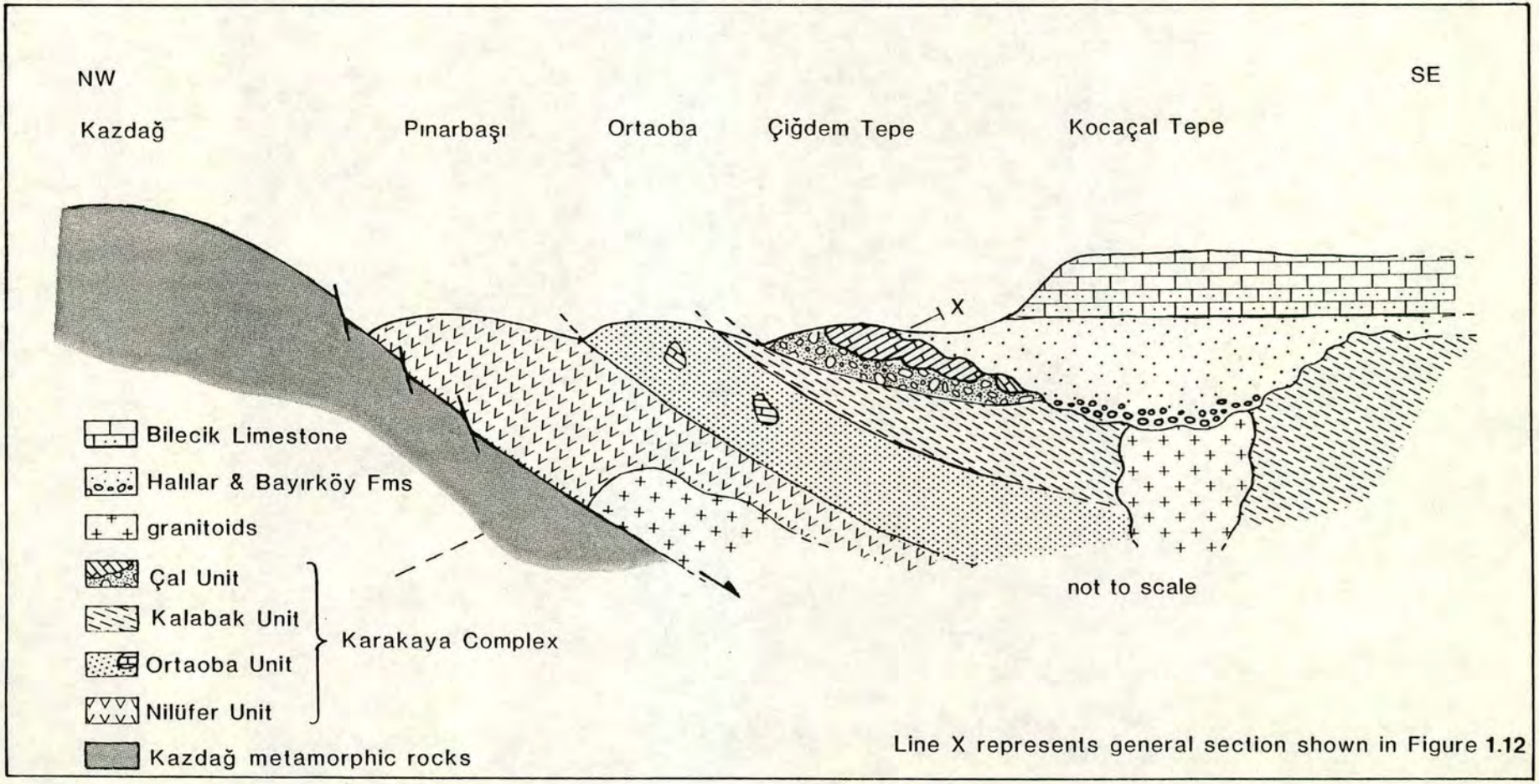

Figure 4.14 Schematic cross-section of the Edremit region, showing the relationship of the Çal Unit with the tectonically underlying Kalabak Unit and the overlying sedimentary cover.

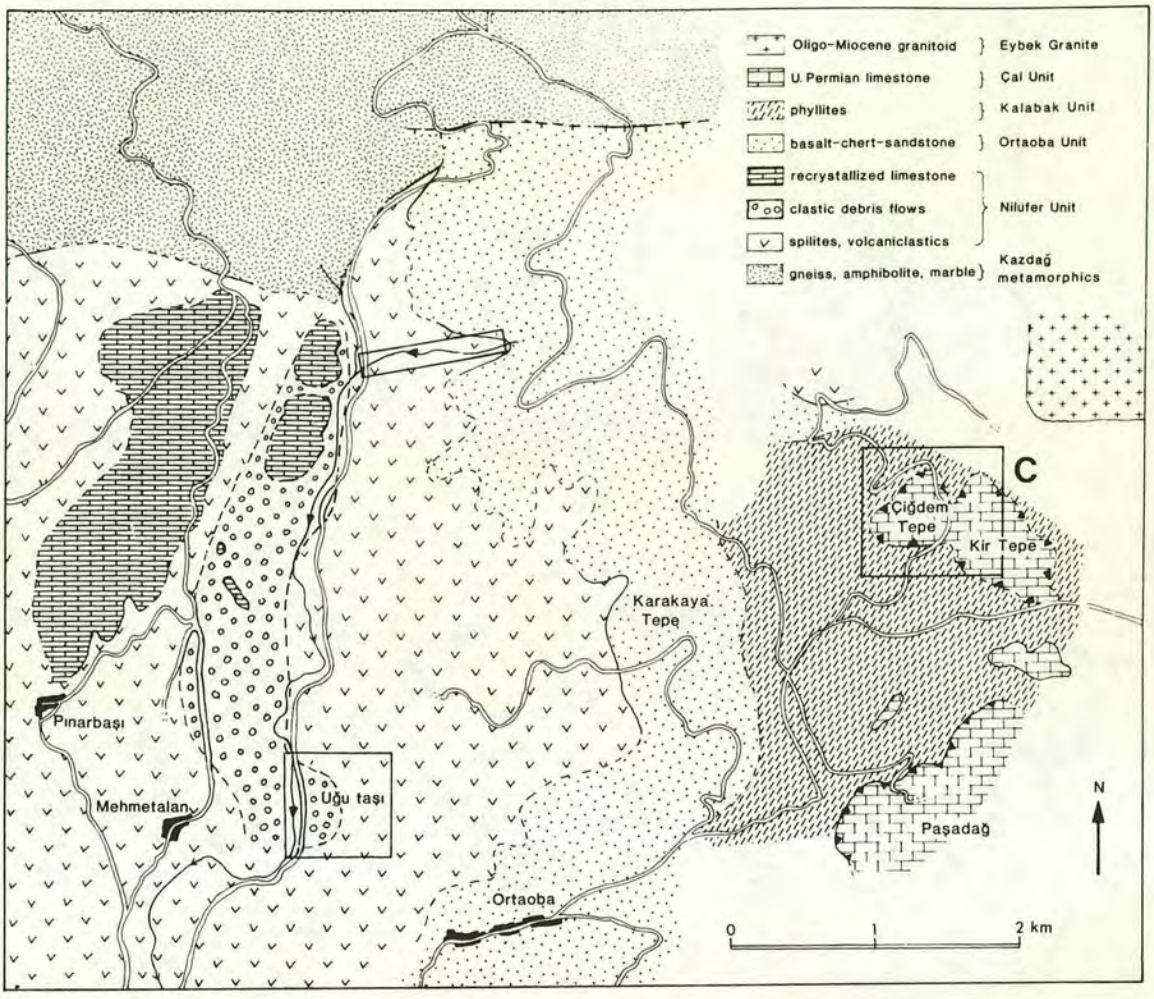

Figure 4.15 Geological map of the region north of Edremit (based on my own fieldwork and an unpublished map by Okay *et al.*, 1991). The box marked C marks the best exposure of the Çal Unit in this region and is shown in more detail in Figure 4.16.

small poorly exposed outcrop in the road. The outcrops on Çigdem Tepe are too small to display any features diagnostic of a debris flow.

4.7.1 Çigdem Tepe

Limestone facies of the Çal Unit are best exposed along the track which runs around the east flanks of Çigdem Tepe, 1.5km northeast of the village of Ortaoba (Figures 4.16 and 4.17).

a) Limestone

The limestone which crops out on the hills north of Edremit displays varying degrees of recrystallization but is mostly massive, pale grey and fossiliferous. The limestone contains a rich assemblage of thin-shelled bivalves, calcispheres, bryozoa, red algae, echinoids and foraminifera (especially fusulinids). The faunal assemblages are described in more detail in Section 4.7.3. The limestone is predominantly micritic with extensive sparry replacement in places. In the more micritic parts excellent sedimentary structures and redeposited fossil debris were observed. An outcrop of limestone on the east side of Çigdem Tepe was studied in detail. The limestone at this locality contains a sequence of thin- to medium-bedded micrite, clearly defined by alternating layers of shelly micrite and finer-grained bioclastic micrite, as shown in Fig. 4.18. The shelly layers are mid grey in colour and contain abundant curved shell fragments which have no preferred way-up. The alternate layers are lighter grey and consist of fine-grained bioclastic debris in a micritic matrix. One layer contains a discontinuous band of ooids, foraminfera and molluscan shell debris (Figure 4.19a). The ooids are irregular and consist of sparry calcite nuclei with thin cortices of brown micrite. The cortices generally consist of one to a few concentric micritic laminae. The ooids and fossils lie in matrix-supported sparry calcite.

Laterally discontinuous horizons of matrix-supported limestone conglomerate occur within the bedded sequence. One of these is shown in Fig. 4.17b. The types of limestone which form clasts in these bands include oolite, finely-laminated bioclastic micrite, shell-rich micrite, homogenous micrite and one stromatolitic fragment. The clasts are angular and commonly rectangular and represent broken and redeposited fragments of thin beds. Many clasts are at a high angle to bedding, implying that they were deposited in a high energy environment. The matrix to the clasts is fine-grained bioclastic micrite with evidence of small-scale channelling. An example is shown in Fig. 4.17b where a small channel has cut into the top of the breccia layer. The infill is

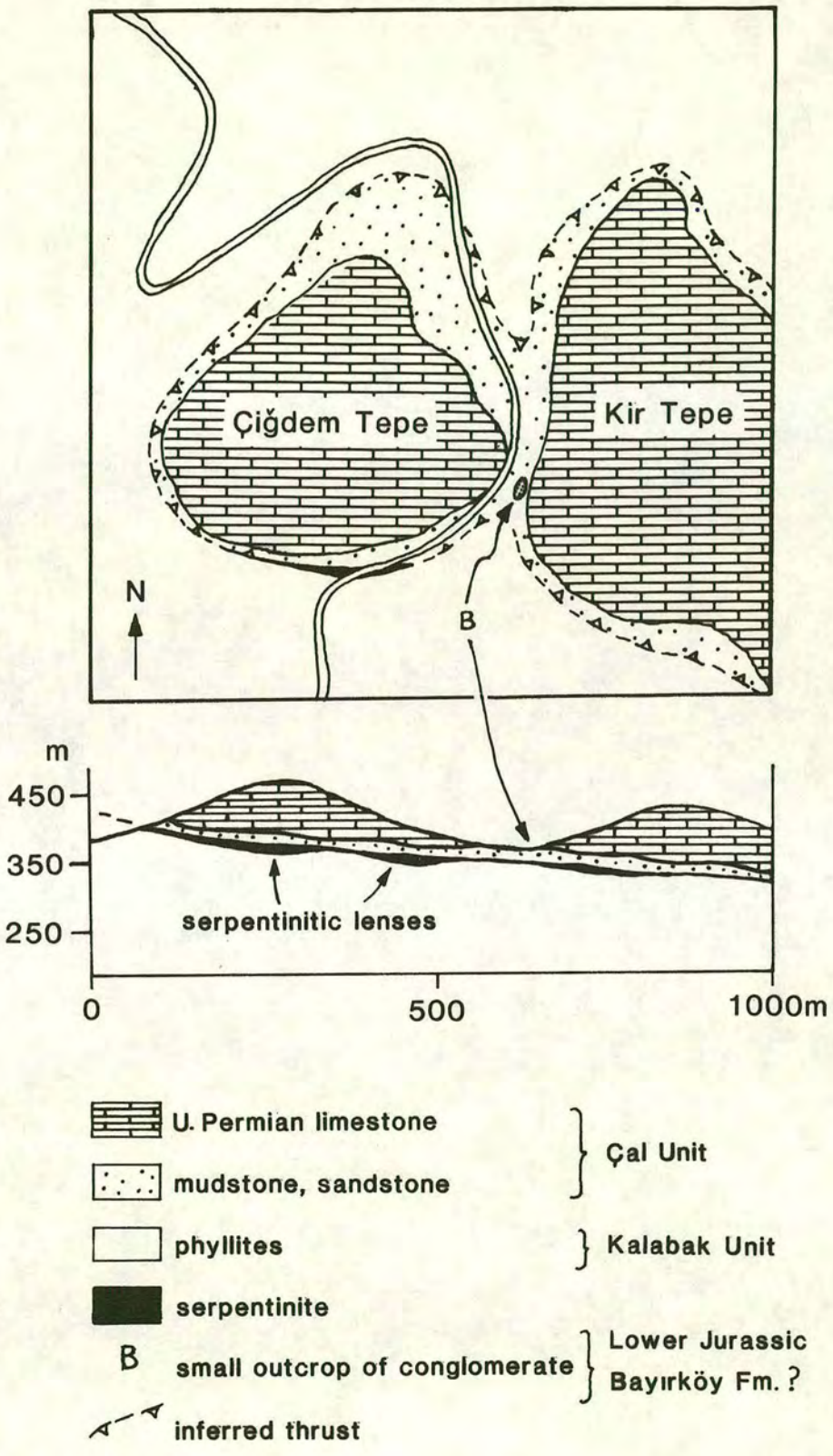

Figure 4.16 Sketch map and cross-section of the region around Çiğdem Tepe and Kir Tepe (based on my own fieldwork and an unpublished map by Okay *et al.*, 1991).

Figure 4.17

(a) View of Çigdem Tepe and Kir Tepe from the south. The sketch of the photograph shows the position of the inferred thrust between the Çal Unit and the underlying Kalabak Unit.

(b) Field photograph of part of a laterally discontinuous horizon of limestone clasts and redeposited bioclastic debris on the east side of Çigdem Tepe. The rectangular clast at a high angle to bedding is comprised of ooids.

a

W

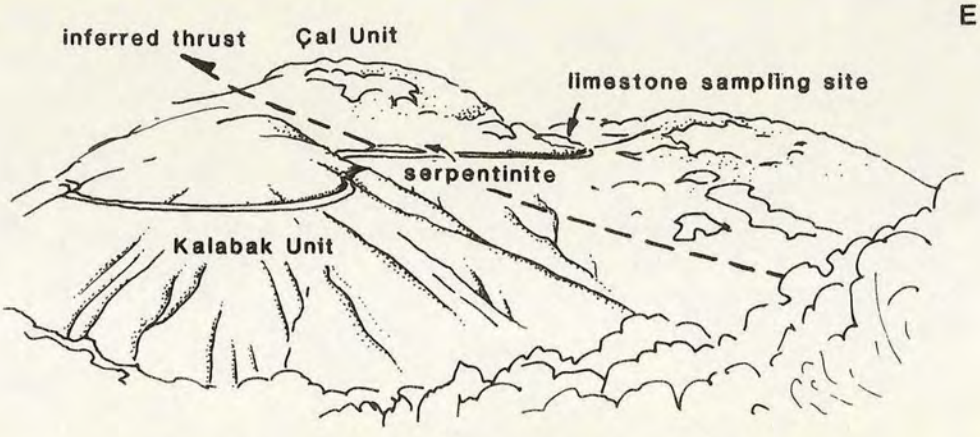
inferred thrust
Çal Unit
limestone sampling site
serpentinite
Kalabak Unit

E

b

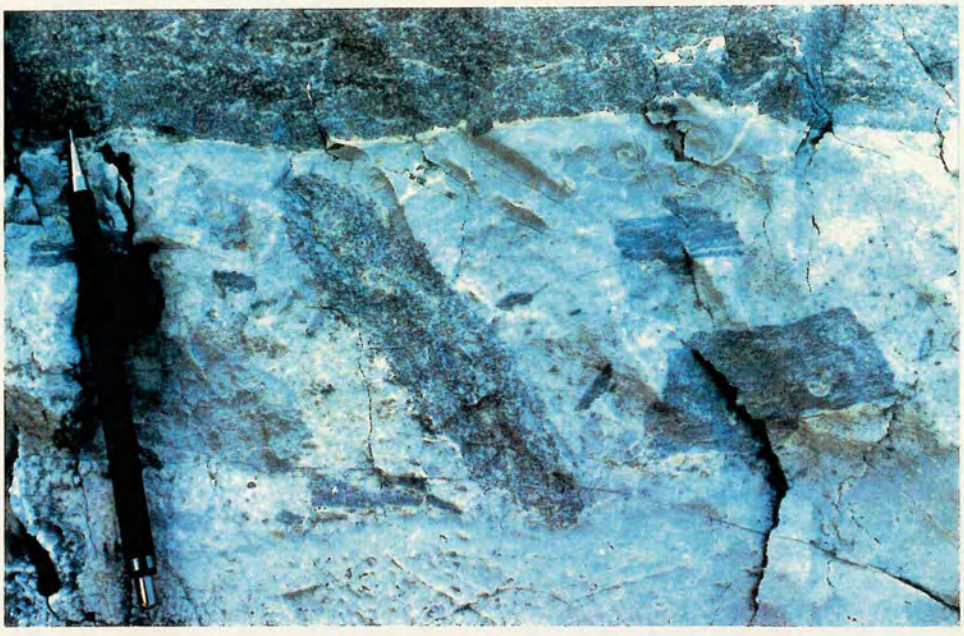

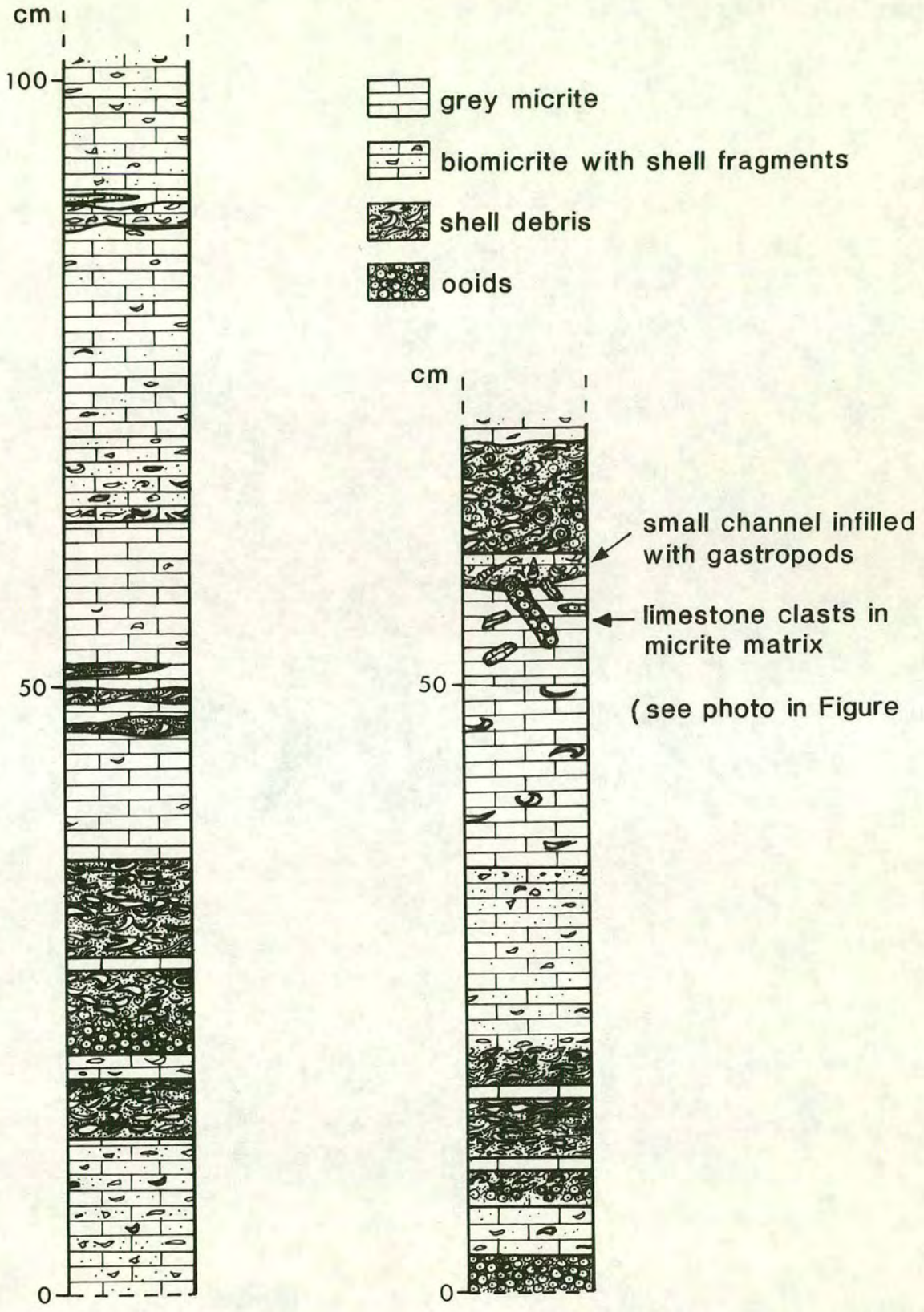

Figure 4.18 Representative logs through the redeposited limestone facies on the east side of Çigdem Tepe.

white micrite and contains gastropods, which display geopetal structures and indicate that the sequence, in this block at least, is the right way up. The large oolite clast can be seen to cut into the channel, implying that it was more lithified than its matrix during formation of the channel and thus was more resistant to winnowing.

On Pasadag the limestone of the Çal Unit is white and recrystallized with little fossil preservation. One sample from this region displays silica replacement and beige dolomitic laminations.

b) Red mudstone

Poor outcrops of red-brown mudstone are found directly below the lowermost limestone outcrop on the east side of Çigdem Tepe. The mudstone contains silt-grade fragments of mica and is unfoliated.

c) Micaceous sandstone

Closely associated with the mudstone (and occurring as blocks within it) is poorly exposed fine- to medium-grained sandstone. The sandstone is dark grey-green and consists predominantly of angular quartz and feldspar grains in a muddy, clay and mica-rich matrix.. The sandstone is immature and poorly sorted and contains quartz, muscovite, biotite, altered alkali feldspar, plagioclase, opaques, lithic clasts and secondary chlorite. The quartz ranges from showing undulose extinction to being very recrystallized. There is a wide range of lithic clast lithologies, including foliated micaschist, shale, basalt, myrmekitic quartz-feldspar and speckled grey material which could be either chert or devitrified basalt. Rare detrital grains of rutile were also observed. The matrix is a grey-brown mixture of fine-grained quartz, clays, opaques and chlorite. Orange-brown rims of clays and opaques are present on many clasts. Stylolitic seams around grains and clay-rich shear zones are common features.

4.7.2 Limestone fauna of the Çal Unit

The limestone which caps the hills of Çigdem Tepe and Kir Tepe contains a rich fauna of pelagic foraminifera and red algae. Fossils were identified by M. Lys (pers. comm., 1991) and include:

Tubiphytes obscurus Maslov, *Climacammina sphaerica*, *Geinitzina* sp., *Colaniella parva*, *Tuberitina* sp., *Reichelina* sp., *Glomospira* sp., *Dagmarita chanakchensis*, *Glomospirella* sp., *Lasiodiscus* sp., *Globivalvulina* sp., *Pachyphloia* sp., *Pachyphloia*

Figure 4.19 Photomicrographs of bioclastic limestone on the east side of Çigdem Tepe (sampling site marked on sketch in Figure 4.17).

(a) Layer of irregular ooids and micrite-coated grains within redeposited bioclastic limestone which predominantly comprises shell fragments, foraminifera and micrite clasts (PPL, field of view: 26mm).

Examples of Upper Permian foraminifera from the Çal Unit on Çigdem Tepe (identified and dated by M. Lys).

(b) *Pachyphloia* sp. (sample 85b/90, PPL, field of view: 1.4mm).

(c) *Dagmarita chanakchensis* (sample 85b/90, PPL, field of view: 5.5mm).

a

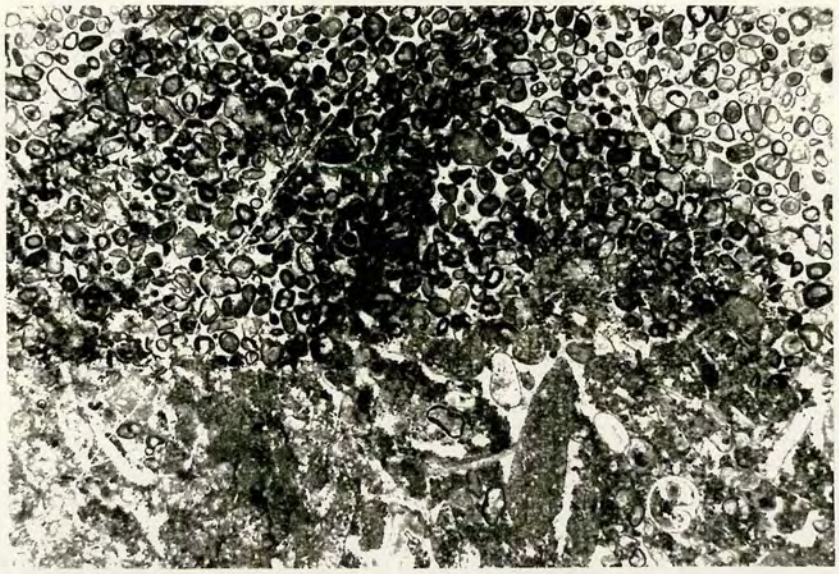

b

c

Figure 4.20

Examples of Upper Permian algae and foraminifera from the Çal Unit on Çigdem Tepe (identified and dated by M. Lys).

(a) The red alga *Tubiphytes obscurus* Maslov (sample 85b/90, PPL, field of view: 7.8mm)

(b) *Climacammina sphaerica* (sample 85b/90, PPL, field of view: 5.5mm).

(c) *Colaniella parva* (sample 85b/90, PPL, field of view: 3.5mm).

a

b

c

Schwageri, *Hemigordius* sp. (affinity with *Hemigordius reicheli* Lys), *Hemigordius longus* and *Paraglobivalvulina* sp. (*mira*?).

Examples of the foraminifera from this site are shown in Figures 4.19 and 4.20. The presence of the photosynthesizing red alga *Tubiphytes* indicates a shallow marine setting and implies that the mainly pelagic faunal assemblage was deposited in a near-shore environment. All the other fossils listed above are pelagic foraminifera, except for *Tuberitina* sp. which is benthic.

An assemblage of corals, brachiopods, gastropods, ostracods and echinoids in limestone blocks from the Çan area (Okay *et al.*, 1991) also indicates a shallow marine setting. Many of the blocks in the upper part of the Karaasik section are coralline and/or algal, which contrasts with the redeposited nature of the Çal limestones near Edremit. A rich foraminiferal assemblage is also present in the Çan area and was described by Okay *et al.* (1991). According to their work samples yielded:

Ammodiscus sp., *Glomospira* sp., *Archaesphaera* sp., *Bisphaera* ? sp., *Tuberitina* sp., *Pachyphloia* sp., *Paleotextularia* sp., *Cribogenerina* sp., *Globivalvulina* sp., *Reichelina* ? sp., *Codonofusiella* ? sp., *Yangchienia* ? sp., *Schwagerina* sp., *Neoschwagerina* sp. and *Pseudovermiporella* sp.

The foraminifera from the Çigdem Tepe site indicate a Late Permian age and, more specifically, Dorashamian, the last stage in the Permian, as indicated by the diagnostic *Colaniella parva* (Figure 4.20c) (identified and dated by M. Lys, 1991). Limestone blocks from the Çan area also yield an Upper Permian assemblage.

4.7.3 Çanlibaba area

The Çal Unit crops out in the valley at Çanlibaba, 2km NE of Edremit (Figure 4.21). It is overlain by Liassic sandstones, shales and limestones of the Bayirköy Formation and Bilecik Limestone. In the bottom of the valley there is a sheared outcrop of red mudstone and green calcareous shale. Lenses of sheared sandstone and blocks of medium- to coarse-grained green sandstone are found within the sheared mudstone. Small duplex structures were observed within the outcrop.

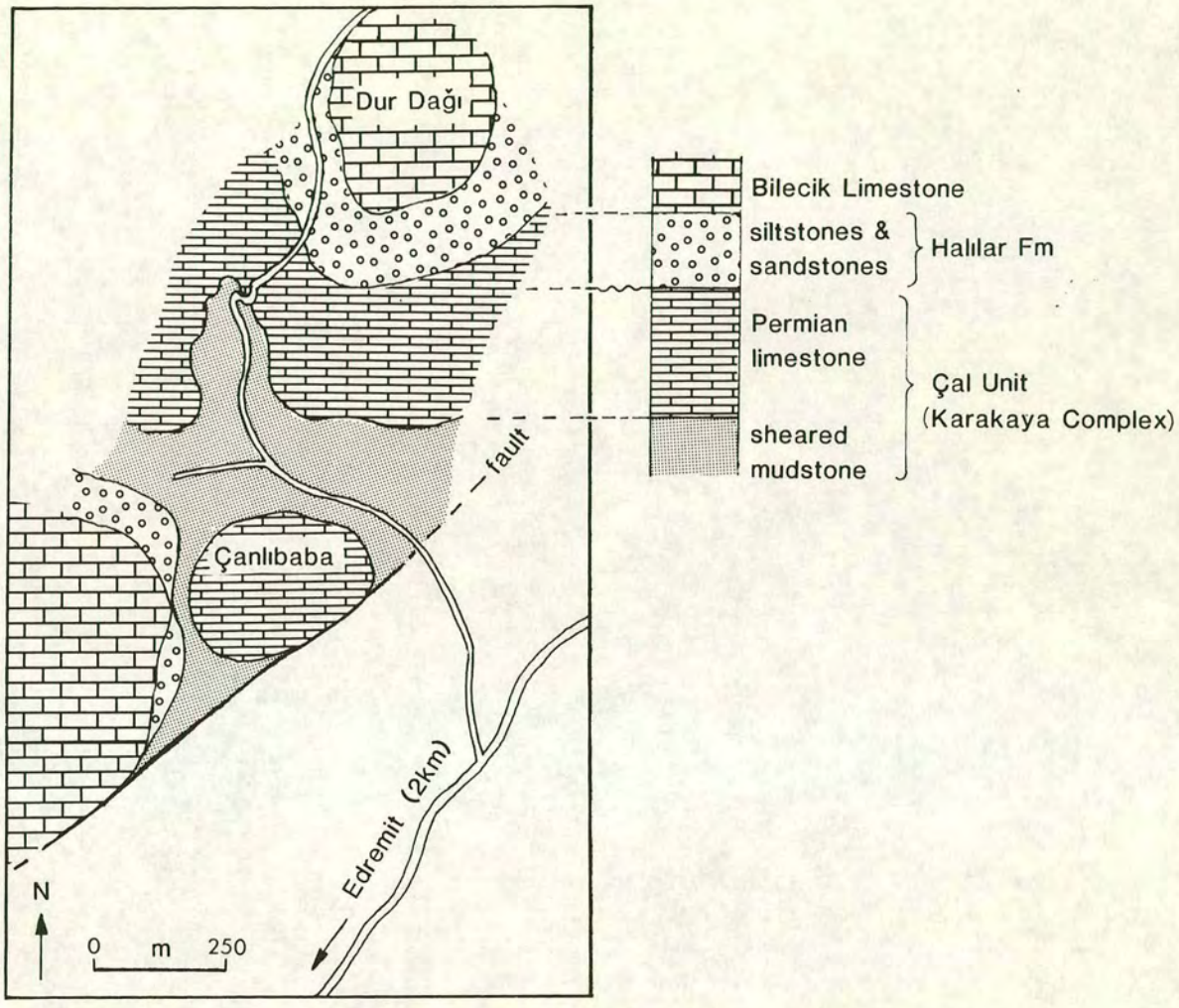

Figure 4.21 Sketch map of the Çanlibaba region 2km NE of Edremit, showing the Çal Unit overlain by clastics of the Upper Triassic-Liassic Halilar Formation (based on my own fieldwork and an unpublished map by Okay *et al.*, 1991).

4.8 Contacts and structure of the Çal Unit

4.8.1 Bergama area

As shown in the map of the area north of Bergama (Figure 4.1), the disrupted carbonate platform which makes up the Çal Unit in this region is thrust over the Nilüfer Unit. A thrust sheet of Permian limestone was observed near the village of Adaköy (Figure 4.3). Clastics containing volcanogenic material and basaltic blocks lie directly beneath the brecciated thrust zone and it is unclear whether they represent a slice of the platform basement or clastic debris flows associated with the upper levels of the Nilüfer Unit. Sheared clastics were also observed near the villages of Hacilar and Halilaga and are interpreted to be the base of the platform. The extent of internal deformation of the platforms is difficult to assess as the limestone is broken up into coherent blocks surrounded by sheared clastics.

4.8.2 Çan area

Near Çalköy in the Çan region the upper contact of the Çal Unit can be clearly observed. A green volcaniclastic debris flow containing basalt blocks is sharply overlain by conglomerates of the Lower Jurassic Bayirköy Formation, which pass up into calcareous sandstones and siltstones. The basal conglomerates contain abundant rounded basaltic clasts which were clearly derived directly from the volcaniclastic debris flows of the underlying Çal Unit.

Below the Çal Unit lie volcanogenic schists, called the Sazak Metatuffs by Okay *et al.* (1991) after the village of Sazak, south of Yenice (Figure 4.8). Okay *et al.* (1991) regarded these metavolcanic rocks as being part of the widespread, predominantly volcanic, Nilüfer Unit (see Chapter 2). Although the contact between the Çal Unit and the Sazak Metatuffs was not observed it is presumed to be tectonic on the basis of the Çal Unit's well-exposed basal tectonic contacts near Bergama and Edremit.

Internal deformation of the Çal Unit is minimal in the Çan area. The well-exposed debris flows along the road to Çalköy display some degree of shearing which is most apparent in the middle and lower parts of the section. Shear planes dip NE and rare duplexes indicate motion to the west. In places the shaly volcaniclastic matrix has a crude foliation which drapes around the volcanic and limestone clasts. Many of the volcanic clasts have slightly phacoidal shapes and smooth surfaces which may

indicate tectonic shearing. Most of the road section however, displays undisturbed primary contacts between various lithological associations. Deformed calcturbidites are found in the central portion of the Çal section. Brittle deformation has given a "broken" appearance to the beds, which are also slightly undulose with an amplitude of 1-2m. A few small-scale folds with NW-dipping axial planes, NE-plunging fold axes and possible vergence towards the SE were observed.

Along the Karaasik road most of the lithologies are likewise relatively undeformed. Figure 4.12 shows a relatively undeformed sequence of red mudstones, yellow-green shales and thin lava flows. The lowest unit observed along the Karaasik road is a sequence of alternating sandstones and mudstones. Despite being fault-bounded the sliver is internally coherent and the lithologies are totally undeformed. Even the mudstones, which would readily record any shearing, show no evidence of foliation development and break with a conchoidal mudstone fracture.

4.8.3 Edremit area

In the Pasadag area near Edremit the Çal Unit lies tectonically over phyllites of the Kalabak Unit, forming the hills of Çigdem Tepe, Kir Tepe, Pasadag and Durdag (Figures 4.15 and 4.21). The contact is shallowly dipping to the ESE and, on Çigdem Tepe, is marked by a zone of highly sheared pale green sepentinitic material (Figure 4.17). Directly below the fault zone are dark phyllites of the Kalabak Unit, while above it lie undeformed sandstones and red siltstones of the Çal Unit. The clastics form a thin layer of a few metres above the fault zone and pass directly into the limestone which forms the bulk of the Çal Unit in the Edremit region. On Pasadag the contact is less sharp and is marked by a zone of intense shearing which incorporates lithologies from both the Çal Unit and the underlying phyllites of the Ortaoba Unit. Folds and shears imply thrusting towards the NW.

The upper boundary of the Çal Unit in the Pasadag region is marked by a small exposure of conglomerate lying stratigraphically above the limestone on Kir Tepe (Figure 4.16). The actual contact is not exposed but is clearly sharp. In the Çanlibaba region just north of Edremit, Çal limestone is overlain by sandstones and mudstones. Similarly, the contact is not exposed but can be located to within 2m on the basis of soil colour and block distribution. As with Çigdem Tepe the main feature of the contact is the sharp difference in metamorphic grade, lithology and deformation.

On Çigdem Tepe there is a marked contrast between the sheared phyllitic rocks of the Kalabak Unit and the tectonically overlying Çal Unit which contains virtually undeformed sandstones and shales. The limestones which make up the bulk of the hill are also undeformed and display excellently preserved bedding and other sedimentary structures such as rafted clasts and scours. Even the individual shell fragments and ooids which make up many beds and clasts have retained their original shapes,despite partial recrystallization in places. Much of the limestone on Kir Tepe and Pasadag is highly recrystallized and devoid of fossils or sedimentary structures as a result. However, as with the well-preserved limestone on Çigdem Tepe, there is no evidence of shearing or deformation of any kind.

At Çanlibaba, however, red mudstones (presumed to be part of the Çal Unit) are highly sheared in places and display a strong foliation with internal asymmetric "fish" structures indicating top-to-NW shearing. This appears to be a fairly local phenomenon and on the whole the Çal Unit is undeformed relative to the other Karakaya units.

4.9 Geochemistry of the Çal Unit

4.9.1 Whole-rock geochemistry of basalt blocks

Volcanic clasts from the debris flows in the Çalköy and Karaasik sections were collected for geochemical analysis. Rare primary volcanic flows were observed in the Karaasik section, but owing to their very weathered and oxidized state only one sample was suitable for analysis by X-ray fluorescence. Highly amygdaloidal and veined clasts were not used, although small amygdales up to 1mm in size were unavoidable.

The SiO_2 values of the basalts are very variable, ranging from 34.97% (a highly altered sample) to 58.99%. The average values, however, are in the range 40-47%. MgO values are also very variable (1.28-11.65%) and tend to decrease up section. Basalts from the lower part of the Çal sequence (i.e. along the Karaasik road) display high MgO values ranging from 8.23% to 11.65%, implying a relatively primitive magma source. An exception is sample 23/8/19 which has an MgO value of 3.95%. Basalts higher in the sequence (i.e. along the Çalköy road) display generally lower MgO values. With the exception of samples 22/8/16, 21/10/2 and 22/8/18 (MgO values of 1.28%, 3.24% and 1.1% respectively) most of the values are in the range

6.06% to 8.77%. As the basalt samples were collected from blocks within chaotic debris flows it is not surprising that both primitive and more evolved types are represented at different levels in the sequence.

The trace elements were plotted on geochemical discrimination diagrams (Figures 4.22, 4.23 and 4.24) and MORB-normalized plots (Figures 4.25 amd 4.26). The Ti-Zr, Zr/Y-Zr and Ti/Y-Nb/Y plots are useful for distinguishing between MORB and WPB. The Cr-Y plot is used for separating IAT from MORB lavas and the Ti/Y-Nb/Y plot separates basalts into tholeiitic, transitional and alkalic varieties. The MORB-normalized plots show the variation of basalts from typical MORB and emphasize relative enrichments or depletions of particular elements within individual samples. The P_2O_5-Zr and Zr/Y-Ti/Y diagrams show that the basalts are alkalic and from a within-plate setting (Figure 4.22). This is confirmed by the other plots which show that they are of WPB geochemical type. On the Ti-Zr diagram the samples (with the exception of one of the Karaasik samples) plot in the WPB field and form a clear Ti-Zr fractionation trend (Figure 4.23b). A within-plate origin is also indicated by the Zr/Y-Zr, Cr-Y and Ti/Y-Ti/Y diagrams (Figures 4.23a and 4.24). The basalts cluster around the transitional/alkalic boundary in the Ti/Y-Ti/Y diagram and plot predominantly in the middle of the WPB field (Figure 4.24a). In most of the diagrams one sample 23/8/19 (from the Karaasik road) has an anomalous position with respect to the rest of the Çal basalts, due in most part to its low Zr, Nb and Ti values.

The within-plate characteristics of the Çal basalts are also apparent on MORB-normalized plots (Figures 4.25 and 4.26). Figure 4.25a shows basalts from the Karaasik road. Sample 23/8/92-4 was taken from a primary basaltic flow near Yukarikaraasik whereas 23/8/92-19 and 23/8/92-24 were from blocks surrounded by red mudstone further down sequence towrads Asagikaraasik. The plots for samples 23/8/92-4 (basalt flow) and 23/8/92-24 (block in debris flow) are almost identical, indicating that the ubiquitous basalt blocks are essentially "intra-clasts" and were derived from the same lava source as the primary flows. Sample 23/8/92-19 however, displays a much flatter pattern with slight HFS depletion and a pronounced Nb trough. Basalts from the road to Çalköy are shown in Figures 4.25b and 4.26 and represent samples taken at three main sites from the base to the top of the exposed sequence. All the plots display typical within-plate "humped" patterns and show enrichment in both LIL and HFS elements. Many of the samples show Ba depletions, possibly reflecting substitution for K in feldspar. A smooth slope downwards from Th to Sc is a characteristic feature of these basalts, especially those from the Karaasik road and

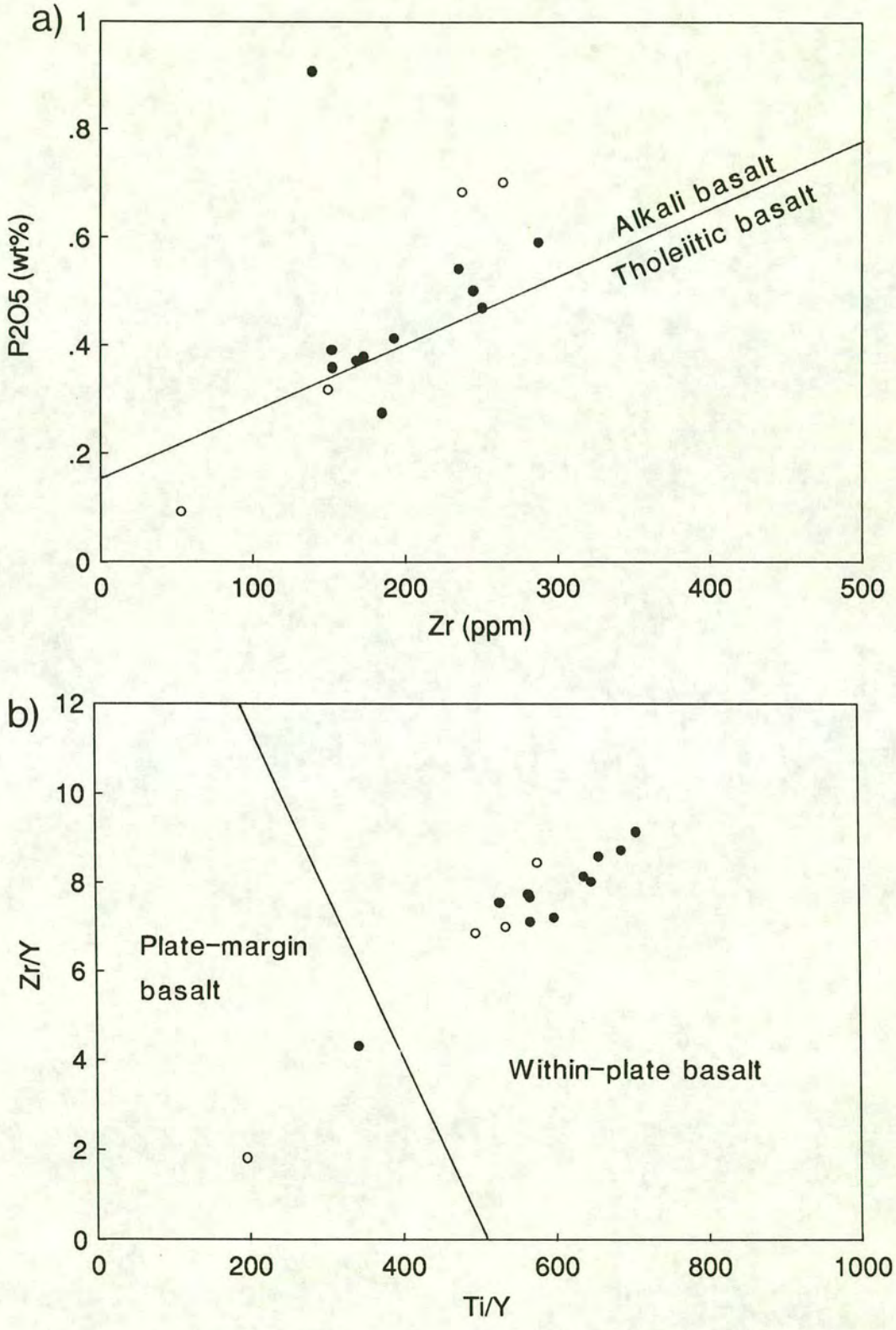

Figure 4.22 Tectonic discrimination diagrams for basalt blocks of the Çal Unit in the Çan region. (a) P_2O_5-Zr plot (fields from Winchester & Floyd, 1976), (b) Zr/Y-Ti/Y plot (fields from Pearce & Gale, 1977). Samples are from the Çalköy road (solid circles) and the Karaaşık road (open circles).

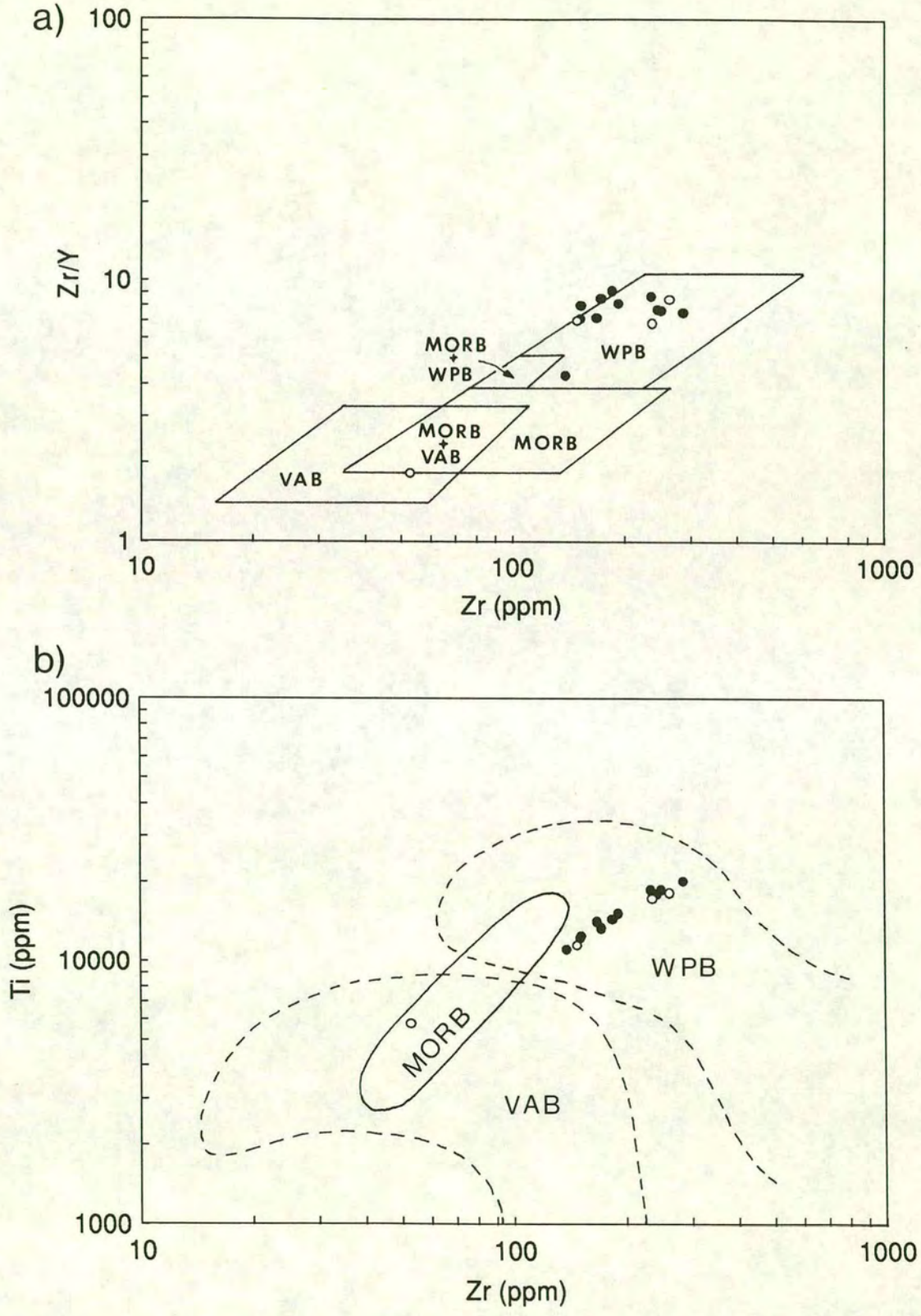

Figure 4.23 Tectonic discrimination diagrams for basalt blocks in the Çal Unit in the Çan region. (a) Zr/Y-Zr plot (fields from Pearce & Norry, 1979), (b) Ti-Zr plot (fields from Pearce, 1982). Samples are from the Çalköy road (solid circles) and the Karaaşık road (open circles).

(MORB: mid-ocean ridge basalt, WPB: within-plate basalt, VAB: volcanic-arc basalt)

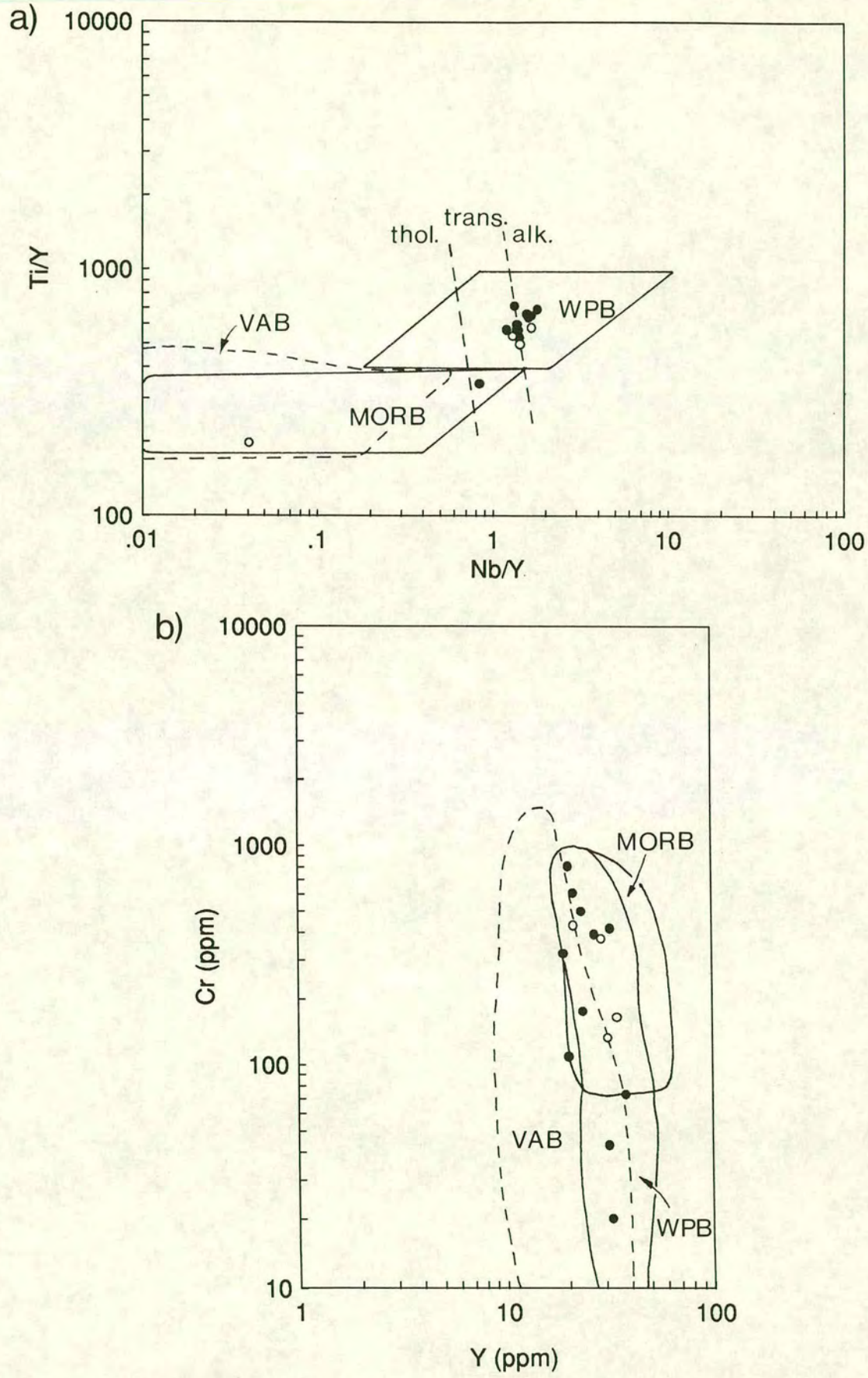

Figure 4.24 Tectonic discrimination diagrams for basalt blocks in the Çal Unit in the Çan region. (a) Ti/Y-Nb/Y plot (fields from Pearce 1982), (b) Cr-Y plot (fields from Pearce, 1982). Samples are from the Çalköy road (solid circles) and the Karaaşık road (open circles).

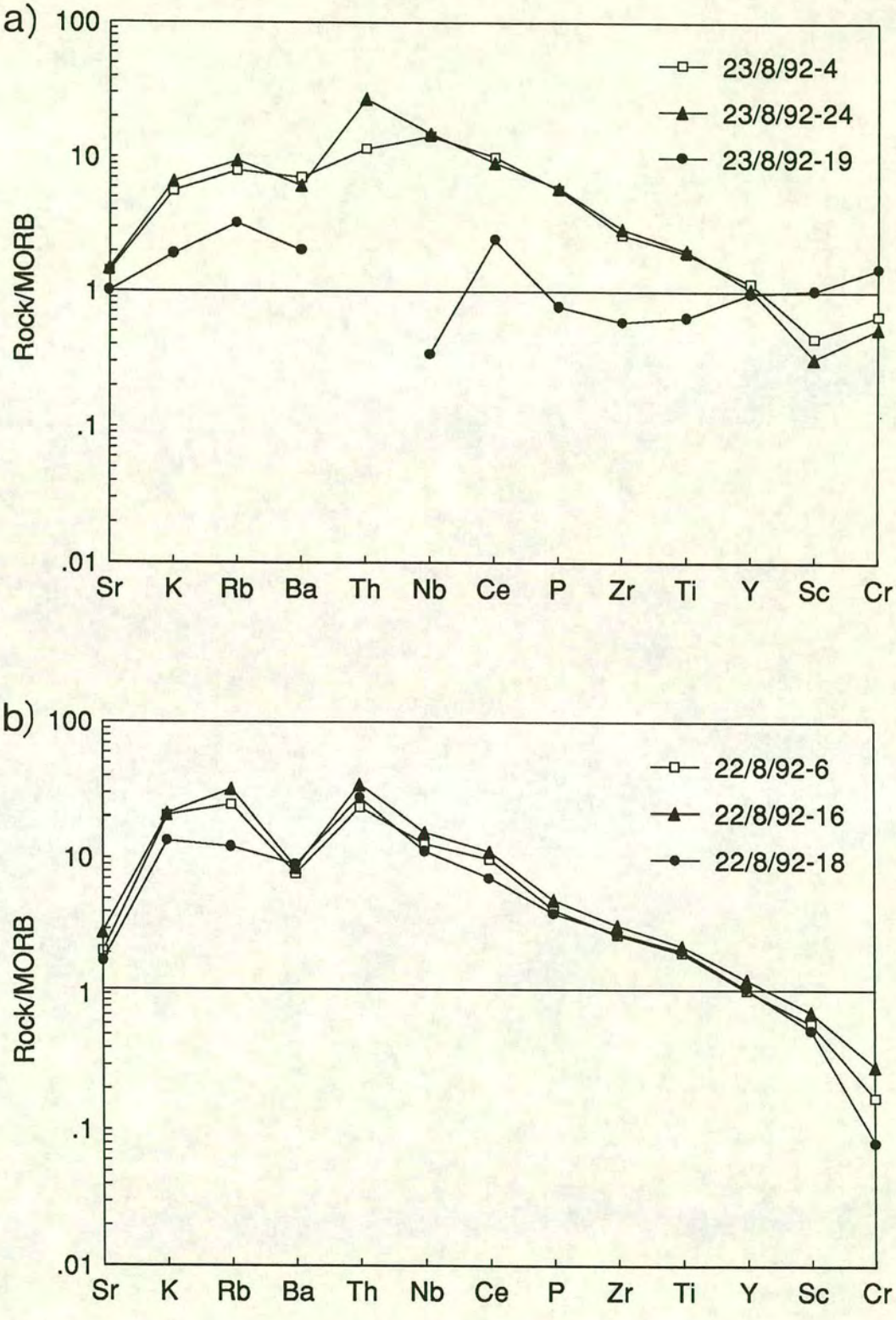

Figure 4.25 MORB-normalized multi-element plots for basalts from (a) the Karaaşik road and (b) the Çalköy road. All samples are from blocks within debris flows except for sample 23/8/92-4 which was taken from a primary basaltic flow. Normalizing values from Pearce (1982, 1983) (Appendix **4**).

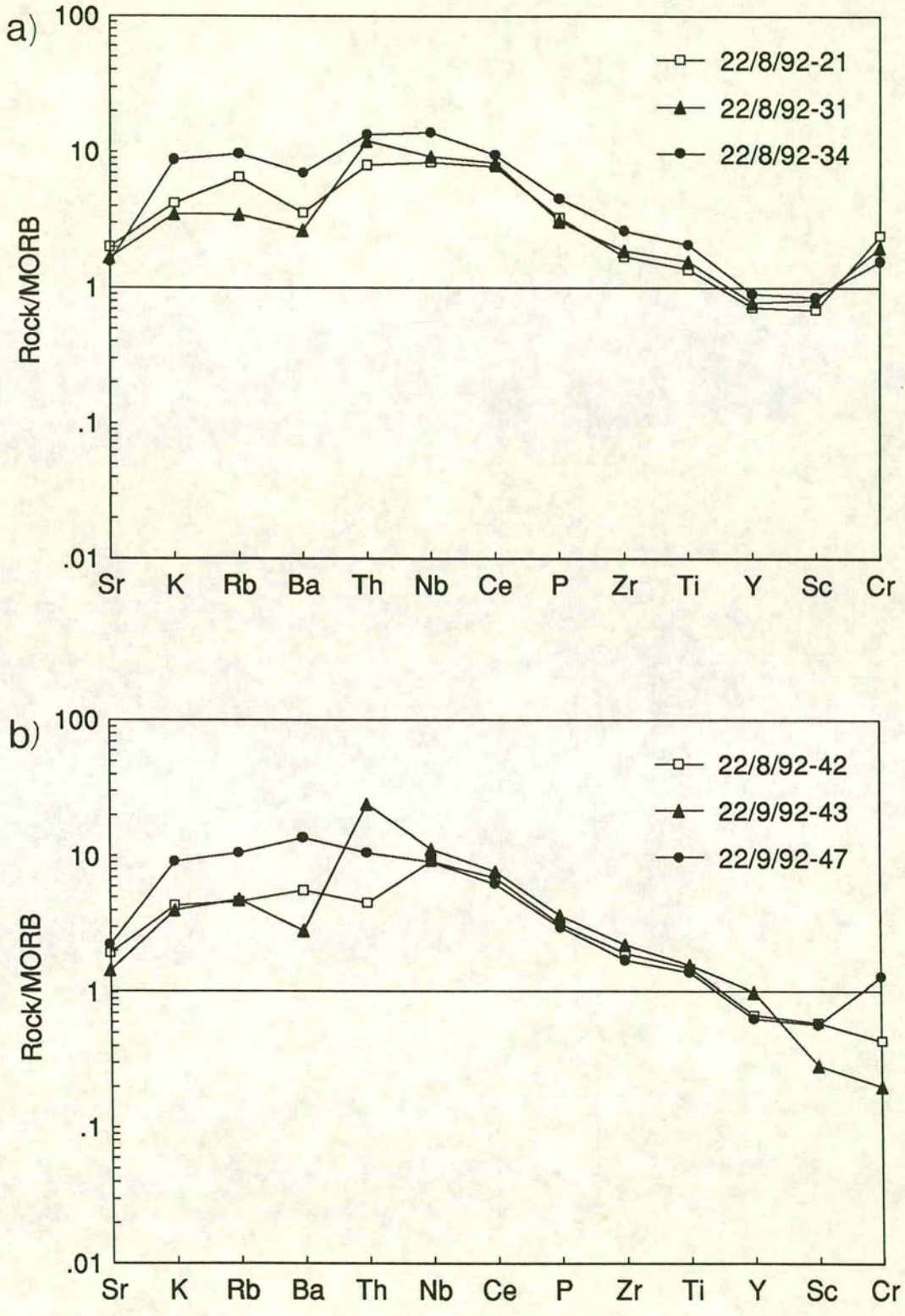

Figure 4.26 MORB-normalized multi-element plots for basalt blocks from the debris flows along the Çalköy road. Normalized as for Figure 4.25.

those from the higher levels of the Çalköy road sequence. Cr displays both depleted and enriched values. The enriched values displayed by the samples in Figure 4.26a together with the high Ni values of these samples may indicate derivation of the parental magma from a peridotite mantle source. Basalts higher in the sequence (Figure 4.25b) show strongly depleted Cr values and also lower Ni values, possibly implying clinopyroxene and olivine fractionation, or the simultaneous crystallization of olivine- and Cr-rich spinel (Basaltic Volcanism Study Project, 1981).

4.9.2 Microprobe analysis of clinopyroxenes

As outlined in more detail in Chapter 2 clinopyroxene geochemistry is a useful discriminant for basalts from different tectonic settings. Clinopyroxene phenocrysts in basaltic blocks from debris flows of the Çal Unit in the Çan area were analyzed by electron microprobe. Unlike the predominantly sub-ophitic textures of basalts from the Nilüfer and Ortaoba Units, the Çal basalts are porphyritic and glomeroporphyritic. Clinopyroxenes are very fresh and range from small groundmass crystals to large glomero-phenocrysts. Both cores and rims of phenocrysts were analyzed and plotted as triangles (rims) and circles (cores) on the (Ca+Na) versus Ti discrimination diagram of Leterrier *et al.* (1982) (Figure 4.27), which discriminates between alkali basalts (A) and tholeiitic and calc-alkali basalts (T). Basalts which plot in field T can be separated further using other diagrams devised by Leterrier *et al.* (1982). The results for clinopyroxenes from the Çal Unit plot predominantly in the alkali basalt field and are therefore not suitable for further discrimination using the digrams of Leterrier *et al.* (1982). This result agrees with the alkalic nature indicated by the whole-rock geochemistry of the basalts.

4.9.3 Geochemistry of sedimentary rocks from Edremit area

Two samples of red-brown siltstone (78C/9o and 79B/90) and one sample of fine-grained sandstone (78B/90) were collected from Çigdem Tepe in the Edremit area and analyzed by X-ray fluorescence. Results were normalized to NASC (North American Shale Composite: Gromet *et al.*, 1984) which can be regarded as an average continental composition. The siltstone results are shown in Figure 4.28a. The samples display patterns relatively close to the normative values (i.e. a terrigenous signature) with slight enrichment of Sc, V, Cr, Ni, Nb and Ce and slight depletion of Sr, Y, Zr and Ba. The enrichment of Cr and Ni may indicate the involvement of a mafic component. The low Sr probably reflects a lack of calcite and/or variations in

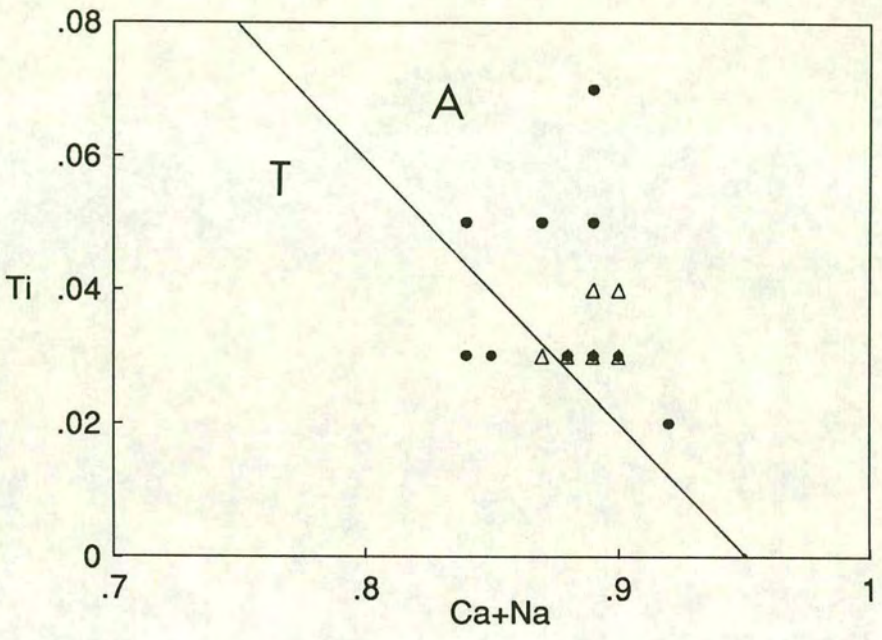

Figure 4.27 Ti vs (Ca+Na) tectonic discrimination diagram for clinopyroxenes in basalts from the Çal Unit, showing the fields for alkali basalts (A) and tholeiitic and calc-alkali basalts (T) (fields from Leterrier *et al.*, 1982). Clinopyroxene compositions are expressed in cations per six oxygens. Circles represent phenocryst cores and triangles represent rims.

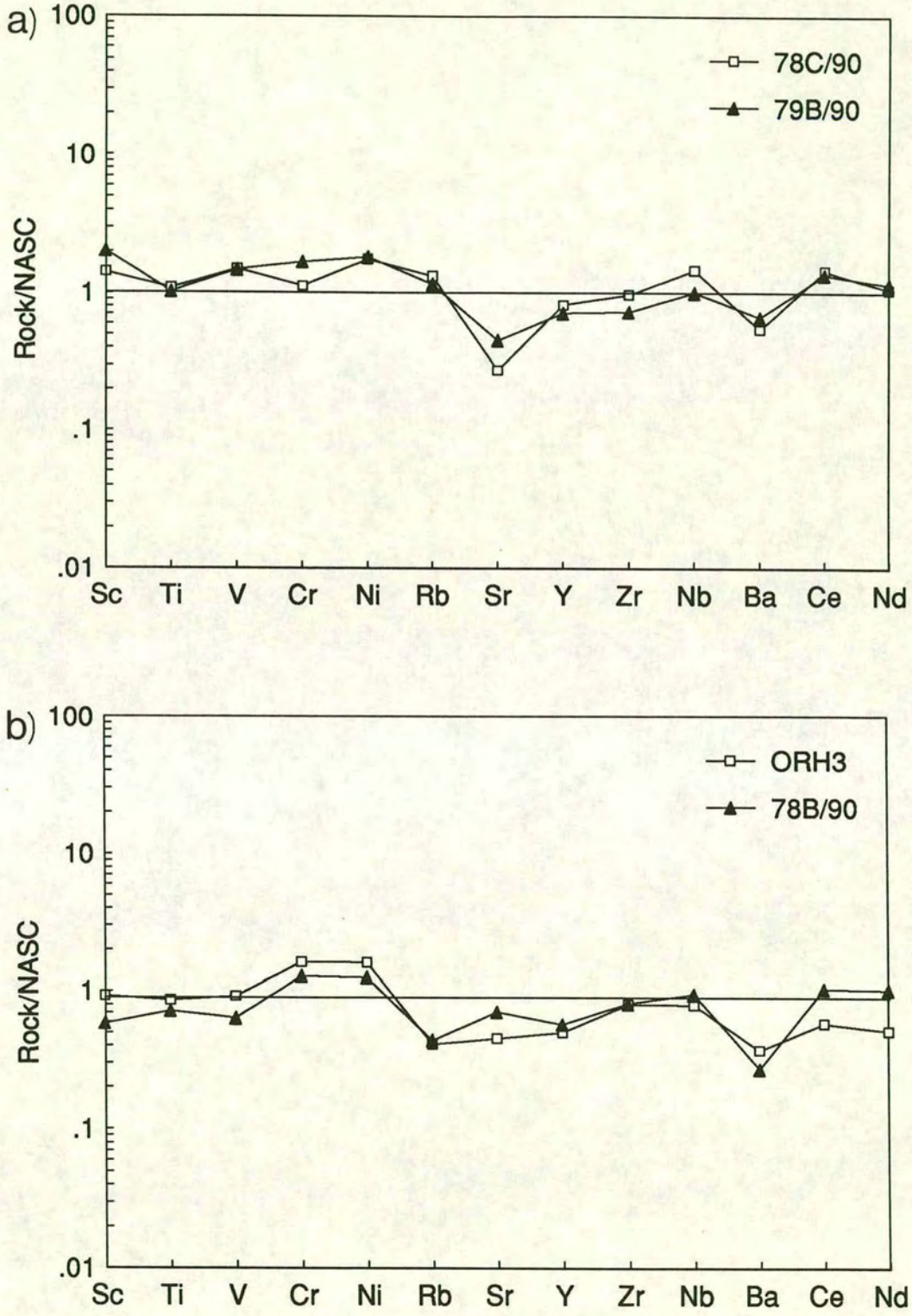

Figure 4.28 NASC-normalized multi-element plots for (a) Çal Unit mudstones on Çiğdem Tepe and (b) a sandstone from the Çal Unit (78B/90) and the Orhanlar Greywacke (ORH3). Normalizing values from Gromet *et al.* (1984) (Appendix **4**).

plagioclase content relative to average crust. In general, however, the siltstones exhibit a typical terrigenous trace-element signature. The sandstone (sample 78B/90 in Figure 4.28b) also displays a terrigenous pattern with slight Cr and Ni enrichment relative to NASC, possibly indicating a small amount of mafic input. It is slightly depleted in Sc, Ti, V, Rb, Sr, Zr and Ba.

4.9.4 Interpretation of geochemistry

The basalt blocks within the Çal Unit are alkalic and have a distinct within-plate signature. Although all the samples are blocks rather than *in situ* flows (with the exception of sample 23/8/4) they nevertheless display a general upwards transition from relatively primitive to slightly more evolved magmas with higher MgO values. Alkali basalts are commonly found in intra-plate tectonic settings such as oceanic islands and the early stages of intra-continental plate rifts. Taken alone, the within-plate geochemistry of the Çal volcanics cannot distinguish clearly between the two settings. Sample 23/8/19 from the Karaasik road displays very different geochemical characteristics; it is tholeiitic and displays MORB/VAB characteristics.

Despite the complete lack of terrigenous blocks within the Çal Unit the geochemistry of the siltstone and sandstone in the Edremit region appears to indicate a predominantly terrigenous source with a minor mafic component.

4.10 Regional comparisons and correlations

Fragmented Permian platform sequences are a common feature of NW Turkey. As well as those described in this chapter, there are Permian platforms beneath the Denizgören and Lesbos Ophiolites and also within the Chios allochthon (see Chapters 7 and 8 respectively). Where observed, the basements of these platforms are invariably clastic and terrigenous, implying a common origin of probable continental affinity.

Similar lithological associations to those which form the debris flow part of the Çal Unit have also been reported from the Karakaya-type sequences of the Ankara region. Okay *et al.* (1991) briefly described a unit which consists of spilitized basic volcanics, volcanogenic sandstone, chert and debris flows. The unit in the Ankara region is known variously as the Dösemedere Formation, Dirlarkaç Member, and the Ortaköy Formation (Okay *et al.*, 1991 and references therein). Debris flows are less common

in this unit than in the Çal Unit of the Biga Peninsula and contain Triassic, as well as Permian, limestone blocks (Okay *et al.*, 1991). In the Biga Peninsula only Upper Permian limestone blocks have been identified.

A poorly exposed, structureless sandstone unit called the Orhanlar Greywacke by Okay *et al.* (1991) may also be associated with the Çal Unit. This unit crops out in the Balya region but was little studied in this project. It consists predominantly of poorly sorted, muddy sandstone, rich in angular quartz, feldspar, volcanic and metamorphic clasts. Figure 4.28a is a NASC-normalized plot showing a sample of this unit from near the village of Orhanlar (ORH3) and a Çal sandstone from Edremit (78B/90) for comparison. The two are remarkably similar, despite being from outcrops over 50km apart. Okay *et al.* (1991) found abundant Lower Carboniferous limestone blocks within the Orhanlar Greywacke in this region.

4.11 Interpretation

The Çal Unit, as described in this thesis, consists predominantly of disrupted Permian platform carbonates and volcanic- and limestone-rich debris flows. The ubiquitous limestone blocks within the debris flows indicate reefal build-ups and the reworking of shallow-marine limestones into bedded slope facies. Most of the blocks contain transported assemblages. After its deposition and lithification, the limestone became incorporated into slope talus and debris flows with a matrix of mud and volcanic debris. The multiple debris flows of the Çal section imply a steep slope with both volcanic and limestone sources. The sandstone-shale sequence may be a fault-bounded block which was incorporated into the unit during subsequent accretion processes.

Taken on their own, the volcanic- and limestone-rich debris flows of the Çal Unit, together with the within-plate geochemistry of the basalt blocks, could be interpreted as one of two main tectonic settings.

a) An open-ocean seamount setting or,
b) A rift setting

Within-plate basalt geochemistries are characteristic of both settings, as are debris flows and pelagic sediments. The close association of basalt and limestone is a common seamount assemblage, as is their incorporation into multiple debris flows.

However, NASC-normalized mudstone plots from the Çal Unit lie close to the normalizing line, indicating a considerable terrigenous source and effectively ruling out an open-ocean seamount setting. The limestone and basalt debris flows of the Nilüfer Unit, by contrast, are devoid of terrigenous material and hence can be viably interpreted as an open-ocean seamount. Unlike the Nilüfer Unit, the volcanic "core" of a potential Çal seamount is not observed. However, this does not preclude a seamount origin as the core may have been subducted intact whilst its slope apron of debris flows and breccia was offscraped and preserved within the accretionary complex. The presence of Upper Permian blocks in the debris flows and the abundance of Upper Permian platform carbonates in the field area have led to their being included in the same unit. The clastic basement to the platform carbonates also argues against an open-ocean seamount setting. The most likely scenario, therefore, is that of a rifted carbonate platform in which the debris flows and pelagics near Çan represent an intra-platform basin. Similar pelagic associations observed in the Bergama and Edremit regions may record the formation of other small basins within a large carbonate platform. The precise mechanism of formation of the debris flows is uncertain. The volcanic and limestone "conglomerates of conglomerates" near Çalköy may record initial talus formation at the base of a slope and subsequent incorporation of the talus into a debris flow. Alternatively, slope talus may have been reworked into debris flows at a much later stage; for example, on arriving at a trench.

The carbonate platforms and debris flows which characterize the Çal Unit may be interpreted as an oceanic plateau with intra-platformal rifts. The platform carbonates in the Bergama, Ezine and Balya regions would be remnants of this plateau (or several smaller edifices), while the volcanic- and limestone-rich debris flows in the Çan area represent rift basins which formed within the platform(s). The fact that the debris flows and associated clastics in the Çan area contain terrigenous material suggests that the basement of the plateau was continental. This hypothesis is supported by the clastic nature of the basement beneath the carbonate sequences in the Bergama, Ezine and Balya regions. In this scenario the lava flows and abundant volcanic clasts within the Çal debris flows may have been derived from localized rift-related volcanism.

4.12 Analogues in the Eastern Mediterranean

Intra-platform rift sequences have also been recognized in the Argolis Peninsula of Greece (Clift & Robertson, 1990). The Argolis Peninsula preserves remnants of relatively in situ carbonate platforms and collapsed intra-platform basins, representing

part of a carbonate platform bordering a Mesozoic ocean basin (Clift & Robertson, 1990). The Asklipion Unit of Argolis comprises Anisian andesitic volcanics and deep-water carbonates, interpreted by Clift & Robertson (1990) to record Middle Triassic rifting related to opening of the Neotethys and subsequent deposition of calciturbidites in a deep basinal setting.

The Kargi Complex in the Central Pontides of Turkey is also believed to represent a carbonate-capped oceanic plateau (Ustaömer, 1993), and thus may reflect a similar tectonic setting to the platform units observed in Argolis and the Çal Unit. The basement of the carbonate platform is not exposed, although quartzitic conglomerates observed at the base of the succession preclude an open-ocean seamount setting (Ustaomer, 1993). This led to his interpretation of the Kargi unit as a continental fragment which rifted off Gondwana during the Palaeozoic and became accreted to the active Eurasian margin during the Late Permian-Early Triassic. A very similar scenario is illustrated by the present-day Eratosthenes Seamount which lies due south of the Aegean-Cyprus active margin. This structure has been interpreted as a horst formed in the Mid-Upper Triassic by rifting of the north margin of Gondwana to form the Neotethys ocean (Robertson *et al.*, 1994). Dredging suggests that carbonate platforms built up on the seamount during the Mesozoic/Early Tertiary. The northern and margin of the seamount is interpreted as part of the seamount plateau that has been downfaulted, associated with thrusting beneath Cyprus.

CHAPTER 5

UPPER TRIASSIC-JURASSIC SEDIMENTARY COVER: A PERCHED ACCRETIONARY PRISM-TOP BASIN

5.1 Introduction

In the Biga Peninsula the Karakaya Complex is unconformably overlain by undeformed Upper Triassic to Lower Jurassic clastic sequences, which pass up into the Lower-Upper Jurassic Bilecik Limestone. Near Havran, in the SE part of the peninsula, a clastic succession up to 1000m thick (the Halilar Formation) has a very localized distribution. Further east, in the Bursa-Bilecik region, Lower Jurassic clastics (the Bayirkoy Formation) lie unconformably on deformed Karakaya-type units. The Bilecik Limestone which overlies these sequences is the most common and widely distributed Early Mesozoic lithology in NW Turkey. It caps the underlying Karakaya units, with or without, the intervening clastics of the Halilar and Bayirkoy Formations.

The Halilar and Bayirkoy Formations of the Biga Peninsula were investigated, owing to their position immediately above the Karakaya Complex and the fact that the ages of the clastics near the base of the sequence are relatively close to those obtained for parts of the Karakaya Complex itself. The lithological characteristics of the clastic part of the sequence provide invaluable information regarding the setting of the Karakaya Complex and the later stages of its evolution. The overlying Jurassic limestone constrains the timing of the cessation of Palaeotethyan tectonic activity and indicates the establishment of stable Neotethyan platforms, a new phase in the evolution of this region. Most of this chapter is concerned with the clastic-limestone sequence near Havran, owing to its thickness and excellent exposure (Figure 5.1). Equivalent and related units which occur in the Edremit, Çan and Balya regions are also discussed.

5.2 Distribution of Upper Triassic-Jurassic sequences in NW Turkey

Upper Triassic to Jurassic rocks are widely distributed throughout NW Turkey. They are found in the Biga Peninsula and also in the regions of Bursa-Bilecik, Mudurnu-Nallihan, Aktas-Cerkes and Ankara, as outlined by Altiner *et al.* (1991) in Figure 5.2. The sequences are exposed as scattered outcrops along a broad belt, which trends

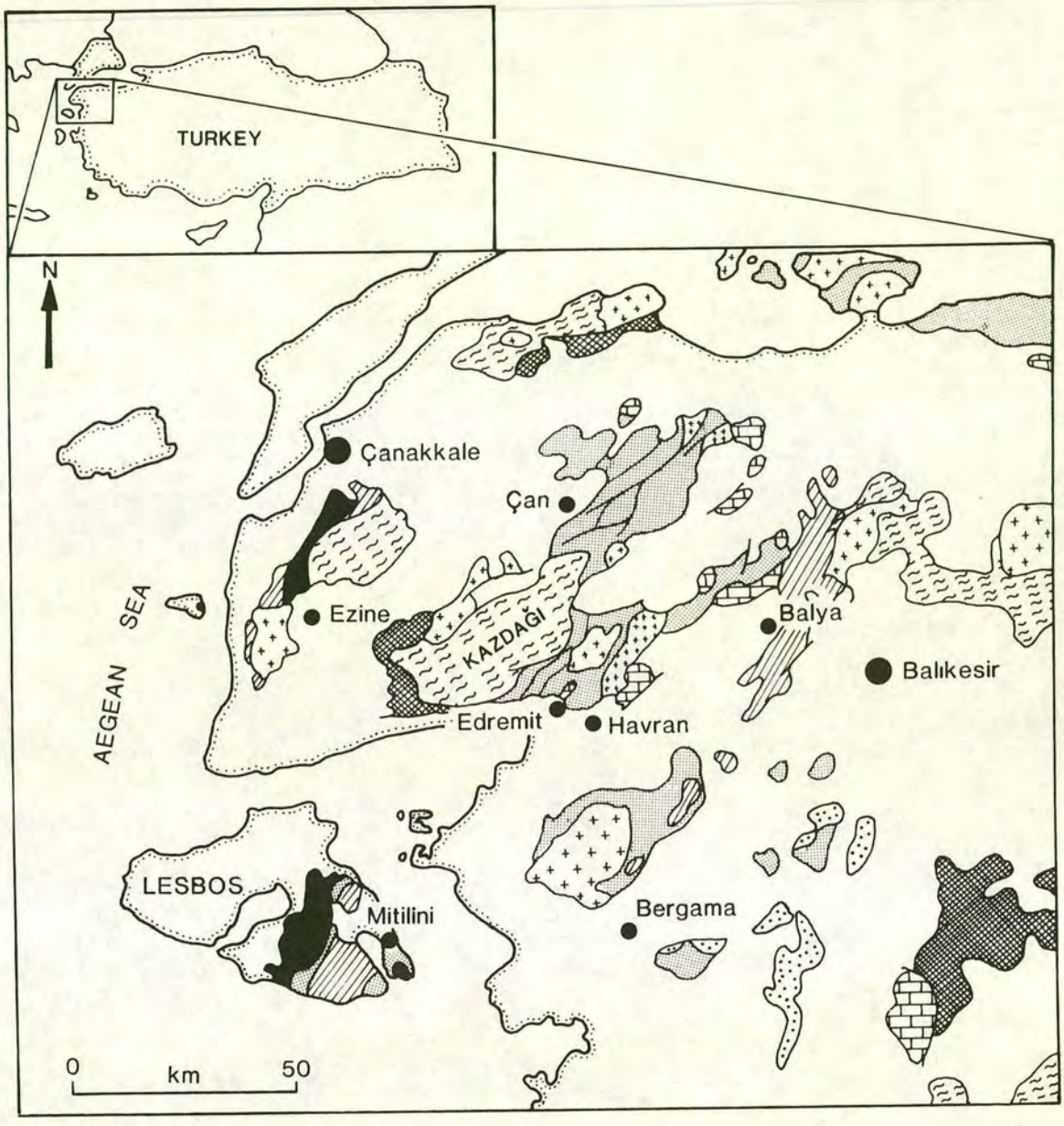

Figure 5.1 Generalized geological map of the Biga Peninsula and surrounding regions.

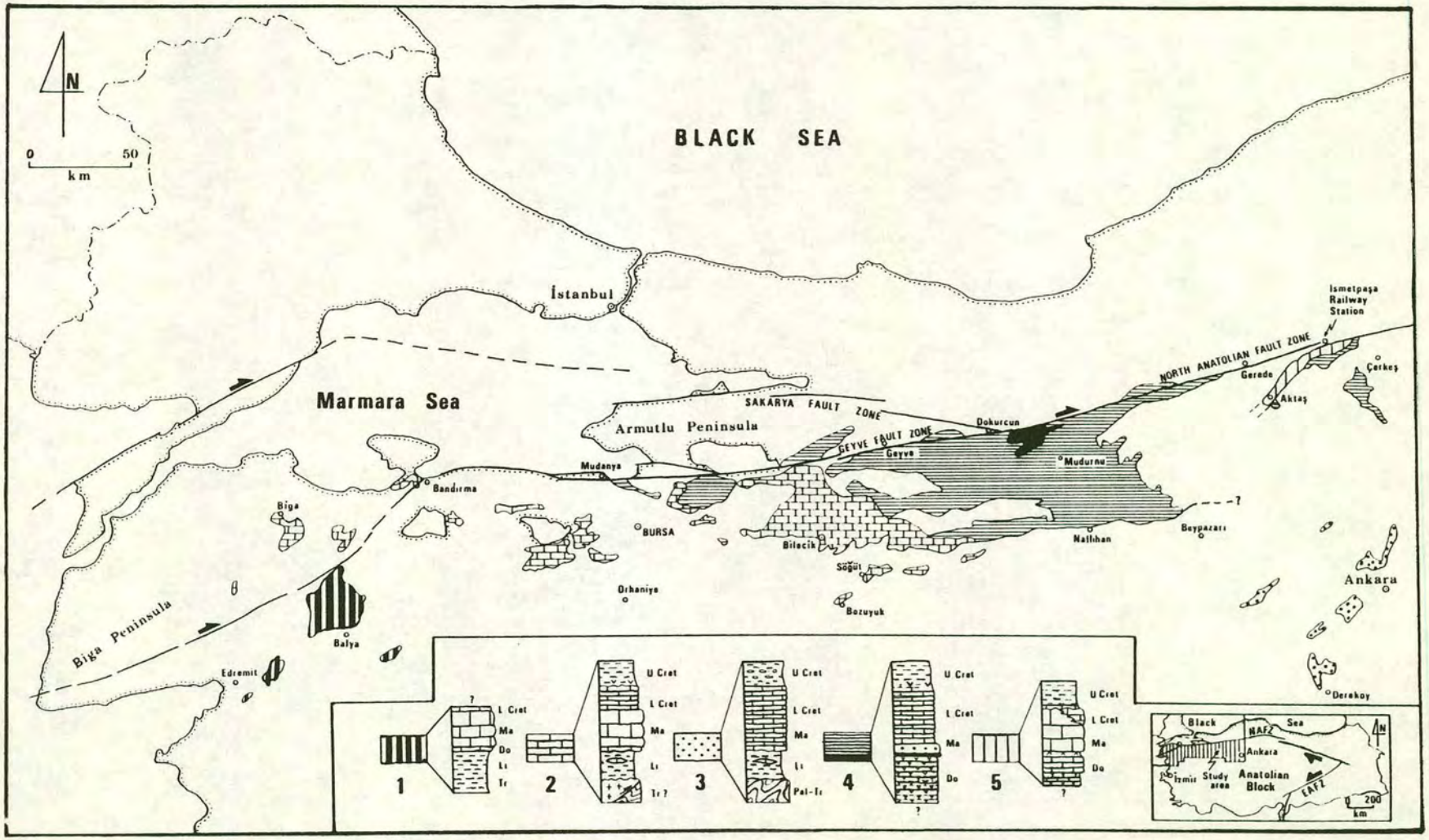

Figure 5.2 Distribution of Upper Triassic-Jurassic sedimentary sequences in NW Turkey. (sequences from 1: Edremit-Balya, 2: Bursa-Bilecik, 3: Ankara, 4: Mudurnu-Nallıhan, 5: Aktaş-Çerkes). From Altıner *et al.* (1991).

approximately E-W along the line of the North Anatolian Fault and extends from the Mudurnu-Nallihan region to the Biga Peninsula in the west. Isolated exposures of Lower Jurassic to Upper Cretaceous sequences are also found further south, in the region around Ankara. Exposure is most extensive in the area between Bilecik and Mudurnu.

5.3 Previous work

a) Upper Triassic-Lower Jurassic clastics

The clastic Triassic-Lower Jurassic sequences of the southern Biga Peninsula region have been the subject of study, since Triassic rocks were first recognized in the Balya area by Neumayr (1887) and Bittner (1890). Subsequent studies in the Biga Peninsula included descriptions and palaeontological determinations by Aygen (1956), van der Kaaden (1957), Gumus (1964) and Aslaner (1965). The Upper Triassic-Lower Jurassic clastic sequence in the southern Biga Peninsula region was named the Hasanlar Formation by Bingol *et al.* (1973) and was subsequently mapped as the Halilar Formation by Krushensky *et al.* (1980), who divided the formation into three informal members (lower, middle and upper). The Halilar Formation was renamed the Halilar Group by Altiner *et al.* (1991) and divided into the Bagcagiz and Sakarkaya Formations.

The Lower Jurassic sandstones of the Bilecik area were informally called the "gres de Beyerkey" by Granit & Tintant (1960) and subsequently named the Bayirkoy Formation by Altinli (1973a). Okay *et al.* (1991) correlated this unit with Lower Jurassic clastic rocks in the Biga Peninsula.

With the exception of Altiner *et al.* (1991) and Okay *et al.* (1991), most of the workers outlined above have only carried out limited stratigraphical and palaeontological studies on the clastic sequences. Very little work has been done on the detailed sedimentary facies associations or their environmental and tectonic settings, especially in relation to surrounding units.

b) Jurassic Limestone

Jurassic limestone has long been recognized in the Edremit-Havran area and is recorded in the literature as the unnamed limestone of Aygen (1956), van der Kaaden (1957), Gumus (1964) and Aslaner (1965). The limestone in the southern part of the

Biga Peninsula was named the Alancik Formation by Bingol *et al.* (1973) and the Kocacaltepe limestone by Krushensky *et al.* (1980).

In the Bilecik area, Granit & Tintant (1960) named the carbonates overlying their "gres de Beyerkey", the "calcaires de Yediler" and the "calcaires de Bilecik". Okay *et al.* (1991) correlated the Jurassic limestones of the Bilecik and Biga regions and called the limestone of the Biga Peninsula the Bilecik Limestone, after the original name of Granit & Tintant (1960). Altiner *et al.* (1991) renamed the unit the Bilecik Group and divided it into two formations, the Tascibayiri Formation and the Gunoren Formation. The limestone studied in this project corresponds mainly to their Tascibayiri Formation which is the lower of the two formations.

5.4 Nomenclature used in this thesis and in the literature

In this study the Upper Triassic-Lower Jurassic clastic sequence in the Havran region is referred to as the Halilar Formation, after the nomenclature of Krushensky *et al.* (1980). Although the overlying Jurassic limestone has been subdivided into several formations and members by Altiner *et al.* (1991), it is referred to in this thesis as the Bilecik Limestone, following Granit & Tintant (1960). This informal nomenclature is used because the Bilecik Limestone was only briefly studied at one locality, and the facies described were not all *in situ*. Hence, the accurate assignment of lithologies to particular stratigraphic units was not possible.

During fieldwork the Halilar Formation was logged along the Pinar Dere stream section near Kocaçal Tepe (Figures 5.3 and 5.4), and was divided into Lower, Middle and Upper Units on the basis of lithological characteristics (Figure 5.5). All descriptions of the Halilar Formation given in this chapter are made with reference to these three informal units. It is almost impossible to correlate these units with those devised by other workers (e.g. Kushensky *et al.*, 1980; Okay *et al.*, 1991; Altiner *et al.*, 1991), owing to widely differing interpretations regarding the structure and lithologies of the area. For example, the lower member of Krushensky *et al.* (1980) is actually part of the Camlik Metagranodiorite, which they misidentified as an arkosic sandstone. The Halilar sequence of Altiner *et al.* (1991) is approximately 300m thick compared to my 1000m (Figure 5.5), owing to their very different structural interpretion of the area which involves folding and thrusting. However, it appears that their Bacagiz Formation roughly corresponds to the Middle Unit described in this study, and their Sakarkaya Formation corresponds to the Upper Unit. The Lower

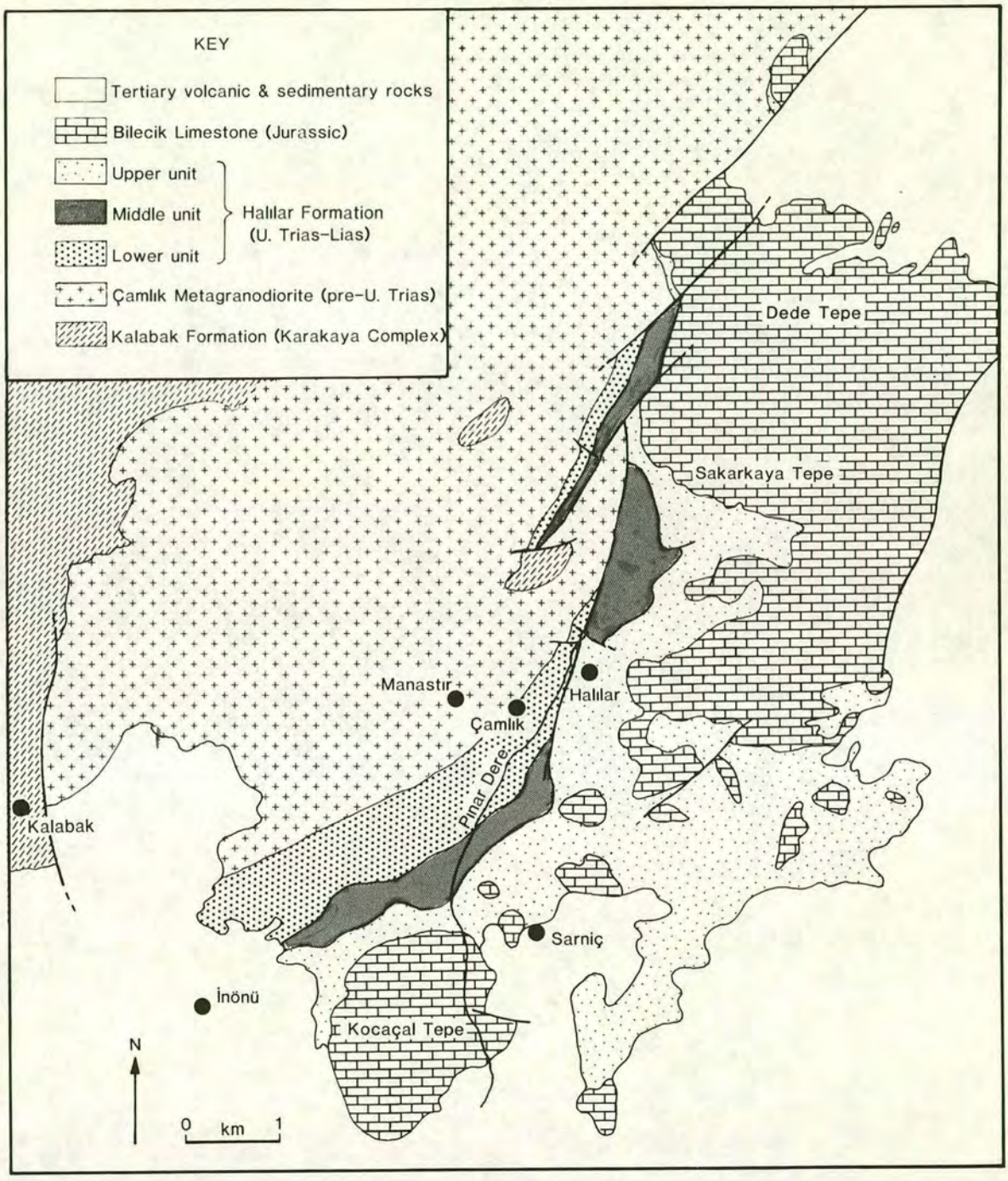

Figure 5.3 Geological map of the Kocaçal Tepe region, showing the distribution of the Halılar Formation and the Bilecik Limestone. Modified after Gümüs (1964), Krushensky *et al.* (1980) and Okay *et al.* (1991).

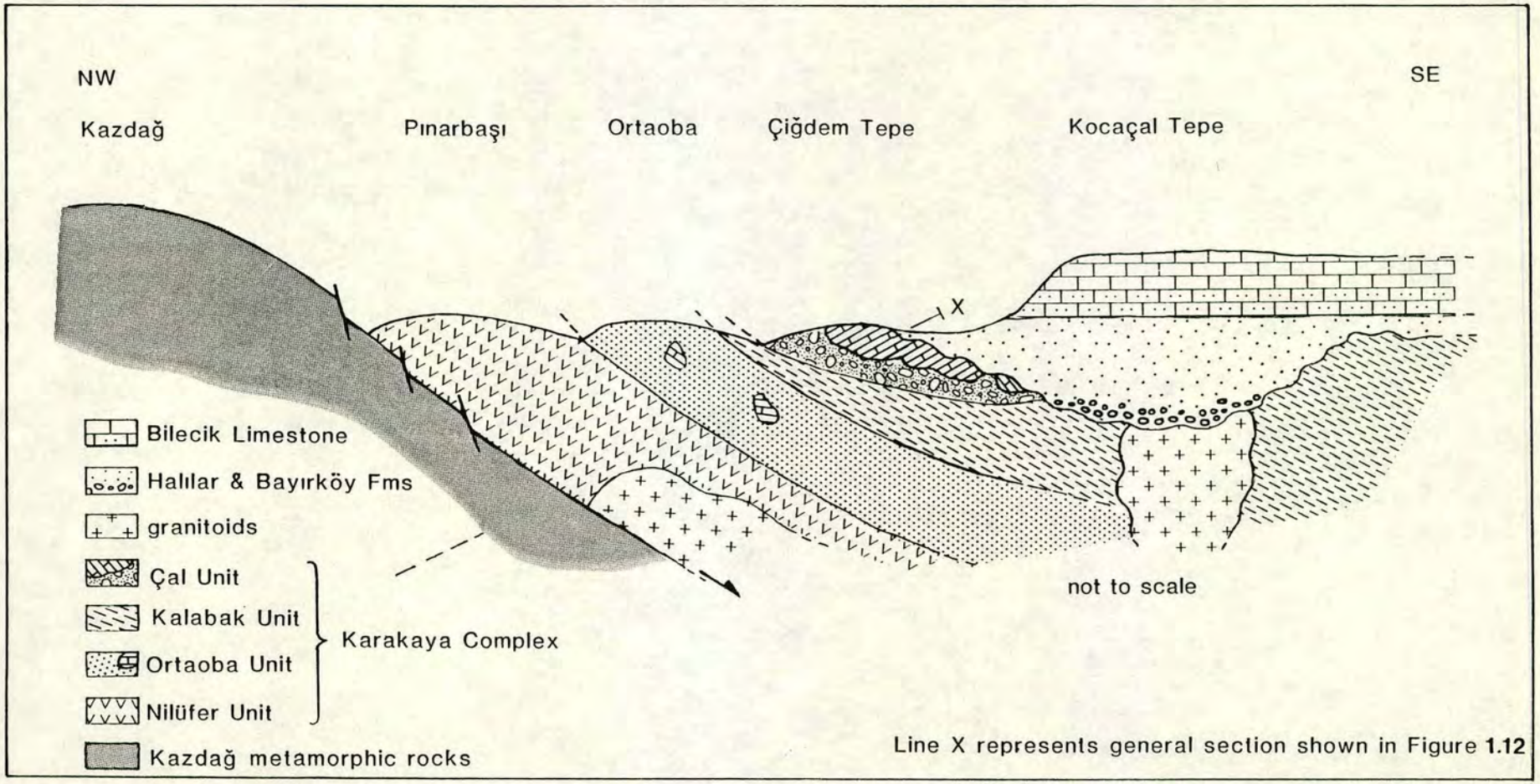

Figure 5.4 Schematic cross-section of the Edremit-Havran region, showing the relationship of the Upper Triassic-Jurassic clastic and carbonate sequences with the underlying Karakaya Complex.

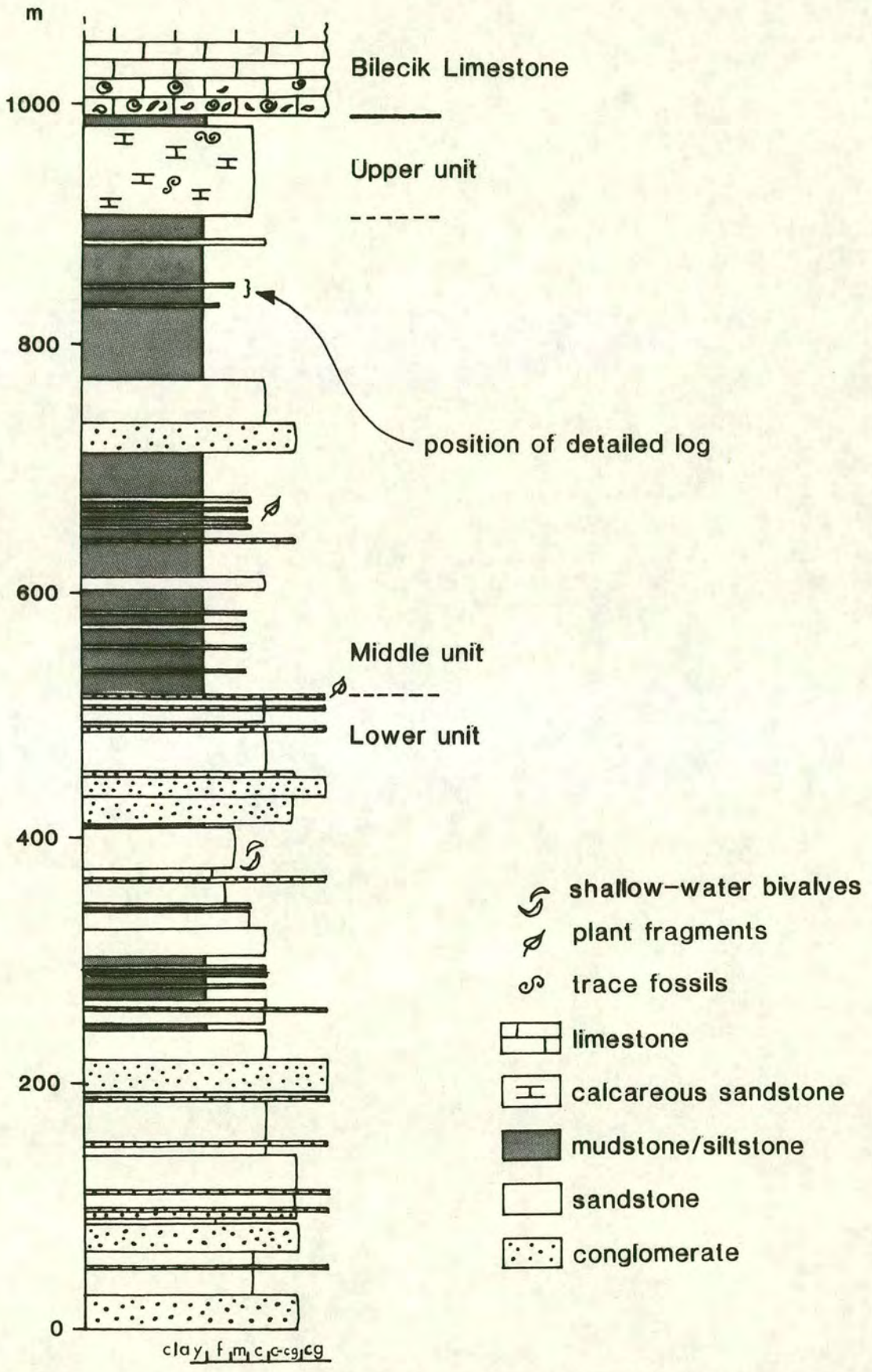

Figure 5.5 Generalized stratigraphic column through the Halılar Formation along Pınar Dere between Çamlık and Kocaçal Tepe.

Unit, however, also falls within their Sakarakaya Formation owing to their interpretation of thrust repetition. Problems also arise when trying to correlate the Halilar Formation with work by Okay *et al.* (1991). They assigned the Upper Triassic clastics to their widespread "Hodul Unit", described by them as part of the Karakaya Complex and which also incorporates the Ortaoba Unit described in Chapter 3. In this thesis the Karakaya Complex is regarded strictly as the deformed, metamorphosed, accretionary units which lie *below* the Halilar Formation. The great differences in metamorphic grade, lithologies and extent of deformation between the Ortaoba Unit and the Triassic clastics near Havran makes the nomenclature of Okay *et al.* (1991) meaningless in this case. A pilot illite crystallinity study carried out on mudstones from the Halilar Formation and the underlying Karakaya units clearly displays the difference in metamorphic grade between the Karakaya units and the overlying Halilar Formation, thus supporting the nomenclature used here.

Correlation of the Bayirkoy Formation is also problematic. In the Bilecik region (its type area) Okay *et al.* (1991) correlated the Bayirkoy Formation with Upper Liassic clastic rocks from the Çan region of the Biga Peninsula (Figure 5.1). In the Çan region a thin sequence of clastic and calcareous rocks overlies the Çal Unit of the Karakaya Complex. The epifaunal bivalve *Posidonia,* which indicates a probable Toarcian-Aalenian age, has been found in the upper part of this sequence (Okay *et al.*, 1991) and also in the Bacagiz Formation (Altiner *et al.*, 1991), indicating age correlation between the Can sequence and the Middle Unit of the Halilar Formation. However, the Bayirkoy Formation in its type area has been assigned a Hettangian-Pliensbachian age (Altiner *et al.*, 1991), which predates the probable age of the *Posidonia*-bearing sequence in the Çan area. For this reason the Upper Liassic clastics near Çan are described, but not assigned to any formal stratigraphic units.

5.5 Illite crystallinity

A pilot illite crystallinity study was carried out in order to compare the mudstones of the Halilar Formation with those of the underlying Karakaya Complex (see Appendix 1). In particular, the aim was to supplement field and petrographic evidence which clearly shows that the Halilar Formation unconformably overlies the Karakaya Complex and is not part of it, as postulated by Okay *et al.* (1991). The X-ray diffraction response of illite can be used to give an indication of the burial history of a sedimentary rock. The method is based on the fact that there is an increase in the degree of crystallinity and a change in the chemical composition of illite in the late

diagenetic-early metamorphic realm (e.g. Hardy & Tucker, 1988). The degree of illite crystallinity is given by the parameter Hbrel which is based on the width of the illite diffraction peak at half height. The illite peaks become sharper and narrower with progressively greater depths of burial and are reflected by decreasing Hbrel values.

Typical illite peaks for two Halilar mudstones from the Upper Unit of the Halilar Formation, together with their Hbrel values plotted with respect to the diagenetic-anchizone division, are shown in Figure 5.6. The illite peaks are clearly much wider than those of the Karakaya units (Figure 5.7) and their Hbrel values are correspondingly much greater and plot well inside the diagenetic zone. The results obtained from this preliminary study thus support the field observations which indicate that the Halilar Formation is lying as a relatively undeformed sequence on top of the accretionary Karakaya Complex.

5.6 Structure of the Halilar-Bilecik sequence near Havran

5.6.1 Folding

The Halilar Formation is relatively undeformed, although folding in the Upper Unit can be observed at one locality along the Pinar Dere stream, near the contact with the overlying Bilecik Limestone of Kocacal Tepe. At this locality the folding has a broken, discordant appearance owing to later high-angle faulting, but is clearly tectonic rather than slump-related. Due to its inaccessibility, the outcrop was not investigated. Krushensky *et al.* (1980) used the folding of the upper part of the Halilar Formation as evidence for their hypothesis that the Bilecik Limestone is not *in situ* but was emplaced over the Upper Triassic clastic rocks by gravity sliding. They also described the presence of "fault breccias" at the contact between the Halilar Formation and the Bilecik Limestone. Breccias do exist, but they are cemented limestone talus, probably of relatively recent age, and clearly do not indicate any kind of tectonic or gravity emplacement.

Open folds with wavelengths up to 2km and NNE-SSW trending fold axes have been mapped in the Halilar Formation and Bilecik Limestone of this region by Gumus (1964) and Krushensky et al. (1980). An example of an open fold was observed during palaeomagnetic sampling of the Bilecik Limestone on Kocacal Tepe (see Chapter 9).

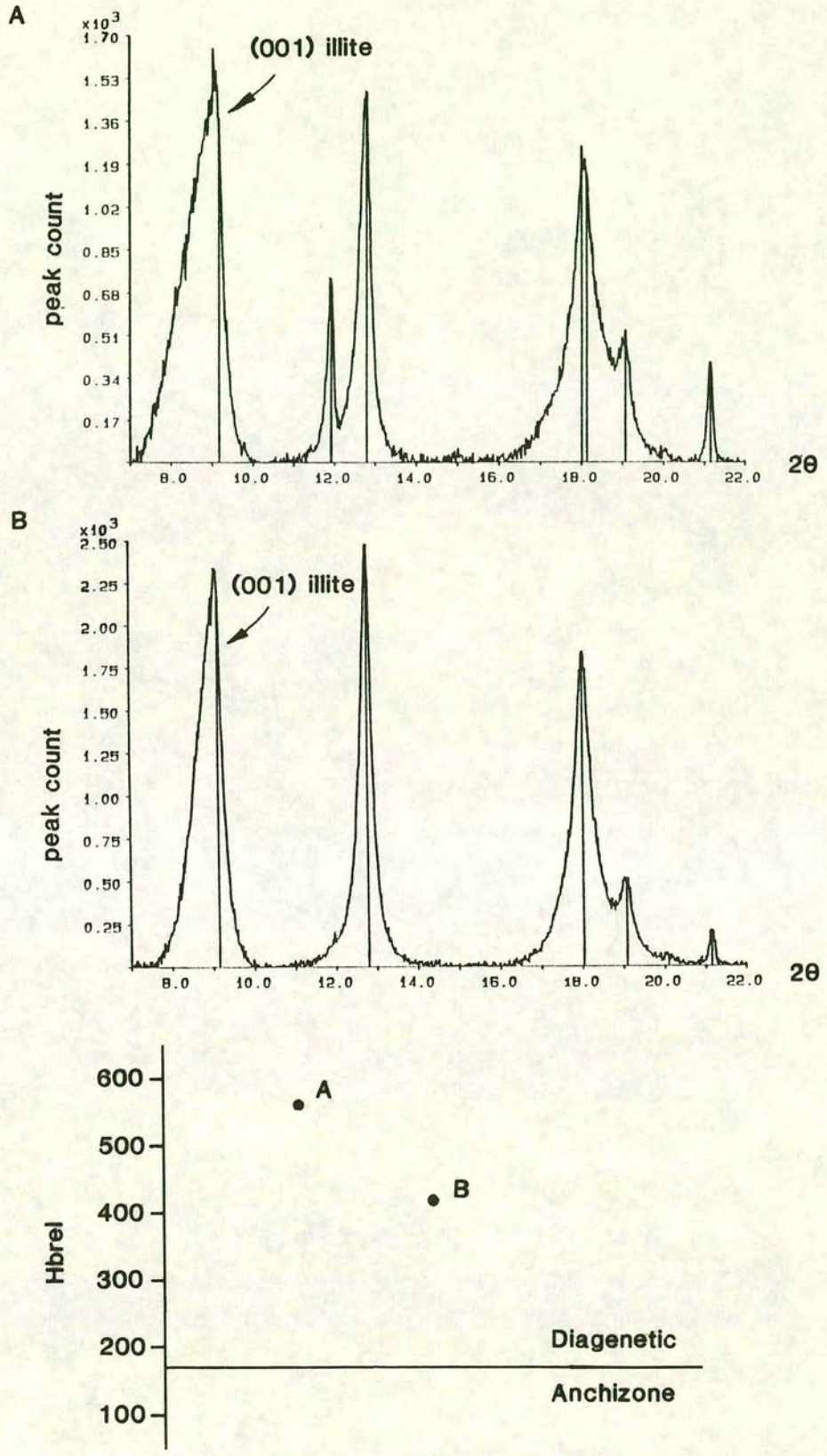

$$\text{Hbrel} = \frac{\text{(half width for (001) illite)}}{\text{(half width for (100) quartz)}} \times 100$$

Figure 5.6 Illite crystallinity plots for two samples of mudstone from the Upper Unit of the Halılar Formation near Kocaçal Tepe. Note the wide illite peaks and the Hbrel values which plot well within the diagenetic zone.

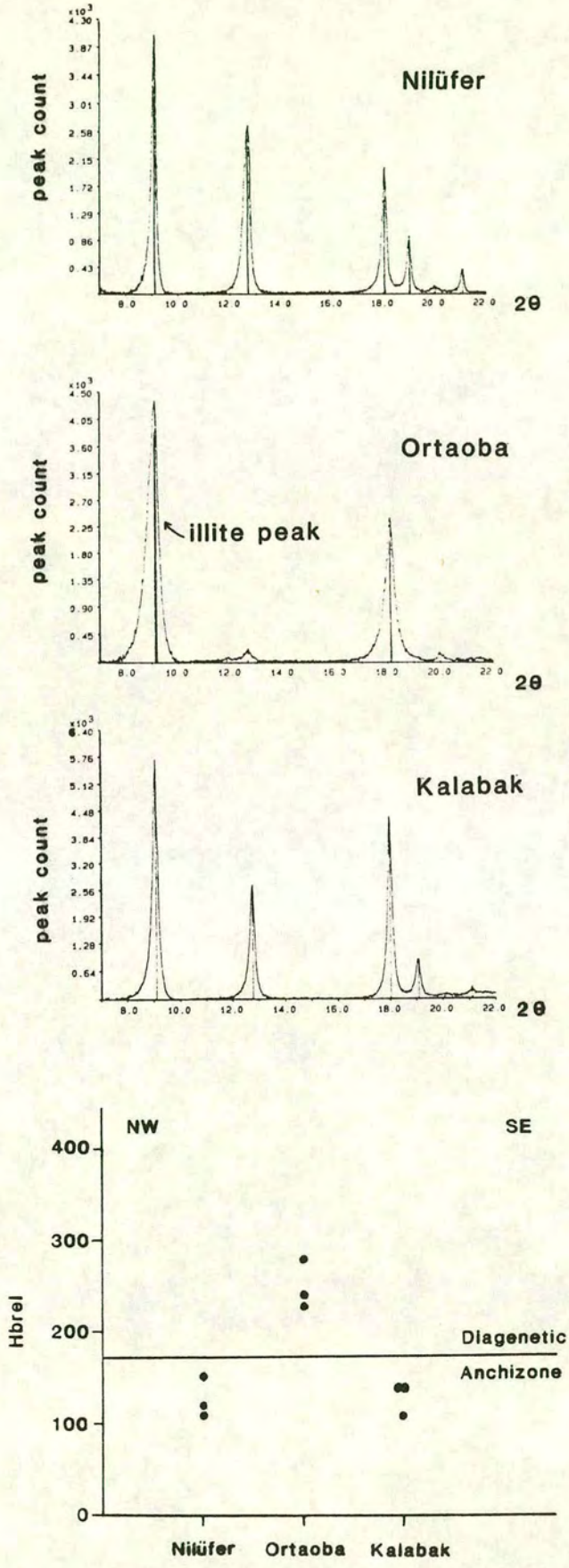

Figure 5.7 Illite crystallinity plots for shales from the units of the Karakaya Complex in the Edremit region. Note the attenuated and sharp illite peaks and the Hbrel values which plot in the low diagenetic or anchizone zones (c.f. Figure 5.6).

5.6.2 Faulting

Faults with steep, SE-dipping fault planes were locally observed in the Halilar Formation. Slickensides indicate normal, dip-slip movement, although rare SE-dipping faults display slickensides which plunge towards the south, implying a possible component of dextral strike-slip. One of these faults cuts silicified limestone, on a hill east of Halilar village. As silicification probably occurred during Oligo-Miocene magmatic activity in this region, the age of the faulting is thus younger than the volcanism. Steep faults with E- to SE-dipping fault planes and SSE-plunging slickensides occur near the contact of the Halilar Formation with the Camlik Metagranodiorite near the village of Halilar. These faults are highly mineralized, a feature which led some previous workers (e.g. Altiner *et al.*, 1991) to interpret the Çamlik Metagranodiorite as an intrusion into the Halilar Formation. This is, however, not the case, as explained in section 5.7.1.

5.7 The Halilar Formation

The Halilar Formation comprises approximately 900-1000m of conglomerates, sandstones and shales which are well exposed in the Pinar Dere river which runs southwards and cuts through the hill of Kocacal Tepe near the village of Sarniç (Figure 5.3). Bedding orientation is locally difficult to determine and hence the true thickness may be less than the estimate given above. The river bed does, however, provide the best section through all the various lithologies of the Halilar Formation and allows distinct facies to be distinguished. The formation is here divided into Lower, Middle and Upper Units, on the basis of lithological characteristics (Figure 5.5).

5.7.1 Lower Unit

The Lower Unit unconformably overlies a weathered granitoid (the Camlik Metagranodiorite of Okay *et al.*, 1991, and the Duztarla Granite of Altiner *et al.*, 1991) and is characterized by a coarse basal conglomerate. Altiner *et al.* (1991) described the presence of quartz veins and extensive ore mineralization (galena, chalcopyrite, pyrite) along the boundary and proposed that the contact is intrusive. However, the area they studied (along the upper portion of the Pinar Dere stream), contains a sub-vertical, anastomosing fault running between the granite and the sandstones of the Halilar Formation. Fluids along this fault are likely to have been

responsible for the mineralization and the quartz veining. Near the village of Çamlik (Figure 5.3) an unconformity between the granite and the Halilar Formation is clearly exposed. A conglomerate containing large granite clasts up to 8cm in size can be observed overlying the granite. South of the village of Manastir, 0.5 km to the west, the contact is between granite and black mudstone rich in small brachiopods. The variation in lithologies may be due to onlap against an undulose granite erosion surface with the deposition of conglomerates as channel lags within a predominantly quiet, muddy shallow-marine setting. Alternatively there may have been minor faulting along the boundary which cut out the conglomerate and produced the rather sheared and rubbly appearance of the mudstones near the contact.

This unit is predominantly composed of a monotonous sequence of coarse-grained beige to grey sandstones, with common horizons of conglomerate. The poorly sorted sandstone is rich in white mica, quartz, alkali feldspar and plagioclase with a matrix of quartz, sericite and clays. Calcareous fragments and rare laminated quartzose lithic clasts were also observed in thin-section. The sandstones commonly have a slightly ferruginous, reddish matrix. Beds range from 12cm to 1m in thickness. The thinner beds tend to be medium-grained, whereas the 1m-thick beds are coarse-grained and commonly contain conglomeratic bands with clasts up to 8cm in diameter.

The matrix of the conglomerates is the same sandstone as described above and the larger clasts include white quartz (mostly polycrystalline or with undulose extinction), grey quartzite, granite, fine-grained sandstone, opaques, and angular fragments of finely banded, silvery-grey quartzose schist and calcareous siltstone. One thin-section contained several clasts of a dark grey, microcrystalline speckled mineral which was difficult to identify. (Similar clasts in sandstones from the Ortaoba Unit were analyzed by microprobe and found to be both quartz and albite). The clasts are rounded to angular depending on their lithology. Granitic and quartzite clasts are generally rounded, whereas the schist and siltstone clasts are angular. The granitic clasts display well-preserved igneous textures including myrmekitic and graphic intergrowths. Very few sedimentary structures were observed within these massive sandstones and conglomerates, apart from possible imbrication in the coarser conglomerates. Rusty films of iron oxide on clasts are very common throughout this unit, especially in the more conglomeratic horizons.

Many of the conglomerates and sandstones are rich in carbonaceous fragments, including well-preserved woody material and reed-like leaves. Lower in the unit

broken thick-walled bivalve shells are preserved among the large clasts of a non-ferruginous conglomerate horizon (Figure 5.8a). A thin black bed with associated black seams perpendicular to the bedding is interpreted as some kind of carbonaceous layer with associated rootlets. In thin-section the black material is opaque, implying oxide replacement of what may have originally been a coal layer.

5.7.2 Middle Unit

The Middle Unit comprises thick sequences of black mudstone, siltstone and shale intercalated with beds of sandstone and conglomerate which are identical to those of the Lower Unit. A typical outcrop is shown in Figure 5.8b. The lower boundary is taken as the appearance of the thicker shale sequences, although this is rather artificial as the only change is the relative proportions of the lithologies rather than the lithologies themselves. The upper boundary is not well exposed along the river bed and an area of poor outcrop separates this unit from the Upper Unit. However, there is no evidence of faulting, so the contact is assumed to be stratigraphic and probably conformable.

The mudstones of this unit are generally soft and undeformed and have a characteristic conchoidal fracture. Nodular concretions of relatively indurated mudstone (often calcareous) weather out. Thin beds of siltstone and fine-grained sandstone are ubiquitous throughout the mudstones and they locally have a rich fauna of brachiopods. A certain degree of deformation has taken place in some parts of the exposed Halilar Formation, producing a slight foliation in the mudstones. The sandstones are largely undeformed except for recrystallization in places. Towards the top of the unit turbiditic sandstone intercalations occur within a thick mudstone sequence, as shown in the detailed log in Figure 5.9. These intercalations display partial Bouma sequences. Rounded grey mudstone clasts up to 30cm in diameter are present within the conglomerates and indicate a high energy environment with deposition relatively close to the mud source. High energy is also implied by the climbing ripples and the planar laminations of the Bouma upper laminar flow regime. The thinner beds display good fining-upward sequences with muddy laminae near the tops of the beds, which grade into the intervening mudstone intercalations. This entire sandy horizon within the mudstones represents a sequence of turbidites ranging in thickness from a few cm to 2m. Cross-bedding, climbing ripples and sole marks were used as palaeocurrent indicators and indicate a dominantly S to SE-directed flow (see Figure 5.10c). The sole marks are bulbous flutes, their original shape probably

Figure 5.8

(a) Conglomerate from the Lower Unit of the Halilar Formation, along the Pınar Dere stream section. Note the rounded quartzitic and granitic clasts and the thick-shelled bivalves. The large shell in the upper central region of the picture is probably a megalodont.

(b) A typical outcrop of the Middle Unit of the Halılar Formation, showing the characteristic interbedded sandstones and black mudstones.

(c) Massive sandstone bed along Pınar Dere, in the upper part of the Middle Unit. Mudstone rip-up clasts are a common feature of this part of the sequence.

a

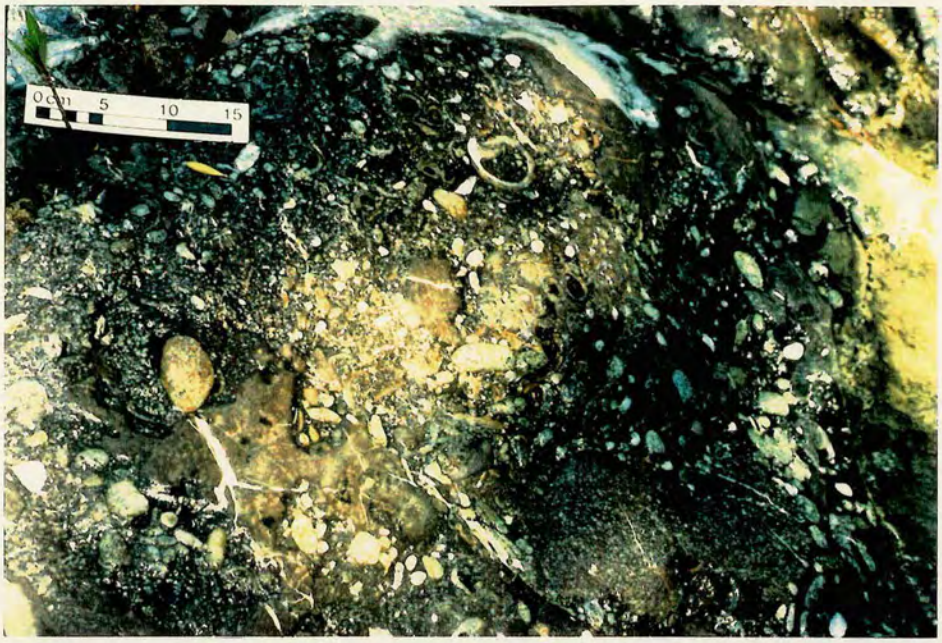

b

c

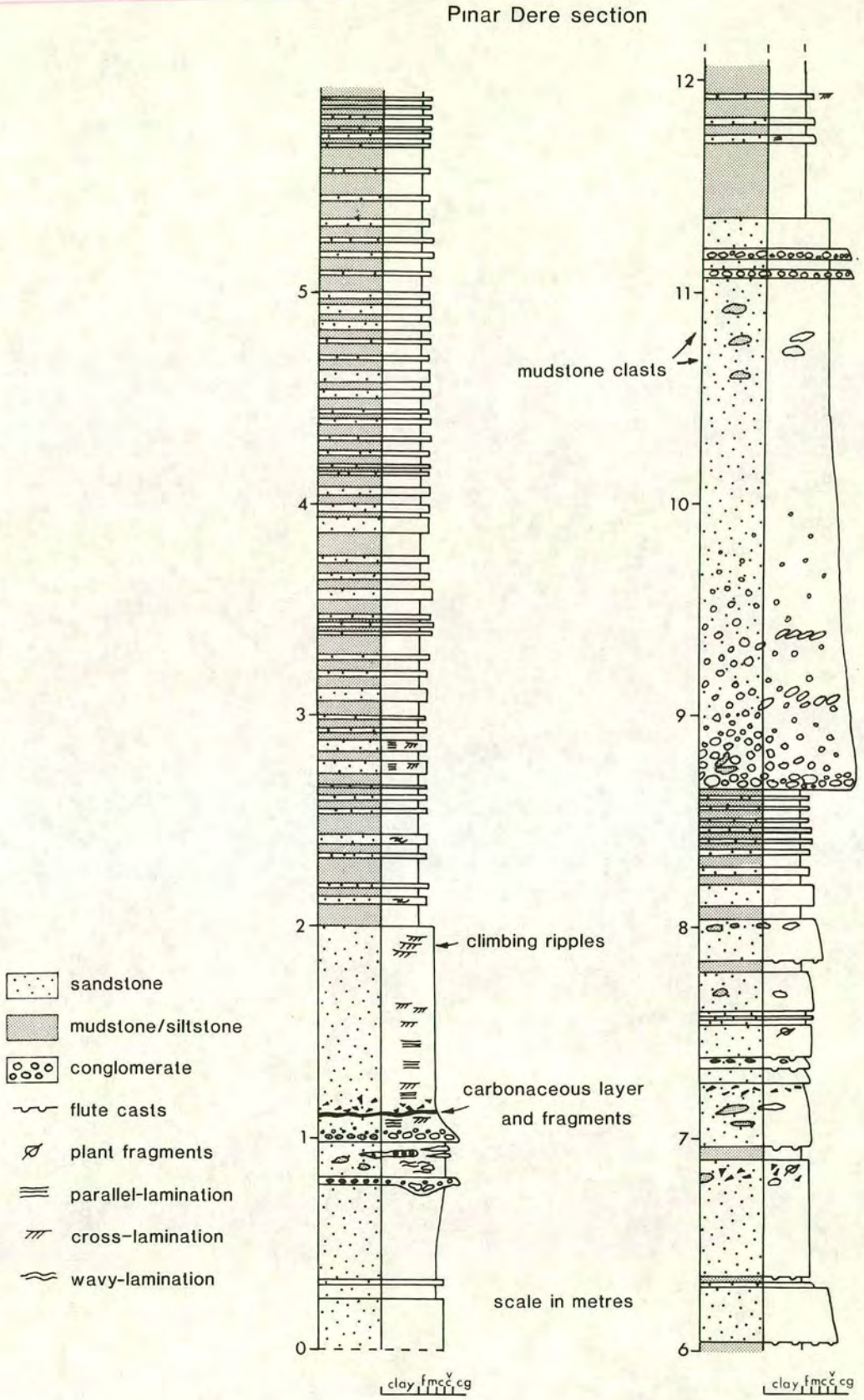

Figure 5.9 Detailed log through a sandstone interval in the upper part of the Middle Unit, as indicated on the general log in Figure 5.5.

Figure 5.10

(a) Small-scale erosional scour features in massive sandstone in the Middle Unit. Apart from its grain-size the conglomerate is identical to the sandstone.

(b) Climbing ripples near the top of a turbidite sequence in the Middle Unit (indicated on the log in Figure 5.9).

(c) Rose diagram showing S and SE flow directions, as measured from a limited number of cross-beds and flutes in the Middle Unit.

a

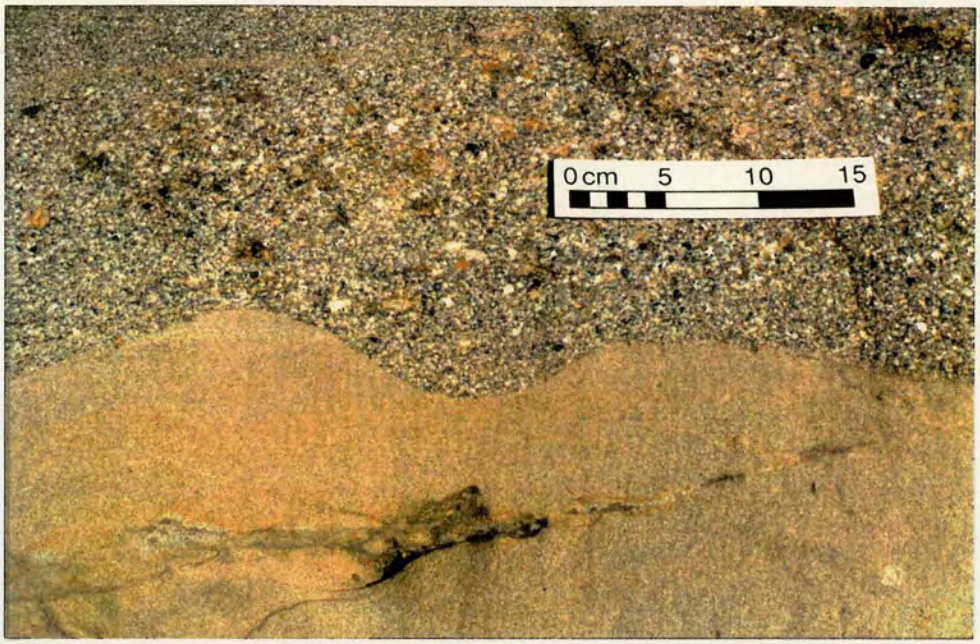

b

c

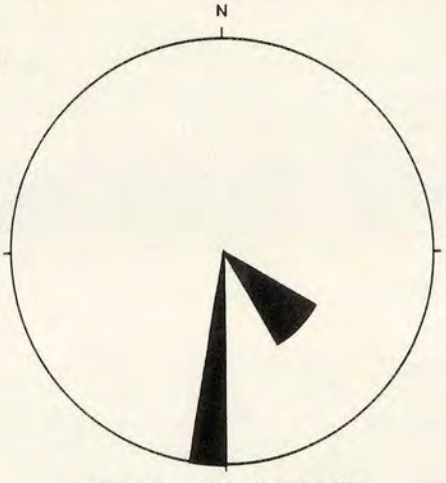

Values: 5 Interval: 10° Radius:40%

enhanced by slight load cast formation. Imbrication of pebbles within the conglomerates was also observed and gives a similar direction. The actual azimuth of the flow was determined from distinctly directional features such as cross-bedding, asymmetrical ripples and pebble imbrication. Distinctive features of the middle unit will be considered below.

The sandstones in this unit are generally poorly sorted and contain angular grains of white mica, quartz, alkali feldspar, perthite, biotite, plagioclase, sparry calcite and a speckled dark grey mineral (microcrystalline quartz or highly altered feldspar) in a matrix of recrystallized quartz, clays, biotite, sericite and replacement calcite. Some sandstone horizons are slightly ferruginous and many display calcitic cements. The main lithologies of clasts within the conglomerates of the Middle Unit include granitoid, opaque white vein quartz, grey quartzite, silvery-grey phyllite and grey mudstone. The clast-supported conglomerate in Figure 5.8a contains clasts up to 15cm in diameter and is rich in shell fragments, which were derived from thick-shelled bivalves. Other clasts include limestone, rounded granitoid cobbles, gneissic fragments and crinoid fragments in a micaceous and calcareous grey sandstone matrix. The chaotically dispersed shells imply that this may represent a rapidly deposited storm bed. The deposit broadly fines upward and displays slight imbrication near its base. A conglomerate higher in the sequence contains many clasts of recrystallized sandy blue-grey limestone.

Black carbonaceous imprints are a common feature of the sandstones in the middle part of the sequence. They have a woody appearance and are up to 5cm long. They are observed on bedding planes and display a crude alignment in some cases.

The sandstone interval near the top of the middle unit (as shown in Figure 5.9) comprises a 10m-thick sequence of sandstone layers displaying turbiditic features, which separates massive sandstone from overlying dark shales and mudstones. At the top and bottom of this subunit are thick sandstone and conglomerate horizons, both of which contain impressive mudstone rip-up clasts (Figure 5.8c). The lower sandstone layer displays a turbidite succession which passes up from scour deposits (Figure 5.10a) into massive sandstone with cross- and planar-laminations and, near the top of the unit, climbing ripples (Figure 5.10b). The sandstone units at the top and bottom of this intercalation are separated by 4m of interbedded sandstones and shales and, above this, 3m of thickly bedded sandstones with thin shale intercalations.

The thickly bedded sandstones also display features indicative of turbidites, such as good fining-upward sequences and mud rip-up clasts. Sole structures are also common and are intermediate between flute and load casts.

Altiner *et al.* (1991) reported an abundance of the pelagic bivalve *Bositra buchii*, in the uppermost part of their Bagcagiz Formation, which is largely equivalent to the Middle Unit described above.

5.7.3 Upper Unit

The contacts of the Upper Unit are not exposed in the river section and the unit is defined solely on the basis of its lithology. The unit is locally folded and thus its true thickness is difficult to gauge. Calcareous, beige to grey medium-grained sandstone is the dominant rock type. It is poorly sorted, thin- to medium-bedded and intercalated with thin shaly intervals. Clasts are angular and lithologies include quartz (polycrystalline, strained and unstrained varieties), alkali feldspar, perthite, white mica, biotite, dark grey recrystallized quartz or feldspar and carbonate clasts. The carbonate clasts include a punctate brachiopod fragment and echinoderm debris. One clast of a myrmekitic granitic rock was also observed. The matrix is predominantly sparry calcite. Bedding planes are very rich in mica flakes and small black carbonaceous fragments. Slight grading can be observed in some beds, indicating that the unfolded parts of the unit are the right way up.

Trace fossils are a characteristic feature of this unit and are present on bedding planes as well-preserved burrows and feeding traces, including *Thalassinoides*, *Chondrites, Ophiomorpha, Planolites* and *Skolithos*. *Thalassinoides* and *Ophiomorpha* are particularly diagnostic of shallow water conditions. Very few sedimentary structures other than grading are present within this unit. Figure 5.11 shows a representative section through part of this sequence. A field photograph of the logged outcrop is shown in Figure 5.12a. Blocks of cream-coloured limestone up to 1m long are present within the bedded sequence (Figure 5.12b). Although superficially resembling large clasts they are may be *in situ* concretions. In thin-section the carbonate has no internal structure or fauna and has a very amorphous texture, consistent with a concretionary origin. The carbonate is similar in appearance to the lower part of the Bilecik Limestone, but lack of fossils makes its origin difficult to ascertain.

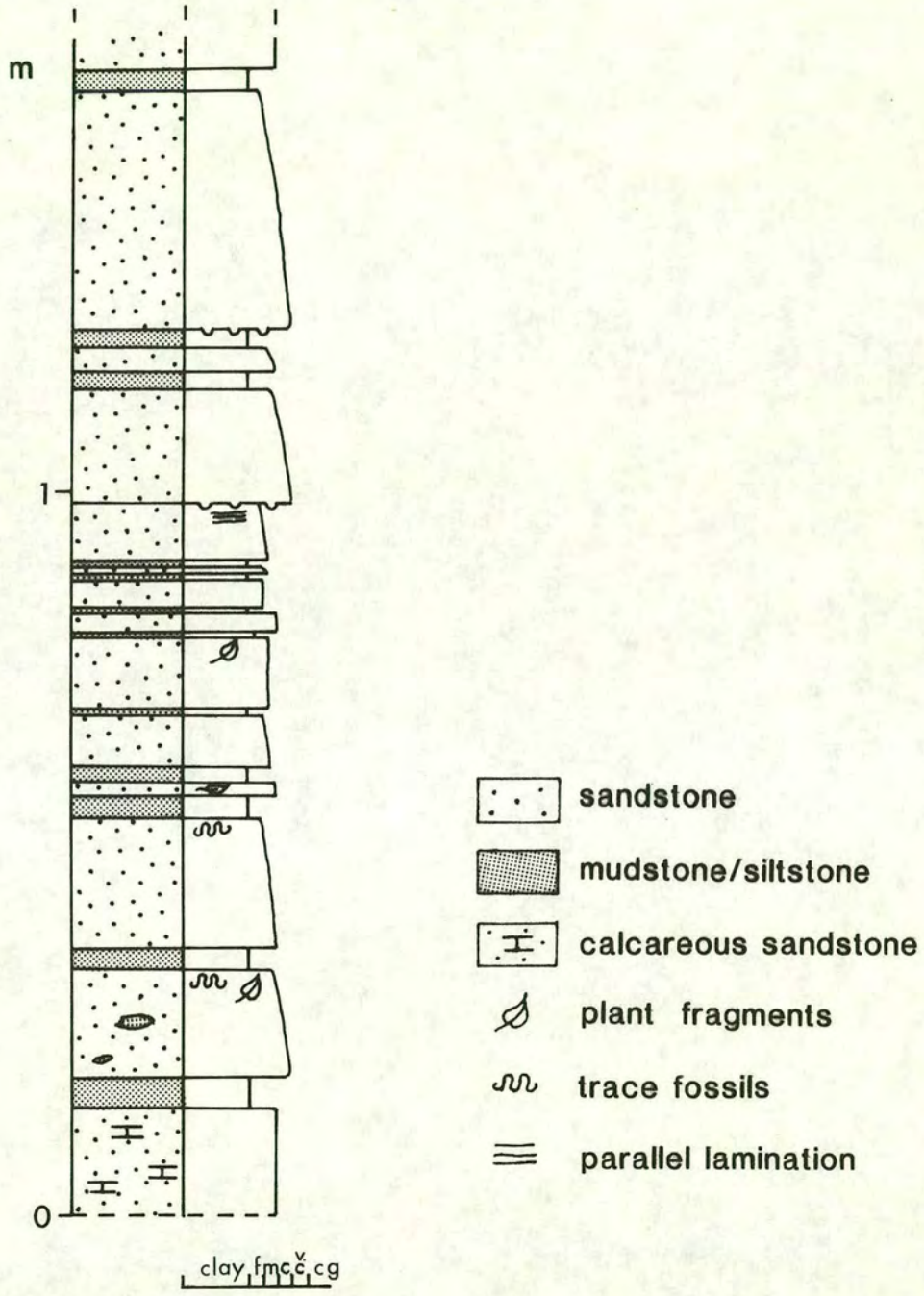

Figure 5.11 Representative short log through part of the Upper Unit of the Halılar Formation at the point where Pınar Dere meets Kocaçal Tepe.

a

b

Figure 5.12

(a) Field photograph of the Upper Unit as logged in Figure 5.11, showing the characteristic alternation of sandstone and calcareous sandstone with grey mudstone. The bedding planes at this locality are rich in shallow-water trace fossils.

(b) Large carbonate concretion within the Upper Unit.

Up section, the calcareous sandstones pass into yellow marls, although the contact is not exposed. The marls are very calcareous and contain belemnites and ammonites, heralding the appearance of the overlying Bilecik Limestone. The increasingly calcareous nature of the clastic sequence is good evidence for a sedimentary contact with the Bilecik Limestone and disproves the fault hypothesis of Krushensky *et al.* (1980). Grey-green mudstones, similar to those lower in the Halilar Formation, occur above the marls, implying that the change from predominantly clastic sedimentation to carbonate deposition was not instantaneous. This is borne out by the basal *Ammonitico Rosso* of the Bilecik Limestone, which contains rare fragments of green calcareous shale in a micritic pink matrix.

5.8 Subsidence history

A highly simplified subsidence curve for the Halilar Formation was generated using data collected by Altiner *et al.* (1991) from the Havran region and a programme written by J. Turner at Edinburgh University (Figure 5.13). Backstripping and decompaction were carried out according to the method devised by Sclater & Christie (1980) and the results were plotted against the timescale of Harland *et al.* (1990). Water depth and subsidence are shown at the top of the graph while sedimentation rate is shown at the bottom. The dotted line represents the depth to basement at different times (i.e. the subsidence). The filled circles represent the depth to basement with minimum and maximum water depth corrections and the shaded area represents the water depth correction itself.

The curve is based on the logs of Altiner *et al.* (1991), rather than my own, as I did not carry out detailed palaeontological age determinations. The mudstone-rich unit in the central part of the succession is reflected by the intervals of increased water depth and decreased sedimentation rate shown on the plot. The subsidence curve indicates a steady rate of subsidence from the Late Triassic to the Mid Jurassic, although this is extremely general as the dating does not allow better resolution.

5.9 Interpretation of the Halilar Formation

The carbonaceous black shales and sandstones which occur in the Lower and Middle Units of the Halilar Formation in the Havran region were probably deposited in a restricted marine environment, close to a vegetated landmass. The basin experienced regular influxes of coarse-grained clastics, resulting in the deposition of massive

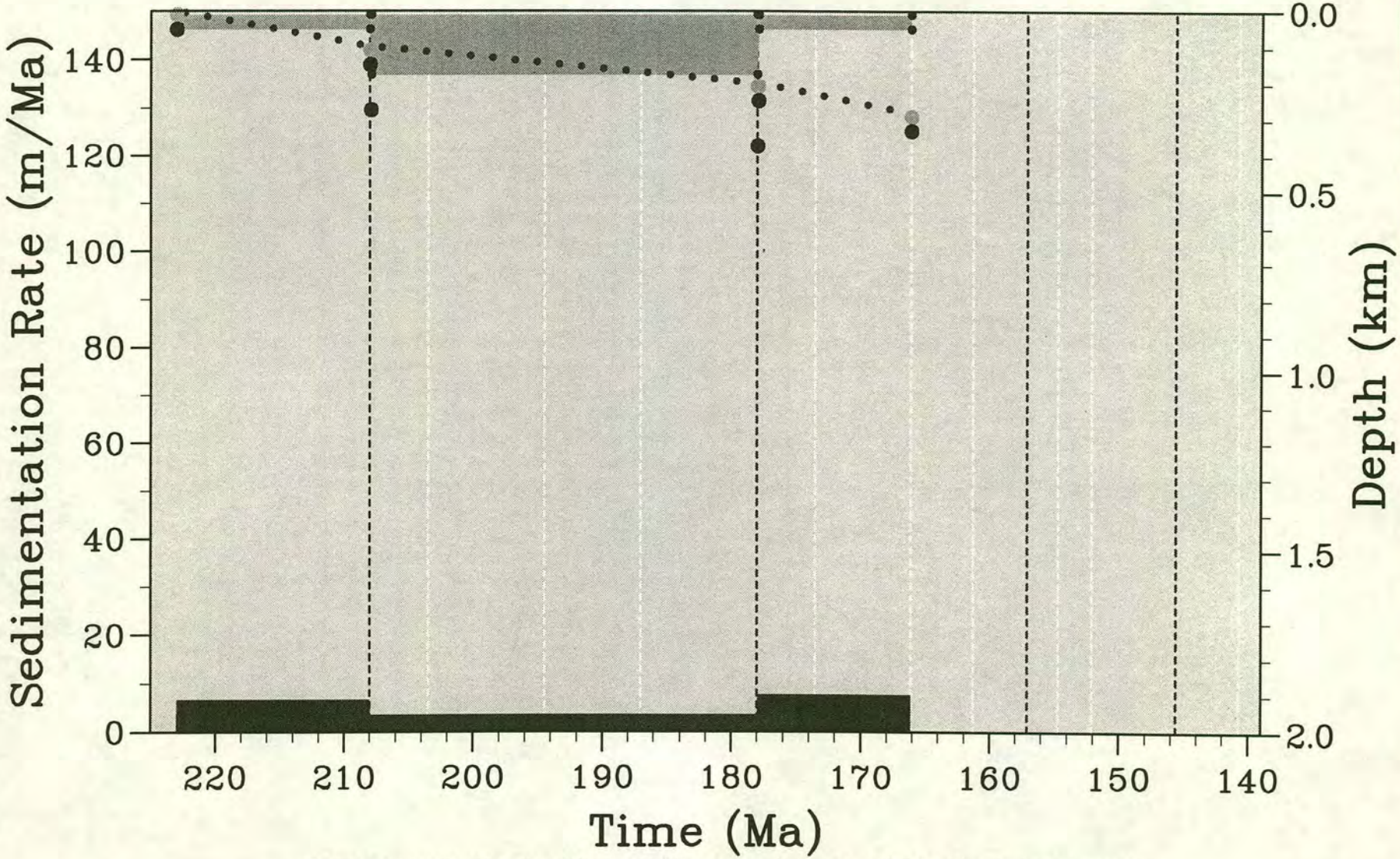

Figure 5.13 Highly simplified subsidence curve for the Halılar Formation, based on the measured sections and dates of Altıner *et al.* (1991). (subsidence programme: J. Turner, 1994).

sandstones, conglomerates and turbidite horizons. The clastic material was derived from relatively proximal metamorphic, plutonic and sedimentary sources. Plutonic components are abundant in the Lower and Middle Units, but only occur as rare clasts in the Upper Unit. Metamorphic clasts, especially strained quartz, occur throughout the Halilar Formation. Sedimentary clasts, especially fine-grained clastics, also occur throughout the sequence. Many of the thick conglomerates contain plant debris and ferruginous coatings on clasts, features indicative of a terrestrial or marginal-marine setting. Another conglomerate contains the same clast types but is non-ferruginous and rich in oyster fragments. These features may imply a laterally shifting, fluvial to shallow marine environment. Many of the massive sandstones contain thin, laterally discontinuous, conglomerate horizons, a characteristic feature of traction deposits. Large mud rip-up clasts are also common, especially in the Middle Unit, implying a relatively proximal source of semi-lithified mud and high energy currents. The turbidites in the upper part of the Middle Unit indicate a significant slope with a proximal source of mud and lithic clasts. Rare palaeocurrent indicators within these turbidites imply S- and SE-directed currents. Higher in the sequence the turbiditic horizons and massive sandstones give way to the bedded calcareous sandstones and shales of the Upper Unit of the Halilar Formation. These were probably deposited in a shallow-marine setting, as evidenced by shallow-water trace fossils and sparry calcite cements. The sandstones are rich in dark carbonaceous matter and mica flakes which indicate that a terrigenous source was still relatively close during this time. The quartz, feldspar and mica grains which constitute most of the clasts indicate that a plutonic and/or metamorphic source was still providing clastic material to the basin. The calcitic nature of the sandstone matrix and the presence of large carbonate concretions indicate the establishment of shallow conditions and herald the onset of carbonate deposition. Carbonate content increases upwards into the micritic lower levels of the Bilecik Limestone. Clastic supply did not cease suddenly, as the *Ammonitico Rosso* and nodular limestone facies do contain small grains of quartz.

Thus it appears that two periods of shallow water deposition (represented by the Lower and Upper Units) were separated by a period of relative deepening (the Middle Unit), as shown in the upper part of the plot in Figure 5.13. However, as there are no palaeobathymetric indicators for the Middle Unit it is impossible to make any definite statements. Initial shallow marine to fluvial deposition was followed by the accumulation of dark muds and sporadic coarse clastic influxes and turbidite flows. The establishment of shallower conditions was accompanied by incipient carbonate deposition and an abundant shallow marine fauna which created trace fossils. As the

clastic supply decreased, carbonate production increased and the Bilecik carbonate platform began to build up.

5.10 Upper Triassic-Lower Jurassic clastics in adjacent areas

Undeformed Early Mesozoic clastics are also exposed in the neighbouring regions of Çan, Edremit and Balya. Whereas the Havran sequence displays a continuous, or near continuous succession from Upper Triassic to Jurassic age, in the adjacent areas of Çan and Edremit, the Upper Triassic is missing and Lower Jurassic sedimentary rocks directly overlie the Karakaya basement. Near Balya, Upper Triassic shales and sandstones are overlain by clastics rich in Upper Permian limestone blocks, which are overlain in turn by Lower Jurassic clastics. The blocky horizons have been interpreted both as a stratigraphically conformable part of the sequence (Okay *et al.*, 1991) and as a nappe emplaced by gravity sliding (Aygen, 1956). On the basis of reconnaissance fieldwork in the Balya region, together with comparisons with similar sequences in the Bergama region, the gravity-emplaced nappe hypothesis seems more viable. However, much more work is necessary before this problem can be resolved.

5.10.1 Çan area

Jurassic clastic rocks, described as the Bayirköy Formation by Okay *et al.* (1991), are exposed in the Çan region as an 8m-thick horizon overlying spilitized volcaniclastic flows of the Karakaya Complex. The sequence is best exposed just outside the village of Çalköy (see Chapter 4; Figure 4.8) and is shown in the log in Figure 5.14a. Conglomerate with a calcitic cement forms the lowest horizon. Most of the clasts are well-rounded basalt pebbles with a wide variety of textures visible in thin section, including intersertal, intergranular, seriate, spherulitic, vesicular and porphyritic textures (Figure 5.14b). The clasts are set in a sparry calcitic matrix and have very sharply defined edges. There is no evidence of deformation, except for slight flattening of clasts where they are in contact with each other. Other clasts include clinopyroxene crystals and echinoderm fragments. The conglomerate passes up into a horizon of lenticular sandy limestone beds intercalated with thin siltstones. The sandy limestone passes up into green-brown shale and siltstone which contain the epifaunal bivalve *Bositra bronni* of Upper Liassic age (Okay *et al.*, 1991).

Approximately 5km NNW of Çalköy, the clastic sequence described above is absent and Bilecik Limestone directly overlies the Karakaya Complex (Okay *et al.*, 1991).

Figure 5.14

(a) Section through the Upper Liassic clastic/carbonate sequence overlying debris flows of the Çal Unit near the village of Çalköy in the Çan region.

(b) Photomicrograph of the basal conglomerate as logged in (a), showing basaltic clasts set in a sparry calcite matrix (PPL, field of view: 4.5mm).

(c) Photomicrograph of conglomerate overlying the Çal Unit on Kir Tepe in the Edremit region. Fine-grained basalt and micrite clasts lie within a sparry calcite matrix. Echinoderm and shell debris is clearly visible within the matrix (PPL, field of view: 12mm).

a

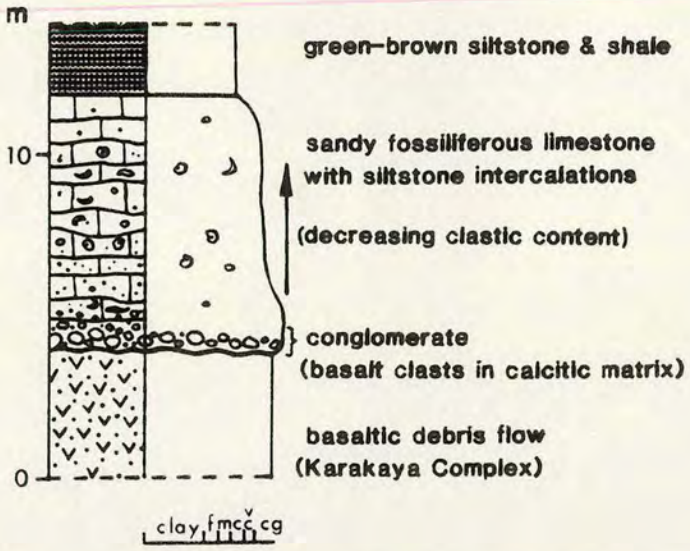
m
10
0
green–brown siltstone & shale
sandy fossiliferous limestone
with siltstone intercalations
(decreasing clastic content)
conglomerate
(basalt clasts in calcitic matrix)
basaltic debris flow
(Karakaya Complex)
clay f m c v cg

b

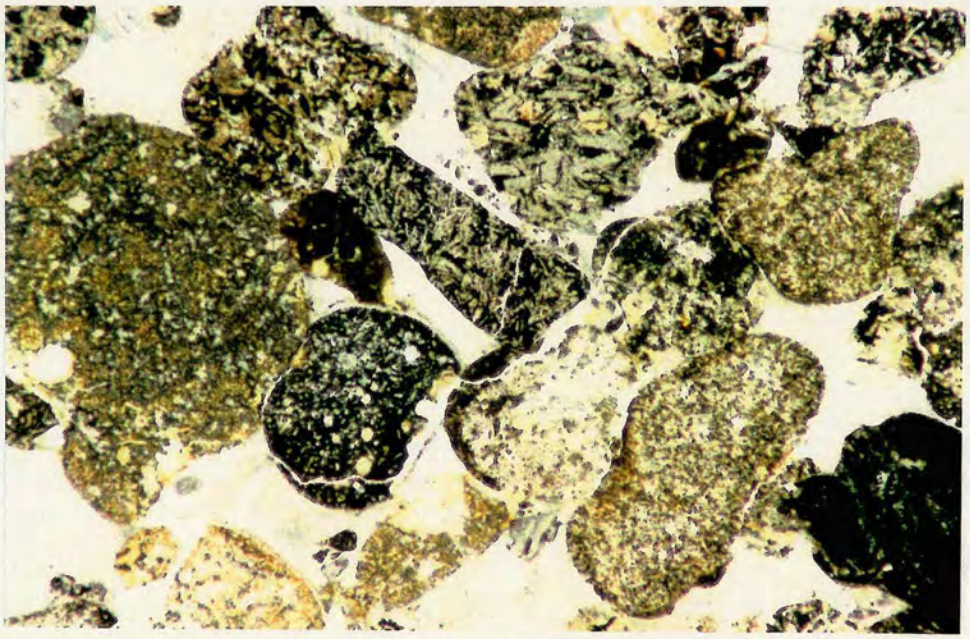

c

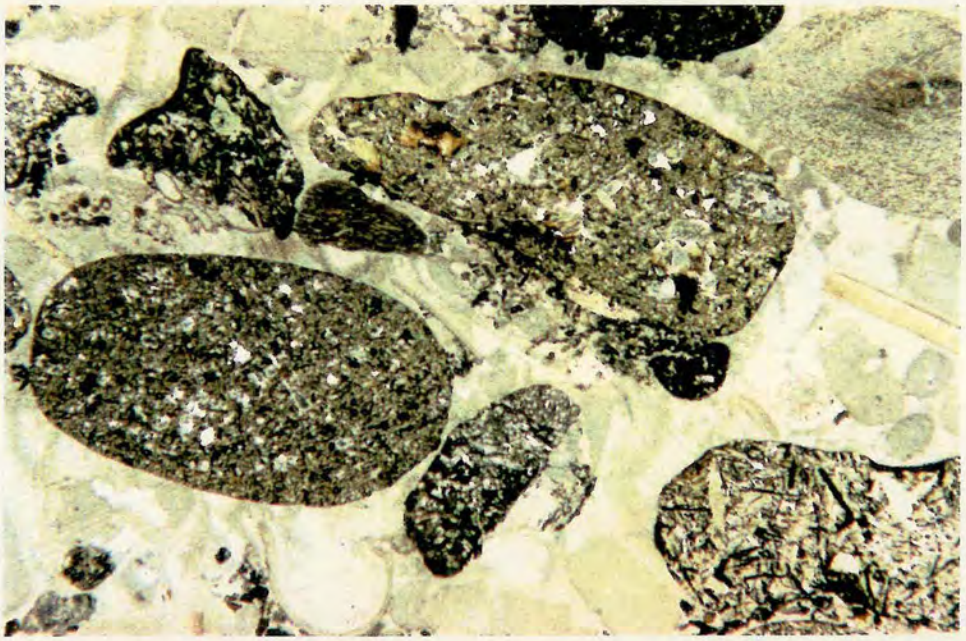

5.10.2 Edremit area

On the hill of Kir Tepe, north of Edremit (Figure 4.16), small outcrops of conglomerate similar to that exposed at Çalköy overlie Permian limestone of the Çal Unit (the upper unit of the Karakaya Complex). Definite correlation with the sequence near Can could not be made owing to the lack of any fossils at this locality. However, in thin-section the two conglomerates are very similar and, owing to their positions immediately above the Çal Unit, are interpreted to be part of the same sequence. Thin-section study reveals clasts of basalt, spherulitic glass, clinopyroxene crystals, shell and echinoderm debris and micrite in a sparry calcite matrix (Figure 5.14c). The basalt clasts display doleritic, trachytic and seriate textures. Rare large clasts of sandstone were also observed. They contain fragments of angular quartz, mica-rich schist, opaques, detrital biotite (altering to chlorite), devitrified volcanics and feldspar (e.g. plagioclase and perthite) in a dark red ferruginous matrix. The quartz is strained and shows undulose extinction and sub-grain formation. Many of the grains have calcite overgrowths. This conglomerate is correlated with the conglomerate observed near Çan, despite the absence of the rest of the sequence. The conglomerates from both sites are lithologically extremely similar and occupy positions directly above the Karakaya Complex.

At Çanlibaba, 2km NE of Edremit, poorly exposed clastics overlie recrystallized limestone of the Çal Unit and are overlain, in turn, by the Jurassic Bilecik Limestone (Figure 5.15). The lower clastics comprise grey-green siltstones and sandstones, rich in mica and plant debris, which pass up into medium- to coarse-grained sandstones in which individual beds display fining-upward sequences. In places the sandstone becomes conglomeratic. A clast of amphibolite was found within sandstone near the inferred unconformable contact with the underlying, deformed Karakaya Complex. No contacts are exposed, although it was possible to constrain them to within a few metres on the basis of soil colour and boulder distribution. From the outcrop pattern, it can be seen that the sandstone and siltstone sequence has a variable thickness. I found no evidence of faulting and deduced that the thickness variation is a primary sedimentary feature.

5.10.3 Balya area

The clastic sequence north of Balya comprises hundreds of metres of arkosic sandstones which pass up, through a few tens of metres of muddy sandstone, shale,

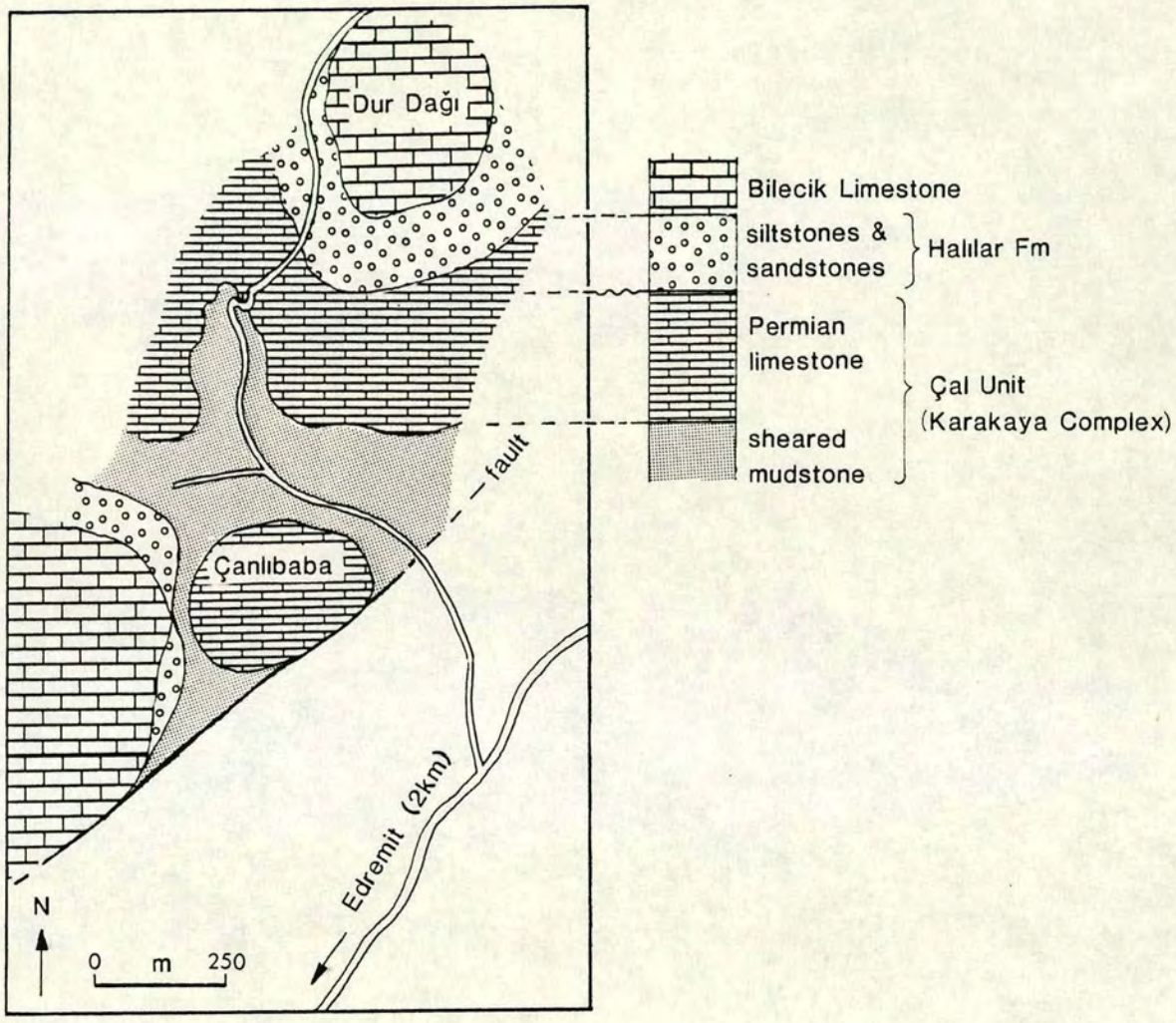

Figure 5.15 Sketch map of the Çanlıbaba area 2km NE of Edremit, showing Triassic-Jurassic clastics and carbonates overlying the Karakaya Complex.

chert and calcturbidite, into debris flows rich in Upper Permian limestone blocks (Okay *et al.*, 1991). The transition from arkosic sandstones to debris flows was observed by Okay *et al.* (1991) near the village of Gerdeme, southwest of Gönen. I did not investigate this northern part of the Balya region.

Near Balya black shales containing the pelagic bivalve *Halobia neumayri* Bittner (Aygen, 1956), pass up into yellow-brown sandstones and siltstones, rich in plant debris, brachiopods, bivalves and ammonites (Okay *et al.*, 1991). Aygen (1956) described an Upper Triassic fauna from these shales and sandstones. The 100m-thick sandstone and shale sequence is overlain by conglomerates rich in Upper Permian limestone clasts (Okay *et al.*, 1991). The conglomerates are interbedded with coarse-grained sandstones and contain rounded clasts of grey and white limestone, beige siltstone and coarse-grained arkosic sandstone. Good exposures of conglomerate are also found a few kilometres north of Balya and a representative log is shown in Figure 5.16. The conglomerate is clast-supported, poorly sorted and has crude bedding. The clasts are well-rounded and include crinoidal limestone, algal limestone, basalt, black chert, green mudstone rip-up clasts, conglomerate, sandstone and pale green felsic volcanics. The maximum clast size is about 30cm. Green volcanics and crinoidal limestone are the most common clast types. The conglomerate horizon is approximately 24m thick and overlies micaceous, green siltstone and sandstone. The conglomerates pass up through a region of poor exposure into recrystallized limestone of Permian age, which is discussed in Chapter 4. Owing to the juxtaposition of Permian rocks over Triassic rocks this contact probably represents a major tectonic boundary. During emplacement some disruption may have occurred, producing the disrupted limestone sequences and debris flow horizons. Okay *et al.* (1991) reported that the limestone debris flows of the Balya region are unconformably overlain by calcareous sandstones of the Jurassic Bayirkoy Formation.

5.11 Age of the clastic sequences

Krushensky *et al.* (1980) and van der Kaaden (1959) reported Late Triassic (probably Norian-Rhaetian) bivalves and brachiopods from the lower part of the Halilar Formation in the Havran area. The abundance of the pelagic bivalve *Bositra buchii* in the middle portion of the Halilar Formation may indicate an Early Dogger (Aalenian-Bajocian) age (Altiner *et al.*, 1991). Since the lowest levels of the Bilecik Limestone are Bajocian in age (Altiner *et al.*, 1991), the Halilar Formation may be assigned to the Norian-Bajocian.

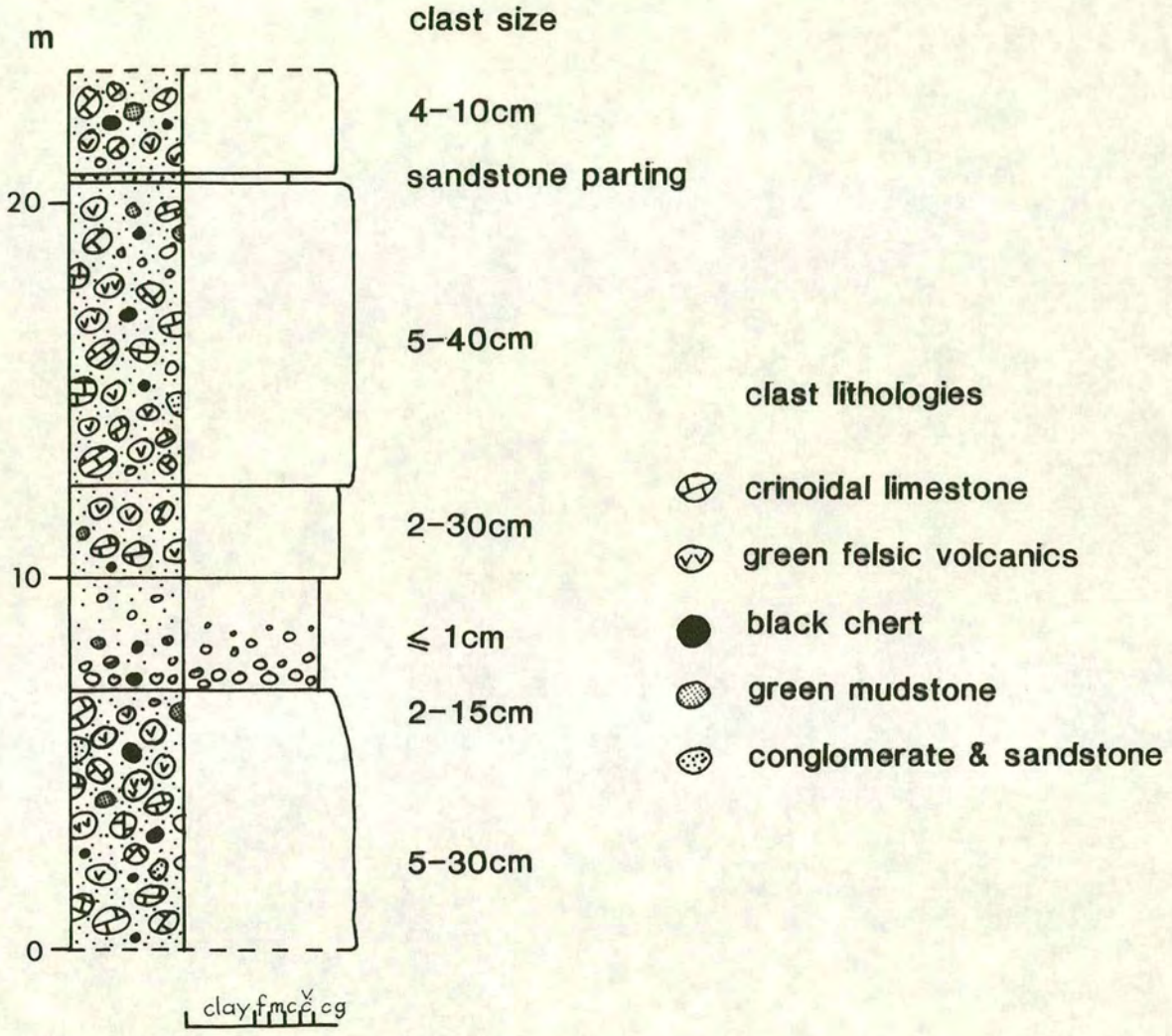

Figure 5.16 Representative log through conglomerate of probable Upper Triassic age, north of Balya.

In the Çan and Bursa-Bilecik areas Upper Triassic sequences are absent and the Karakaya Complex is directly overlain by clastics of Lower Jurassic age (Bayirköy Formation in the literature). In the Çan area the clastic sequence contains the bivalve *Bositra bronni* which indicates an Upper Liassic age (Okay *et al.*, 1991). In the Bursa-Bilecik area the upper part of the Bayirköy Formation is dated on the basis of Jurassic foraminifera which are older than the overlying Upper Sinemurian-Lower Pliensbachian *Ammonitico Rosso* of the Bilecik Limestone (Altiner *et al.*, 1991). Thus, a Hettangian or Sinemurian age is probable.

5.12 Provenance of the clastic sequences

A wide range of metamorphic, plutonic and sedimentary components have been identified within the Halilar Formation. The large undeformed granodiorite clasts which characterize the Lower and Middle Units imply that a plutonic source dominated during the early history of the sequence and was probably the eroded granodiorite pluton (Çamlik Metagranodiorite) over which the sequence was laid down. A metamorphic source was also present, as indicated by the presence of abundant strained quartz as well as phyllite, quartzite, schist and gneiss clasts. Sedimentary components are present as mudstone clasts and relatively rare siltstone and sandstone clasts. Surprisingly, no volcanic clasts derived from the underlying Karakaya Complex were observed. This may imply a very localized source area for the Halilar Formation.

By contrast, volcanic clasts were the most abundant clast type in the Upper Liassic rocks near Çan and Edremit. In both these areas the volcanic clasts were probably derived from the underlying basaltic debris flows of the Çal Unit. Echinoderm debris observed in these rocks was probably reworked from local Liassic carbonate build-ups (marking the start of Bilecik Limestone deposition). Similar fossil debris is also present in the Upper Unit of the Halilar Formation, but is also unfortunately undatable. Upper Triassic clastics in the Balya region are also rich in volcanic (including both basaltic and felsic varieties) and carbonate clasts.

5.13 The Bilecik Limestone

The Bilecik Limestone is the most common and widely distributed Early Mesozoic lithology in NW Turkey. It caps the underlying Karakaya units with or without an intervening clastic sequence, such as those described above. In the Havran area the

Bilecik Limestone is separated from the underlying Karakaya Complex by at least 900m of Upper Triassic-Jurassic clastics, whereas near Can it overlies debris flows of the Karakaya Complex with an intervening clastic sequence of only a few metres. North of Edremit, on Durdag hill, there is a similar situation, with only a few metres of clastics between Permian limestone blocks of the Çal Unit and the Jurassic Bilecik Limestone (Figure 5.15). Extensive exposure of the Bilecik Limestone occurs further east near its type locality, the town of Bilecik. This study deals in the most part with the outcrops which are found in the Edremit-Havran region of the Biga Peninsula (Figure 5.1).

5.13.1 Limestone facies at Koçacal Tepe

The gorge running approximately N-S through the hill of Kocaçal Tepe, near the village of Sarniç (Figure 5.3), provides the best exposures of the Bilecik Limestone in the Edremit-Havran area. Fossiliferous, bedded, pink and grey limestone passes up into the massive white limestone which forms the impressive cliffs of the gorge and Kocaçal Tepe itself. Most of the exposed rock within the gorge is inaccessible, but good outcrops of the Bilecik Limestone can be observed at the northern end of the gorge where Pinar Dere cuts into Kocaçal Tepe. The limestone at this locality represents the lower horizons of the Bilecik Limestone, as suggested by its proximity to the underlying clastics and confirmed by the pink colour of the micrite and the presence of loose blocks of *Ammonitico Rosso*-type limestone.

The best examples of *Ammonitico Rosso*-type facies are found among the loose boulders, up to several metres in size, which litter the northern end of the gorge. The blocks have clearly not been transported far and provide an excellent indication of the range of facies which originally formed the lower levels of the Bilecik Limestone in this area. Altiner *et al.* (1991) reported the presence of a 1-1.5m-thick stromatolitic and pelletal limestone layer at the base of the Bilecik Limestone which was not observed at this locality. Most of the *in situ* exposure of Kocaçal Tepe gorge consists of bedded grey micrite and nodular pink micrite, both containing ammonite-rich horizons. The range of facies observed within the northern part of the gorge are described below.

a) Dark red micrite with ammonites

This facies is pink to dark red and contains micrite fragments, ammonites, belemnites and thin-shelled bivalves in a pink/red micritic matrix (e.g. Figure 5.17a). The matrix

Figure 5.17

(a) *Ammonitico Rosso*-type facies in the Kocaçal Tepe gorge, showing a well-preserved ammonite in a slightly nodular pink and red micritic matrix.

(b) Photomicrograph of grey biomicrite from the section shown in Figure 5.18. An ammonite with a micrite infill, a belemnite and several bioclastic clasts are enclosed within a fine-grained bioclastic matrix which contains thin-shelled bivalves, echinoderm plates and foraminifera (PPL, field of view: 24mm).

(c) Field photograph of grey biomicrite nodules in a slightly marly, orange biomicrite matrix. Despite their clast-like appearance the nodules are diagenetic.

a

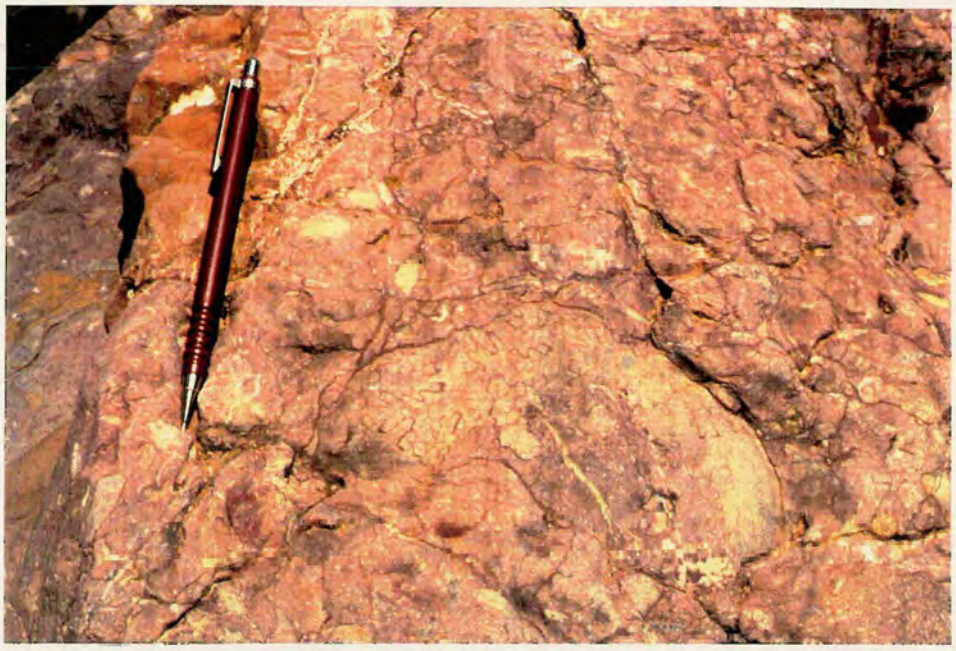

b

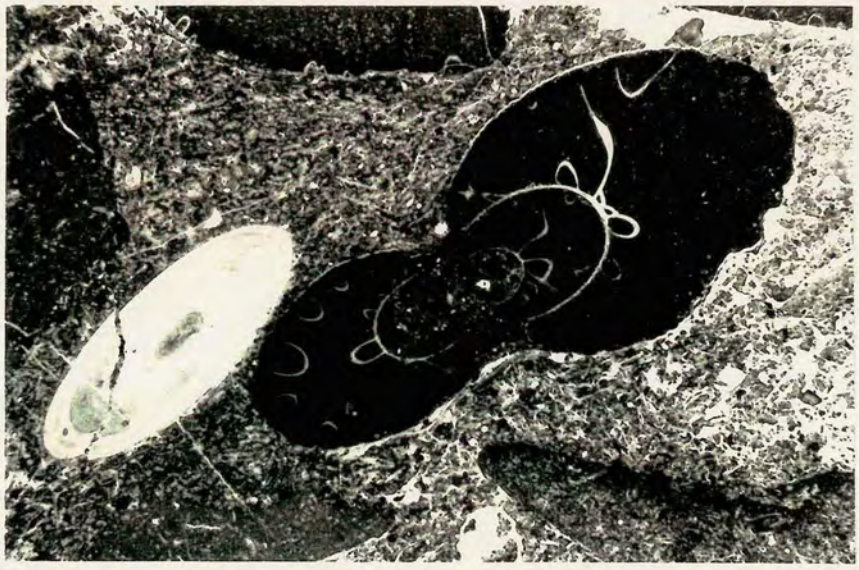

c

is rich in echinoderm fragments, bryozoa, micrite fragments, small angular quartz clasts and glauconitic grains. Several "clasts within clasts" were also observed; for example, one micrite clast contains a smaller micrite clast which itself contains echinoderm fragments and quartz grains. This facies was not found *in situ* in this area and was only observed at Kocaçal Tepe as a large loose boulder within the gorge.

b) Nodular pink biomicrite with ammonites

The pink biomicrite facies contains no exotic clasts and has a nodular appearance. It is rich in small ammonites, echinoderm debris, thin-shelled bivalves and foraminifera. The ammonites contain micritic infills which are slightly more ferruginous than the rest of the limestone and which contain abundant shell fragments and foraminfera. Rare micrite clasts were also observed. It alternates with fossiliferous grey biomicrite on a 10cm scale. There is a complete spectrum between the pink and grey biomicrite facies.

c) Pink micrite breccia

This facies was not observed as an *in situ* exposure, only as large blocks at the mouth of the gorge. The facies comprises intraformational, clast-supported breccias of angular pink and light grey micrite fragments, surrounded by seams of pink to red micrite. Various stages of brecciation are represented, from fractured micrite to separate micrite clasts in a red carbonate matrix.

d) Nodular, bedded grey biomicrite with ammonites

This was the most commonly observed facies. Light grey micrite, rich in ammonites and generally slightly nodular, is bedded on a 30cm scale. It is also found interbedded with pink nodular biomicrite. Loose boulders of very dark grey, nodular, bedded micrite containing large ammonites (up to 10cm across) were found within the gorge and may represent a more organic-rich part of the same facies. The grey micrite commonly contains alternations of relatively homogeneous micrite and very fossiliferous horizons which comprise chaotic shell debris, belemnites and ammonites (Figure 5.17b). Foraminifera, thin-shelled bivalves, calcispheres, echinoderm and bryozoa fragments, and small, angular quartz clasts were also observed in thin section. Figure 5.18 shows a representative log through this facies and the orange biomicrite facies described below.

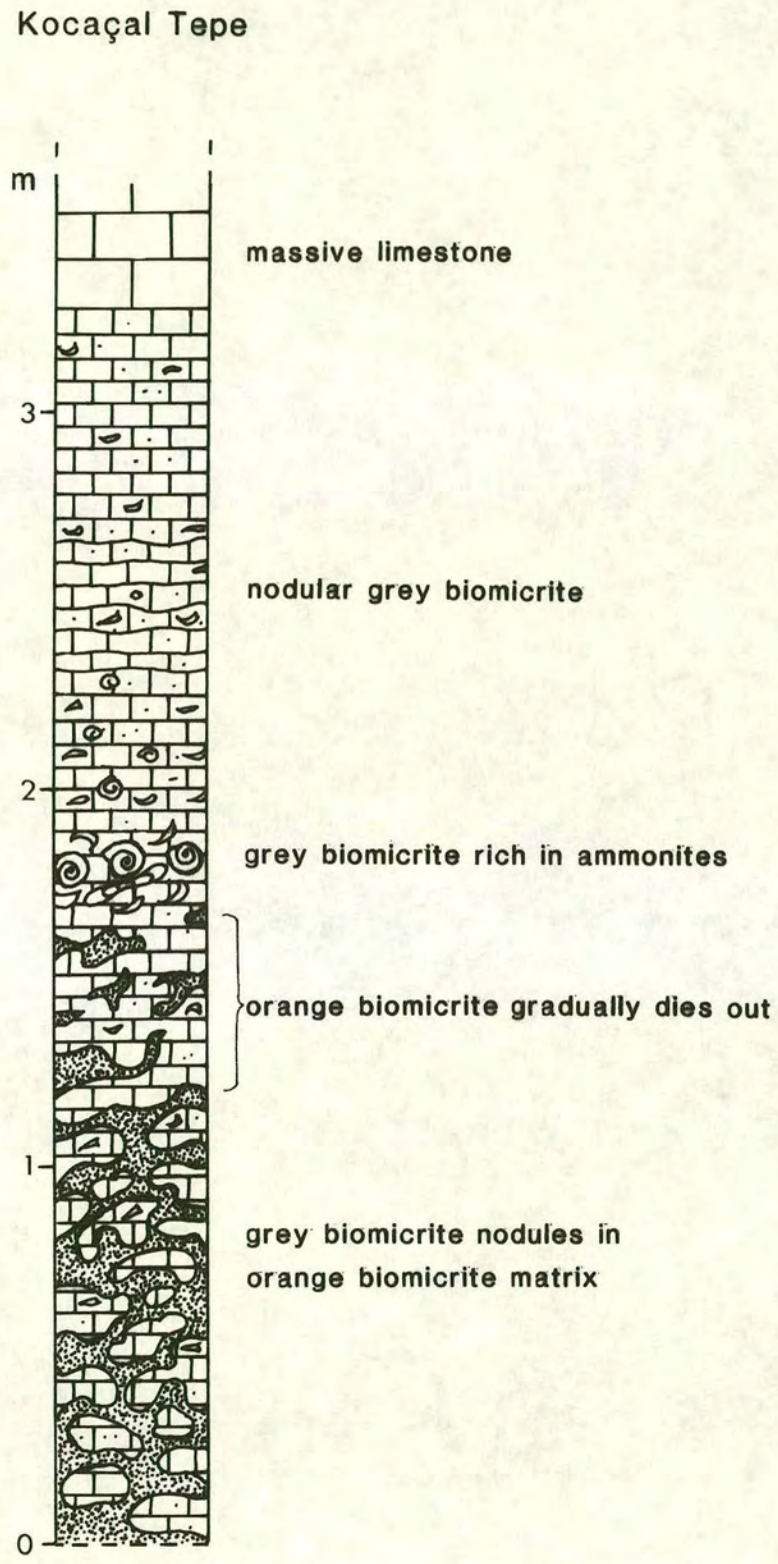

Figure 5.18 Section measured through the lower levels of the Bilecik Limestone on Kocaçal Tepe, showing limestone facies (d) and (e) described in the text.

e) Diagenetic orange biomicrite

Orange biomicrite is intimately associated with the grey biomicrite facies, forming outcrops with a conglomeratic appearance. Patches of the two types of facies form very rounded amorphous shapes with sharp boundaries which initially look like clasts and matrix, as shown in Figure 5.17c. However, a belemnite was observed which crosses the boundary between a "clast" and "matrix", proving the diagenetic nature of their association. The lithologies of the orange and grey facies are almost identical, although the orange biomicrite is slightly coarser grained and more marly than the grey biomicrite.

f) Silicified limestone with relict brecciation

Silicified limestone is a common lithology, capping the tops of the hills in this region and occurring as loose boulders in the Kocaçal Tepe gorge. It has a brecciated and slightly translucent appearance, and is orange in colour. Originally, it was probably a micrite which became brecciated and silicified by hot fluids during the extensive volcanic activity which occurred in NW Turkey during the Oligo-Miocene. It cannot therefore be properly considered as a truly separate limestone facies.

5.13.2 Fossil asemblages of the Bilecik Limestone

Detailed palaeontological work was carried out on the Bilecik Limestone of NW Turkey by Altiner *et al.* (1991) and is summarized below.

The lowest 92m of the Bilecik Limestone, which defines the Tascibayiri Formation of Altiner *et al.*(1991), is very rich in ammonites, thin-shelled bivalves and foraminifers. They have identified stephanoceratid ammonites and *Garantiana* sp. which indicate Middle and Upper Bajocian ages respectively. Another ammonite found in these levels, *Prohectinoceras retrocostatum*, indicates the Upper Bathonian (Cope, 1991). Altiner *et al.* (1991) also observed thin-shelled bivalves (*Bositra*?) and the foraminifers *Globuligerina* gr. *oxfordiana*, *Palaeomiliolina* sp., *Ophthalmidium* sp. and *Globochaete alpina*; and, in the upper levels, *Tubiphytes morronensis*, *Lenticulina* sp., *Spirillina* sp., Ataxophragmiidae, Miliolidae, corals and echinoids. These fossil assemblages indicate a Bajocian to early Kimmeridgian age.

The overlying Gunören Formation (260m thick) of Altiner *et al.* (1991) is rich in coral boundstones and bioclastic packstones. Altiner *et al.* (1991) identified scleractinian corals, *Tubiphytes morronensis*, *Lithocodium* sp. and bryozoa within the massive

limestones. They also found *Valvulina* sp., Ataxophragmiidae and Miliolidae. Altiner *et al.* (1991) attributed a possible Kimmeridgian-Tithonian age to the Gunören Formation owing to the absence of a Cretaceous fauna.

Dating of ammonites, belemnites and foraminifers by Altiner *et al.* (1991) in their Tascibayiri Formation (approximately the lower 100m of the Bilecik Limestone in the Havran area) has yielded a Middle Bajocian to Early Kimmeridgian age range. The basal condensed levels are limited to a Bajocian-Bathonian age (Altiner *et al.*, 1991). Athough the absence of any Cretaceous elements in the overlying Gunoren Formation has led to the assignation of a possible Kimmeridgian to Tithonian age for this unit (Altiner *et al.*, 1991), the upper age limit of the Bilecik Limestone in the Biga Peninsula is not well constrained, owing to incomplete sequences. In the more complete sequences of the Bilecik region the upper levels of the Bilecik Limestone contain foraminifers from the Hauterivian of the Early Cretaceous (Altiner *et al.*, 1991).

5.14 Interpretation of the Bilecik Limestone

The condensed nodular limestones and *Ammonitico Rosso*-type facies which characterize the lower levels of the Bilecik Limestone in the Havran area are typical continental plateau or seamount facies (Bernoulli & Jenkyns, 1974; Jenkyns, 1986). These facies develop as a result of the curtailment of pelagic and some benthic carbonate deposition by strong currents. Similar facies are also present in the Bursa-Bilecik area, implying that the sequence developed over a relatively wide region, probably a plateau rather than an isolated seamount. The presence of pelagic oolites (as described by Altiner *et al.*, 1991) implies an open marine, shallow setting with relatively strong wave action. The stromatolites reported by Altiner *et al.* (1991) also confirm that the basal part of the Bilecik Limestone developed in a very shallow marine environment. The abundance of pelagic fossils such as ammonites, belemnites and globigerinids throughout the nodular facies near the base of the Bilecik Limestone indicates an open marine setting. The presence of small angular quartz clasts in these facies indicates a proximal terrigenous source and indicates an environment in which clastic input competed with carbonate production. The sequence passes upwards into the coralline and algal build-ups described by Altiner *et al.* (1991), which represent more stable conditions and the full establishment of the carbonate platform.

5.15 Cretaceous limestones in the Biga Peninsula and adjacent areas

In the Biga Peninsula the Bilecik Limestone extends as far up as the Aptian (Altiner *et al.*,1991). It is overlain disconformably by the Vezirhan Formation of Altinli (1973b) which comprises about 30m of thin- to medium-bedded white and pink pelagic limestones (Okay *et al.*, 1991). Okay *et al.* (1991) described the formation from various localities, including south of Biga and north of Balya (Figure 5.2). The formation has been dated on the basis of radiolaria and *Hedbergella* sp., which are characteristic of the Aptian-Maastrichtian, and one sample of *Banetocardiella conoidea* which indicates an Albian-Cenomanian age (Okay *et al.*, 1991).

Lower Cretaceous limestone, possibly equivalent to the Vezirhan Formation, has also been recognized in the Bursa-Bilecik region and was called the Sogukcam Limestone by Altinli (1973b). According to Altiner *et al.* (1991) the sequence has a condensed lower portion which passes up into thin- to medium-bedded, pink and white porcelaneous limestones with chert nodules and planktic foraminifers. Planktonic and benthic foraminifera of Late Hauterivian age are found in the condensed levels and Barremian-Late Aptian planktic foraminifers occur in the porcelaneous limestone (Altiner *et al.*, 1991).

5.16 Correlation with Upper Triassic-Jurassic units in adjacent areas

Comparison of Upper Triassic-Jurassic sequences studied in this thesis with those investigated by other workers elsewhere in NW Turkey reveals several important differences. Most importantly, the sequence below the Bilecik Limestone in the Havran region is very different from those observed anywhere else in NW Turkey. The Halilar Formation indicates continuous clastic deposition from Late Triassic to Bajocian/Bathonian times, a sequence which is not observed elsewhere. By contrast, in the Bursa and Bilecik regions, the Upper Triassic is absent and Hettangian-Sinemurian clastics lie directly on Karakaya-type basement followed by a Pliensbachian-Bajocian hiatus (Altiner *et al.*, 1991). However, above the condensed Bajocian and Bathonian horizons of the Bilecik Limestone the Callovian-Upper Jurassic stratigraphy of the Havran and Bursa-Bilecik areas is almost identical (Altiner *et al.*, 1991), indicating that the Havran "basin" had been entirely filled by this time.

The pre-Cretaceous successions of the Biga Peninsula and Bursa-Bilecik regions differ markedly from the Mudurnu-Nallihan sequence further east. The Lower Jurassic is missing from the Mudurnu-Nallihan sequence which, unlike the sequences further west, includes volcanics and volcaniclastics. The age of the volcanics corresponds approximately to the Pliensbachian-Bajocian hiatus of the Bursa-Bilecik sequence. Although carbonate deposition began in the Callovian it was interrupted by debris flows, slumps and redeposited calcturbidites.

5.17 Interpretation of Triassic-Jurassic sequences in terms of tectonic setting

The Halilar Formation may represent a "perched" fore-arc basin sequence which developed on top of the "Karakaya" accretionary complex. This postulation is based on the age of the sequence, its relatively undeformed nature, and its unconformable position immediately above the Karakaya Complex. Such basins have been recognized in modern convergent settings by seismic profiling (e.g. the Columbia fore-arc, SW Caribbean Plate, Lu & McMillen, 1983; the Sunda fore-arc, Stevens & Moore, 1985; the Japan Trench, von Huene & Arthur, 1982). Accretionary-top basins from the Sunda fore-arc have dimensions ranging from 3 by 1km and a few hundred metres of sediment fill, to 21 by 4km with greater than 600m of sediment fill (Stevens & Moore, 1985). The Halilar "basin" contains 900-1000m of sediment and thus, compared with the Sunda fore-arc basins, would represent a large perched fore-arc basin. However, there are several features of the Halilar sequence which differ from both the predicted and observed characteristics of accretionary-top basins. Pickering *et al.* (1989) have shown how supra-accretionary prism basins may develop a shallowing- and coarsening-upward sequence as such a basin is simultaneously uplifted and transported away from the trench. They also postulated that internal deformation, although gentle, should increase with depth and towards the margins of the basins. In the Halilar sequence the large scale coarsening-up succession which would be expected for a progressively uplifted basin is not observed. Although the calcareous sandstones in the Upper Unit are certainly shallow-water deposits, the conglomerates at the base of the sequence also appear to have been laid down in very shallow conditions. The intervening mudstones reflect deeper, more restricted conditions. As regards deformation, the lower levels of the Halilar Formation display no evidence of the folding or shearing one would expect if the basin had been forming on an actively deforming accretionary prism. This may imply that deposition only started after the cessation of accretionary tectonics, or at least a considerable distance from the active deformation front.

The basin was clearly relatively localized as indicated by its restricted range of clast lithologies (a large basin would probably have sampled a greater range of Karakaya lithologies) and by the absence of the Upper Triassic in any of the other clastic sequences in the Biga Peninsula and surrounding regions. The Lower Jurassic clastic sequences in the Çan, Edremit and Bursa-Bilecik areas probably represent "background" sedimentation in NW Turkey during this time. These Lower Jurassic clastics are ubiquitous over NW Turkey and indicate reworking and redeposition of lithologies from the accretionary complex in a shallow sea. The presence of carbonates within these clastics implies some carbonate production, possibly as relatively isolated build-ups. By the Mid Jurassic the extensive Bilecik Limestone carbonate platform had been established. Figure 5.19 shows a series of cartoons (after Altiner *at al.,* 1991) illustrating the possible palaeogeographic evolution of NW Turkey from the Hettangian to the Oxfordian.

5.18 Analogues for the Halilar Formation

A similar sequence to the Halilar Formation occurs in the Neotethyan Maden Complex of SE Turkey. The Palaeocene-Eocene Hazar Group forms part of the Maden Complex and overlies the deformed and eroded Upper Cretaceous Güleman ophiolite. It comprises, in ascending order, red conglomerates and sandstones (Ceffan Formation), flysch (Simaki Formation) and pelagic or redeposited limestones (Gehroz Formation). Aktas & Robertson (1984) have interpreted the red conglomerates of the Ceffan Formation as sub-aerial clastics, laid down as small, alluvial fans. They interpreted the sandstones as channelized, braided stream deposits. A transgression, accompanied by subsidence, led to the deposition of flysch-type deposits of the Simaki Formation, together with minor lavas. The Gehroz Formation either unconformably overlies the Simaki Formation, or is directly above the ophiolitic basement. The sequence consists of pelagic and bioclastic limestones and has been interpreted as representing both basinal and coastal settings (Aktas & Robertson, 1984). Aktas & Robertson (1984) have interpreted the Hazar Group as a sequence recording the gradual peneplanation of a rugged landmass, followed by rapid differential subsidence. The resulting flysch sequence was bordered by carbonate build-ups which progressively infilled the basin. In terms of tectonic setting, they envisaged it as a subsiding fore-arc basin above a northward-dipping Neotethyan subduction zone.

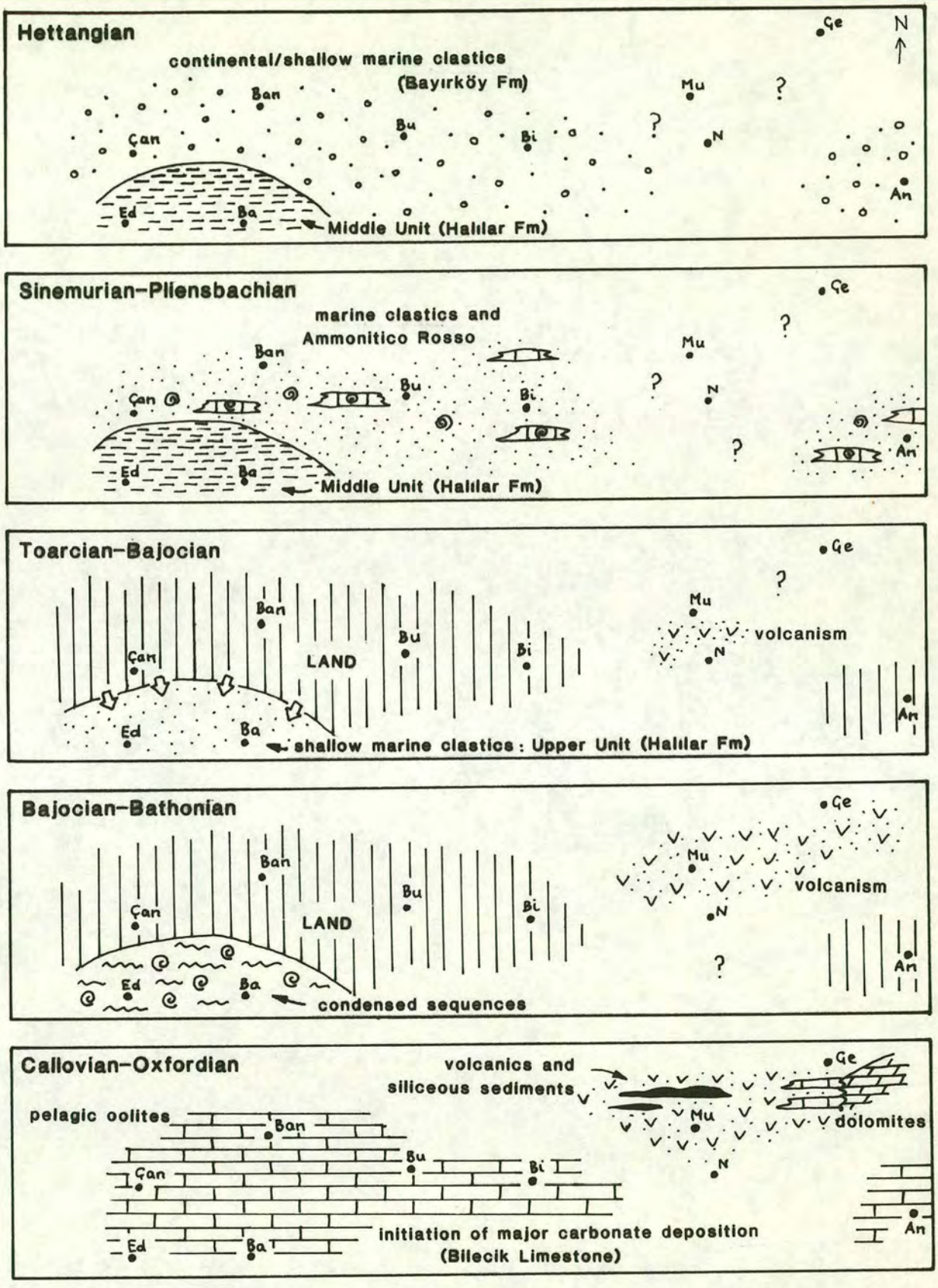

Figure 5.19 Cartoon maps showing the Jurassic palaeogeographic evolution of NW Turkey. (Ed: Edremit, Ba: Balya, Ban: Bandırma, Bu: Bursa, Bi: Bilecik, Mu: Mudurnu, N: Nallıhan, Ge: Geyve, An: Ankara) (see Figure 5.2 for map of region). Slightly modified after Altıner *et al.* (1991).

The Hazar Group as a whole bears many similarities to the Halilar-Bilecik sequence. The red conglomerates and massive sandstones of the Lower Unit of the Halilar Formation may be equivalent those of the Ceffan Formation, whereas the Middle and Upper Units may reflect similar depositional conditions to the Simaki Formation. The uppermost part of the sequences, in both cases, are represented by shelf limestone successions (Bilecik Limestone and Gehroz Formation respectively). Unlike the Hazar Group, however, volcanic rocks do not occur in the Halilar-Bilecik sequence. The Hazar Group and Halilar-Bilecik sequence also differ in the nature of their basements. The Hazar Group is largely floored by the deformed and eroded Upper Cretaceous Guleman ophiolite, whereas the Halilar-Bilecik sequence overlies the Karakaya Complex and the Camlik Metagranodiorite which intrudes it. The lack of volcanic material implies that the Halilar "basin" was not formed adjacent to a volcanic arc, unlike the Hazar Group. The Karakaya basement to the Halilar sequence also indicates a position above an accretionary complex, rather than behind it, as in the case of the Hazar Group. This suggests the unusual scenario of a subsiding, accretionary-top basin, contrary to what one would expect for a basin formed on a growing accretionary complex (e.g. Pickering *et al.*, 1989). A possible explanation could be that subduction and accretion ceased during deposition of the Halilar Group, leading to subsidence of the underlying accretionary basin.

The "Cambria slab" in central California may also represent a ponded trench-slope basin which formed on an accretionary complex (e.g. Cloos & Apted, 1979). The Cambria slab sequence comprises 4km of massive, thick-bedded greywacke with minor interbedded shale. The sandstones overlie metamorphosed melanges of the Franciscan Complex, but are themselves unmetamorphosed and contain well-preserved sedimentary structures. At the Franciscan-Cambria slab contact, blocks of the Cambria slab are incorporated into the Franciscan melanges (Smith *et al.*, 1979), implying that the underlying accretionary complex was actively deforming during deposition of the sequence. The predominance of coarse-grained, massive sandstone and the abundance of soft-sediment deformation structures have been interpreted as indicators of rapid deposition in a channelized mid-fan environment (Cloos & Apted, 1979).

Other examples of inferred perched fore-arc basins are present within the metamorphic belts of Japan. For example, thick Cretaceous sandstone sequences within the Shimanto Belt (e.g. the Muroto-hanto Group) have been interpreted as submarine channel and fan complexes formed in basins lying on an accretionary

complex (Taira *et al.*, 1982). Similar lithological associations are also present in the Eocene to Oligocene parts of the Shimanto Belt (e.g. the Kumage Group). These rocks are considerably deformed but, nevertheless, display the characteristic thickening- and coarsening-upwards cycles of many perched fore-arc basins (Taira *et al.*, 1982).

5.19 Conclusions

1. The Karakaya Complex in the Biga Peninsula and Bursa-Bilecik areas is overlain unconformably by Upper Triassic-Lower Jurassic (Halilar Formation), or Lower Jurassic (Bayirkoy Formation) clastic sequences, which are in turn overlain by the Jurassic Bilecik Limestone.

2. The Lower and Middle Units of the Halilar Formation comprises interbedded sandstones, conglomerates and mudstones which display features characteristic of a predominantly shallow marine environment, which often experienced deposition by mass flow and possibly turbidity currents. A predominance of dark mudstone in the Middle Unit may be evidence for a period of relative deepening. The sandstones in the Upper Unit of the Halilar Formation were laid down in a shallow marine environment, as evidenced by shallow marine trace fossils and calcitic cements.

3. Lower Jurassic sequences from the Can and Edremit areas contain carbonate fragments and basaltic clasts derived from the underlying Karakaya Complex, in a sparry calcite matrix. Clastic content decreases upward, indicating the gradual establishment of conditions favourable for carbonate production.

4. The Middle-Upper Jurassic Bilecik Limestone overlies the Halilar and Bayirkoy Formations. Nodular limestones and *Ammonitico Rosso*, both containing lithic and quartz clasts, pass up into bedded grey biomicrite. The upper levels of the Bilecik Limestone comprise coralline and algal boundstones. The Bilecik Limestone is interpreted as a carbonate sequence which built upwards from basal *Ammonitico Rosso* and other condensed facies into massive coralline and algal build-ups, reflecting the establishment of a stable platform environment.

5. The Halilar sequence is tentatively interpreted as the clastic fill of a perched fore-arc basin lying on top of the " Karakaya" accretionary complex. Cessation of subduction-accretion tectonics led to the formation of a stable platform, the Bilecik Limestone.

CHAPTER 6

THE KAZDAG MASSIF: A METAMORPHIC CORE COMPLEX

6.1 Introduction

The Kazdag Massif (Mount Ida in Homer's Iliad) is a NE-SW trending mountain range situated north of the Gulf of Edremit (Figure 6.1). It is approximately 50km by 20km in size and rises to the peaks of Sarikiz Tepe, Babadag and Kirklar Tepe, up to 1774m above sea level. It forms an impressive range which dominates the coastal plains to the northwest (the site of ancient Troy) and the rolling hills of the Edremit-Havran region to the southeast.

The Kazdag Massif comprises a sequence of metamorphic rocks which are folded into an anticline which has a broadly domal shape. On its eastern side the Kazdag Massif is tectonically juxtaposed against volcanic rocks of the Karakaya Complex. To the west it has a faulted contact with an Upper Cretaceous mélange (the Çetmi Mélange of Okay *et al.*, 1991) and, along its western margin, is intruded by the Evciler Granodiorite of probable Late Tertiary age. The base of the Kazdag Massif is not exposed and a total structural thickness of over 10km has been estimated by Okay *et al.* (1991).

Banded quartzo-feldspathic gneiss intercalated with marble and amphibolite forms the most common lithological association in the Kazdag Massif. Outcrops at the summit of Kazdag reveal rocks from the core of the dome, including metagabbro, metaharzburgite, plagiogranite and amphibolite. Although an age determination for the gneisses indicates a possible Upper Triassic age (Bingöl, 1971), isotopic dating of these rocks has as yet proved very inconsistent and the ages appear to have been reset by Oligo-Miocene magmatic activity in the region.

Detailed petrographic, metamorphic and structural investigations of the Kazdag rocks were not made during this study. Rather, work was aimed at deducing the general structure of the Kazdag Massif, its relationship with surrounding units and its significance in terms of the evolution of this region of NW Turkey. A general description of the main lithologies is followed by a brief discussion of the structural features of the massif.

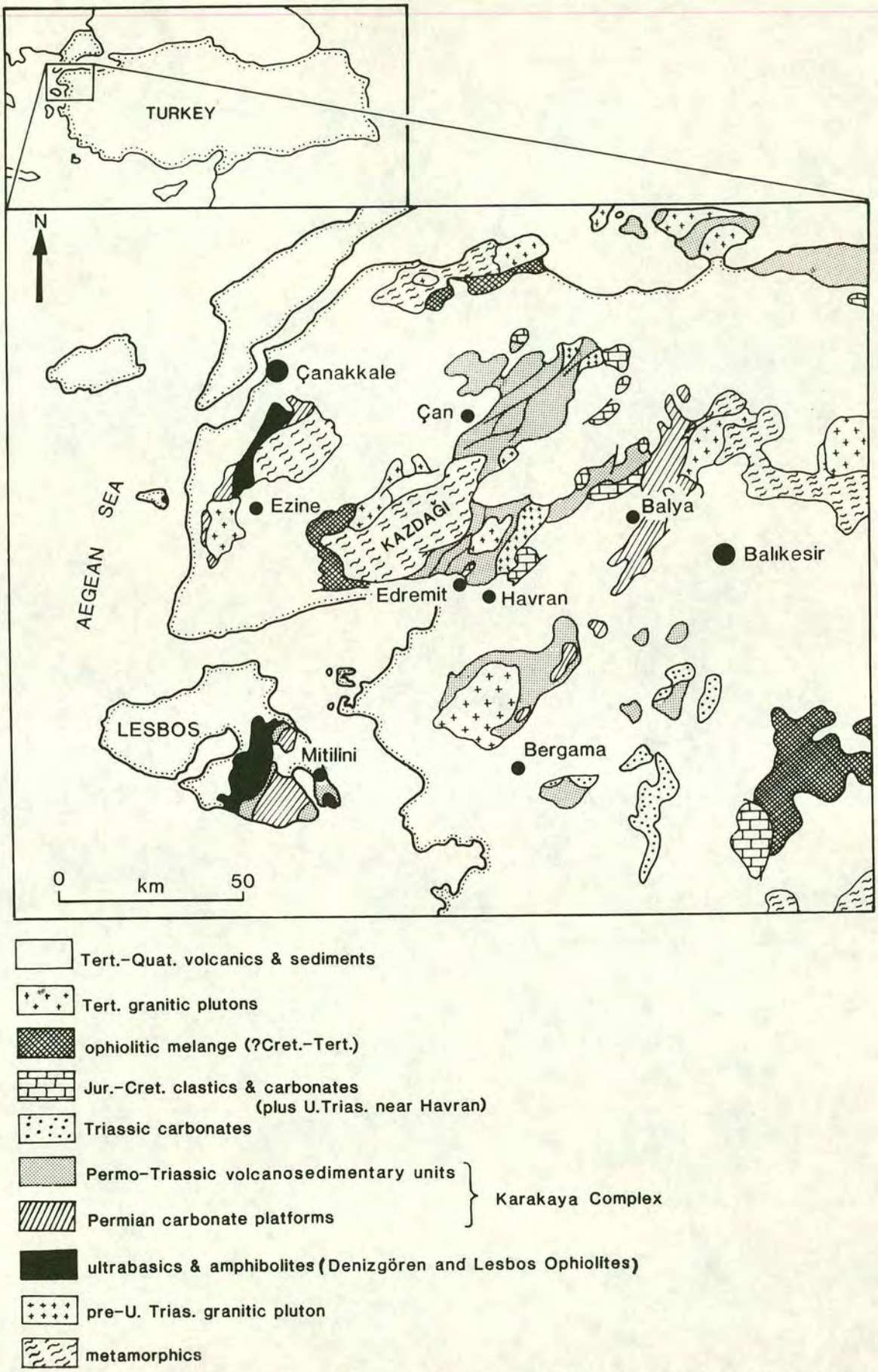

Figure 6.1 Generalized geological map of the Biga Peninsula. The Kazdağ Massif lies directly NW of Edremit.

6.2 Previous work

The rocks of the Kazdag Massif were first described by Diller (1883) as part of his geological study of the Troad (synonymous with the Biga Peninsula). He recognized the domal structure of the massif and reported the exposure of the oldest rocks near the summit of the mountain. The Kazdag Massif, together with Uludag near Bursa, were studied by van der Kaaden (1959) who described the lithologies and general structural trends. The earliest detailed petrographic and metamorphic studies of the Kazdag Massif were carried out by Schuiling (1959), Bingöl (1968), Bingöl (1971) and Bingöl *et al.* (1973). Schuiling (1959) made a generalized map of the Kazdag Massif and identified structural trends such as the widespread N-S lineation. Bingol (1968) mapped the massif to the north of Altinoluk and also described some of the surrounding units to the southeast, naming them the Karakaya Formation. Bingöl *et al.* (1973) named the metamorphic rocks the Kazdag Group. More recently, Okay *et al.* (1991), summarized the structure and lithologies of the Kazdag metamorphic rocks and suggested that the range may represent deeply buried levels of the Karakaya Complex which were subsequently exhumed. In this chapter the Kazdag rocks are informally referred to as the Kazdag metamorphic rocks.

6.3 The Kazdag metamorphic rocks

The Kazdag metamorphics as described in this thesis include all the metamorphic rocks found within the Kazdag Massif; from the predominantly ultrabasic rocks in the core of the mountain to the thick succession of gneisses which forms the bulk of the massif. The "core" rocks are found near the summit of Kazdag and represent the lowest exposed levels of the Kazdag metamorphics. They comprise ultrabasic rocks and amphibolites and are overlain by a thick succession of banded quartzo-feldspathic gneisses, the most common rock type in the massif. The gneisses are intercalated with amphibolite and marble horizons, especially in the lower levels. Figures 6.2 and 6.3 show the general structure and lithological succession through the Kazdag Massif.

6.3.1 "Core" rocks

The core of the massif consists predominantly of harzburgite, dunite, metagabbro and amphibolite schists. Good outcrops are found near the Kazdag summit plateau (the region around the peaks of Sarikiz Tepe, Babadag and Kirklar Tepe; Figure 6.4), underlying a marble horizon at least 100m thick. Figure 6.5 is a photograph of the

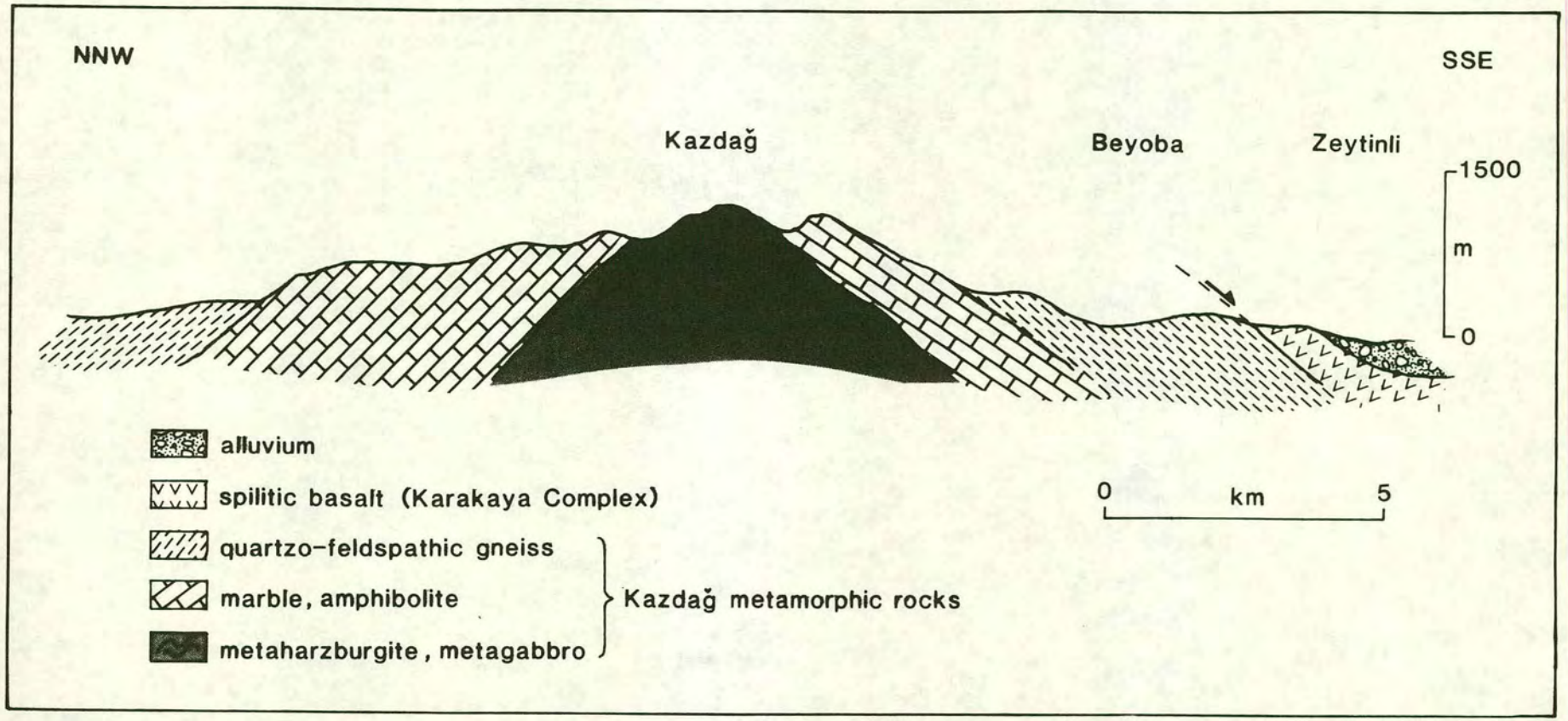

Figure 6.2 Schematic cross-section through the Kazdağ Massif (line of section shown in Figure 6.4).

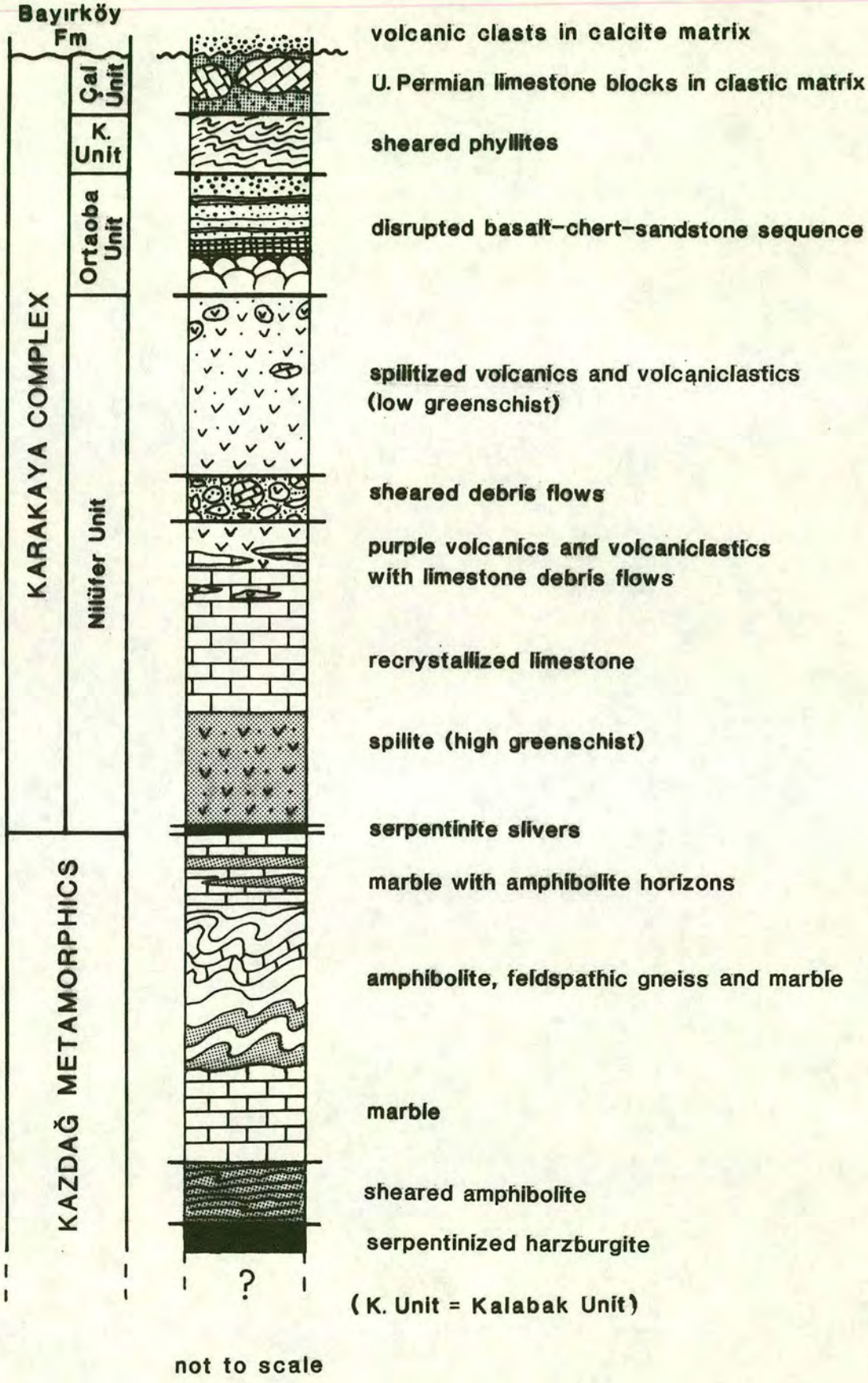

Figure 6.3 Generalized succession through the Kazdağ Massif and the overlying Karakaya Complex in the Edremit area.

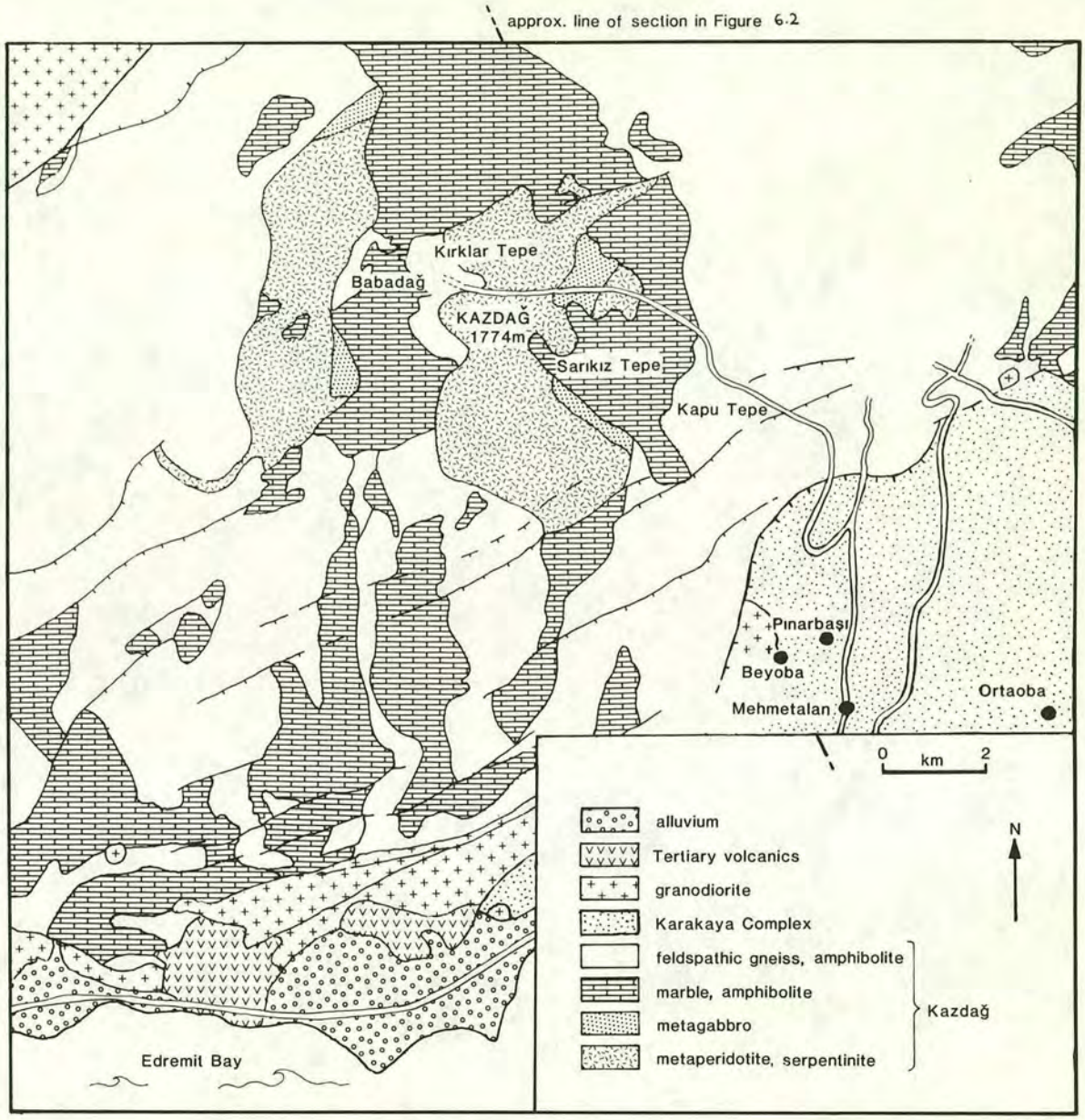

Figure 6.4 Geological map of the southeastern part of the Kazdağ Massif showing the contact with the Karakaya Complex at its eastern margin. The distribution of the Kazdağ rocks is taken from Bingöl (1971).

Figure 6.5 View from the forestry station on Kapu Tepe, looking W-SW across the summit plateau of the Kazdag Massif. The sketch of the photograph shows the position of the ultrabasic and amphibolitic rocks in the core of the antiform, with the inferred continuation of the overlying marble and gneiss horizons shown as dotted lines. The line of impressive white cliffs in the centre right part of the picture comprise marble and form a mantle over the core. Their continuation can be seen in the distant cliffs on the left of the picture. For scale, the exposed "core" is approximately 2-3km wide.

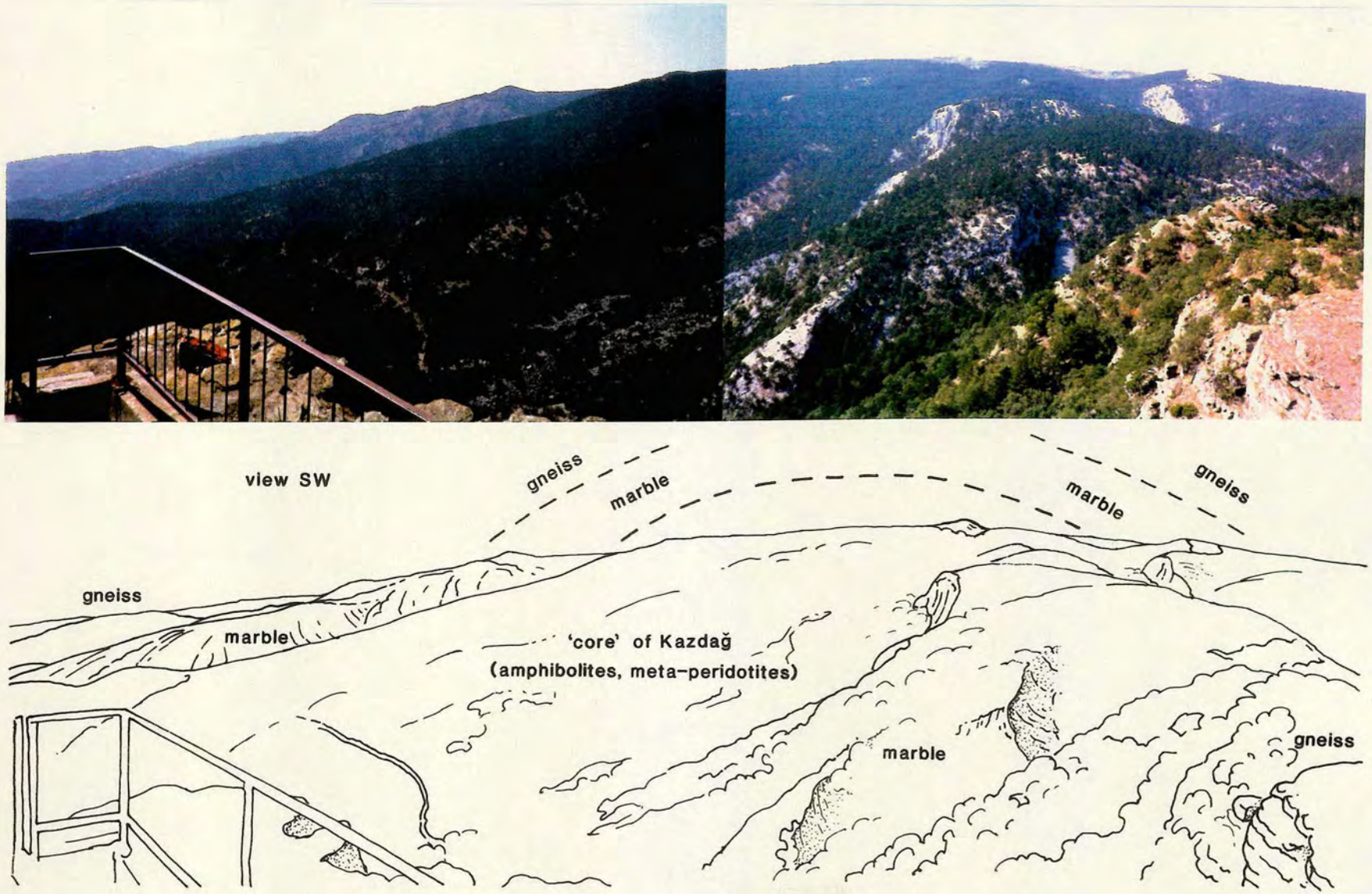
view SW
gneiss
marble
marble
gneiss
gneiss
marble
'core' of Kazdağ
(amphibolites, meta-peridotites)
marble
gneiss

Kazdag summit plateau, taken from Kapu Tepe and looking approximately W to SW. The photograph shows the "core" rocks cropping out in the centre of the plateau, beneath thick horizons of marble and, further up section, gneiss. The estimated continuations of these layers are shown as dotted lines. The contact region between the marble and the ultrabasic rocks was not observed owing to inaccessibility. Harzburgite, garnet-rich ferrogabbros, meta-gabbros, plagiogranites, meta-pegmatites and loose boulders of actinolite-rich rocks were observed along the mountain track which links the summit plateau with the road running north from Mehmetalan village. Figure 6.6a shows an outcrop of coarse-grained meta-pegmatite and Figure 6.6b is a photomicrograph of a garnet amphibolite from Sarakiz Tepe. Peridotites near the summit of Sarikiz displays tectonite fabrics. They are highly serpentinized and in thin-section some display a sheared mesh texture, indicative of an olivine (i.e. dunitic) precursor. The rocks possess a strong shear fabric defined by strands of serpentinite and wispy stringers of opaques. Intense shearing and folding are characteristic of the core rocks. Tight to isoclinal folds are common within the amphibolites and meta-gabbros of the summit plateau near the summits of Sarikiz Tepe and Babadag. Garnets were observed in the hinge zones of folded amphibolite and are a common feature of many of the core amphibolites.

Coarse-grained, speckled amphibolites form a horizon between the core rocks and the banded gneisses and marbles which form the bulk of the Kazdag metamorphic complex. Similar amphibolites also occur within the overlying gneisses and the two sets were sampled with the aim of distinguishing different sources.

6.3.2 Amphibolite

Amphibolite occurs as coarse-grained outcrops within, or close to, the core of the massif and also as dark green intercalations within the overlying gneiss and marble sequence. The amphibolite within the latter rocks comprises hornblende, plagioclase, sphene, diopside and opaques and commonly occurs as foliation-parallel lenses and veins. The amphibolite layers are very common towards the core of the massif and often display necking and boudinage parallel to the general gneissic foliation. Amphibolite veins are invariably parallel to the foliation, unlike the felsic veins which are commonly at high angles to the foliation. Amphibolite intercalations are common along both the eastern and western flanks of the Kazdag Massif.

Figure 6.6 Examples of Kazdağ lithologies.

(a) Coarse-grained meta-pegmatite from the "core" sequence on Sarıkız Tepe.

(b) Photomicrograph of garnet amphibolite from Sarıkız Tepe (gt: garnet, hbl: hornblende, plag: plagioclase, op: opaques) (PPL, field of view: 4mm).

(c) Typical quartzo-feldspathic banded gneiss from the "cover" sequence, 5km north of Mehmetalan.

a

b

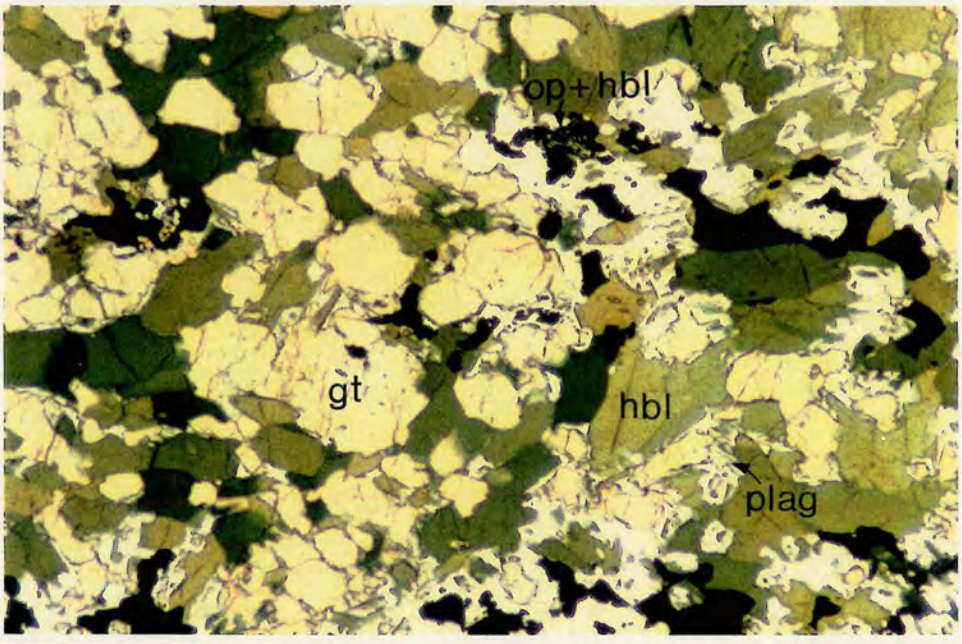

c

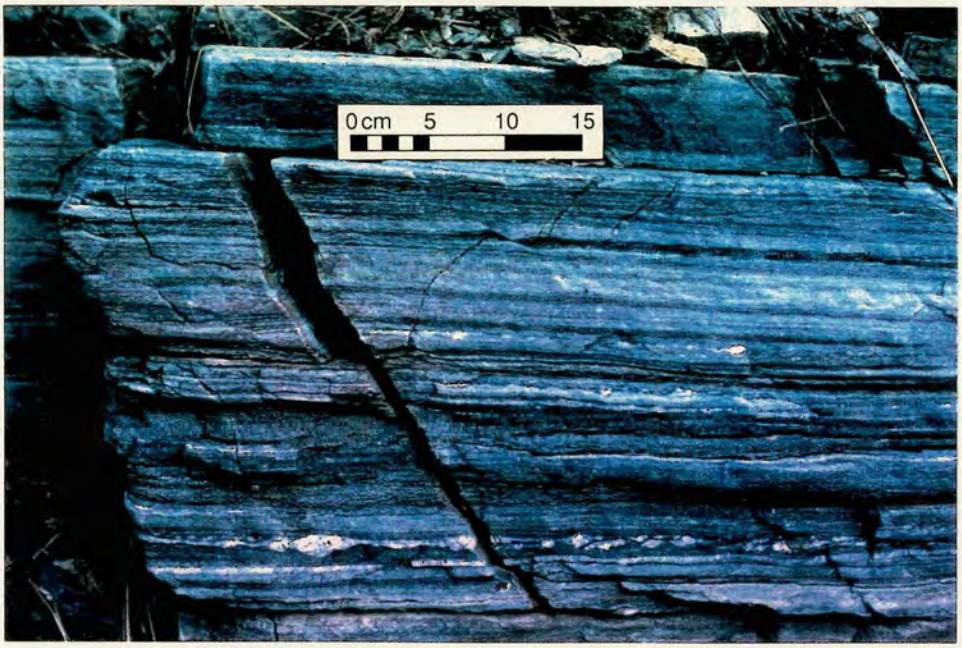

The hornblende which forms the amphibolite layers comprises well-formed crystals with strong cleavages and green to khaki-green pleochroism. Similar to the core amphibolites, many crystals have blue-tinged rims and also display blue-green overgrowths with little or no cleavage and a more amorphous form. In one crystal small quartz and/or feldspar grains define the outline of an earlier crystal edge and mark the division between green and green-blue hornblende.

6.3.3 Banded gneiss

The most common lithology in the Kazdag metamorphic sequence is banded grey gneiss. The gneiss consists predominantly of quartz, plagioclase alkali feldspar, biotite and hornblende with lesser amounts of diopside, garnet, sphene and opaques. Staurolite, kyanite and sillimanite have also been reported (Bingöl, 1968). The gneisses are light to medium grey in colour and medium- to coarse-grained. Banding is on a scale of centimetres to tens of centimetres and is caused by higher concentrations of the ferromagnesian minerals. The gneisses are generally lighter in colour towards the top of the sequence. Those near the core are medium to dark grey owing to the abundance of hornblende. Up section the amount of hornblende decreases until the gneisses are pale grey and almost entirely made up of quartz and feldspar. Figure 6.6c shows a typical outcrop of quartzo-feldspathic gneiss. The gneisses commonly contain intercalations of marble and amphibolite which are described in sections below. Rocks in the highest levels of the Kazdag Massif have a strong schistosity, owing to an abundance of white mica. These micaschists are pale beige in colour and are best observed at the northern end of the valley north of Zeytinli.

6.3.4 Marble and calc-silicates

Marble is a very common lithology and near the summit of Kazdag forms a massive banded horizon up to 100m thick. Figure 6. 5 shows the impressive cliffs formed by this horizon and the underlying ultrabasic and amphibolitic rocks. Marble is also found as thinner intercalations (from <1cm to several metres) throughout the rest of the Kazdag Massif. The marble horizons are composed of calcite with minor quartz and phyllosilicates and generally display a fine (mm-scale) banding defined by thin dark seams. In thin section the bands are revealed as thin layers of hornblende crystals surrounded by calcite. Hornblende crystals are also present as isolated grains within non-banded marble. Marble is commonly intercalated with amphibolite,

forming distinctive green and white outcrops along the road to the summit (e.g. Figure 6.7a) and also on the western flanks of the Kazdag range. Owing to competency contrasts the marble was deformed in a relatively ductile fashion, whereas gneissic and amphibolite bands within the marble were segmented into angular boudins. Near Beyoba, marble forms a mylonitic horizon up to several metres thick which contains blocks of gneiss rimmed by garnets. The marble has a streaky foliation defined by bands of impurities, which drapes around the "porphyroblasts" of gneiss.

Calc-silicate assemblages which contain little or no carbonate are also a common feature of the Kazdag metamorphics. A calc-silicate band within gneisses on the western flanks of Kazdag contains an assemblage of calcic plagioclase, diopside, scapolite, apatite, biotite and hornblende. The biotite, hornblende and plagioclase are concentrated in discontinuous "hydrous" layers up to 5mm wide.

6.4 Geochemistry of Kazdag rocks

6.4.1 Study of garnet amphibolite from core sequence

A sample of garnet amphibolite (KAZ6a) was collected north of Sarikiz Tepe, from a very fresh outcrop along the road which runs across the summit plateau. The amphibolite consists of garnets, plagioclase, amphiboles and opaques (as shown in Figure 6.6b). Several garnets and amphiboles from this sample were analyzed by electron microprobe.

a) Garnets

The garnets are equant and up to 3mm across. They are pale pink with grey interference colours and weak birefringence. They have slightly darker pink rims and, apart from a few small inclusions, are very clean. Many of the garnets are rimmed by irregular zones of plagioclase. The garnets are concentrated in distinct bands but are also present in lesser quantities throughout the rock. The cores and rims of six garnets from sample KAZ6a were analyzed by electron microprobe (Appendix 3). The garnets are almandine-rich, although the moderately high Ca contents (9.58-11.34 in the cores) may indicate a complex solid solution of predominantly almandine component with a minor amount of pyrope and subsidiary grossular and/or spessartine components.

a

b

Figure 6.7

(a) Marble intercalated with lenses of amphibolitic gneiss 2km SE of Kapu Tepe.

(b) Ductile folding within Kazdağ gneisses on Kapu Tepe.

The garnet rims are generally slightly enriched in Si, Mg and Ca, and depleted in Al, Mn and Fe, relative to the cores. Mn depletion in the rims is particularly marked and may be the result of fractionation of Mn into garnet when it first appeared, as explained by Atherton & Edmonds (1966) and Hollister (1966). As garnet growth continued, the Mn-content of the reactant phases would have become lower, thereby creating Mn-depleted rims.

b) Plagioclase

Plagioclase occurs as irregular "pools" around many of the garnets and forms embayments into the amphiboles. The conversion of garnet to plagioclase is a typical feature of garnet-bearing rocks which have been uplifted.

c) Amphiboles

The amphiboles are euhedral, with strong pleochroism (emerald green to khaki-green), low birefringence and well-developed cleavages. A blue-green tinge locally marks the rims of some crystals and also characterizes many smaller, less well-formed crystals. This feature is not apparent in the photomicrograph in Figure 6.6b.

Six crystals were analyzed. Their Ca values (10.37-11.55) are significantly greater than their Na values (2.4-2.54), thus placing them in the calcic amphibole sub-group. On the basis of this and their appearance in thin-section they can be identified as hornblendes. Blue-green rims surrounding green cores may indicate a period of metamorphism followed by a later, lower grade metamorphic event as blue-green hornblende is usually the lowest grade hornblende to appear during the metamorphism of basic rocks.

d) Opaques

Complex intergrowths of pyrite, chalcopyrite and ilmenite form up to 20% of this sample. They also form intimate intergrowths with the hornblende as indicated at the top of Figure 6.6a.

6.4.2 Whole-rock geochemistry of amphibolites

A small number of amphibolites were collected for analysis by X-ray fluorescence. Five samples were taken from the upper levels of the core region and four were from within the gneisses immediately overlying the core rocks. The association of the Kazdag amphibolites with meta-gabbros and other meta-plutonic rocks means that a

gabbroic, rather than basaltic, origin for the amphibolites is likely. For this reason basaltic discrimination diagrams are probably inappropriate in this case. Geochemical data were therefore plotted on variation diagrams to investigate fractionation trends. Variation diagrams are shown in Figure 6.8. The plots of MgO against TiO_2, Zr, Nb and Ce show distinct fractionation trends towards lower values of MgO. With one exception, the "core" amphibolites form a high-MgO (in the range 10-12%) cluster and may be candidates for a suite of parental gabbros. The "cover" amphibolites and one of the "core" amphibolites lie along trends away from this cluster and probably represent a suite of rocks which evolved from the gabbros. A detailed discussion of these fractionation trends and their implications is outside the scope of this study. Amphibolites from both core and cover sequences were also plotted on MORB normalized multi-element plots as shown in Figure 6.9. The core rocks are shown in plot (a) and are clearly more depleted than the cover amphibolites shown in (b). The cover amphibolites display patterns which are closely parallel to the normalizing line, implying a normal MORB-type source. Sample 10/10/92-b3, which displays an enriched pattern probably represents a more evolved version of the other cover samples in plot (b).

6.5 Structural features of the Kazdag Massif

6.5.1 General structure

The Kazdag Massif is a NE-SW trending anticlinal structure which forms a broad dome (Figure 6.2). The deepest levels of the massif are exposed at the summit of Kazdag and the highest levels are exposed on the outer flanks. The well-developed gneissic foliation of the Kazdag metamorphics dips away from the centre of the massif, giving the massif its elongate domal structure. Although the massif as a whole strikes NE-SW the dominant structural fabric is a ubiquitous N-S trending lineation associated with N and S directed shearing and strong flattening. The structurally deeper levels of the massif are highly deformed and contain abundant granitic dykelets and veins. The upper levels are less deformed and do not contain any intrusive rocks. Extensional faults and shear zones which cut the foliation are present throughout the gneissic sequence and range from large detachment faults to micro-scale shear zones.

Much of the Kazdag Massif is difficult to reach owing to dense forests, steep gorges and very few roads. For this reason fieldwork concentrated along a few mountain

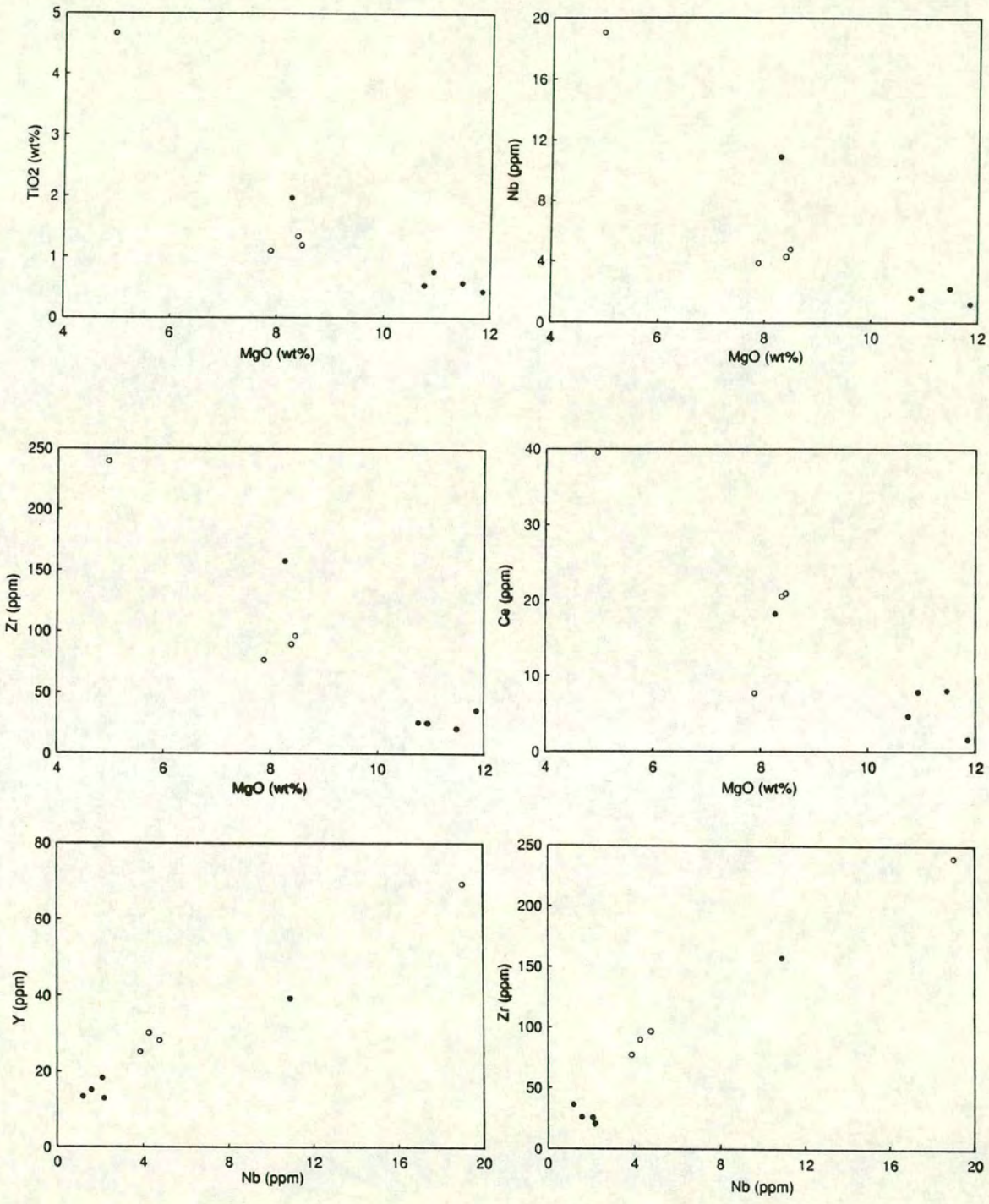

Figure 6.8 Variation diagrams for amphibolites from the Kazdağ core (closed circles) and the cover (open circles) sequences.

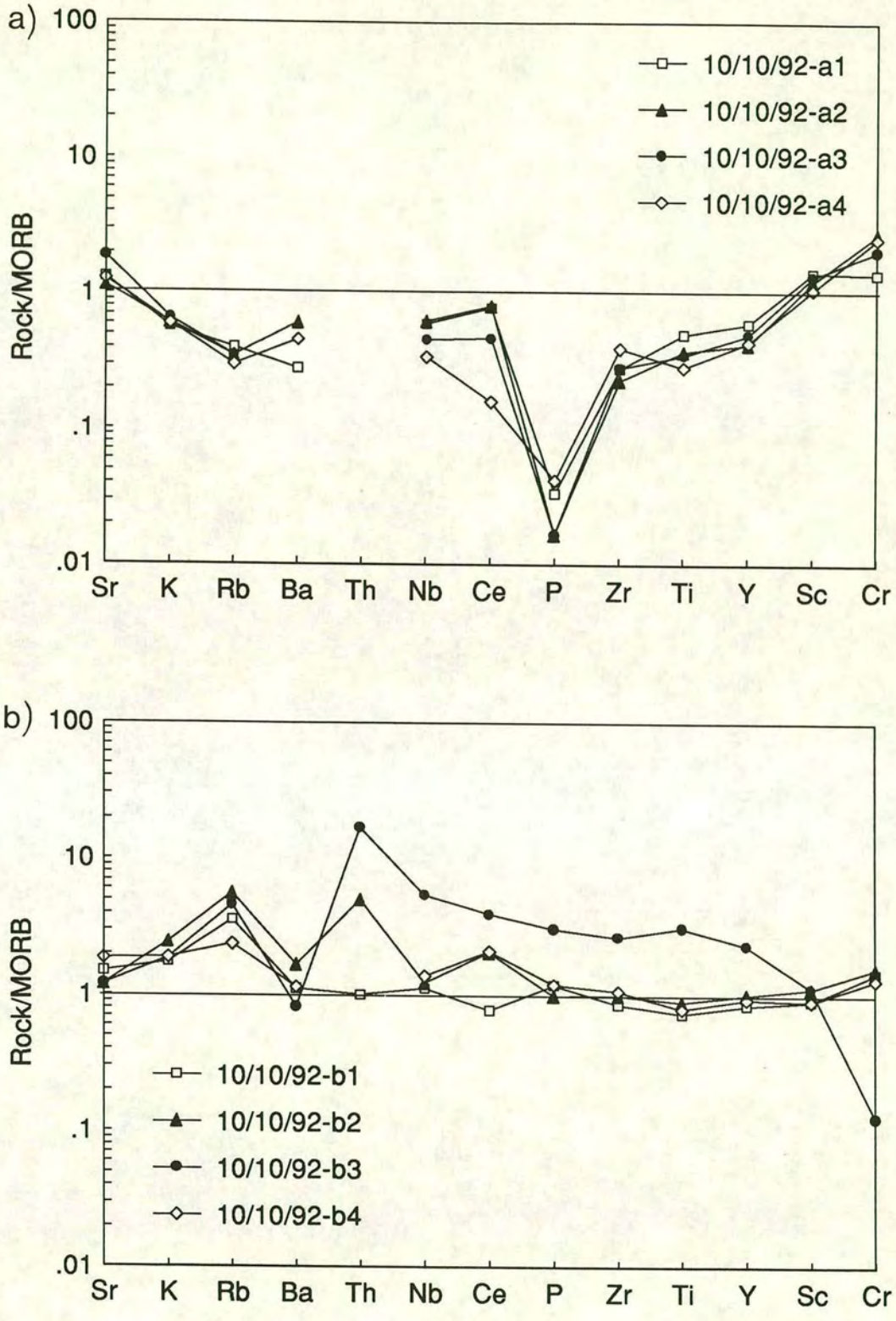

Figure 6.9 MORB-normalized multi-element plots for amphibolites from (a) the Kazdag core and (b) the structurally overlying gneissic sequence. Normalizing values from Pearce (1982 & 1983) (Appendix **4**).

tracks which, between them, give a good section through the lithologies and structures of the massif as a whole. Study of individual outcrops along these tracks has allowed the construction of a tentative sequence of events and the qualitative determination of the conditions under which the various structures formed. In particular, outcrops along the forestry track which runs past Kapu Tepe to the summit peaks of the Kazdag Massif (Figure 6.4) display a wide range of structures and degrees of deformation. In this section brief descriptions of the characteristic structural features of the Kazdag Massif (e.g. foliations, lineations, folding) are followed by a discussion of the wide range of younger extensional features and their implications for the evolution of the massif.

6.5.2 Planar fabrics

a) Gneissic foliation and schistosity

A pervasive foliation which dips consistently away from the core occurs throughout the Kazdag Massif and defines the pseudo-bedding which is such a characteristic feature of the Kazdag Massif. Most of the Kazdag gneisses, when viewed under the microscope, display a domainal schistosity which defines the foliation. Lenticular domains of quartz and feldspar aggregates are surrounded by anastomosing films of mica which have a strong preferred orientation so that their long axes are parallel or sub-parallel to the foliation. Domainal-type schistosity is generally described as schistosity as long as the mica-rich domains are anastomosing. This is gradational with gneissic layering which is defined by a more marked differentiation between felsic and mafic minerals. An example of gneissic layering found in the Kazdag Massif is shown in the outcrop in Figure 6.6c which is found along the road running due north of Mehmetalan.

Foliation defined by elongate lenses and bands of amphibolites, occurs within the thick carbonate sequences of the Kazdag Massif and reflects the gneissic foliation. Poles to foliation, measured on both the eastern flanks of the massif, are shown in Figure 6.10.

b) Tectonite fabrics

Planar tectonite fabrics were observed within the serpentinized harzburgites and associated amphibolites of the Kazdag Massif "core". These fabrics are defined by mineral segregations and dip predominantly NW-NE.

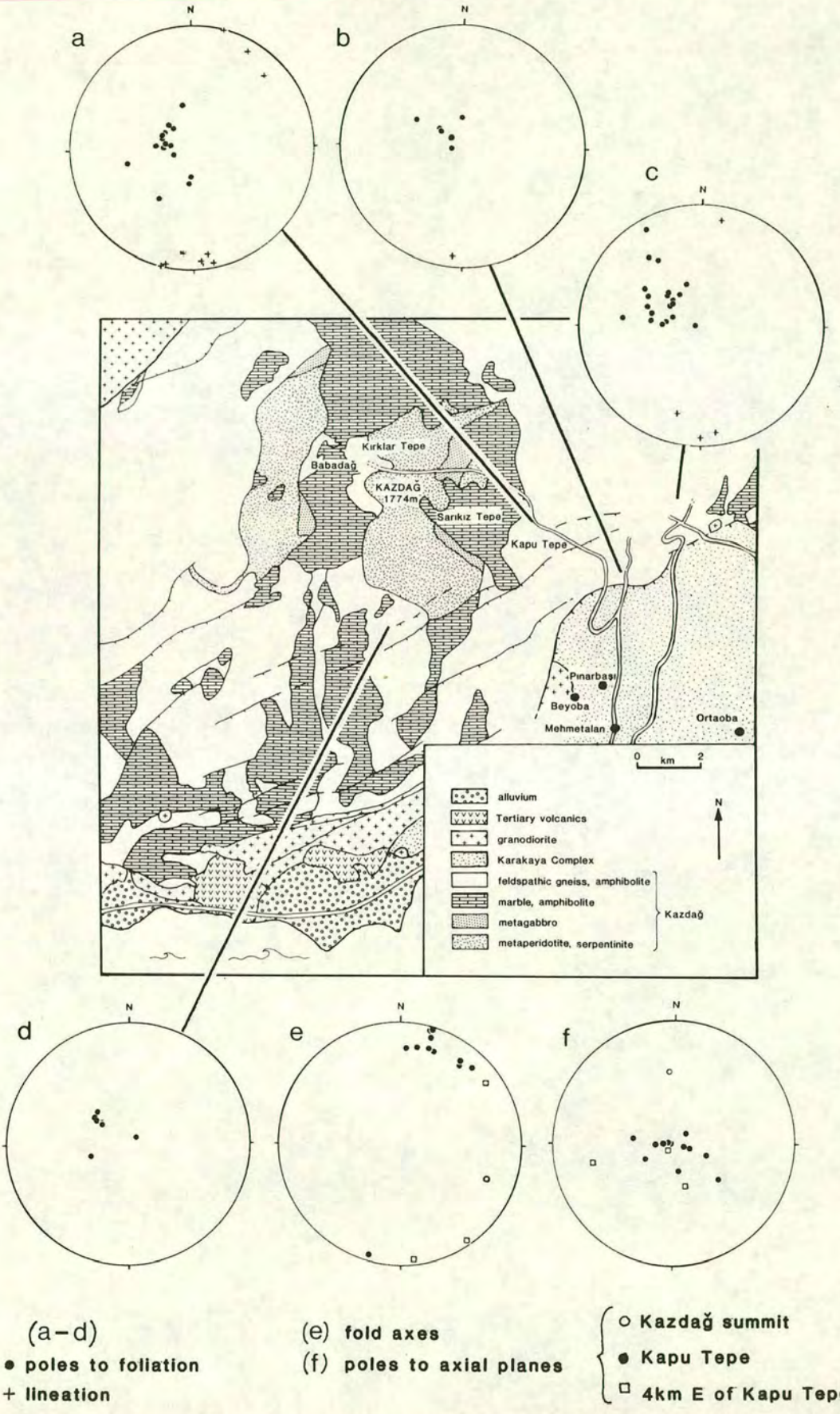

Figure 6.10 Stereoplots of the foliations, lineations (plots a-d) and fold data (plots e, f) measured on the eastern flanks of the Kazdag Massif.

6.5.3 Linear fabrics

A well-developed mineral and/or stretching lineation defined by streaky quartz and mica is ubiquitous throughout the Kazdag Massif. It is best developed on foliation planes within the banded gneisses and has a consistent N-S to NNE-SSW trend (Figure 6.10). Quartzo-feldspathic pods observed within the gneisses near Kapu Tepe are also elongate in this direction. The Çamlica Micaschists to the NW of the Kazdag Massif also display a N-S lineation and may represent the uppermost levels of the massif.

6.5.4 Folding

The core rocks are highly folded and display isoclinal folds with steep axial planes. The few axial planes measured dip towards the south with fold axes plunging to the E and SE. The gneisses directly above the core contain ductile, disharmonic folds which close in opposite directions and may reprsent sheath folds. An example of the folding along the road near Kapu Tepe is shown in Figure 6.7b. Owing to the two-dimensional nature of the outcrop surface and the extremely ductile appearance of the folds, measurements could not be taken. On passing up the structural section away from the core (i.e. travelling east along the road past Kapu Tepe; see map in Figure 6.4), the folds become increasingly less ductile in appearance. The folds tend to have NNE-plunging fold axes (Figure 6.10) and predominantly close towards the west. This westward-closing is also observed in folds near the contact with the Kazdag metamorphics and the Karakaya Complex north of Mehmetalan.

6.5.5 Deformed veins and dykes

Banded gneisses near the core of the massif are cut by several generations of aplitic and pegmatitic veins, most of which are at a high angle to the gneissic foliation. Many have been considerably deformed and now display structural features such as ptygmatic folding, buckling, boudinage and shearing. Foliation-parallel, slightly diffuse and boudinaged veins indicate an earlier generation of veining. Figure 6.11a shows an "early" vein which has been boudinaged and, at the top of the picture, a younger granitic vein. The earlier veins are rich in hornblende, whereas the younger, cross-cutting veins have a fresh granitic mineral assemblage of feldspar, quartz and biotite and have very sharp boundaries with the gneissic country rock. This implies that intrusion was occurring during deformation and that the intruding rocks evolved

Figure 6.11

(a) Veins within gneisses on Kapu Tepe. The lower, amphibolitic, vein is foliation-parallel and represents an earlier phase of injection than the granitic vein above.

(b) Foliation-parallel green epidote veins and granitic veins at a high angle to the foliation. The sketch of the photograph shows that although the epidote appears to cross-cut one margin of a granitic vein, the other margin encloses the epidote, indicating that they are probably almost synchronous. Note the vein with the foliated core and unfoliated margins which is further discussed in the text.

a

b

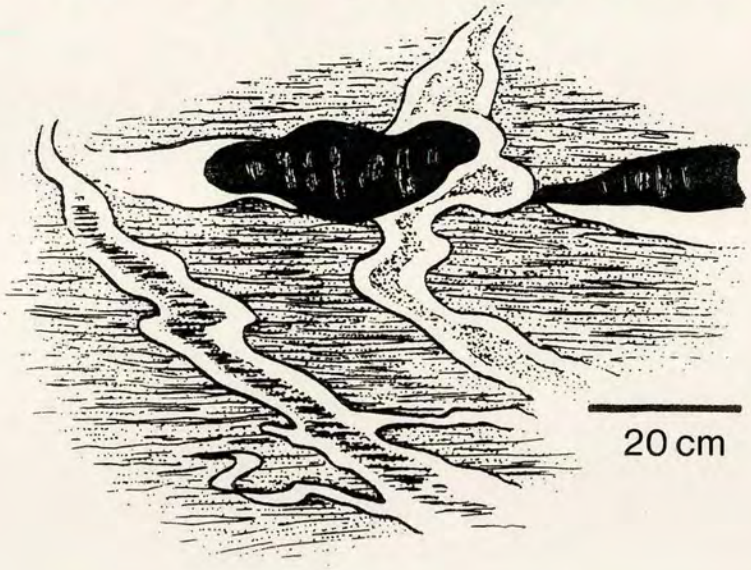

from intermediate to granitic compositions. The granitic veins have also undergone deformation which produced buckle folding and stretching. A few late-stage granitic veins with composite selvages display little or no deformation. Deformation was probably occurring during injection of some veins. This is evidenced by outcrops in which a range of degrees of deformation affecting different veins can be observed. The two main generations of veins indicated by cross-cutting relationships are listed below in their likely order of injection. They have been divided according to their conformity (Phase 1) or non-conformity (Phase 2) with the gneissic foliation.

Phase 1. foliation-parallel hornblende/epidote-rich lenses (e.g. Figure 6.11a).
foliation-parallel quartz veins.
foliation-parallel boudinaged felsic veins.
boudinaged epidote bands (e.g. Figure 6.11b).

Phase 2. pegmatitic/aplitic veins/dykelets with pinch and swell structures.
thin, relatively undeformed aplitic veins.

The relationships between the veins within the first generation are complex and not clear. Textures imply that many veins were injected during deformation, thereby producing the wide range of degrees of deformation observed within single outcrops. Competency contrasts between the veins and country rock are also important and will produce varying degrees of buckling or boudinage. Another point to be considered is the fact that some of the undeformed, thin aplitic veins, in the absence of cross-cutting relationships, may not be as young as one would expect. They would solidify quickly and would therefore not have time to acquire the foliation or buckling displayed by other, thicker veins of the same age.

Towards the centre of the Kazdag Massif deformation becomes increasingly ductile. Folds with opposite senses of closing are well exposed in banded gneisses along the road to the summit plateau, near Kapu Tepe and may reflect sheath folds veiwed down the shear direction. This road, which runs approximately westwards to the summit peaks of the Kazdag range, displays an excellent section through the central part of the Kazdag Massif. Along the road deformation increases dramatically over 200m and is well recorded by the nature of the felsic veins which cut the gneisses. The gneisses give way to the amphibolite, meta-intrusive rocks and harzburgite which constitute the core of the range.

The wide range of degrees of extension observed within the veins of individual outcrops implies that deformation was occurring during injection of the veins. Attenuation, buckling and rotation into parallelism with the foliation were all recorded from single exposures. Many pegmatitic veins have composite selvages and foliated cores, implying that the cores cooled slowly enough to acquire the typical Kazdag foliation or that they crystallized relatively competent feldspar and mica at the margins and ductile quartz in the core. The less competent quartz took the strain and hence acquired a foliation. Boudinage parallel to the foliation is a common feature of many veins and dykelets. In the case of the epidote veins shown in Figure 6.11b the foliation drapes around the boudins. Extensional cracks within the epidote, at right angles to the gneissic foliation, may indicate late-stage extension which post-dated the initial extension but which was still in essentially the same direction.

The obvious explanation for the syn-deformational injection of veins is that the Evciler Granodiorite (of probable Late Tertiary age; Okay *et al.*, 1991) on the western margin of Kazdag, and possibly the Eybek pluton to the east, are extension-related. Deformation appears to be synchronous with magmatic intrusions and with the evolution of magmas towards acidic (i.e. aplitic and pegmatitic) compositions. The metamorphic core complexes of the western USA also display a close temporal relationship between extension and magmatism. Wernicke *et al.* (1987) stressed the consistent relationship between the timing of onset of extension and the intensity of the plutonic history in their study of the tectonomagmatic evolution of Cenozoic extension in the North American Cordillera.

6.6 Extensional structures associated with the Kazdag Massif

Extensional structures are present within the Kazdag Massif on a range of scales and representing a range of conditions of formation. Structures ranging from massif-bounding detachment faults to mesoscopic and microscopic faults and shear zones were observed. The structures are described below according to their scale.

6.6.1 Faults along the massif margins

The Kazdag Massif is fault-bounded on both its eastern and western margins. The southernmost faults of the eastern margin are major normal faults which form the northern boundary of the Gulf of Edremit graben. On its east and west flanks the Kazdag Massif is juxtaposed against surrounding non-metamorphic units by shallow

faults associated with thick mylonite zones and also by steeper serpentinitic faults with much narrower zones of deformation. Mylonite zones are well exposed along the SE margin of the massif near the village of Beyoba (Figure 6.4) and to the NW around the village of Alakeçi (not shown).

a) Beyoba fault zone

A shallowly dipping fault plane (024/22 SE) was observed along the eastern margin of the massif, near the village of Beyoba (Figure 6.12). Slickensides form a series of N-S trending (e.g. 15/186, 18/183), rounded corrugations up to 3cm wide which reflect the ubiquitous N-S Kazdag lineation. A much fainter, uncorrugated lineation was also observed, perpendicular to the fault plane strike and at a high angle to the N-S lineation (e.g. 20/108). Cross-cutting relationships between the two lineations were not visible. The lineation at a high angle to the N-S lineation (i.e. 20/108) probably reflects later, normal slip down a surface which was reactivated as normal fault.

The fault surface itself is a smooth, shallowly dipping, corrugated plane which comprises streaky mylonitized marble and pale green gneiss, with minor fault gouge. The hanging wall at this locality consists of very weathered and fractured granodiorite which has been considerably disrupted by its proximity to the fault. Previous workers claimed that the granitoid pluton intrudes the Kazdag gneisses (e.g. Okay *et al.*, unpublished map). However, field observations in the region of Beyoba have shown that that the pluton only intrudes spilites of the Karakaya Complex and is clearly faulted against the metamorphics. The continuation of this fault is also exposed at the Kazdag-Karakaya contact 3km north of the village of Mehmetalan (Figure 6.4). There, the fault zone predominantly comprises mylonitized marble as shown in Figure 6.13a.

The smooth fault plane near Beyoba forms the upper part of a thick mylonite zone. Altered, crumbly granodiorite and granodiorite-derived fault gouge lie above the fault plane. A small block (20cm by 30cm) of blue-green amphibolitized metaspilite was found within the granodiorite near the fault plane. This is identical to the spilitic country rock, proving that the pluton intruded the Karakaya spilites. The abrupt termination of the granitoid against the fault and its incorporation within the underlying mylonite zone indicates that it does not intrude the Kazdag Massif as was previously thought. About 0.5km north of the well exposed fault surface near Beyoba, the hanging wall consists of highly sheared and folded green volcaniclastics, presumably part of the Karakaya Complex. Although the detachment itself is not

Figure 6.12 Field photo and sketch of the fault zone near Beyoba, between the Kazdağ Massif (on the left of the picture) and the granodiorite which intrudes the Karakaya Complex (on the right).

a

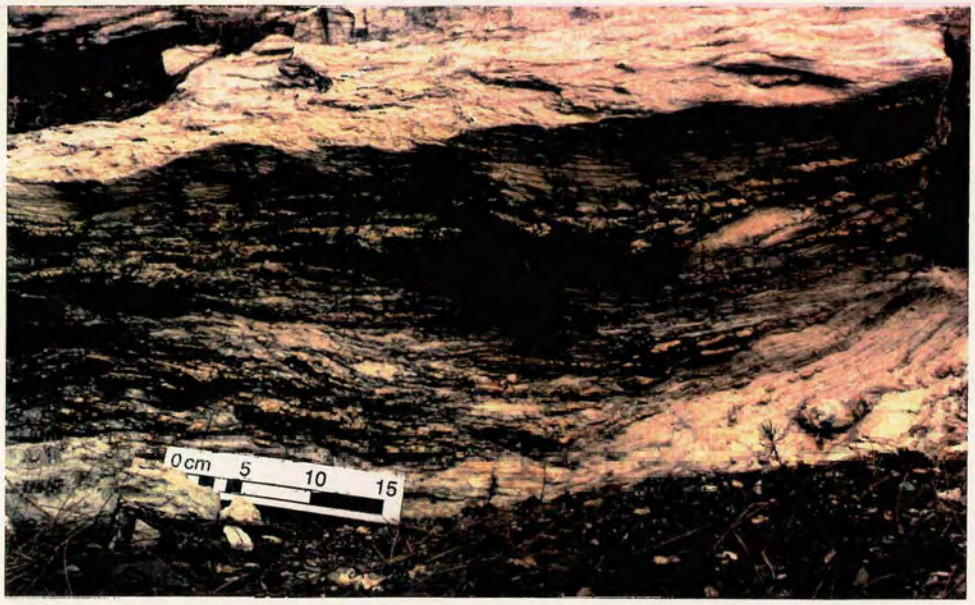

b

Figure 6.13

(a) Mylonitized Kazdağ marble at the contact between the Kazdağ Massif and the Karakaya Complex north of Mehmetalan.

(b) Amphibolitic and granitic "porphyroblasts" within calcite mylonite 50m below the Beyoba detachment shown in Figure 6.12.

exposed it is clear that the foot wall comprises sheared and mylonitized gneisses and marble.

Immediately below the fault plane lies at least 10m of highly sheared gneiss, granodiorite, green spilite and marble. Isolated marble and gneiss blocks lie within a rubbly matrix of sheared gneiss, granodiorite and possibly spilite. Mylonitization can be found within the Kazdag gneisses up to at least 50m below the fault plane. Deformation shows a distinct progression from brittle-ductile to purely ductile behaviour away from the fault. Spectacular carbonate mylonite is observed in the river gorge immediately to the west of the fault. Large clasts of gneiss and amphibolite, still preserving their original foliations, are enclosed in a carbonate matrix (Figure 6.13b). The carbonate has a streaky foliation which drapes smoothly around the clasts. Many of the clasts have lensoid shapes and some display boudinage. Garnets are common around clast edges and garnet clusters are present within the carbonate matrix. This carbonate mylonite forms a distinct horizon several metres thick between mylonitic gneisses.

North of the Beyoba fault, further along the eastern boundary of Kazdag, the contact between the metamorphics and the Karakaya Complex can again be observed. Unlike the shallow fault contact near Beyoba the contact is relatively steep (dips range from 40° to 75°) and is characterized by extremely shiny, undulose, serpentinitic fault planes. Slickensides indicate normal-slip movement towards the SSE. Within the Kazdag gneisses below these normal faults lies a horizon of carbonate mylonite, probably equivalent to that observed near Beyoba. Thicknesses are very difficult to gauge but the mylonite is several 100m below the contact. This contrasts with the situation near Beyoba where the carbonate mylonite is about 50m below the detachment.

When considered with the micro- and meso-scale extensional structures it is likely that the Beyoba fault is a low angle normal fault, possibly comparable with the shallow, extensional detachment surfaces described from the Basin and Range terrane in the USA. Structural and lithological features associated with the Kazdag fault are remarkably similar to those described from the middle Tertiary extensional Basin and Range Province (Hamilton, 1987). Characteristically, mylonitized gneiss-mylonite-cataclasite-gouge sequences can be observed on passing towards detachments. Examples of such sequences may be found in the carapaces beneath the Ruby

Mountains and Riverside Mountains detachment faults. There is very little deformation in the upper plates.

b) Alakeçi Mylonite Zone

Along the western boundary of the Kazdag massif Okay *et al.* (1991) recognized a 2km-thick mylonite zone, (their Alakeçi Mylonite Zone) which they described as a thrust-related structure. They described the mylonite as consisting of mylonitized gneisses with the characteristic Kazdag N-S lineation. In outcrop the mylonites are pale grey and streaky, and break into pencils and elongate slaty fragments. They have a characteristic non-fissile foliation. Strongly boudinaged quartz veins up to 0.5m thick were observed parallel to the foliation and, towards the top of the mylonite zone, quartzitic intercalations are common. The mylonites contain large (up to 4km long) slivers of serpentinite which themselves contain rare microgabbro lenses (Okay *et al.*, 1991). The serpentinitic rocks are very dense and green-grey in colour. The mylonite is also associated with banded, grey, recrystallized limestone. The contact of the mylonite with the underlying Kazdag metamorphics appears to be gradational, implying that the mylonite is a progressively deformed version of the Kazdag metamorphic rocks. The mylonite contains semi-horizontal shear zones. The upper boundary of the mylonite zone is sharp and juxtaposes dense serpentinitic rocks and fault gouge against recrystallized white limestone which may be part of the Çetmi Ophiolitic Mélange (a Cretaceous-Tertiary mélange on the SW margin of the massif which was described by Okay *et al.*, 1991). The zone of fault gouge which marks this contact is up to 20m thick.

Near the village of Çaldag, which is situated towards the upper levels of the Alakeçi Mylonite Zone, streaky marble and fine-grained purple volcanics are exposed. This association is identical to the marble and purple volcanics which are well exposed within the Nilüfer Unit north of Mehmetalan. It thus appears that the same lithological association occurs above the mylonite zones on both flanks of the domed Kazdag massif. This implies that a unit including this distinctive marble/purple volcanic shale association was faulted down from a higher structural level along shallow detachment faults.

This zone may be the westren boundary equivalent to the calcite and gneissic mylonites described from the eastern boundary near Beyoba. The mylonites dip shallowly towards the northwest, which may indicate the presence of a shallow detachment fault. Work in the Basin and Range region has revealed that domiform or

undulating detachment faults extend over much greater areas than originally reported. If a similar phenomenon is present in the Kazdag region then the same detachment fault may crop out on either side of the Kazdag massif, having originally passed over the massif. Alternatively the mylonite zone and the Beyoba calcite mylonites may represent different fault zones which dip shallowly in opposite directions. In either case they are probably large-scale extensional faults along which Kazdag was exhumed.

6.6.2 Smaller-scale extensional structures within the massif

a) Mesoscopic structures

Boudinage is pervasive in the lower levels of the Kazdag Massif. Asymmetrical boudinage structures such as ductile normal shear zones are particularly common. Symmetrical necking and boudinage also exists, especially in amphibolite veins within the gneisses. The gneisses and marbles of the Kazdag Massif are cut by numerous small extensional faults and shear zones which consistently dip NW or SE. Figure 6.14 shows stereoplots of extensional faults and shear zones near the western margin of the Kazdag Massif which show a consistent SE dip. Listric and planar faults are both observed, often in the same outcrop. Common structures are listric normal faults up to a few cm in length. The gneissic foliation is displaced by a small amount (up to 1cm) and is deflected towards the curved fault in the hanging wall. The foot- and hanging-walls of the faults are fused together leaving only a sealed trace of the original plane of displacement. Planar normal faults are also common and differ from the listric faults in that they displace the foliation without deflecting it and their planes of displacement are generally quartz-filled or open. Examples of extensional faults within the Kazdag Massif are shown in Figure 6.15. Small planar faults are also observed in marbles of the Nilüfer Unit on the eastern flanks of Kazdag (near Pinarbasi). They produce a domino effect, dipping in the same SE and NW directions as the Kazdag Massif examples (Figure 6.16a).

b) Microscopic fabrics

Extensional structures are also present as microstructural elements in Kazdag metamorphic rocks. Thin-section studies of orientated samples from both the eastern and western flanks of the Kazdag Massif show that the sense of shear is normal in all cases and dips away from the core of the massif (i.e. towards the SE and NW). Features observed in thin-section include S-C fabrics, mica fish and asymmetric tails on quartz and feldspar porphyroblasts. These features are best observed in sections

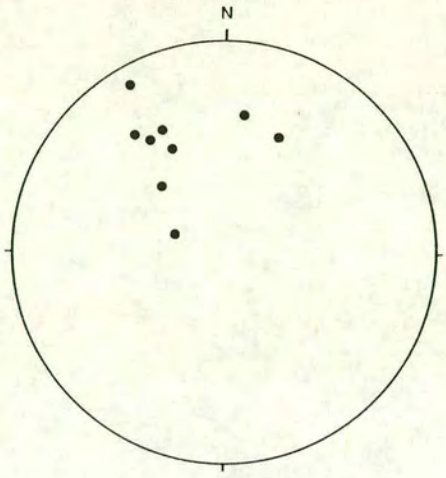

small (cm-scale) extensional shear zones in gneisses along road past Kapu Tepe and to the east of Kapu Tepe

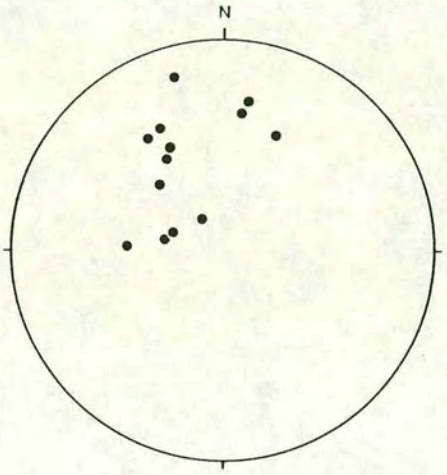

normal faults in gneisses along road past Kapu Tepe

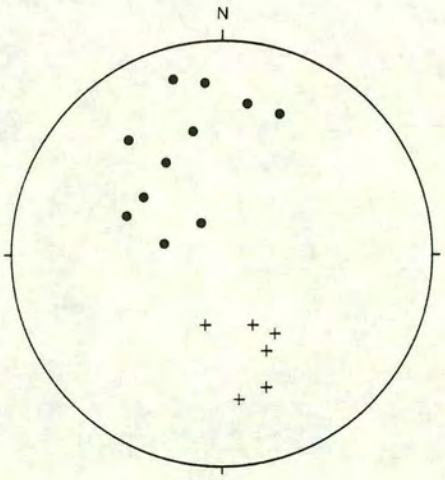

polished serpentinitic fault planes at contact between Kazdağ Massif and the Karakaya Complex north of Pınarbaşı

● poles to fault planes

\+ slickensides (motion down-dip)

Figure 6.14 Stereoplots of extensional faults in the western Kazdag Massif area.

Figure 6.15 Examples of extensional faults within the Kazdağ Massif.

(a) Extension in marbles on the western flank of the Kazdağ Massif, 5km south of the summit. The more coherent grey layer has deformed by faulting, whereas the surrounding marble has behaved in a more ductile fashion. The faults dip NW.

(b) Small extensional faults in gneisses north of Mehmetalan. The faults dip to the SE, a direction reflected by a series of faintly visible fractures. One of the small faults has been infilled by a quartz vein.

(c) Planar extensional fault in banded gneisses near Kapu Tepe.

a

b

c

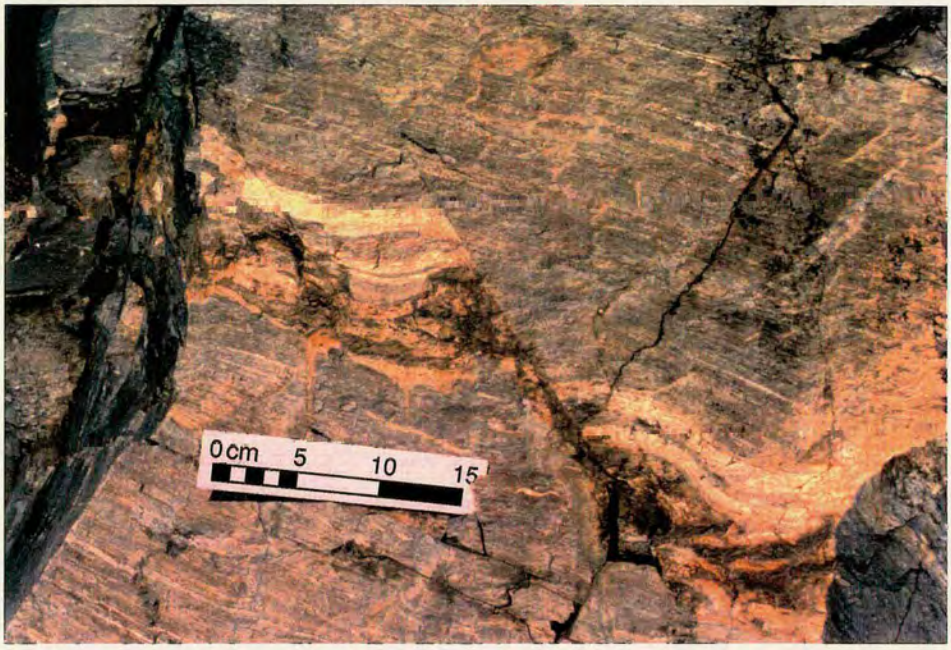

a

b

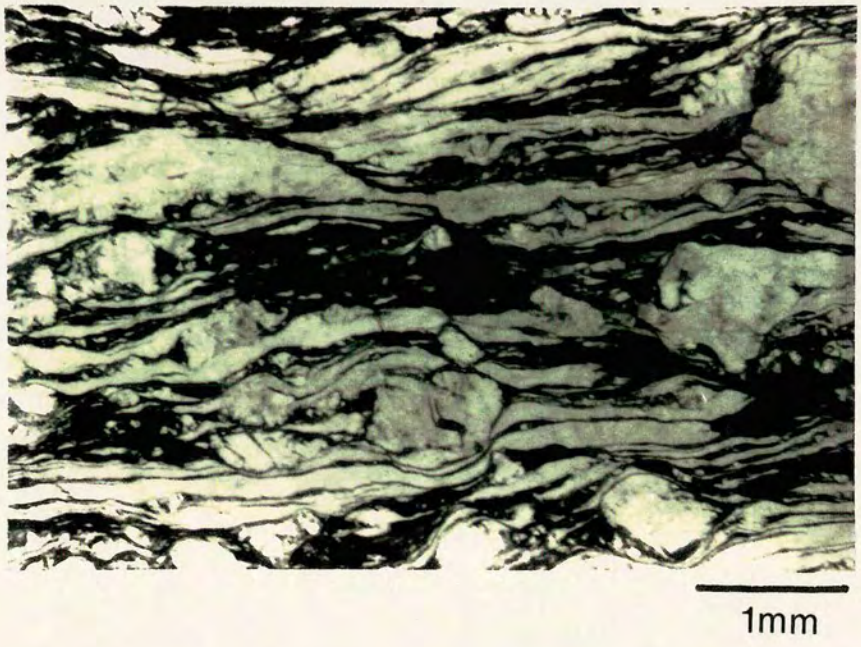

Figure 6.16

(a) NW-dipping domino faulting in recrystallized limestone of the Nilüfer Unit near Pınarbaşi.

(b) Photomicrograph of an extensional shear zone in mylonitic gneiss near the contact between Kazdağ and Karakaya rocks along the road past Kapu Tepe. The section is cut parallel to the lineation and indicates a normal sense of shear to the right of the picture (i.e. to the SE).

cut parallel to the strongly developed N-S lineation which is a ubiquitous feature of the Kazdag metamorphics. This lineation is a mineral and/or stretching lineation and is defined on foliation surfaces by streaky quartz and mica. Similar structures are also observed in sections cut parallel to the dip direction of the foliation and also indicate motion to the SE or NW. Sections cut parallel to the lineation display the best structures as the lineation is probably a direct result of the normal shear which produced the microstructures. Figure 6.16b is a photomicrograph of a mylonitic gneiss near the contact between Kazdag and Karakaya rocks along the road past Kapu Tepe. The section is cut parallel to the lineation and indicates a normal sense of shear to the SE.

6.7 Discussion

By investigating many individual outcrops in detail a sequence of extensional events can be outlined. Cross-cutting relationships are the obvious way of relating events, correlating between outcrops and ultimately producing such a sequence. The extensional faulting events clearly post-date the foliation, vein injection, boudinage and folding which characterize the deeper levels of the Kazdag Massif. This implies a progression of the extension from ductile shearing to semi-brittle or brittle faulting with the same sense of transport. The obvious conclusion from this is that continuing uplift raised the metamorphics from a region with a ductile regime to levels where semi-brittle and brittle processes were dominant. This deduction is supported by the presence of two main kinds of small normal fault as outlined above. The listric faults which display a deflection in the adjacent foliation were formed in a more ductile regime than the planar faults which display no such deflection. Higher levels may be indicated by conjugate joint systems which indicate a general NW-SE extension direction. It is interesting to note the change in the dominant extension direction from N-S to NW-SE, reflecting a later phase of strike-slip and extension.

Thus it can be seen that Kazdag displays extensional structures from ductile extension through semi-ductile mylonite formation to brittle faulting and fracturing. As ductile structures from deeper levels were uplifted they were cut by higher-level brittle faults in an ongoing regime of extension. Ductile faults may have been reactivated as more brittle structures as they reached higher crustal levels. Thus low-angle detachments such as that observed near Beyoba may have been obliterated by steep normal faults in the area further north described above. Presumably the complex had risen to high crustal levels where further low-angle slip was not possible. Subsequent extension

was accommodated by steep, rotating fault blocks and new detachment faults developed at depth. The slickensides on the steep normal faults indicate dip-slip motion towards the SE to SSE, whereas the grooves observed on the shallow Beyoba detachment are parallel with the N-S Kazdag lineation.

The discovery of the shallow Beyoba fault and the extensional nature of the Kazdag lineation and associated microstructures has important implications for the origin of the Kazdag metamorphics. An origin as an exhumed core complex has been suggested (Okay *et al.*, 1991) but not investigated using structural data. Data collected from fault zones and lineations is concordant with formation as a metamorphic core complex. Extensional features range from S-C fabrics on a scale of millimetre- to centimetre-scale domino faulting and large detachment fault zones as described above. These structures are generally shallowly dipping except for domino-style faulting which characteristically has a steep dip of 60°. Microstructural studies of S-C fabrics show that this lineation represents the main extensional direction within the massif.

Petrological features within the amphibolite described in Section 6.4.1 also support an origin as an exhumed core complex. The garnets are embayed and surrounded by plagioclase, a typical assembalge of de-pressured garnet-bearing rocks. Hornblendes in both the core and gneissic sequences display rims and overgrowths of lower grade blue-green hornblende, possibly indicating retrogression caused by uplift to higher crustal levels.

6.8 Tertiary-Recent tectonics

Uplift of the Kazdag Massif has been postulated as being of post-Miocene and probably of Pliocene age by Okay et al (1991) and can thus be considered as part of the overall Miocene-Recent Aegean arc extensional regime. The dating of Kazdag uplift is based mainly on the faulted contact of the massif with Miocene siltstones and shales at the southern edge of the mountain (Siyako *et al.*, 1989). These Miocene sediments were probably deposited in small, fault-bounded basins during the extensive Early-Mid Miocene calc-alkaline volcanism which occurred in this region of northwestern Anatolia (Siyako *et al.*, 1989). Cessation of volcanic activity in the Late Miocene was followed by deposition of shallow marine sandstones and, in the Pliocene and Quaternary, by fluvial sediments and lacustrine carbonates.

Uplift of the massif occurred along normal faults which probably included both low-angle detachments as described in Section 6.6.1 and the steeper graben-bounding faults of the Gulf of Edremit which now enclose a Quaternary basin. As Okay et al (1991) suggested, this implies that the Kazdag Massif may have originally formed the lower levels of the Karakaya Complex and was exhumed during the Tertiary by processes similar to those which formed the metamorphic core complexes of regions such as the Basin and Range Province of the southwestern USA.

Strike-slip faulting probably also played a significant role in the uplift of the Kazdag Range. A NE-SW zone of strike-slip faulting trends across the Biga Peninsula from the Bay of Edremit to Bandirma and is probably an Early Miocene to Recent strike-slip zone. The Kazdag Range, bounded to north and south by strike-slip faults, may be a compressive segment within this zone and hence is probably still undergoing uplift. A NE-SW striking graben in the Yenice-Gonen region, with dextral displacement (Schindler, 1993) is part of this zone and is directly along strike from the Kazdag Massif. Strong earthquakes in 1953 and 1969 in the Yenice-Gönen region indicate that deformation is continuing today.

Along the western edge of the Biga Peninsula, Upper Miocene sedimentary rocks are linked to NE striking dextral-normal faults (Schindler, 1993). This area is dominated by N-S and NE-SW striking faults. The NE-SW striking faults may be influenced by the North Anatolian Fault although this is little understood.

The uplift of the Kazdag Massif must be considered in relation to related metamorphic complexes such as the Uludag Massif just south of Bursa. Mount Uludag (2543m above sea level) is also a region of major tectonic uplift. Contemporaneous Neogene sediments are exposed at different altitudes, implying neotectonic activity. Uludag also displays an increase in metamorphic grade towards its central part. NW-SE and N-S striking faults which juxtapose different metamorphic units are assumed to be related to the neotectonic stress regime (Schindler, 1993). They described horizontal fault striae on polished surfaces which indicate late dextral strike-slip movement.

6.9 Metamorphic core complexes

6.9.1 Formation of metamorphic core complexes

Most high-pressure metamorphic terrains or "core complexes" have probably been formed in subduction-zone settings or in collisional orogenic belts, as summarized by Platt (1993). In active margin settings, high pressure terrains generally lie oceanward of a magmatic arc, commonly accompanied by relatively low P/T ratio metamorphism (the paired metamorphic belts of Miyashiro, 1961). The two belts may be separated by a sedimentary fore-arc basin which is generally unmetamorphosed and invariably displays a major tectonic contact with the underlying metamorphic terrain. An example of such a situation is the Coast Range fault in California which separates the Coast Range ophiolite and the overlying fore-arc basin from the underlying Franciscan Complex (e.g. Ernst, 1970). A similar situation is found in the Alps where a tectonic contact separates the Austroalpine complex from the underlying high-pressure Pennine Zone and represents a pressure gap of 4-13kb (Platt, 1986). The stratigraphic repetition across these major tectonic boundaries clearly indicates that thrusting has occurred. However, the jump in pressure suggests that at a later stage the contacts have been reactivated or crosscut by extensional structures. This "late" extensional phase has clearly taken place in the Kazdag Massif where both micro-shears and metres thick mylonite zones testify to a period of extension.

As summarized by Platt (1993), there is no single mechanism that can explain the exhumation of all metamorphic terrains. A combination of extension and erosion may account for the uplift and exposure of many bodies of high-pressure metamorphic rocks. In his review paper, Platt (1993) outlined a variety of possible extensional geometries in orogenic wedges which may lead to the exhumation of high-pressure rocks. The models assume the formation of a thrust or accretionary complex above a rigid underthrust plate, with a rigid buttress at the rear. Underplating at depth thickens the wedge and increases the surface slope, requiring extension in the rear of the wedge to maintain a stable geometry. Extension of the lithosphere may also occur in the core of a collisional orogen as a result of convective removal of the lithospheric root, as illustrated for the Alboran Sea by Platt (1993).

6.9.2 General characteristics and examples

Metamorphic core complexes were defined by Davis (1987) as "mountain-size geological exposures of regional, upward-tapering ductile-brittle shear zones" which are marked by the presence of thick, low-angle zones of mylonites that give way upwards to cataclasites and, ultimately, to regional low-angle detachment faults and associated normal faults. Such mylonitic zones and detachment faults are especially well exposed in the Basin and Range Province of the southwestern USA, where they have been extensively studied.

Dome-shaped or undulating detachment faults have been recognized in many parts of the Basin and Range Province. Their characteristics can be illustrated by the Tucki Mountain detachment fault in the Panamint Mountains of California (Hamilton, 1987). The detachment is dome-shaped with shallow flank dips and is sub-parallel with the layering in the lower-plate metamorphic rocks. The detachment is marked by breccia and gouge and lies above a retrograde mylonitic zone. The upper plate consists of unmetamorphosed rocks of varying ages. Using other examples from Nevada and California, Hamilton (1987) described the typical "gouge-cataclasite-mylonite-mylonitic gneiss" sequence which extends downwards from many detachment faults . Gouge is commonly found directly on a polished chloritic shear plane which typically caps a zone of cataclasite several metres thick. The cataclasite may grade downward into tens of metres of sheared chloritic, epidotitic rock. Beneath these rocks are laminated mylonites which record more ductile shear. These ductile zones may extend downwards for tens or even up to hundreds of metres and grade into mylonitic gneisses.

It is generally agreed that the detachment faults and associated cataclasites in the core complexes of the southern part of the Basin and Range are the products of Tertiary extensional deformation. The more ductile mylonites, however, are more controversial and there is much debate on whether thrust-related ductile carapaces were affected by later extension, or were formed by early extensional slip that evolved into detachment faults. The consensus among many workers (e.g. Davis, 1987; Hamilton, 1987) is that the mylonites are part of the detachment system and were formed in shear zones which accommodated extension of the crust. Davis (1987) invoked a ductile-brittle continuum of deformation and related the formation of the mylonites by shearing at depth to the development of cataclasites, detachment faults

and normal faults at shallower levels. The deeper level mylonitic gneisses may, however, reflect deformation events older than the extension.

Core complexes, mylonitic shear zones and shallow-dipping detachment faults have also been recognized in many other regions. For example, islands in the Cylcadic archipelago of the Aegean Sea contain elongate domes and display major shallow-dipping shear zones (e.g. Lister *et al.,* 1984; Avgiad & Garfunkel, 1991). Lister *et al.* (1984) pointed out the many similarities between the Cyclades and the core complexes of the Basin and Range Province. Avigad & Garfunkel (1991) stressed the role of low-angle normal faulting in the exhumation of the Cycladic blueschist terrains, a feature which has also been recognized in the Alps (Platt, 1986).

6.10 Comparison of the Kazdag Massif with Basin and Range core complexes

The overall shape of the Kazdag Massif is that of an elongate dome, 50km by 20km in size, with gently dipping flanks which reflect the pervasive gneissic foliation. These dimensions resemble those of Basin and Range detachments which are typically 10-20km by 20-40km (Hamilton, 1987).

The faulted margins of the Kazdag Massif have many features in common with the mylonitic zones and detachment faults that characterize the core complexes of the Basin and Range Province of the USA. In particular, the Beyoba fault zone at the southeastern margin of Kazdag displays a well exposed detachment plane and a distinct brittle-ductile downward sequence which passes from fault gouge to cataclasites and mylonites. The hard, polished fault plane near Beyoba with its gentle dip of 22° is typical of many detachment faults. Rounded fault grooves and ridges, parallel to the mineral lineation in the Kazdag gneisses, are present on the fault surface. Similar fault grooves are present along the Catalina-Rincon detachment in southeastern Arizona and are also parallel to the regional gneissic lineation. There, fault grooves up to metres in wavelength, perfectly parallel to the mineral lineation in nearby mylonite gneiss, have been described (Davis, 1987). The gouge-cataclasite-mylonite sequence below the Beyoba fault also bears a striking similarity to the Catalina-Rincon detachment sequence where cataclasite, microbreccia and mylonitic gneiss lie beneath the fault in a sequence which displays evidence of increasingly ductile deformation down section (Davis, 1987). The horizon of calcite mylonite below the Beyoba fault is very similar in composition and appearance to a mylonite which was described from the carapace beneath the Ruby Mountains detachment fault

in Nevada by Hamilton (1987). Both examples were derived from marble and contain boudins and rotated blocks of gneiss and amphibolite in a streaky calcitic matrix.

A large proportion of the Kazdag gneisses are mylonitic and very strongly layered. Aligned, asymmetric feldspar porphyroblasts and quartz laminae are parallel to the foliation, implying extensional shear. Microstructures such as S-C fabrics consistently indicate normal-slip simple shear as described in Section 6.6.2. Pervasive fabrics such as these are characteristic features of metamorphic core complexes in southeastern Arizona. For example, the Catalina and Rincon Mountains, site of the detachment zone described above, display S-C fabrics in mylonite gneiss which indicate normal-slip simple shear (Davis, 1987). A strongly developed penetrative mineral lineation with extraordinary preferred orientation is also present. The Kazdag lineation is similarly well developed and penetrative, and also possesses a remarkably consistent N-S trend throughout the dome-shaped massif.

6.11 Related metamorphic rocks

The Kazdag Massif is probably an along-strike continuation of the Uludag Massif near Bursa. Uludag, like Kazdag, contains metamorphic rocks and an aureole of Karakaya-type metavolcanics and metavolcaniclastics. The volcanics have been metamorphosed to a higher grade of greenschist facies than those in the Kazdag region, possibly as a result of baking by the Uludag pluton which makes up a large proportion of the massif.

The Çamlica Micaschists as described by Okay *et al.* (1991) may also have affinities with the Kazdag metamorphic rocks. This unit occurs to the east of the Denizgören Ophiolite and comprises a monotonous sequence of poorly exposed micaschists. The schists have a N-S lineation which may relate them to the Kazdag gneisses. Similar rocks are not observed on the east side of Kazdag, possibly as a result of cut-out by normal faults. The micaschists may, alternatively, have no affinities with the Kazdag Massif and were merely affected by the same extensional event and thus acquired a similar lineation. The Kazdag Massif has also been correlated with metamorphic assemblages elsewhere in the Tethyan realm. Papanikolaou & Demirtasli (1987), (as described in Papanikolaou, 1989 and Okay *et al.*, 1991) correlated Kazdag and Uludag with the Rhodope Massif in Greece and the overlying Nilüfer Unit of the Karakaya Complex with the Circum-Rhodope Belt in Greece.

CHAPTER 7

THE DENIZGÖREN AND LESBOS OPHIOLITES, THEIR METAMORPHIC SOLES AND THE UNDERLYING CARBONATE PLATFORMS

7.1 Introduction

The Denizgören Ophiolite is exposed 5km north of the town of Ezine in the western part of the Biga Peninsula (Figure 7.1). It is almost entirely composed of serpentinized harzburgite. The other elements of a classic ophiolite succession are absent and for this reason it should more correctly be termed an ultrabasic body. It forms a narrow band, 2-3km wide and 25-30km long, trending in a SSW-NNE direction.

On its western margin the ultrabasic slab tectonically overlies the Karadag Unit, a Permian carbonate platform sequence. Amphibolite forms a well-preserved metamorphic sole unit at the base of the slab and is described below for the first time. The sole grades abruptly downwards into sheared metasedimentary and metavolcanic rocks which lie at the top of the Karadag Unit. To the east, the Denizgören Ophiolite has a steep, possibly strike-slip, contact with a poorly exposed, monotonous sequence of micaschists (the Çamlica Micaschists). The localities discussed in this chapter are situated along the main Çanakkale-Izmir road north of Ezine.

A similar ultrabasic body and associated amphibolite sole unit are exposed on the Greek island of Lesbos which lies just off the Turkish mainland, south of the Biga Peninsula (Figure 7.1). This ophiolitic nappe lies directly along strike from the Turkish example and is excellently exposed NW of Agiassos, on the slopes of Mount Olympos. It covers a large area of eastern Lesbos and forms a smaller exposure south of the island's major town, Mitilini. The Lesbos Ophiolite and its metamorphic sole tectonically overlie a volcanosedimentary sequence which contains crystalline carbonate intercalations of Lower-Middle Triassic age.

The geographical position, constituent lithologies and geochemistry of the Denizgören and Lesbos Ophiolites all indicate that they originally formed part of the same ophiolitic body. This chapter treats them as part of an originally single entity (i.e. a Denizgören-Lesbos ophiolite sheet) and deals with their equivalent components in

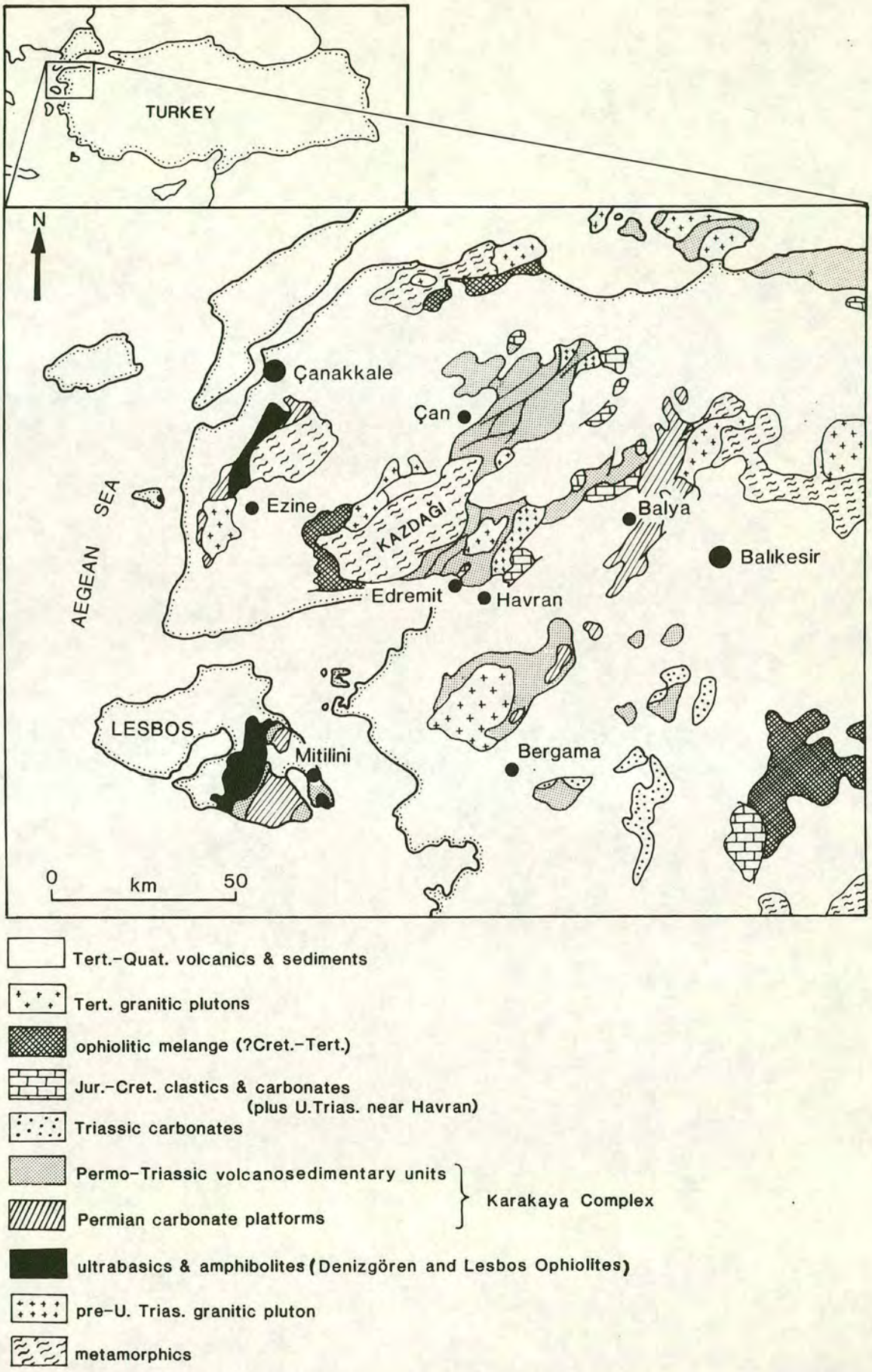

Figure 7.1 Generalized geological map of the Biga Peninsula and the Greek island of Lesbos, showing the location of the two ophiolites.

turn, starting with the ultrabasics and then the metamorphic sole units. The structure and geochemistry of the ophiolites and their metamorphic soles were investigated with the aim of elucidating their tectonic setting and their role in the evolution of the Palaeotethys Ocean in NW Turkey. The structurally underlying carbonate platforms are discussed at the end of the chapter.

7.2 Previous work

The first mention of ultrabasic rocks in the western part of the Biga Peninsula was by Diller (1883). He reported "serpentine" in the Karadag region and deduced that it had been derived from "olivine-enstatite rocks of a truly eruptive nature". Although shown on the current MTA map of NW Turkey, relatively little subsequent work has been carried out on the ultramafic unit near Ezine. Kalafatçioglu (1963) described the ultramafics as "serpentines" and postulated a Permian age on the basis of the apparent intercalation of the serpentines with the flysch and limestones of the Permian Karadag Unit. He dated the Karadag Unit as Upper Permian using foraminifera and algae. Okay (1987) recognized the tectonic nature of the contact between the ultramafics and the Permian sedimentary rocks and postulated a Permo-Triassic ophiolite obduction based on the similarity of the flysch to Lower Triassic sequences elsewhere in northwest Turkey. Okay (1987) also suggested the possible equivalence of the ultrabasics with those on the island of Lesbos. More recently, Okay *et al.* (1991) mapped the ultrabasic unit and named it the Denizgören Ophiolite. Although not an ophiolite *sensu stricto* the ultrabasic body will hereafter be referred to as the Denizgören Ophiolite after Okay *et al.* (1991). Okay *et al.* (1991) also made a detailed map of the various intervals within the Karadag platform sequence and confirmed the Upper Permian age deduced by Kalafatçioglu (1963).

The SE part of Lesbos was mapped during the 1970s (maps published by IGME, the Geological Survey of Greece) but the maps were unfortunately unavailable during the period of this thesis due to restricted availability. More recently, work was carried out on the ophiolitic nappe by Katsikatsos *et al.* (1982), as referenced in Migiros (1992). The Permian carbonate sequence of Lesbos was mapped and described by Hecht (1972, 1974, 1975) and Katsikatsos *et al.* (1982) as part of their general studies of the geology of the island.

The amphibolites which form a horizon beneath the Denizgören Ophiolite have not been previously been studied and are described in this chapter for the first time. An

equivalent unit on Lesbos has been recognized and was tentatively interpreted as metamorphosed gabbros from an oceanic environment (Migiros, 1992). In this thesis the interpretation is taken a step further with the interpretation of the amphibolitic units as an intact metamorphic sole to the Denizgören-Lesbos ophiolite sheet.

7.3 General structure of the Denizgören Ophiolite

7.3.1 Contacts

The western contact of the ultramafic unit is marked by a metamorphic sole which is 100-125m thick (Figures 7.2 and 7.3). The amphibolites of the sole become progressively sheared downwards, towards the Permian platform and grade into the sheared greenschist-grade clastics which form the highest level of the Karadag Unit. A very pronounced foliation is observed. The foliation becomes vertical to overturned near the top of the Figli Dag ridge where the contact of the metamorphic sole with the underlying limestones can be located to within 1m.

The eastern contact of the Denizgören Ophiolite is less well exposed. It has a definite tectonic contact with the Çamlica Micaschists (Figure 7.3), described by Okay *et al.* (1991) as the Ovacik Thrust. The affinity and origin of the schists are unknown although their distinct N-S trending lineation may indicate an affinity with the Kazdag metamorphic rocks. The contact between the two units is very steep and is vertical south of the village of Derbendbasi (Figure 7.2). Vertical, anastomosing foliations enclosing sheared lenses of serpentinite suggest strike-slip displacement. Towards the north the dip of the contact shallows to 30°, possibly indicating thrusting and implying that the boundary may be characterized by at least two styles of faulting of unknown age.

7.3.2 Structures within the ultrabasic rocks

The ultrabasic rocks of the Denizgören Ophiolite are cut by numerous anastomosing shear planes and a dense network of joints and fractures. The joints are commonly infilled with green serpentinite and carbonate which form veneers up to 0.5cm thick on the joint walls. Structural analysis of the joints and shear planes on a well-exposed rock face did not lead to any conclusive results. Most of these structures probably formed after serpentinization and therefore are unlikely to reflect original tectonic transport directions. Towards the eastern boundary of the ophiolite serpentinite

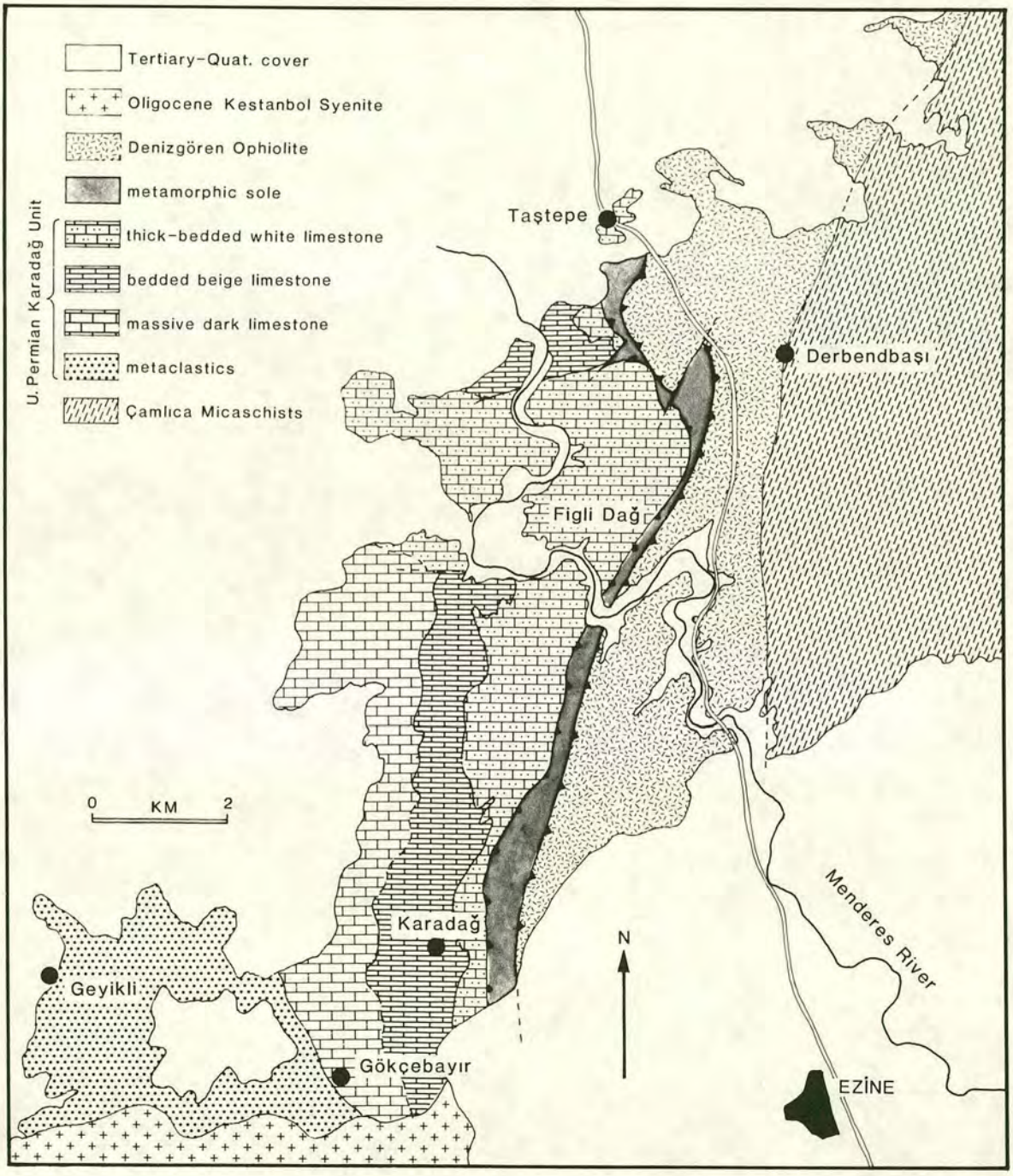

Figure 7.2 Geological map of the region north of Ezine, showing the Denizgören Ophiolite, its metamorphic sole and the underlying carbonate lithologies of the Karadağ Unit (after Okay *et al.*, 1991).

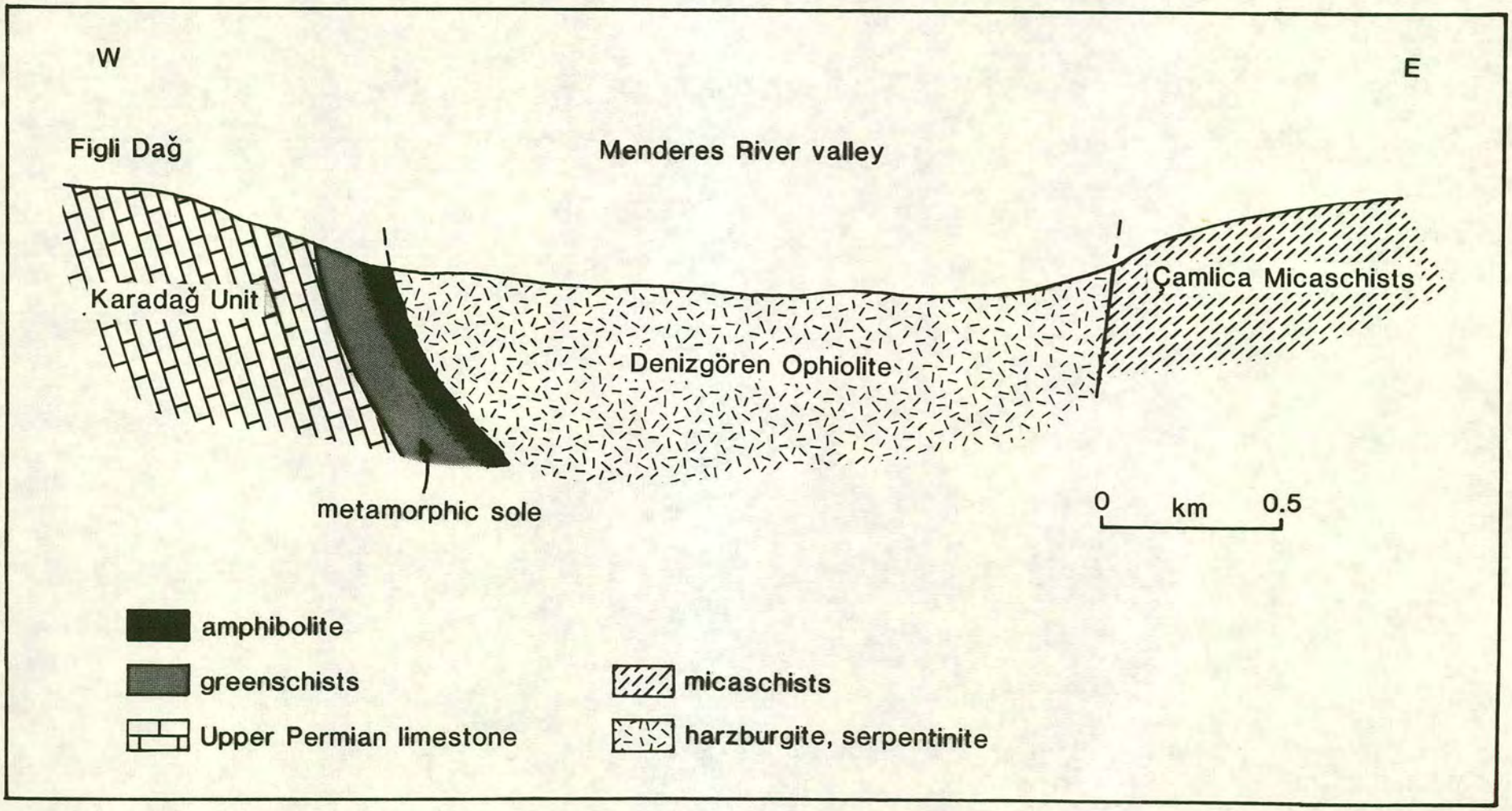

Figure 7.3 Schematic cross-section through the Denizgören Ophiolite.

becomes predominant and the rock also becomes increasingly deformed. Within 50m of the contact with the micaschists, the ophiolite comprises a pale, rubbly serpentinitic matrix containing polished phacoidal "clasts" of more coherent material. Within a few metres of the fault zone the foliation steepens towards the vertical.

The outcrops in the road cuttings along the main road display a large-scale structural grain which dips towards the SE. The foliation is defined by the alternation of pale serpentinitic bands with dark, more coherent layers of ultrabasics.

7.3.3 Structures within the metamorphic sole and underlying Karadag Unit

The Denizgören Ophiolite and its metamorphic sole tectonically overlie the Karadag carbonate platform. Close to the contact between the sole and the platform the foliated greenschist metasedimentary/metavolcanic rocks are very steeply dipping and are locally overturned (Figures 7.4). On moving eastwards, away from the contact, the dip of the foliation shallows. In the amphibolites the foliation dips at approximately 50° towards the southeast. The limestone at the top of the platform is very recrystallized and streaky with a foliation which reflects that of the metamorphic sole. Near Karadag village thin red streaks within the foliation of the limestone directly below the metamorphic sole are folded asymmetrically towards the NW (see Section 7.17.2). Faint lineations parallel to the strike of the foliation planes were observed within both the amphibolites and greenschists. It is not clear whether this lineation represents a separate tectonic event or, alternatively, reflects kink fold axes related to the NW-vergent folds observed in the underlying limestone. Figure 7.5 shows stereograms of the foliations and lineations observed in the metamorphic sole and the underlying limestone.

The vertical to overturned nature of the metasedimentary sequence may be the result of large scale folding, or post-emplacement tilting of individual fault blocks whose boundaries are not observed in the field. This structural feature has led to the mistaken interpretation on the published M.T.A. map that the platform is structurally above the ophiolite. The way-up of the ultramafic-sole sequence implies that this is unlikely as it would require the entire ophiolitic slab to be upside down. Moreover, the sole sequence is only locally observed to be overturned. Away from the contact the platform has relatively shallowly dipping beds, implying that the overturning is a structural feature confined mainly to the zone around the contact. This may imply some fault control along the contact, although this was not observed in the field. The

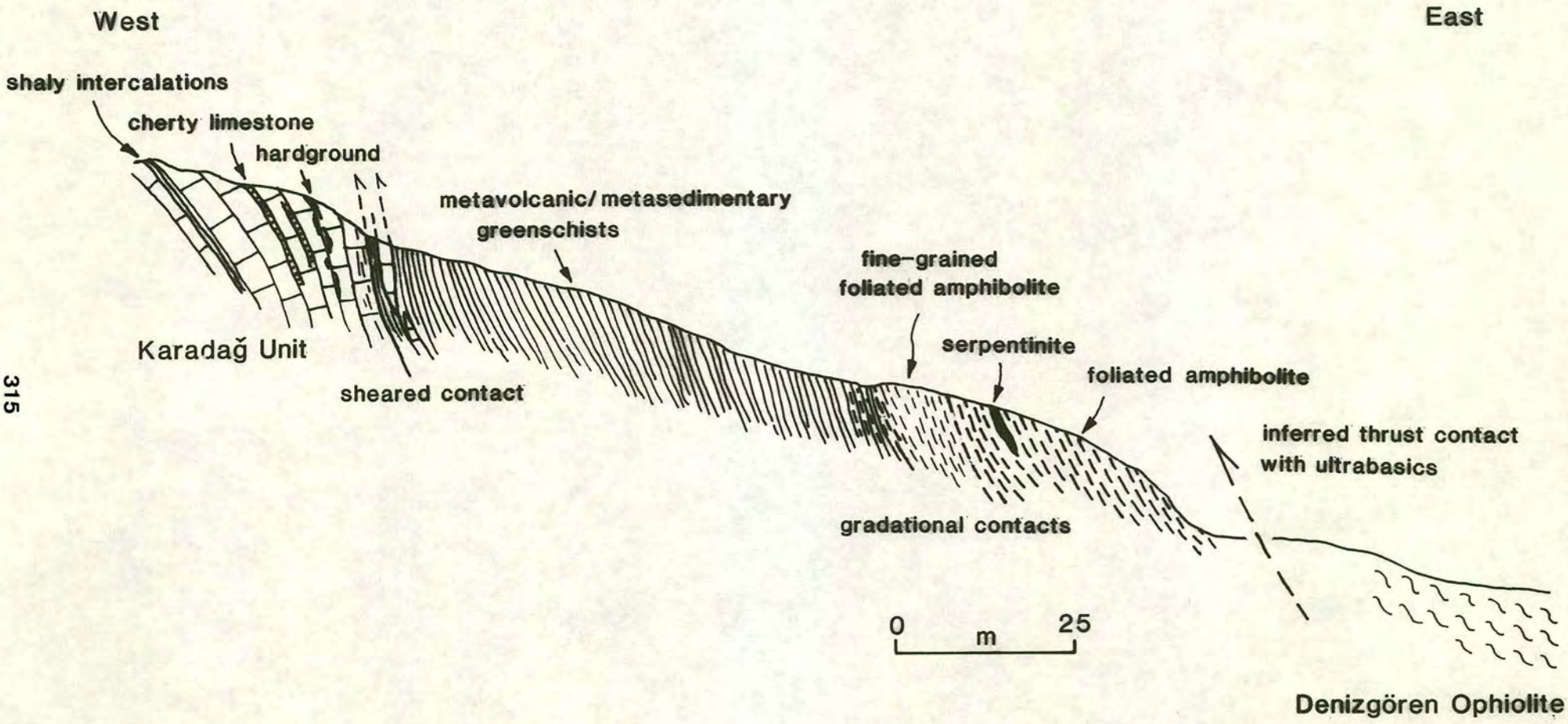

Figure 7.4 Sketch of the eastern slopes of Figli Dağ, showing the metamorphic sole and its relationship with the underlying carbonate platform.

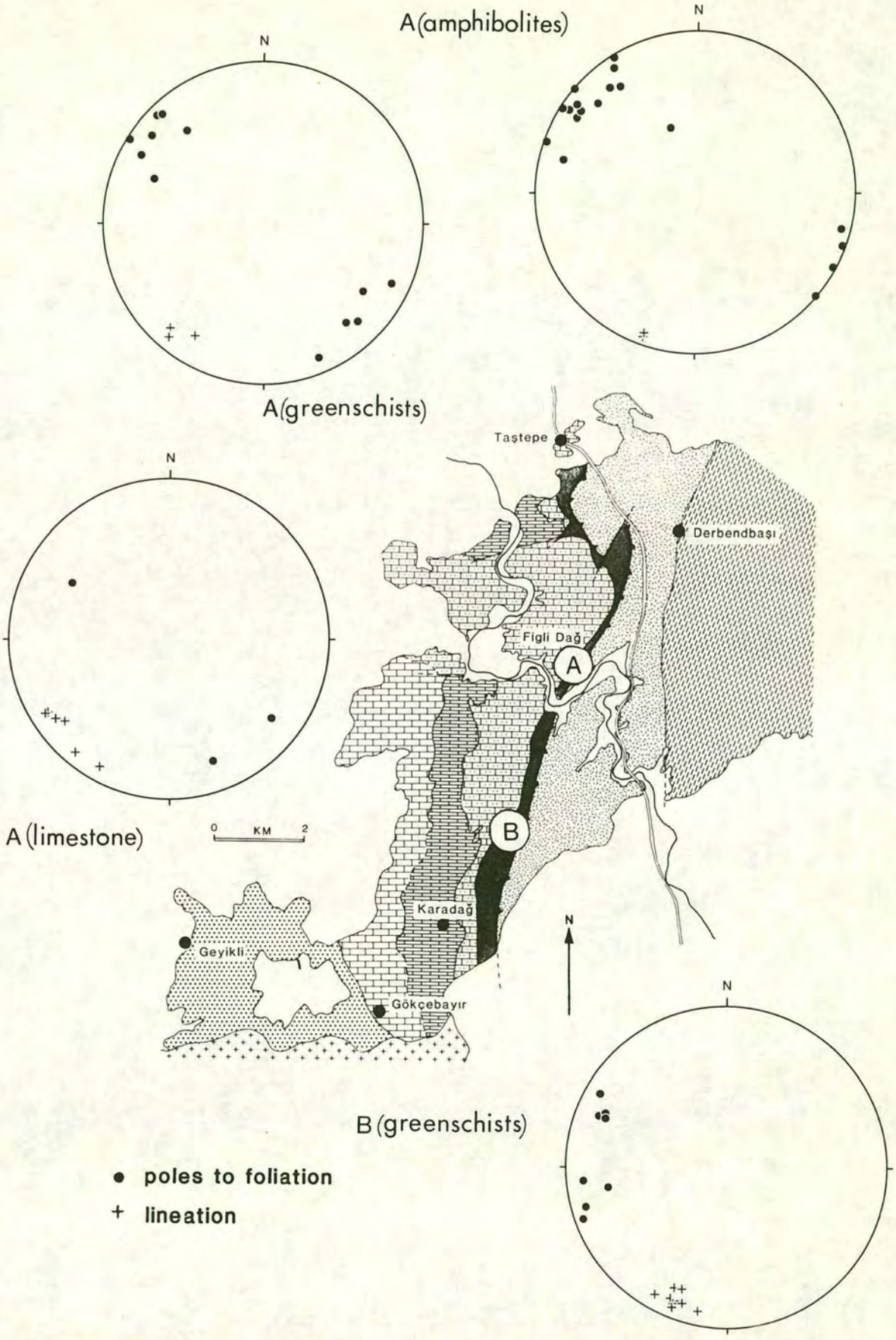

Figure 7.5 Stereoplots of the foliations and lineations measured in the metamorphic sole and the underlying limestone. The letters on the plots refer to the sites on the map.

section below describes in more detail the uppermost limestone of the Karadag Unit near its contact with the overriding metamorphic sole.

7.4 General structure of the Lesbos Ophiolite

7.4.1 Contacts

As with the Denizgören Ophiolite the Lesbos Ophiolite has a tectonic boundary at its base, marked by the presence of a metamorphic sole (Figure 7.6). The amphibolitic part of the metamorphic sole overlies sheared volcanosedimentary rocks of Triassic age which are equivalent to the sheared greenschists below the Denizgören amphibolites. This contact dips towards the northwest and trends NE-SW across the southeastern part of the island. To the west, the ophiolitic nappe is unconformably overlain by thick Neogene and Quaternary volcanic sequences. Investigations have focused on the metamorphic sole of the ophiolite, west of Agiassos (Figure 7.6).

7.4.2 Structure of the metamorphic sole

The metamorphic sole of the Lesbos Ophiolite was little studied, although it clearly contains evidence of several phases of folding. Relatively late kinks and open folds are superimposed on the traces of earlier centimetre-scale isoclinal folds with steeply plunging axial planes. The asymmetrical isoclinal and the kink folds close westwards whereas the open folds apparently close NE. On the basis of field relations near Agiassos structures can be tentatively placed in the following order of formation:

1. Isoclinal folds with steep axial planes. (W-closing).
2. Tight high angle kink folds. (W-closing).
3. Poorly defined open folds. (?NE-closing).
4. Late multi-phase brittle faulting.

Locally, C-S fabrics and rotated porphyroblasts with a sense of motion towards the east were also observed within sheared meta-lavas of the metamorphic sole. It is unclear where they fit into the sequence above, although their association with E-closing folds may place them within stage 3. The highest greenschists of the metamorphic sole also contain evidence of eastward directed motion. Small intrafolial folds and later crenulation folds, some of which are asymmetrical to the east, were observed, although there appeared to be no consistent sense of vergence.

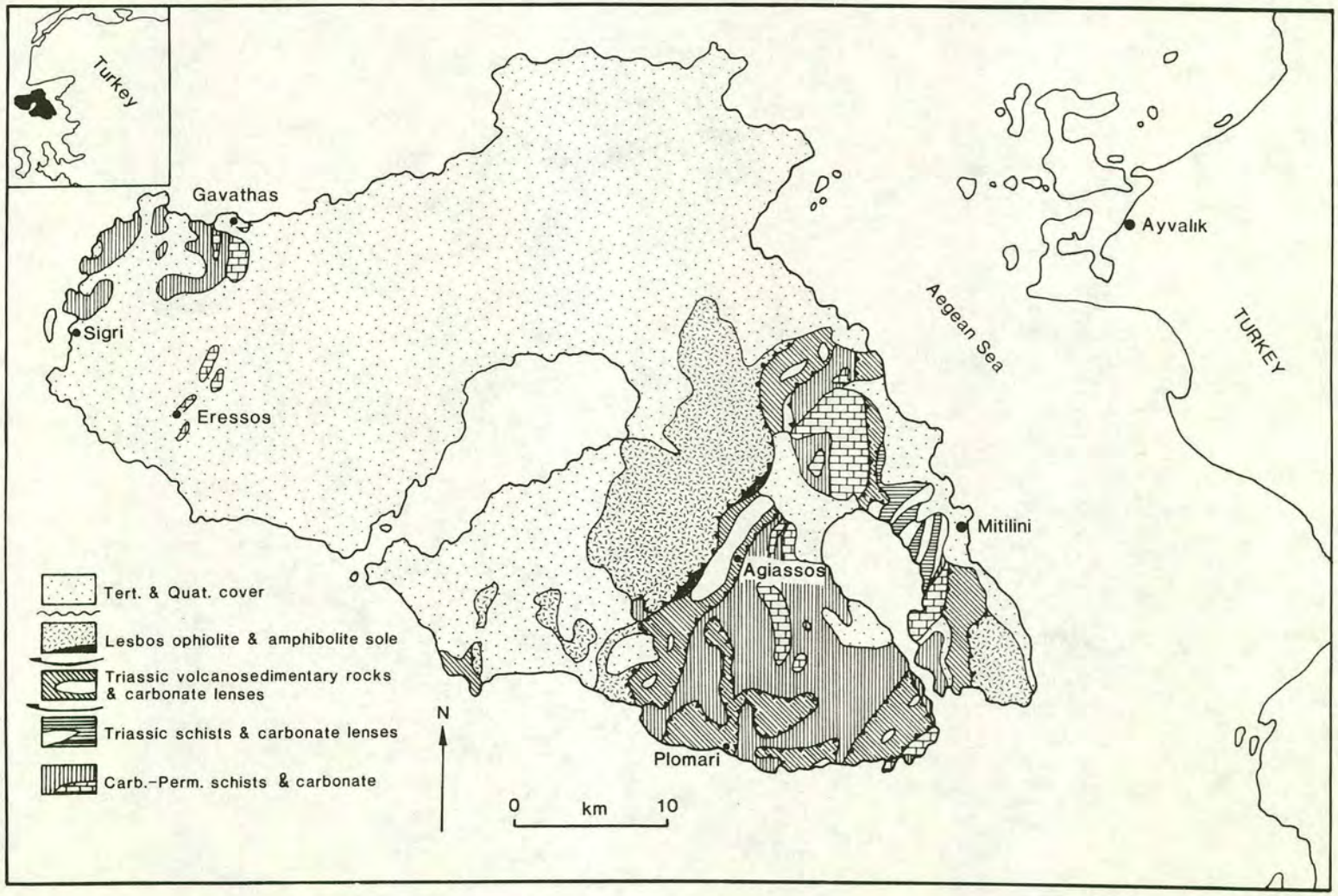

Figure 7.6 Geological map of Lesbos showing the ophiolitic sheet and the amphibolitic sole (redrawn after Katsikatsos *et al.,* 1982).

An open fold within the marble underlying the metamorphic sole closes west, the same direction as the folds within the limestone beneath the Denizgören sole. Thus it appears that the Lesbos Ophiolite has undergone both westward- and eastward-directed movement. The sequence of events outlined above would suggest that an earlier event of westward transport was followed by movement in the opposite direction. However, rotated porphyroblasts observed in meta-lavas along the road from Agiassos to Mount Olympos clearly indicates that E-directed motion was *followed* by W-directed motion. Fold asymmetry in the amphibolitic part of the sole appears to be the result of westward motion followed by eastward motion, whereas in the lower, greenschist part of the sequence, the sense of motion appears to be eastwards only. However, owing to the reconnaissance nature of my visit to Lesbos this discussion is very tentative and a great deal more structural data is required before any clear structural history for the Lesbos Ophiolite can be put forward.

7.5 The Denizgören and Lesbos ultrabasic rocks

In this section the peridotites of the Denizgören and Lesbos ophiolites are described. Despite forming the bulk of both ophiolites the ultrabasic rocks are too highly serpentinized to be particularly informative. However, several less altered samples were taken for XRF analysis and electron probe analysis of chromian spinels, the results of which are presented in Sections 7.6.2 and 7.6.3.

7.5.1 Denizgören ultrabasic rocks

The bulk of the ultrabasic rocks of the Denizgören Ophiolite comprise harzburgite in various stages of serpentinization. Minor gabbro has also been observed (Okay *et al.*, 1991), although their description probably refers to the amphibolites of the metamorphic sole identified during fieldwork for this study. A large-scale fabric dipping E to SE at 55-70°, is defined by broad colour changes in the harzburgite which reflect the degree of serpentinization. The bands which define this fabric are up to many metres wide and are best observed along the main road north of Ezine, just north of the bridge over the Menderes River (Figure 7.7a). The more serpentinized regions tend to be shiny and very light green-grey in colour, whereas the fresher rock is darker and more massive. The harzburgite is generally highly serpentinized and in thin-section consists predominantly of mesh-textured serpentine and altered orthopyroxene. A few fresh crystals of olivine and clinopyroxene were observed. The clinopyroxenes are very fresh in some cases and display exsolution lamellae of

a

b

Figure 7.7

(a) Large-scale E to SE-dipping fabric in serpentinized harzburgite, 1km east of Figli Dağ. Pale coloured, highly serpentinized shear zones separate darker, more coherent bands.

(b) Compositional banding in ultrabasics near Karadağ, defined by alternating concentrations of serpentinized olivine (grey) and altered orthopyroxene crystals (brown).

orthopyroxene, parallel to a very strong cleavage. The harzburgite locally contains disseminated chromian spinel and chromium-rich magnetite clusters.

A tectonite fabric defined by parallel alignment of orthopyroxene crystals was observed in several outcrops. Near Karadag village a small outcrop of banded harzburgite was observed which has escaped the total serpentinization which affects much of the ophiolite (Figure 7.7b). Banding on a 0.5cm scale is defined by an alteration of green-grey and yellow-brown layers. Thin-section study reveals that this was originally caused by alternating concentrations of olivine and orthopyroxene crystals. The grey layers comprise mesh-textured serpentine, a characteristic alteration product of olivine. The brown layers consist of highly altered fibrous orthopyroxene with sharply defined exsolution lamellae of fresh clinopyroxene parallel to the cleavage. Fresh clinopyroxene and olivine crystals were also observed.

7.5.2 Lesbos ultrabasic rocks

The ophiolitic nappe of Lesbos (Figure 7.6) is composed entirely of serpentinized peridotites which are locally cut by veins of pyroxenite and gabbro (Migiros, 1992). He also reported that the ultrabasic nappe is at least 1000m thick in places. On the basis of reconnaissance fieldwork in SE Lesbos it appears that, as with the Denizgören Ophiolite, the bulk of the Lesbos Ophiolite is serpentinized harzburgite. Tectonite fabrics were observed in the harzburgite.

7.6 Geochemistry of the peridotites

7.6.1 Introduction to ophiolite settings

The main aim of carrying out geochemical analyses on the rocks of the Denizgoren and Lesbos ophiolites was to determine the likely tectonic environments of their protoliths and to gain information regarding their subsequent evolution. Although the origin of ophiolites is still a matter of much debate it has been confirmed that they can form in tectonic settings, broadly classified as supra-subduction (SSZ) and mid-ocean ridge basalt (MORB) settings (e.g. Pearce *et al.*, 1984).

SSZ ophiolites differ from MORB ophiolites in their geochemistry and in the depleted nature of their mantle sequences. They also contain more chromite deposits and a higher abundance of wehrlite relative to troctolite in their cumulate sequences which

is a result of the crystallization of clinopyroxene before plagioclase (Pearce *et al.*, 1984). Despite these discriminating criteria it is often difficult to assign incomplete or fragmentary ophiolitic sequences to either a SSZ or a MORB setting, especially in cases where crustal sequences are not observed. The Denizgoren and Lesbos ophiolites consist predominantly of harzburgite with minor dunite.

The main differences between SSZ and MORB ophiolites and the criteria by which they may be distinguished are presented in Pearce *et al.* (1984). Their criteria include chemical signatures, crystallization sequences, type of mantle residue, presence or absence of chromite pods, ophiolite structure and the nature of the sedimentary cover. The main distinguishing criteria may be summarized as follows:

1. Immobile trace-element analysis of ophiolite lavas and dykes can be used to broadly distinguish SSZ volcanics, which have island-arc geochemical characteristics, from MORB volcanics which have mid-ocean ridge geochemistry. This is achieved by comparing the lava geochemistry with data from known settings using basalt discrimination diagrams.

2. The cumulates of SSZ and MORB ophiolites usually exhibit distinct crystallization sequences. In SSZ ophiolites pyroxenes tend to crystallize before plagioclase, whereas the reverse occurs in MORB ophiolites. Thus in SSZ cumulate sequences, basal dunites are followed by lherzolites, wehrlites, norites and gabbros. Dunites are usually followed up section by troctolites and gabbros in MORB ophiolites.

3. Cumulate chromite-dunite bodies are more common in SSZ ophiolites than in MORB ophiolites. Although small podiform chromites do exist within MORB ophiolites all the known major chromite deposits occur within inferred SSZ ophiolites, possibly as a result of subduction-derived water leading to expansion of the olivine and spinel phase volumes.

4. Harzburgite is the predominant lithology of the ultramafic tectonites (mantle sequences) of SSZ ophiolites and usually comprises 80-90% of the total exposure. The remainder includes pods of dunite, lherzolite and pyroxenite. The mantle sequences in MORB ophiolites contain both harzburgite and lherzolite, in widely varying proportions. Also, the harzburgite of MORB ophiolites is generally less depleted than that of SSZ ophiolites and contains more Al, Ca and Ti.

Other ophiolite characteristics such as ophiolite structure and the nature of sedimentary cover sequences have also been investigated as possible indicators of SSZ or MORB settings and are discussed in Pearce *et al.* (1984). With regard to structure, the thicknesses of the crustal and lava sequences do not correlate well with ophiolite type. The proportion of intermediate and acid rocks may provide a better discriminant. SSZ ophiolites such as Troodos and Vourinos contain a greater proportion of intermediate to acid lavas than MORB ophiolites, although the SSZ Semail ophiolite is intruded by diorite-plagiogranite bodies and contains many andesites and rhyolites in its lava sequences. Sedimentary cover rocks cannot directly be used to discriminate between SSZ and MORB ophiolites, but volcanosedimentary sequences which indicate the presence of an adjacent volcanic arc may help to confirm a SSZ setting. The Coast Range ophiolite in central California provides a good example of a situation where the presence of an adjacent arc is indicated by the thick volcaniclastic sediment cover of the ophiolite (Robertson, 1989).

The Denizgören and Lesbos Ophiolites are slabs of ultrabasic rock, fault-bounded and lacking cumulates, extrusive sequences or a sedimentary cover. Owing to their fragmentary nature many of the criteria outlined above are inapplicable and deductions must be made largely on the basis of geochemistry; for example, peridotite and chromian spinel composition.

Both ophiolites comprise predominantly harzburgite, a common feature of the lower levels of many ophiolites. Dunite pods have been observed in the Denizgören Ophiolite (Okay *et al.*, 1991), a common phenomenon in harzburgite-dominated ophiolites. Chromian spinel occurs as disseminated grains within the harzburgite and one sample from the Denizgören Ophiolite was analysed by electron microprobe. Chromian spinel is a useful indicator of the original composition of the melt owing to its highly refractory nature and several studies have been made on the composition of ophiolitic chromian spinels. A few samples of peridotite from the Denizgören ophiolite were analyzed by XRF, although the usefulness of the composition of peridotites is limited.

7.6.2 Whole-rock analysis of peridotites

Several samples of peridotite were collected from the Denizgören Ophiolite for whole-rock XRF analysis (Appendix 2). The least sheared exposures along the main Çanakkale-Izmir road were selected for sampling. Results were plotted on the Cr-

TiO_2 plot for tectonized ultramafic rocks (Pearce *et al.*, 1984) which separates SSZ from MORB ophiolites on the basis of TiO_2 content (Figure 7.8a). SSZ ophiolite mantle residue tends to be more depleted (i.e. it is more "residual") than that of MORB ophiolites, having been derived by higher degrees of melting of a similar source, or by similar degrees of melting of a less fertile source, than the mantle sequences of MORB ophiolites (Pearce *et al.*, 1984). They contain less Ti, Ca and Al than those from MORB settings. The Denizgören samples plot mainly in the SSZ-MORB overlap zone, but by comparison with other, better understood Tethyan ophiolites (Figure 7.8b) they appear to have most affinity with SSZ ophiolites, especially those from the Troodos and Semail Ophiolites.

7.6.3 Microprobe analysis of chromian spinels

Chromian spinel $(Mg,Fe^{2+})(Cr,Al,Fe^{3+})2O_4$ is an accessory phase in many basalts and peridotites and has proved to be a sensitive indicator of melt composition and pressure of crystallization (e.g. Dick & Bullen, 1984 and references therein). Spinel composition fields in genetically related basalts and peridotites from ophiolites and the oceans are very similar, implying that spinels may reflect the degree of melting in the mantle source region. During fractional crystallization or partial melting, Cr and Mg are strongly partitioned into the solid, while Al is strongly partitioned into the melt. Partitioning of Mg and Fe^{2+} between spinel and silicate melts is strongly dependent on temperature and the Fe^{2+}/Fe^{3+} ratio is sensitive to changes in fO_2. As a result of these features, spinel compositions can vary considerably during crystallization, melting or re-equilibration and hence provide an extremely sensitive indicator of host rock petrogenesis.

Studies have been carried out to compare spinel compositions from mid-ocean ridge basalts and peridotites with those from various ophiolite complexes. Dick & Bullen (1984) classified peridotites from ophiolite complexes according to the similarity of their spinel chemistry to that of spinels from mid-ocean ridge rocks. Spinels from Type I peridotites share chemical characteristics (in particular, variation in Cr and Al as described below) with mid-ocean ridge spinels, whereas the spinels of Type III peridotites fall largely outside this range. Peridotites transitional between these two are classed as Type II.

The most significant compositional variation of spinel is a large reciprocal variation of Cr and Al, with a strong correlation of increasing Cr/Cr+Al (Cr#) and decreasing

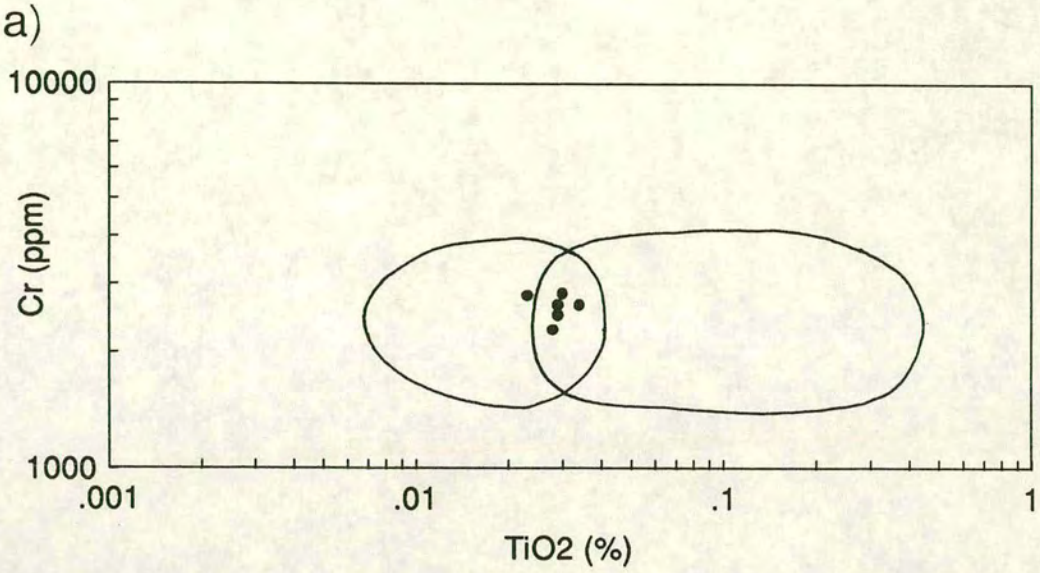

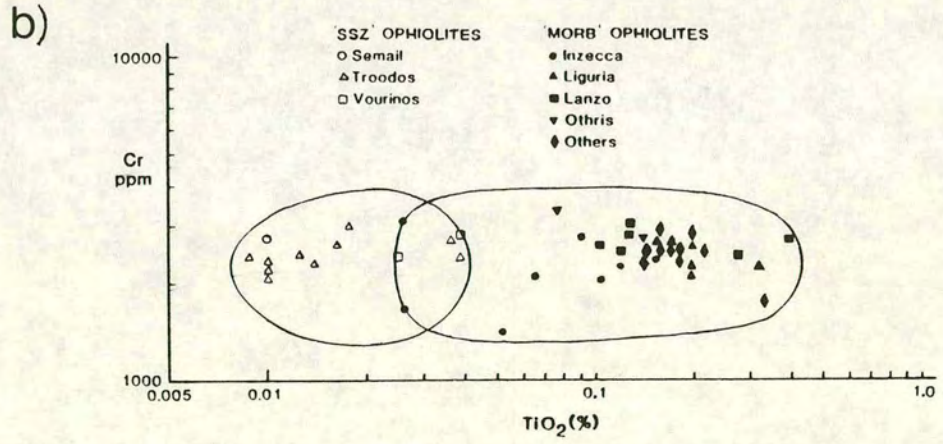

Figure 7.8 Cr-TiO_2 plots for tectonized peridotites from (a) the Denizgören Ophiolite and (b) other Tethyan ophiolites (from Pearce *et al.*, 1984).

$Mg/Mg+Fe^{2+}$ (Mg#) (Dick, 1978; Hamlyn & Bonatti, 1980). Increasing values of Cr# reflect increasing degrees of partial melting in the mantle. This ratio forms the basis of the classification outlined above. Type I peridotites and associated volcanics contain spinels with Cr#<0.60; Type III peridotites and associated volcanics contain spinels with Cr#>0.60, and Type II peridotites and volcanics are transitional and contain spinels spanning the ranges of the former two types.

As described by Dick & Bullen (1984), spinels in mid-ocean ridge peridotites lie wholly within the Type I field, implying that ophiolites containing Type I peridotites probably represent oceanic lithosphere formed at a mid-ocean ridge. Dick & Bullen (1984) interpreted a sub-volcanic arc petrogenesis for most Type III peridotites as modern analogues for this category are found in arc-related volcanic and intrusive rocks, continental layered intrusions and oceanic plateau basalts. Type II peridotites indicate large variations in degree and provenance of melting which may reflect composite origins and multi-stage melting histories.

Chromian spinel can occur in peridotites as a cumulus phase and also as isolated interstitial grains with irregular shapes. Interstitial grains of chromian spinel were observed in a sample of peridotite from the Denizgören Ophiolite. In thin-section they form small (up to 0.5mm across) amorphous clusters of grains, characteristically deep red to black in plane-polarized light. The spinel occurs together with small clusters of interstitial Cr-rich magnetite.

Twelve spinels from a peridotite sample (Den1) were analyzed by electron microprobe. Cores only were analyzed in spinels 1-7 and both cores and rims were analyzed in spinels 8-12. The Fe^{2+} concentration was calculated on the basis of stoichiometry after the method of Droop (1987). Core and rim compositions were plotted on the Cr# against Mg# diagram shown in Figure 7.9 (fields from Dick & Bullen, 1984). Also shown on the diagram are the composition fields for chromian spinels from abyssal alpine-type peridotites (i.e. MORB-type), island-arc basalts and boninites. According to the classification of Dick & Bullen (1984) the Denizgören peridotite strictly lies in the Type I category, as the spinels have Cr# values ranging from 0.51 to 0.56 (i.e. less than 0.60). However, most of the spinels lie just outside the high Cr end of the mid-ocean ridge (abyssal) spinel range and therefore the peridotite can be assigned to the transitional Type II category.

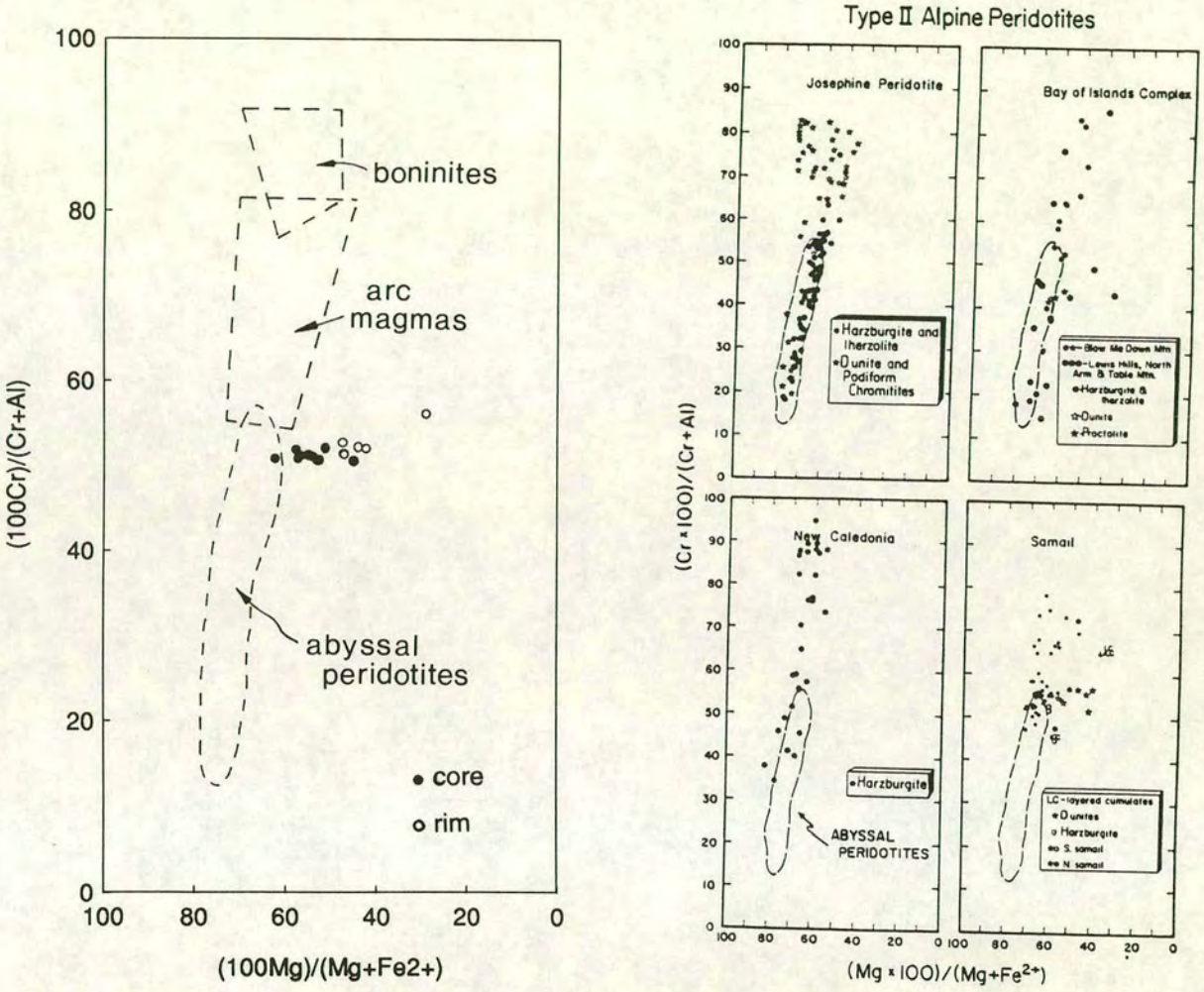

Figure 7.9 Chromian spinel compositions plotted on the Cr# vs Mg# diagram of Dick & Bullen (1984). (a) serpentinized peridotites of the Denizgören Ophiolite and (b) examples of Type II alpine-type peridotites (from Dick & Bullen, 1984).

Examples of peridotites which fall into the Type II category are shown in Figure 7.9 (Dick & Bullen, 1984). The petrogenesis of Type II peridotites is the most complex and consequently least understood of the three types. Chromian spinels from the Denizgören Ophiolite are compositionally most similar to those from the southern part of the Semail Ophiolite which is classified as Type II category. These spinels lie more or less within the Cr# range of abyssal spinels, consistent with the mid-ocean ridge origin proposed by Pallister & Hopson (1981). Those from the north lie far outside the abyssal field and this marked north-south difference was interpreted by Dick & Bullen (1984) as recording different stages in the opening and evolution of back-arc basins or continental rifts.

7.6.4 Interpretation of peridotite geochemistry

Although the Denizgören Ophiolite peridotite samples plot in the SSZ-MORB overlap zone of the Cr-TiO_2 diagram they appear to be mainly of SSZ affinity, having relatively low TiO_2 values compared to most of the Tethyan "MORB" ophiolites shown for reference in Figure 7.8b (from Pearce *et al.*, 1984). Those from the supra-subduction Troodos and Vourinos ophiolites occupy similar positions to those from the Denizgören Ophiolite, by analogy implying a possible SSZ origin, or at least the involvement of a SSZ component.

A SSZ component for the Denizgören Ophiolite is also indicated by the chromian spinel geochemistry (Figure 7.9). The chromium spinels have Cr# values of less than 0.60, which should strictly place them in the Type I (MORB) category of Dick & Bullen (1984). However, most of the spinels lie outside the high Cr end of the mid-ocean ridge (abyssal) spinel range and therefore the peridotite should be assigned to the transitional Type II category which may represent rocks with composite origins and multi-stage melting histories. Chromian spinels from the Denizgören Ophiolite are compositionally most similar to those from the southern end of the Semail Ophiolite in Oman, thus confirming their place within the Type II category and indicating a possible SSZ component.

7.7 Other supra-subduction zone ophiolites in the Eastern Mediterranean

Supra-subduction zone (SSZ) ophiolites probably form in response to short-lived spreading events (5-7 Ma) above young oceanic subduction zones, before the establishment of arc volcanism (Natland & Tarney, 1982). Subduction initiation is

followed by "roll-back" of dense lithosphere which allows asthenosphere to well up and cause spreading in the fore-arc region. Continuing subduction results in the construction of a volcanic arc on the initial SSZ lithosphere.

Following the summary by Robertson (1994), an ideal supra-subduction zone ophiolite would comprise a depleted harzburgitic mantle section, a sheeted dyke complex and IAT and/or boninitic extrusives. If subduction continued after boninitic "pre-arc" spreading, a volcanic arc edifice would build up and be recorded by high-level plagiogranite intrusives and acidic extrusives. A thick volcanic and volcaniclastic sequence may also be present.

The most complete example of this type of ophiolite in the Eastern Mediterranean region occurs within the Jurassic eastern part of the Mirdita Zone in Albania (Shallo *et al.,* 1990), where depleted mantle harzburgites, layered cumulates, massive gabbros, sheeted dykes, plagiogranites and IAT/boninitic extrusives are overlain by acidic extrusives and volcaniclastics.

The Troodos ophiolite in Cyprus also displays IAT and boninitic lavas in the upper extrusives and is widely regarded as a SSZ ophiolite (e.g. Pearce, 1980; Gass, 1990). Other examples of inferred SSZ ophiolites in the Eastern Mediterranean region include the Jurassic Pindos and Vourinos ophiolites (northern Greece) and the Cretaceous Hatay, Baer-Bassit and Guleman ophiolites in northern Syria and SE Turkey (Pearce *et al.,* 1984; Jones *et al.,* 1991).

Although no modern example of active "pre-arc" spreading is known, a wide range of rock-types similar to those in inferred SSZ ophiolites (e.g. harzburgites, boninites), has been discovered in the modern Mariana-Bonin fore-arc (e.g. Ishii, 1984; Crawford *et al.,* 1989).

7.8 Metamorphic sole rocks

In this section the metamorphic rocks observed below the ultrabasic sequences are discussed. By comparison with other sub-ophiolitic units around the world, their tectonic position and constituent lithologies indicate that they represent a metamorphic sole to the Denizgören and Lesbos ophiolitic sheets. The Denizgoren sole tectonically overlies an Upper Permian carbonate sequence and the Lesbos sole is emplaced onto a Middle-Upper Triassic clastic and carbonate succession. This may

imply a diachronous emplacement. However, this is an inference and no sole dates are available as yet. The general characteristics of metamorphic soles, based on field observations, are briefly mentioned below. This is followed by a discussion of the lithologies and geochemistry of the Denizgören and Lesbos sole units.

7.9 Characteristic features of metamorphic soles

The existence of metamorphic rocks at the base of many ophiolitic bodies has long been recognized (Williams & Smyth, 1973; Woodcock & Robertson, 1977). Seemingly regardless of age and geographical position, these metamorphic rocks or "metamorphic soles" have many features in common. Searle and Malpas (1980) outlined the common features of metamorphic soles based on investigations of several ophiolites and peridotite bodies, including the sub-ophiolitic metamorphic sheets beneath the Bay of Islands Complex in Newfoundland.

1. Metamorphic rocks occupy a constant stratigraphic position at the base of the ophiolite and underlie a thick ultramafic unit.

2. They exhibit a decreasing metamorphic grade with depth beneath the peridotite.

3. The metamorphic complexes characteristically have a narrow width, suggesting a high geothermal gradient.

4. There is a general lack of intrusive phenomena (e.g. dykes, xenoliths, chilled margins) associated with the contact between the ultramafic and the metamorphic rocks.

5. Where there has been no dismemberment, orientations of metamorphic fabrics and the conditions of their formation are essentially the same in the basal ultramafic rocks and the metamorphic rocks.

The metamorphic units present beneath the Denizgören and Lesbos ophiolites conform well to the criteria outlined above and, unlike some sole units (e.g. Pindos; Jones & Robertson, 1991), are relatively intact and *in situ*. In this respect the metamorphic soles of the Denizgoren and Lesbos ophiolites resemble those of the

Vourinos and Semail ophiolites. The components of the Denizgören and Lesbos metamorphic soles are discussed below.

7.10 Denizgören metamorphic sole

The sub-ophiolitic rocks of the Denizgören Ophiolite can be broadly divided into two main groups: amphibolites and foliated metasedimentary/metavolcanic rocks (greenschists). The amphibolites lie directly beneath the ultrabasic rocks and pass gradationally downwards into foliated greenschists which overlie the Karadag Unit (Figures 7.3 and 7.4).

7.10.1 Amphibolites

Directly beneath the ultrabasics lies an approximately 25m-thick horizon of amphibolite which is coarse-grained and displays a well-developed preferred orientation of amphiboles. The best exposure of this horizon is south of the hill of Figli Dag, near the Menderes River, where the entire sub-ophiolitic sequence can be observed up the hillside (Figure 7.4). In the field the amphibolite is speckled dark green and white and has a sparkling appearance on fresh surfaces. It has a banded appearance as shown in Figure 7.10a. In thin-section the constituent minerals are revealed as hornblende, zoisite and epidote. The hornblendes are strongly pleochroic, green and blue-green in colour and considerably bent and broken in places. The zoisite is colourless with an anomalous blue-grey colour in cross-polarized light. It forms both interstitial masses and individual crystals. Some zoisite crystals contain inclusions of an amphibole. Epidote is common and occurs as crystals as well as within small veins. Clinozoisite may also be present in some veins. Figure 7.10b shows a photomicrograph of a typical amphibolite from the Figli Dag region, showing predominantly hornblende with scattered clusters and individual crystals of colourless zoisite.

7.10.2 Greenschists

Approximately 100m of highly foliated, green metasedimentary/metavolcanic rocks of greenschist facies overlie the amphibolite horizon. A sedimentary origin can be deduced for at least some of the greenschists from rare lenses and relict beds of sandstone preserved in the lower parts of the unit. The presence of sheared limestone blocks within the greenschists also testify to a sedimentary origin. A few cherty

Figure 7.10

(a) Banded amphibolite from the metamorphic sole near Figli Dağ. Banding is defined by alternating hornblende- and zoisite-rich layers.

(b) Photomicrograph of amphibolite from Figli Dağ, showing hornblende (hbl) with clusters of colourless zoisite (zs) concentrated in bands trending from top right to bottom left of picture (sample DEN A, PPL, field of view: 4mm).

(c) Photomicrograph of amphibolite from the metamorphic sole west of Agiassos showing the same mineral assemblage as the sample above (sample LS5, PPL, field of view: 9mm).

a

b

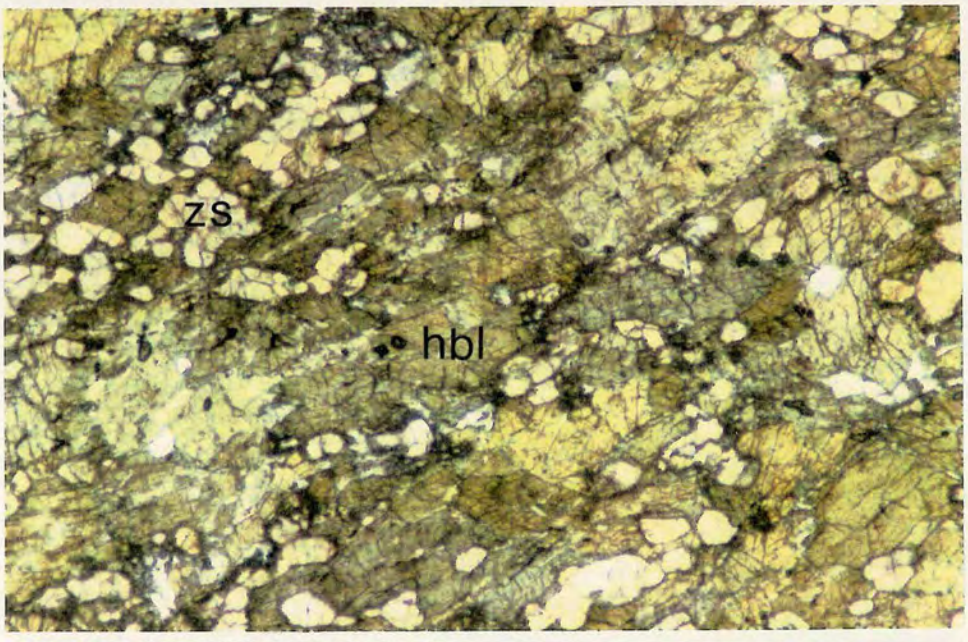

c

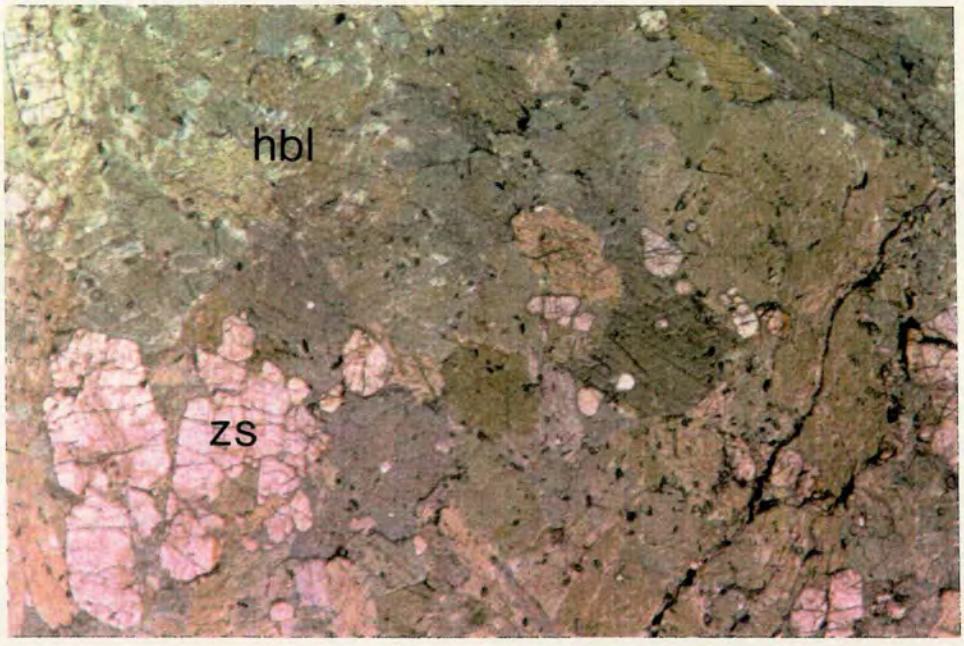

layers were also observed, especially in the lower part of the sequence. In the most part, however, sedimentary features have been obliterated by intense shearing and the development of the strong fissility. There is no sharp contact between the amphibolites and the metasedimentary rocks. They are gradational over a relatively small distance (a few metres). Down section the amphibolites become progressively finer grained and start to show a foliation. Further down sequence the amphibolites become indistiguishable from the foliated greenschists. The basal contact of the greenschists is very sheared but relatively sharp, although there is no sharp break in metamorphic or deformational gradient. The underlying carbonates are highly sheared and recrystallized and are characteristically streaky white, grey and pink.

7.11 Lesbos metamorphic sole

The metamorphic sole of the Lesbos Ophiolite is best observed west of the town of Agiassos (Figure 7.11). As with the Denizgören Ophiolite the sole can be divided into an amphibolitic unit and a basal greenschist unit consisting of metasedimentary and metavolcanic rocks (Figure 7.12).

7.11.1 Amphibolites

Amphibolites at the base of the ultrabasic section are very similar to those found in the Denizgören Ophiolite. They have a green and white speckled appearance and display hornblende and zoisite in thin-section (Figure 7.10c). Pumpellyite (possibly with some prehnite) can be observed in veins. The hornblende displays exsolution lamellae of a second amphibole (?cummingtonite), an unusual feature. Banding defined by the preferred orientation of hornblendes is locally well-preserved. The amphibolites have a well-developed foliation with a constant dip over tens of metres. The estimated stratigraphic thickness of the amphibolite horizon is 80-100m. Folds and a ductile shear band were observed within the amphibolite. Structures within the sole are described in more detail in Section 7.11.2.

7.11.2 Greenschists

Structurally below the amphibolites are buff schists with a well-developed cleavage. These pass down into sheared and folded green and blue-green volcaniclastics with thin marble and metachert intercalations, and dark grey metalavas, locally including deformed pillows and lava breccias. These greenschists contain marble lenses up to

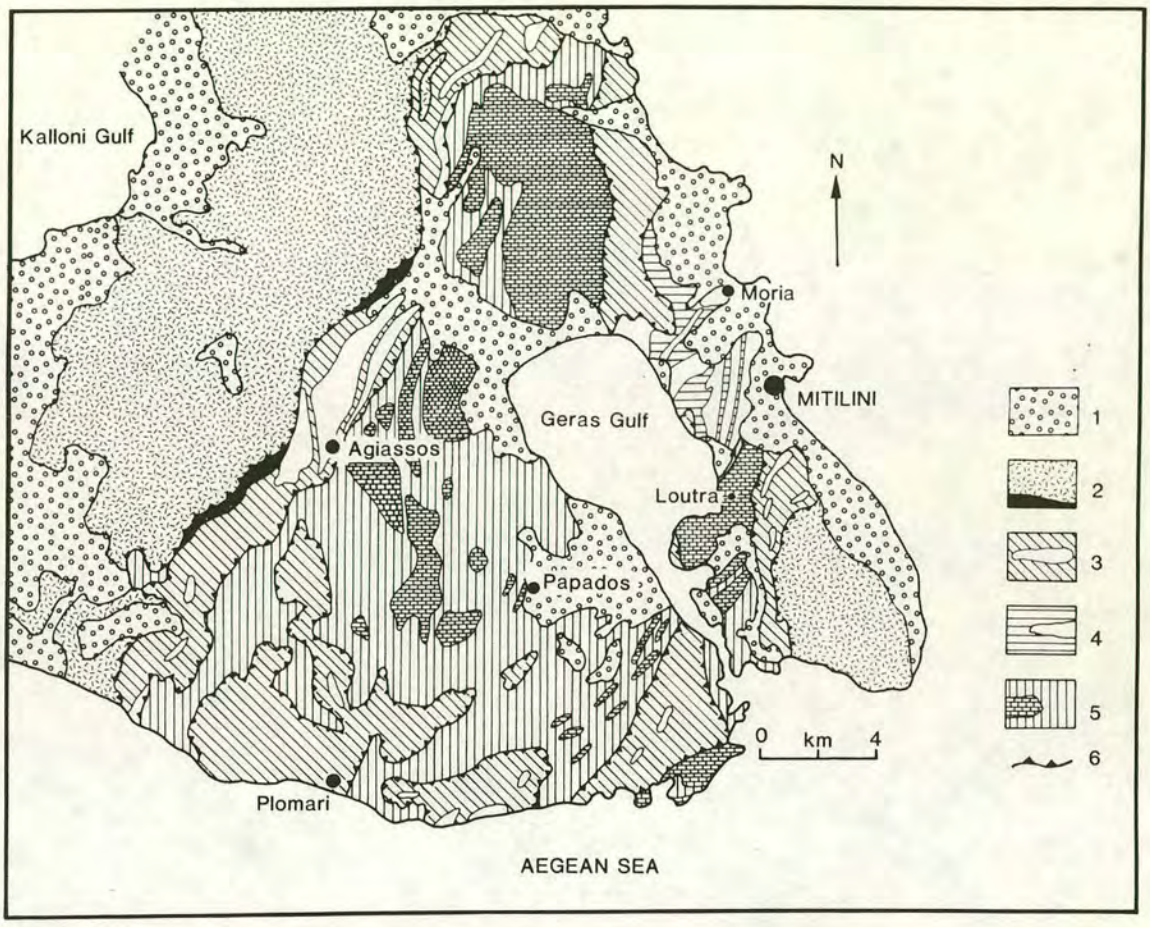

Figure 7.11 Geological map of SE Lesbos (redrawn after Katsikatsos *et al.,* 1982). (1: Quaternary-Neogene deposits, 2: Ultrabasic rocks with amphibolitic sole, 3: Triassic volcanosedimentary units with carbonate lenses, 4: Triassic schists with carbonate lenses, 5: Carboniferous-Permian schists and carbonate, 6: Thrust). Samples of amphibolites were collected from the metamorphic sole directly east of Agiassos.

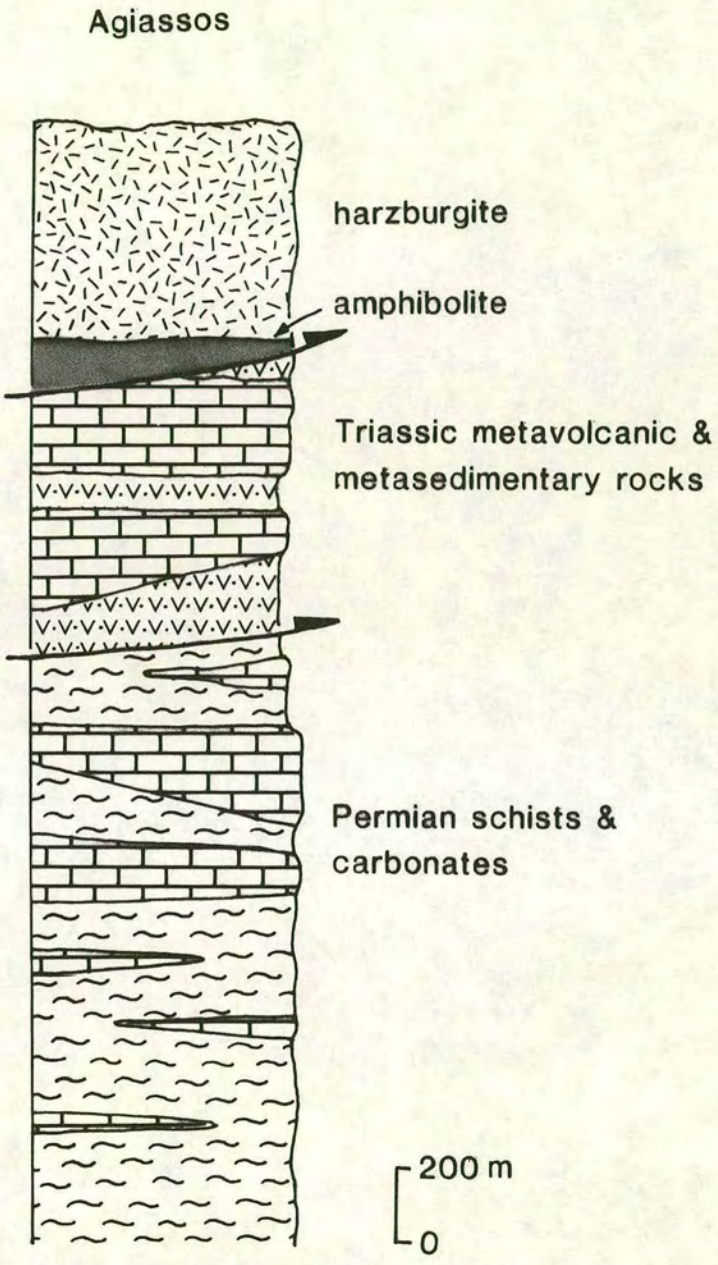

Figure 7.12 Simplified section through the Lesbos metamorphic sole in the Agiassos area (after Migiros & Pavlopoulos, 1992). The Triassic metavolcanic and metasedimentary unit represents the lower levels of the metamorphic sole.

50-100m long. At the base of the sequence are highly sheared debris flows which consist of deformed marble clasts in a purple-green muddy matrix. They lie immediately above Permian limestones which are equivalent in age and structural position to the Karadag Unit in Turkey. The size of the marble clasts within the debris flows increases upwards to 5m in diameter. The total thickness of this metasedimentary/metavolcanic unit is approximately 500m.

7.12 Geochemistry of sole rocks

7.12.1 Whole-rock analysis of amphibolites

Suites of amphibolites were collected from the metamorphic sole units of both the Denizgoren and Lesbos Ophiolites for whole-rock X-ray fluorescence analysis. Their geochemical compositions indicate basaltic or gabbroic precursors (Appendix 2) which were probably part of an oceanic crustal sequence which became the decollement zone along which the ophiolite was originally emplaced. Several of the amphibolites from both the Denizgören and Lesbos metamorphic soles are extremely depleted in immobile elements, especially Zr, P, Ti and Y. As a result of this they plot well outside the volcanic-arc basalt fields of tectonic discrimination diagrams (Figure 7.13) and display dish-shaped MORB-normalized patterns (Figures 7.14-7.16). This trough ranges from being very shallow and only dipping slightly below MORB (e.g Figure 7.15a), to a pronounced U-shape (e.g. Figure 7.15b). Patterns such as these are often characteristic of boninites (e.g Hickey & Frey, 1982). Boninites are high-MgO (>6%) andesites and andesitic basalts whose depleted trace-element geochemistry indiactes a refractory and depleted source. Based on evidence from the southern Troodos transform fault, Murton (1989) described the essential conditions for boninite genesis:

a) A mantle source that is extremely depleted in the incompatible trace-elements.
b) An extensional tectonic regime in which the source area can be melted.
c) A process whereby the the peridotite solidus can be sufficiently lowered to allow source melting.

The first two conditions may be met by the oceanward migration of a subduction zone and the resulting extension of the fore-arc region. In such a case oceanic crustal generation above the subduction zone will leave upper mantle material that has been depleted by the extraction of both MORB and SSZ oceanic crust. This material will

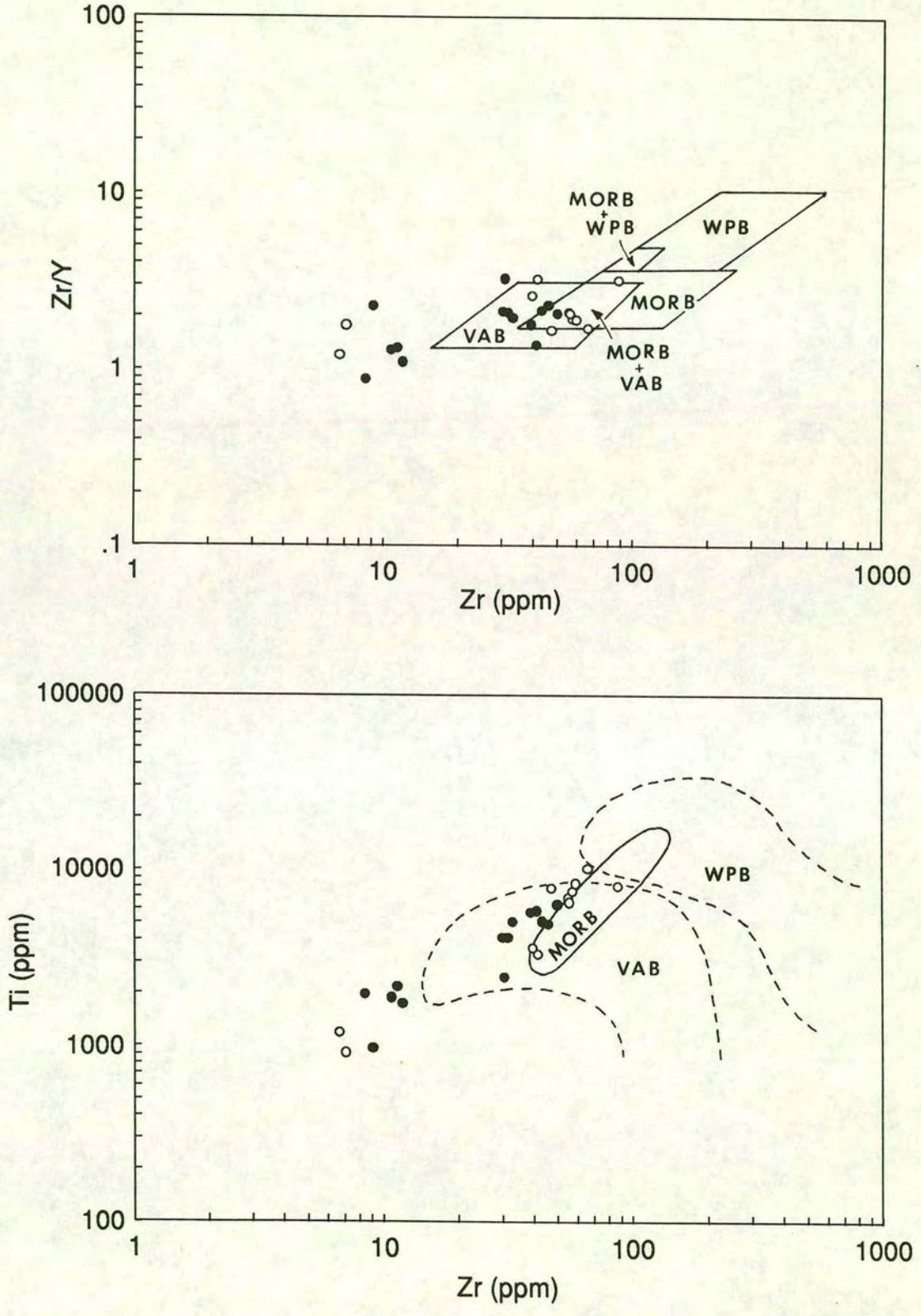

Figure 7.13 Amphibolites plotted on tectonic discrimination diagrams. (a) Zr/Y-Zr plot (fields from Pearce & Norry, 1979), (b) Ti-Zr plot (fields from Pearce, 1982). Samples are from the metamorphic soles of the Denizgören Ophiolite (solid circles) and the Lesbos Ophiolite (open circles).

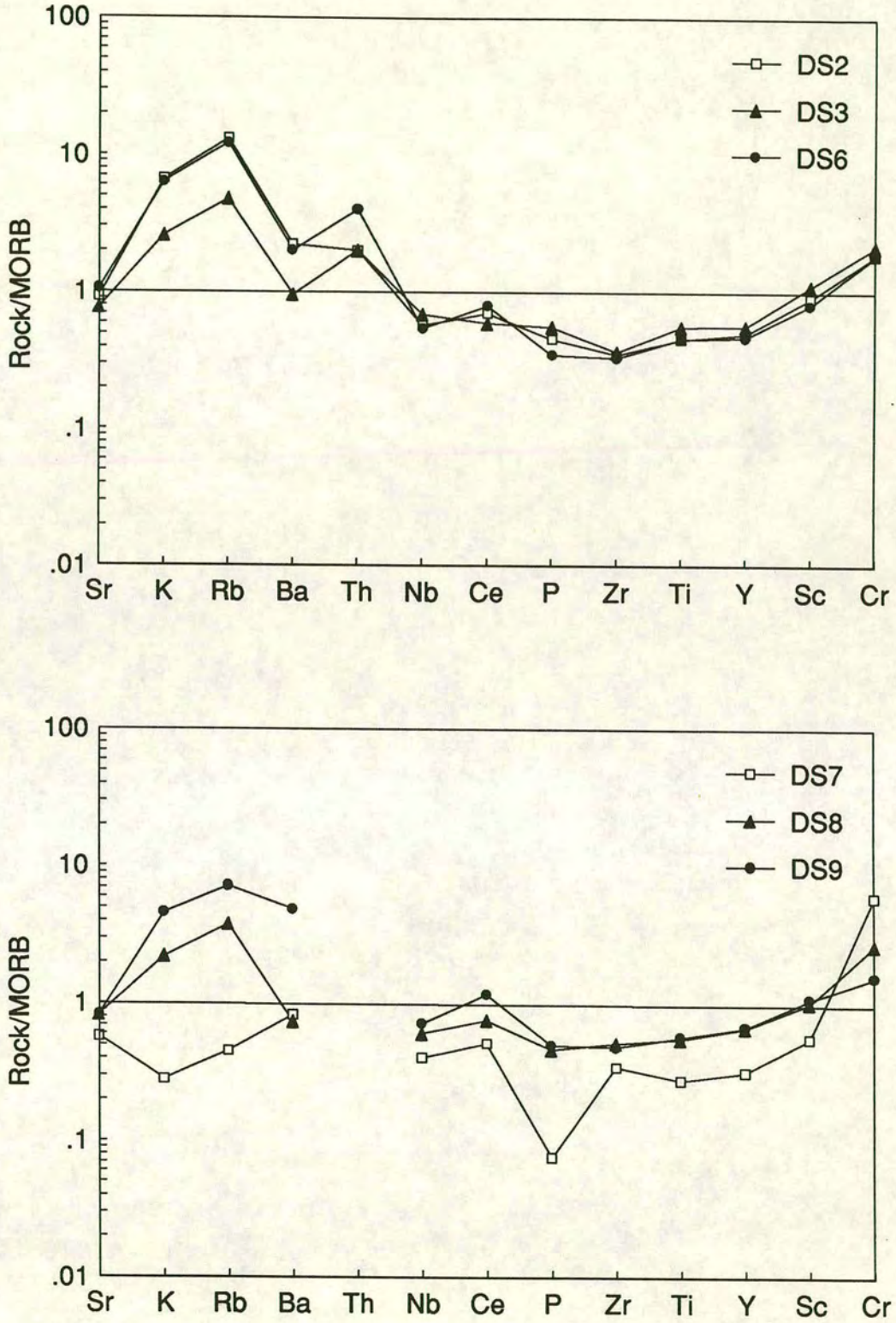

Figure 7.14 MORB-normalized multi-element plots for amphibolites from the metamorphic sole of the Denizgören Ophiolite. Normalizing values from Pearce (1982 & 1983) (Appendix **4**).

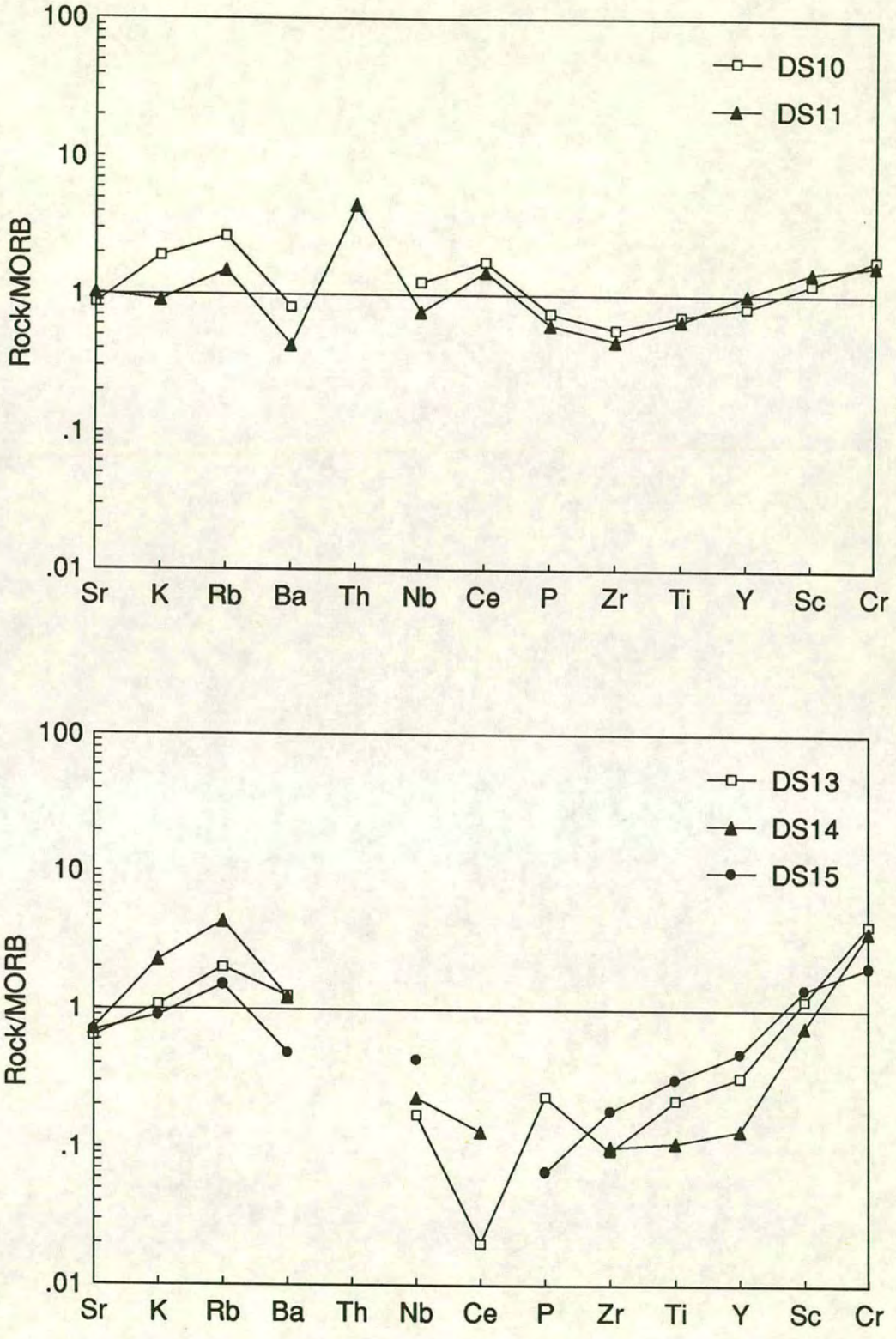

Figure 7.15 MORB-normalized multi-element plots for amphibolites from the metamorphic sole of the Denizgören Ophiolite. Normalized as for Figure 7.14.

thus have a very depleted composition which could, if melted, produce boninites. The final condition may be accomplished by the introduction of a hydrous fluid phase such as those which would be released from the subducting slab. The fact that all three conditions need to be met at the same time may explain the erratic spatial and temporal nature of boninite occurrences in the present-day oceans (e.g. the isolated exposures found on the Marianas inner trench wall and within the fore-arc region; Crawford *et al.*, 1983).

Thus, if the multi-element plots shown in Figures 7.14-7.16 reflect a boninitic precursor, this has important implications for the origin of the amphibolites and the mechanism of their incorporation into a metamorphic sole.

However, an important point which must be noted is that it is not easy to determine whether the protoliths of the amphibolites were basalts or gabbros. If the amphibolites originated from basalts then discrimination diagrams shown in Figure 7.13 may be used to provide information on their likely tectonic setting. However, if the protoliths were gabbroic then the picture is more complex and basalt discrimination diagrams are not appropriate. The range of MORB-normalized patterns, from highly depleted to MORB-type signatures, may merely indicate progressive evolution from a parental suite of cumulate gabbros by fractional crystallization. This scenario is favoured by the marked variation in MgO, Al_2O_3 and CaO, consistent with an originally variable modal mineralogy. This variation is not reflected by the trace elements, suggesting that the major and trace elements are essentially decoupled, a feature characteristic of gabbros. Thus, it is possible that the metamorphic sole may represent highly deformed slivers of cumulate gabbros from a straightforward MORB setting, rather than depleted forearc volcanics.

Geochemical data from the Denizgören and Lesbos amphibolites were plotted on variation diagrams in order to investigate the fractionation processes which may have produced the suite of rocks which comprise the lower parts of the metamorphic soles (Figures 7.17 and 7.18). MgO, rather than SiO_2, was used as abscissa owing to its wide variation as a result of the breakdown of magnesian phases during partial melting or their removal during fractional crystallization (e.g. Rollinson, 1993). The plots of MgO against TiO_2, Zr, Ce and Nb show distinct fractionation trends away from a cluster of amphibolites which may be candidates for a suite of parental gabbros. Plots of Y and Zr against Nb also show clear fractionation trends away from the same cluster of depleted samples (Figure 7.18).

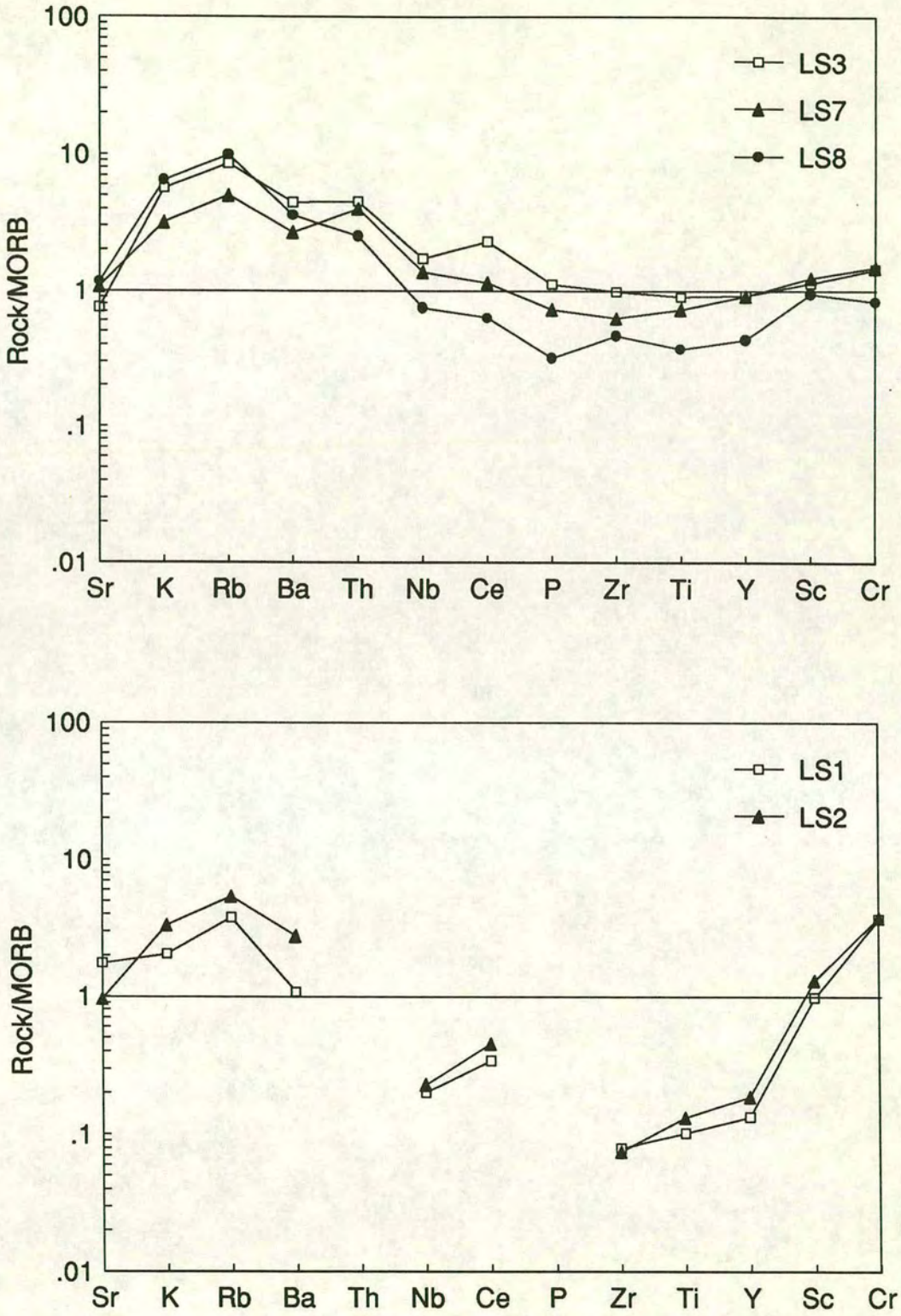

Figure 7.16 MORB-normalized multi-element plots for amphibolites from the metamorphic sole of the Lesbos Ophiolite. Normalized as for Figure 7.14.

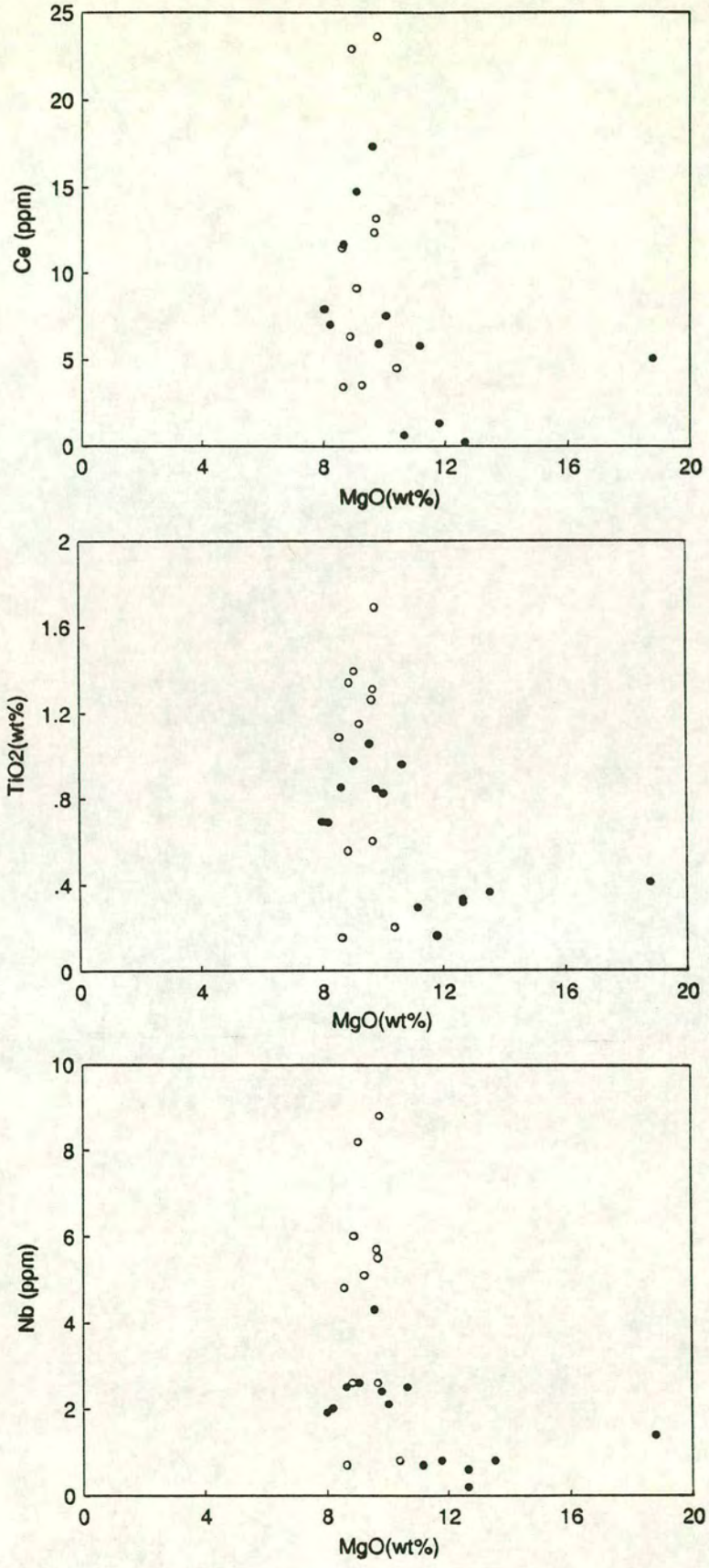

Figure 7.17 MgO variation diagrams for amphibolites from the metamorphic soles of the Denizgören (closed circles) and Lesbos (open circles) Ophiolites.

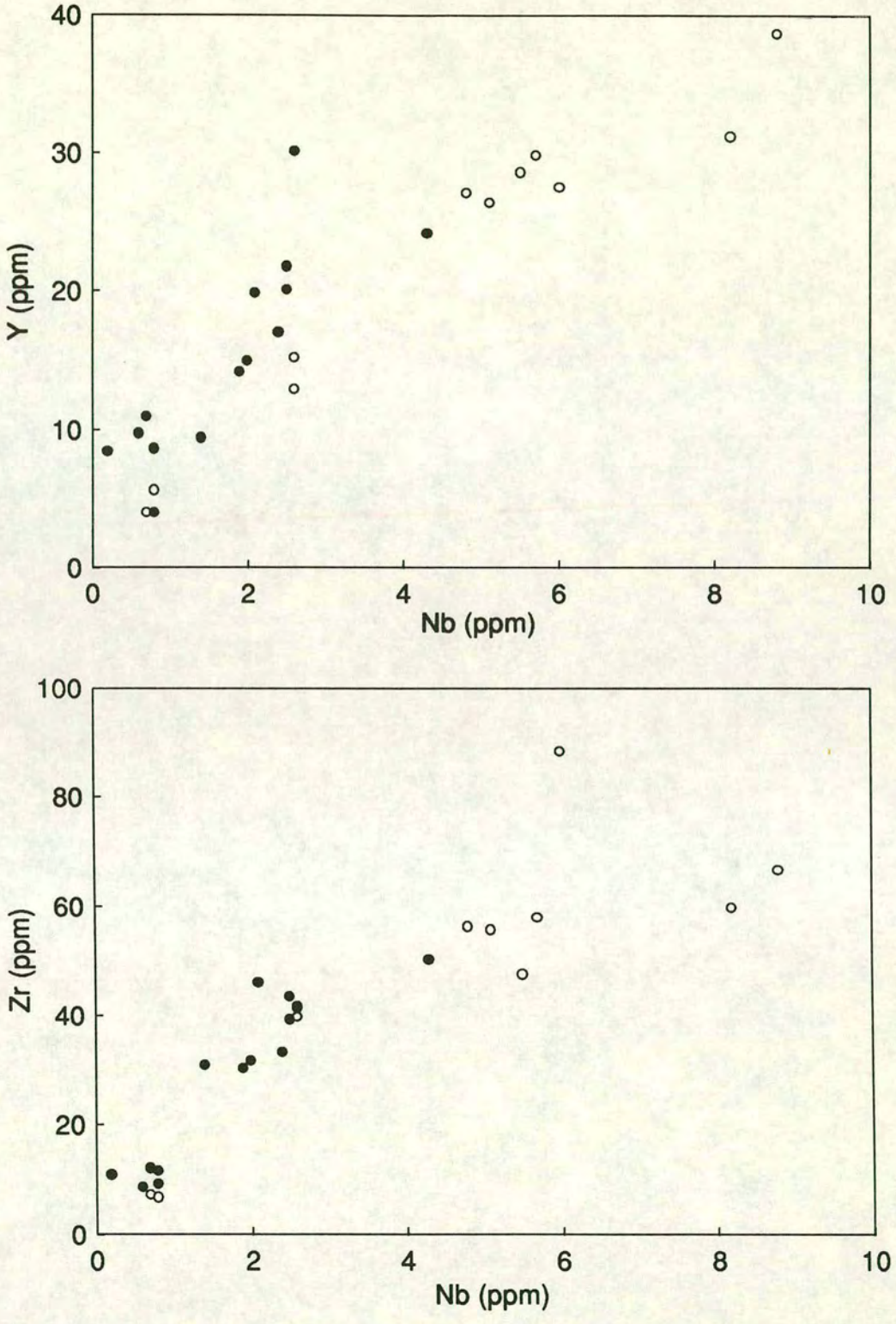

Figure 7.18 Y-Nb and Zr-Nb variation diagrams for amphibolites from the metamorphic soles of the Denizgören (closed circles) and Lesbos (open circles) Ophiolites.

7.12.2 Interpretation of amphibolite geochemistry

Interpretation of the amphibolite geochemistry depends to a large degree on the amphibolite protoliths (i.e. whether they represent basalts or cumulate gabbros). If they are considered as basaltic, then a SSZ signature may be invoked, thereby implying that they may have been generated in a similar tectonic setting to the peridotites. The highly depleted nature of some samples (e.g. Figures 7.15b and 7.16b), together with their high MgO content may be evidence for boninite generation in a fore-arc setting. The occurrence of SSZ components in a metamorphic sole is relatively rare and has only been observed in a few of the Eastern Mediterranean ophiolites (e.g. Euboea; Robertson, 1991 and Pindos; Jones & Robertson, 1991). Robertson (1991) explained the apparent subduction zone signature in some of the amphibolites below the Euboea ophiolite by suggesting that the leading edge of the supra-subduction slab collapsed and was overridden by hot peridotite. This scenario may also explain the presence of a supra-subduction signature in both the peridotite and amphibolite sole of the Denizgoren-Lesbos ophiolite.

However, if the amphibolites record fractionation of gabbros (and it is probably more likely that they do) it is difficult to assign any particular tectonic setting. The amphibolites may record a suite fractionated from a cumulate gabbro in a MORB setting, but nevertheless a subduction zone setting is still a possibility. If a non-subduction setting is invoked for the sole rocks then it is possible that the SSZ ophiolite sheet caught up slivers of "normal" MORB crust, rather than fore-arc volcanics,during its obduction.

7.13 Metamorphic soles associated with other ophiolites

Metamorphic rocks at the base of ophiolitic complexes, have been described from all over the world. In particular, Mesozoic ophiolites within the Tethyan realm have well preserved metamorphic soles (e.g. Woodcock & Robertson, 1977). The Semail ophiolite of Oman is perhaps the best example of a well-developed metamorphic sole beneath an ultrabasic thrust sheet (e.g. Searle & Malpas, 1980). Metamorphic sole rocks have also been identified in the Mesozoic complexes of Albania, Greece, Yugoslavia and southern Turkey, and below the Baer-Bassit ophiolite of Syria. Some of the best documented Eastern Mediterranean examples are in Greece where Mid Jurassic metamorphic soles have been recorded beneath the Pindos, Vourinos, Othris and Euboea ophiolites (reviewed by Spray *et al.*, 1984). The amphibolites beneath the

ophiolitic rocks of the Pindos Mountains in Greece provide a particularly good example of a metamorphic sole (Jones & Robertson, 1991). An example from the Mesozoic of Turkey is a fragmentary amphibolite and greenschist unit in the Antalya region, interpreted as the remnants of a metamorphic sole to the Kizil Dag ophiolite by Robertson *et al.* (1991). Neotethyan ophiolites, such as those described above, have reasonably well preserved and well documented metamorphic soles, whereas Palaeotethyan examples are relatively poorly known. The Elekdag ophiolite and its basal eclogitic melange in the central Pontides of Turkey may be one such Palaeotethyan example (Ustaömer, 1993). Sub-ophiolitic metamorphic rocks have also been described from Palaeozoic ophiolite complexes such as the Bay of Islands Complex in Newfoundland (e.g. Jamieson, 1980, 1981).

7.14 Summary of ophiolite and metamorphic sole geochemistry

In summary, peridotite and Cr-spinel analysis suggest that the Denizgoren and Lesbos ophiolites originated in a transitional MORB/SSZ setting. The amphibolites from the metamorphic soles may have originally been tholeitiic basalts formed during intra-oceanic thrusting and subsequent ophiolite obduction. Their geochemical characteristics may indicate MORB to IAT affinities and several samples are extremely depleted, suggesting a possible boninitic origin. Basaltic precursors may have been derived from relatively primitive magmas, generally depleted with respect to MORB. Alternatively, the amphibolites may record the fractionation of cumulate gabbros and, in this case, a supra-subduction zone setting is not required to explain their depleted characteristics. The lack of distinct Nb depletions favours this hypothesis. These two alternatives have different implications for metamorphic sole generation and ophiolite obduction. Established models of metamorphic sole formation are outlined below and followed by a discussion of their application to the Denizgören and Lesbos Ophiolites.

7.15 Models of metamorphic sole formation

Many mechanisms have been proposed for metamorphic sole generation, the key requirement for which is the juxtaposition of hot crust against older, cooler crust. It is probable that ophiolitic sole rocks can form in a range of tectonic settings and the various alternatives were summarized by Robertson & Dixon (1984) and Jones (1990). Four alternative models for metamorphic sole formation are discussed briefly below. The first model invokes low-angle thrusting of oceanic crust near a subduction

zone (Nicolas & Le Pichon, 1980; Whitechurch *et al.*, 1984). The second model suggests that decoupling occurred along the lithosphere/asthenosphere bounday at a spreading ridge (Nicolas & Le Pichon, 1980; Spray, 1984) and has been postulated for the formation of the Semail ophiolite sole (e.g. Boudier *et al.*, 1982). The third model was proposed by Lippard *et al.* (1986) for the metamorphic sole of the Semail ophiolite, and involves thrusting along the boundary between old and new oceanic lithosphere in supra-subduction crust. However, as pointed out by Jones (1990), the fore-arc crust envisaged in this model is not found preserved in Oman and amphibolites analyzed by Searle & Malpas (1982) do not show a supra-subduction zone signature. Nevertheless, this model remains a viable mechanism for metamorphic sole generation. In the fourth model Casey & Dewey (1984) proposed that metamorphic soles may have formed during initiation of subduction. In this model, the sole becomes accreted to the base of the overriding plate and is preserved in this position during emplacement.

It is likely that many metamorphic soles have undergone multi-stage histories and may record events from more than one of the models outlined above. A well documented example is the Loumnitsa Unit, the metamorphic sole of the Pindos ophiolite, which undewent two stages of metamorphic sole formation within the Neotethyan Pindos ocean (Jones, 1990; Jones & Robertson, 1991). One possibility which they explored is the accretion of the sole onto the overriding plate during the initiation of subduction (i.e. model 4) followed by thrusting along the boundary between older fore-arc and supra-subduction zone crust and mantle, above an established SW-dipping subduction zone (i.e. model 1).

7.16 Application of models to the Denizgören-Lesbos metamorphic sole

If the depleted signatures of the Denizgoren and Lesbos metamorphic soles are taken to reflect forearc volcanism then the soles were probably accreted during deep-seated displacement of crust and mantle in a fore-arc setting (i.e. models 1 or 3; Section 7.15). This would account for the presence of amphibolites with very depleted, boninitic-type geochemistries within the sole. The fact that MORB/IAT volcanics are also present in the sole may indicate that older, back-arc crust was also involved in its generation (see model 3). As yet, there is insufficient structural data from the Denizgören/Lesbos metamorphic soles to allow the resolution of distinct tectonic events, although the incorporation of both highly depleted (?boninitic) and MORB/IAT volcanics into the metamorphic sole may imply accretion from at least

two sources. A more likely possibility is that the amphibolites simply record different positions on a fractionation trend from a parental suite of cumulate gabbros, rather than reflecting subduction components. In this case, the metamorphic sole could have been derived from the oceanic crust of the descending (i.e. "MORB") slab which became accreted to the base of the ophiolite during obduction.

The sheared volcanic and sedimentary sequence in the greenschist part of the sole may be equivalent to the melanges described from the soles of many Mesozoic Tethyan ophiolites. Such melanges are commonly tectonically "sandwiched" between the underlying passive margin and the overriding ophiolite (e.g. the Pagondas Complex below the Euboea ophiolite; Robertson, 1991). Limestone blocks observed in the Denizgören and Lesbos sole rocks may reflect accretion of seamount material or detritus from the approaching platform.

7.17 The Karadag Unit

The Karadag Unit is a predominantly carbonate sequence which crops out near the western shore of the Biga Peninsula, adjacent to the Denizgören Ophiolite. Okay *et al.* (1991) named the unit after the village of Karadag north of Ezine. The Karadag Unit comprises a carbonate platform sequence built up on a clastic basement and thus is probably part of the Cal Unit, as defined in Chapter 4. The Karadag Unit tectonically underlies the Denizgören Ophiolite and its associated metamorphic sole. It has been described in most detail by Okay *et al.* (1991) who mapped its various components (Figure 7.2).

7.17.1 Lithologies

According to Okay *et al.* (1991) the Karadag Unit can be broadly divided into five main intervals which are, from base to top:

a) Metaclastic and metacarbonate rocks
b) Massive/thick-bedded dark unfossiliferous limestone
c) Thin/medium-bedded grey/beige recrystallized limestone with fusulinids
d) Massive/thick-bedded white limestone
e) Greenschist facies metaclastic/metavolcanic rocks

The general lithologies of these components are briefly discussed below, based on the descriptions of Okay *et al.* (1991) and my observations in the field. My own fieldwork concentrated mainly on the middle part of the carbonate sequence (as exposed in a quarry south of Tastepe) and on the uppermost limestone horizons near their contact with the greenschists. I regard the greenschist facies rocks at the top of the sequence as part of the metamorphic sole unit of the Denizgören Ophiolite.

a) Metaclastic and metacarbonate rocks

This interval crops out east of the village of Geyikli and comprises grey, brown and green shales, pink sandstone with quartz pebbles, white metaquartzite and calcschist. Limestone and shale intercalations at the top of this unit mark the transition into the overlying carbonate sequence. This metaclastic unit was not studied as part of this thesis.

b) Massive/thick-bedded dark unfossiliferous limestone

Massive to thick-bedded limestone up to 650m thick conformably overlies the metaclastics. The limestone is dark grey and unfossiliferous.

c) Thin/medium-bedded grey/beige recrystallized limestone with fusulinids

The unfossiliferous limestone passes up into a 600m-thick succession of thin- to medium-bedded recrystallized limestone which ranges from dark grey to beige in colour. This unit is well exposed in the large quarry south of Tastepe near the Küçük Menderes River where fusulinid-rich bands up to 6cm thick are a common feature (Figure 7.19a). Colour changes define the banding which gives a streaky appearance to the limestone in the field. Parts of the limestone are grey and micritic, but grey to creamy beige recrystallized limestone is the most common lithology.

Fusulinid-rich limestone from the quarry near Tastepe was studied in thin-section. The fusulinids are composed of sparry calcite with faintly preserved internal structures. They are set in a matrix of beige micrite. The matrix contains many sparry fragments which are aligned parallel to bedding. Rounded remnants of algae and bryozoa were also recognized. Samples have yielded *Mizzia velebitana* Schubert, *Glomospira* sp., *Neoschwagerina* cf. *craticulifera* Schwager and *Hemigordius* sp., (Kalafatçioglu, 1963); *Neoschwagerina* sp. and *Stafella* sp. (Okay *et al.*, 1991). All these are indicative of the Upper Permian.

Figure 7.19

(a) Photomicrograph of recrystallized and compressed fusulinids from the Karadağ Unit at Taştepe (PPL, field of view: 22mm).

(b) Metalliferous partings within the Karadağ Unit (interpreted as a hardground) near its contact with the tectonically overlying metamorphic sole at Figli Dağ.

(c) Photomicrograph of the limestone shown in (b) showing stylolitic seams of opaque metalliferous material (PPL, field of view: 12.5mm).

a

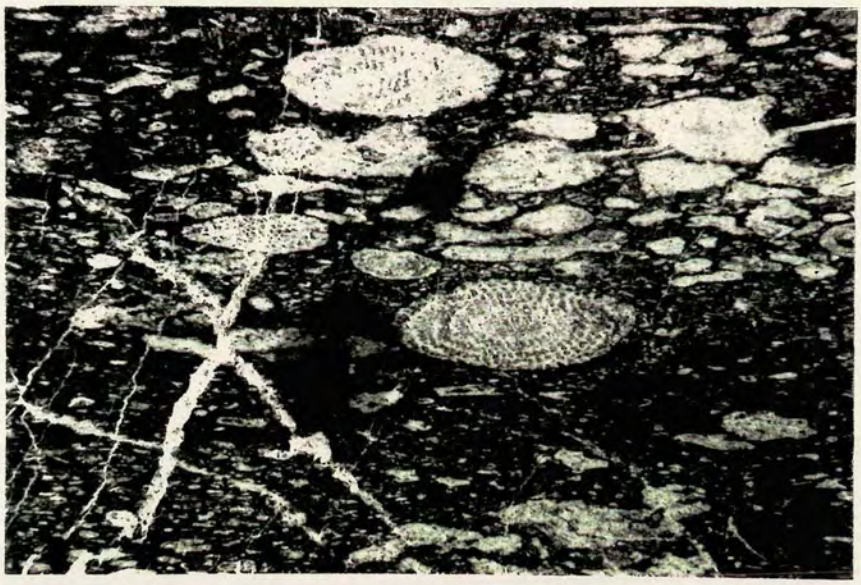

b

c

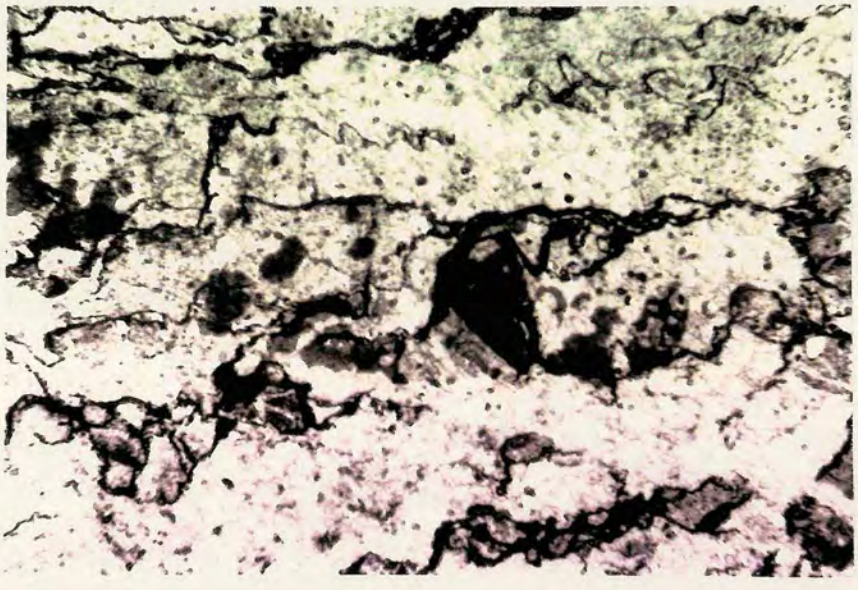

d) Massive/thick-bedded white limestone

The fusulinid-bearing limestones are overlain by 350m of massive to thick-bedded white limestone which contains the alga *Mizzia* sp. in its upper levels.

e) Greenschist facies metaclastic/metavolcanic rocks

Overlying the carbonate succession described above is a sequence of sheared and foliated green metaclastics and/or metavolcanics. This sequence varies in thickness and attains 350m in its thickest part. The sequence comprises foliated green shale, sheared beige sandstone beds, calcturbidites and siliceous limestone. Okay *et al.* (1991) also reported the presence of limestone and basic volcanic olistoliths, although these were not observed during my own fieldwork. Although this interval forms the top of the Karadag Unit it also constitutes part of the metamorphic sole unit to the Denizgören Ophiolite and is discussed more fully as such in Section 7.10.

7.17.2 Top of the Karadag carbonate platform

a) Locality near Izmir-Çanakkale highway

The uppermost limestone of the Karadag Unit is very recrystallized and highly sheared in places. The contact with the overlying greenschists, here interpreted as part of the metamorphic sole to the ophiolite, is very sharp and can be located to within 2m. The limestone near the contact has a grey and white streaky texture. Streaky pink colouring and swirly black manganiferous partings are common near the contact (Figure 7.19b). In thin-section recrystallized limestone is intercalated with streaky black material which is opaque in thin section and is probably a manganiferous oxide. Stylolitic seams which contain the opaque mineral and biotite altering to chlorite drape around calcite grains (Figure 7.19c).

Cherty bands 0.5-1cm wide are also a common feature. Approximately 10m below the top of the carbonate sequence lies a red ferruginous crust interpreted as a hardground. Limestone immediately above the crust is thinner bedded and more cherty than that below. The pink cherty limestone above the crust is overlain by a shale intercalation. Just below the hardground lies an intraformational breccia of angular limestone clasts set in red micrite (Figure 7.20a). The breccia is laterally discontinuous and grades into fractured limestone with red fracture-infills. Below the breccia is a sequence of intercalated green shales (similar to those in the overlying greenschists of the metamorphic sole), cherty beds and limestone with cherty partings. All these facies are sheared and foliated.

a

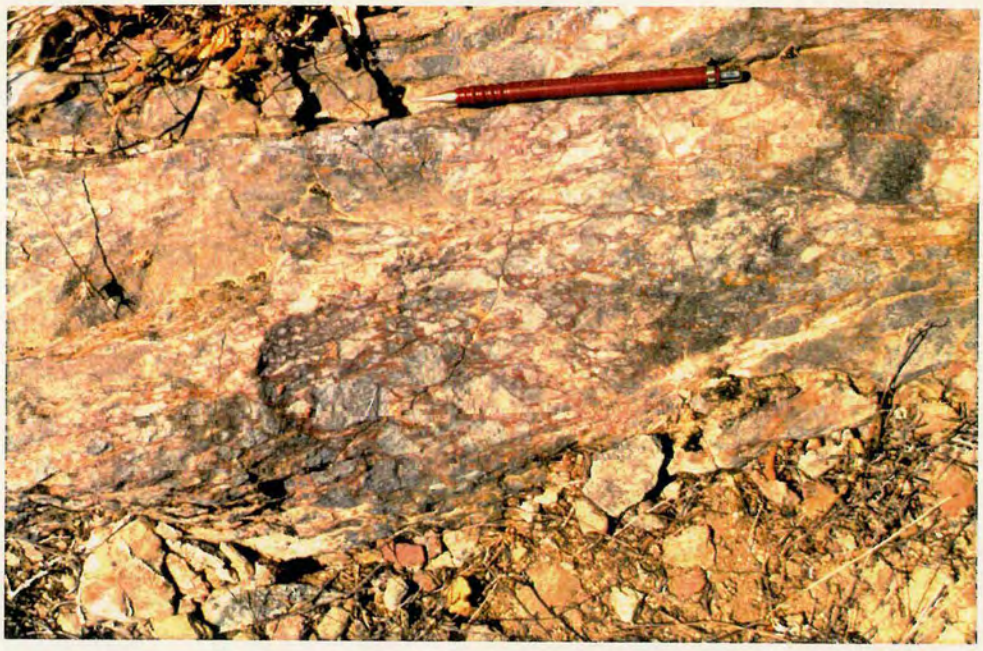

b

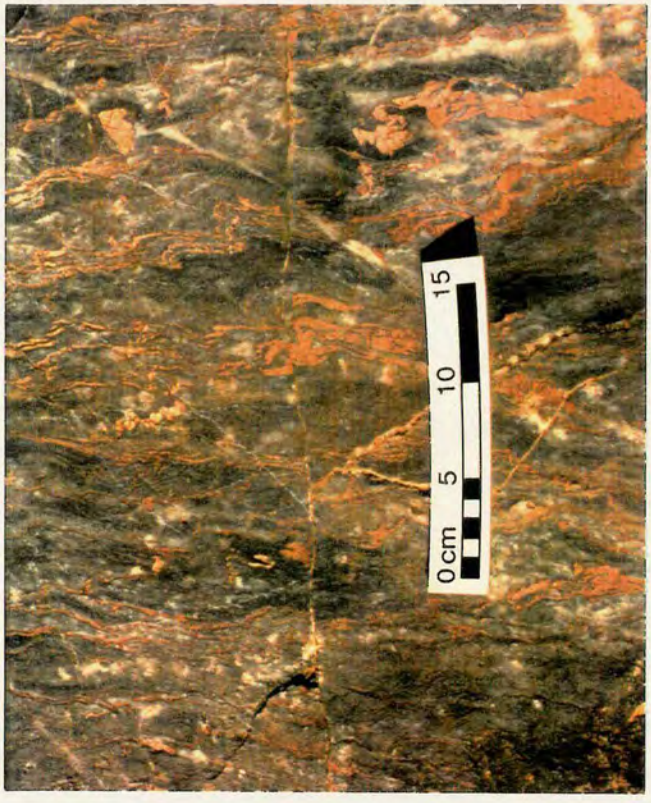

Figure 7.20

(a) Brecciated limestone with hematitic seams a few metres from the contact of the Karadag Unit with the metamorphic sole at Figli Dağ.

(b) Sheared limestone near Karadağ. Pink bands pick out small asymmetrical folds which verge towards the W/NW (i.e left of picture).

The brecciated limestone near the top of the platform is completely recrystallized into sparry calcite with a sugary texture in hand specimen. The limestone contains many small, highly angular quartz grains which display sharp extinction and abundant inclusions. A few grains display very undulose extinction and sub-grain development. Some quartz grains show replacement by calcite. Rare feldspar fragments are also present, one displaying a perthitic texture. The sparry calcite also contains disseminated red-brown hematite which also locally act as a matrix to angular pieces of sparry calcite and rare clasts of quartzitic sandstone. The sandstone clasts comprise recrystallized quartz, perthite and white mica. In places this ferruginous "matrix" is being replaced by sparry calcite and also contains quartz grains and a few wisps of white mica. The opaques are amorphous and have a slightly laminated texture in places.

b) 0.5km from Çamköy on road to Karadag

The top of the platform is also exposed along the minor road to Camköy and Karadag. The limestone is sheared and streaky and contains asymmetrically folded thin pink bands (Figure 7.20b). Their sense of asymmetry is approximately towards the W/NW. Foliated greenschists overlie the limestone and are themselves overlain by massive crystalline amphibolites.

7.17.3 Interpretation of Karadag Unit

The Karadag Unit is interpreted as an *in situ*, relatively intact limestone platform which was constructed on a clastic basement of sandstone and shale. The Karadag Unit is thus very similar to the platform units of the Çal Unit and is probably part of the same platform(s). A transitional boundary between the basement and the limestone indicates a gradual change from predominantly terrigenous input to a shallow-marine environment suitable for extensive and prolonged carbonate deposition. The lowest limestone is dark grey and unfossiliferous. This may indicate a high organic and/or mud content. Up sequence, the limestone becomes paler and more fossiliferous, possibly reflecting progressively shallower conditions as the platform built up. Fusulinid-rich layers are common in the middle levels of the sequence, implying open marine conditions and reworking. Reworking is also indicated by the presence of well rounded fragments of algae and bryozoa. The top of the Karadag Unit records a rapid deepening event interpreted as being caused by the approach of the obducted Denizgören Ophiolite and its metamorphic sole. Material shed off the ophiolite onto the platform was subsequently incorporated into the upper

parts of the metamorphic sole, together with limestone blocks from the platform and cherty limestone which was deposited in the deeper conditions. Only the uppermost levels of the platform are affected by the ophiolite obduction, testifying to the rapid nature of the event. The limestone is brecciated, sheared and contains evidence of hardground formation.

7.18 The Permian platform of Lesbos

The Permian of the island of Lesbos is part of a continuous Permian to Upper Triassic sequence which distinguishes it from the Permian successions of NW Turkey. The Permian sequence forms the autochthon of Lesbos and comprises intercalated metaclastic rocks and recrystallized limestone. The base of the sequence is predominantly clastic, comprising sandstones and schists with intercalations of limestone rich in Upper Carboniferous and Permian fossils (Migiros & Pavlopoulos, 1992). Permian carbonates are best exposed near the towns of Gavathas, Eressos, Agiassos and Papados.

7.18.1 Lithologies

a) Gavathas

Permian carbonates form large white outcrops on the hills and overlie metasandstones and schists. A disused quarry near Gavathas provides the best exposure. The limestone is light grey and very recrystallized with a streaky marble-like appearance in places. Cracks within the limestone are filled with red bauxite which also contains clasts of limestone. The limestone-bauxite contact appears to be normal although it is faulted in many places. On the beach near Gavathas redeposited, laminated limestone contains flattened intraclasts up to many cm long containing crinoid ossicles. Migiros & Pavlopoulos (1992) described foraminifera, algae, sea urchins, bivalves, gastropods and brachiopods from this locality. The foraminifera include *Pachyphloia ovata* Lange, *Globivalvulina graeca* Reichel, *Climacammina major* Morozova, *Climacammina spaerica* Potievskaya, *Globivalvulina aff. vonderschmitti* Reichel, *Geinitsina* sp., *Colaniella* sp., *Dunbarula* sp., *Neoschwagerina* sp. and *Stafella* sp. The upper levels of the limestone at this locality contain corals, dasyclad algae and sea urchins (Migiros & Pavlopoulos, 1992).

b) Eressos

Near Eressos in NW Lesbos medium-bedded Permian limestone is interbedded with shale. The limestone is dark grey and veined and has a fissile, shaly texture indicating a high mud content. The limestone contains abundant fusulinids and ooids. A fauna of Ammodiscidae, Miliolidae, *Permocalculus* and *Colaniella* was described by Migiros & Pavlopoulos (1992). A conglomerate containing clasts of silicic green volcanics, grey quartzite, pink limestone, grey limestone and ooidal limestone in a matrix of grey-green shale is exposed nearby, although the contact was not observed.

c) Agiassos

Near Agiassos the Permian limestone is intercalated with dolomitic limestone and contains a rich Permian fauna of the alga *Mizzia velebetana*, *Permocalculus* sp., ostracods, bivalves and gastropods (Migiros & Pavlopoulos, 1992).

d) Papados

The exposures of Permian limestone near Papados are similar to those near Eressos. The limestone is dark, veined and fossiliferous and contains foraminifera, algae and brachiopods (Katsikatsos et al., 1982; Migiros & Pavlopoulos, 1992).

7.18.2 Interpretation of the Lesbos platform

The Permian limestone succession on the island of Lesbos represents an intact carbonate platform formed on a clastic basement. Typical shallow-water indicators such as ooids, corals, dasyclad algae, ostracods fusulinids and miliolids are present throughout the sequence. Dasyclad algae tend to occur in shallow, protected lagoonal areas of the present-day tropics (Tucker, 1981) and are well known in shallow, inner platform settings throughout the Permian Tethys. Fusulinids, ostracods and miliolids are also typical of relatively sheltered inner platform environments. The presence of ooids in the sequence near Eressos may indicate a shallow environment with a higher energy regime, perhaps at the shelf edge. The Permian succession on Lesbos passes directly up into Triassic schists, clastics and carbonates which are overthrust by the ophiolitic nappe. The Permian part of the sequence is probably analogous to the Karadag Unit on the Turkish mainland. Both sequences represent intact Permian platforms and tectonically underlie ophiolitic slabs.

7.19 Emplacement of the Denizgören and Lesbos Ophiolites

Ophiolite emplacement directions play a critical role in the interpretation of the tectonic evolution of a region and, when combined with other regional geological data, also provide valuable insights into the mode of origin and original tectonic setting of the ophiolites. Structural data were collected from the two ophiolites with this aim in mind. By attempting to determine the emplacement direction(s) and interpreting geochemical data, it was hoped that a coherent picture of the nature and origin of this dismembered ophiolite would emerge. The ultrabasic rocks of the Denizgören-Lesbos ophiolite are largely structureless, apart from a dense network of joints. As a result structural investigations focused on the metamorphic soles and the upper levels of the underlying deformed sedimentary sequences.

7.19.1 Emplacement of the Denizgören Ophiolite

Very few structures were found in the Denizgören metamorphic sole other than the ubiquitous pervasive foliation. However, E-dipping greenschists outside the village of Karadag contain small duplexes which give a sense of motion towards the west. Limestone at the top of the Karadag Unit is highly recrystallized and contains streaky pink and grey bands. Small-scale folds are well picked out by these coloured layers as shown in Figure 7.20b. Although the folds could not be accurately measured owing to the polished surface of the outcrop, their vergence is clearly approximately NW, similar to the direction indicated by the duplexes near Karadag. The overall foliation of the metamorphic sole dips towards the SE. The ultrabasic rocks themselves display a crude SE-dipping fabric on a scale of many metres. The steep NW-dipping foliation present near the contact between the sole and the Karadag Unit is a result of localized overturning in the contact region. In summary, therefore, it appears that the Denizgören Ophiolite may have been emplaced onto the Karadag platform from the SE to the NW. However, the scarcity of shear sense criteria makes this very tentative and more detailed structural studies need to be carried out before any definite statements regarding emplacement directions can be made.

7.19.2 Emplacement of the Lesbos Ophiolite

In Lesbos the ophiolite lies as a shallowly dipping slab on the metasediments and marbles of the underlying "Neopalaeozoic formations". Unlike the Denizgören Ophiolite it generally dips gently northwest. The opposing dips of the two ophiolitic

bodies may imply that they both formed part of the same relatively flat-lying ultrabasic sheet which has subsequently been tilted to different angles depending on the localized tectonic regimes of the two areas. Sense of shear criteria within the metamorphic soles of the two ophiolites are likely to be much more indicative of the original direction of emplacement. The Lesbos Ophiolite appears to have undergone both NW and SE directed events and it is tentatively suggested that the NW-directed motion came first.

7.19.3 Discussion of emplacement direction

It therefore appears that both the Denizgören and Lesbos ophiolites underwent a northwestward-directed event. Unlike the Denizgören Ophiolite, the Lesbos Ophiolite also shows clear evidence of an eastward-directed, probably later, thrusting event which is reflected by the overall NW-dipping nature of the Lesbos thrust sheet. It is therefore possible that the original emplacement direction was towards the W or NW; a direction which is consistent with the structural trend of the Karakaya Complex in the Biga Peninsula and surrounding regions. A subsequent event caused the Lesbos Ophiolite to be thrust back towards the SE. Whether the Denizgören Ophiolite was also affected by this is not clear from field evidence. The eastern tectonic contact of the Denizgören Ophiolite (the Ovacik Thrust of Okay *et al.*, 1991) dips NW along its northern portion and may be equivalent to the NW-dipping thrust which forms the eastern boundary of the Lesbos Ophiolite.

7.20 Possible correlation with the Kazdag Massif and the Central Pontides

7.20.1 The Kazdag Massif

Mantle peridotites and associated amphibolites are also present within the Kazdag Massif, approximately 50km to the SE (Figure 7.1). The core of the massif is composed of highly deformed amphibolites, harzburgites, dunites, metagabbros and plagiogranites. This assemblage has previously been described as a meta-ophiolite sequence by Okay *et al.* (1991). Structural relationships in the core of the massif are very difficult to determine, owing to the fact that many of the lithologies are not *in situ*. Amphibolites collected from the core of the massif display similar geochemistries to those from the sole of the Denizgören Ophiolite (see Chapter 6 for a discussion of the Kazdag metamorphic rocks). A very tentative inference may be that the Denizgören-Lesbos and Kazdag "ophiolites" are related and may represent part of

the same oceanic fragment. However, far more work on these two ultrabasic bodies, especially the lithologies and structural relations of the Kazdag Massif, is required before any detailed models can be put forward.

7.20.2 The Elekdag Ophiolite (Central Pontides)

The Elekdag Ophiolite, of probable Late Palaeozoic-Early Mesozoic age, in the Central Pontides of Turkey is interpreted by Ustaömer (1993) as supra-subduction Palaeotethyan ocean crust and could be a possible eastern equivalent of the Denizgören-Lesbos ophiolite. Analysis of chromian spinels by Usatömer (1993) has revealed a clear subduction zone signature (IAT to boninitic) for the Elekdag Ophiolite. Similar studies carried out on the Denizgören Ophiolite show a less pronounced subduction zone signature, although peridotite geochemistry and the predominance of harzburgite does indicate a SSZ origin. The eclogitic blocks in the melange at the base of the Elekdag Ophiolite display distinct MORB characteristics (Ustaömer, 1993). The Denizgören and Lesbos metamorphic sole rocks do display MORB geochemistry, although the depleted rocks are more problematic in that their apparent boninitic signatures may actually reflect fractionation of gabbros rather than subduction components.

7.21 Interpretation

On the basis of geochemical studies the Denizgören Ophiolite is interpreted as a supra-subduction zone ophiolite which formed above a subduction zone in a similar manner to the Semail Ophiolite of Oman or the Troodos Ophiolite of Cyprus. The harzburgites represent the lower parts of an oceanic mantle sequence, the upper levels of which have been eroded or tectonically removed. The metamorphic sole of amphibolites probably represents the metamorphosed part of an upper crustal sequence of basaltic or gabbroic rocks, which became the decollement zone along which the ophiolite was emplaced. The geochemistry of these amphibolites indicates either the involvement of MORB/IAB basalts and highly depleted IAB/boninitic basalts or the fractionation of cumulate gabbros. In either case, an oceanic crustal sequence (derived from a forearc setting or from the subducting slab) was overridden by a SSZ peridotite slab. In this model east to southeastwards intra-oceanic subduction was accompanied by eruption of supra-subduction zone basalts, including boninites. The Denizgoren-Lesbos ophiolite probably formed in a marginal basin or fore-arc setting behind this subduction zone. As subduction continued, MORB-type

basalts, lava-derived clastics and deep-sea sediments were incorporated into an accretionary melange, now represented by the sheared sedimentary and volcanic greenschist units. Accretionary complexes have been observed below other ophiolites, including the Euboea (Robertson, 1991) and Semail (e.g. Robertson & Searle, 1990) ophiolites. As the passive margin approached the subduction zone, the ophiolite was detached and thrust northwestwards over the accretionary complex, generating the amphibolite sole. The occurrence of boninitic components within the sole implies that detachment probably occurred within the fore-arc region and the ophiolite overthrust fore-arc extrusives as well as accretionary material. The accretionary melange and the overriding metamorphic sole and ophiolite were then emplaced onto the Karadag carbonate platform. The resulting subsidence of the platform led to hardground formation and ferruginous oxide precipitation.

CHAPTER 8

CHIOS AND THE KARABURUN PENINSULA: RIFT AND PASSIVE MARGIN SEQUENCES

8.1 Introduction

The Greek island of Chios which lies off the Aegean coast of Turkey and the Karaburun Peninsula on the Turkish mainland, both lie at the eastern end of the Izmir-Ankara-Erzincan Suture Zone. This broad Neotethyan zone of ophiolites and ophiolitic mélanges trends across northern Turkey (Figure 1.5) and, in the west, lies directly south of the Karakaya Complex of the Bergama region.

The sequences in both areas are characterized by thick Triassic carbonate platforms which overlie mélange (Chios) and Carboniferous limestone (Karaburun). The tectonic affinities of the two areas are uncertain and various interpretations have been proposed for their origin. Their position to the south of the Karakaya Complex makes them critical to the wider tectonic interpretation of NW Turkey.

The description of the Chios succession is based on observations made during a Geological Society of Greece field excursion and during my own fieldwork on the island. The geology of northern Chios basically comprises an "autochthonous" unit and an "allochthonous" unit (e.g. Besenecker *et al.,* 1968, 1971, Papanikolaou & Sideris, 1992 and references therein). The "autochthonous" unit is best described as "relatively autochthonous" as it comprises a mélange, containing blocks of lava, chert and Silurian, Devonian and Carboniferous limestone in a clastic matrix. The mélange is unconformably and/or gradationally overlain by a Triassic platform. The allochthonous unit occurs as a nappe in the NE of the island and comprises a Permian sequence unconformably overlain by Liassic sediments.

On the Karaburun Peninsula, Lower-Middle Carboniferous limestone of the Alandere formation is unconformably overlain by the Lower Triassic Denizgiren Group which comprises chert, clastics, mafic volcanics and pelagic limestones. The Upper Carboniferous and Permian are absent. The description of the Karaburun sequence given in this chapter is based on my own reconnaissance fieldwork and an excursion with Dr. B. Erdogan from the Dokuz Eylül University, Izmir.

The position of the Karaburun and Chios sequences, directly south of the Karakaya Complex, make them critical elements in the complex tectonic mosaic that characterizes NW Turkey. Chios, in particular, is critical to tectonic reconstructions, owing to the thick mélange which forms the lower part of the Chios autochthon. Whether this is part of the Karakaya Complex or is, in fact, from a completely different setting is a question which has not yet been satisfactorily answered.

In this chapter I describe the sequences observed on the Karaburun Peninsula and Chios, before interpreting them in terms of their relationship with the Karakaya Complex and their possible role in the pre-Jurassic tectonic evolution of NW Turkey as a whole. More detailed geochemical and sedimentological work needs to be done before this can be fully understood, although the studies carried out as part of this thesis have revealed many interesting features which may pave the way for further work.

8.2 Previous work

The geology of Chios has been studied by many workers, as reviewed by Papanikolaou & Sideris in Papanikolaou *et al.* (1992). The island has also been mapped in detail by I.G.M.E. (maps by Besenecker *et al.*, 1971). The general geology of Chios, especially in the northern part of the island, is described by Papanikolaou & Sideris in Papanikolaou *et al.* (1992) and references to more specific studies are given therein.

Phillipson (1911) prepared the first map of the Karaburun Peninsula and paved the way for several subsequent studies. Erdogan (1990) made a comprehensive review of the previous work and the reader is referred to his paper and the references therein. Erdogan (1990) also made detailed sedimentological and palaeontological descriptions of the entire Karaburun succession, together with a brief tectonic interpretation of the Karaburun Peninsula.

The tectonic setting of the autochthon of Chios and the Karaburun Peninsula has been the subject of recent debate. Baud *et al.* (1991) interpreted the relatively autochthonous sequence of Chios as an accretionary complex and, in their recent synthesis of Tethyan margins, Stampfli *et al.* (1991) described the autochthon of Chios as the imbricated outer slope of a Palaeotethyan accretionary complex. This hypothesis contrasts with that of Erdogan (1990 & pers. comm., 1992) who

interpreted the Karaburun peninsula and, by analogy, Chios, as passive margin sequences deformed during formation of the Cretaceous-Tertiary Izmir-Ankara-Erzincan suture zone (IAESZ). He postulated that the Karaburun and Chios sequences were incorporated into the Bornova flysch of the IAESZ as huge coherent blocks many tens of kilometres in size.

8.3 Chios

The Greek island of Chios is basically made up of a "relatively autochthonous" unit and an overthrust allochthonous unit (Figures 8.1 and 8.2). The autochthonous sequence comprises a thick mélange unit overlain by Triassic clastics and a carbonate platform. The allochthonous unit occurs as a nappe in the NE part of the island and consists of a Permian carbonate platform overlain by Lower Jurassic clastics and limestones.

8.3.1 Mélange of the Chios autochthon

Beneath the Triassic carbonate platform, the autochthonous unit of Chios is composed of a deformed sequence of sandstone and shale, 3-4km thick. The sequence is referred to here as a mélange, owing to the abundant blocks of limestone, conglomerate, volcanics and chert which occur in distinct horizons within a predominantly clastic matrix (Figure 8.2). The term "mélange" is thus used here as a purely descriptive, non-genetic field term for a pervasively mixed unit, irrespective of whether mixing was caused by sedimentary or tectonic processes. The limestone blocks range in age from Silurian to Carboniferous (Papanikolaou & Sideris, 1983). The limestone and volcanic blocks range in size from small clasts up to 1km in size (e.g. near Kampia; Figure 8.3). According to Papanikolaou & Sideris (1983) the blocks are concentrated in four "olistostrome" horizons which they named, from base to top, the Melanios, Nenitouria, Drymonas and Agrelopos Units (Figures 8.2 and 8.3). They also noted the predominance of Silurian limestone blocks in the upper (Agrelopos) unit and of Carboniferous blocks in the lowest (Melanios) unit. Although these horizons certainly exist and are referred to in the following descriptions, it is not clear whether they actually do represent a series of olistostromes. The blocks could also represent a succession of tectonic slices within an accretionary-type complex or a highly tectonized, formerly intact, sedimentary succession. The parallel bands formed by these blocky horizons in map view (Figure 8.3) could be due either to the presence of

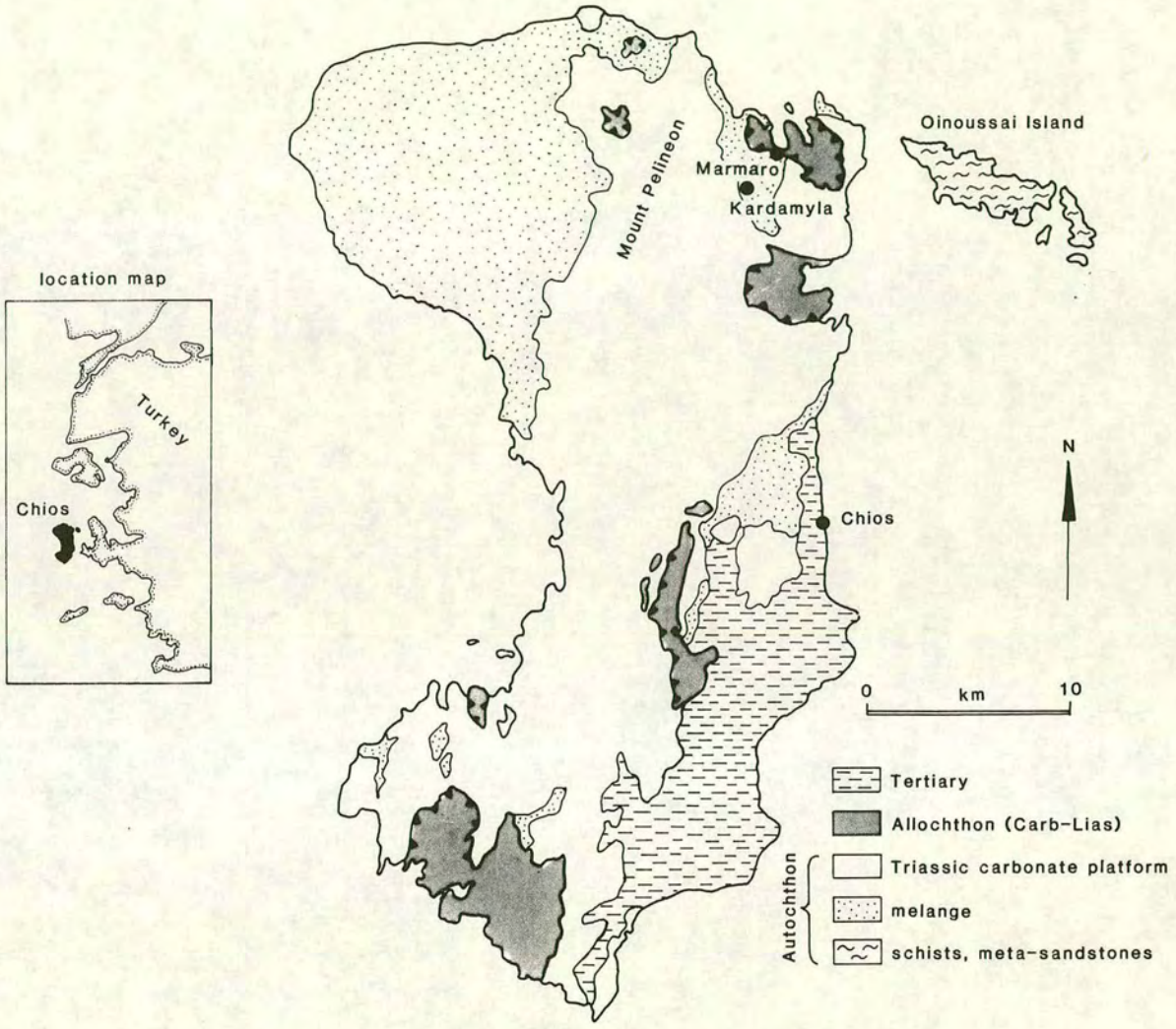

Figure 8.1 Geological map of Chios (modified after Besenecker *et al.*, 1968).

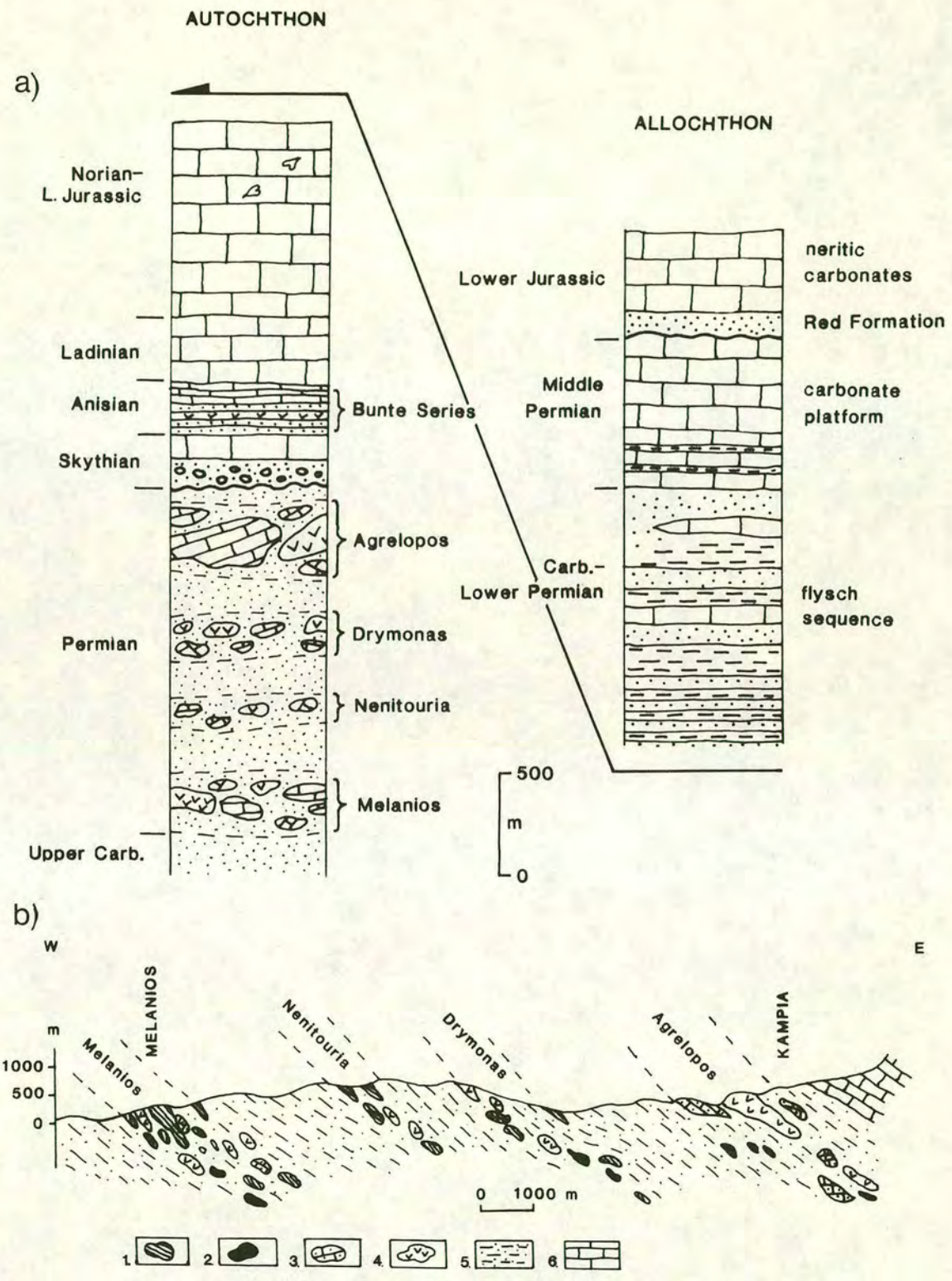

Figure 8.2

(a) Schematic stratigraphical sections through the autochthonous and allochthonous units of Chios (redrawn after Papanikolaou & Sideris, 1992).

(b) Cross-section through the mélange unit of the "autochthon" in NW Chios (1: Carboniferous limestone, 2: Devonian limestone, 3: Silurian limestone, 4: volcanics, 5: clastics, 6: Triassic carbonate platform) (after Papanikolaou & Sideris, 1992).

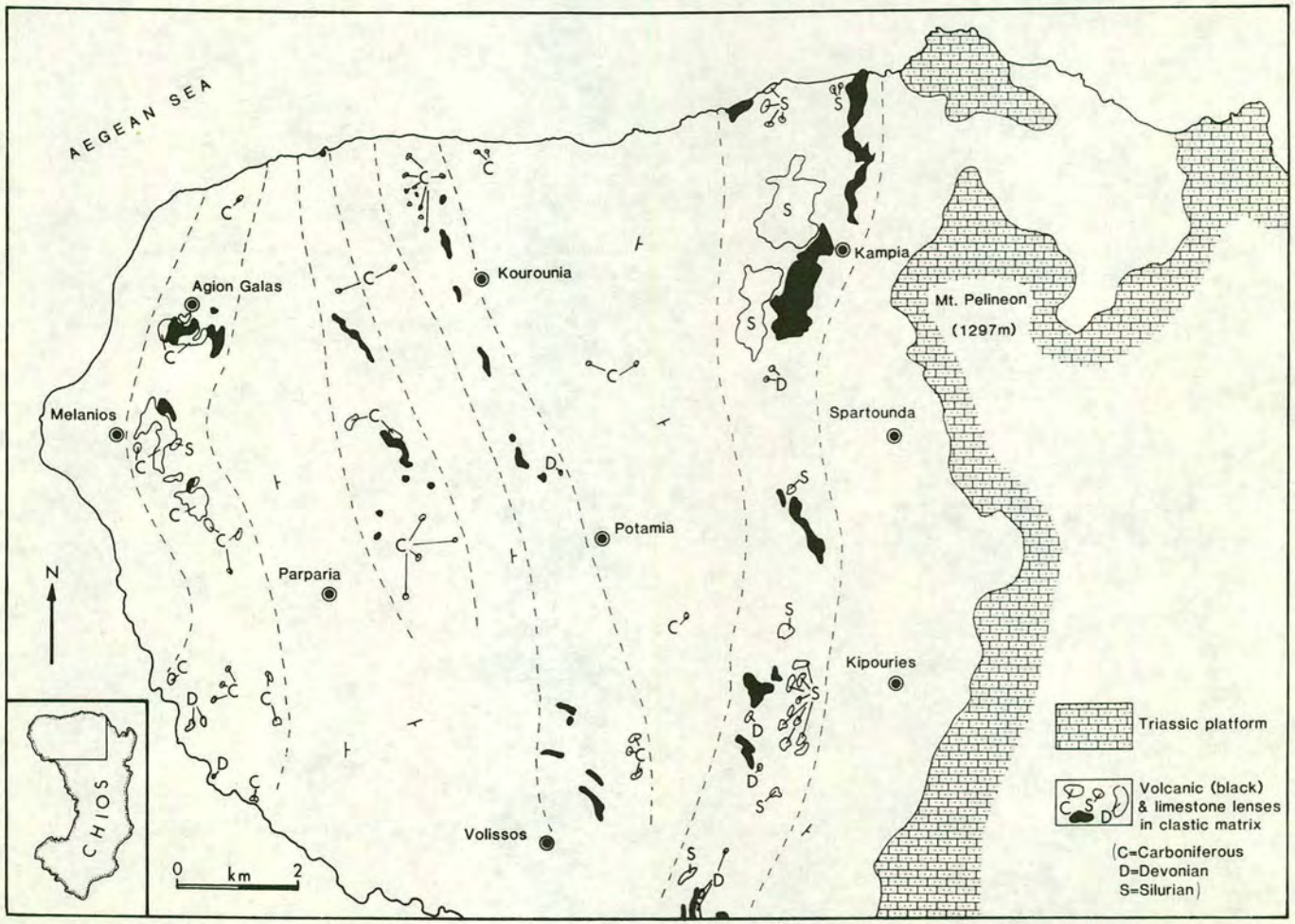

Figure 8.3 Geological map of NW Chios, showing the mélange unit with its distinctive bands of volcanic and limestone blocks (modified after Besenecker *et al.*, 1971 and Papanikolaou & Sideris, 1992).

several discrete layers, or to the erosion of one originally highly folded horizon. The mélange is best exposed in three regions of NW Chios as described below.

a) Kipouries

Southwest of the village of Kipouries, in the region known as Sgourou Nero, the uppermost mélange unit (Agrelopos Unit) is excellently exposed (Figure 8.3). Numerous limestone, quartzitic conglomerate and volcanic blocks crop out on the valley sides to the west of the road as shown in the sketch in Figure 8.4. The larger limestone blocks are over 50m across. The lithologies of the limestone blocks include brecciated limestone with buff marly infills, grey and pink micrite, marly limestone and limestone conglomerates. One block consists of crinoidal, coralline and oolitic fragments with laminated micrite interstices, possibly representing lithified reef talus (Figure 8.5a). Besenecker *et al.* (1968) dated these limestones as Ludlovian-Middle Devonian. Near the valley floor the contact between quartzitic conglomerate and a large limestone block can be observed. The limestone block is mantled by up to 10m of limestone breccia which grades from breccia to slightly fractured limestone with marly infills at the edges of the block. Laterite-filled fissures up to 3m wide cut across the limestone and the surrounding limestone breccias, but do not cut the quartzitic conglomerates (Figure 8.5b). The laterite is laminated parallel to the fissure edges and contains blocks of limestone. The contact between the quartzitic and limestone conglomerates is marked by a ferruginous crust. Seams and patches of buff marly material cut across the laterite fissures but do not cut the quartzitic conglomerate. Red partings within the buff material may represent reworked laterite from the previous phase of fissure-infill. Thus, on the basis of the limestone block shown in Figure 8.5a an interpretative sequence of events can be outlined:

1. Reef talus was lithified and subaerially exposed, leading to karstic weathering and laterite formation.
2. This assemblage was detached and reworked as a coherent block.
3. Break-up at the edges of the block led to fracturing and infilling by the buff marly material.
4. The block was deposited along with quartzitic conglomerate and blocks of volcanics.

Quartzitic conglomerates are well exposed near the valley floor. They are clast-supported and comprise rounded cobbles of arkosic sandstone, acidic volcanics, grey quartzite, white vein quartz and micaceous quartzite, up to 15cm across. Muddy

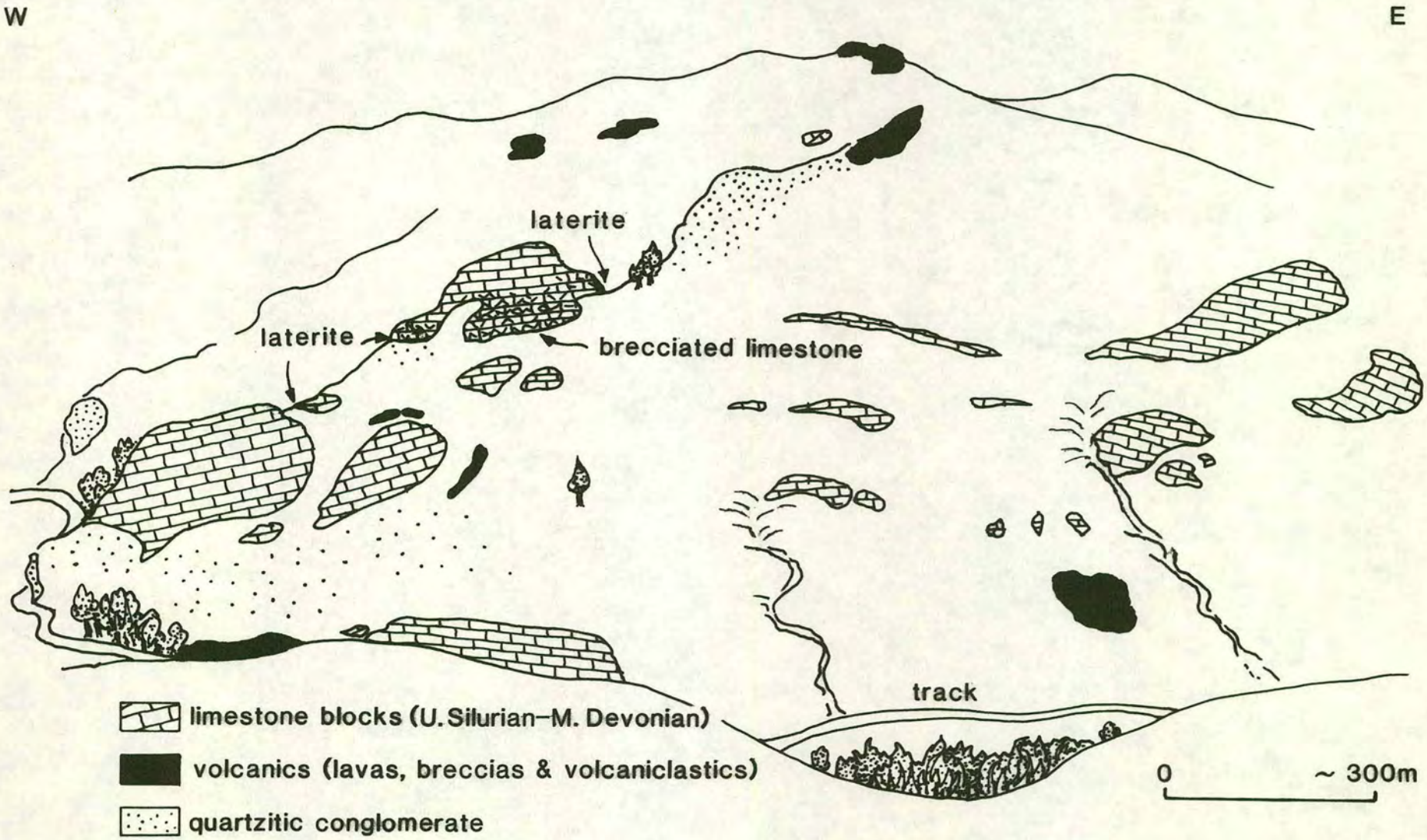

Figure 8.4 Field sketch of the upper mélange unit (Agrelopos Unit), SW of Kipouries.

Figure 8.5

(a) Brecciated limestone block from the hillside sketched in Figure 8.4. The limestone comprises reefal fragments with laminated micrite interstices. The buff marly infills visible in the picture represent a later phase of brecciation.

(b) Laterite-filled fissure cutting across a limestone block at the same location as (a).

(c) Flute casts on the base of a sandstone bed within the mélange north of Volissos.

a

b

c

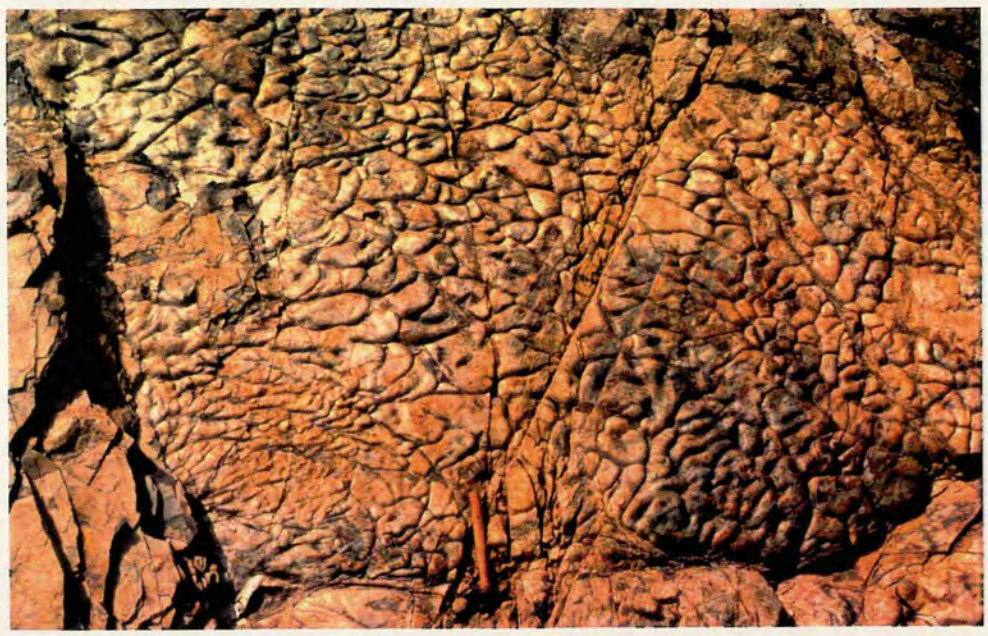

interbeds occur within the conglomerate near its contact with the limestone block. The conglomerates appear to form a matrix to the large limestone blocks at this locality, although it is possible that some of the conglomerate outcrops also represent blocks. The contacts between the limestone blocks and the coarse clastic matrix are relatively diffuse, with intervening zones (up to several metres wide) of brecciated limestone and calcareous conglomerate.

The volcanic blocks at near Kipouries predominantly comprise breccias of angular volcanic fragments up to 10cm in size. Most clasts are phenocryst-rich and/or vesicular. The phenocrysts are commonly clinopyroxene and are up to 3mm across. Vesicles are 0.5-1mm across on average, although in some clasts they attain 6mm.

b) Kampia

The Agrelopos Unit is also well exposed in the area known as Agrelia, west of Kampia (Figure 8.6). The large limestone block to the left of the picture (west) is fossiliferous and has been dated as Silurian-Lower Devonian (Papanikolaou & Sideris, 1983). The limestone is very similar to the limestone blocks at Sgourou Nero in that it is karstified and cut by laterite fissures. A laterite layer up to 10m thick marks the base of the limestone block and is the site of an old galena and sphalerite mine (Papanikolaou & Sideris, 1992). Several samples were collected from this horizon and analyzed by X-ray fluorescence (Appendix 2). The laterite samples are very rich in Fe (14-23.77%) and Pb (over 20000ppm in samples Ch-lat1 and Ch-lat3). Grading and load structures in the interbedded sandstones and shales at the base of the limestone and laterite block indicate that the sequence is overturned.

The grey-green crag on the right (east) of Figure 8.6 is almost entirely volcanic, comprising over 200m of lava, volcanogenic sediments and volcanic breccias. The top of the hill is made up of coarse-grained, structureless mafic rock, possibly a sill. A simplified section measured up the hillside is shown in Figure 8.7. The volcanic breccias are identical to those which form the blocks near Kipouries. The bottom of the valley between the two hills is characterized by conglomerates containing sandstone, chert, limestone, green volcanics and reworked laterite. One limestone "clast" is 10m across and contains a laterite fissure. Thin-bedded redeposited carbonate also occurs within the sequence at this level. The conglomerates contain rounded cobbles of quartzite, volcanics and chert, identical to those near Kipouries.

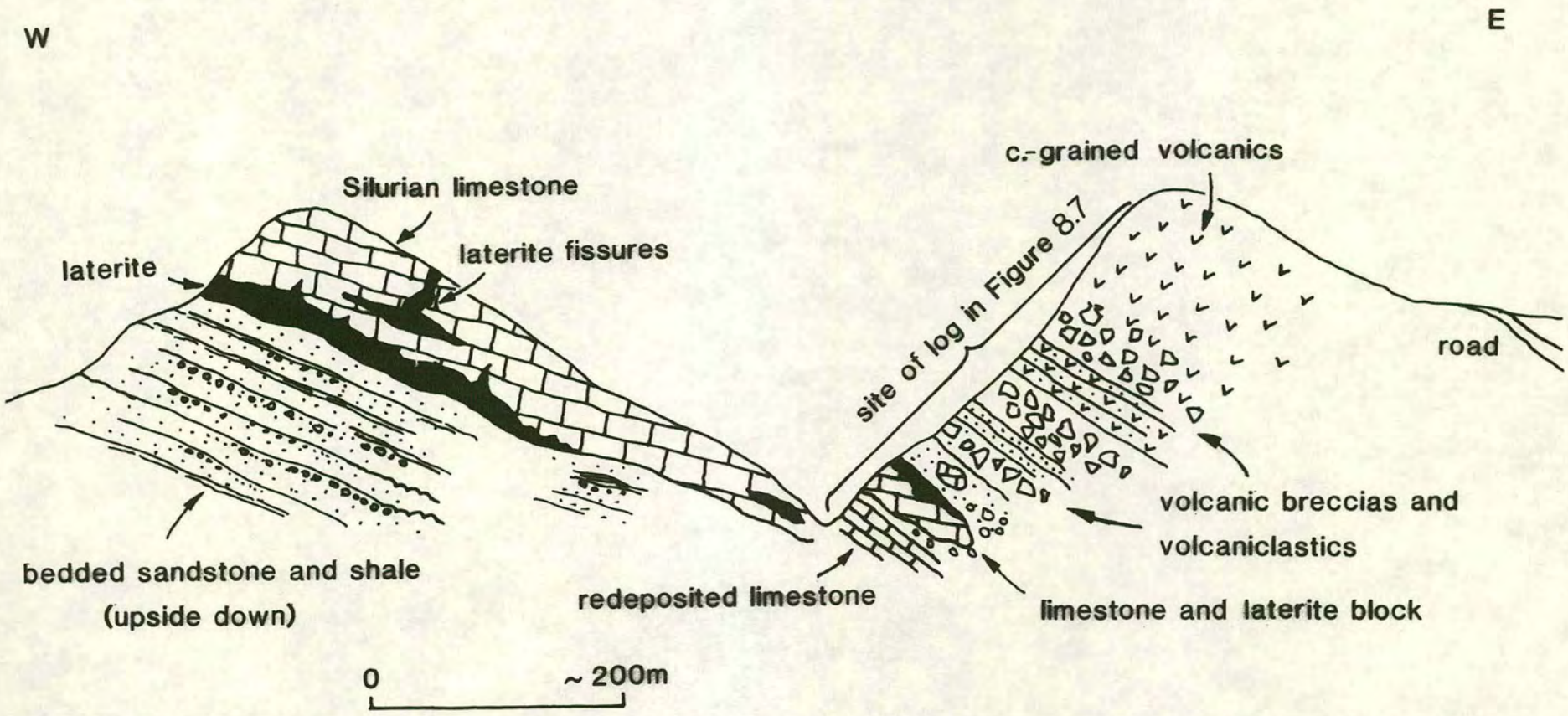

Figure 8.6 Sketch of the Agrelopos Unit west of Kampia.

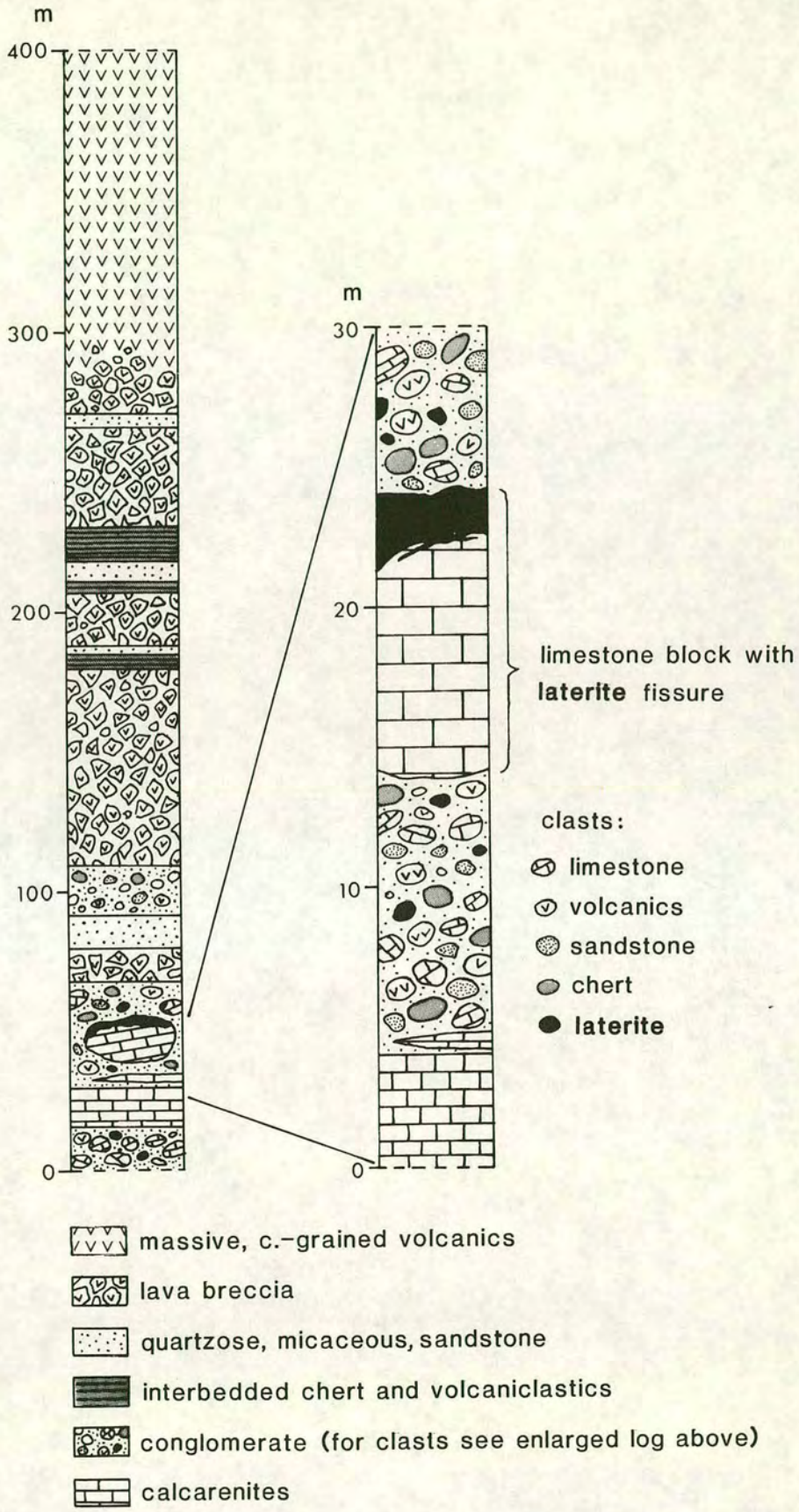

Figure 8.7 Logs through the Agrelopos Unit on the hillside shown in Figure 8.6.

c) Melanios

The lowermost mélange horizon, the Melanios Unit, is exposed south of Melanios village. At this locality blocks of volcanic breccia and lenses of limestone were observed. The limestone blocks at this site have been dated as Silurian and Lower Carboniferous (Papanikolaou & Sideris, 1983). Approximately 2km north of Melanios, near the village of Agion Galas, the same unit is exposed. There, a thick sequence of volcaniclastic sandstones and shales contains sheared blocks and lenses of Carboniferous limestone. Just outside the village an old monastery is built on one of these large limestone blocks.

d) Selada

The autochthonous mélange unit is also exposed in the NE part of the island (Figure 8.12). South of Nagos Bay, mélange is exposed near the tectonic contact with the overlying allochthon. Blocks of sheared black chert and sandstone up to many metres in size are well exposed. The complete lack of detrital material in the chert blocks implies that the two lithologies were deposited separately and were subsequently tectonically intersliced. The bedded chert is boudinaged and chevron-folded and contains numerous shear zones. One shear zone indicates normal motion towards the SW which contrasts with the clear NW direction of thrusting observed east of Nagos. Papanikolaou & Sideris (1992) assumed the black cherts (their "lydites") to be Devonian, by analogy with Devonian black cherts elsewhere in Europe.

8.3.2 General structure of the mélange

The mélange forms an eastward-dipping stack of folded sandstone and shale with horizons of large blocks of limestone, volcanics and conglomerate (Figure 8.2). Structures within the bedded sandstones and shale sequence include asymmetrical folds with wavelengths up to many metres.

The roads running north of Volissos and west of Spartounda display extensive exposures of bedded sandstone with well-preserved sedimentary structures. These structures allowed the determination of fold facing. Meso-scale, west-verging folds lie along the road west of Spartounda. Grading and load casts indicate the folds to be west facing with the western limbs overturned. Folded shales interbedded with the sandstone also display asymmetry towards the west. Turbiditic sandstones at the locality shown in Figure 8.6 dip eastward and are overturned, also indicating west-facing folding on a scale of many metres.

8.3.3 Palaeocurrents

As well as helping to deduce the structural vergence of the mélange, the well-preserved sedimentary structures in the clastic mélange matrix along the roads running north of Volissos and west of Spartounda allowed accurate palaeocurrent determinations. The structures observed include normal grading, lamination, cross-lamination, load casts, grooves, prods, flute casts and orientated plant fragments. Measurements were taken of numerous orientated plant fragments, groove marks and flute casts. The general orientation of these structures is approximately N-S to NNE-SSW. Directional structures such as the well-preserved flute casts in Figure 8.5c show that currents flowed predominantly from north to south. Figure 8.8 shows palaeocurrent rose diagrams for the structures measured at various localities. Southward directed palaeocurrent indicators (cross-bedding) were also observed in the overlying sandstone and conglomerate near the base of the Triassic platform at Mesorachi and also north of Siderounta, possibly implying that both the sandstones within the mélange and the overlying clastics were formed under the same long-lived regime. The palaeocurrents are parallel to the current strike of the Triassic carbonate platform to the east and may represent axial currents along the platform margin.

8.3.4 Basalt geochemistry

Samples were collected from three volcanic blocks on the hillside near Kipouries (Figure 8.4). They were analyzed by X-ray fluorescence and shown to be predominantly andesitic in composition (Appendix 2). For this reason they were not suitable for basalt discrimination diagrams, although the data were plotted on MORB-normalized trace-element plots to give a general idea of relative enrichments and depletions and for comparison purposes (Figure 8.9). The samples display a variety of patterns, depending on which "block" they were collected from in the field. Three blocks were sampled and, correspondingly, three distinct patterns emerge on normalizing to MORB. The C45 samples (A, C and D) have "humped" traces, showing considerable enrichment in LIL elements and a gradual slope down to Y and Sc. By contrast, the samples from a neighbouring block (i.e. the C40 samples) all display a sharp trough at Nb and depletion of Zr, Ti, Y and Cr relative to MORB. Samples C37, C38 and C39 were collected from a third basaltic block and also display a distinct trough at Nb with depletion of several HFS elements with respect to MORB. The results from the "C45" block, however, are very similar to those obtained from many of the Nilüfer and Çal basalts.

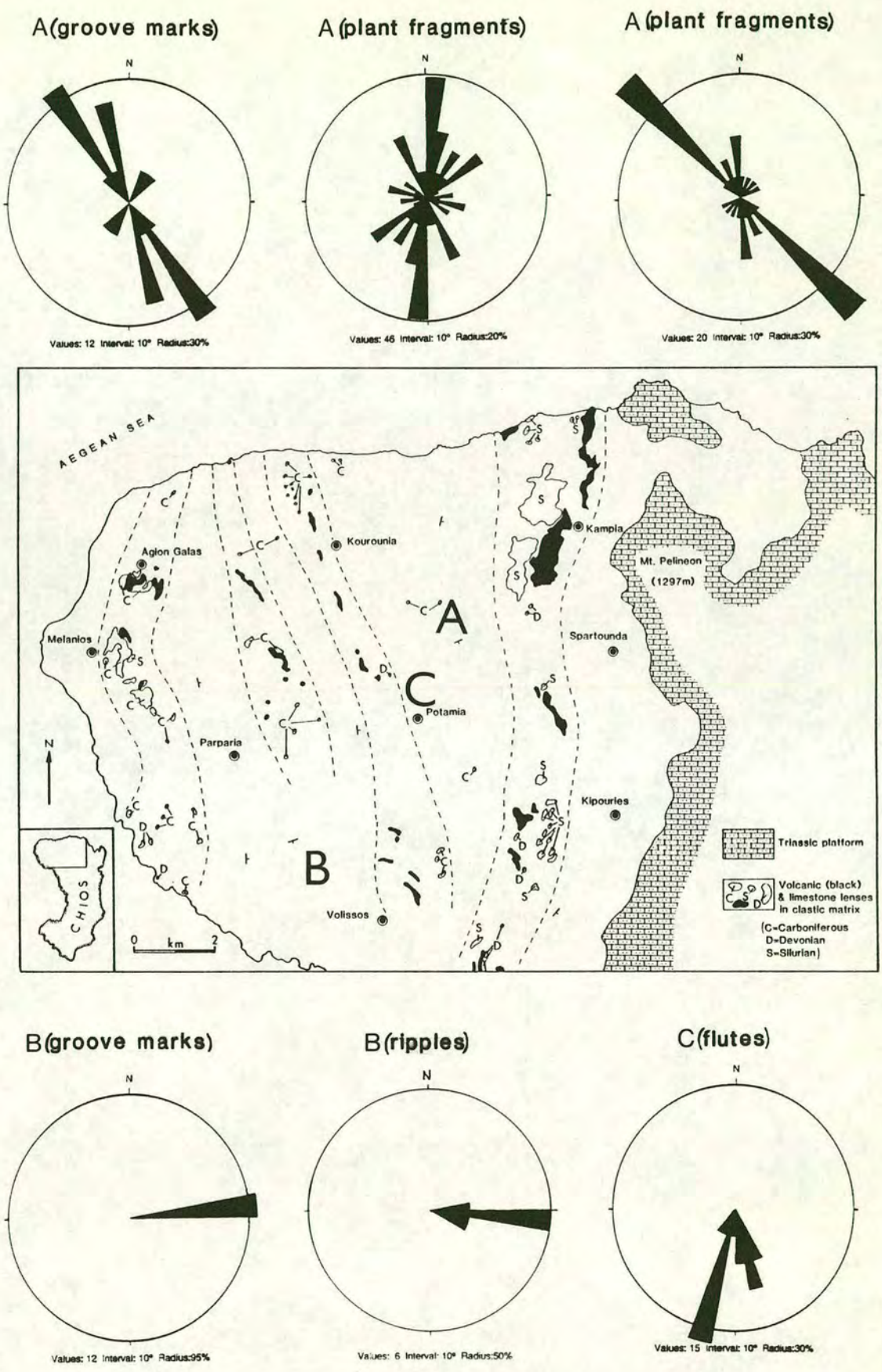

Figure 8.8 Rose diagrams showing the palaeocurrent directions given by various sedimentary structures at three localities within the clastic matrix of the mélange.

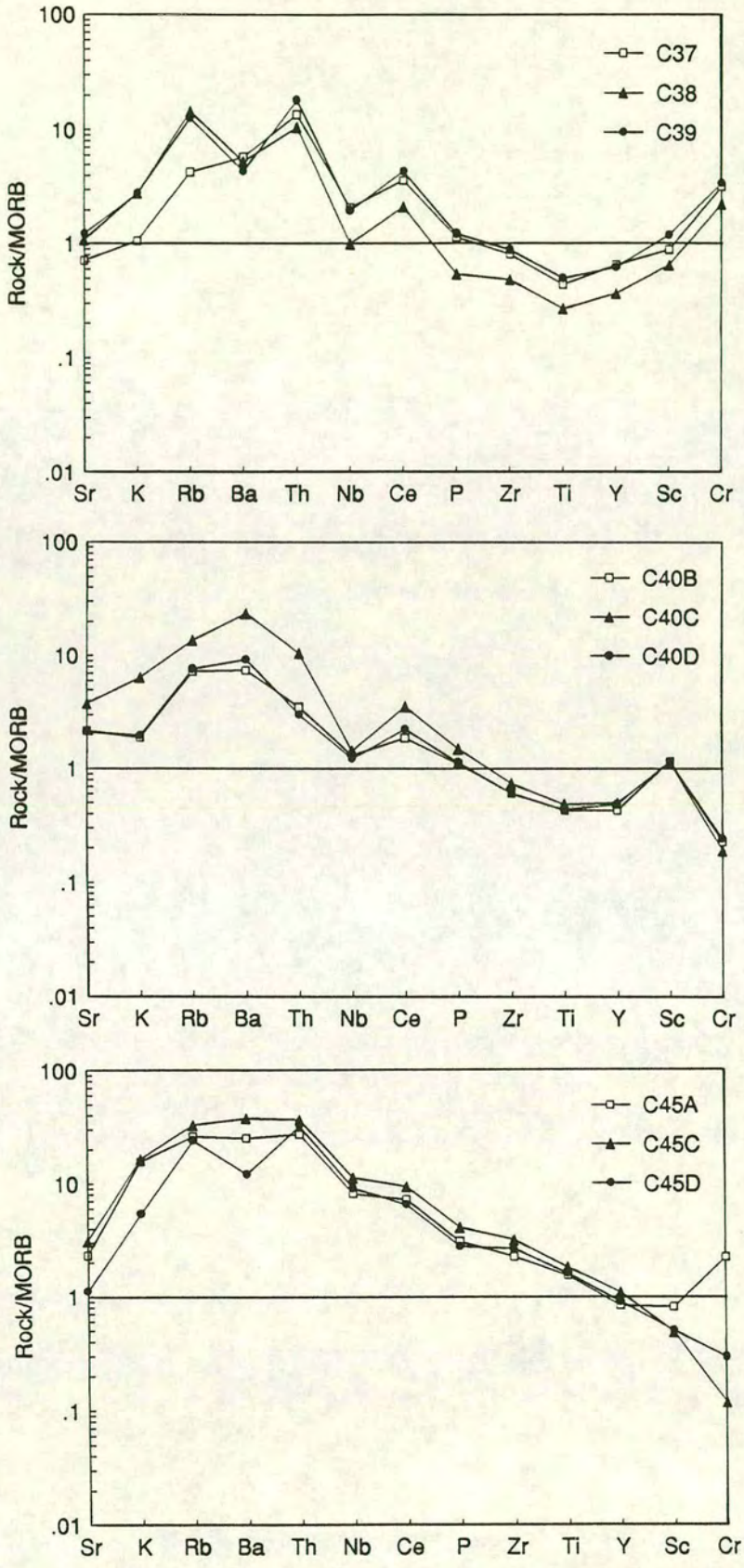

Figure 8.9 MORB-normalized multi-element plots for basaltic andesites from the hillside SW of Kipouries (normalizing values from Pearce, 1983, 1982). Each of the three plots corresponds to a separate volcanic block within the mélange.

8.3.5 Interpretation of geochemistry

Although the samples are andesitic and thus not strictly appropriate for normalizing against MORB, the plots obtained do display features of interest. Samples from the two of the volcanic blocks (Figure 8.9a and 8.9b) display a distinct Nb depletion with respect to Ce, along with LIL enrichment and HFS depletion. The LIL enrichment is as expected for these more evolved rocks, although the strong Nb depletion is probably a primary feature, characteristic of arc-related volcanism and recording a subduction component. By contrast, the block from which the C45 samples were taken displays a "humped" within-plate pattern with no evidence of a subduction component. Owing to the andesitic nature of the volcanics, these results cannot be used to determine palaeotectonic settings. Nevertheless, they do reflect a variety of magmatic processes, and include extrusives that were possibly formed in a subduction-related environment.

8.3.6 Triassic platform

Northern Chios is dominated by the high white ridge of Mount Pelineon (1297m) which represents the Triassic carbonate platform at its thickest extent (Figure 8.10a). The platform is exposed as a N-S trending ridge and is best studied along its margins. The clastics at the base of the platform are well exposed in the Mesorachi area, along the main road from Chios town to Marmaro. The basal conglomerate of the platform is also exposed in an isolated outcrop by the church of Aghios Andreas on the headland west of Marmaro Bay.

a) Mesorachi section

In the Mesorachi area, the base of the Triassic platform is represented by a Skythian-Anisian sequence, stratigraphically overlying sheared mélange. The base of the sequence is marked by sheared dark grey/green mudstone which is gradational with the underlying mélange. The mudstone passes up into an intraformational conglomerate of chert fragments in green-grey and red cherty mudstone. The conglomerate is interbedded with fine-grained sandstone and mudstone. The chert conglomerate passes up into massive and thick-bedded clast-supported conglomerates containing abundant rounded white quartz clasts (1mm-3cm in size). Other clast lithologies include medium- to coarse-grained sandstone, black chert, green volcanics, green mudstone and conglomerate. The maximum clast size is 12cm. The conglomerate is interbedded with medium- to coarse-grained sandstone which

Figure 8.10

(a) The Triassic carbonate platform of Chios viewed from the west. In this picture the platform forms Mount Pelineon, the highest mountain on Chios (1297m). In the foreground are the clastics which form the matrix of the mélange.

(b) Conglomerate rich in black chert and quartzite clasts at the base of the Triassic platform near Mesorachi (see Figure 8.11 for location). Cross-bedding is present in the sandstone intercalation.

(c) Nodular pink and grey limestone near the top of the lower Anisian "Bunte Series".

a

b

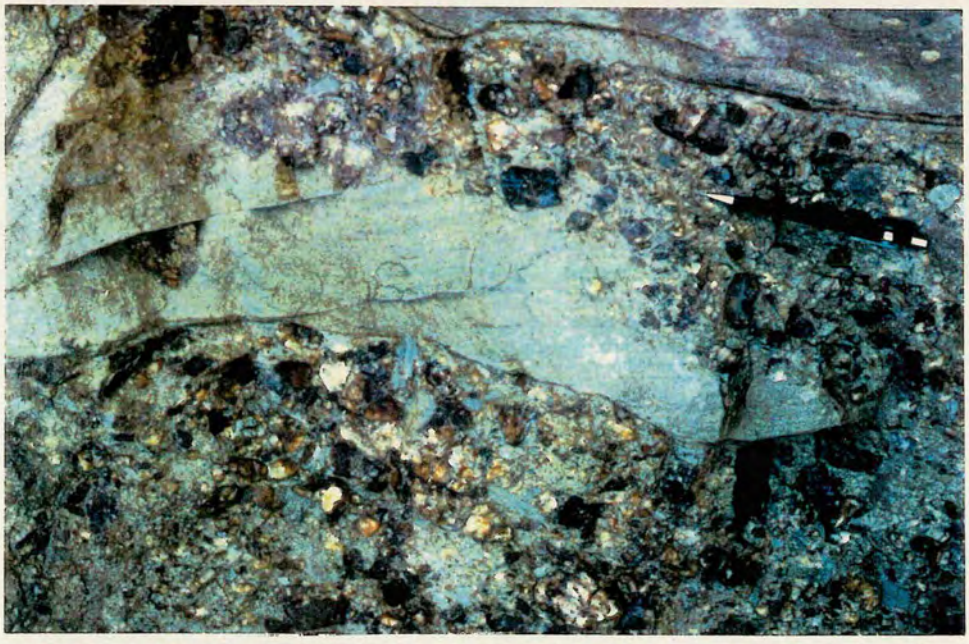

c

contains traces of cross-bedding (Figure 8.10b). Red and green mudstone are also interbedded with the conglomerates. The conglomerates are laterally discontinuous and grade into sandstone over a few metres.

Up sequence the conglomerates become matrix-supported and pass into medium-grained sandstone. The sandstone passes into sheared olive-green mudstone with grey calcarenite lenses. The calcarenite becomes pinkish with red mudstone partings and locally a nodular texture. It passes up into the basal intraformational conglomerate of the "Bunte Series" which was dated as lower Anisian on the basis of conodonts (Kauffman, 1969). The conglomerate is reddish and contains angular dolomite fragments in a muddy matrix. It is overlain by red shales and cherts with bands of silicic conglomerate and pale tuff bands which pass up into nodular limestone containing gastropods (Figure 8.10c). The "Bunte Series" is overlain by massive Ladinian dolomites and algal limestones of Ladinian-Carnian age, which mark the establishment of the platform proper. The platform is over 1000m thick and extends up into the Lower Jurassic. The I.G.M.E maps indicate that the platform displays at least three emersion horizons which are characterized by intercalations of conglomerate and sandstone. Laterite horizons are also present (Papanikolaou & Sideris, 1992 and references therein).

South of the Mesorachi sequence, near Delphini, Triassic limestone is tectonically overlain by highly folded Carboniferous-Lower Permian clastics of the allochthon. The Triassic limestone near the contact is also very folded and appears to be locally overturned. Box folds in the limestone are common and may have been caused by back-thrusting and pop-up as the limestone decolled along the contact with the underlying mélange.

b) Kipouries

Silicic conglomerates very similar to those of the Mesorachi region are also exposed north of Siderounta. Conglomerates containing fining-upwards sequences and sharp bases are interbedded with purple-grey sandstone (Figure 8.11). The conglomerate is predominantly made up of clasts of opaque white quartz (which forms 80-90% of the clasts) with minor amounts of grey limestone, laterite and black chert clasts. White mica, schist, fine-grained sandstone, and basalt clasts were also observed in thin-section. At the top of the logged section the conglomerate contains coarser bands. The purple-grey sandstone at the base of the section contains a large-scale foreset. A thick sequence of bedded purple-grey sandstones is also exposed along the track

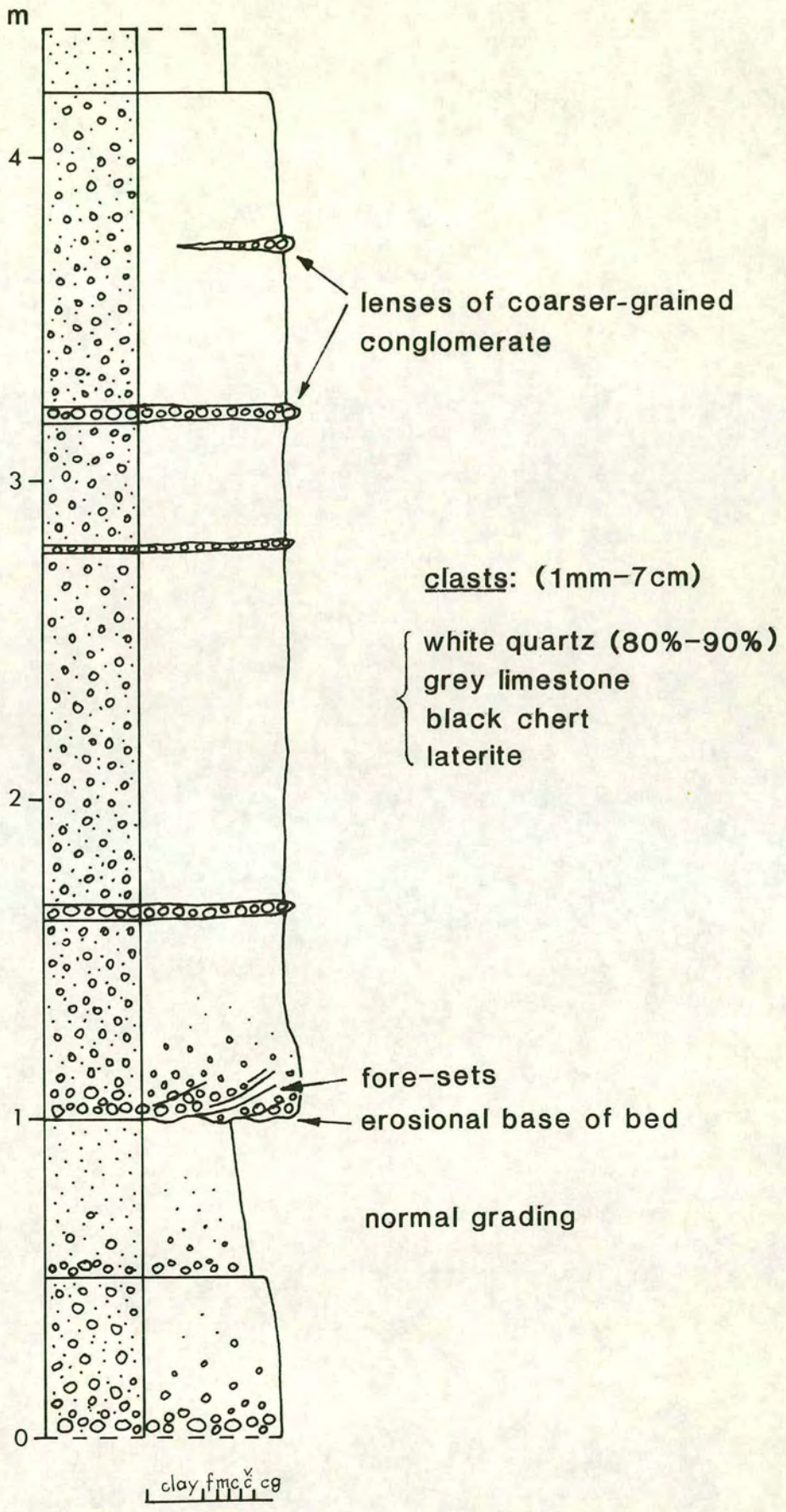

Figure 8.11 Log through siliciclastic conglomerates north of Siderounta.

which runs down into the valley at Sgourou Nero. They crop out on the opposite side of the valley to the underlying Agrelopos Unit (as shown in Figure 8.4). Thin-section study reveals the presence of abundant lithic grains, including devitrified porphyritic andesite/dacite, glassy basalt, fine-grained sandstone, quartzite, mica schist and granodiorite. All the grains are surrounded by dark red to opaque ferruginous material which also appears as seams within some of the grains.

c) Aghios Andreas church

Aghios Andreas church (Figure 8.12) is built on conglomerates, bedded calcarenites and coarse-grained sandstones which belong to the Upper Skythian Basal Series of the Triassic-Jurassic platform (Papanikolaou & Sideris, 1992). These rocks unconformably overlie sheared greywackes of the mélange sequence. The calcarenites are oolitic and cross-bedded. The conglomerates are well exposed along the small track to the church. They contain cobbles (up to 10cm) of black chert, coarse-grained sandstone, pale green quartzite and rare white quartz. The clasts are generally angular and are distributed in discontinuous traction deposits. Thick-bedded to massive limestones overlie this clastic sequence.

8.3.7 Discussion of Triassic platform

The Triassic platform of Chios displays a well-preserved basal section which indicates that the carbonates were established on a clastic basement. At Mesorachi the basal clastics are sheared and appear to have a sedimentary contact with the underlying mélange. The Mesorachi section represents relatively deep-marine conditions, as evidenced by the cherts and red mudstones. An intraformational chert breccia indicates reworking within the basin and the sporadic coarse clastic layers may reflect influxes of coarse material by storm currents. The fining-upwards sequences within the clastics north of Siderounta are typical coarse-grained proximal turbidites. The clasts within these conglomerates and sandstones reflect both sedimentary and volcanic sources. Opaque white quartz is the most abundant clast type and may have originated as vein quartz related to volcanic activity. At Aghios Andreas the clastics underlying the platform limestones include oolitic calcarenites, indicating progressive shallowing and heralding the initiation of carbonate deposition. The base of the platform is characterized by dolomites and algal limestones, indicating the establishment of very shallow-marine conditions. Coarse-grained clastic horizons and bauxites indicate periodic emergence of the platform .

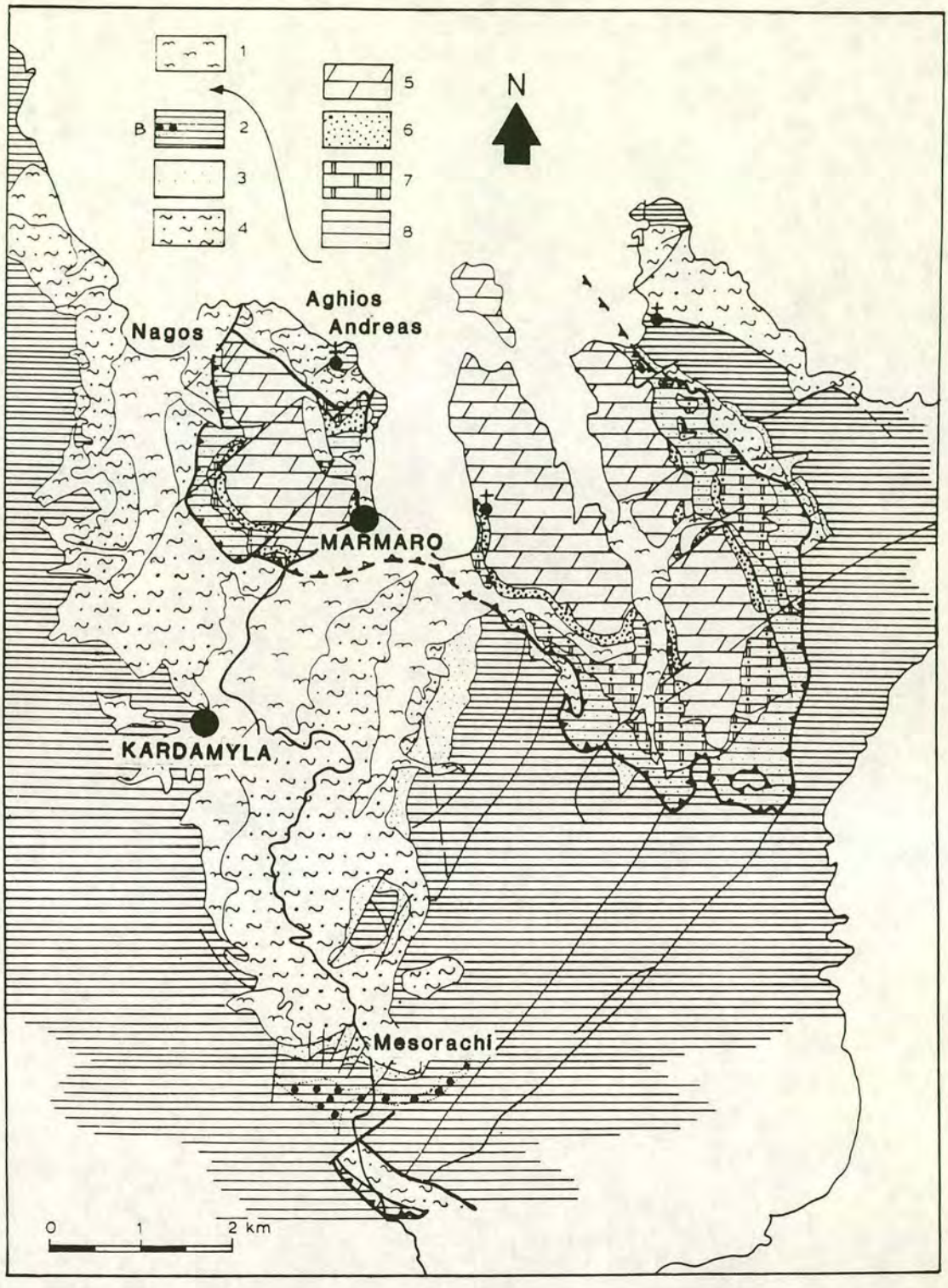

Figure 8.12 Geological map of NE Chios, showing the allochthonous unit emplaced over the autochthon around Marmaro. 1: alluvial deposits, 2: Triassic carbonate platform (B: "Bunte Series"), 3: Basal conglomerate and sandstones of the Triassic platform, 4: clastics of the autochthon, 5: Liassic carbonate platform, 6: Red Liassic clastic formation, 7: Middle Permian limestone, 8: Carboniferous-Lower Permian flysch-type sequence (after Besenecker *et al.,* 1971 and Papanikolaou & Sideris, 1992).

8.3.8 Chios allochthonous unit

The NE part of the island of Chios is characterized by a nappe (the "allochthonous unit of Chios" according to Migiros, 1992) which tectonically overlies the autochthon (Figure 8.12). In the nappe sequence Carboniferous to Lower Permian clastic rocks are overlain by a carbonate platform of Middle Permian age. The sequence is capped by Lower Jurassic red sandstones and shales which are in turn overlain by Lower Jurassic carbonates.

a) West of Delphini

The Carboniferous-Lower Permian part of the allochthon is exposed west of Delphini, along the main road which runs from Chios to Marmaro (Figure 8.13a). At this locality interbedded green sandstones, calcarenites and shales are thrust over Triassic limestone of the autochthonous platform and are themselves tectonically overlain by overturned Jurassic limestone from the upper part of the allochthon. The intervening Middle Permian flysch and Liassic Red Formation have been tectonically cut out. The clastic sequence is highly folded and faulted. Many of the folds are chevron folds with "noses". The asymmetrical folds display north- to NW-ward vergence and well-preserved grading indicates that the sequence is the right way-up. Duplexes and thrust faults within the folded outcrop also indicate thrusting towards the NW.

b) Marmaro Bay

The allochthonous unit is exposed in the NE part of the island around the town of Marmaro. Figure 8.13b is a view showing the allochthon thrust over the autochthon. In this region Middle Permian limestone overlies Carboniferous-Lower Permian flysch-type sediments. The limestone crops out as a well-bedded, fossiliferous sequence on the east side of Marmaro Bay. Grey silty limestone beds (15cm-1m thick) are intercalated with dark shale and are cut by a dense network of veins. Bioturbated muddy horizons, diagenetic concretions and thin yellow layers of echinoderm spines are common. Some beds contain abundant gastropods and ammonites. Geopetal structures indicate that the sequence is the right way up. The limestone displays considerable internal shearing. Lags up to 1m thick, containing fusulinids, crinoids, ammonoids and shelly debris were observed. One 0.5m-thick bed contains abundant oncoliths up to 3cm in diameter, fusulinids, crinoids, occasional ammonoids and shell debris. Small ammonoids and fusulinids form the nuclei of several oncoliths (Figure 8.13c). Fossils found within the limestones by Kauffmann

Figure 8.13

(a) Carboniferous-Lower Permian sandstones and shales of the allochthon west of Delphini.

(b) View eastwards from Aghios Andreas church, north of Marmaro, showing the allochton thrust over the autochthon with the inferred direction of thrusting.

(c) Middle Permian limestone containing abundant oncoliths, from the east side of Marmaro Bay. Small ammonoids and fusulinids form the nuclei of the oncoliths.

a

b

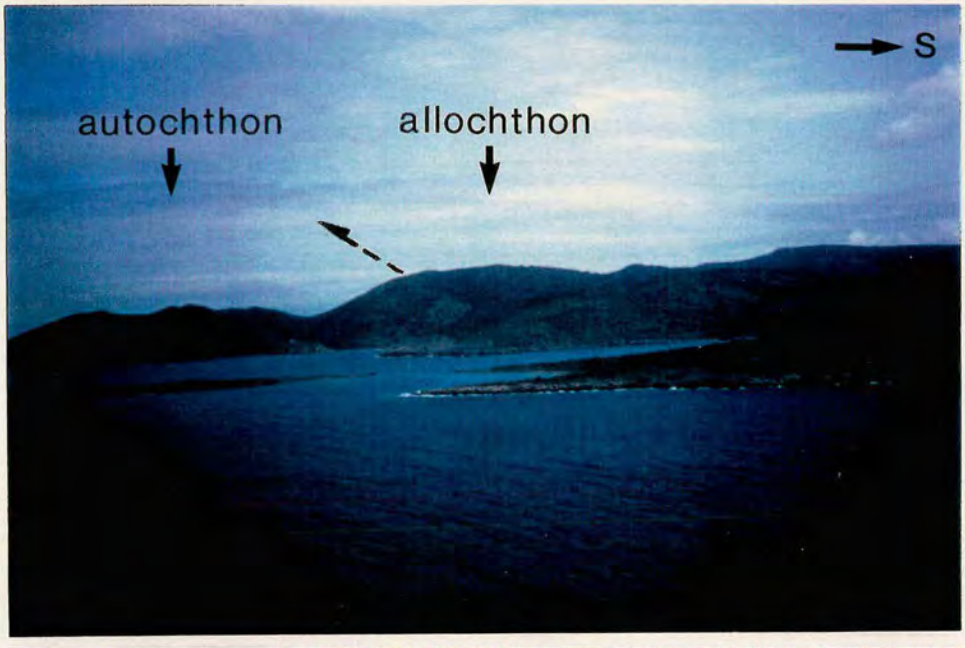

c

(as referenced in Papanikolaou & Migiros, 1992) include fusulinids, calcareous algae, corals and brachiopods as listed below:

fusulinids: mainly *Nankinella*
calcareous algae: *Girvanella* sp., *Mizzia velebitana*, *Permocalculus texanum*, *Velebitana triplicata*, *Vermiporella nipponica*, *Gymnocodium bellerophontis*
corals: *Sinopora*
brachiopods: *Linoproductus* cf. *lineatus*, *Richthofenia* cf. *lawrencia*, ?*Costispinifera ovalis*, ?*Krotovia* cf. *opuntia*, *Oldhaminia* sp., ?*Striatifera* cf. *compressus*

The upper part of the bedded limestone series is thin- to medium-bedded and dolomitic, with shelly lags and redeposited benthic foraminifera. The Permian limestones are overlain by the Lower Jurassic Red Formation which consists predominantly of thin-bedded red mudstones and siltstones interbedded with greenish sandstones. The clastics pass up into Lower Jurassic limestone. Buff partings and a slight nodular texture are common. A few layers of redeposited shelly material and limestone intraclasts indicate deposition on or near a slope.

c) Nagos Bay

On the western side of the bay green sandstone and conglomerate are overlain by fossiliferous, bedded grey limestone which is very similar in appearance to that exposed in Marmaro Bay. The limestone contains shelly coquinas rich in gastropods and probably represents part of the allochthonous Permian sequence rather than the "Palaeozoic autochthon" as described in Papanikolaou & Sideris (1992).

d) Scardana

Near Scardana well-bedded Mid Permian dolomitic limestones are exposed. These represent the upper part of the Permian carbonate sequence and at this locality are overlain by Liassic clastics and limestone. Below the dolomites the Permian limestone is dark and marly and contains shelly lags rich in transported benthic foraminifera.

8.3.9 Interpretation of the Chios Permian platform

The Mid Permian carbonates on the island of Chios conformably overlie a Carboniferous to Lower Permian succession of intercalated limestones and flysch-

type sediments and are interpreted as a platform developed on a clastic basement. The Mid Permian succession contains a predominantly shallow-marine fauna of fusulinids, algae, corals and brachiopods. The presence of shelly coquinas and lags within the platform sequence may record storm events and suggest an open shelf environment which experienced periodic storms. Localized coral build-ups, probably at the shelf edge, supplied detritus to the shelf. The muddy nature of the lower part of the platform sequence indicates input from a terrigenous source, possibly as a result of fine-grained deltaic material spreading across a carbonate shelf during storm events. The dolomitic limestones higher in the sequence may record a shallower and more stable shelfal environment.

8.3.10 Emplacement of allochthon

The tectonic contact between the autochthon and the allochthon is well exposed east of Nagos Bay (Figure 8.12). Near the contact, thin-bedded black cherts of the underlying autochthonous sequence are highly folded and sheared. The shear zones and general fabric of the outcrop dip moderately to the SE and are associated with small duplexes which indicate motion towards the NW. The shear zones cut chevron folds with axial planes which also dip SE, at slightly steeper angles than the shears. The folds verge NW and have NE-trending axes. On the basis of this outcrop it appears that emplacement was towards the NW, rather than the south as suggested by Papanikolaou & Sideris (1992).

8.4 The Karaburun Peninsula

The pre-Tertiary geology of the Karaburun Peninsula basically comprises a Middle Carboniferous-Cretaceous sequence, whose upper levels are incorporated into the Maastrichtian-Danian Bornova Mélange (part of the Izmir-Ankara-Erzincan Suture Zone) (Figure 8.14). The sequence is continuous and unbroken between the Scythian and the Lower Cretaceous and, with the exception of Scythian-Anisian cherts, clastics and volcanics, is totally comprised of carbonates. East-dipping thrust faults cause some tectonic repetition on the eastern side of the peninsula.

8.4.1 Alandere Formation (Lower-Middle Carboniferous)

The lowest part of the Karaburun Peninsula sequence comprises Lower-Middle Carboniferous limestones of the Alandere Formation. This unit is exposed near Ildir

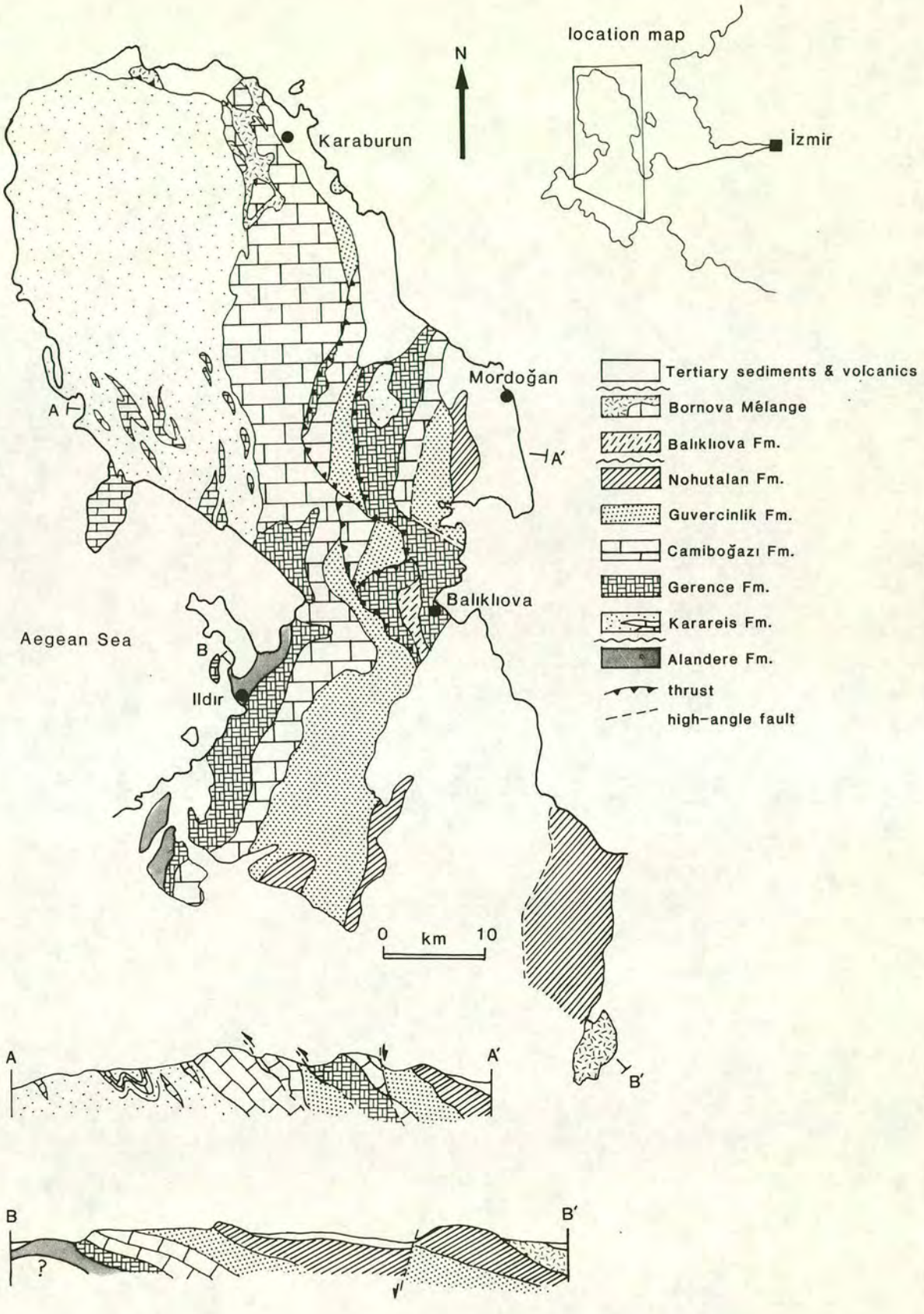

Figure 8.14 Geological map and cross-sections of the Karaburun Peninsula (redrawn after Erdoğan, 1990).

and is made up of fossiliferous, dark grey limestone. The limestones of this unit are rich in crinoids, ooids and corals and also contain rounded clasts which are themselves bioclastic. The clasts have micrite rinds and include gastropod fragments, echinoderm plates, red algae, molluscs and ooids. Rare quartzite and calcareous sandstone clasts were also observed. Detailed palaeontological investigations by Erdogan (1990) have revealed the presence of abundant Early-Middle Carboniferous fossils in the Alandere Formation.

To the north of Ildir, the limestone is associated with green sandstone and limestone conglomerates. The lower boundary of the Alandere Formation is not exposed on the Karaburun Peninsula and the total thickness of the exposed sequence has been estimated as 300m (Erdogan, 1990). The upper contact can be observed along the road north of Ildir. There, dark grey limestones of the Alandere Formation are overlain by Lower Triassic light grey limestone of the Denizgiren Group. The Upper Carboniferous and Permian are absent. Karstic weathering and ferruginous oxidation along the contact indicate subaerial exposure. The contact can again be observed east of the village of Reisdere where the Alandere Formation is overlain by thin-bedded limestones and chert intercalations. The limestones contain intraformational breccias.

8.4.2 Denizgiren Group (Lower Triassic)

The Mesozoic of the Karaburun Peninsula is represented by a continuous succession from the Lower Triassic to the Albian. The Lower Triassic consists of the Denizgiren Group which has been divided into the laterally equivalent and gradational Karareis and Gerence Formations. The Gerence Formation which crops out in the south consists of thin-bedded limestone, ammonitic red limestone of Anisian age, red and green chert, pink dolomite and mafic tuffs. The Karareis Formation lies to the north and consists of sandstone, chert, manganiferous chert, mafic volcanics, Carboniferous limestone blocks and pelagic limestone lenses of probable Lower Triassic age. Pilot geochemical studies of the manganiferous chert and volcanics were carried out and are briefly discussed below.

a) Manganiferous chert

Chert horizons within the Karareis Formation contain ore grade material and were once mined for manganese (B. Erdogan, pers. comm., 1992). The Mn imparts a characteristic dense, black appearance to the chert and, in places, a metallic lustre. Five samples of the chert were collected and analyzed by X-ray fluorescence

(Appendix 2). The MnO concentrations are extremely variable within this small sampling site and range from 0.89% to 51.61%, implying highly localized concentrations. Samples 6/10/92-1 and 6/10/92-4 contain 51.61% Mn and 40.79% Mn respectively. The high degree of Mn enrichment in these samples is illustrated by comparison with the average Mn concentration of 16.78% in abyssal nodules (Glasby, 1977). By contrast, abyssal nodules are much richer in Fe than the analyzed black chert. The Fe concentrations in the Karaburun cherts range from 1.08% to 2.63%, whereas the average Fe content of abyssal nodules is 17.27% (Glasby, 1977).

Manganiferous sedimentary rocks are a distinctive feature of many Tethyan passive margin sequences and are widely believed to be associated with volcanic hydrothermal systems. For example, Degnan (1992) carried out detailed studies on the Upper Jurassic Mn-rich cherts in the Pindos Zone in Greece and concluded that Mn-enrichment was primarily caused by the precipitation of Mn-rich phases from hydrothermal fluid exhalations. A similar origin was proposed for Mn-rich deposits above Upper Triassic lavas in the Antalya Complex, SW Turkey (Robertson, 1981) and in the Troodos Mountains, Cyprus (e.g. Robertson & Boyle, 1983). Robertson & Boyle (1983) also noted that Upper Jurassic to Lower Cretaceous manganiferous accumulations reflect renewed volcanism along the passive margins of Turkey (Antalya Complex), Oman (Hawasina Complex), Cyprus (Mamonia Complex) and Syria (Baer-Bassit).

b) Basalt geochemistry

On Karaburun vesicular volcanics were sampled from a road section on the west of the peninsula, north of Ildir, where they stratigraphically underlie the Triassic carbonate platform. The samples were analyzed by X-ray fluorescence and found to be basaltic andesites. On MORB-normalized diagrams the Karaburun samples display a distinctive "spiky" pattern with LIL enrichment and HFS depletion relative to MORB (Figure 8.15). The spiky appearance of the plots is largely due to a trough at Nb. Nb is depleted relative to Ce, but is enriched with respect to MORB. Ce is very enriched relative to MORB and Ti is depleted. With the exception of Cr, the other HFS elements, P, Zr, Y and Sc are almost at the normalizing line.

Although the strong Nb trough implies the involvement of a subduction component, it is impossible, without further detailed geochemical and regional studies, to determine the nature and age of the subduction zone. Many other Triassic rift-related basalts in the Tethyan realm possess a subduction signature of uncertain affinity.

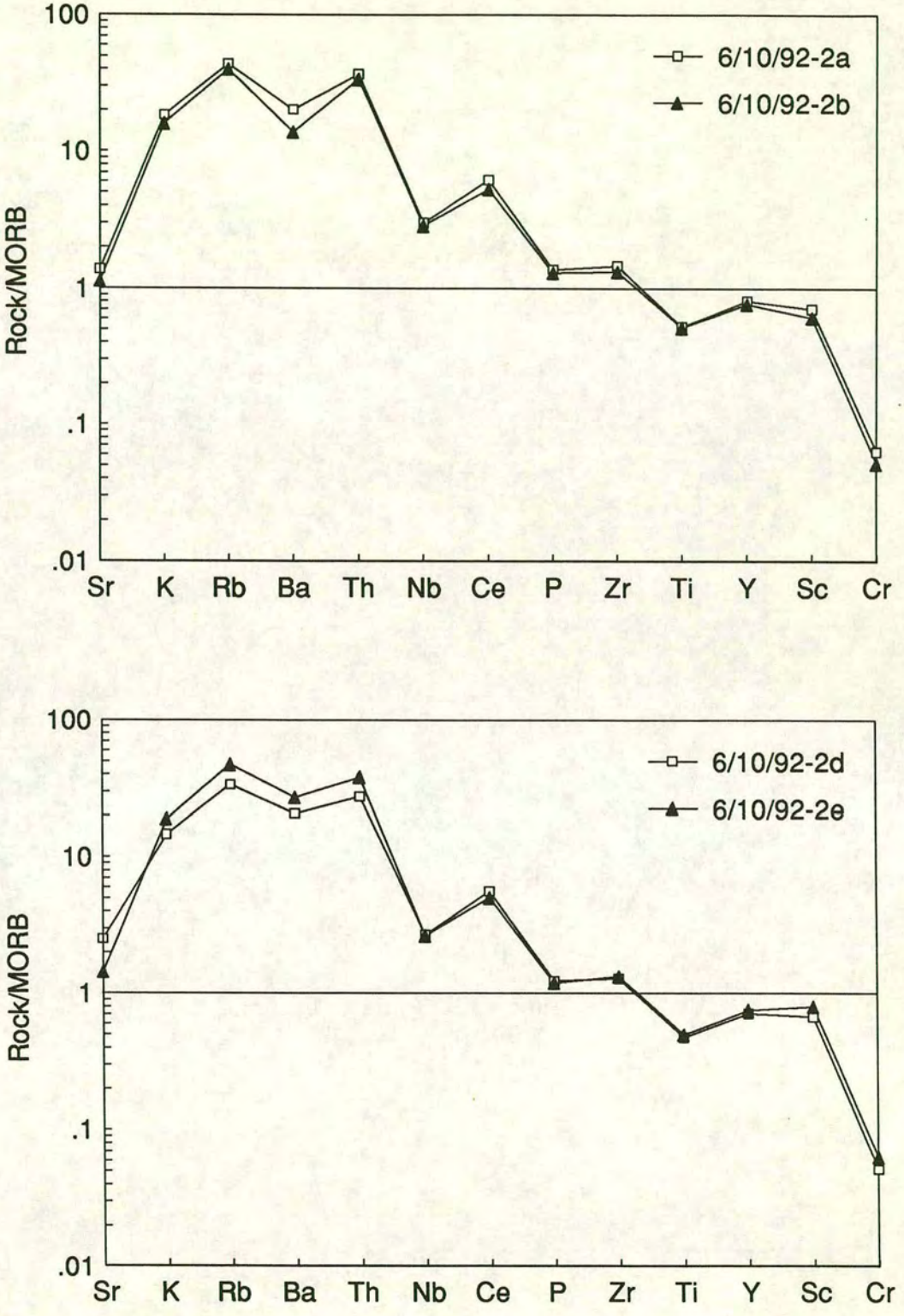

Figure 8.15 MORB-normalized multi-element plots for basaltic andesites from the Karaburun Peninsula (normalizing values from Pearce, 1983, 1982).

8.4.3 Middle Triassic-Lower Cretaceous carbonate platform

The Gerence and Karareis Formations are gradationally overlain by a continuous Triassic carbonate platform sequence up to 3km thick which forms the imposing mountain of Akdag ("white mountain" in Turkish) and comprises the Camibogazi Formation (Ladinian-Carnian) and the Guvercinlik Formation (Norian-Rhaetian). The base of the platform is well exposed in the north where upper Anisian limestone overlies plagioclase- and clinopyroxene-phyric basaltic andesites. The limestone comprises thin-bedded calciturbidites and contains well-preserved *Daonella,* a deep water bivalve (Figure 8.16a). The limestone beds are laminated and very fossiliferous. Alternating bands of radiolarian-rich limestone and shelly packstone were observed in thin-section. The packstone consists of micritic shell debris, bryozoan fragments and redeposited ooids in a sparry matrix. Replacement chert occurs along laminations in the carbonate becomimg less common up section. Normal grading indicates that the sequence is the right way up. The chert eventually dies out and the limestone becomes massive. The equivalent unit to the south is an ammonite-rich red limestone horizon. The lowest limestone of the platform is Lower Ladinian-Carnian in age. A complete unbroken sequence exists from the Ladinian to the Aptian-Albian.

A Norian to Lower Jurassic limestone section is excellently exposed along the shore near Balikliova. Buff stromatolitic limestone is interbedded with dolomitic micrite layers. The limestone contains undulose laminoid fenestrae (elongate cavities) up to 2mm thick and irregular fenestrae ("birdseyes"), both filled with sparry calcite. In thin-section the carbonate has a particulate, slightly pelletal texture, probably caused by algal trapping and binding of fine-grained carbonate sediment. Towards the top of the section the limestone contains megalodonts and red stylolitic seams and is pink in certain horizons (Figure 8.16b). Red sandstone lenses and intercalations are found throughout the sequence. The sandstone consists mainly of highly strained, subrounded to angular quartz grains displaying strong undulose extinction and strings of inclusions. Rare schist and devitrified volcanic grains were also observed. The more conglomeratic layers contain clasts of black ?chert and white quartz up to 3cm in size. Large-scale cross beds and conglomeratic traction deposits are common. These clastics are very similar in lithology and stratigraphic position to the Çayir Formation in the Antalya Complex, SW Turkey. The Çayir Formation forms a distinct interval in the Mesozoic Anamas Dag carbonate platform and comprises red and orange quartzose sandstones, conglomerates, siltstones, mudstones and pisolithic

a

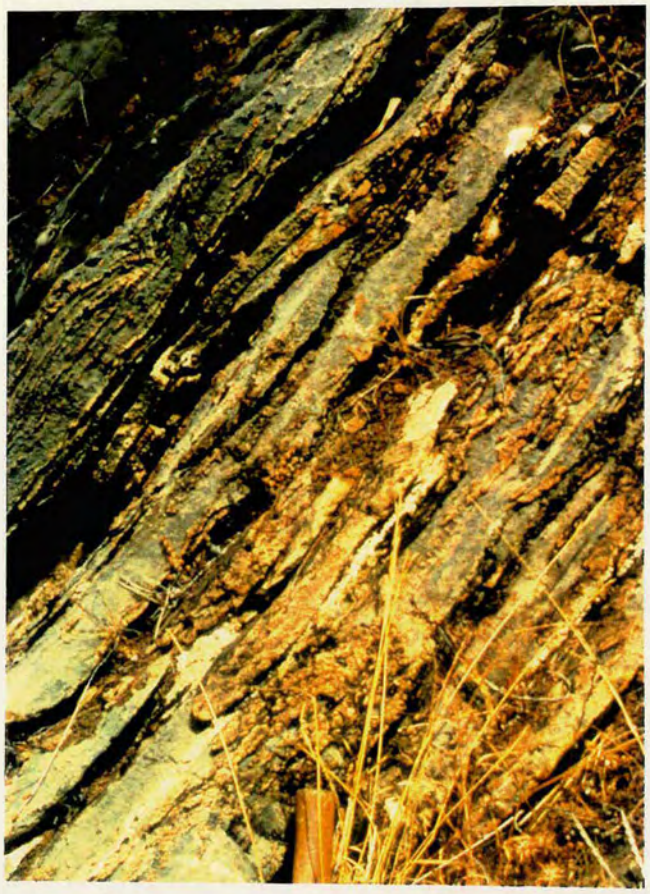

b

Figure 8.16

(a) Calciturbidites at the base of the Triassic carbonate platform on the Karaburun Peninsula. Replacement chert can be seen along laminations within the limestone.

(b) Megalodonts in the Norian limestone near Balıkliova.

ironstones (Monod & Akay, 1984). Like the red sandstones on Karaburun, the Çayir Formation occurs within an Upper Triassic shallow-water limestone sequence which is overlain conformably by Lower Jurassic limestones. The clasts in the Çayir Formation include schist and quartzite from a metamorphic terrain, Upper Permian platformal limestone and chert from a more basinal setting (Robertson, 1993). With the exception of the Upper Permian limestone clasts, the clasts from the Karaburun sandstones are extremely similar to those of the Çayir Formation.

There is a gradational boundary between the Triassic and the Lower Jurassic. At its base, the limestone of the Lower Jurassic-Albian Nohutalan Formation is very similar to the Triassic and also contains megalodonts, albeit smaller than those of the Triassic. The Nohutalan Formation is unconformably overlain by the Campanian-Maastrichtian Balikliova Formation which comprises thick-bedded limestones in its lower levels and, up-section, thin-bedded cherty limestone passing into intercalated sandstones and mudstones. The Balikliova Formation also directly overlies parts of the Lower Triassic succession with a marked angular unconformity.

8.4.4 Discussion of the Karaburun sequence

The Triassic sequence of the Karaburun Peninsula represents an overall shallowing-upward sequence. The cherts, pelagic limestones and volcanics of the Gerence and Karareis Formations were laid down in deep water, around or above the CCD. Localized manganiferous cherts indicate hydrothermal activity in a deep marine environment, probably related to extrusion of the Karareis Formation volcanics. The limestone at the base of the overlying platform also records deep water conditions as indicated by the presence of *Daonella* and chert within the bedded limestone. The progression from cherty calcturbidites to massive limestone indicates that conditions had shallowed sufficiently for platform carbonates to become established. The Upper Triassic-Lower Jurassic part of the platform displays characteristic features of intertidal-supratidal flats (e.g. birdseyes, cryptalgal laminae). The dolomitic micrite layers may represent tidal-channel levee deposits and the dolomite is probably penecontemporaneous in origin. This lithologies in this sequence are almost identical to the fenestral, dolomitic limestones of the Alpine Triassic, the so-called "Loferites" (Fischer, 1964). The local lenses of red sandstone may represent land-derived channel fills. The red stylolitic seams near the top of the sequence may represent periodic subaerial, karst environments. This predominantly tidal flat environment would have been regularly to rarely covered by water and subjected to weak currents and wave

action. Tidal flats are commonly found shoreward of lagoons and in this case the tidal flat sequence may represent the landward equivalent of the main reefal carbonate build-up. Evaporites and evaporite pseudomorphs are not associated with these limestones, suggesting that the climate was relatively humid.

8.5 Correlation of the Chios and Karaburun sequences

The Mesozoic platformal sequences of Chios and Karaburun are undoubtedly part of an originally continuous carbonate platform. Both areas display thick successions of shallow-water Triassic to Cretaceous limestone constructed on deep-sea pelagic limestones, cherts and volcanics. The underlying sequences of both areas also display many common features which can be correlated. The Carboniferous limestone blocks within the Chios mélange may represent a dismembered version of the Lower-Middle Carboniferous Alandere Formation on Karaburun. The other components of the mélange are very similar to many of the lithologies within the Denizgiren Group (comprising the Karareis and Gerence Formations) of Karaburun. Both units contain clastics, black chert, limestone and mafic volcanics. Carboniferous limestone blocks are common to both sequences and were probably derived from a Palaeozoic basement which is now only exposed on Karaburun as the Alandere Formation. The presence of karstic weathering and ferruginous oxidation within both the Alandere Formation and many of the Chios mélange blocks supports this hypothesis. The Chios mélange also contains Silurian and Devonian limestone blocks, a feature not observed within the Denizgiren Group. The thick clastic sequences present within the Chios mélange are not observed on Karaburun, although sandstone is common within the middle levels of the Karareis Formation. Sheared and folded intervals of black chert are a distinctive feature of both the Chios and Karaburun sequences. On Chios this lithology has clearly been tectonically disrupted or sliced into the sequence.

The allochthonous unit of Chios is absent on the Karaburun Peninsula and its origin is as yet unknown. Permian rocks are absent from both the Chios autochthon and the Karaburun sequence. It is interesting to note that in both the Chios autochthon and throughout NW Turkey, Permian limestone platforms form the highest structural levels and occur as relatively shallow-dipping thrust sheets (c.f. Çal Unit in Edremit and Bergama regions). The highest levels in the Chios allochthon are Liassic, indicating that emplacement occurred in post-Liassic times. Limited structural measurements made near Marmaro suggest that the nappe was emplaced from SE to NW, although more data are needed to confirm this.

8.6 Alternative tectonic models for Chios and Karaburun

The tectonic evolution of the Chios-Karaburun region, and its role in the wider setting of the Palaeotethyan system, is a complex problem which requires a great deal more work, especially detailed structural studies and geochemistry. Nevertheless, reconnaissance fieldwork carried out as part of this project has revealed many interesting features which have important implications for the interpretation of Palaeotethyan evolution in NW Turkey.

Of particular importance is the intriguing, but poorly understood, "mélange" unit which forms the lowest part of the Chios autochthon. This thick clastic sequence with its abundant blocks of Palaeozoic limestone and volcanics is overlain by a Triassic carbonate platform which shallows upwards from a deep-water chert, tuff and clastic sequence. On the Karaburun Peninsula, by contrast, Carboniferous limestone forms the lowest unit. The overlying cherts, sandstones and volcanics of the Denizgiren Group form the base of a thick Triassic carbonate platform, equivalent to that on Chios. Thus, from Triassic times the histories of the two regions were broadly similar and involved the establishment of shallow conditions and the construction of thick carbonate sequences. The tectonic setting of the Chios mélange and the Denizgiren Group of Karaburun are of vital importance to the testing of radically different models, which invoke accretionary processes above a south-dipping subduction zone (Baud *et al.*, 1991; Stampfli *et al.*, 1991) and disruption of a north-facing passive margin (Erdogan, 1990 & pers. comm., 1992), respectively. Several possible alternative origins of the mélange are discussed below.

8.6.1 Subduction-accretion setting

In this alternative, the Chios mélange unit could be interpreted as a Palaeotethyan accretionary complex and this hypothesis forms the basis of the models of Baud *et al.* (1991) and Stampfli *et al.* (1991). In this scenario the volcanic and limestone blocks would represent fragments of oceanic seamounts and the clastics would be trench-fill or trench-slope basins. The age of these "seamounts" (Silurian-Carboniferous), however, is considerably older than any equivalent sequences within the Karakaya Complex (c.f. the Mid Triassic seamount near Bergama). Their position to the south of the Karakaya Complex could indicate a general younging of the accretionary complex towards the north caused, for example, by a southward dipping subduction zone. However, despite the folding described in Section 8.3.2, the sandstone

sequences within the mélange are relatively little deformed, displaying perfectly preserved sedimentary structures and no evidence of low-grade metamorphism. This is in marked contrast to the Karakaya Complex in the Biga Peninsula, where most sedimentary structures have been obliterated by intense shearing, layer-parallel extension and recrystallization.

A further problem with the accretionary hypothesis is the fact that the Chios mélange matrix does not consist of predominantly deep-sea sediments. The clastic matrix predominantly comprises coarse terrigenous clastics which contain carbonaceous plant material and were clearly derived from a continental source. The limestone blocks are shallow-water and display evidence of subaerial exposure. The black cherts near Nagos are tectonic slivers and therefore do not necessarily represent matrix. It is possible that the mélange does not represent an "ideal" oceanic accretionary complex. An example of a "non-ideal" accretionary complex is the Upper Triassic-Jurassic Avdella Mélange in the Pindos Mountains of Greece. Jones & Robertson (1991) pointed out that the components of the mélange were mainly derived from marginal units rather than oceanic accretion. The early Tertiary Ermioni Complex in Argolis, southern Greece, is another example of an accretionary complex containing a large proportion of non-oceanic elements. During eastward-directed subduction of the Neotethyan Vardar Ocean, the passive margin of the Pelagonian microcontinent collided with the trench and lower-slope units became incorporated into the accretionary complex (Clift & Robertson, 1990).

8.6.2 Deformed passive margin/rift setting

Alternatively, the deep-water successions of chert, pelagic limestone and volcanics which characterize the base of the platforms may be interpreted as rift sequences. The Carboniferous Alandere Formation at the base of the Karaburun section may represent a fragment of rifted Gondwanan margin. This rifting event may have caused the shedding of the abundant Carboniferous and older limestone blocks now present in the Chios mélange. Huge volumes of clastics and volcanic blocks, which now form a large proportion of the Chios mélange were also shed off the margin. In this scenario, the volcanic blocks within the Chios mélange are unrelated to Triassic rifting as rift volcanics would be erupted within the rift rather than high on the margins. The volcanic blocks were thus derived from the rifted Palaeozoic basement, along with the clastics and Palaeozoic limestone blocks.

The Triassic platform is relatively undeformed, implying that most of the structures within the mélange were formed before the build-up of the Triassic platform. It is therefore possible that a "Neotethyan" passive margin sequence (i.e the Triassic sequences of Chios and Karaburun) built up on the deformed remants of an older, Palaeotethyan, passive margin (i.e. the Chios mélange and the Denizgiren Group on Karaburun). It is interesting to note that both the Alandere Formation and many of the limestone blocks in the Chios mélange display evidence of subaerial exposure. In the limestone blocks at Sgourou Nero, laterite cuts the limestone and surrounding limestone conglomerate, implying that subaerial exposure occurred during break-up of the limestone into blocks. A tentative explanation may be rift margin uplift, a major feature of many rift systems (e.g. the East African Rift System; Morgan, 1983). Subsequent erosion of the faulted rift flanks may have caused the shedding of large blocks of subaerially weathered limestone into the basin, along with clastics and volcanics. The resulting sedimentary mélange is now represented by the Chios mélange. Clastics eroded off the Gondwanan continental mass form a large proportion of the mélange components. Sedimentary structures are abundant and indicate southward-directed flow, parallel to the trend of the platform. Deep-water cherts, pelagic limestones and tuffs stratigraphically overlie the mélange and may reflect the establishment of deep conditions and the initiation of rift volcanism. This episode of pelagic sedimentation and rift volcanism is also represented on the Karaburun Peninsula by the Denizgiren Group.

The similarity of the Karaburun and Chios successions to many other well-documented Triassic rift-related sequences, also adds credence to this hypothesis. Good examples of well-preserved Eastern Mediterranean rift and passive margin sequences are found in mainland Greece and in the Antalya Complex, SW Turkey, as discussed briefly below.

8.7 Comparison of Chios and Karaburun with Triassic sequences in Greece and Antalya, SW Turkey

8.7.1 Pelagonian Zone, Greece

Rift-related units, very similar to the Chios and Karaburun sequences, are widely exposed in the Pelagonian Zone of southeast Greece (as reviewed by Robertson et al., 1991). For example, on Euboea in southeast Greece, thick successions of Mid Triassic andesitic volcanics are overlain by an Upper Triassic carbonate platform.

South of Euboea, andesites are depositionally overlain by pelagic limestones which pass up into calciturbidites and, finally, shallow-water carbonate platform facies. Near Beletsi, 20km north of Athens, a succession which passes up into Triassic dolomitic and megalodont-rich limestone was described by Clement (1977). As observed in the basal section of the Chios platform, Anisian limestone is overlain by red radiolarites, tuffs and sandstones. The tuffs and sandstones of both successions are overlain by Upper Triassic dolomitic limestones and, in the Beletsi sequence, an iron-rich nodular horizon. Similarly, on the Karaburun Peninsula, the volcanics and clastics of the Lower Triassic Denizgiren Group are gradationally overlain by Upper Anisian cherty limestones. The base of the overlying platform is Lower Ladinian in age and passes up into the Aptian-Albian with no break. The base of the platform is dolomitic, a feature also found in the Chios and Beletsi sections.

8.7.2 Antalya Complex, SW Turkey

The Triassic Chios and Karaburun platform sequences also display many features in common with the Antalya Complex in SW Turkey. In the Antalya region, Early-Mid Triassic rifting, followed by final break-up in the Late Triassic, formed a narrow ocean basin (e.g. Robertson, 1993; Robertson *et al.,* 1991). Late Triassic basalts were erupted in both the axial zones and along the rift margins and are now exposed in the Antalya region and around the margins of the "Isparta angle". The Triassic extrusives are associated with deep-sea radiolarites, hemipelagic *Halobia* limestones, turbiditic quartzose sandstones and patch reefs (Robertson & Waldron, 1990). In the northeast part of the Antalya area, Upper Triassic basalts are associated with proximal terrigenous sediments and platform-slope carbonates (Waldron, 1981). The sequence is overlain by massive, coralline limestones.

Many of the thick, Mesozoic, passive margin sequences in the Antalaya Complex can be closely correlated with the Chios and Karaburun carbonate platforms. For example, the Anamas Dag unit exhibits an intact Mesozoic succession which passes up from shallow-marine clastics into Upper Triassic dolomites and limestones. The platform is interrupted by the distinctive red clastic Cayir Formation (see Section 8.4.3) which is overlain by shallow-water Lower Jurassic limestones and, finally, Upper Cretaceous pelagic limestones (Robertson, 1993). Upper Triassic dolomitic limestones are also observed within the Chios and Karaburun successions. Red clastics form horizons within the Upper Triassic Karaburun platform and, as in the Anamas Dag succession, are overlain by shallow-water Liassic limestones.

8.8 Discussion

On the basis of the reconnaissance fieldwork carried out on the sequences of Chios and Karaburun it is not possible to make definite interpretations regarding their tectonic settings. However, tentative interpretations can be made and several features indicate that an accretionary origin is unlikely. The Palaeozoic age of the limestone blocks within the Chios mélange and the general lack of intense deformation may indicate that these blocks were derived from an established Palaeozoic margin, and, together with large volumes of coarse clastics, were transported into a rifted basin by mass wasting processes. Strike-slip activity is also possible mechanism for accumulating these thick clastic sequences. The rift-related sediments and volcanics were then overlain by a Triassic carbonate platform sequence. The apparent subduction component displayed by the volcanics is a feature that is common to many Triassic rift volcanics in the Eastern Mediterranean region (e.g. Bernoulli & Jenkyns, 1974; Robertson & Dixon, 1984; Robertson *et al.,* 1991) and the question of whether the Tethyan Triassic rifts were ultimately related to subduction zones needs a great deal of further investigation.

The rift and accretionary models both have problems as outlined above, and it is likely that a variety of processes contributed to the formation of the Chios mélange. In view of the predominantly sedimentary nature of the block-matrix contacts in the Chios mélange and the relatively undeformed nature of the clastic matrix, a rift-related setting seem more likely. However, the presence of sheared and boudinaged chert slivers near Nagos in the north of the island mean that accretionary processes, at least locally, cannot be ruled out.

8.9 Tectonic model

On the basis of the points outlined above, it is most likely that the Chios and Karaburun sequences developed in a rift setting, closely analogous to the well documented sequences further south in the Antalya Complex (e.g. Robertson, 1993). Within this framework, a rifted Gondwanan continental margin is the most likely explanation for the voluminous terrigenous clastics which dominate the Chios mélange. Normal faulting along this margin would have exposed many levels of continental basement, hence explaining the variety of Palaeozoic limestone blocks present within the mélange. The volcanic and chert blocks within the mélange were probably also derived from this Palaeozoic source. Similarly, on the Karaburun

Peninsula, the Denizgiren Group contains Carboniferous blocks derived from the underlying Alandere Formation which may represent a relict of a rifted Gondwanan block. Further rifting and deepening of the rift basin also led to extrusion of volcanics and the deposition of chert and pelagic limestone.

On the Karaburun Peninsula, the sediments and volcanics of the Denizgiren Group pass stratigraphically up into a Triassic carbonate platform, interpreted here as a passive margin carbonate sequence which built up directly over earlier rift facies. However, any overall tectonic model for the formation of the Karaburun and Chios sequences must also explain the fact that although the Triassic platform on Chios is relatively undeformed, shearing and box-folds do occur near Mesorachi, along the contact with the underlying mélange (Section 8.3.6). Despite this, a major tectonic contact is unlikely as the well-exposed road section at this locality displays an apparently stratigraphical, albeit sheared, contact between the mélange and the chert and tuff sequence at the base of the platform. A possible explanation for this, on Chios at least, may be large-scale gravity sliding of the Triassic platform over the debris flows, blocks and clastics of the underlying mélange. In this scenario, most deformation would have been taken up by the incoherent mélange and the immediately adjacent platform, in a relatively diffuse zone. The mobility of the mélange would not facilitate the formation of a sharp tectonic decollement. Box-folding within the overlying Triassic limestone may have been caused by a later tectonic event which reactivated the old gravity slide zone.

The clear stratigraphical correlation of Chios and Karaburun with sequences in the Antalya Complex and Greece suggests that they all originally formed elements within the same southern Neotethyan mosaic of carbonate platforms and rifted basins. The poorly understood Menderes Massif, which separates Karaburun and Chios from the Lycian Nappes and the Antalya Complex, is a metamorphic core complex (Verge, 1993) which may represent a relatively young structure generated by collision-induced crustal thickening (Sengör *et al.,* 1984).

CHAPTER 9

PALAEOMAGNETIC STUDY OF THE BILECIK LIMESTONE

9.1 Introduction

Palaeomagnetism is one of the most powerful tools for deciphering the motion histories of fault-bounded regions as it can be used to detect both latitudinal motions and vertical-axis rotations. Palaeomagnetic studies have thus proved invaluable in unravelling the complex tectonic histories of numerous tectonostratigraphic terranes. It was therefore intriguing to see whether a palaeomagnetic study on rocks from NW Turkey could provide a better understanding of the Karakaya Complex and of the evolution of the Tethyan realm as a whole. Field structural studies usually only provide information about relative horizontal crustal movements such as thrusting, since vertical-axis rotations are often not apparent in the field. Hence, without knowing if such rotations have occurred, the structures within the Karakaya Complex tell us little about the original direction of thrusting. Tectonic rotations which occurred *after* formation of the Karakaya Complex would have rotated all the original structures, hence leading to spurious interpretations regarding the tectonic evolution of NW Turkey.

As described in Chapter 5 the Lower-Middle Jurassic Bilecik Limestone forms a cap over the deformed Karakaya Complex in the Biga Peninsula and regions to the east. Owing to a general lack of deformation and the well-bedded, micritic nature of the limestone, the unit was considered potentially suitable for a palaeomagnetic study. With this in mind, a few pilot samples were collected during the field season of 1991. Measurements made on two of these samples in Edinburgh indicated that the lithology was suitable for palaeomagnetic measurements and that they appeared to have undergone a significant amount of anticlockwise rotation. In the light of this, further palaeomagnetic sampling was carried out the following year with Dr. E. Platzman from the Department of Earth Sciences, Oxford University. The aim was to deduce the position of this region of Turkey during deposition of the Bilecik Limestone in the Jurassic, and also to measure and hopefully constrain any tectonic rotations which may have occurred in this region since that time. Any rotations found to have affected the Bilecik Limestone will necessarily have affected the underlying Karakaya Complex, thus allowing a more accurate interpretation of the present-day structural trends within the complex.

Sampling of the Bilecik limestone was carried out in conjunction with an extensive sampling programme by E. Platzman of the Tertiary volcanic rocks in NW Turkey. Sample measurement and data analysis were carried out at the Department of Earth Sciences, Oxford University with the permission and help of Drs E. McClelland and E. Platzman respectively. In this chapter, the results of this study and their implications for the tectonic evolution of the Karakaya Complex are discussed, after a brief introduction to the origin and analysis of magnetization in rocks.

9.2 Introduction to natural remanent magnetization (NRM)

9.2.1 NRM

The magnetism present in a rock is known as the natural remanent magnetization (NRM). It is commonly composed of at least two components; a primary NRM acquired during the formation of the rock and secondary magnetization(s) acquired during subsequent thermal and tectonic events. Most palaeomagnetic investigations are concerned with the separation and interpretation of these magnetic components. The primary magnetization is often referred to as the characteristic remanent magnetization (ChRM). A primary NRM acquired by igneous rocks when they cool through the blocking temperatures of constituent magnetic minerals is described as a thermo-remanent magnetization (TRM). The magnetization acquired as a result of chemical change (e.g. formation of ferromagnetic minerals by weathering or precipitation) is called chemical remanent magnetization (CRM). Grains possessing a primary TRM or CRM may become involved in sedimentation and will tend to become aligned with the ambient geomagnetic field whilst the sediment is unconsolidated. Subsequent compaction and lithification will "freeze" this direction into the rock as a detrital remanent magnetization (DRM). Rocks may also acquire an unstable secondary magnetization called a viscous remanent magnetization (VRM) as a result of being exposed to the small, ambient magnetic field of the Earth. Unstable magnetizations adjust themselves to each new ambient field after geologically short time periods. The typical period over which this realignment takes place is related to what is known as the relaxation time of a magnetization. Magnetizations with short relaxation times of seconds to millions of years (i.e. VRMs) are very common and owing to their instability are usually found in directions parallel to the present-day geomagnetic field. The relaxation time for stable magnetizations may be greater than several billions of years.

9.2.2 Demagnetization of NRM

In order to recognize the presence of primary and secondary magnetic components in a rock, "cleaning" or demagnetization techniques must be applied to isolate and determine these components. These methods serve to gradually eliminate the magnetizations with lowest relaxation times and leave those with long relaxation times which are most likely to contain the bulk of the primary remanence. Demagnetization techniques depend on the rock type being analyzed and include chemical leaching, heating in an oven (thermal demagnetization) and the application of alternating fields (AF demagnetization).

Thermal demagnetization was the principal demagnetization method used in this study. This technique involves heating a specimen to an elevated temperature T and then cooling it to room temperature in a zero magnetic field. This causes the grains with a blocking temperature (temperature at which magnetization is frozen into a grain) less than or equal to T to lose their NRM. In effect, the magnetization of these grains is randomized. Successive steps of thermal demagnetization treatment remove the different components of remanent magnetizations.

The results of the progressive thermal demagnetization process is a set of measurements of NRM remaining after increasing temperature levels. Progressive changes in the direction and magnitude of the NRM are best shown on vector component diagrams. The sequence of NRM declinations and inclinations are projected onto horizontal and vertical planes respectively which are then combined to give a single vector component diagram or Zijderveld plot. In such diagrams the base of the NRM vector is placed at the origin and the tip of the vector is projected onto two orthogonal planes. The intensity of each NRM vector is proportional to the distance of each data point from the origin.

9.3 Magnetic mineralogy of marine limestones

A detailed review by Lowrie & Heller (1982) of the magnetic properties and mineralogy of marine limestones forms the basis for the following summary. The most common carriers of remanence magnetization in limestones are the ferromagnetic minerals, magnetite, hematite and goethite.

a) Magnetite

The primary remanence in many limestones is a postdepositional remanence (pDRM) carried by detrital magnetite, although biogenic magnetite can also be important. The study of magnetite grains extracted from modern carbonate sediments suggests that terrigenous detritus is the most important source for magnetite in limestones. The orientation of grain magnetic moments by the ambient magnetic field should result in a depositional remanent magnetization (DRM). However, Keen (1963) found that bioturbation destroys most DRM in modern deep-sea sediment and discovered that the remanence directions of soft sediment slumps has commonly been reset, thus explaining pDRM acquisition in limestones.

b) Hematite

By contrast, most hematite in limestones is thought to be diagenetic rather than detrital and its remanence is thus a CRM. The characteristic Mesozoic pink and red limestones of the Tethyan realm (e.g. *Scaglia Rossa* and *Ammonitico Rosso* facies) contain pigmental hematite which probably formed as an early diagenetic product of directly precipitated goethite (Lowrie & Heller, 1963). It has been established that hematite can form from a goethite precursor at a very late stage of diagenesis in which limestones have been exposed to surface weathering in a subtropical climate (Heller, 1978b). Heating to 450-650°C causes reduction of hematite and the subsequent formation of new magnetite which acquires unwanted VRMs.

c) Goethite

Goethite is also a common magnetic mineral in limestones. It can be precipitated directly from seawater or be produced by pyrite alteration. The alteration of pyrite may be diagenetic or the result of subaerial weathering. Goethite rapidly dehydrates to hematite if heated above 300°C and thus leads to problems in isolating primary DRM carried by magnetite.

9.4 Introduction to isothermal remanent magnetization (IRM)

The acquisition of isothermal remanent magnetization (IRM) is used to identify and distinguish between the magnetic carriers described above. This method is based on the fact that the common ferromagnetic minerals have distinctive, characteristic coercivities and thermomagnetic properties (Lowrie, 1990). Coercivity is a measure of the resistance of the domain structure to changes in magnetic field and can usually be thought of as the magnetic field required to demagnetize a magnetization. IRM is

induced by exposing a sample to a magnetizing field. The resulting IRM is measured and the procedure is repeated using progressively higher magnetizing fields until saturation is reached. The rate of acquisition of IRM can provide an effective measure of the coercivity spectrum of the magnetic mineralogy of the sample and thus is a useful diagnostic technique. For example, magnetite usually saturates at <150mT while hematite requires fields from 200mT (specular hematite) to 2T or more (pigmentary hematite). For more conclusive interpretations this method is combined with studies of the temperature dependence of IRM which involve destruction of the IRM by thermal demagnetization.

9.5 Geological setting of the sampling sites

9.5.1 Kocaçal Tepe (sites BJ01-BJ03)

Sites BJ01, BJ02 and BJ03 are all situated within gorges which cut through Kocaçal Tepe, a hill entirely composed of Middle-Upper Jurassic Bilecik Limestone (see Chapter 5) near the village of Sarniç in the Havran region (Figures 9.1 and 9.2). Around the edges of the western and northern flanks of Kocaçal Tepe the limestone stratigraphically overlies clastic rocks of the Upper Triassic-Lower Jurassic Halilar Formation. The contact is poorly exposed but appears to be conformable or near conformable. The southern and eastern margins of Kocaçal Tepe are characterized by onlapping Oligo-Miocene volcanic rocks and Quaternary-Recent alluvium. The volcanic sequences comprise the Bagburun and Hallaçlar Formations which predominantly consist of dacites and andesites. The volcanics infill the valleys of a pre-Oligo-Miocene topography which existed in the Upper Triassic to Jurassic sequence. Limestone adjacent to the volcanics is commonly entirely silicified. Despite its extensive distribution on the hills of the Havran region the Bilecik Limestone is commonly recrystallized, poorly exposed and displays little or no bedding. The deeply incised gorges of Kocaçal Tepe, however, contain excellent outcrops of well-bedded, micritic limestone and were thus chosen as potentially good sites for palaeomagnetic sampling. These two gorges cut through the eastern and southern parts of Kocaçal Tepe. Site BJ01 is situated at the northern end of the N-S trending gorge, close to the base of the Bilecik Limestone, while BJ02 and BJ03 lie in the E-W trending gorge to the south (Figure 9.3).

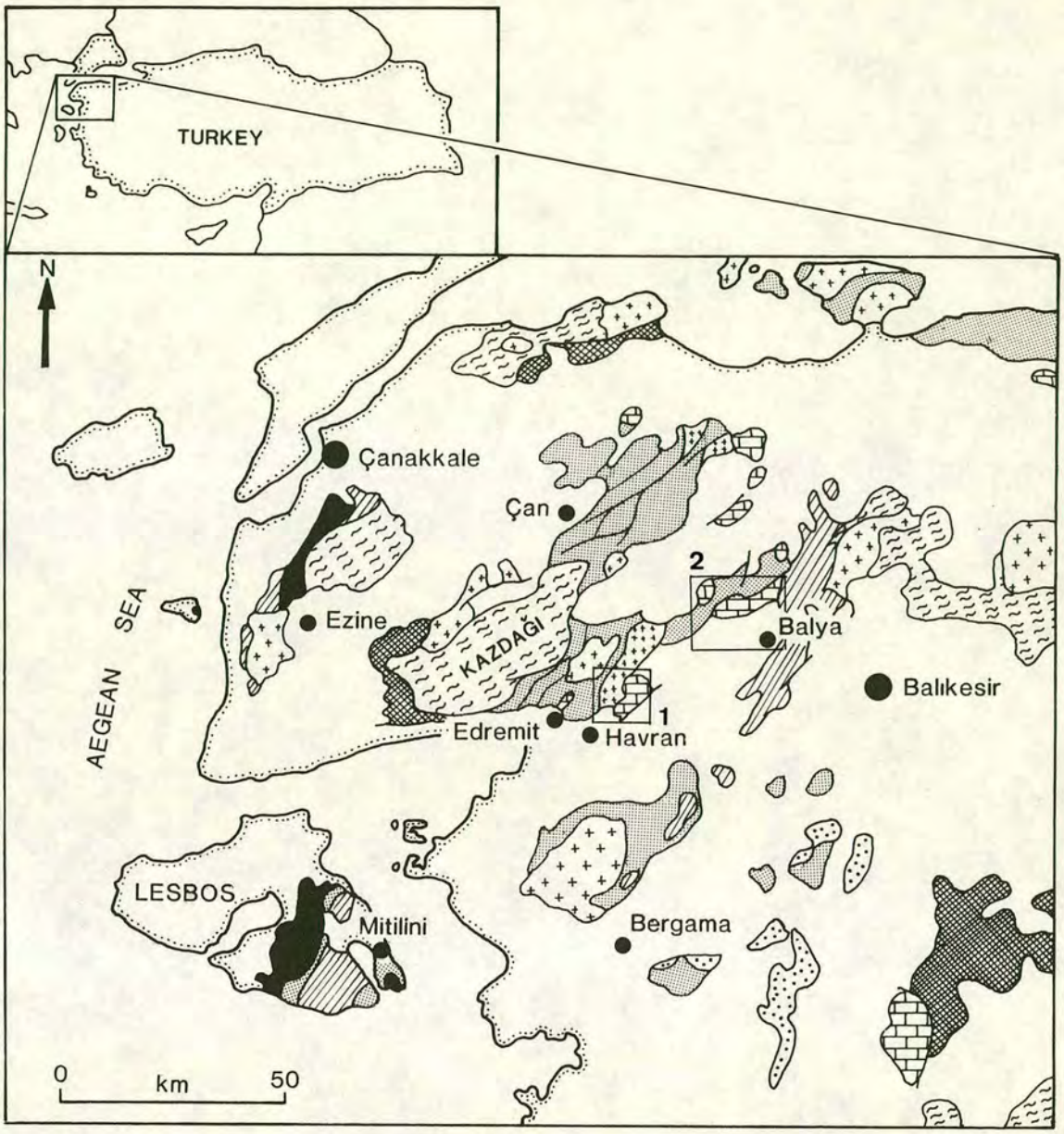

Figure 9.1 Generalized geological map of the Biga Peninsula and surrounding regions. Boxes 1 and 2 mark the locations of palaeomagnetic sampling. Geological maps of these areas are shown in more detail in Figures 9.2 and 9.4.

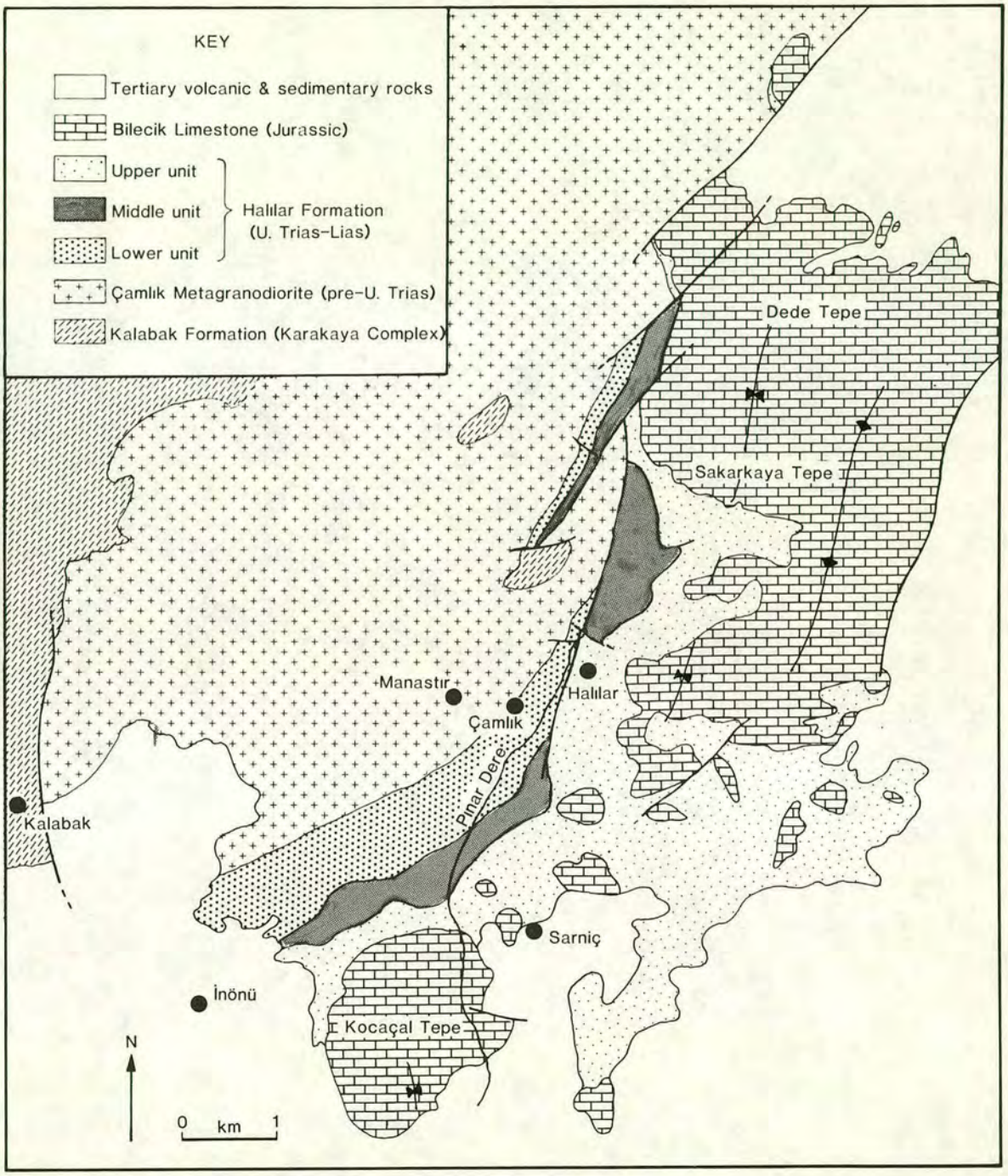

Figure 9.2 Geological map of the Kocaçal Tepe region (box 1 in Figure 9.1).

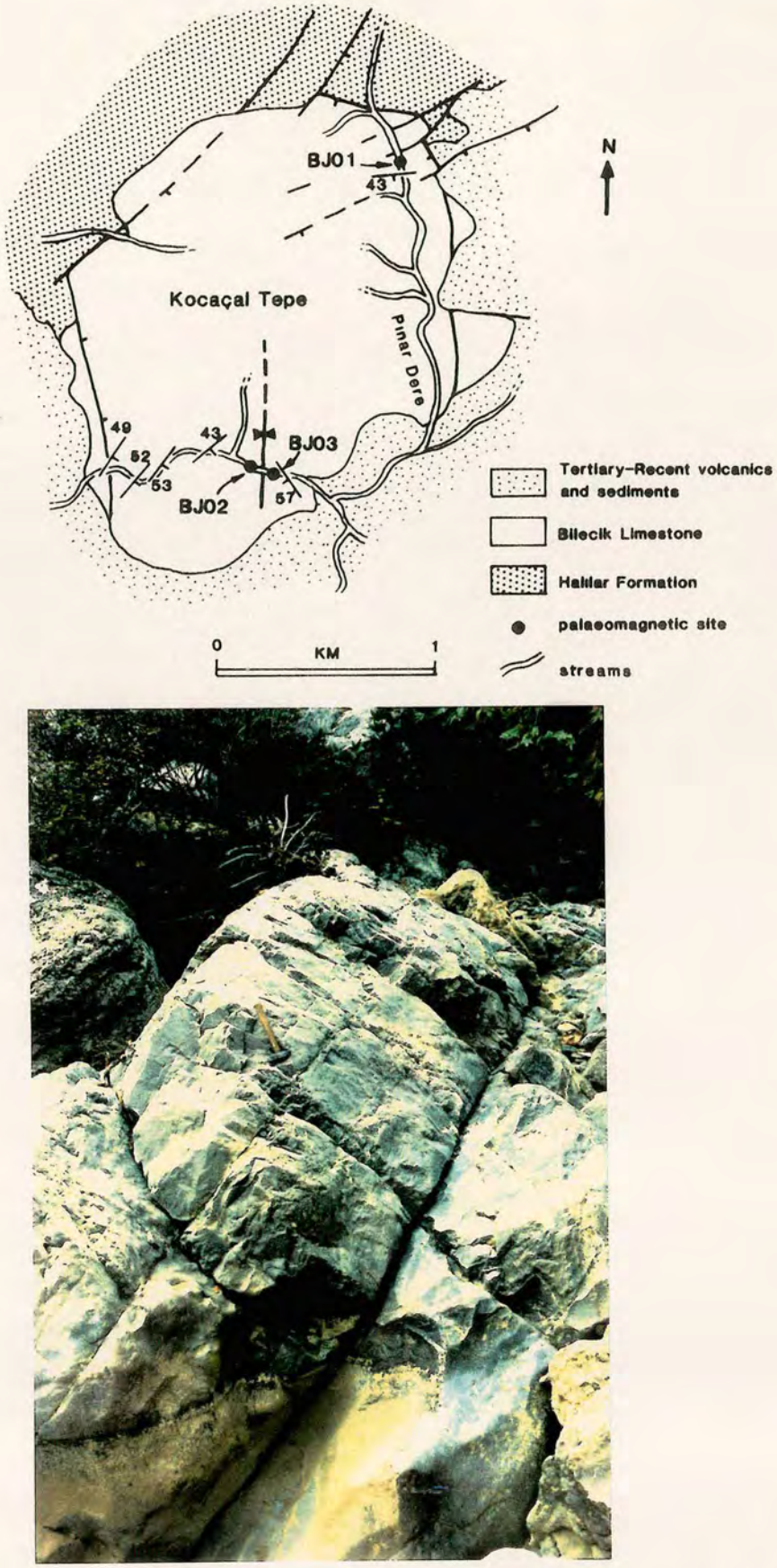

Figure 9.3 Map of Kocaçal Tepe, showing the palaeomagnetic sites BJ01, BJ02 and BJ03. The photograph shows bedded micritic limestone at site BJ01 (looking W).

a) Site BJ01

Site BJ01 is characterized by well-bedded limestone with beds up to 0.75m thick. The limestone is fossiliferous, micritic and pale pink to grey in colour. The well-bedded micrite of site BJ01 is shown in the field view in Figure 9.3. Ammonites and diagenetic nodular textures are common features of the limestone at this site. The limestone beds dip SW at approximately 25°-50°. A slight but abrupt change in bedding strike within the area of the sampling is probably due to localized fracturing or minor faulting. No folding was apparent.

b) Sites BJ02 and BJ03

Sites BJ02 and BJ03 are located on the limbs of a shallow syncline in the gorge which runs through the southern part of Kocaçal Tepe, as shown in Figure 9.3. The limestone is well-bedded and micritic. It forms beds up to 20cm thick and is uniformly pale to mid-grey. It does not show the pink coloration of the limestone at BJ01, nor does it contain ammonites or nodular horizons. The positions of the sites were chosen with the aim of applying a fold test of palaeomagnetic stability. The two sites are situated 100-150m apart, on the western (BJ02) and eastern (BJ03) limbs of the syncline. The fold is open and has a wavelength of approximately 200m. The fold axis runs approximately N-S and the beds of BJ03 and BJ02 dip SE and SW respectively. The direction of the fold axis reflects the trends of other folds in the Havran region, as mapped by Gümüs (1964) and Krushensky *et al.* (1980). Gümüs (1964) mapped folds with a wavelength of up to 2000m and NNE-SSW trending fold axes in the Bilecik Limestone of Sakarkaya Tepe and Dede Tepe, approximately 6km NE of Kocaçal Tepe (as shown in Figure 9.2). The folds do not affect the surrounding Oligo-Miocene volcanics. A 1:50 000 map of this region by Krushensky *et al.* (1980) also shows that the folding in the Bilecik Limestone and the underlying Halilar Formation does not affect the volcanic sequence, thereby constraining the age of the folding to between the Early Jurassic and the Oligo-Miocene.

9.5.2 Balya-Çan road (sites BJ04-BJ06)

Sites BJ04, BJ05 and BJ06 are located in an area of patchily-exposed Bilecik Limestone, surrounded by Oligo-Miocene volcanic rocks, along the main road between Balya and Çan (Figures 9.1 and 9.4). In this region the limestone is generally very poorly exposed except for a few well-bedded outcrops near the villages of Alincik and Pinaroba. These outcrops were chosen as sampling sites because of their easy accessibility and well-preserved bedding planes. They are, however, slightly

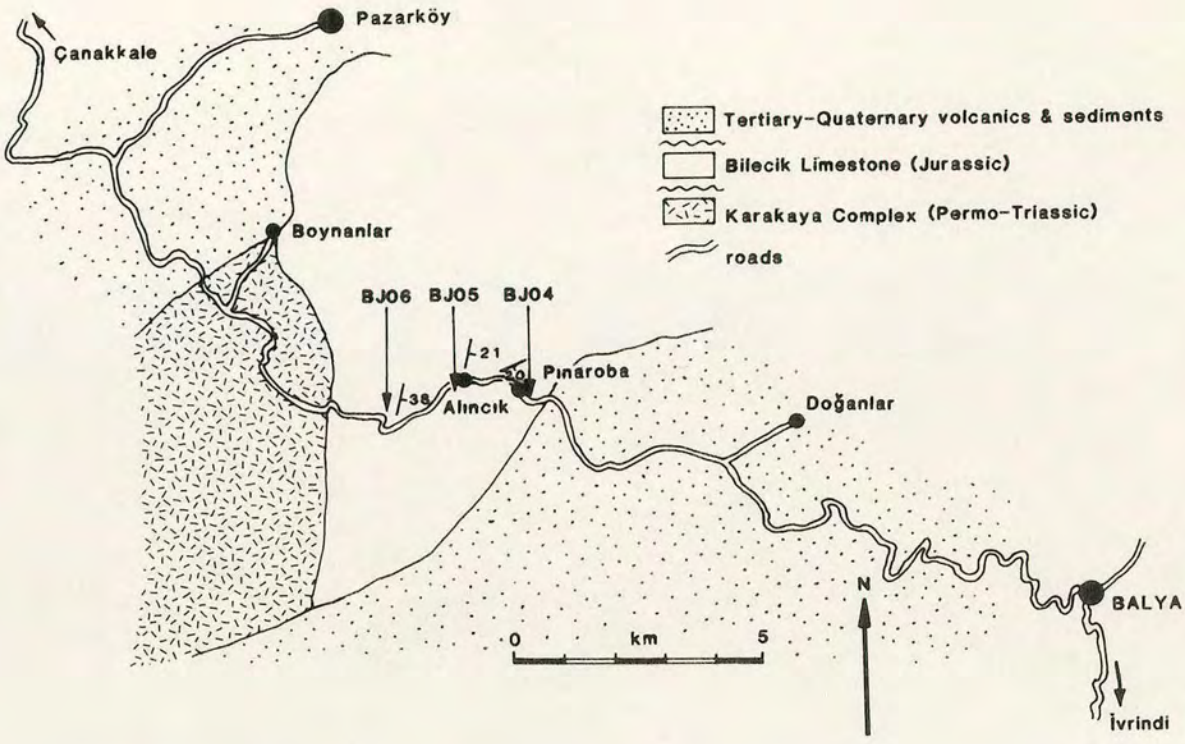

Figure 9.4 Map of the area NW of Balya (box 2 in Figure 9.1), showing the positions of palaeomagnetic sites BJ04, BJ05 and BJ06. The sampling site BJ05 is shown in the photograph (looking S).

more recrystallized than those at Kocaçal Tepe, a feature which is reflected in the generally poorer quality of the palaeomagnetic data from these sites compared to the data from the Kocaçal Tepe sites. The structural control on these sites is very poorly constrained, owing to a lack of continuous outcrop and the unavailability of detailed geological maps.

a) Site BJ04

Site BJ04 is located on the SE edge of the village of Pinaroba along the road between Balya and Çan (Figure 9.4). The limestone is slightly recrystallized, and is grey to beige in colour. Thin seams of orange-brown Fe oxides were observed in some samples. Beds are up to 0.5m thick and are gently warped. An open anticline with a poorly defined fold axis trending approximately E-W, was observed. Samples were taken from both limbs of the fold with the aim of applying a fold test.

b) Site BJ05

Site BJ05 is located on a small crag to the south of the main road just outside the village of Alincik, 2km west along the road from site BJ04. Pale grey, micritic limestone forms well-preserved beds up to 20cm thick. Slight recrystallization was observed in places. Bedding dips gently to the east. No folding was observed.

c) Site BJ06

Site BJ06 is situated further west along the Balya-Çan road from site BJ05. The limestone is very similar to that at site BJ05 and forms beds up to 20cm thick. Bedding dips moderately to the SE and no folding was observed.

9.6 Sampling

A suite of limestone samples was collected from the sites described above. Standard drilling, orientation and collection techniques were employed as outlined in Appendix 5. Samples were collected from a total of 6 sites, only 5 of which yielded viable palaeomagnetic results (BJ04 results were discarded). Sampling was carried out in sites where recrystallization of the limestone appeared to be at a minimum and also where bedding was clearly discernible. Visibly weathered and karstified exposures were avoided. Samples were only collected when an accurate bedding tilt correction could be defined. Sites BJ01, BJ02, BJ03 and BJ04 were sampled by drilling, whereas sites BJ05 and BJ06 were sampled by hammer and chisel. Between 6 and 14

independent cores were collected from sites BJ01 to BJ04, and 6 and 4 large orientated hand specimens were taken from sites BJ05 and BJ06 respectively.

9.7 NRMs and demagnetization results

The NRMs of all the samples, including sub-samples from single cores, were measured on the Oxford Earth Sciences Department two-axis cryogenic CCL magnetometer. Some samples displayed extremely weak magnetizations (e.g. 0.03-0.04mA/m in samples from sites BJ03 and BJ04) which, on demagnetizing, were soon below the detection limit of the magnetometer (approximately 0.01mA/m). Many of these samples were discarded at this point. The selected samples were divided into 3 batches for demagnetization. Initially, both thermal and alternating field demagnetization techniques were tried as different rocks commonly respond better to one or other of these two methods. It was found that AF demagnetization did not fully isolate the components of magnetization and therefore thermal demagnetization was the principal method employed in this study.

Figures 9.5 to 9.11 show typical Zijderveld plots (in geographic coordinates) for thermally demagnetized samples from the Bilecik Limestone sites. Solid data points indicate projection onto the horizontal plane (i.e. declination) and open data points indicate projection onto the E-W orientated vertical plane (i.e. inclination). Selected temperatures used in the thermal demagnetization process are shown along the declination trace. Also shown on the diagrams are plots of normalized NRM intensity versus temperature which give a clearer idea of the changes in NRM magnitude with increasing temperature. Data are also shown on Wulff nets which provide another method for displaying and analyzing the changes in magnetization direction. Ideally, a single component of remanence plots at one point and points making up great circles record the changing from one vector component to another.

9.7.1 Site BJ01

Samples from site BJ01 yielded NRMs in the range 0.2-1mA/m and generally responded very well to thermal demagnetization. Although the magnetic intensity of a few samples had dropped to about 0.01mA/m (the magnetometer detection limit) by 450°C, most samples did not lose their NRM until 550°C-600°C or above. Most of the Zijderveld plots are characterized by well-defined, two-component vectors displaying a low-temperature component which reflects the present-day magnetic field

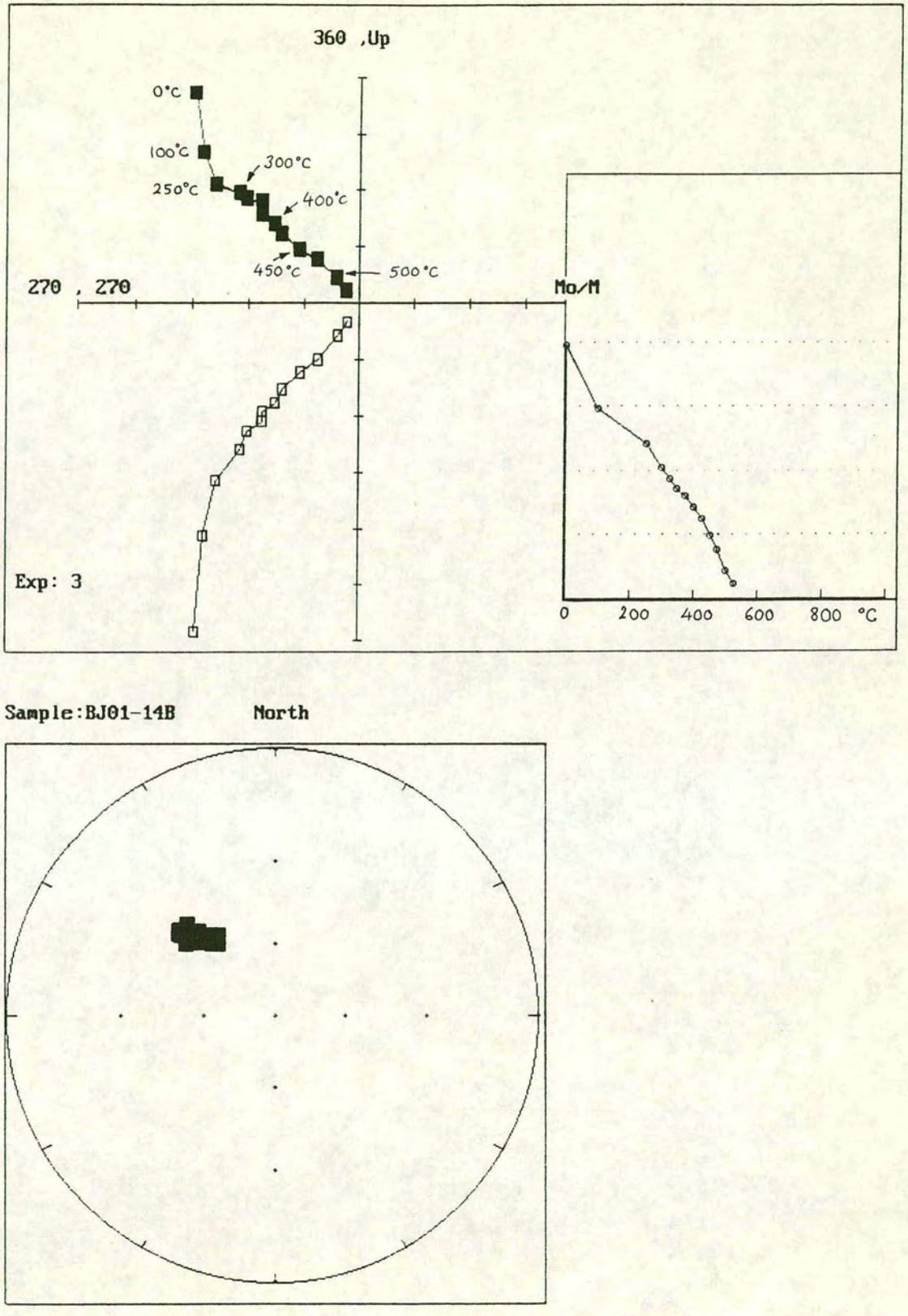

Figure 9.5 Zijderveld plot and Wulff net (in geographic coordinates) for sample BJ01-14B. The inset plot shows the changes in NRM intensity with increasing temperature.

(i.e. north-directed) and a second, higher temperature component (here referred to as the characteristic vector) with a consistent direction from the NW to the origin. A typical example is shown in Figure 9.5 with the characteristic vector clearly defined on the Wulff net.

9.7.2 Site BJ02

Samples from site BJ02 had initial NRMs which ranged from 0.2 to 0.6mA/m. During thermal demagnetization the samples lost most of their magnetic intensity between 400 and 425°C or between 500 and 575°C. The magnetization components of samples from BJ02 are generally less well-defined than those from BJ01, although their directions are very similar. Figure 9.6 is a typical plot, showing three components of remanent magnetization; the present-day field, the "characteristic" vector observed in BJ01 samples, and also a poorly defined higher temperature component (becoming apparent in the temperature range 475-575°C) which is shown in the enlarged plot (b). This higher temperature component is attempting to decay to the origin from the opposite direction, i.e. the SE rather than the NW and probably had the opposite polarity to the lower temperature vectors. Unfortunately this more primary vector is difficult to define.

9.7.3 Site BJ03

Samples from site BJ03 had initial NRMs which ranged from 0.04 to 0.3mA/m. The magnetic intensities measured during the thermal demagnetization process were much weaker than those from sites BJ01 and BJ02. As a result most of the samples had lost their NRMs by 300 to 400°C. Vectors obtained for these samples are less well defined than those of BJ02, probably owing to fewer magnetic minerals or possibly to the more recrystallized nature of the limestone. Vectors similar to the characteristic BJ01 and BJ02 vectors were identified, along with a higher temperature component. The sample in Figure 9.7 displays a curved trace which probably reflects overlap in the unblocking temperature spectra of the characteristic and present-day field components. On magnifying the area around the origin, it can be seen that the trace passes the origin, turns and tries to approach the origin from the opposite direction, thus indicating the presence of a higher temperature component (in the approximate range 400-550°C) (Figure 9.8). As with the poorly defined, high temperature vector shown in Figure 9.6, this vector is also very difficult to isolate.

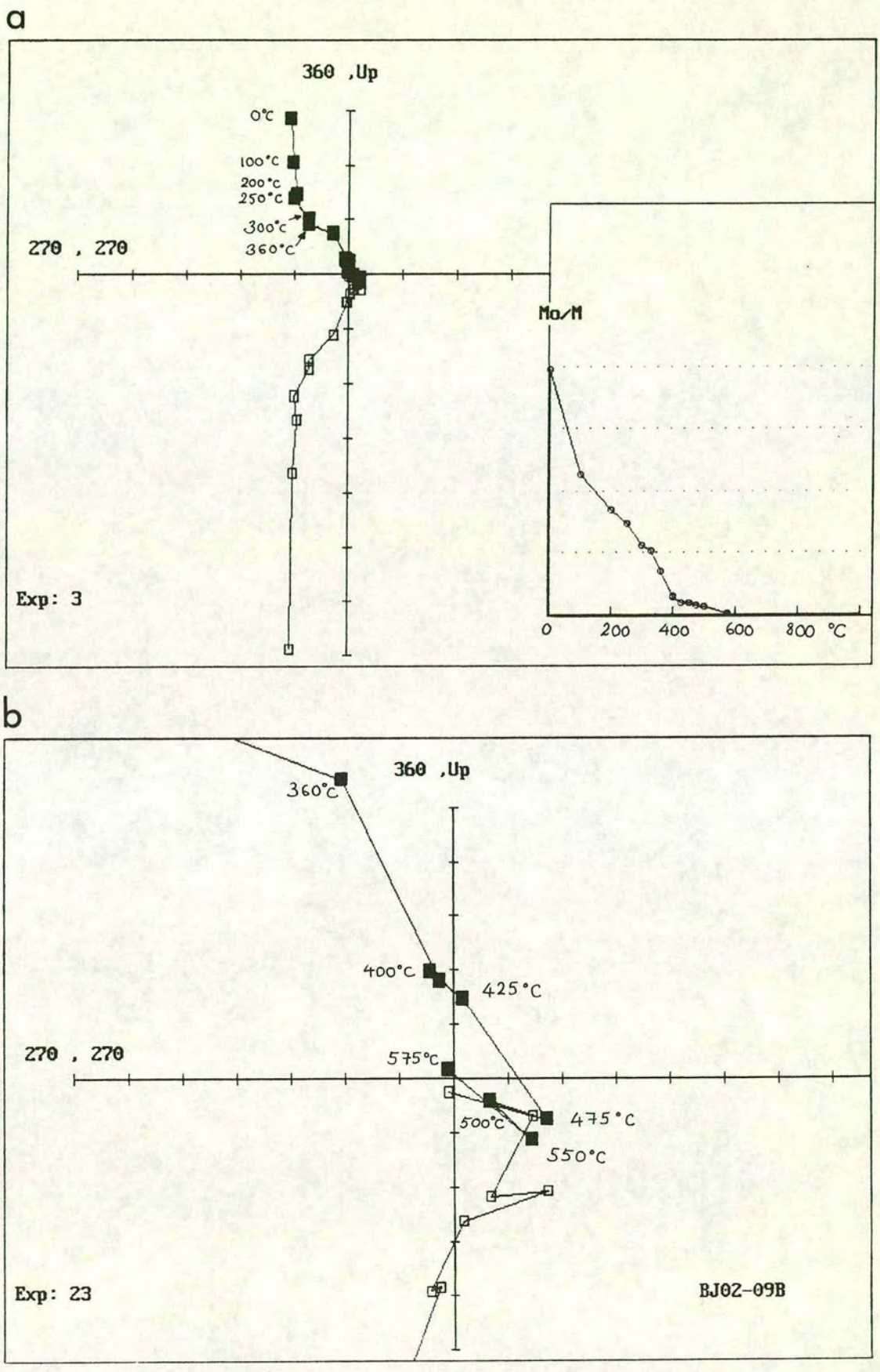

Figure 9.6 Zijderveld plots (in geographic coordinates) for sample BJ02-09B. Plot (b) is a magnified view of the region around the origin in plot (a), showing the poorly defined higher temperature component (approximately 475°C to 575°C).

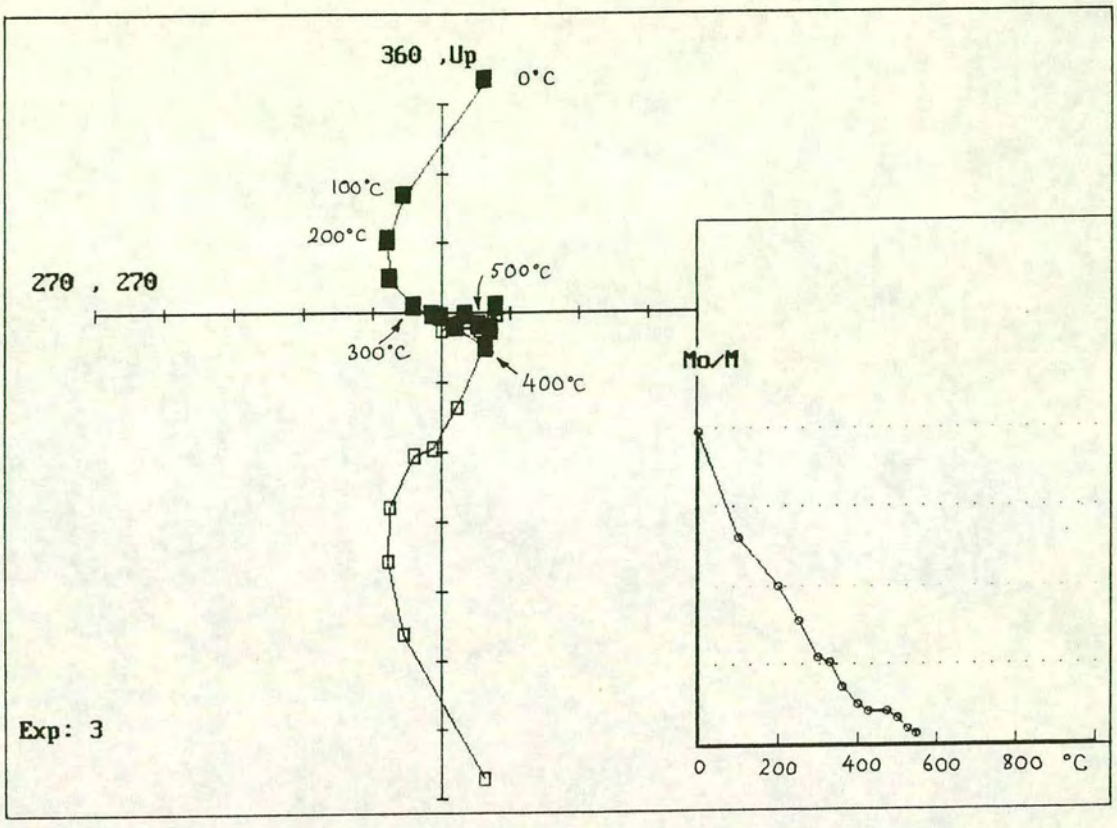

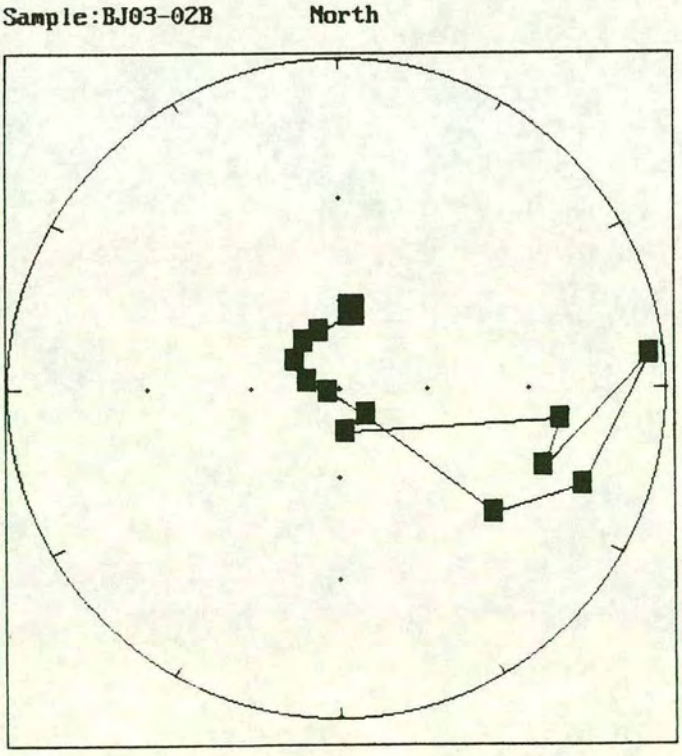

Figure 9.7 Zijderveld plot and Wulff net (in geographic coordinates) for sample BJ03-02B. The curved trace may indicate overlap in the unblocking temperature spectra of the characteristic and present-day components.

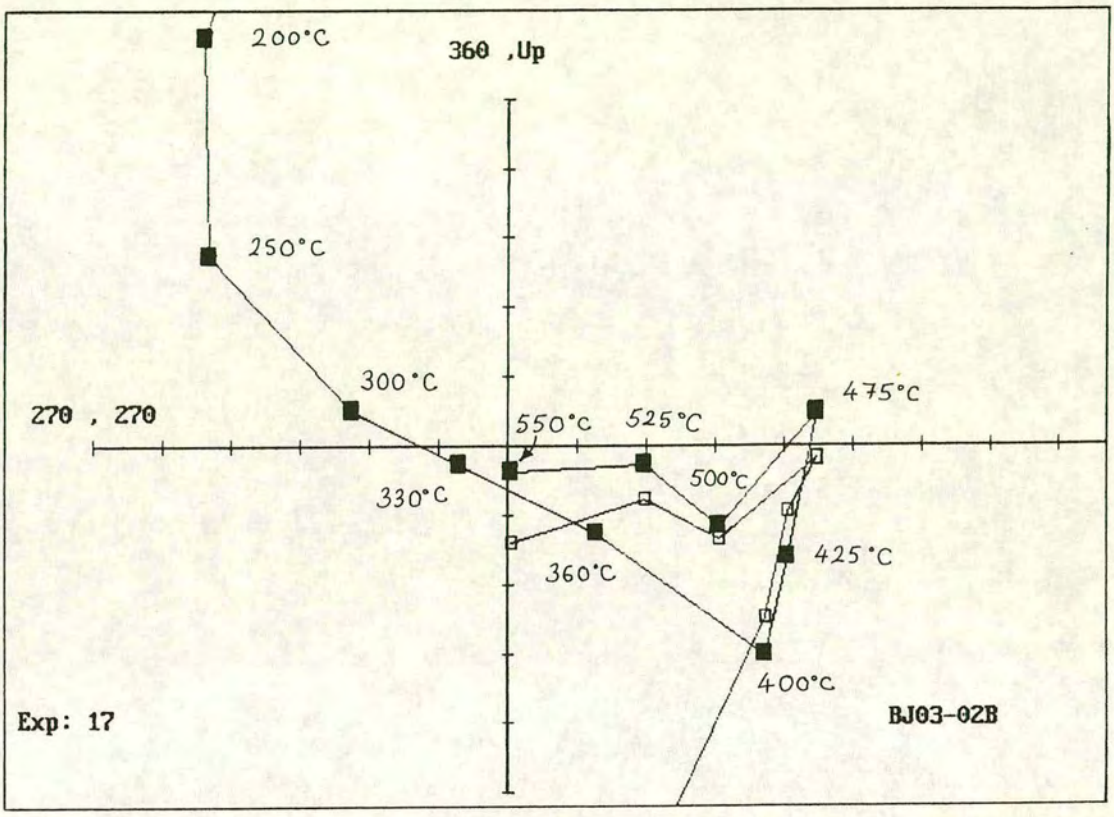

Figure 9.8 A magnified view of the area around the origin of the plot in Figure 9.7, showing the poorly defined higher temperature component (approximately 400° C to 550°C) which is difficult to isolate.

9.7.4 Site BJ04

The initial NRMs of samples from site BJ04 (0.03 to 0.7mA/m) were obliterated after just a few thermal demagnetization steps. The NRMs of most samples were reduced to 0.01mA/m or less on reaching 300-400°C. Apart from two samples which gave similar vectors to those from the BJ01-BJ03 sites, the rest gave Zijderveld plots which were either undecipherable or displayed only the present-day field (Figure 9.9). The results from this site were not used in any further analysis owing to their poor quality and unreliability.

9.7.5 Site BJ05

Samples from site BJ05 yielded relatively high NRMs (1.7-6mA/m). However, magnetic intensities were reduced to 0.01mA/m or less on reaching the temperature range 450-550°C. Many of the Zijderveld plots from this site yield unusual two-component patterns (three-components if present-day field is counted), as shown in the magnified plot and Wulff net in Figure 9.10. The higher temperature component is similar to the characteristic vector of sites BJ01-BJ03 and, in a few of the BJ05 plots, is the only distinguishable vector. The lower temperature vector trends in the opposite direction to the "characteristic" vector and sharply separates the higher temperature vector from the ubiquitous present-day field component.

9.7.6 Site BJ06

Samples from this site gave relatively high initial NRM values of 0.3-3mA/m which were not obliterated until over 550°C in most cases. However, the Zijderveld plots yielded generally relatively poor palaeomagnetic data from which very few good vectors could be picked out. Howver, one Zijderveld plot (Figure 9.11) shows a similar pattern to those from BJ05, in that it comprises the characteristic vector of the other sites (isolated between 425 and 500°C) and also a lower temperature vector (300-400°C) which has an opposite direction from the characteristic component. In most cases however, a strong present-day field vector tends to obliterate most features.

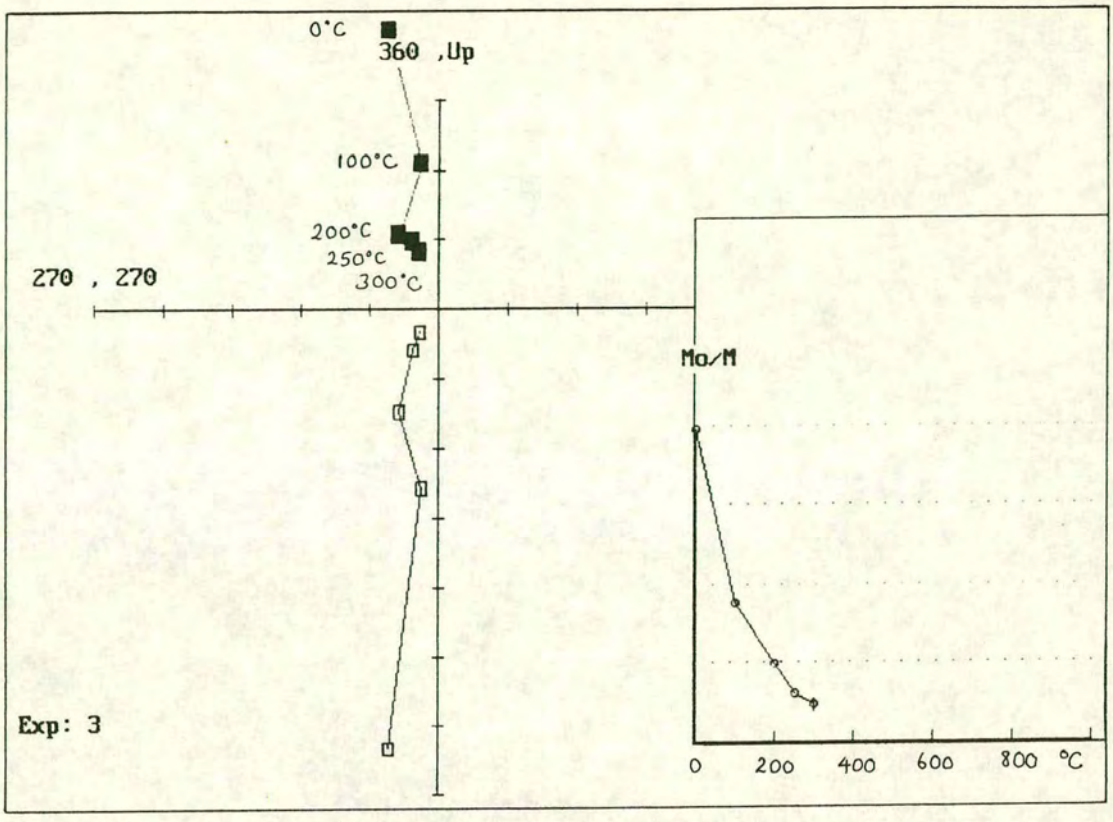

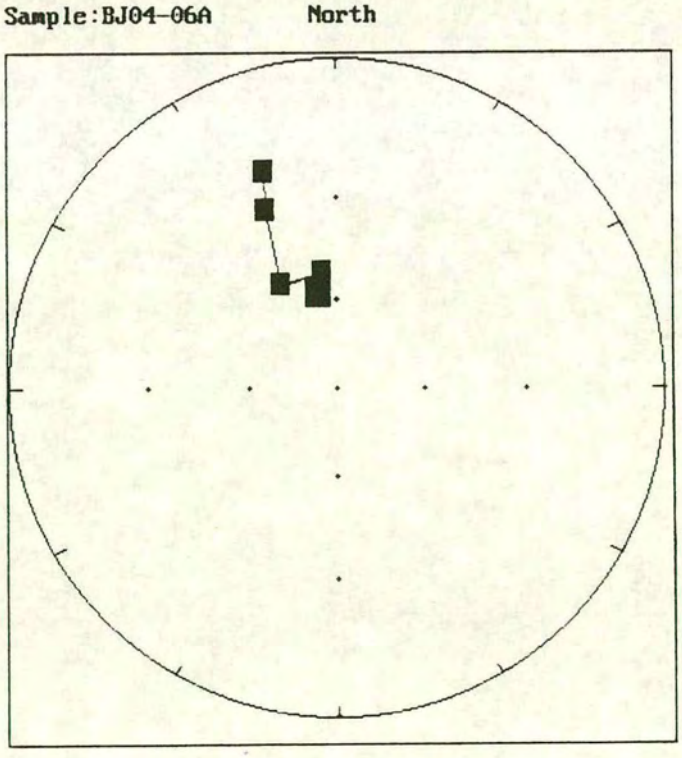

Figure 9.9 Zijderveld plot and Wulff net for sample BJ04-06A (in geographic coordinates) showing a predominantly present-day field (i.e. north-directed).

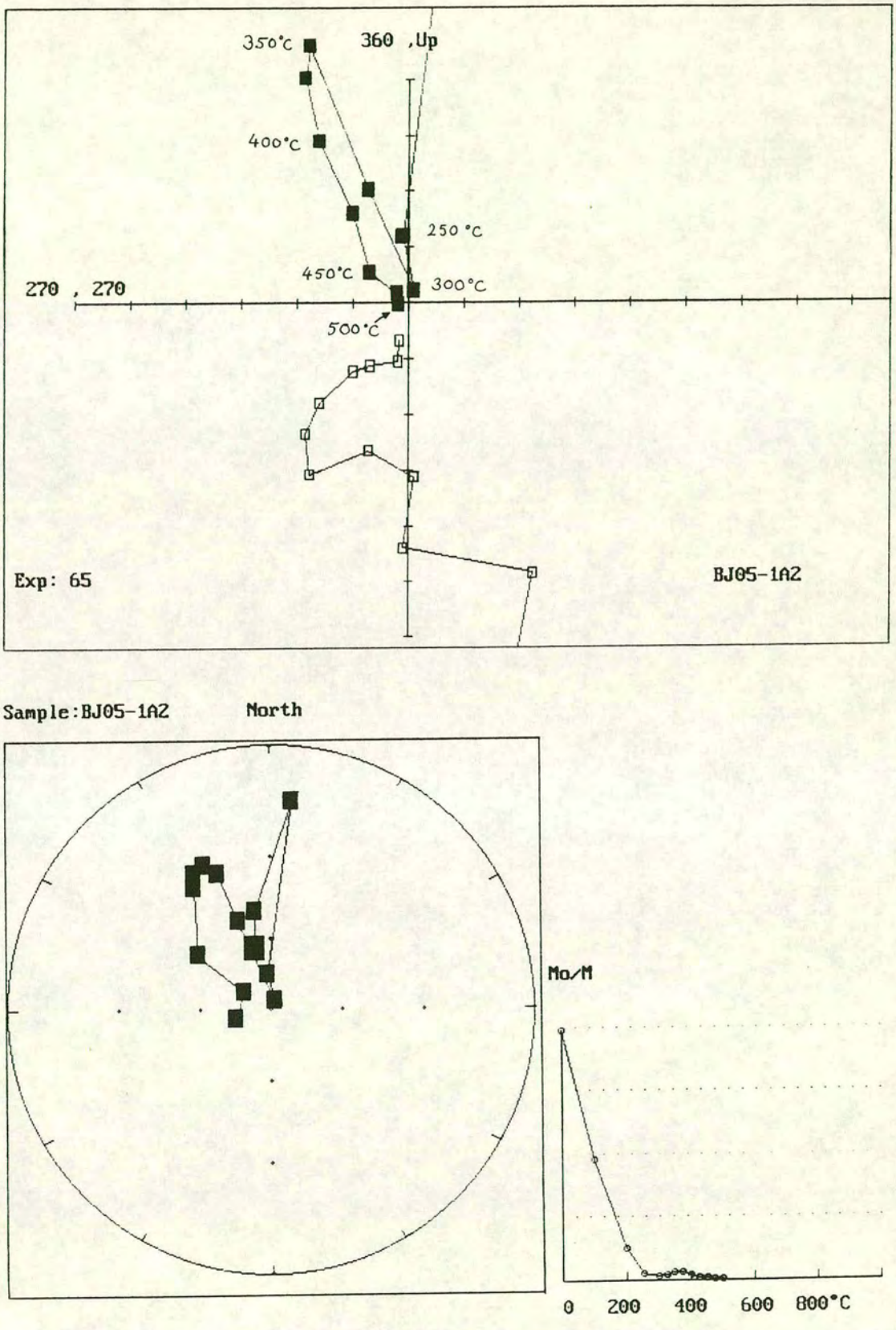

Figure 9.10 Magnified Zijderveld plot and Wulff net (in geographic coordinates) for sample BJ05-1A2, showing three components of magnetization.

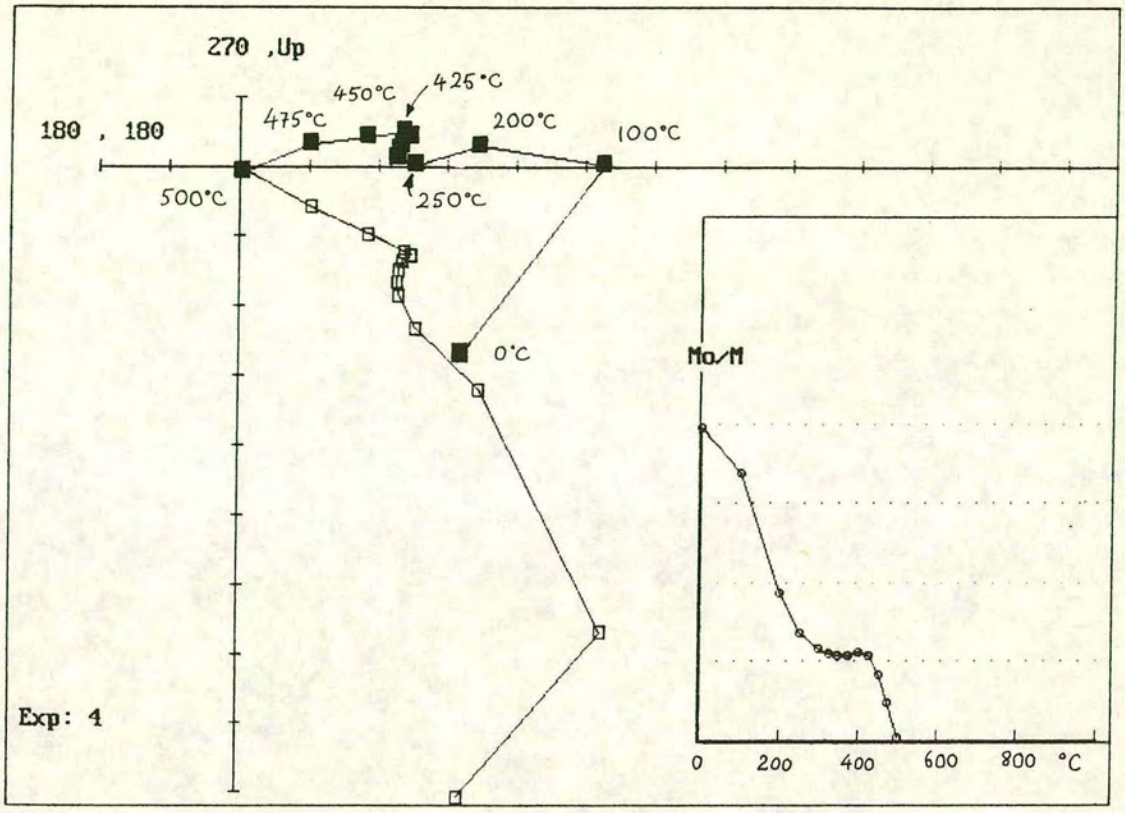

Sample:BJ06-1A1 North

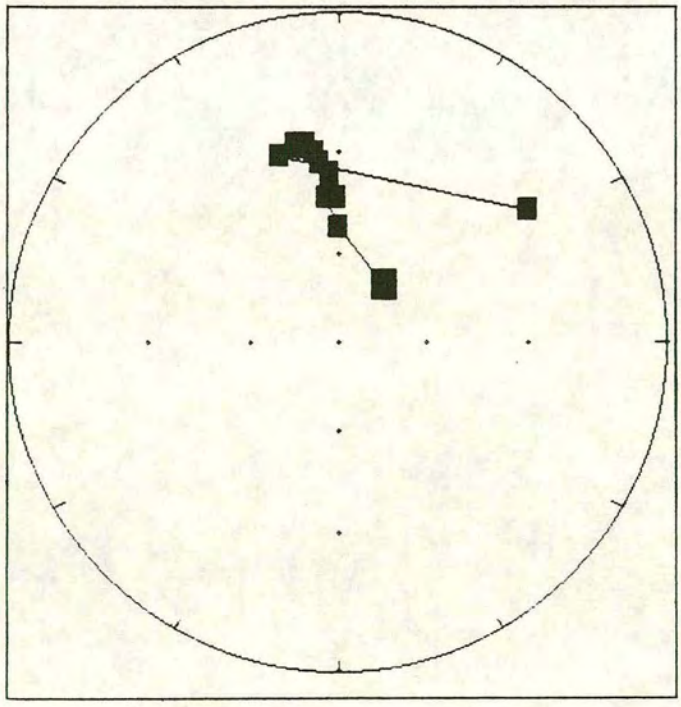

Figure 9.11 Zijderveld plot and Wulff net (in geographic coordinates) for sample BJ06-1A1.

9.7.7 Summary of results

The Zijderveld plots and Wulff nets indicate that there is a characteristic component of remanent magnetization which is observed in samples from all the sites. This component was invariably lies in the NW quadrant and may or may not reach the origin. In those cases where the trace passes the origin it usually turns and starts to decay towards the origin from the opposite direction, thus indicating the likely presence of a higher temperature, and hence more primary, component in the SE quadrant. Unfortunately this high temperature component, although apparent on Zijderveld plots, is very messy and cannot be isolated. Most of the samples also display a present-day field component which can be easily isolated from the more significant higher temperature components.

9.8 Bulk susceptibility measurements

Chemical changes which occurred in the magnetic mineral phases during thermal demagnetization were monitored by carrying out bulk susceptibility measurements. All substances acquire a magnetic moment when placed in a magnetic field and this ability is known as their magnetic susceptibility. In effect, magnetic susceptibility can be regarded as the "magnetizability" of a substance. Bulk susceptibility is the net susceptibility resulting from the contributions of all the magnetic minerals in a rock. The "magnetizability", and hence the bulk susceptibility, of a sample falls when magnetic minerals are destroyed and rises when new magnetic species are created. If bulk susceptibility measurements are carried out throughout the thermal demagnetization process the temperatures at which such chemical changes occur can be determined and the growth of new magnetic minerals can be monitored.

In this study susceptibility measurements were carried out on 2 of the 3 batches of samples (36 samples in total). Bulk susceptibility measurements were made throughout the thermal demagnetization process, after each heating step and subsequent measurement of NRM. Figure 9.12 shows examples of bulk susceptibility plots for the Bilecik Limestone samples. The plots display the typical bulk susceptibility changes exhibited by the Bilecik Limestone during thermal demagnetization. Upturns in the curve at higher temperatures are a common feature of the plots and indicate the growth of new magnetic minerals. For example, upturns occurring in the range 450-600°C may reflect the reduction of hematite to new magnetite which readily acquires VRMs.

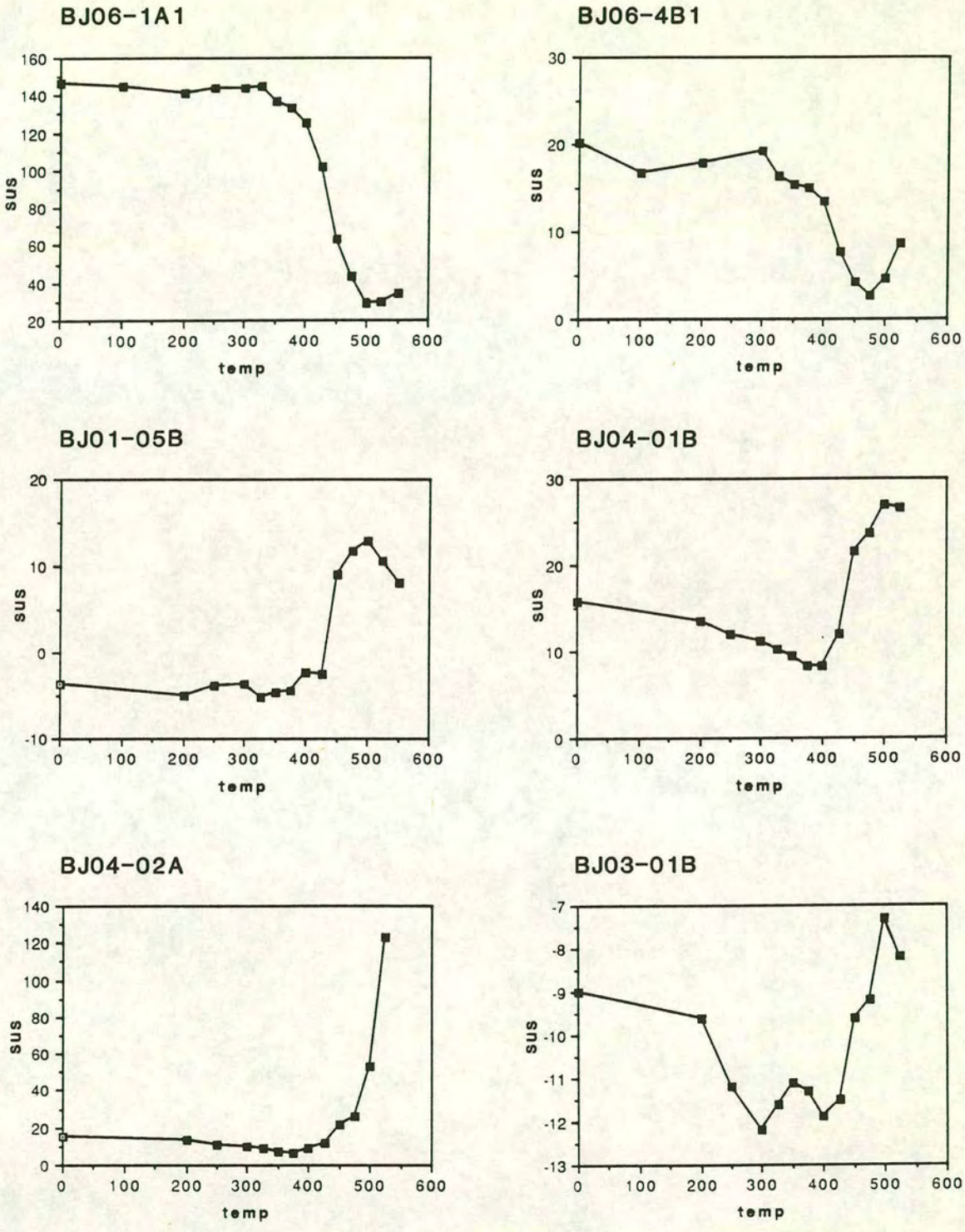

Figure 9.12 Examples of bulk susceptibility plots, showing typical changes exhibited by the Bilecik Limestone when thermally demagnetized.

9.9 Identification of remanent components

The methods of vector subtraction and great circle analysis were used to identify and define the various remanent components isolated by thermal demagnetization. Vector subtraction from Zijderveld plots was the most commonly used technique in this study and the results obtained by this method are shown in Table 9.1. The results given in the table are for the charateristic component, (referred to as mid T in the cases of BJ05 and BJ06) and also the distinct low temperature component (low T) identified in samples from BJ05 and BJ06.

9.9.1 Vector subtraction from Zijderveld plot

This method involves choosing (usually by eye) characteristic vectors (or ChRMs) from Zijderveld plots. Examples of Bilecik Limestone Zijderveld plots with their characteristic vectors are shown in Figure 9.5 to 9.11. The directions of the chosen characteristic vectors were defined in terms of declination and inclination and were plotted as points on stereograms (Figures 9.13 and 9.14). From these the mean of the magnetization directions for each site (the site mean ChRM) was calculated, both before and after tectonic correction. Site mean ChRMs do not necessarily represent primary components, as indicated by Zijderveld plots of the Bilecik Limestone from all 6 sites. In addition to the relatively well-constrained, characteristic vectors displayed on the ChRM plots, many of the plots display a short, very messy high temperature vector which probably represents the primary component, or at least, a more primary component than the ChRM. Unfortunately it was impossible to define this vector by this method in practically all cases, owing to extremely low magnetization intensities and overprinting caused by growth of new magnetic minerals during heating. Many samples also display a very low temperature component which is near parallel to the north axis on the Zijderveld plots. This is a VRM reflecting the present-day geomagnetic field and was not used in the calculation of site mean ChRMs. Figures 9.13 and 9.14 show stereograms for the characteristic vectors from the 6 sites (as well as lower temperature vectors for BJ05 and BJ06, and poorly defined higher temperature vectors for BJ02), both before and after tectonic correction. The statistics shown on the two sets of plots are those used in the fold test discussed in Section 9.11 below.

Table 9.1 Table of results for the palaeomagnetic sites BJ01-BJ06. The low temperature and mid temperature results for BJ05 and BJC6 refer to the two main components picked from Zijderveld plots.

Site	N	Dec_b	Inc_b	α95	k	Dec_a	Inc_a	α95	k	av. dip/d.dir. (sample nos)
BJ01	13	317	49	7.4	32.7	262	57	9.0	22.0	50/196 (1-9) 25/172 (10-14)
BJ02	12	309	43	9.9	20.4	263	82	12.2	13.5	43/138
BJ03	5	313	45	7.0	121.1	288	13	10.3	55.8	50/245
BJ04	2	319	37	116.8	7.1	304	51	67.9	15.7	25/172 (1-6) 16/135 (9-12)
BJ05 (low T)	10	153	7	7.3	45.1	152	-3	6.8	51.1	21/095
BJ05 (mid T)	9	334	24	8.8	35.6	344	34	8.4	38.2	as above
BJ06 (low T)	5	147	14	29.7	7.6	147	-17	33.3	6.2	40/109
BJ06 (mid T)	3	349	21	18.8	44.1	8	31	17.6	50.3	as above

N number of samples
k precision parameter
Dec mean declination
Inc mean inclination
(subscripts a and b indicate before and after bedding correction)

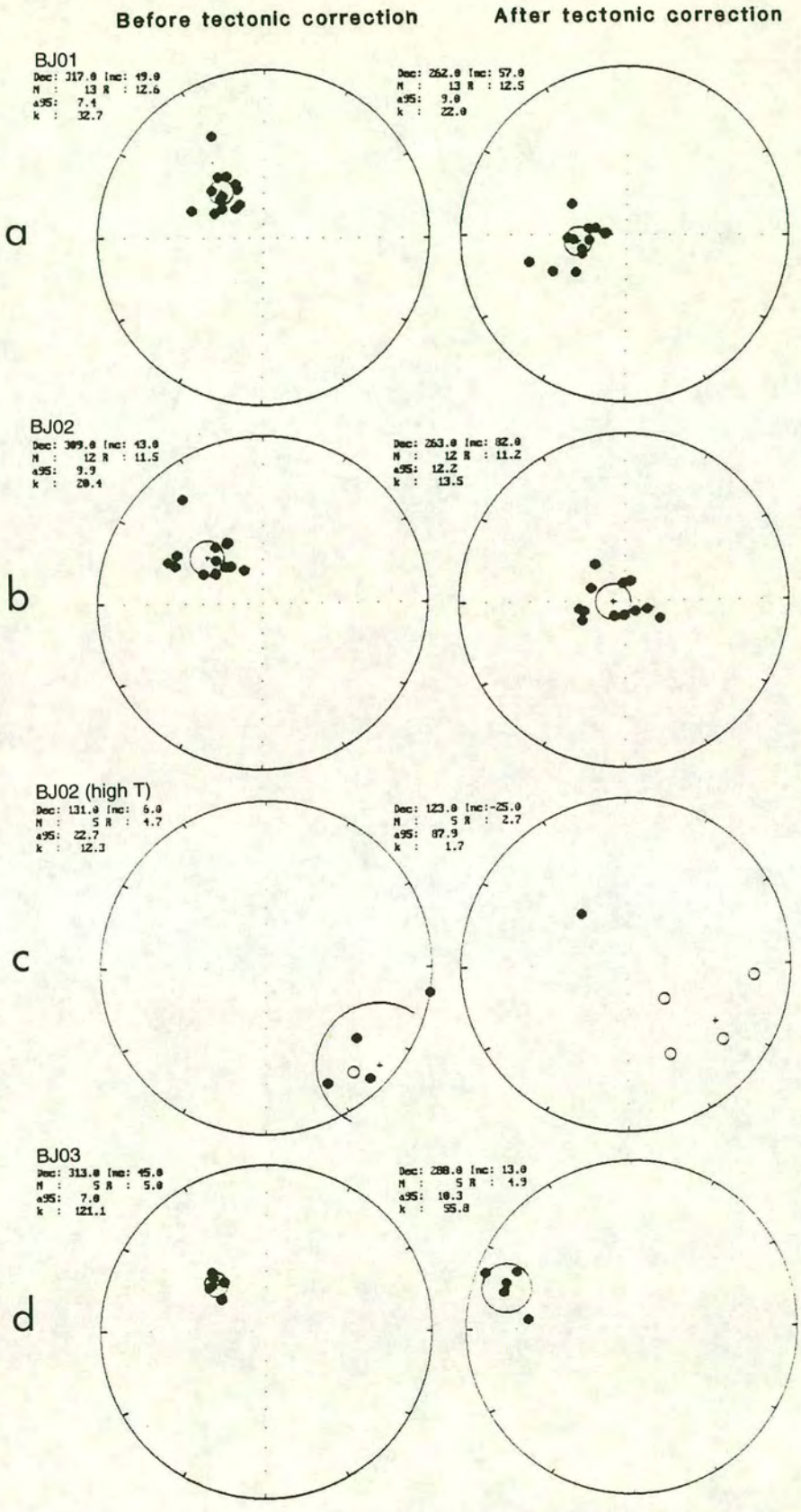

Figure 9.13 Stereograms showing the characteristic vectors for sites BJ01, BJ02 and BJ03, before and after tectonic correction. Plot (c) shows the position of the poorly defined higher temperature component observed in samples from site BJ02.

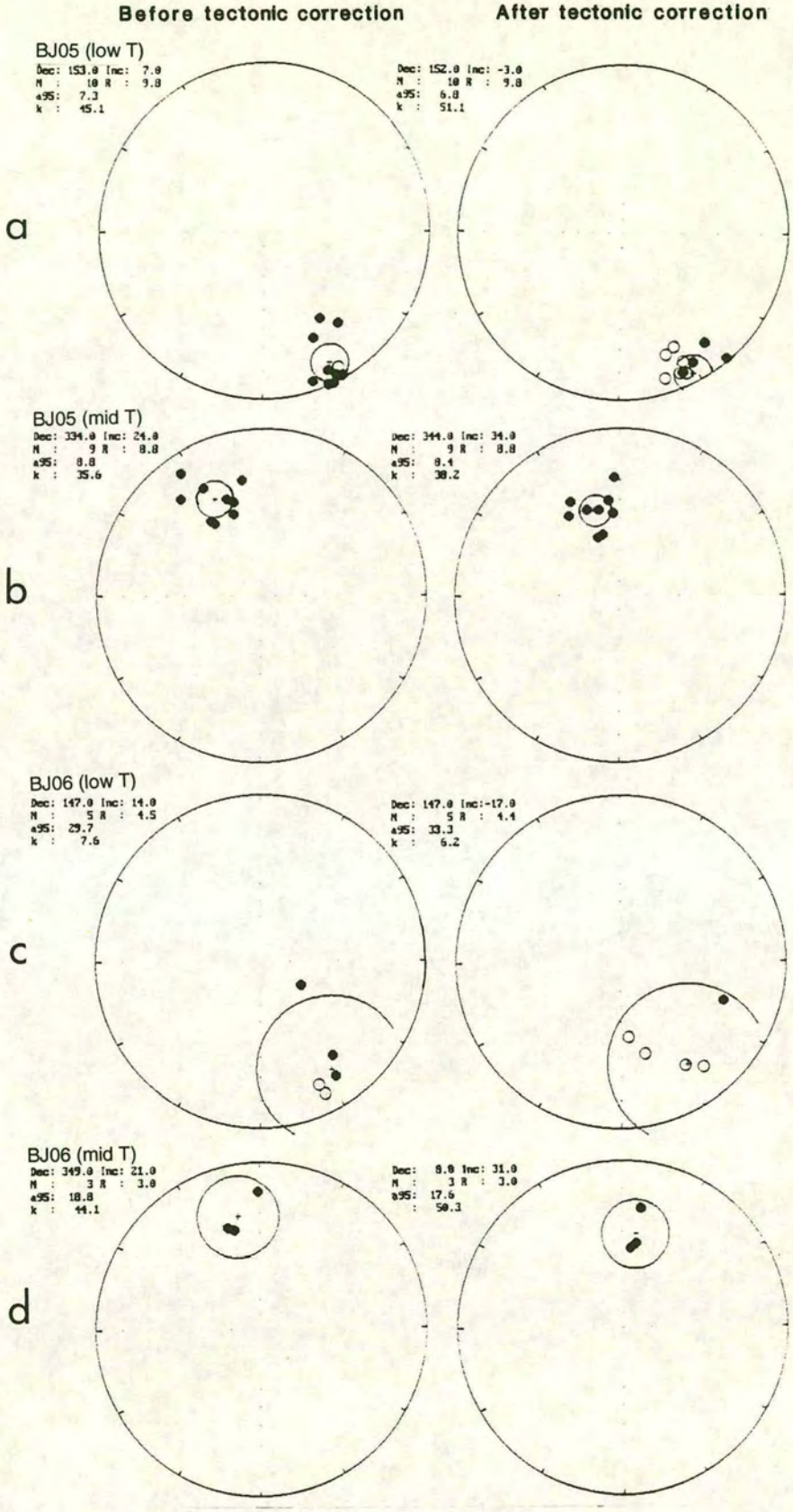

Figure 9.14 Stereograms showing vectors of magnetization for sites BJ05 and BJ06, before and after tectonic correction. Plots (b) and (d) show the characteristic (mid T) vectors for these sites, whereas (a) and (c) represent the distinct lower temperature component (low T) observed in the samples.

9.9.2 Great-circle analysis

Great circle analysis can be an effective way of separating components in cases where the blocking temperature or coercivity spectra of the superimposed remanences are overlapping to the extent that more conventional techniques (e.g. vector subtraction) cannot be applied (Halls, 1978). This method is based on converging great-circles of magnetization. If a rock carrying two superimposed components is demagnetized, the successive NRM directions will lie along a great-circle on a stereonet, provided that there is a difference between the blocking temperature or coercivity spectra (in this case, blocking temperature spectra). The intersection point of great-circles from a group of samples yields an estimate for the mean direction of the component. Great-circle analysis carried out before and after tectonic correction can potentially isolate components of secondary and primary magnetization respectively.

Great-circle analysis was carried out, using site BJ02 as an example, in order to try and isolate the very poorly defined high temperature component which was observed, but not isolated, on the Zijderveld plots. This component is also present on several of the Zijderveld plots from other sites. Figure 9.15 shows the great-circle diagrams (before and after tectonic correction) for site BJ02 which were obtained using McElhinny great-circle programmes. The uncorrected diagram successfully defines the secondary component (the ChRM in this case) and confirms the vector already obtained using the vector subtraction technique. The tectonically corrected version, however, completely fails to isolate the higher temperature component. This component proved impossible to define by either vector subtraction or great-circle analysis. Therefore, other than to say that a more primary magnetization than the ChRM *did* exist, it is unfortunately impossible to incorporate it into any palaeomagnetic interpretation.

9.10 IRM results

To investigate the magnetic aquisition properties of the Bilecik Limestone the IRM of six samples (1 from each site) were measured by placing them in a steady magnetic field whose strength was progressively increased in steps up to 800mT (Figure 9.16). IRM aquisition curves for limestones whose main remanence carrier is magnetite are generally characterized by a steep initial increase and by saturation or drastic flattening of the slope at fields of 300mT or less (Lowrie & Heller, 1982). These characteristics are clearly observed in the Bilecik Limestone samples as shown in

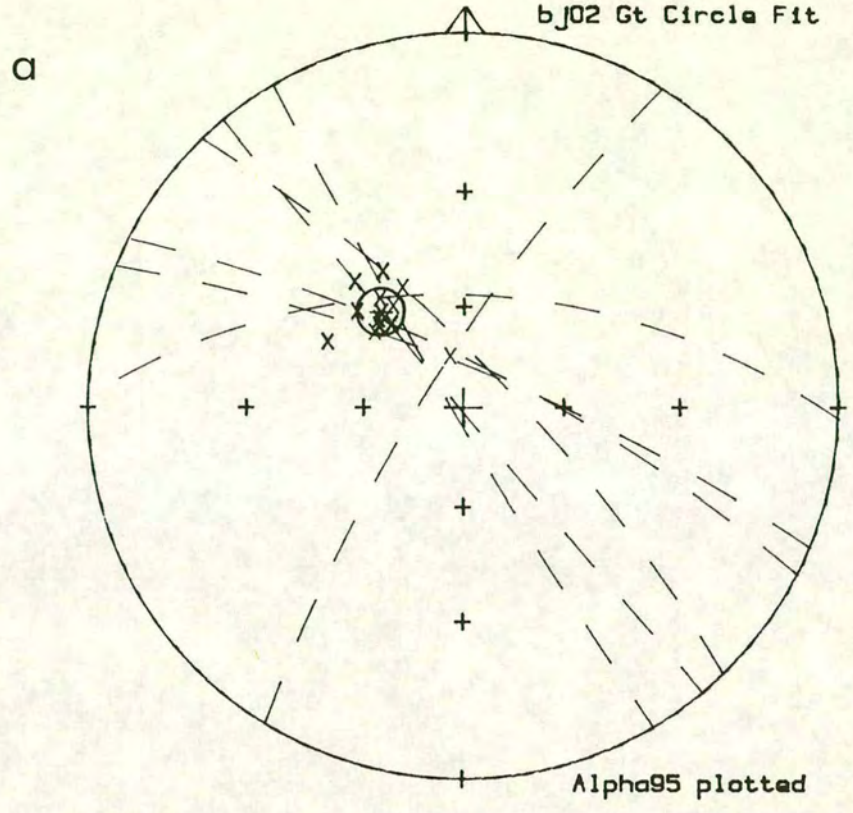

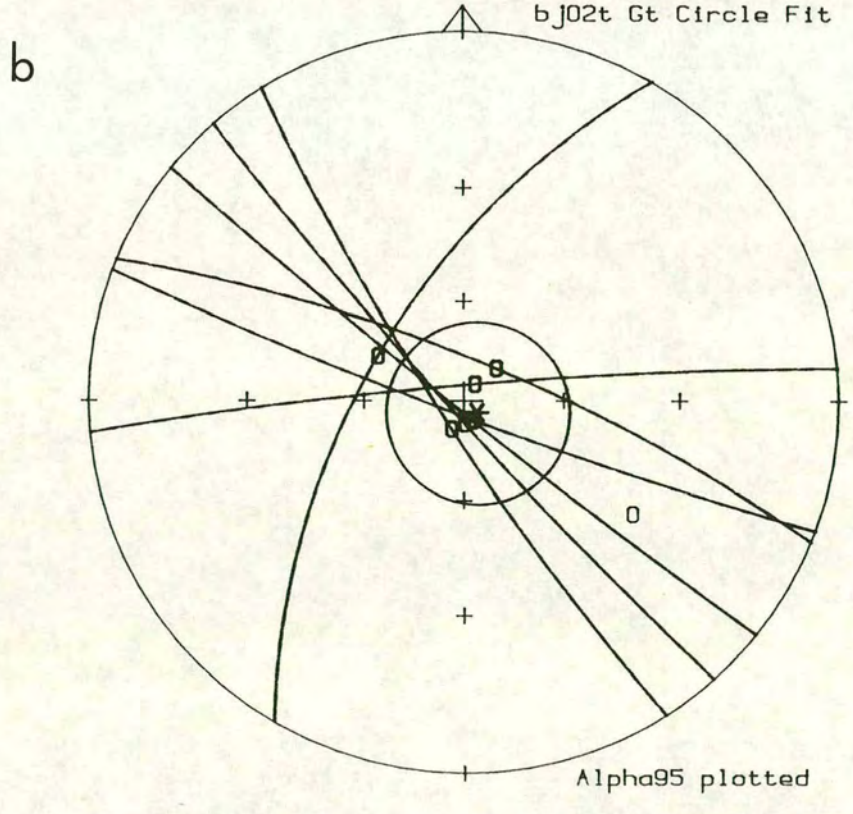

Figure 9.15 Stereoplots showing circles of remagnetization for site BJ02, (a) before and (b) after tectonic correction. Crosses (in plot a) and crosses (in plot b) represent vectors picked using Zijderveld plots.

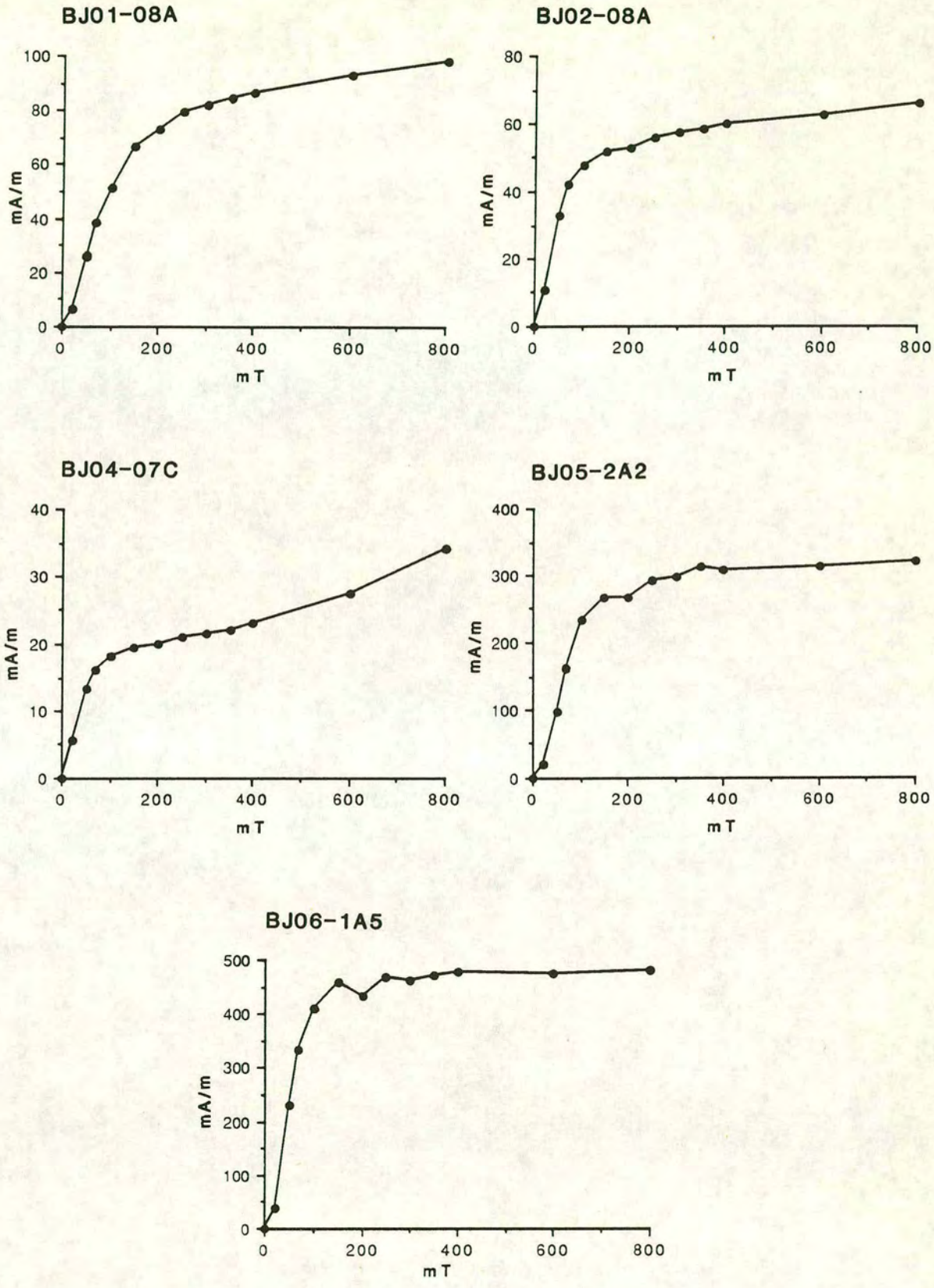

Figure 9.16 Examples of IRM acquisition curves for the Bilecik Limestone.

Figure 9.16. The IRM acquisition curves are characterized by steep initial curves which flatten out to form flat or shallowly rising plateaux. The steep parts of the curves start to shallow out at around 100mT and continue to rise gradually. In the case of samples BJ06-1A5 and BJ05-2A2 a flat plateau is reached by around 400mT. The steep initial part of the curve and its subsequent rapid flattening is interpreted to be due to the presence of magnetite. However, the IRM acquisition curves for samples BJ01-08A and BJ02-08A are more rounded than the characteristic magnetite curve described above and reach saturation at much higher fields, indicating the presence of a higher coercivity mineral phase which is probably hematite. The curve for BJ01-08A illustrates this well and as the limestone at site BJ01 is slightly pink in colour it is probable that hematite is responsible for the higher field part of the curve. Although it is often hard to distinguish between hematite and goethite, both of which have saturation fields well above 500mT, goethite curves may display slightly concave initial curves, a feature which is not present in any of the Bilecik samples.

The interpretation of magnetic mineralogy by IRM analysis is enhanced by the subsequent progressive thermal demagnetization of the acquired IRM. Heating was carried out in successive steps up to a maximum temperature of 680°C. Thermal demagnetization of IRM shows a smooth and gradual reduction in the magnetization up to a maximum unblocking temperature of around 600°C (Figures 9.17 and 9.18). These curves are characteristic of Ti-poor magnetite and closely resemble curves obtained by Lowrie & Heller (1982) for *Scaglia Rossa* sediments.

9.11 Fold tests

The fold test provides a powerful test of the stability of magnetic remanence and can be used to determine the timing of acquisition of remanence. It is based on the premise that if the magnetization was acquired *before* folding, tectonic correction improves the grouping of the magnetization directions and the fold test is said to be positive. The fold test was introduced by Graham (1949) and statistically refined by McElhinny (1964), McFadden & Jones (1981) and McFadden (1990). In the McElhinny (1964) fold test the statistical improvement is measured by the change in the precision parameter from k1 (before tectonic correction) to k2 (after tectonic correction). If the ratio k2/k1 exceeds a critical value then the fold test is statistically significant or positive. If, however, the magnetization was secondary and acquired *after* folding, correction increases the scatter of the directions (i.e k2/k1 is lower than the critical value) and the fold test is negative. More recent studies (McFadden &

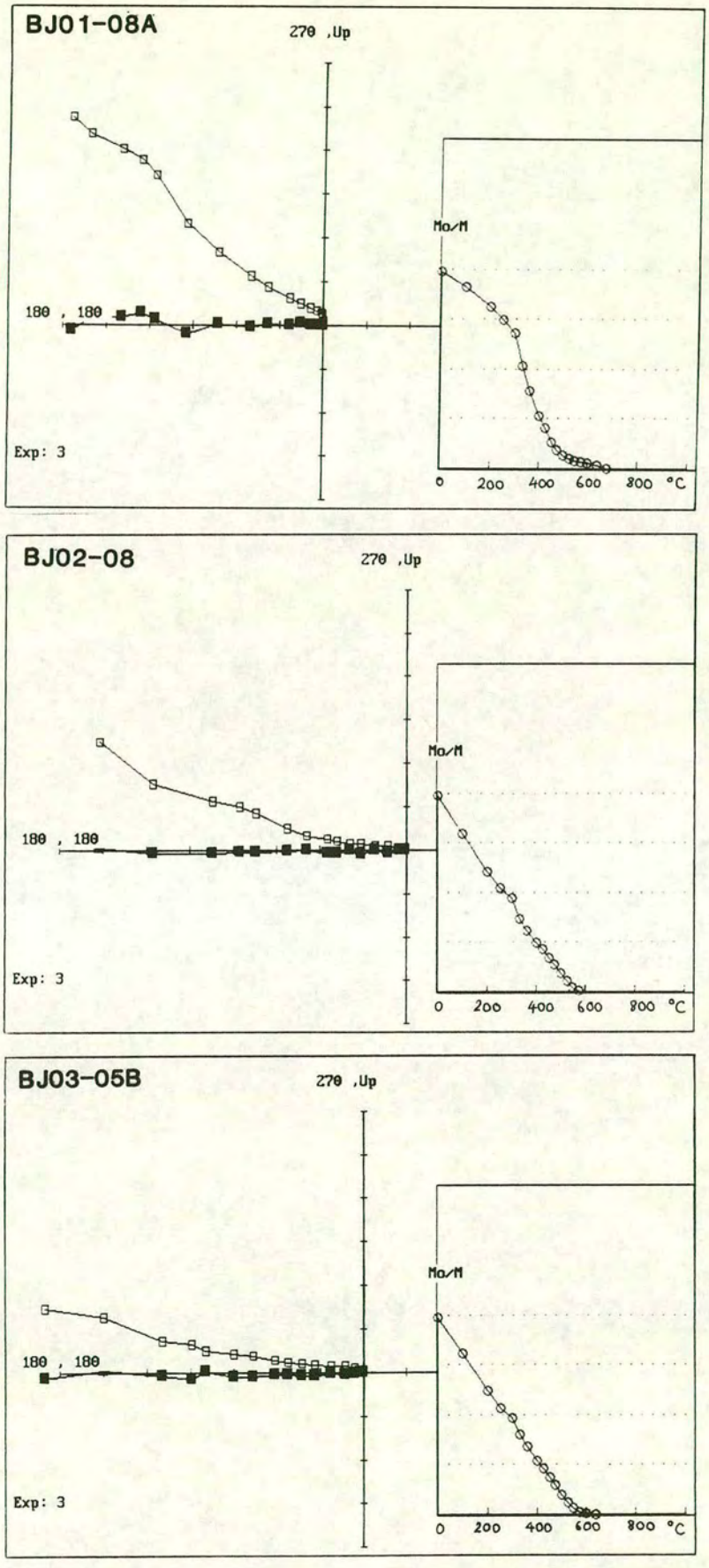

Figure 9.17 Zijderveld plots of thermal demagnetization (in core coordinates) of samples with acquired IRMs from sites BJ01, BJ02 and BJ03.

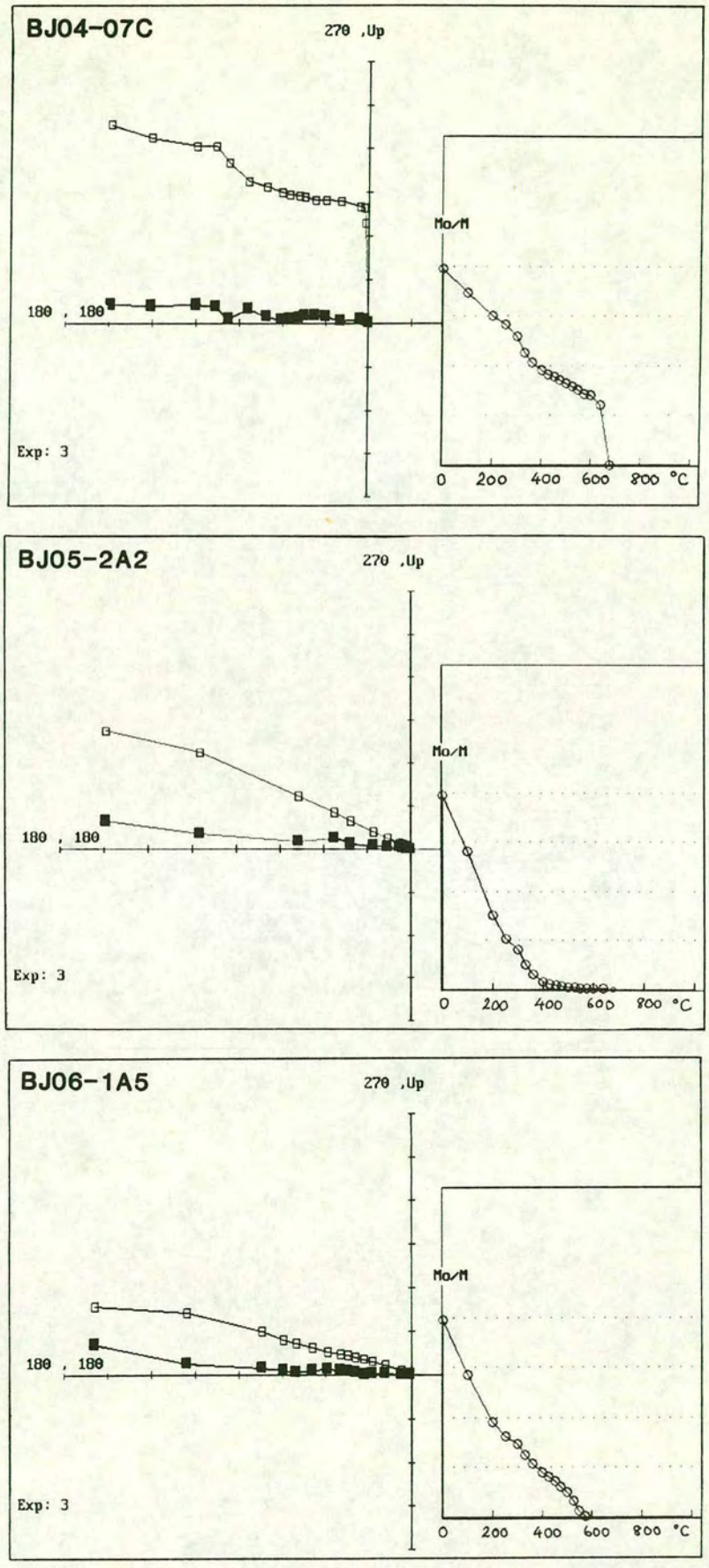

Figure 9.18 Zijderveld plots of thermal demagnetization (in core coordinates) of samples with acquired IRMs from sites BJ04, BJ05 and BJ06.

Jones, 1981 and McFadden, 1990) have suggested that the McElhinny fold test is statistically invalid and too stringent. However, it is a useful initial test of stability as long as it is followed up with more sophisticated tests such as those developed by McFadden & Jones (1981) and McFadden (1990). The McFadden (1990) fold test is based on a correlation between the distribution of magnetic directions and the tectonic information. Both the McElhinny and McFadden fold tests were applied to the Bilecik Limestone data and the results are presented below.

9.11.1 Results of the McElhinny (1964) fold test

Table 9.2 gives the result of the McElhinny (1964) fold test for the calculated ChRM values of the sampled sites. Folds were only observed in the field at sites BJ02/BJ03 and BJ04 and these results are underlined. However, the fold test was also applied to other sites and combinations of sites in case their different strikes were due to large-scale folding not apparent in the field. The values k1 and k2 are the precision parameters before and after tectonic correction and N is the number of magnetizations involved. The critical k2/k1 values given by McElhinny (1964) at 95% and 99% confidence limits for different values of N are tabulated in Appendix 6. The test results are for both 95% and 99% confidence limits.

In all cases the fold test is conclusively negative at both 95% and 99% confidence limits. This can be visually confirmed by looking at the stereoplots showing the magnetization directions before and after correction. Figure 9.19 shows plots for data from sites BJ02 and BJ03, before and after correction. It is clear that tectonic correction drastically increases the scatter of the directions (i.e. k2/k1 is much lower than the critical value), thus confirming that the fold test is negative.

9.11.2 Results of the McFadden (1990) fold test

Data from sites BJ02/BJ03 and BJ04 were also analyzed using the more statistically valid and slightly less stringent McFadden (1990) fold test. Versions 1 and 2 of the McFadden (1990) fold test programme (which use slightly different statistical parameters) were used and both gave negative or inconclusive results.

Table 9.2 Results of the McElhinny (1964) fold test for the calculated ChRM values of the sampled sites. The test results given below are for both 95% and 99% confidence limits. Folds were only observed in the field at sites BJ02/BJ03 and BJ04 and these results are underlined.

	N	k1	k2	k2/k1	Result
Possible within-site folding					
BJ01	13	32.7	22.0	0.7	negative
BJ02	12	20.4	13.5	0.7	negative
BJ03	5	121.1	55.8	0.5	negative
BJ04	2	7.1	15.7	2.2	negative
BJ05	9	35.6	38.2	1.1	negative
BJ06	3	44.1	50.3	1.1	negative
Possible folding between sites					
BJ01/BJ02	25	24.9	12.6	0.5	negative
BJ01/BJ03	18	40.9	9.3	0.2	negative
BJ02/BJ03	17	27.7	4.9	0.2	negative
BJ01/02/03	30	29	7.3	0.3	negative
BJ04/BJ05	11	22.9	18.7	0.8	negative
BJ04/BJ06	5	11.6	7.3	0.6	negative
BJ05/BJ06	12	32.2	27.9	0.9	negative
BJ04/05/06	14	22.3	16.3	0.7	negative

a

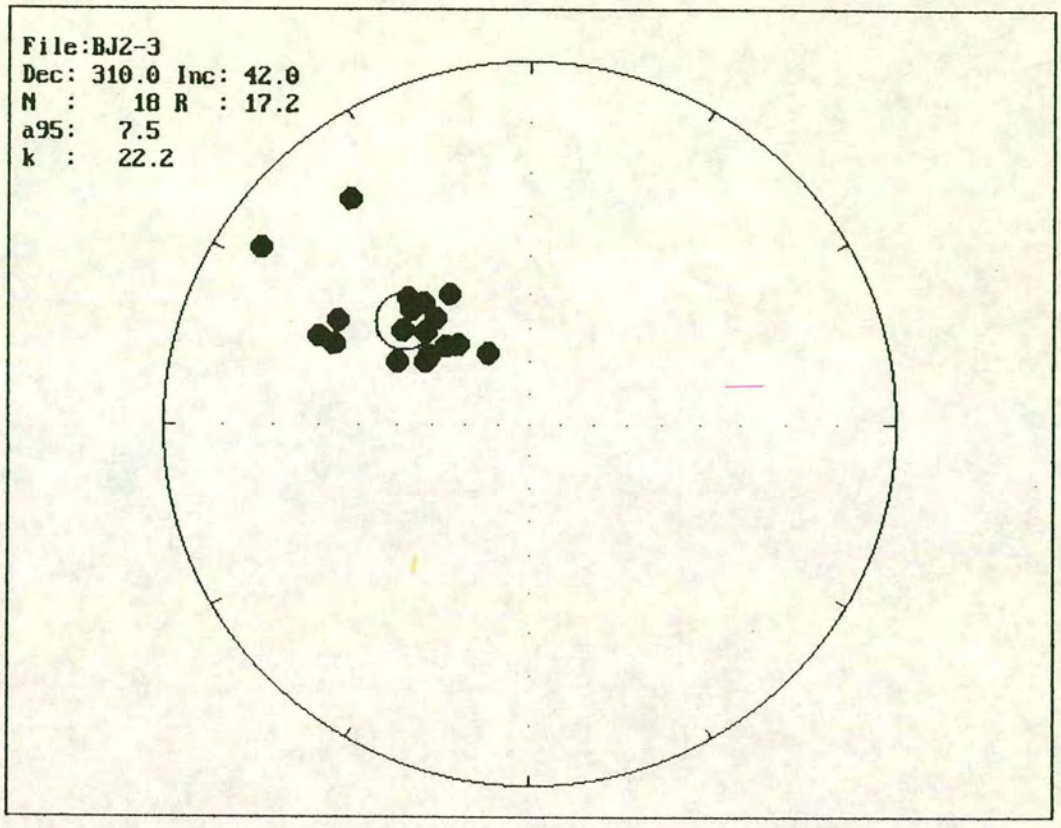

b

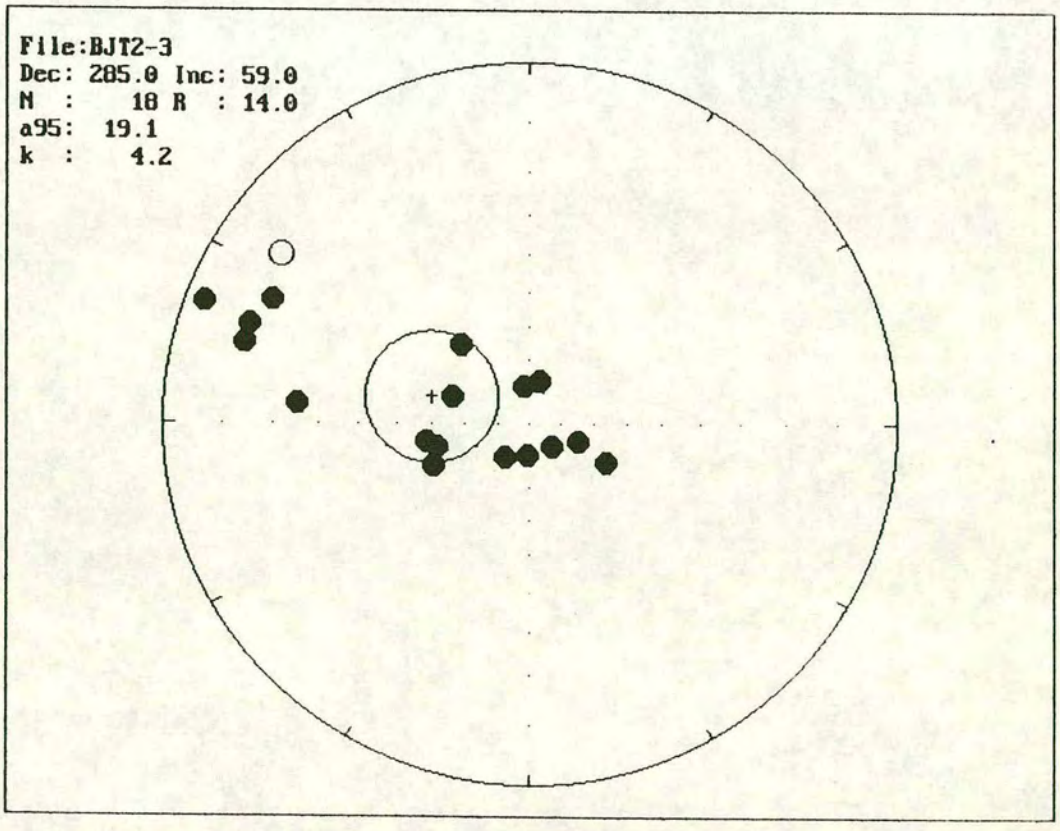

Figure 9.19 Magnetization directions for sites BJ02 and BJ03 (a) before and (b) after tectonic correction, showing an increase in scatter *after* correction (i.e. negative fold test result).

9.11.3 Discussion of fold test results

The fact that the observed folds at sites BJ02/BJ03 and BJ04 give negative results with both the McElhinny and McFadden fold tests is strong evidence that the ChRM of these limestones was acquired *after* folding. The ChRM is therefore a secondary magnetization and cannot give any information regarding the geomagnetic field at the time of formation of the Bilecik Limestone. However, secondary magnetizations can provide useful information as long as constraints can be placed on the age of folding and subsequent geological events. In this case the fold trends reflect the general NNE-SSW structural grain of the Biga Peninsula which was probably produced as a result of compression associated with the Early Tertiary closure of the Neotethys Ocean. The fold axes are consistent with a Neotethyan origin as they parallel the strike of the melanges and ophiolites which lie in the Izmir-Ankara-Erzincan Suture Zone to the south. If this is the case then the folds in the Kocaçal Tepe region probably date from the Early Tertiary. As a result of Neotethyan subduction and subsequent collision extensive sequences of Oligo-Miocene volcanic rocks were extruded in NW Turkey between the Izmir-Ankara-Erzincan zone and the Black Sea. Remagnetization of the Bilecik Limestone could have occurred as a result of either the folding or volcanic activity.

9.12 Virtual geographic poles (VGPs) and palaeolatitudes: a comparison with Eurasia and Gondwana

A virtual geographic pole (VGP) can be defined as the position of the pole of a geocentric dipole that can account for the observed magnetic field at one location and at one point in time (Butler, 1992). Thus a VGP can be calculated from a single observation of the direction of the present geomagnetic field at a particular locality. VGPs can be also be calculated for ancient geomagnetic fields. A site-mean ChRM is a record of a past geomagnetic field direction and, if the time of acquisition of the ChRM (ideally a short interval) is known, then a VGP can be calculated. A palaeolatitude, which can be calculated once the inclination of a magnetization direction is known, is the latitude at which the magnetization was acquired. The fact that the samples conclusively fail the fold test means that magnetization was acquired after folding, thus making tectonic corrections are meaningless. Therefore, when calculating VGPs, the uncorrected ChRM values were used.

A series of VGP values for Eurasia and Africa (Gondwana) were compared with those obtained in this study to try and deduce the most likely setting for the Bilecik Limestone during the Early Tertiary. Plots (a) and (b) in Figure 9.20 show the polar wander curves for Eurasia and Gondwana (with reference to site BJ01) and were plotted using VGPs from the Middle Jurassic to the Quaternary (values from Westphal *et al.*, 1986). The Middle Jurassic is the earliest possible age of the magnetization as it is the age of the limestone itself. However, given that the magnetization post-dated folding it is very unlikely that the magnetization is as old as the Middle Jurassic. The age of folding is thus crucial for the interpretation of the magnetization directions and the tectonic evolution of the region as a whole. Folding is most likely to have occurred during the compressive regime of Neotethyan closure in the Early Tertiary. The palaeolatitudes (before tectonic correction) for sites BJ01-BJ03 were calculated to be 30°, 24° and 26° respectively, and were then compared with the Eurasian and Gondwanan palaeolatitude curves of Westphal *et al.* (1986) for the Early Tertiary period. The Bilecik palaeolatitudes lie approximately between the two curves, precluding the assignation of the Bilecik Limestone to either a definite Eurasian or Gondwanan position during the Early Tertiary. The palaeolatitudes obtained for sites BJ05 and BJ06 are anomalously low (12° and 10° respectively). The shallow inclinations which produced these results could have been caused by a sedimentary or tectonic fabric or, alternatively, by post-fold tilting. Such palaeolatitudes imply a position far south of Gondwana, a scenario which clearly cannot be true and is hard to explain.

9.13 Rotations

The site mean declinations and inclinations for all the sites except BJ04 are plotted in Figure 9.20c with their $\alpha 95$ values plotted as circles of confidence. The present magnetization directions of sites BJ01-BJ03 could have been achieved by approximately 47° of anticlockwise rotation away from either a Eurasian or Gondwanan setting. The alternative, a clockwise rotation of 313°, is very unlikely. The inclination of the magnetization directions implies an original position which corresponds closely to the Tertiary positions for both continental masses, supporting the idea that the magnetization was acquired during the Oligo-Miocene magmatism of NW Turkey. According to Platzman (pers. comm., 1993) Oligo-Miocene volcanics elsewhere in the Biga Peninsula show an average value of 26° of anticlockwise rotation. This is similar to the anticlockwise rotations (average 30°) measured in Eocene and Miocene volcanics near the North Anatolian Fault Zone (NAF), NW of

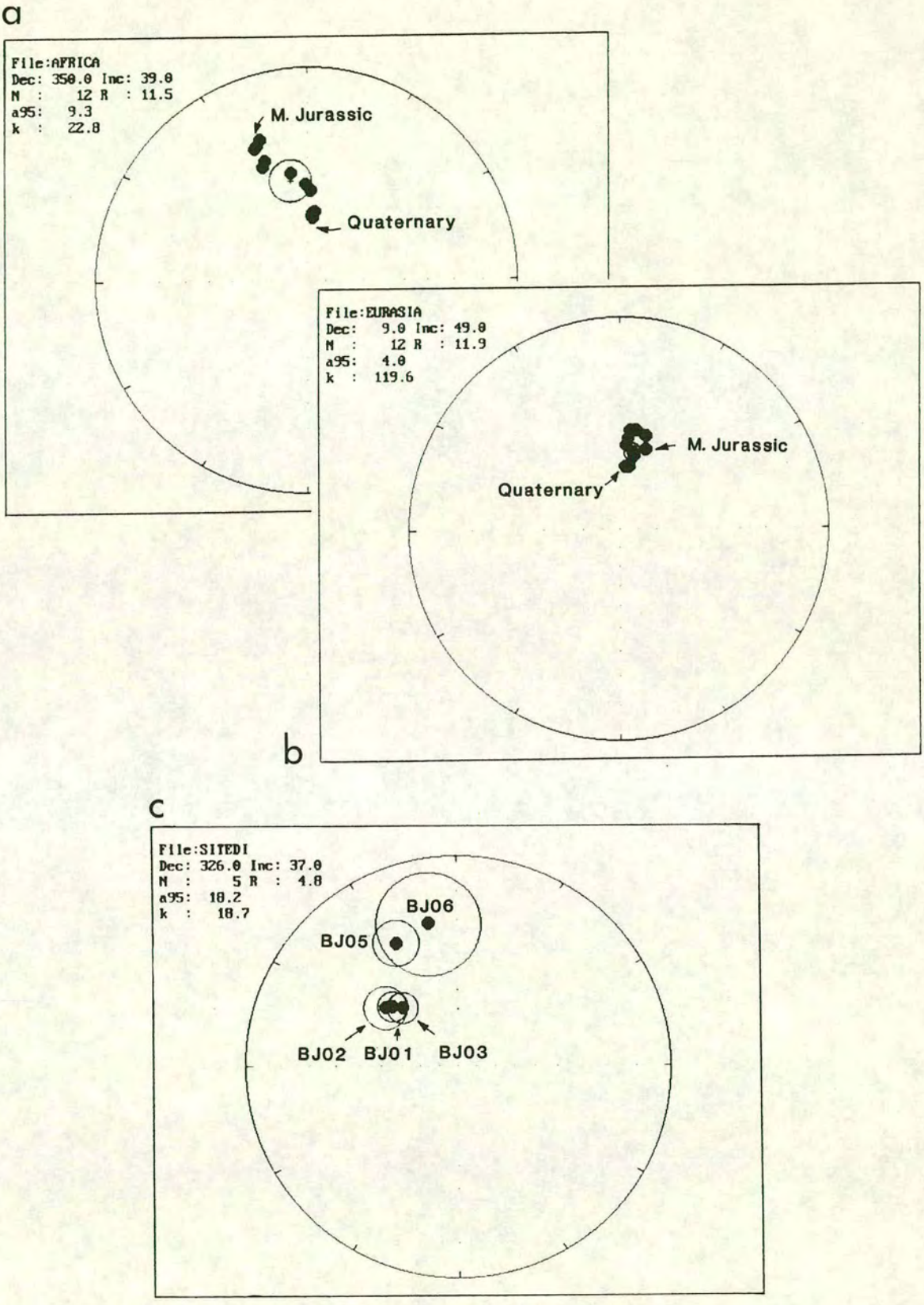

Figure 9.20 Polar wander curves for (a) Africa and (b) Eurasia (with reference to site BJ01) which were plotted using VGPs from the Mid Jurassic to the Quaternary (values from Westphal *et al.*, 1986). Plot (c) shows site mean ChRMs for sites BJ01, BJ02, BJ03, BJ05 and BJ06 with their $\alpha 95$ values plotted as circles of confidence.

Ankara (Platzman *et al.*, in press). These results are unexpected in that the rotations occurred in close proximity to the NAF, a major zone of dextral strike-slip. One explanation, as postulated by Platzman *et al.*, (in press), is that the anticlockwise rotations in northern Turkey may be accommodating deformation resulting from the northward motion of Arabia with respect to Anatolia since the Mid Miocene.

9.14 Implications for interpretation of the Karakaya Complex

The fact that a rotation was measured in the Bilecik Limestone samples clearly has implications for the interpretation of the Karakaya Complex in this region. The strike of the complex ranges from NNE-SSW to NE-SW and this orientation must partly reflect the rotation described above. An anticlockwise rotation of 47° in the Early Tertiary implies a pre-rotation structural trend of E-W to ENE-WSW, concordant with an origin as an accretionary complex forming parallel to the subduction zone of an approximately E-W trending Palaeotethys Ocean. The extensional faults within the Kazdag Massif strike NE-SW, parallel to the structural grain of the Karakaya units, and were therefore probably rotated together with the Karakaya Complex into their present position. According to Okay *et al.* (1991) the Kazdag faults are post-Miocene and probably Pliocene in age. This implies that the rotation measured in the Bilecik Limestone in the Havran region may be Pliocene or post-Pliocene. If this is the case then the rotation post-dates the age of initiation of the dextral North Anatolian Fault in the Mid Miocene. A full discussion of the timing and implications of the measured rotation is beyond the scope of this chapter and the reader is referred to Platzman *et al.* (in press) for further discussions on the relationship of tectonic rotations to the North Anatolian Fault and the collision of Arabia and Anatolia.

9.15 Conclusions

The results of this study show that the characteristic magnetization was acquired *after* folding and *before* an anticlockwise rotation of approximately 47°. The pre-magnetization folding in the Bilecik Limestone of Kocaçal Tepe reflects the general NNE-SSW structural grain of the Biga Peninsula which was probably produced as a result of compression associated with the Early Tertiary closure of the Neotethys ocean to the south. If this is the case then the folds in Kocaçal Tepe probably date from the Early Tertiary and the subsequent magnetization and rotation occurred after this time as a result of tectonic or volcanic activity. It is possible that the limestone was remagnetized during the Oligo-Miocene as a direct result of the extensive

volcanic activity which was occurring at this time. The proximity of limestone to volcanics at all the sampled sites and the presence of silicified limestone around Kocaçal Tepe make this hypothesis highly likely. The observed anticlockwise rotations were probably produced as the result of the motions of a fault-bounded block. In summary, a tentative sequence of events from the Jurassic to the Tertiary can be summarized as:

1. Deposition of the shelfal Bilecik Limestone in shallow Neotethyan seas during the Middle-Late Jurassic. Continuation of limestone deposition into the Cretaceous.

2. Closure of the Neotethys by the Early Tertiary, causing folds with approximately NE-SW trending axes in the Bilecik Limestone. Some remagnetization of the Bilecik Limestone may have occurred during tectonic activity at this time.

3. Extensive arc/post-collisional magmatism in NW Turkey during the Oligo-Miocene. The acquisition of magnetic remanence by the Bilecik Limestone is likely to have predominantly occurred during this volcanic episode.

4. An anticlockwise rotation of 47°, affecting the underlying Karakaya Complex, and causing fold axes in the Bilecik Limestone to become orientated N-S/NNE-SSW.

CHAPTER 10

SYNTHESIS

10.1 Introduction

The aim of this study was to shed new light on the Late Palaeozoic-Early Mesozoic tectonic units of NW Turkey and to test the different tectonic models proposed for their evolution. Although these models were based on basic geological mapping, further detail was missing. Sedimentological, geochemical and structural data were collected from a wide area of NW Turkey during the course of this study. Although further work needs to be done before detailed tectonic reconstructions can be confirmed, this project has elucidated the various tectonic settings represented by the units in the Biga Peninsula region of NW Turkey.

A major part of the project was to establish the setting of formation of the various igneous and sedimentary units, especially the Permo-Triassic Karakaya Complex, the Denizgoren-Lesbos Ophiolite and the sequences of Chios and Karaburun. The tectonic settings of the studied tectonostratigraphic units have been interpreted individually on the basis of their lithological associations and geochemistries. These separate stories must be amalgamated if large scale tectonic reconstructions are to be made. Owing to sparse exposure between the main fieldwork areas, incorporation of the various units into one coherent tectonic model is very difficult and the interpretation given in this chapter is a tentative one. In this chapter the main findings of the previous chapters are first summarized and interpretations are made.

10.2 The Karakaya Complex of NW Turkey

10.2.1 Nilüfer Unit

The Nilüfer Unit comprises a thick sequence of green spilitic basalts, volcaniclastic debris flows, ignimbrites and volcanogenic sedimentary rocks which is well exposed in the Edremit and Bergama regions. A distinctive feature of the unit is the presence of redeposited carbonates within the volcanics, locally dated as Mid Triassic in the Bergama region on the basis of conodonts (Kaya *et al.,* 1992). Discrete limestone blocks up to 10m in size, limestone debris flows and calciturbidites form horizons within the volcanic pile. The lower parts of the unit consist of massive, unpillowed

basalts and ignimbritic debris flows. Geochemical analysis of basalts from the Edremit, Bergama and Bursa regions reveals a within-plate signature. The unit becomes progressively more sediment-rich towards the upper levels, with the appearance of volcanogenic sandstones and cherty mudstones. However, terrigenous clastic material is noticeably absent. In the Bergama region, green spilites and redeposited limestone lenses grade structurally downwards into strongly foliated, highly sheared grey schists and marble, a feature which can also be observed near Edremit. Here, volcaniclastics and limestone debris flows grade structurally downwards into the green amphibolites and marbles which comprise the upper levels of the Kazdag metamorphic massif.

The Nilüfer Unit is interpreted as a Triassic seamount sequence in which an internal core of massive basalt is overalin by flank facies of debris flows and sediments. A carbonate cap to the seamount is indicated by horizons of redeposited limestone and discrete blocks. Complete absence of terrigenous clastics implies formation in the open ocean, away from any terrigenous sources.

10.2.2 Ortaoba Unit

North of Edremit, to the southeast of the Kazdag Massif, a disrupted clastic sequence is tectonically emplaced over the Nilüfer Unit described above. A thickening- and coarsening-upward sandstone sequence overlies approximately 10m of bedded grey chert, which is floored by pillow lava and hyaloclastite. Geochemical analysis of the basalt indicates a MORB origin. The sequence is strongly disrupted and the cherts and basalt occur only in rare tectonic slices. Considerable tectonic repetition occurs throughout the unit. Most of the unit is made up of feldspathic sandstones and interbedded dark shales. Strong layer-parallel extension and re crystallization have obliterated most sedimentary structures, although normal grading, debris flow horizons and slump folds can still be observed.

The Ortaoba Unit is interpreted as a trench sequence, recording deposition of trench turbidites on ocean-floor basalts and cherts. Slumping indicates a significant slope and the coarsening-upward nature of the succession is typical of trench deposits, recording progressive migration of the depositional site towards the trench.

10.2.3 Kalabak Unit

The Kalabak Unit comprises dark grey phyllites, quartzo-feldspathic schists and rare horizons of deformed conglomerate and recrystallized limestone. The unit has a well-developed foliation and displays kink folding, shearing and duplexes. Northeast of Edremit phyllites of the Kalabak Unit are intruded by a granodiorite pluton. Exposure of the intrusion is patchy and very altered, making contacts difficult to establish. However, the pluton is definitely pre-Late Triassic, owing to the presence of an unconformity overlain by an undeformed Upper Triassic sequence. There is a similar phyllitic sequence further south, in the Kinik region.

The fine-grained phyllites may indicate pelagic deposition on ocean floor away from the supply of coarse clastics to the trench.

10.2.4 Çal Unit

In this thesis the Çal Unit comprises disrupted fragments of Upper Permian carbonate platforms with clastic basements and debris flows containing volcanic clasts and Upper Permian limestone blocks. The disrupted Upper Permian carbonate platforms are exposed in the Ezine, Bergama and Balya regions and the debris flows are exposed locally near Edremit and Çan. In the Çan region, the matrix of the debris flows is volcaniclastic or, more rarely, extrusive igneous in nature. Thin horizons of pink pelagic limestone and mudstone occur within the debris flows and volcanics. The debris flows range from limestone-rich conglomerates with interstitial volcanic material to flows containing volcanic clasts only. At the base of the unit there are medium-bedded micaceous sandstones and shales. This clastic sequence is separated from the dominantly volcanic succession by a fault and also appears as tectonic slivers higher in the sequence. Above the sandstones and shales, red mudstones are interbedded with pelagic limestones and thin basalt flows. The highest part of the sequence comprises the debris flows described above. Scattered outcrops of the unit also occur north of Edremit where Upper Permian limestone, associated with micaceous sandstone, basalt and red mudstone, form klippen on the tops of hills. The limestone is probably one large disrupted block within a muddy matrix, which also contains rare basalt blocks. The lower contacts of the klippen are much shallower than the characteristically steep structures of the underlying Ortaoba phyllites and are marked by serpentinite.

The Çal Unit is interpreted as an extensive Permian carbonate platform which was constructed on a clastic basement and subsequently rifted to produce intra-platform basins.

10.2.5 Interpretation of the Karakaya Complex as an accretionary complex

By analogy with well-preserved accretionary complexes from around the world, the lithological assemblages of the individual Karakaya units and their structural juxtaposition suggests an origin involving subduction-accretion processes. The lithologies which make up the various tectonostratigraphic units clearly record sedimentation in a variety of marine environments, including seamount, trench, abyssal plain and rifted platform settings (as discussed above). The preservation potential of such sequences is extremely low unless they become incorporated into an accretionary prism at a subduction zone.

The overall structural arrangement of the Karakaya Complex is also suggestive of an accretionary origin. The units form a stack of tectonically bounded slices which are commonly imbricated with each other along their contacts. In the Edremit area, for example, tectonic slivers of Nilufer spilites are found within the Ortaoba Unit and the contact between the Ortaoba and Kalabak Units is a sheared zone containing elements of both units. With the exception of the Cal Unit at the top of the stack, the contacts between the units and also their internal structures are relatively steep, a characteristic feature of many accretionary complexes. Deformational features within the units are pervasive and and include low-grade metamorphism, cleavage formation, duplexes, shearing, folds and stratal disruption. Extensional features are also common and include normal faults and layer-parallel extension of bedding.

Many sedimentary features of the Karakaya Complex, as described below, are also in accordance with an accretionary origin. Soft-sediment deformation and sedimentary blocks within the Ortaoba Unit imply a unstable slope and the coarse polymict debris flows within the Nilufer Unit near Edremit may have been produced in an accretionary setting. The coarsening upward nature of the turbidites in the Ortaoba Unit is consistent with an oceanic plate becoming progressively closer to a trench. A debris flow in the platformal Cal Unit near Can displays two phases of conglomerate formation, possibly recording intra-platform rifting followed by subsequent disruption at a subduction zone.

Subduction-accretion settings similar to the one proposed for the Karakaya Complex are well documented, for example in the circum-Pacific area (e.g. Nankai Trough; Karig, 1988) and on land (e.g. Franciscan Complex; Cloos, 1984). Investigation of complexes such as those in California and SW Japan, whose tectonic evolution is relatively well constrained, allows direct comparison with poorly understood assemblages such as the Karakaya Complex. The Mino terrane, for example, is a Jurassic accretionary complex in SW Japan which is composed of units remarkably similar to those of the Karakaya Complex of NW Turkey. They include a greenstone-carbonate-chert unit, a siliceous pelagite-distal turbidite unit, a proximal turbidite unit and an olistostrome-slump unit (Sano *et al.*, 1992). They are interpreted as remnants of Permian-Jurassic oceanic crust, including dismembered seamounts, ocean-floor sediments, trench turbidites and trench-slope debris flows. Processes of seamount dismemberment are illustrated by the Daiichi-Kashima seamount, an excellent modern analogue for the Karakaya seamounts. Having arrived at the Japan Trench, it is breaking up by processes of normal faulting and subsidence of the fault blocks into the trench (Cadet *et al.*, 1987). Drilling by the Kaiko Project has revealed extensive limestone talus associated with these blocks, illustrating the importance of normal faulting in seamount break-up.

10.3 Associated units in NW Turkey

10.3.1 Triassic-Jurassic cover sequence

In the Edremit-Havran region the Karakaya units are overlain by a relatively undeformed, unmetamorphosed clastic succession, up to 1000m thick. It has a basal, unconformable contact with the granodioritic pluton which intrudes the phyllitic unit. Near its base the sequence comprises thick conglomerates and arkosic sandstones, rich in plant fragments and oyster shells. Up sequence, thick horizons of fossiliferous dark mudstones, containing *Halobia*, *Daonella*, *Posidonomya*, *Neritopsis* (van der Kaaden, 1959) and *Bositra buchii* (Altiner *et al.*, 1991) are intercalated with both massive and bedded turbiditic sandstones. An Upper Triassic age (probably Norian) can be assigned to the mudstone-rich part of the sequence (Krushensky *et al.*, 1980). Near the top of the sequence the sandstones and mudstones contain shallow-water trace fossils such as *Thalassinoides*, *Chondrites* and *Skolithos*. The clastics pass up into the Ammonitico Rosso and nodular limestone facies at the base of the overlying Bilecik Limestone.

The Halilar Formation is interpreted as a perched fore-arc basin, deposited on top of the actively deforming Karakaya accretionary complex. Clastic sequences, interpreted as restricted, perched basin deposits which formed on an accretionary complex, have also been described from the Franciscan Complex of California. Undeformed sandstones and mudstones in the Eastern Unit of the Franciscan Coastal Belt (Bachman, 1982) may be analogous to the clastic succession near Havran.

By the Lias accretionary tectonics had ceased in NW Turkey and the establishment of stable conditions led to the build-up of a thick carbonate platform, the extensive Bilecik Limestone.

10.3.2 Kazdag Massif

The Kazdag Massif comprises a sequence of metamorphic rocks which are folded into an anticline which has a broadly domal shape. On its eastern side the Kazdag Massif is tectonically juxtaposed against volcanic rocks of the Karakaya Complex. To the west it has a faulted contact with an Upper Cretaceous mélange (the Çetmi Ophiolitic Mélange of Okay *et al.,* 1991) and is intruded by an Oligo-Miocene granodiorite. The base of the Kazdag Massif is not exposed and a total structural thickness of over 10km has been estimated by Okay *et al.* (1991).

Banded quartzo-feldspathic gneiss intercalated with marble and amphibolite forms the most common lithological association in the Kazdag Massif. Outcrops at the summit of Kazdag reveal rocks from the core of the dome, including meta-gabbro, meta-harzburgite, plagiogranite and amphibolite. Although an age determination for the gneisses indicates a possible Upper Triassic age (Bingöl, 1971), isotopic dating of these rocks has as yet proved very inconsistent and tends to reflect Oligo-Miocene magmatic activity in the region.

Regardless of its original tectonic setting, the Kazdag Massif is interpreted as a metamorphic core complex which was exhumed along normal faults, detachments and extensional mylonite zones during the Miocene.

10.3.3 Denizgören and Lesbos Ophiolites

The Denizgören Ophiolite is almost entirely composed of serpentinized harzburgite. The other elements of a classic ophiolite succession are absent and for this reason it

should more correctly be termed an ultrabasic body. It forms a narrow band, 2-3km wide and 25-30km long, trending in a SSW-NNE direction.

On its western margin the ultrabasic slab tectonically overlies the Karadag Unit, a Permian carbonate platform sequence. Amphibolite forms a well-preserved metamorphic sole unit at the base of the slab. Geochemical analysis of the amphibolites reveals clear fractionation trends, suggesting that they were derived from gabbroic, rather than basaltic, precursors. The sole grades abruptly downwards into sheared metasedimentary and metavolcanic rocks which lie at the top of the Karadag Unit. To the east, the Denizgören Ophiolite has a steep, possibly strike-slip, contact with a poorly exposed, monotonous sequence of micaschists (the Çamlica Micaschists).

A similar ultrabasic body and associated amphibolite sole unit are exposed on the Greek island of Lesbos which lies just off the Turkish mainland, south of the Biga Peninsula. This ophiolitic nappe lies directly along strike from the Turkish example and is excellently exposed NW of Agiassos, on the slopes of Mount Olympos. The Lesbos Ophiolite and its metamorphic sole tectonically overlie a volcanosedimentary sequence which contains crystalline carbonate intercalations of Lower-Middle Triassic age. The geographical position, constituent lithologies and geochemistry of the Denizgören and Lesbos Ophiolites all indicate that they originally formed part of the same ophiolitic body.

Geochemical analyses of peridotites from the Denizgoren Ophiolite are similar to those from supra-subduction ophiolites around the Eastern Mediterranean. The amphibolites which form the metamorphic sole of both ophiolites had gabbroic precursors and are interpreted as fragments of oceanic crust which were caught up during ophiolite obduction.

10.3.4 Chios and the Karaburun Peninsula

The Karaburun Peninsula and the Greek island of Chios, south of the main area of study preserve thick Mesozoic carbonate platforms which overlie mélange sequences of volcanics, chert, clastics and limestone. The Chios melange comprises both sedimentary and tectonic blocks of lava, chert and Palaeozoic limestone in a clastic matrix. This sequence is overlain by a thick Triassic carbonate platform with a basal horizon of chert, tuff and conglomerates. A similar situation is present on the

Karaburun Peninsula where the Lower Triassic Denizgiren Group, comprising chert, clastics, mafic volcanics and pelagic limestones, is overlain by a thick Triassic-Cretaceous carbonate platform. The base of the platform is marked by a shallowing-up sequence passing from basalts and chert to pelagic limestone and, finally, massive shallow-water limestone.

The mélanges of Chios and Karaburun are interpreted as Palaeozoic Gondwanan continental-related sequences and deformed Triassic rift sequences. Deep-water cherts, pelagic limestones and volcanics lie directly below the overlying Triassic platforms and may reflect the establishment of deep-water conditions and the initiation of rift volcanism. Thick Triassic carbonates built up over the rift successions and record passive margin shallow-water conditions with periodic emergence.

10.4 Palaeomagnetic study of the Bilecik Limestone

A pilot palaeomagnetic study was carried out on the Jurassic Bilecik Limestone in the field area. The aim was to determine Jurassic palaeolatitudes and to try and constrain tectonic rotations which may have affected the underlying Karakaya Complex. The analyses do not give conclusive results regarding palaeolatitudes, but do indicate that the limestone has undergone, at least in the Biga Peninsula, a post-Mid Jurassic anticlockwise rotation of approximately 47°. This result has implications for interpretation of the current structural trends of the Karakaya Complex and is thus incorporated into the dicussions below. The rotation occurred after remagnetization, which was probably caused by extensive magmatism in NW Turkey during the Oligo-Miocene. The magnetization direction acquired during deposition of the limestone (primary component of magnetization) could not be isolated.

10.5 The Karakaya Complex: Palaeotethys ocean or back-arc basin?

The question of whether the Karakaya Complex represents a fully oceanic basin (i.e. the Palaeotethys Ocean itself) or a back-arc basin is crucial to the interpretation of the Palaeotethys Ocean in NW Turkey. Distinguishing between these two tectonic settings is not an easy task, especially when the rocks are highly dismembered within an accretionary complex. The Küre Complex in the northern Pontides illustrates this well. The Küre Complex was previously interpreted as the main Palaeotethys Ocean (e.g. Sengör *et al.*, 1984) but was subsequently reinterpreted as a Palaeotethyan back-

arc basin by Ustaömer (1993) and Ustaömer & Robertson (1994). Their reinterpretation was largely based on the fact that open ocean sediments (e.g. radiolarion cherts), MORB-type extrusives and blueschists are absent from the Kure Complex. Basalts in the Küre Complex are directly overlain by terrigenous, rather than volcanogenic, shales and turbiditic sandstones with no pelagic (e.g. chert) interval, and display a subduction zone signature which is in accordance with a back-arc interpretation. However, many modern back-arc basins do display siliceous sequences (e.g. Leitch, 1984) and so absence or presence of chert cannot be used as a definite criterion for distinguishing between oceans and back-arc basins.

The Karakaya Complex, by contrast, displays MORB basalts overlain by up to 10m of chert (Ortaoba Unit) and thick seamount sequences (Nilüfer Unit) which display clear within-plate geochemistries with no evidence of a supra-subduction component. Although blueschists were not observed within the Karakaya units studied during this project, Okay *et al.* (1991) reported the presence of incipient sodic amphiboles in the Nilufer Unit in the Bursa region.

If the Karakaya Complex in western Turkey had been a back-arc basin, the seamount basalts of the Nilüfer Unit would probably have shown some evidence of a subduction signature, such as depletions in the HFS elements. Interestingly, several of the MORB basalts in the Ortaoba Unit do display slight Nb depletions. Whether this is a fractionation effect or reflects a minor subduction influence is not clear and requires further geochemical studies.

Another point to consider is the fact that the Karakaya Complex does not display any evidence of initial arc splitting and rifting, such as coarse, arc-derived volcaniclastics. Ocean drilling of modern back-arc settings, together with studies of uplifted back-arc basin sequences, have revealed the importance of arc-derived volcaniclastic debris (as reviewed by Carey & Sigurdsson, 1984). For example, they described a sequence drilled through the Parece Vela Basin, west of the West Mariana Ridge in the western Pacific, which reflects:

1. Initial creation of back-arc crust.
2. Influx of volcaniclastics from the active arc.
3. Waning of arc volcanism. Pelagics become interbedded with volcaniclastics.
4. Cessation of arc volcanism. Subsidence of back-arc basin. Ash- and carbonate-poor clay is deposited.

The clastic sequences of the Küre Complex contain both terrigenous and volcaniclastic detritus, as expected for a back-arc basin formed within the Eurasian margin. Although the clastics of the Karakaya Ortaoba Unit contain abundant devitrified acidic volcanic material, coarse arc-derived volcaniclastics are absent. Hydrothermal deposits also provide an additional source of volcanogenic sediments and are found at the base of many back-arc sites in the western Pacific (e.g. in the Philippine Sea; Bonatti *et al.,* 1979). As in major oceans, such deposits are formed and distributed around spreading centres and are thus found mainly at the base of back-arc basin sedimentary sequences. Metalliferous deposits are a distinctive feature of the back-arc Kure Complex. Cupriferous pyrite deposits are found along the lava-sediment interface as both disseminated and massive ores (Ustaömer & Robertson, 1994). Apart from localized, small-scale sulphide deposits at the top of the pillow basalts in the Ortaoba Unit, the Karakaya Complex in NW Turkey contains relatively few ore-bodies.

In summary, the available evidence suggests that the Karakaya Complex represents the remnants of an open oceanic area, rather than a back-arc basin, and is therefore here interpreted as an accretionary complex formed by closure of the Palaeotethys Ocean itself. However, more work needs to be done on the complex, especially in the regions to the east of the field area, before this can be confirmed.

10.6 Tectonic models for the evolution of the Karakaya Complex within the framework of the Palaeotethys Ocean

The models put forward for Eastern Mediterranean Palaeotethyan evolution tend to polarize into two radically different end-members, invoking both northward (e.g. Robertson & Dixon, 1984) and southward (e.g. Sengör *et al.,* 1984) subduction of the Palaeotethys Ocean (see Chapter 1). These alternative hypotheses have very different implications for the studied units within the Palaeotethyan framework.

In the light of the evidence presented above, the Karakaya Complex is interpreted as an accretionary complex formed by closure of a major ocean (i.e. the Palaeotethys). In this respect any models presented in this thesis will differ radically from the model postulated by, for example, Sengor *et al.* (1984) which is based on the premise that the Palaeotethys subducted south (in the Eastern Mediterranean region) and that the Karakaya Complex was a relatively small back-arc basin. Nevertheless, given the predominant northward vergence of the Karakaya Complex, southward subduction is

still a viable option and is accordingly discussed below. Despite its incompatibility with the overall structure of the Karakaya Complex, northward subduction also has points in its favour. The points for and against the two main scenarios are briefly discussed below.

10.6.1 Southward subduction of Palaeotethys

Southward subduction of the Palaeotethys Ocean is the most obvious way of producing the present structure of the Karakaya Complex and also the similar northward vergence of the Denizgören Ophiolite. Northward-vergent structures within the Karakaya Complex are ubiquitous, in NW Turkey at least, and strongly support a predominant southward subduction process during formation of the complex.

However, southward subduction does not fit with the widely accepted view of an active Eurasian margin and a passive Gondwanan margin (e.g. Dercourt *et al.*, 1986). In particular, a southward subduction scenario does not fit with the model postulated by Ustaömer (1993) for the Central Pontides, directly east of the field area. In his model northward subduction of the Palaeotethys Ocean was accompanied by back-arc basin formation. The back-arc basin (Küre Complex) was subsequently subducted southwards, producing a suture zone to the north of his main Palaeotethyan suture. It is important to emphasize that despite its fragmentary nature in central northern Turkey, the Karakaya Complex *clearly lies to the south of both these sutures, thus reflecting tectonic events which must have occurred either within the Palaeotethys Ocean or towards its southern margins, rather than at the Eurasian margin.*

10.6.2 Northward subduction of Palaeotethys

Northward subduction of the Palaeotethys Ocean fits with the broad picture of an active Eurasian margin and a passive Gondwanan margin (e.g. Chios and Karaburun) and agrees with the models of Robertson & Dixon (1984) and Ustaömer (1993) for the Central Pontides. Northward subduction of the Palaeotethys would also explain the presence of abundant Upper Permian carbonate platforms with clastic basements which are found associated with Palaeotethyan accretionary units in NW Turkey. Carbonate platforms with clastic basements are characteristic of the Mesozoic Tethys and have been interpreted as continental fragments which were rifted off Gondwana (e.g. Robertson *et al.*, 1991). It is therefore likely that the older platforms of NW

Turkey were similarly derived from the Gondwanan margin. The Upper Carboniferous-Permian Kargi Complex in the central Pontides is also thought to represent a Gondwanan fragment which drifted north across the Palaeotethys (Ustaömer, 1993). Several possible analogies to the Kargi Complex are found in the Biga Peninsula and surrounding regions (e.g. Karadag Unit, Çal Unit).

However, a major problem with this model is that a northward subduction model cannot be used to explain the ubiquitous northward vergence of the Karakaya Complex and associated units such as the Denizgören Ophiolite.

10.7 Discussion

As the current arrangement of the Karakaya Complex and other related units (e.g. Denizgören Ophiolite, Kazdag Massif, Küre Complex) cannot be fully explained by either north- or south-directed subduction alone, it seems most likely that elements of both were involved during closure of the Palaeotethys Ocean in the Late Palaeozoic-Early Mesozoic. A tentative model which could explain the current arrangement of tectonic units in the Biga Peninsula and surrounding regions is shown in Figure 10.1 and is explained more fully below.

Owing to the clear northward vergence of the Karakaya Complex, southward subduction was probably the predominant mechanism during its formation. However, invoking southward subduction zone to form the Karakaya Complex does not preclude an earlier, northward subduction zone beneath an active Eurasian margin. By analogy with the Mesozoic Tethys it seems likely that the numerous carbonate-capped slivers within the Palaeotethys Ocean were derived from the Gondwanan margin. Thus, northward drift of carbonate-capped continental slivers from the Gondwanan margin and northward subduction at the Eurasian margin may have been followed by later, southward, subduction and the formation of the Karakaya Complex. Oceanic crust, trench sequences, seamounts, abyssal sediments and intra-oceanic platforms were accreted and incorporated into the Karakaya Complex. A shallow-marine, perched fore-arc basin developed on top of the accretionary complex. As southward subduction of the Palaeotethys Ocean does not appear to have occurred in the central Pontides (except during closure of the Kure back-arc basin) it may be a feature confined to the extreme western end of the Palaeotethys Ocean. Cessation of north-dipping subduction and the initiation of south-dipping underthrusting may have been caused by "jamming" of the original trench by large oceanic plateau or many

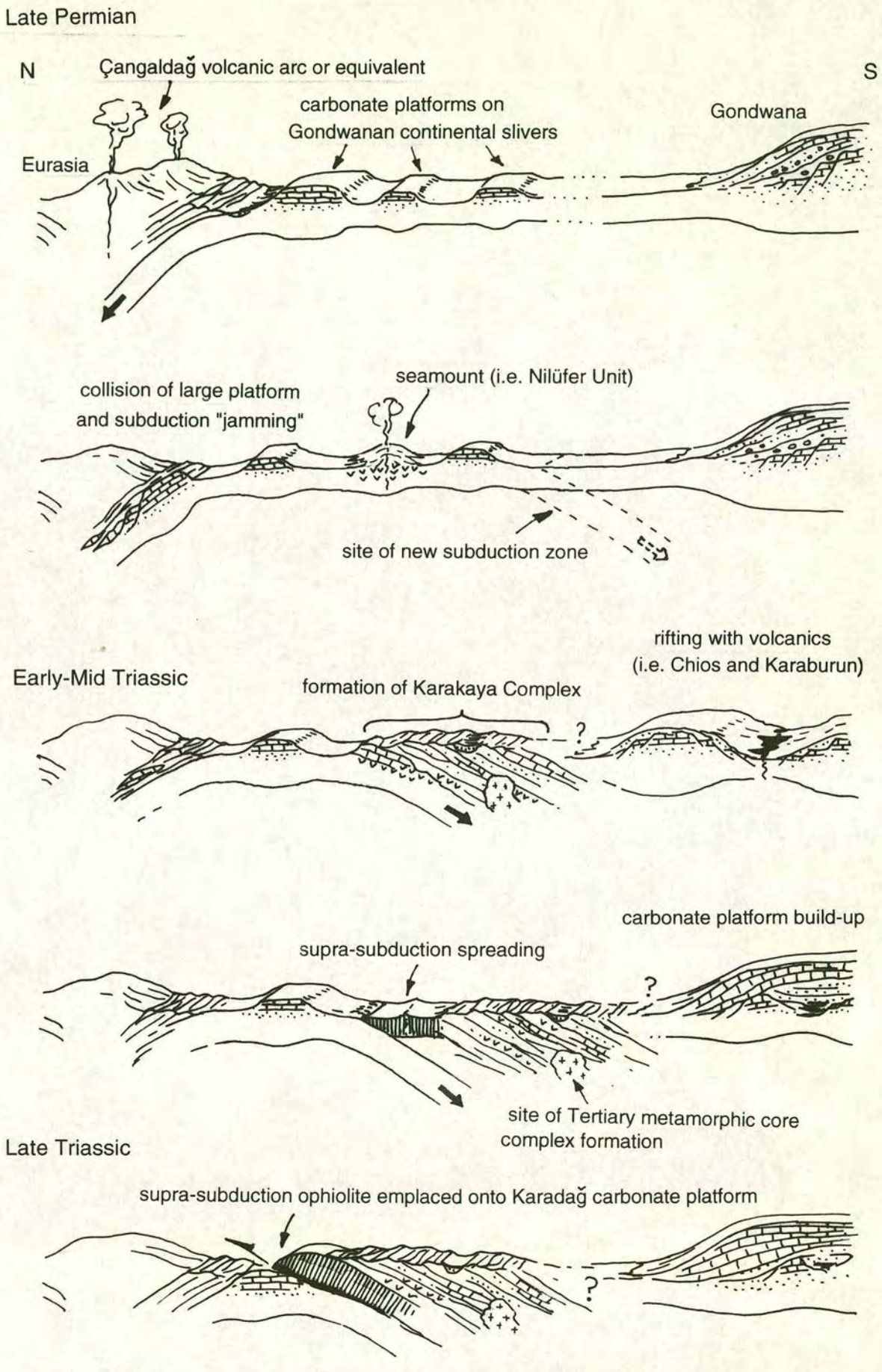

Figure 10.1 Tentative tectonic evolution of the Palaeotethys Ocean in NW Turkey from the Late Palaeozoic to the Late Triassic.

small platforms, perhaps features similar to the Kargi Complex in the Central Pontides. An analogous situation may have occurred in the SW Pacific during the Mid or Late Miocene. The Ontong Java Plateau collided with the West Melanesian Trench (SW subduction) in Mid or Late Miocene, effectively blocking further subduction at this trench system. As a result of this collision plate boundaries readjusted and NE subduction was initiated along the SW margin of the New Ireland-Solomon Island archipelago (Weissel *et al.,* 1982). A similar, although not analogous, situation may be present south of Cyprus where the Eratosthenes Seamount is apparently wedged between the converging African and Eurasian plates. In this case, northward subduction of the seamount was followed by southward underthusting beneath the Levantine Basin, owing to collision-related compression (Robertson *et al.,* 1994). Unlike the Eratosthenes example, the switching of subduction polarity within the Palaeotethys did not involve direct collision between the two continental masses. Nevertheless, this example serves to show that the direction of underthrusting may reverse if large oceanic/continental fragments impinge on a subduction zone.

The presence of terrigenous material within the Karakaya Complex implies that this inferred southward subduction occurred towards the Gondwanan margin, possibly beneath a rifted continental fragment which may, or may not, have developed minor arc volcanism. The general absence of arc volcanics (other than devitrified acidic volcanic clasts of possible arc affinity within the Ortaoba Unit) implies that a major arc did not develop.

Thus, northward subduction probably shaped the large scale plate tectonic arrangement of the Eastern Mediterranean region (producing the well-documented Gondwanan passive margin and an active Eurasian margin to the north), while the northward vergence which characterizes the pre-Jurassic of NW Turkey, was produced by a subsequent southward subduction event of unknown extent.

The Denizgören Ophiolite was probably both formed and emplaced to the north of the Karakaya Complex. This hypothesis is based on the fact that the Upper Triassic perched fore-arc sequence (Halilar Formation) lying on top of the Karakaya Complex in the Biga Peninsula is unmetamorphosed, relatively undeformed and completely lacking in ophiolite detritus. The supra-subduction zone (SSZ) characteristics of the ophiolite suggest that the south-dipping subduction zone which formed the Karakaya Complex may have "stepped back", causing SSZ spreading in front of the Karakaya Complex. Such a phenomenon could be caused by arrival at the trench of large

edifices such as seamounts. Tomoda & Fujimoto (1983) described the effects of the interference between trenches and seamounts. They concluded that large seamounts or rises which are difficult to subduct may cause a new subduction zone to form seaward of the original trench. This has been documented in the Early Cretaceous Kamuikotan tectonic belt of Hokkaido, Japan (Watanabe & Maekawa, 1985). A similar situation may be present in the Mediterranean where continental crust of the Eratosthenes Seamount is currently being subducted beneath Cyprus. Northward underthrusting in the Mid-Late Miocene was followed by a southwards jump of the active decollment zone, giving rise to a small sedimentary basin (Robertson *et al.*, 1994). The Nilüfer "seamount(s)", may have caused this type of subduction step-back. The position of the Nilüfer Unit at the base of the Karakaya Complex thrust stack also supports this hypothesis. At this point the Karakaya Complex would have become isolated from the trench and thus ceased to be an active accretionary complex. Subsidence of the accretionary complex led to deeper water sediments being laid down in the perched fore-arc basin. Arrival of a further Gondwanan platform (the clastic-carbonate Karadag Unit) at the trench initiated emplacement of the ophiolite over the platform. Thrusting caused the incorporation of oceanic sediments and gabbros into the metamorphic sole beneath the ophiolite. Northward emplacement of the ophiolite over the platform was accompanied by northward thrusting of the Karakaya Complex as a whole. An influx of very shallow marine clastics at the top of the perched fore-arc basin sequence may reflect this uplift of the Karakaya Complex. Tectonic activity had ceased by the Mid Jurassic when the shelfal Bilecik Limestone was laid down over much of NW Turkey.

The model described above can also explain the presence of meta-ophiolitic lithologies within the core of the Kazdag Massif metamorphic core complex. If the Karakaya Complex was carried along on the back of the Denizgören Ophiolite then presumably parts of the ophiolite lie beneath the deepest levels of the Karakaya Complex. This appears to be the case, as exhumation of the Kazdag Massif during the Tertiary has revealed a thick sequence of metamorphosed Karakaya-type lithologies with an ophiolitic remnant at its core.

Following the definition of Ustaömer (1993), the Palaeotethys Ocean is viewed here as an essentially Palaeozoic ocean which only finally closed by northward subduction along the Izmir-Ankara-Erzincan Suture Zone in Late Mesozoic-Early Tertiary times. Thus, the northward emplacement of the Denizgören Ophiolite and Karakaya Complex during the Triassic occurred north of the final suture zone while a large

expanse of Palaeotethys remained to the south. The Tethys reverted to a regime of predominantly northward subduction during the Mesozoic-Tertiary, as documented by many workers in the Eastern Mediterranean (as summarized by Robertson & Dixon, 1984). The "Neotethys" was formed by basins that rifted in the Late Palaeozoic-Early Mesozoic along the Gondwanan margin and was destroyed in Late Mesozoic-Early Tertiary times as Palaeotethys continued to close. Forceful suturing of the Palaeotethys is unlikely as relatively little deformation is recorded by the Triassic carbonate platforms of Chios and Karaburun.

Although it can explain the arrangement of the Karakaya Complex and associated units, this model does not yet adequately explain what occurred at the two continental margins during the Late Palaeozoic-Early Mesozoic. The evolution of the Eurasian and Gondwanan margins in western Turkey and surrounding regions during this time are beyond the scope of this project, but need to be further studied if the model presented here is to be fully tested.

10.8 Summary

The key points regarding the origin of the various units and their tentative tectonic reconstruction are listed below. It must be recognized, however, that the model postulated here is basically a two dimensional one and that strike-slip may have played a significant role.

1. During the Late Permian, the Palaeotethys Ocean was subducting northwards beneath an active Eurasian margin, as recorded in the Central Pontides of Turkey (Ustaömer & Robertson, 1994). Continental slivers derived from Gondwana drifted northwards to become accreted at the Eurasian margin. These slivers comprised carbonate platforms on clastic basements, such as the Kargi Complex and the Karadag and Çal Units.

2. A large platform "jammed" the subduction zone, or at least slowed down the subduction process, and a new southward-dipping subduction zone was initiated further south during the Late Permian-Early Triassic, possibly beneath a rifted Gondwanan fragment. This new subduction zone caused further rifting within the Gondwanan margin to create a north-facing passive margin (now represented by Chios and Karaburun).

3. Oceanic units and Gondwana platforms were accreted at the south-dipping subduction zone, thereby generating the Karakaya Complex. Tectonostratigraphic units within the complex include Triassic seamount(s) (Nilüfer Unit), trench sequences (Ortaoba Unit), abyssal plain (Kalabak Unit) and Permian carbonate platforms with intra-platform basins (Çal Unit). These units were tectonically juxtaposed and form a south-dipping thrust stack. The dismembered seamounts and intra-platform basin lavas have within-plate geochemical signatures, whereas the basalts flooring the trench sequence are predominantly MORB. Subduction-accretion processes were accompanied by the formation of perched basins (e.g. the Halilar Formation) on top of the accretionary complex.

4. Large Mid Triassic seamounts (e.g. the Nilüfer Unit) arrived at the trench and caused the subduction zone to "step back" to the north. Fore-arc spreading above the new subduction zone created SSZ harzburgitic crust. Intra-oceanic thrusting led to metamorphic sole formation and eventual emplacement of the ophiolite over a carbonate platform.

5. Impingement of a further large carbonate platform (the Karadag Unit) may have caused the initiation of ophiolite emplacement over the platform. A metamorphic sole was generated as the harzburgitic slab overthrust fore-arc volcanics and accretionary units near the trench. The ophiolite was emplaced northwestwards onto Permian (Karadag Unit) and Permo-Triassic (Lesbos) carbonate-clastic units.

6. Emplacement of the ophiolite was accompanied by northwards thrusting of the Karakaya Complex as a whole.

7. By the Early-Mid Jurassic tectonic activity had ceased and extensive shelf carbonate sequences (Bilecik Limestone) were established over much of NW Turkey.

8. The Kazdag Massif represents a metamorphic core complex composed of deeply buried levels of the Karakaya Complex and parts of the Denizgoren-Lesbos Ophiolite. Exhumation of the core complex occurred along normal faults and large-scale mylonitic detachments and was initiated during the Miocene. Amphibolites in the core of the massif are interpreted as part of the Denizgören Ophiolite and indicate protoliths which formed in both MORB and SSZ settings.

6. Tertiary tectonics caused an approximate 47° anticlockwise rotation of the Biga Peninsula region. However, timing cannot be well constrained.

REFERENCES

Adamia, Sh. A., Chkhotua, T., Kekelia, M., Lordkipanidze, M., Shavishili, I. & Zakariadze, G. 1981. Tectonics of the Caucasus and adjoining regions: implications for the evolution of the Tethys ocean. J. Struct. Geol. 3 (4), 437-447.

Adamia, Sh. A., Belov, A. A., Kekalia, M. A. & Shavishili, I. D. 1987. Paleozoic tectonic development of the Caucasus and Turkey. In: Fingel, Sassi, & Grecula (eds) Pre-Variscan and Variscan events in the Alpine-Mediterranean Mountain Belts. Mineralia Slovaca Monograph, 23-50.

Adamia, Sh. A. & Belov, A. A. 1989. Problems on the Paleozoic geodynamic domains and their alpidic evolution in the Caucasus. In: Papanikolaou, D. J. & Sassi, F. P. (eds) IGCP Project No. 276. Newsletter 1. Geol. Soc. Greece Spec. Publ. 1, 11-18.

Akartuna, M. 1968. Armutlu yarimadasinin jeolojisi. Istanbul Universitesi Fen Fakultesi Monografileri, sayi 20, 105pp.

Aktas, G. & Robertson, A. H. F. 1984. The Maden Complex, S.E. Turkey: evolution of a Neotethyan active margin. In: Dixon, J. E. & Robertson, A. H. F. (eds) The Geological Evolution of the Eastern Mediterranean. Geol. Soc. Spec. Publ. No. 17, 375-402.

Akyurek, B. & Soysal, Y. 1993. Biga Yarimadasi (Savastepe-Kirkagac-Bergama-Ayvalik) temel jeoloji ozellikleri. M.T.A. Derg., 95/96, 1-12.

Alt, J. C., Laverne, C. & Muehlenbachs, K. 1985. Alteration of the upper oceanic crust: Mineralogy and processes in DSDP Hole 504B, Leg 83. In: Anderson, R. N., Honnorez, J., Becker, K. et al. (eds) Initial reports of the Deep Sea Drilling Program, 83, 217-247.

Altiner, D., Kocyigit, A., Farinacci, A., Nicosia, U. & Conti, M. A. 1991. Jurassic-Lower Cretaceous stratigraphy of the southern part of north-western Anatolia (Turkey). Geologica Romana, vol. 27, 13-80.

Altinli, I. E. 1973a. Bilecik Jurassic (Turkey). In: Doyran, S. (ed). Papers, Congress of Earth Sciences on the occasion of the 50th anniversary of the Turkish Republic. M.T.A., 105-114.

Altinli, I. E. 1973b. Geology of the Middle Sakarya River (Turkey). In: Doyran, S. (ed). Papers, Congress of Earth Sciences on the occasion of the 50th anniversary of the Turkish Republic. M. T. A., 161-196.

Anderson, R. N. & Hobart, M. A. 1976. The relation between heat flow, sediment thickness, and age in the eastern Pacific. J. Geophys. Res. 81, 2968-2989.

Aslaner, M. 1965. Etude geologique et petrographique de la region d'Edremit-Havran (Turquie). M.T.A. Publ., 119, 1-98.

Atherton, M. P. & Edmonds, W. M. 1966. An electron microprobe study of some zoned garnets from metamorphic rocks. Earth Planet. Sci. Lett. 1, 185-193.

Avgiad, D. & Garfunkel, Z. 1991. Uplift and exhumation of high pressur metamorphic terrains: the example of the Cycladic blueschist belt (Aegean Sea). Tectonophysics, 188, 357-372.

Aygen, T. 1956. Etude geologique de la region de Balya (Turquie). M.T.A. Publ., D, 11, 1-95.

Bachman, S. B. 1982. The Coastal Belt of the Franciscan: youngest phase of northern California subduction. In: Leggett, J. K. (ed) Trench-Forearc Geology. Geol. Soc. London Spec. Publ. No. 10, 401-417.

Ballard, R. D., Holcombe, R. T. & van Andel, T. H. 1979. The Galapagos Rift at 86°W; sheet flows, collapse pits, and lava lakes of the rift valley. J. Geophys. Res. 84, 5407-5422.

Basaltic Volcanism Study Project. 1981. Basaltic volcanism on the terrestrial planets. New York, Pergamon Press, 1286pp.

Baud, A., Jenny, C., Papanikolaou, D., Sideris, Ch. & Stampfli, G. 1991. New observations on Permian stratigraphy in Greece and geodynamic interpretation. Bull. Geol. Soc. Greece, 25 (1), 187-206.

Bechennec, F., Le Metour, J., Rabu, D., Bourdillon-de-Grissac, C. H., De Wever, P., Beurrier, M. & Villey, M. 1990. The Hawasina Nappes: stratigraphy and structural evolution of a fragment of the south-Tethyan passive continental margin. In: Robertson, A. H. F., Searle, M. P. & Ries, A. C. (eds) The Geology and Tectonics of the Oman Region. Geol. Soc. London Spec. Publ. No. 49, 213-223.

Berger, W. H. & Winterer, E. L. 1974. Plate stratigraphy and the fluctuating carbonate line. In: Hsu, K. J. & Jenkyns, H. C. (eds) Pelagic sediments: on land and under the sea. Spec. Publ. Int. Ass. Sediment, 1, 11-48.

Bernoulli, D. & Jenkyns, H. C. 1974. Alpine, Mediterranean and North Atlantic Mesozoic facies in relation to the early evolution of the Tethys. In: Dott, R. H. & Shaver, R. H. (eds) Modern and Ancient Geosynclinal Sedimentation. Spec. Publ. Soc. Econ. Paleont. Miner. 19, 129-160.

Besenecker, H., Durr, S., Herget, G., Jacobshagen, V., Kauffmann, G., Ludtke, G., Roth, W. & Tietze, K.-W. 1968. Geologie von Chios (Agais). Geologica et Palaeontologica, 2, 121-150, Marburg.

Besenecker, H, Durr, S., Herget, G., Kauffmann, G., Ludtke, G., Roth, W. & Tietze, K.-W. 1971. 1:50000 Geological map of Chios (2 sheets: northern and southern), Athens.

Bhatia, M. R. & Crook, K. A. W. 1986. Trace element characteristics of geywackes and tectonic discrimination of sedimentary basins. Contrib. Mineral. Petrol. 92, 181-193.

Bingol, E. 1968. Contribution a l'etude geologique de la partie centrale et SE du massif de Kazdag (Turquie). Ph.D. Thesis. Univ. of Nancy, France.

Bingol, E. 1971. Fiziksel yas tayini metodlarini siniflama denemesi ve Rb-Sr ve K-Ar metodlarinin Kazdag'da bir uygulamasi. Turkiye Jeol. Kur. Bult. 14, 1-16.

Bingol, E. 1989. Geological Map of Turkey. 1: 2000 000. M. T. A. Ankara.

Bingol, E., Akyurek, B. & Korkmazer, B. 1973. Geology of the Biga Peninsula and some characteristics of the Karakaya Formation. In: Doyran, S. (ed). Papers, Congress of Earth Sciences on the occasion of the 50th anniversary of the Turkish Republic. M. T. A., 71-77.

Bittner, A. 1890. Brachiopoden der Alpinen Trias. Abhandl. d. K. K. geol. Reichsanstalt, Band 14, Wien.

Blanc, P. 1965. Serie stratigraphique de Cal Koy (Anatolie Occidentale, Turquie): presence de spilites dans le Permien. C. R. Soc. Geol. France, 3, 100-102.

Bonatti, E., Kolla, V., Moore, W. S. & Stern, C. 1979. Metallogenesis in marginal basins: Fe-rich basal deposits from the Philippine Sea. Mar. Geol. 32, 21-37.

Boudier, F., Nicolas, A. & Bouchez, J. L. 1982. Kinematics of oceanic thrusting and subduction from basal sections of ophiolites. Nature 296, 825-828.

Brown, K. M. & Westbrook, G. K. 1987. The tectonic fabric of the Barbados Ridge accretionary complex. Marine Petroleum Geol. 4, 71-81.

Busby-Spera, C. J. 1987. Lithofacies of deep marine basalts emplaced in a Jurassic back arc apron, Baja California (Mexico). J. Geol. 95, 671-686.

Busby-Spera, C. J. 1988. Evolution of middle Jurassic marginal basin, Cedros Island, Baja California: evidence from a marine volcaniclastic apron. Geol. Soc. Am. Bull. 100, 218-233.

Butler, R. F. 1992. Paleomagnetism: magnetic domains to geologic terrains. Blackwell Sci. Pubs.

Cadet, J-P., Kobayashi, K., Aubouin, J., Boulegue, J., Deplus, C., Dubois, J, von Huene, R., Jolivet, L., Kanazawa, T., Kasahara, J., Koizumi, K., Lallemand, S., Nakamura, Y., Pautot, G., Suyehiro, S., Tokuyama, H. & Yamazaki, T. 1987. The Japan Trench and its juncture with the Kuril Trench: cruise results of the Kaiko project, Leg 3. Earth Planet. Sci. Lett. 83, 267-284.

Cann, J. R. 1969. Spilites from the Carlsberg Ridge, Indian Ocean. Journal of Petrology 20, 244-267.

Carey, S. W. 1958. The tectonic approach to continental drift. In: Carey, S. W. (ed) Continental Drift, A Symposium, Geology Department, University of Tasmania, Hobart, 177-356.

Carey, S. & Sigursson, H. 1984. A model of volcanogenic sedimentation in marginal basins. In: Kokelaar, B. P. & Howells, M. F. (eds) Marginal Basin Geology. Geol. Soc. London Spec. Publ. No. 16, 37-58.

Cas, R. A. F. & Wright, J. V. 1987. Volcanic successions. Unwin Hyman, London.

Casey, J. F. & Dewey, J. F. 1984. Initiation of subduction zones along transform and accretionary plate boundaries, triple junction evolution, and fore-arc spreading centres: implications for ophiolite geology and obduction. In: Gass, I. G., Lippard, S. J. & Shelton, A. W. (eds). Ophiolites and Oceanic Lithosphere. Geol. Soc. London Spec. Publ. No. 14, 269-290.

Chaput, E. 1932. Voyages d'etudes geologiques et geomorphologiques en Turquie. Paris.

Clement, B. 1977. Du Parnasse a l'Attique. Bull. Soc. geol. France 7 (14) 1, 66-70.

Clift, P. D. 1990. Mesozoic/Cenozoic sedimentation and tectonics of the southern Greek Neo-Tethys (Argolis Peninsula). Unpub. Ph.D. Thesis. Univ. of Edinburgh.

Clift, P. D. & Robertson, A. H. F. 1989. Evidence of a late Mesozoic ocean basin and subduction-accretion in the southern Greek Neo-Tethys. Geology 17(6), 559-563.

Clift, P. D. & Robertson, A. H. F. 1990. A Cretaceous Neo-tethyan carbonate margin in Argolis, southern Greece. Geol. Mag. 127 (4), 299-308.

Clift, P. D. & Robertson, A. H. F. 1990. Deep water basins within the Mesozoic carbonate platform of Argolis, Greece. J. Geol. Soc. Lond. 147, 825-836.

Cloos, M. 1984. Flow melanges and the structural evolution of accretionary wedges. Geol. Soc. Am. Sp. Paper 198, 71-80.

Cloos, M. & Apted, M. 1979. Guidebook to the Southern Coast ranges: Geology and Plate Tectonics. Esso Guidebook 10. Univ. of California at Los Angeles.

Clube, T. M. M. & Robertson, A. H. F. 1986. The palaeo-rotation of the Troodos microplate in the Late Mesozoic-Early Cenozoic plate tectonic framework of the Eastern Mediterranean. Surv. Geophys., 8, 375-437.

Cope, J. C. W. 1991. Middle Jurassic to Lower Cretaceous ammonites from the Pontide Mountains, northern Anatolia. Geologica Romana, vol. 27, 327-345.

Crawford, A. J., Falloon, T. J. & Green, D. H. 1989. Classification, petrogenesis and tectonic setting of boninites. In: Crawford, A. J. (ed) Boninites Unwin Hyman, London, 1-49.

Davidsen, E. K. & Cloos, M. 1985. Petrology and structure of greenstone blocks encased in Franciscan mud-matrix melange near San Simeon, California: dismembered subducted seamounts in an accretionary prism. Geol. Soc. Am. Bull. 17 (7), 559.

Davis, G. H. 1987. A shear-zone model for the structural evolution of metamorphic core complexes in southeastern Arizona. In: Coward, M. P., Dewey, J. F. & Hancock, P. L. (eds) Continental Extensional Tectonics. Geol. Soc. Spec. Publ. No. 28, 247-266.

Degnan, P. J. 1992. Tectono-sedimentary evolution of a passive margin: the Pindos Zone of the Peloponnese, Greece. Unpub. PhD. thesis, University of Edinburgh.

Dercourt, J., Zonenshain, L. P., Ricou, L. E., Kazmin, V. G., Le Pichon, X., Knipper, A. L., Grandjacquet, C., Sbortshikov, I. M., Geyssant, J., Lepvrier, C., Pechersky, D. H., Boulin, J., Sibuet, J. C., Savostin, L. A., Sorokhtin, O., Westphal, M., Bazhenov, M. L., Laver, J. P. & Biju-Duval, B. 1986. Geological evolution of the Tethys Belt from the Atlantic to the Pamirs since the Lias. Tectonophysics 123, 241-315.

Dewey , J. F., Pitman III, W. C., Ryan, W. B. F. & Bonnin, J. 1973. Plate tectonics and the evolution of the Alpine system. Geol. Soc. Am. Bull. 84, 3137-3180.

Dick, H. J. B. 1989. Abyssal peridotites, very slow spreading ridges and ocean ridge magmatism. In: Saunders, A. D. & Norry, M. J. (eds) Magmatism in the Ocean Basins. Geol. Soc. Spec. Publ. No. 42, 71-105.

Dick, H. J. B. & Bullen, T. 1984. Chromian spinel as petrogenetic indicators in abyssal and Alpine-type peridotites and spatially associated lavas. Contrib. Mineral. Petrol. 86, 54-76.

Diller, J. S. 1883. Note on the geology of the Troad. Quart. Journ. Geol. Soc., no. 156, London.

Dimitriadis, S. & Asvesta, A. 1993. Sedimentation and magmatism related to the Triassic rifting and later events in the Vardar-Axios Zone. In: Proceedings of the 6th Congress of the Geological Society of Greece, 25-27 May, 1992, Athens, 149-168.

Doubleday, P. A., Leat, P. T., Alabaster, T., Nell, P. A. R. & Tranter, T. H. 1994. Allochthonous oceanic basalts within the Mesozoic accretionary complex of Alexander, Antarctica: remnants of proto-Pacific oceanic crust. J. Geol. Soc. London 151, 65-78.

Droop, G. 1987. A general equation for estimating Fe3+ concentrations in ferromagnesian silicates and oxides from microprobe analyses using stoichiometric criteria. Mineral. Mag. 45, 201-209.

Eaton, S. & Robertson, A. H. F. 1993. The Miocene Pakhna Formation, southern Cyprus and its relationship to the Neogene tectonic evolution of the Eastern Mediterranean. Sedimentary Geology 86, 273-296.

Erdogan, B. 1990. Geology of Karaburun Peninsula. Guide book for the International Earth Sciences Congress on Aegean regions, 1-6 October 1990, Izmir, pp. 45.

Ernst, W. G. 1970. Tectonic contact between the Franciscan melange and the great Valley Sequence-crustal expression of a Late Mesozoic Benioff Zone. J. Geophys. Res. 75, 886-901.

Fischer, A. G. 1964. The Lofer cyclothems of the Alpine Triassic. In: Merriam, D. F. (ed) Symposium on cyclic sedimentation. Bull. Geol. Surv. Kansas 169, 107-149.

Floyd, P. A. 1993. Geochemical discrimination and petrogenesis of alkalic basalt sequences in part of the Ankara melange, central Turkey. Journal Geol. Soc. London 150 (3), 541-550.

Floyd, P. A. & Winchester, J. A. 1975. Magma-type and tectonic setting discrimination using immobile elements. Earth Planet. Sci. Lett. 27, 211-218.

Gass, I. G. 1990. Magmatic processes at and near constructive plate margins as deduced from the Troodos (Cyprus) and Semail Nappe (N. Oman) ophiolites. In: Saunders, A. D. & Norry, M. J. (eds) Magmatism in the ocean basins. Geol. Soc. London. Spec. Publ. 42, 1-16.

Gillis, K. M. & Robinson, P. T. 1990. Multistage alteration in the extrusive sequence of the Troodos ophiolite, Cyprus. In: Malpas, S., Moores, E. M., Panayiotan, A. & Xenophontos, C. (eds.) Ophiolites: Oceanic Crustal Analogues. Cyprus Geol. Surv., 655-664.

Glasby, G. P. (ed) 1977. Marine manganese deposits. Elsevier, Amsterdam, pp 523.

Goncuoglu, M. C., Erendil, M., Tekeli, O., Aksay, A., Kuscu, I. & Urgun, B. M. 1987. Geology of the Armutlu Peninsula. In: Guide book for the field excursion along western Anatolia, Turkey. M.T.A. Publ.

Graham, J. W. 1949. The stability and significance of magnetism in sedimentary rocks. J. Geophys. Res. 54, 131-167.

Granit, Y. & Tintant, H. 1960. Observations preliminaires sur le Jurassique de la region de Bilecik (Turquie). C. R. Acad. Scien. Paris 251, 1801-1803.

Gromet, L. P., Dymek, R. F., Haskin, L. A. & Korotev, R. L. 1984. The "North American Shale Composite": its compilation, major and trace element characteristics. Contrib. Mineral. Petrol. 80, 160-182.

Gumus, A. 1964. Contribution a l'etude geologique du secteur septentrional de Kalabak Koy-Eymir Koy (region d'Edremit, Turquie). M. T. A. Publ. 117, 1-109.

Halls, H. C. 1978. The use of converging remagnetizion circles in palaeomagnetism. Physics of the Earth and Planetary Interiors 16, 1-11.

Hamilton, W. 1987. Crustal extension in the Basin and Range Province, southwestern United States. In: Coward, M. P., Dewey, J. F. & Hancock, P. L. (eds) Continental Extensional Tectonics. Geol. Soc. Spec. Publ. No. 28, 155-176.

Hardy, R. & Tucker, M. 1988. X-ray diffraction of sediments. In: Tucker, M. (ed) Techniques in Sedimentology. Blackwells Scientific Publications, 191-228.

Harland, W. B., Armstrong, R. L., Cox, A. V., Craig, L. E. & Smith, A. G. 1990. A Geologic Time Scale 1989. Cambridge University Press.

Hecht, J. 1972. Geological map: Plomari-Mytilini sheet. 1:50000 IGME.

Hecht, J. 1974. Geological map: Polychnitos sheet. 1:50000 IGME.

Hecht, J. 1975. Geological map: Eressos sheet. 1:50000 IGME.

Heller, F. 1978. Rock magnetic studies of Upper Jurassic Limestones from Southern Germany. J. Geophys. 44, 595-543.

Hickey, R. L. & Frey, F. A. 1982. Geochemical characteristics of boninite series volcanics: implications for their source. Geochim. Cosmochim. Acta 46, 2099-2115.

Hollister, L. S. 1966. Garnet zoning: an interpretation based on the Rayleigh fractionation model. Science 154, 1647-1651.

Hopson, C. A., Mattinson, J. M. & Pessagno, E. A. 1981. Coast Range ophiolite, western California. In: Ernst, W. G. (ed). The geotectonic development of California: Rubey Volume 1, New Jersey, Prentice Hall, 418-510.

Hsu, K. J. 1977. Tectonic evolution of the Mediterranean basins. In: Nairn, A. E. M, Kanes, W. H. & Stehl, F. G. (eds) The Ocean Basins and Margins, 4A, The Eastern Mediterranean, Plenum, New York, 29-75.

Hudson, T. & Plafker, G. 1979. Paleogene anatexis along the Gulf of Alaska margin. Geology 7, 573-577.

Humphris, S. E. & Thompson, G. 1978. Hydrothermal alteration of oceanic basalts by seawater. Geochimica et Cosmochimica Acta 42, 107-125.

Jamieson, R. A. 1980. Ophiolite emplacement as recorded in the dynamothermalaureole of the St. Anthony Complex, north-western Newfoundland. In: Panaiotou, A. (ed). Proceedings of the International Ophiolite Symposium, Cyprus, 1979. Cyprus Geol. Surv. 620-627.

Jamieson, R. A. 1981. Metamorphism during ophiolite emplacement. The petrology of the St. Anthony Complex. J. Geol. 22(3), 297-449.

Jenkyns, H. C. 1986. Black shales and carbon isotopes in pelagic sediments from the Tethyan Lower Jurassic. Sedimentology 33, 87-106.

Jones, G. 1990. Tectonostratigraphy and evolution of the Pindos Opiolite and associated units, north-west Greece. Unpublished Univ. of Ed. thesis. 397pp.

Jones, G. & Robertson, A. H. F. 1991. Tectono-stratigraphy and evolution of the Mesozoic Pindos ophiolite and related units, northwestern Greece. J. Geol. Soc. Lond. 148, 267-288.

Jones, G., Robertson, A. H. F. & Cann, J. R. 1991. Genesis and emplacement of the supra-subduction zone Pindos ophiolite, northwestern Greece. In: Peters, T. J., Nicolas, A. & Coleman, R. G. (eds) Proceedings of the Ophiolite Conference, Oman 1990: Ophiolite Genesis and Evolution of the Oceanic Lithosphere, 779-807.

Jones, G., Sano, H. & Valsami-Jones, E. 1993. Nature and tectonic setting of accreted basalts from the Mino Terrane, central Japan. J. Geol. Soc. Lond. 150, 1167-1181.

Jones, J. G. 1966. Intraglacial volcanoes of south-west Iceland and their significance in the interpretation of the form of the marine basaltic volcanoes. Nature, 212, 586-588.

Kalafatcioglu, A. 1963. Geology around Ezine and Bozcaada and the age of the limestones and serpentines. M. T. A. Publ. 60, 61-70.

Karig, D. E. 1988. The framework of deformation in the Nankai Trough. In: Kagami, H., Karig, D. E. et al. (eds). Initial Reports, DSDP, 87, 927-940.

Karl, S. M. 1984. Sedimentologic, diagenetic, and geochemical analysis of Upper Mesozoic ribbon cherts from the Franciscan assemblage at the Marin Headlands, California. In: Blake, M. C. (ed) Franciscan Geology of Northern California. Pacific Section, S. E. P. M. California, 71-88.

Katsikatsos, G., Matarangas, D., Migiros, G. & Triantaphyllis, M. 1982. The geological structure of Lesvos Island. IGME Report. 95pp.

Kauffman, G. 1969. Die Geologie von Nordost-Chios(Agais). Diss. Marbourg, 212, Marbourg.

Kaya, O., Wiedmann, J. & Kozur, H. 1986. Preliminary report on the stratigraphy, age and structure of the so-called Late Paleozoic and/or Triassic "melange" or "suture zone complex" of north-western and western Turkey. Yerbilimleri, Hacattepe Univ., 13, 1-16.

Kaya, O., Ozcocak, O. & Lisenbee, A. 1989. Stratigraphy of the pre-Jurassic blocky sedimentary rocks to the south of Bursa, NW Turkey. M. T. A. Bull. 109, 15-24.

Kaya, O. & Mostler, H. 1992. A Middle Triassic age for low-grade greenschist facies metamorphic sequence in Bergama (Izmir), western Turkey: the first paleontological age assignment and structural-stratigraphic implications. Newsl. Stratigr. 26 (1), 1-17, Stuttgart.

Keen, M. J. 1963. The magnetization of sediment cores from the eastern basin of the North Atlantic Ocean. Deep Sea Res. 10, 607-622.

Kissel, C. & Laj, C. 1988. The Tertiary geodynamical evolution of the Aegean arc: a paleomagnetic reconstruction. Tectonophysics 146, 183-201.

Kobayashi, K., Cadet, J-P., Aubouin, J., Boulegue, J., Dubois, J., von Huene, R., Jolivet, L., Kanazawa, T., Kasahara, J., Koizumi, K., Lallemand, S., Nakamura, Y., Pautot, G., Suyehiro, K., Tani, S., Tokuyama, H. & Yamazaki, T. 1987. Normal faulting of the Daiichi-Kashima Seamount in the Japan Trench revealed by the Kaiko I cruise, Leg 3. Earth Panet. Sci. Lett. 83, 257-266.

Krushensky, R. D., Akcay, Y. & Karaege, E. 1980. Geology of the Karalar-Yesiller area, northwest Anatolia, Turkey. Geol. Surv. Am. Bull. 1461, 1-72.

Lallemand, S. & Le Pichon, X. 1987. Coulomb wedge model applied to the subduction of seamounts in the Japan Trench. Geology 15, 1065-1069.

Laubscher, H. P. & Bernoulli, D. 1977. Mediterranean and Tethys. In: Nairn, A. E. M, Kanes, W. H. & Stehl, F. G. (eds) The Ocean Basins and Margins, 4A, The Eastern Mediterranean, Plenum, New York, 1-28.

Leggett, J. K., McKerrow, W. S. & Casey, D. M. 1982. The anatomy of a Lower Palaeozoic accretionary forearc: the Southern Uplands of Scotland. In: Leggett, J. K. (ed) Trench-Forearc Geology. Geol. Soc. Spec. Publ. No. 10, 495-520.

Leitch, E. C. 1984. Marginal basins of the south-west Pacific and the preservation and recognition of their ancient analogies: a review. In: Kokelaar, B. P. & Howells, M. F. (eds). Marginal Basin Geology. Geol. Soc. Spec. Publ. No. 16, 97-108.

Le Pichon, X., Iiyama, T., Chamley, H., Charvet, J., Faure, M., Fujimoto, H., Furuta, T., Ida, Y., Kagami, H., Lallemant, S., Leggett, J., Murata, A., Okada, H., Rangin, C., Renard, V., Taira, A. & Tokuyama, H. 1987. Nankai Trough and the fossil Shikoku Ridge: results of Box 6 Kaiko survey. Earth Planet. Sci. Lett. 83, 186-198.

Leterrier, J., Maury, R. C., Thonon, P., Girard, D. & Marchal, M. 1982. Clinopyroxene composition as a method of identification of the magmatic affinities of palaeo-volcanic series. Earth Panet. Sci. Lett. 59, 139-154.

Lippard, S. J., Shelton, A. W., & Gass, I. G. 1986. The Ophiolite of Northern Oman. Geol. Soc. London Memoir No. 11. 178pp.

Lister, G. S., Banga, G. & Feensta, A. 1984. Metamorphic core complexes of Cordilleran type in the Cyclades, Aegean Sea, Greece. Geology 12, 221-225.

Lowrie, W. 1990. Identification of ferromagnetic minerals in a rock by coercivity and unblocking temperature properties. Geophys. Res. Lett. 17, 159-162.

Lowrie, W. & Heller, F. 1982. Magnetic Properties of Marine Limestones. Reviews of geophysics and space physics, 20, 171-192.

Lu, R. S. & McMillen, K. J. 1983. Multichannel seismic survey of the Columbia Basin and adjacent margins. In: Watkins, J. S. & Drake, C. L. (eds) Studies in continental margin geology. Am. Assoc. Petrolm. Geol. Mem. 34, 395-410.

Malpas, J. G., Xenophontas, C. & Robertson, A. H. F. 1987. Mamonia Complex and its relationship to the Troodos Complex. In: Xenophontas, C & Malpas, J. G. (eds) "Troodos-87", Ophiolites and Oceanic Lithosphere, Field Excursion Guidebook. Cyprus Geol. Dep., 234-259.

Malpas, J. G., Xenophontas, C. & Williams, D. 1992. The Atia Vavvara Formation of S.W. Cyprus: a product of complex collisional tectonics. Tectonophysics, 212, 193-241.

McElhinny, M. W. 1964. Statistical significance of the fold test in palaeomagnetism. Geophys. J. R. astr. Soc. 8, 338-340.

McFadden, P. L. 1990. A new fold test for palaeomagnetic studies. Geophys. J. Int. 103, 163-169.

McFadden, P. L. & Jones, D. L. 1981. The fold test in palaeomagnetism. Geophys. J. R. astr. Soc. 67, 53-58.

Meschede, M. 1986. A method of discriminating between different types of mid-ocean ridge basaltss and continental tholeiites with the Nb-Zr-Y diagram. Chem. Geol. 56, 207-218.

Migiros, G. P. 1992. Introduction to the geology of Lesbos Island. In: Papanikolaou, D. J., Migiros, G. P. & Sideris, Ch. (eds) Guide book for post-congress field trip to Chios-Lesvos. 5th meeting of IGCP Project 276, Athens, 25-31 May 1992, 1-15.

Migiros, G. & Pavopoulos, A. Description of the itinerary. In: Papanikolaon, D. J., Migrios, G. P. & Sideris, Ch. (eds). Guide book for post-congress field trip to Chios-Lesvos. 5th meeting of IGCP Project 276, Athens 1992, 20-27.

Miyashiro, A. 1961. Evolution of metamorphic belts. J. Petrol. 2, 277-311.
Monod, O. & Akay, E. 1984. Evidence for an Upper Triassic-Early Jurassic orogenic event in the Taurides. In: Dixon, J. E. & Robertson, A. H. F. (eds) The Geological Evolution of the Eastern Mediterranean. Geol. Soc. Spec. Publ. No. 17, 113-128.

Moore, G. F., Curray, J. R. & Emmel, F. J. 1982. Sedimentation in the Sunda Trench and forearc region. In: Legget, J. K. (ed) Trench-forearc geology: modern and ancient active margin plate margins. Geol. Soc. Spec. Pub. No. 10, 245-258.

Moore, J. C., Mascle, A., Taylor, E., Andreieff, P., Alvarez, F., Barnes, G., Beck, C., Behrmann, J., Blanc, G., Brown, K., Clark, M., Dolan, J., Fisher, A., Gieskes, J., Hounslow, M., McLellan, P., Moran, K., Ogawa, Y., Sakai, T., Schoonmaker, J., Vrolijk, P., Wilkens, R. & Williams, C. 1988. Tectonics and hydrogeology of the northern Barbados Ridge: Results from Ocean Drilling Program Leg 110. Geol. Soc. Am. Bull. 100, 1578-1593.

Morgan, W. J. 1983. Hotspot tracks and the early rifting of the Altantic. Tectonophysics 94, 123-139.

Murton, B. J. 1989. Tectonic controls on boninite genesis. In: Saunders, A. D. & Norry, M. J. (eds) Magmatism in the Ocean Basins. Geol. Soc. Spec. Publ. No. 42, 347-377.

Natland, J. H. & Tarney, J. 1982. Petrological ecolution of the Mariana arc and back-arc basin system, a synthesis of drilling results in the South Phillipine Sea. Initial Reports of the DSDP, U.S. Government Printing Office, Washington D.C. 60, 877-908.

Neumayr, M. 1887. Ueber Trias und Kohlenkalkversteinerungen aus dem westlichen Kleinasien. Anz. d. Kais. Akad. d. Wiss., Wien.

Nicolas, A. & Le Pichon, X. 1980. Thrusting of young lithosphere in subduction zones with special reference to structures in ophiolitic peridotites. Earth Plan. Sci. Lett. 46, 397-406.

Nilsen, T. H. & Zuffa, G. G. 1982. The Chugach Terrane, a Cretaceous trench-fill deposit, southern Alaska. In: Leggett, J. K. (ed) Trench-Forearc Geology. Geol. Soc. Spec. Publ. No. 10, 213-227.

Nisbet, E. G. & Pearce, J. A. 1977. Clinopyroxene composition in mafic lavas from differenr tectonic settings. Contrib. Mineral. Petrol. 63, 149-160.

Ogawa, Y. 1985. Variety of subduction and accretion processes in Cretaceous to Recent plate boundaries around southwest and central Japan. Tectonophysics 112, 493-518.

Okay, A. I. 1984. The geology of the Agvanis metamorphic rocks and neighbouring formations. M. T. A. Bull. 99/100, 16-36.

Okay, A. I. 1987. Ophiolite obduction on a Permian carbonate platform in northwest Turkey (abstr.). Terra Cognita 7, 100.

Okay, A. I., Siyako, M. & Burkan, K. A. 1991. Geology and tectonic evolution of the Biga Peninsula, northwest Turkey. Bull. Tech. Univ. Istanbul 44, 191-256.

Okay, A. I. & Siyako, M. 1993. The new position of the Izmir-Ankara Neo-Tethyan Suture between Izmir and Balikesir. In: Turgut, S. (ed) Proceedings of the Okan Sungurlu Symposium, Tectonics and hydrocarbon potential of Anatolia. Ankara.

Pallister, J. S. & Hopson, C. A. 1981. Samail ophiolite plutonic suite; field relations, phase variation, cryptic variation and layering, and a model of a spreading ridge magma chamber. J. Geophys. Res. 86, 2593-2644.

Papanikolaou, D. J. 1989.Are the Medial Crystalline Massifs of the Eastern Mediterranean drifted Gondwanian fragmenst? Geol. Soc. Greece Spec. Publ. 1, 63-90.

Papanikolaou, D. J. & Demirtasli, E. 1987. Geological correlations between Alpine segments of the Hellenides-Balkanides and Taurides-Pontides. In: Flugel, F. P., Sassi, P. & Grecula, P. (eds) Pre-Variscan and Variscan events in the Alpine-Mediterranean mountain belts, 387-396.

Papanikolaou, D. J., Migiros, G. P. & Sideris, Ch. 1992. Guide book for post-congress field trip to Chios-Lesvos. 5th meeting of IGCP Project 276, Athens, 25-31.

Papanikolaou, D. J. & Sideris, Ch. 1992. Introduction to the geology of Chios Island. In: Papanikolaou, D. J., Migiros, G. P. & Sideris, Ch. (eds) Guide book for post-congress field trip to Chios-Lesvos. 5th meeting of IGCP Project 276, Athens, 25-31 May 1992, 17-27.

Pearce, J. A. 1980. Geochemical evidence for the genesis and eruptive setting of lavas from Tethyan ophiolites. Proc. Int. Ophiolite Symp., Cyprus 1979. Institute of Mining and Metallurgy, 261-272.

Pearce, J. A. 1982. Trace element characteristics of lavas from destructive plate boundaries. In:Thorpe, R. S. (ed) Andesites, 525-548. John Wiley & Sons.

Pearce, J. A. 1983. Role of the Sub-continental Lithosphere in Magma Genesis at Active Continental Margins. In: Hawkesworth, C. J. & Norry, M. J. (eds) Continental basalts and mantle xenoliths, 230-249. Shiva geology series.

Pearce, J. A. & Cann, J. R. 1973. Tectonic setting of basic volcanic rocks determined using trace element analysis. Earth Planet. Sci. Lett. 19, 290-300.

Pearce, J. A. & Gale, G. H. 1977. Identification of ore-deposition environment from trace element geochemistry of associated igneous host rocks. Geol. Soc. Spec. Publ. 7, 14-24.

Pearce, J. A. & Norry, M. J. 1979. Petrogenetic implications of Ti, Zr, Y and Nb variations in volcanic rocks. Contrib. Mineral. Petrol. 69, 33-47.

Pearce, J. A., Harris, N. & Tindle, A. G. 1984. Trace element discrimination diagrams for the tectonic interpretation of granitic rocks. J. Petrology 25 (4), 956-983.

Pearce, J. A., Lippard, S. J. & Roberts, S. 1984. Characteristics and tectonic significance of supra-subduction zone ophiolites. In: Kokelaar, B. P. & Howells, M. F. (eds). Marginal Basin Geology. Geol. Soc. Spec. Publ. No. 16, 77-94.

Phillipson, A. 1911. Reisen und Forschungen im westlichen Kleinasien. Peterm. Mitt., Erg.-Heft 172, 100pp.

Pickering, K. T., Hiscott, R. N. & Hein, F. J. 1989. Deep marine environments. Unwin Hyman, London.

Platt, J. P. 1986. Dynamics of orogenic wedges and the uplift of high-pressure metamorphic rocks. Bull. geol. Soc. Am. 86, 1037-1053.

Platt, J. P. 1993. Exhumation of high-pressure rocks: a review of concepts and processes. Terra Nova 5, 119-133.

Platzman, E. S, Platt, J. P., Tapirdamaz, C., Sanver, M. & Rundle. Why are there no clockwise rotations along the the North Anatolian Fault Zone. In press.

Robertson, A. H. F. 1981. Metallogenesis on a Mesozoic passive continental margin, Antalya Complex, southwest Turkey. Earth Planet. Sci. Lett. 54, 323-345.

Robertson, A. H. F. 1989. Palaeoceanography and tectonic setting of the Jurassic Coast range ophiolite, central California: evidence from the extrusive rocks and the volcaniclastic sediemnt cover. Marine and Petroleum Geology 6(3), 193-288

Robertson, A. H .F. 1991. Origin and emplacement of an inferred late Jurassic subduction-accretion complex, Euboea, eastern Greece. Geol. Mag. 128 (1), 27-41.

Robertson, A. H. F. 1993. Mesozoic-Tertiary sedimentary and tectonic evolution of Neotethyan carbonate platforms, margins and small ocean basins in the Antalya Complex, southwest Turkey. Spec. Publs. Int. Ass. Sediment. 20, 415-465.

Robertson, A. H. F. & Hudson, J. D. 1973. Cyprus umbers: chemical pricipitates on a Tethyan ocean ridge. Earth Planet. Sci. Lett. 18, 93-101.

Robertson, A. H. F. & Boyle, J. F. 1983. Tectonic setting and origin of metalliferous sediments in the Mesozoic Tethys. In: Rona, P. A. (ed) Hydrothermal processes at seafloor spreading centres. NATO Conference Series, Plenum, New York & London, 595-663.

Robertson, A. H. F. & Dixon, J. E. 1984. Introduction: aspects of the geological evolution of the Eastern Mediterranean. In: Dixon, J. E. & Robertson, A. H. F. (eds) The Geological Evolution of the Eastern Mediterranean. Geol. Soc. Spec. Publ. No. 17, 1-74.

Robertson, A. H. F. & Henderson, W. G. 1984. Geochemical evidence for the origins of igneous and sedimentary rocks of the Highland Border, Scotland. Trans. Roy. Soc. Edinburgh: Earth Sciences 75, 135-150.

Robertson, A. H. F. & Searle, M. P. 1990. The northern Oman Tethyan continental margin: stratigraphy, structure, concepts and controversies. In: Robertson, A. H. F., Searle, M. P. & Ries, A. C (eds) The Geology and Tectonics of the Oman Region. Geol. Soc. Spec. Publ. No. 49, 3-25.

Robertson, A. H. F. & Waldron, J. 1990. Geochemistry and tectonic setting of Late Triassic and Late Jurassic-Early Cretaceous basaltic extrusives from the Antalya Complex, SW Turkey. In: Savascin, W. Y & Eronat, A. H. (eds) Proceedings of the International Earth Sciences Congress on Aegean regions 1-6 Oct. 1990, Izmir, 279-299.

Robertson, A. H. F., Clift, P. D, Degnan, P. J. & Jones, G. 1991. Palaeogeographic and palaeotectonic evolution of the Eastern Mediterranean Neotethys. Palaeogeog., Palaeoclim., Palaeoecol. 87, 289-343.

Robertson, A. H. F., Kidd, R. B., Ivanov, M. K., Limonov, A. F., Woodside, J. M., Galindo-Zaldivar, J., Nieto, L. & the Scientific Party of the 1993 "TTR-3" Cruise. In press. Eratosthenes Seamount, easternmost Mediterranean: Evidence of active collapse and underthrusting beneath the Cyprus active margin.

Rollinson, H. R. 1993. Using geochemical data: evaluation, presentation, interpretation. John Wiley & Sons, New York.

Sano, H. 1988. Permian oceanic-rocks of Mino terrane, central Japan. Part 1. Chert facies. Journal. Geol. Soc. Japan. 94 (12), 697-709.

Sano, H. & Kanmera, K. 1988. Paleogeographic reconstruction of accreted oceanic rocks, Akiyoshi, south-west Japan. Geology 16, 600-603.

Sano, H., Yamagata, T. & Horibo, K. 1992. Tectonostratigraphy of Mino terrane: Jurassic accretionary complex of southwest Japan. Palaeogeog., Palaeoclim., Palaeoecol. 96, 41-57.

Saunders, A. D. & Tarney, J. 1984. Geochemical characteristics of basaltic volcanism within back-arc basins. In: Kokelaar, B. P. & Howells, M. F. (eds) Marginal Basin Geology. Geol. Soc. Spec. Publ. No. 16, 59-73.

Schindler, C. 1993. The MARMARA Poly-Project: tectonics and recent crustal movements revealed by space-geodesy and their interaction with the circulation of groundwater, heat flow and seismicity in Northwestern Turkey. Terra Nova 5, 164-173.

Schuiling, R. D. 1959. Uber eine pra-herzynische Faltungsphase im Kazdag Kristallin. M.T.A. Bull. 53, 89-93.

Schweller, W. J. & Kulm, L. D. 1978. Depositional patterns and channelized sedimentation in active eastern Pacific trenches. In: Stanley, D. J. & Kelling, G. (eds) Sedimentation in submarine canyons, fans and trenches. Hutchison & Ross, Dowden, 311-324.

Sclater, J. G. & Christie, P. A. F. 1980. Continental Stretching: An explanation of the Post-Mid-Cretaceous subsidence of the Central North Sea Basin. J. Geophys. Res. 85, 3711-3739.

Searle, M. P., Lippard, S. J., Smewing, J. D. & Rex, D. C. 1980. Volcanic rocks beneath the Semail ophiolite nappe in the northern Oman Mountains and their significance in the Mesozoic evolution of Tethys. J. Geol. Soc. London 137, 589-604.

Searle, M. P. & Malpas, J. 1980. Structure and metamorphism of rocks beneath the Semail Ophiolite of Northern Oman and their significance in ophiolite obduction. Trans. Roy. Soc. Ed. (Earth Sciences) 71, 247-262.

Searle, M. P. & Malpas, J. 1982. Petrochemistry and origin and sub-ophiolitic metamorphic and related rocks in the Oman Mountains. J. Geol. Soc. London 139, 5-24.

Sengör, A. M. C. 1979. Mid-Mesozoic closure of Permo-Triassic Tethys and its implications. Nature 279, 590-593.

Sengör, A. M. C., Yilmaz, Y. & Ketin, I. 1980. Remnants of a pre-Late Jurassic ocean in northern Turkey: Fragments of Permian-Triassic Palaeo-Tethys? Bull. Geol. Soc. Am. 91, 599-609.

Sengör, A. M. C. & Yilmaz, Y. 1981. Tethyan evolution of Turkey: a plate tectonic approach. Tectonophysics 75, 181-241.

Sengör, A. M. C., Satir, M. & Akkok, R. 1984. Timing of tectonic events in the Menderes Massif, western Turkey: evidence of Pan-African basement in Turkey. Tectonics 3, 693-707.

Sengör, A. M. C., Yilmaz, Y. & Sungurlu, O. 1984. Tectonics of the Mediterranean Cimmerides: nature and evolution of the western termination of Palaeo-Tethys. In: Dixon, J. E. & Robertson, A. H. F. (eds) The Geological Evolution of the Eastern Mediterranean. Geol. Soc. Spec. Publ. No. 17, 77-112.

Sengor, A. M. C., Gorur, N. & Saroglu, F. 1985. Strike slip faulting and related basin formation in zones of tectonic escape: Turkey as a case study. In: Biddle, K. T. & Christie-Blick, N. (eds) Strike slip faulting and basin formation. Soc. Econ. Paleontol. Mineral. Spec. Publ. 37, 227-264.

Sengör, A. M. C., Cin, A., Ustaömer, T. & Hsü, K. J. 1988. Origin and assembly of the Tethyside orogenic collage at the expense of Gondwana Land. In: Audley-Charles, M. G. & Hallam, A. (eds) Gondwana and Tethys. Geol. Soc. Spec. Publ. No. 37, 119-181.

Shallo, M., Kodra, A. & Gjata, K. 1990. Geotectonics of the Albanian ophiolites. In: Malpas, J. G., Moores, E. M., Panayiotou, A. & Xenophontas, C. (eds) Ophiolites: oceanic crustal analogues. Proceedings of the symposium "Troodos-87". Nicosia, Cyprus.

Siyako, M. A., Burkan, K. A. & Okay, A. I. 1989. Biga ve Gelibolu yarimadalarinin Tersiyer jeolojisi ve hidrokarbon olanaklari. Turkiye Jeol. Kur. Bult. 14, 1-16.

Smith, A. G. 1971. Alpine deformation and the oceanic areas of the Tethys, Mediterranean and Atlantic. Geol. Soc. Am. Bull. 82, 2039-2070.

Smith, G. W., Howell, D. G. & Ingersoll, R. V. 1979. Late Cretaceous trench-slope basins of central California. Geology 7, 303-306.

Spray, J. G. 1984. Possible causes and consequences of upper mantle decoupling and ophiolite displacement. In: Gass, I. G., Lippard, S. J. & Shelton, A. W. (eds) Ophiolites and Oceanic Lithosphere. Geol. Soc. Lond. Spec. Publ. No. 13, 225-268.

Spray, J. G., Bebion, J., Rex, D. C. & Roddick, J. C. 1984. Age constraints on the igneous and metamorphic evolution of the Hellenic-Dinaric ophiolites. In: Dixon, J. E. & Robertson, A. H. F. (eds) The Geological Evolution of the Eastern Mediterranean. Geol. Soc. Spec. Publ. No. 17, 619-627.

Stampfli, G., Marcoux, J. & Baud, A. 1991. Tethyan margins in space and time. Palaeogeog., Palaeoclim., Palaeoecol. 87, 373-409.

Staudigel, H. & Schmincke, H.-U. 1984. The Pliocene Seamount series of La Palma/Canary Islands. J. Geophys. Res. 89, 11195-11215.

Stevens, S. H. & Moore, G. F. 1985. Deformational and sedimantation processes in trench slope basins of the western Sundra Arc, Indonesia. Marine Geology 69, 93-112.

Stöcklin, J. 1974. Possible ancient continental margins in Iran. In: Burk, C. A. & Drake, C. L. (eds) The Geology of Continental Margins, Springer verlag, Berlin, 873-887.

Suess, E. 1893. Are great ocean depths permanent? Natural Science 2, 180-187.

Sun, S-S. 1980. Lead isotopic study of young volcanic rocks from mid-ocean ridges, ocen islands and island arcs. Phil. Trans. Roy. Soc. Lond. A297, 409-445.

Taira, A., Okada, H., Whitaker, J. H. McD. & Smith, A. J. 1982 The Shimato Belt of Japan: Cretaceous-Lower Miocene active margin sedimentation. In: Leggett, J. K. (ed) Trench-forearc geology. Geol. Soc. Lond. Spec. Publ. No. 10, 5-26.

Taira, A. & Niitsuma, N. 1986. Turbidite sedimantation in Nankai Trough as interpreted from magnetic fabric, grain size and detrial mode analysis. In: Kagan, H., Karig, D. E., Coulborn, W. T. et al. (eds) Initial reports DSDP 1987. U.S. Goverment Printing Office, Washinton D.C., 611-632.
Taira, A., Tokuyama, H. & Soh, W. 1989. Accretion tectonics and evolution of Japan. In: Ben-Avraham, Z (ed) The Evolution of the Pacific Ocean Margins. Oxford Univ. Press, 100-123.

Tekeli, O. 1981. Subduction complex of pre-Jurassic age, northern Anatolia, Turkey. Geology 9, 68-72.

Thornburg, T. M. & Kulm, L. D. 1987. Sedimentation in the Chile Trench: depositional morphologies, lithofacies, and stratigraphy. Geol. Soc. Am. Bull. 98, 33-52.

Tomoda, Y. & Fujimoto, H. 1983. Roles of Seamount, Rise, and Ridge in Lithospheric Subduction. In: Hashimoto, M. & Uyeda, S. (eds) Accretion Tectonics in the Circum-Pacific Regions. Terra Scientific Publ., Tokyo, 319-331.

Tucker, M. E. 1981. Sedimentary petrology: an introduction. Blackwell Scientific Publications.

Turekian, K. K. & Wedepohl, K. H. 1961. Distribution of the elements in some major units of the Earth's crust. Bull. Geol. Soc. Am. 72, 175-191.

Tüysüz, O. 1990. Tectonic evolution of a part of the Tethyside Orogenic Collage: The Kargi Massif, Northern Turkey. Tectonics 9, 141-160.

Ustaömer, T. 1993. Pre-Late Jurassic tectonic-sedimentary evolution of north Tethys: central Pontides, N Turkey. Unpub. Thesis. Univ. Edinburgh. 389 pp.

Ustaömer, T. & Robertson, A. H. F. 1993. A Late Palaeozoic-Early Mesozoic marginal basin along the active southern continental margin of Eurasia: evidence from the Central Pontides (Turkey) and adjacent regions. Geological Journal 28, 219-238.

Ustaömer, T. & Robertson, A. H. F. 1994. Late Palaeozoic marginal basin and subduction-accretion: the Palaeotethyan Kure Complex, Central Pontides, northern Turkey. J. Geol. Soc. London 151, 291-305.

Usumezsoy, S. 1987. The NW Anatolian accretionary orogeny: western termination of Paleo-Tethyan suture belt (in Turkish). Geological. Bull. Turkey 30, 53-62.

van der Kaaden, G. 1959. Age relations of magmatic activity and of metamorphic processes in the northwestern part of Anatolia-Turkey. Bull. Min. Res. Expl. Inst. Turkey 52, 15-33.

von Huene, R. J. & Arthur, M. A. 1982. Sedimantation across the Japan Trench off northern Honshu Island. In: Leggett, J. K. (ed) Trench-Forearc Geology. Geol. Soc. Lond. Spec. Publ. No. 10, 27-48.

Wahrhaftig, C. 1984. Structure of the Marin Headlands block, California: a progress report. In: Blake, M. C. (ed) Franciscan Geology of Northern California. Pacific Section, S. E. P. M. California, 31-50.

Waldron, J. W. F. (1981). Mesozoic sedimentary and tectonic evolution of the northeastern Antalya Complex, Egridir, SW Turkey. Unpub. PhD thesis, Univ. of Edinburgh, 239 pp.

Watanabe, T. & Maekawa, H. 1984. Early Cretaceous dual subduction system in and around the Kamuikotan tectonic belt, Hokkaido, Japan. In: Nasu, N., Kobayashi, K., Uyeda, S., Kushiro, I. & Kagami, H. (eds) Formation of Active Ocean Margins. Terra Scientific Publ., Tokyo, 677-699.

Wegener, A. 1929. Die Entstehung der Kontinente und Ozeane, 4, Auflage Vieweg, Braunschweig, 367 pp.

Weissel, J. K., Taylor, B. & Karner, G. D. 1982. The opening of the Woodlark Basin, subduction of the Woodlark spreading system, and the evolution of northern Melanesia since mid-Pliocene time. Tectonophysics 87, 253-277.

Wernicke, B. P., Christiansen, R. L., England, P. C. & Sonder, L. J. 1987. Tectonomagmatic evolution of Cenozoic extension in the North American Cordillera. In:Coward, M. P., Dewey, J. F. & Hancock, P. L. (eds) Continental Extensional Tectonics. Geol. Soc. Spec. Publ. No. 28, 203-221.

Westphal, M., Bazhenov, M. L., Lauer, J. P., Pechersky, D. M. & Sibuet, J-C. 1986. Tectonophysics 123, 37-82.

Williams, H. & Smyth, W. R. 1973. Metamorphic aureoles beneath ophiolitic suites and Alpine peridotites: tectonic implications with West Newfoundland examples. Am. J. Sci. 273, 594-621.

Wilson, J. T. 1963. Hypothesis of Earth's behaviour. Nature, 198 925-929.

Winchester, J. A. & Floyd, P. A. 1976. Geochemical magma type discrimination: application to altered and metamorphosed basic igneous rocks. Earth Plan. Sci. Lett. 28, 459-469.

Wood, D. A., Joron, J-L.,&Treuil, M. 1979. A re-appraisal of the use of trace elements to classify and discriminate between magma series erupted in different tectonic settings. Earth Plan. Sci. Lett. 45, 326-336.

Woodcock, N. H. & Robertson, A. H. F. 1977. Origins of some ophiolite-related metamorphic rocks of the "Tethyan" belt. Geology 5, 373-76.

Wright, J. V. & Mutti, E. 1981. The Dali Ash, Island of Rhodes, Greece: a problem in interpreting submarine volcanogenic sediments. Bull. Volcanol. 44, 153-67.

Yardley, B. W. D. 1989. An introduction to metamorphic petrology, Wiley & Sons, New York.

APPENDIX 1: GEOCHEMICAL TECHNIQUES

X-ray fluorescence

Whole rock chemical analysis of rock samples was carried out by X-ray fluorescence (XRF) at the Department of Geology & Geophysics, Edinburgh University. After removing veins and weathered surfaces with a diamond saw, rock samples were crushed and ground to a grain size of <200μm. For major element analysis, measured quantities of lithium flux were added to previously ignited rock powder and the samples were fused at 1100°C to obtain glass discs. The samples were analyzed for 10 major elements on a Philips PW 1480 wavelength dispersive sequential XRF spectrometer. For trace element analysis, the rock powders were pressed into pellets and were analyzed for 17 trace elements using the Philips PW 1480 spectrometer. The trace element Nb was measured separately, after recalibration of the machine, to give higher precision data. Samples were calibrated using USGS and CRPG international standards. Further details of preparation procedure are given in Fitton *et al.* (1984) and Fitton & Dunlop (1985).

Sample reproducibility was measured by analyzing six discs and six pellets prepared from one sample of basalt from the Nilüfer Unit (102c/90). The reproducibility of the machine was also measured, by analyzing one disc and one pellet six times each. The results, mean values and standard deviations are presented in the following tables.

Electron microprobe analysis

Samples of basalt, amphibolite and peridotite were analyzed using the Cambridge Instruments Microscan Mark 5 wavelength dispersive electron microprobe at the Department of Geology & Geophysics, Edinburgh University. The samples were prepared as polished, uncovered thin-sections which were carbon-coated under vacuum. Silicate, oxide and pure metal standards were used for calibration. The operating conditions were:

Accelerating potential: 20kv.
Beam current: 30ηa.
Count times: 40 seconds for peaks and 20 seconds for background.
Focused beam diameter: approx. 1-2μm.

Reproducibility test of XRF sample preparation techniques

Six glass discs and six powder pellets were prepared from basalt sample 102c/90 and analyzed by XRF. The results, means and standard deviations are shown below.

							Mean	S.D.
SiO_2	48.20	48.17	48.14	48.20	48.27	48.26	48.21	0.05
Al_2O_3	12.72	12.70	12.67	12.69	12.68	12.67	12.69	0.02
Fe_2O_3	12.71	12.64	12.70	12.68	12.69	12.65	12.68	0.03
MgO	9.34	9.29	9.31	9.32	9.34	9.31	9.32	0.02
CaO	7.59	7.57	7.58	7.55	7.58	7.56	7.57	0.01
Na_2O	3.42	3.41	3.46	3.53	3.45	3.55	3.47	0.06
K_2O	0.265	0.269	0.267	0.269	0.267	0.271	0.268	0.002
TiO_2	2.111	2.096	2.108	2.098	2.093	2.095	2.100	0.007
MnO	0.178	0.181	0.182	0.180	0.177	0.179	0.180	0.002
P_2O_5	0.212	0.212	0.214	0.211	0.215	0.213	0.213	0.001
L.O.I.	3.07	3.11	3.39	3.15	3.16	3.07	3.16	0.12
Total	99.82	99.64	100.02	99.88	99.91	99.83	99.85	0.13
Nb	20.3	20.8	20.9	21.3	20.5	20.7	20.8	0.3
Zr	145.1	144.8	145.2	145.2	145.1	144.6	145.0	0.2
Y	22.6	22.3	22.8	23.0	23.1	22.9	22.8	0.3
Sr	95.0	94.9	95.2	94.8	94.6	94.4	94.8	0.3
Rb	4.4	4.0	3.9	3.9	4.3	4.2	4.1	0.2
Th	4.2	4.4	4.4	4.1	3.2	4.4	4.1	0.5
Pb	1.2	-0.2	-0.4	-0.1	-0.2	-0.7	0.2	0.5
Zn	116.8	115.8	116.5	115.8	114.3	114.7	115.7	1.0
Cu	114.8	112.4	113.7	114.2	116.1	114.8	114.3	1.2
Ni	237.7	235.7	239.9	236.9	238.5	238.1	237.8	1.4
Cr	622.9	629.1	622.3	613.5	610.5	625.1	620.6	7.1
Ce	21.9	28.6	19.1	28.1	26.7	23.5	24.7	3.8
Nd	12.2	19.0	14.5	20.7	15.4	16.5	16.4	3.1
La	7.0	6.1	5.2	6.1	5.2	8.8	6.4	1.4
V	230.6	235.9	236.4	231.8	232.4	233.0	233.4	2.3
Ba	3.4	-3.4	6.6	0.4	3.4	1.8	2.6	2.4
Sc	34.1	32.9	35.8	32.3	34.8	31.9	33.6	1.5

L.O.I. loss of volatiles on ignition
S.D. standard deviation

Reproducibility test of XRF spectrometer

One glass disc and one powder pellet prepared from basalt sample 102c/90 were run six times each on the XRF spectrometer. The results, means and standard deviations are shown below.

							Mean	S.D.
SiO_2	48.27	48.19	48.25	48.21	48.22	48.22	48.23	0.03
Al_2O_3	12.66	12.72	12.71	12.72	12.71	12.70	12.70	0.02
Fe_2O_3	12.68	12.72	12.69	12.68	12.67	12.68	12.69	0.02
MgO	9.32	9.36	9.38	9.35	9.32	9.38	9.35	0.02
CaO	7.56	7.56	7.55	7.59	7.58	7.58	7.57	0.01
Na_2O	3.50	3.44	3.43	3.47	3.46	3.48	3.46	0.03
K_2O	0.269	0.268	0.269	0.266	0.267	0.271	0.268	0.002
TiO_2	2.096	2.116	2.107	2.102	2.096	2.110	2.105	0.008
MnO	0.183	0.176	0.177	0.183	0.180	0.175	0.179	0.004
P_2O_5	0.211	0.211	0.213	0.212	0.209	0.213	0.212	0.002
L.O.I.	3.16	3.16	3.16	3.16	3.16	3.16	3.16	0.00
Total	99.92	99.92	99.93	99.95	99.86	99.97	99.93	0.04
Nb	19.2	19.9	20.1	19.6	19.8	19.4	19.7	0.3
Zr	140.2	140.6	141.2	140.5	140.7	141.1	140.7	0.4
Y	22.6	22.3	22.6	22.4	22.8	22.3	22.5	0.2
Sr	93.4	94.8	94.3	95.1	94.5	94.3	94.4	0.6
Rb	4.2	3.6	3.9	4.0	3.9	4.5	4.0	0.3
Th	3.9	5.4	3.9	5.3	5.1	4.0	4.6	0.7
Pb	1.6	1.7	2.6	2.1	1.7	0.8	1.8	0.6
Zn	115.7	114.1	114.9	114.8	115.6	114.7	115.0	0.6
Cu	115.8	116.0	114.7	113.3	113.8	116.3	115.0	1.2
Ni	236.4	235.2	236.9	235.8	237.2	238.3	236.6	1.1
Cr	646.0	651.6	647.4	649.1	649.5	647.6	648.5	2.0
Ce	23.2	28.2	27.2	26.8	34.1	29.9	28.2	3.6
Nd	20.9	21.0	22.4	20.8	23.0	24.4	22.1	1.5
La	3.2	0.0	4.3	1.6	1.3	0.6	1.8	1.6
V	255.3	256.1	255.6	256.8	258.7	261.3	257.3	2.3
Ba	34.6	33.7	30.2	24.7	39.5	34.0	32.8	5.0
Sc	32.8	31.4	33.6	31.0	31.4	31.8	32.0	1.0

L.O.I. loss of volatiles on ignition
S.D. standard deviation

X-ray diffraction

a) Standard mineralogical determinations

Standard X-ray diffraction (XRD) techniques were carried out on several shale samples. The samples were coarsely ground and packed into pellet-shaped containers for analysis. The powders were analyzed on the Philips PW 1800 diffractometer at the Department of Geology & Geophysics, Edinburgh University. The samples were scanned from 5-60°θ, using a Cu K alpha source. The resulting traces were compared with mineral analyses contained within a databank of standardized minerals and compounds.

b) Illite crystallinity

Fine-grained sedimentary rocks were crushed to a coarse-grained grit and the clay-sized fraction was separated out by mixing with distilled water and using ultrasonic disaggregation and settling columns. The resulting clays in suspension were put into beakers containing glass slides. They were placed in an oven at 60°C until all the water had evaporated. The glass slides with their thin films of sediment were then analyzed using the Philips PW 1800 diffractometer. The samples were scanned from 7-22°θ in steps of 0.2°θ using a Cu K alpha source. A pure quartz standard was run at the beginning and end of the sample analysis.

The widths of the illite and quartz peaks at their half heights were measured and used to calculate the degree of illite crystallinity, after the technique of Weber (1972). The degree of illite crystallinity is defined by the parameter Hbrel:

$$\text{Hbrel} = \frac{\text{(half width for (001) illite)}}{\text{(half width for (100) quartz)}} \times 100$$

APPENDIX 2: WHOLE-ROCK XRF ANALYSES

Spilites of the Nilufer Unit "purple suite" from road N of Mehmetalan

	17/9-B	17/9-C	17/9-D	17/9-E	17/9-F	17/9-G	17/9-H	17/9-I	17/9-J	17/9-K	17/9-L	17/9-N	17/9-Q	17/9-R
SiO2	43.15	64.36	46.01	42.36	45.64	50.28	47.00	48.02	43.78	33.62	46.22	45.53	47.95	44.55
Al2O3	21.78	15.90	13.05	17.02	19.06	18.65	18.77	12.79	14.89	21.06	15.78	15.26	16.05	15.25
Fe2O3	11.48	5.88	8.91	16.76	15.11	14.98	16.07	6.63	11.33	20.68	16.57	13.43	10.44	16.02
MgO	2.70	0.49	2.68	0.62	1.95	1.84	3.73	1.67	1.56	2.68	4.40	7.08	6.67	5.69
CaO	3.11	1.96	10.66	6.07	2.82	0.86	0.45	12.14	10.00	3.74	7.74	5.79	4.41	4.44
Na2O	0.87	8.67	3.82	0.77	2.06	1.75	1.02	3.71	2.70	0.35	2.94	3.56	3.97	3.81
K2O	5.882	0.193	0.917	4.510	4.460	4.329	5.918	1.212	2.859	5.912	0.046	0.334	0.523	0.856
TiO2	4.100	0.036	2.447	4.025	3.115	2.973	2.936	1.525	2.231	4.046	2.841	2.094	2.219	2.131
MnO	0.123	0.050	0.376	0.047	0.162	0.065	0.089	0.332	0.269	0.088	0.155	0.191	0.132	0.104
P2O5	0.857	0.056	0.979	0.676	0.404	0.307	0.270	1.275	0.254	2.059	0.338	0.215	0.267	0.231
LOI	5.53	2.13	9.77	6.71	5.00	3.66	3.84	10.32	10.02	5.01	3.03	6.56	7.18	6.82
Total	99.58	99.72	99.63	99.58	99.78	99.69	100.09	99.63	99.89	99.24	100.07	100.04	99.81	99.88
Nb	157.6	228.1	112.0	154.7	78.5	27.9	32.9	116.6	51.7	261.5	36.3	17.9	29.7	17.7
Zr	532.7	1505.5	401.5	459.7	247.5	162.4	177.6	411.4	159.1	818.3	202.7	119.4	162.9	118.5
Y	33.8	77.7	27.6	35.1	26.4	17.4	24.4	31.0	18.2	56.9	23.7	21.6	19.5	20.6
Sr	103.1	105.2	236.5	106.6	100.4	51.2	15.7	272.5	250.1	119.9	832.5	234.5	66.3	92.2
Rb	158.9	5.0	24.4	124.6	125.1	122.4	104.8	33.3	78.8	163.3	1.1	8.4	15.6	17.4
Th	16.7	28.0	8.5	16.3	11.1	8.9	9.5	8.8	6.2	27.7	6.3	4.4	3.4	4.3
Pb	6.2	0.5	4.4	4.6	6.3	5.3	3.0	2.9	5.6	9.4	1.0	2.0	2.2	2.2
Zn	143.5	45.1	149.8	87.4	118.9	109.6	110.5	94.6	94.6	420.4	102.6	111.9	128.5	110.0
Cu	5.4	10.8	7.8	13.9	10.8	6.7	11.9	7.0	10.1	16.9	20.3	88.4	72.0	12.9
Ni	57.9	10.6	45.4	32.1	42.0	43.7	120.9	30.6	38.3	132.3	46.0	147.4	83.0	179.1
Cr	136.5	-17.7	9.3	85.4	221.4	244.2	138.4	-3.3	174.1	24.3	36.1	354.2	175.5	353.5
Ce	105.8	248.5	121.3	129.0	84.1	54.0	43.0	137.3	68.1	140.4	47.7	25.4	45.5	33.4
Nd	49.9	89.7	56.6	64.4	36.2	22.8	23.9	67.1	30.4	75.4	26.9	15.7	23.9	18.0
La	46.6	135.4	60.5	69.6	45.0	30.8	10.7	71.7	42.8	59.5	19.6	6.8	14.4	10.4
V	272.0	32.1	66.4	175.9	159.4	191.2	44.5	67.2	111.2	280.5	189.4	246.9	235.2	178.8
Ba	1596.4	65.5	297.6	563.1	1284.1	1219.3	544.9	369.8	873.8	1015.3	-31.5	19.0	6.7	60.1
Sc	21.3	-5.7	5.2	11.0	20.9	41.7	37.6	-3.5	16.6	12.5	18.7	35.3	23.5	35.1

Spilites of the Nilufer Unit "green suite" from road N of Mehmetalan

	99A/90	100B/90	102C/90	123A/90	100A/90	102A/90	102B/90
SiO2	38.04	43.87	48.12	47.58	44.19	48.33	47.34
Al2O3	17.99	15.62	12.73	12.62	18.21	12.98	13.12
Fe2O3	14.19	13.09	12.74	11.43	15.06	13.17	13.01
MgO	10.69	7.09	9.35	11.44	0.70	8.43	7.90
CaO	4.53	6.73	7.64	8.92	5.12	6.95	8.04
Na2O	1.23	3.83	3.67	2.75	1.15	3.88	3.76
K2O	0.718	0.414	0.267	0.603	4.775	0.303	0.553
TiO2	2.712	2.047	2.101	1.618	3.657	2.360	2.360
MnO	0.146	0.165	0.180	0.151	0.056	0.151	0.163
P2O5	0.437	0.222	0.227	0.150	1.600	0.265	0.257
LOI	9.79	7.47	2.93	2.37	5.35	3.36	3.24
Total	100.47	100.54	99.95	99.64	99.86	100.18	99.74
Nb	39.5	17.1	20.6	14.3	195.0	22.8	22.8
Zr	226.0	109.3	137.2	97.4	535.2	152.4	153.8
Y	29.5	20.7	20.9	14.8	41.6	26.3	26.5
Sr	110.9	254.3	95.9	78.9	136.8	237.6	228.4
Rb	18.4	8.2	3.8	10.5	133.6	5.0	9.2
Th	3.5	1.2	2.3	0.9	17.6	2.3	2.0
Pb	1.8	2.5	0.9	-0.4	5.2	0.5	2.0
Zn	182.2	102.7	117.2	92.0	71.1	115.8	112.4
Cu	42.9	83.2	120.9	51.7	16.9	119.9	128.5
Ni	277.1	151.3	241.8	313.9	32.4	215.4	180.1
Cr	414.1	360.6	614.7	949.3	88.3	369.8	310.9
Ce	75.6	39.7	31.5	25.0	173.7	45.8	44.3
Nd	36.0	23.9	19.2	12.6	78.3	22.0	21.7
La	27.5	16.1	14.2	10.6	75.0	16.7	18.0
V	294.7	268.9	261.5	241.2	215.9	271.3	280.8
Ba	48.6	73.3	43.6	247.7	738.7	34.7	72.6
Sc	37.1	31.8	34.9	45.7	15.3	35.6	31.9

Spilites of the Nilufer Unit "green suite" from road E of Mehmetalan

	23/90	26/90	30A/90	44A/90	44C/90	46A/90	48A/90	49C/90	51C/90	53E/90	54A/90	56B/90
SiO2	38.88	45.67	50.06	47.38	46.25	44.50	46.18	45.78	41.10	46.82	47.39	44.82
Al2O3	9.75	11.92	11.83	11.89	11.57	16.99	12.94	13.77	6.75	9.76	11.60	15.60
Fe2O3	10.90	13.20	11.65	13.09	13.52	12.75	14.79	12.95	13.98	12.12	11.43	14.50
MgO	12.21	11.11	8.66	11.12	13.09	8.42	5.82	7.53	24.61	14.85	11.29	7.70
CaO	9.74	9.20	7.47	6.23	5.87	5.20	7.11	9.50	4.00	7.41	7.93	4.32
Na2O	1.50	2.22	4.19	3.31	2.65	2.04	4.27	3.16	0.26	2.22	2.33	3.56
K2O	0.203	0.184	0.469	0.387	0.195	3.492	0.605	0.448	0.106	0.099	1.179	0.849
TiO2	2.025	2.182	2.057	2.134	2.083	1.757	3.764	2.638	1.383	1.909	1.993	3.123
MnO	0.159	0.163	0.159	0.158	0.149	0.128	0.170	0.161	0.153	0.156	0.144	0.173
P2O5	0.240	0.247	0.201	0.231	0.231	0.203	0.403	0.301	0.165	0.201	0.319	0.378
LOI	14.98	3.58	3.45	4.17	4.58	4.90	4.57	4.02	8.15	4.48	3.95	4.56
Total	100.59	99.68	100.18	100.10	100.19	100.38	100.63	100.27	100.68	100.02	99.54	99.58
Nb	25.1	23.2	17.8	18.9	16.5	15.7	38.2	27.2	12.4	14.6	19.6	33.2
Zr	142.2	154.9	123.7	132.5	131.8	125.1	236.9	170.8	80.4	115.9	119.6	212.7
Y	19.0	22.9	22.5	24.6	18.0	22.2	31.6	24.8	10.9	20.0	20.6	33.5
Sr	169.6	1231.0	176.0	127.4	77.9	469.3	268.4	456.2	65.7	48.6	323.8	258.1
Rb	3.5	3.9	8.8	5.6	2.4	57.5	14.2	7.5	4.7	1.8	22.4	19.9
Th	1.4	1.5	1.6	1.5	1.5	4.1	3.1	1.3	1.4	0.9	2.1	2.8
Pb	3.3	1.6	3.1	1.9	1.6	1.0	3.4	0.9	0.4	-0.8	2.2	1.6
Zn	91.0	107.2	98.1	113.6	117.2	112.1	143.4	117.8	101.6	82.3	89.8	145.2
Cu	97.3	22.0	118.0	125.6	123.9	97.9	177.0	107.2	72.4	187.2	132.2	167.6
Ni	398.6	415.4	247.7	367.9	567.3	233.3	70.0	141.7	1307.8	692.7	383.2	128.0
Cr	936.9	768.1	564.9	733.3	782.0	388.1	54.5	386.8	1728.3	1151.9	629.4	334.1
Ce	49.2	45.3	35.9	35.5	31.1	35.7	71.1	56.1	31.5	29.8	45.9	52.7
Nd	23.7	22.9	15.4	19.6	16.9	19.6	36.0	29.5	13.1	14.9	23.8	28.8
La	17.4	13.0	12.8	13.3	8.2	8.8	23.3	17.8	9.2	8.9	13.5	22.6
V	240.8	254.7	251.7	250.6	226.2	296.6	357.6	291.7	159.2	223.8	236.8	304.6
Ba	118.3	67.4	60.0	59.5	43.0	510.2	280.9	114.2	242.1	54.5	348.2	195.4
Sc	28.3	32.9	34.9	34.1	30.8	25.8	39.4	36.0	26.2	31.5	29.1	40.7

Spilites of the Nilufer Unit "green suite" from road E of Mehmetalan (cont.)

	56C/90	57A/90	58B/90	108C/90	17/10/01
SiO2	42.79	48.38	45.91	40.94	40.43
Al2O3	15.27	10.31	14.73	10.17	11.69
Fe2O3	14.46	8.95	12.61	11.96	10.91
MgO	8.42	10.25	8.41	12.85	6.98
CaO	7.66	9.58	9.63	9.38	13.23
Na2O	2.47	2.92	2.88	1.06	2.01
K2O	0.846	0.785	0.620	0.064	1.657
TiO2	2.790	1.863	2.512	1.648	2.116
MnO	0.197	0.121	0.160	0.171	0.187
P2O5	0.348	0.235	0.295	0.189	0.240
LOI	5.00	6.88	3.20	11.72	9.86
Total	100.24	100.29	100.96	100.16	99.30
Nb	37.6	20.4	26.0	15.0	27.2
Zr	206.3	125.7	163.2	105.6	148.9
Y	35.6	17.8	25.6	18.3	20.8
Sr	468.1	256.8	436.5	504.9	491.7
Rb	19.2	18.6	9.8	1.9	38.6
Th	3.2	1.4	1.7	1.0	2.7
Pb	4.7	1.7	1.3	0.8	4.0
Zn	148.8	75.9	108.4	89.1	89.4
Cu	162.6	47.5	123.5	105.3	115.9
Ni	154.8	303.5	146.6	338.7	164.5
Cr	428.2	562.1	410.8	818.8	383.2
Ce	66.4	32.4	54.2	27.4	43.8
Nd	37.3	16.9	28.4	16.1	18.9
La	21.3	14.6	18.8	8.9	17.3
V	302.7	228.1	262.6	258.3	276.4
Ba	225.3	243.7	158.6	67.6	209.7
Sc	46.1	28.0	38.9	35.0	33.2

Spilites from the Nilufer Unit in the Bergama region

	21/9/92-12	21/9/92-18a	21/9/92-18b	21/9/92-18c	21/9/92-18d	21/9/92-18e	22/9/92-10	21/9/92-19a	21/9/92-19b	21/9/92-19c	21/9/92-19d
SiO2	59.81	44.70	45.20	44.72	44.12	46.66	46.61	46.11	48.58	46.43	46.95
Al2O3	19.15	10.50	11.23	10.73	11.52	10.39	14.23	13.98	12.31	14.09	14.36
Fe2O3	8.03	10.37	11.37	12.49	13.79	11.59	13.30	13.76	13.26	13.14	12.79
MgO	2.76	10.49	15.40	16.19	13.64	14.64	7.69	7.29	8.97	6.95	7.31
CaO	0.25	12.63	7.40	7.92	7.55	7.91	7.87	7.98	8.67	7.54	7.69
Na2O	1.10	3.10	2.10	1.70	2.11	2.14	3.82	2.58	2.56	1.59	2.99
K2O	3.196	0.058	0.179	0.142	0.514	0.090	0.194	2.350	0.487	4.177	2.046
TiO2	0.864	1.626	2.030	1.812	2.256	1.894	2.751	2.797	2.084	2.693	2.737
MnO	0.122	0.161	0.158	0.175	0.150	0.154	0.152	0.164	0.149	0.146	0.165
P2O5	0.133	0.185	0.228	0.214	0.273	0.226	0.335	0.326	0.174	0.316	0.320
LOI	4.43	5.69	4.59	4.67	4.10	4.12	2.95	2.54	2.86	2.82	2.58
Total	99.84	99.50	99.89	100.78	100.02	99.80	99.89	99.88	100.11	99.90	99.93
Nb	15.5	21.3	24.4	22.5	25.6	24.3	24.7	34.3	14.7	33.4	33.2
Zr	170.9	109.3	127.1	116.8	148.3	126.7	190.1	196.6	119.6	189.9	190.3
Y	27.1	19.4	19.1	16.6	20.5	18.4	32.7	29.4	22.5	29.4	30.1
Sr	71.4	299.2	66.9	100.1	181.9	296.2	276.8	221.3	170.9	318.2	406.6
Rb	116.1	1.0	3.3	3.4	11.5	2.3	2.2	59.8	8.6	47.4	102.3
Th	12.5	0.8	0.8	1.6	1.9	1.4	1.9	5.1	1.2	4.0	7.1
Pb	4.9	1.4	0.7	0.7	1.4	1.4	1.7	2.0	1.0	0.6	1.2
Zn	103.6	72.5	102.2	107.4	107.2	91.2	111.6	123.3	129.4	128.3	104.2
Cu	49.3	87.9	83.6	84.6	113.5	93.2	131.8	129.8	61.6	151.6	104.3
Ni	61.4	333.2	595.2	809.1	796.6	529.4	218.4	92.4	224.3	84.1	87.1
Cr	106.1	511.1	839.1	1168.7	1046.5	815.4	363.2	151.5	198.8	147.1	151.1
Ce	64.3	27.7	28.1	32.3	50.2	38.1	52.3	56.6	24.6	53.2	53.5
Nd	19.9	18.0	16.8	17.6	25.3	17.0	25.3	30.0	16.5	29.3	31.5
La	24.2	10.2	12.6	11.6	19.6	15.9	10.6	20.7	5.9	19.9	20.1
V	188.2	271.7	223.2	247.9	242.1	240.0	310.6	332.6	195.7	347.1	352.7
Ba	450.4	51.7	83.4	26.9	71.4	30.8	60.6	151.0	100.4	202.4	353.6
Sc	28.6	24.4	27.5	30.0	24.5	29.5	32.7	33.4	22.9	30.8	32.4

Spilitic basalts from the Bergama region (cont.)

	21/9/92-19e	21/9/92-19f	21/9/92-19g	21/9/92-19h	25/9/92-8	25/9/92-10
SiO2	47.66	48.65	48.36	45.66	42.29	45.35
Al2O3	13.79	14.89	14.33	14.19	16.43	16.30
Fe2O3	13.59	13.06	13.01	13.98	15.86	14.65
MgO	6.54	6.51	5.61	7.49	8.10	7.79
CaO	8.62	6.07	7.90	7.51	6.50	3.81
Na2O	4.14	4.13	4.17	2.54	2.95	3.74
K2O	0.720	0.568	1.374	2.493	0.222	0.198
TiO2	2.515	2.349	2.708	2.847	2.775	2.543
MnO	0.163	0.149	0.154	0.162	0.147	0.135
P2O5	0.278	0.253	0.337	0.332	0.303	0.287
LOI	2.06	2.83	1.80	2.77	4.54	4.45
Total	100.08	99.46	99.76	99.98	100.16	99.26
Nb	32.9	16.8	34.2	35.1	28.5	28.0
Zr	179.2	133.7	193.5	199.1	203.3	181.3
Y	27.5	27.7	29.0	30.4	29.7	28.0
Sr	326.2	150.7	360.3	246.0	478.1	250.1
Rb	10.5	6.9	21.4	61.5	3.4	2.3
Th	2.3	1.0	2.6	4.8	2.8	2.0
Pb	3.7	0.7	2.1	3.0	2.4	0.9
Zn	115.9	130.0	122.7	132.8	155.7	145.2
Cu	124.5	80.0	115.3	148.3	81.4	71.2
Ni	98.6	236.0	82.7	87.1	272.2	247.2
Cr	177.0	224.5	140.9	157.0	344.1	299.9
Ce	57.1	35.4	54.1	58.2	54.0	46.1
Nd	29.0	18.7	28.3	30.2	32.9	26.5
La	22.7	8.5	22.3	18.9	16.1	20.9
V	262.5	231.9	272.6	373.7	259.8	224.0
Ba	130.6	125.3	238.0	212.6	58.6	60.8
Sc	29.6	25.5	30.6	32.3	21.0	22.5

Spilites from the Nilufer Unit in the Bursa region

Spilitic basalts from the Nilufer Unit in the Bandirma region

	Nil 1	Nil 4	Nil 5	Nil 6	Nil 7	30/8/92-1	30/8/92-3	30/8/92-4
SiO2	46.63	45.96	47.28	46.96	47.14	48.48	48.80	41.15
Al2O3	12.80	12.41	12.65	12.20	12.52	15.52	13.71	11.89
Fe2O3	13.14	13.10	12.40	12.55	12.93	12.12	12.01	10.28
MgO	10.00	10.99	9.28	10.36	10.35	7.40	5.94	6.45
CaO	7.58	7.52	8.25	8.11	7.25	5.88	10.04	15.61
Na2O	2.81	2.61	3.10	2.83	3.05	3.60	2.47	2.69
K2O	0.510	0.329	0.286	0.256	0.298	0.384	0.291	0.160
TiO2	2.144	1.976	2.119	1.991	2.100	1.810	2.024	1.571
MnO	0.171	0.175	0.162	0.168	0.172	0.132	0.142	0.157
P2O5	0.258	0.236	0.251	0.238	0.247	0.164	0.254	0.166
LOI	3.59	4.13	3.51	3.64	3.53	3.74	3.76	8.95
Total	99.62	99.44	99.28	99.30	99.59	99.23	99.45	99.07
Nb	21.1	18.7	16.1	18.9	19.3	14.1	15.6	13.3
Zr	154.0	138.8	153.6	138.8	146.7	116.3	130.9	101.6
Y	24.5	23.1	23.7	22.6	23.2	22.2	24.6	19.4
Sr	377.2	166.2	491.3	259.8	310.8	186.2	277.6	252.3
Rb	6.3	3.4	3.6	2.8	4.7	5.3	4.9	1.3
Th	2.0	1.6	2.2	1.6	1.9	0.8	1.3	0.4
Pb	1.9	1.1	3.1	1.4	0.6	1.7	0.2	1.8
Zn	119.3	114.6	111.9	112.2	115.8	101.7	100.8	87.7
Cu	102.7	99.7	105.0	108.1	99.2	77.0	100.9	79.6
Ni	335.9	370.7	276.3	349.4	317.3	71.6	86.1	232.5
Cr	492.9	525.6	444.8	539.6	514.9	111.9	163.2	477.9
Ce	50.3	38.2	50.2	44.8	45.1	42.0	41.1	37.2
Nd	23.2	22.6	25.3	19.6	21.2	19.3	20.1	17.3
La	13.6	14.1	14.4	16.3	11.1	12.1	8.2	8.4
V	245.7	243.2	254.0	240.5	250.7	261.9	267.7	212.7
Ba	107.3	85.0	62.4	66.5	75.5	59.6	64.8	26.6
Sc	32.6	26.3	30.3	28.6	28.7	33.3	38.3	28.7

Basalts of the Ortaoba Unit (along road by Karakaya Tepe; site C in Figure 3.1)

	18/10/91-7	18/10/91-7	8/10/91-15a	8/10/91-15b	18/10/91-16	LOG2/90	124A/90
SiO2	49.71	47.34	45.68	49.67	46.60	47.17	46.63
Al2O3	16.94	13.93	14.36	13.26	14.09	13.23	13.58
Fe2O3	9.79	9.93	12.52	12.68	12.20	14.25	12.57
MgO	5.79	6.30	6.66	6.86	6.78	6.30	7.21
CaO	6.68	11.09	6.94	7.79	9.38	9.41	9.25
Na2O	5.21	3.99	3.10	3.76	2.57	3.33	3.35
K2O	0.047	0.022	0.116	0.076	0.242	0.202	0.129
TiO2	1.305	1.158	1.574	1.452	1.547	1.954	1.654
MnO	0.123	0.146	0.209	0.209	0.223	0.189	0.216
P2O5	0.117	0.098	0.170	0.164	0.195	0.159	0.199
LOI	3.87	6.00	9.24	4.60	5.85	4.00	5.07
Total	99.58	100.01	100.57	100.51	99.69	100.19	99.86
Nb	1.6	2.1	12.5	9.6	12.9	2.6	14.6
Zr	67.8	60.5	93.7	96.3	102.1	110.1	108.3
Y	32.6	28.5	28.8	30.2	30.1	46.9	31.8
Sr	189.9	156.7	303.9	173.9	209.5	230.8	191.8
Rb	1.5	0.8	2.5	4.6	5.9	5.4	2.6
Th	-0.3	0.0	1.7	0.3	0.8	0.7	1.7
Pb	0.2	0.2	0.5	4.0	1.2	-0.1	1.4
Zn	106.1	88.4	95.9	97.8	100.8	130.5	99.8
Cu	119.5	107.5	84.6	99.6	82.2	103.6	86.7
Ni	98.1	76.9	37.3	58.9	51.6	59.7	57.2
Cr	280.9	220.9	41.3	164.9	165.0	91.8	175.5
Ce	8.3	10.2	21.4	23.9	26.3	13.0	26.9
Nd	9.7	6.2	13.4	12.7	13.1	12.4	13.5
La	5.8	3.4	9.3	12.3	11.1	3.1	14.5
V	380.8	345.3	335.0	406.1	370.9	458.1	372.4
Ba	45.5	29.7	65.1	49.3	218.6	28.6	91.3
Sc	63.2	55.9	46.7	55.3	48.7	47.6	52.8

Basalts from the Ortaoba Unit (road east of Karakaya Tepe; site A on Figure 3.1)

	22/10/91-1	22/10/91-2	22/10/91-3	22/10/91-4	22/10/91-7	22/10/91-9	22/10/91-18	LOG1/90	22/10/91-6	22/10/91-13	71A/90
SiO2	49.95	47.58	48.59	42.10	47.88	46.47	43.78	55.95	43.92	46.76	47.15
Al2O3	17.10	18.26	14.58	11.99	13.76	13.64	12.06	14.25	13.93	14.85	14.03
Fe2O3	11.74	10.78	12.76	12.57	14.26	13.48	13.23	8.68	13.59	13.08	12.42
MgO	4.90	3.86	6.44	6.05	5.99	6.48	11.41	4.11	5.68	6.17	6.44
CaO	6.97	12.52	6.67	12.19	9.49	9.54	7.84	7.12	8.06	7.58	6.68
Na2O	4.00	0.72	4.04	2.47	3.71	3.57	2.37	4.78	2.80	4.49	4.03
K2O	1.274	0.792	0.045	0.030	0.036	0.085	0.417	0.864	0.638	0.082	0.794
TiO2	0.838	0.782	1.557	1.675	1.606	1.784	2.216	1.379	1.829	2.011	2.250
MnO	0.155	0.173	0.581	0.286	0.192	0.191	0.169	0.189	0.216	0.148	0.190
P2O5	0.250	0.278	0.181	0.192	0.127	0.145	0.259	0.078	0.146	0.163	0.326
LOI	2.96	4.88	5.17	9.92	2.86	4.23	5.69	2.25	9.24	4.82	5.66
Total	100.14	100.64	100.61	99.47	99.92	99.62	99.44	99.64	100.05	100.16	99.97
Nb	2.6	2.1	14.6	10.1	2.7	2.5	24.9	2.3	2.9	2.4	37.9
Zr	97.0	64.5	100.8	111.3	84.2	100.2	146.8	72.7	98.8	109.3	181.0
Y	20.0	16.4	30.1	36.0	38.3	42.5	23.9	28.1	42.6	43.4	38.2
Sr	657.1	520.5	280.5	315.0	121.9	273.8	273.6	123.8	213.2	133.7	232.9
Rb	32.8	20.9	0.3	0.6	1.0	3.5	5.9	28.1	23.4	2.5	20.3
Th	3.9	2.2	0.4	0.5	0.5	0.7	1.5	0.9	1.8	0.5	2.5
Pb	3.3	6.1	12.6	1.4	0.2	1.1	1.4	-2.0	0.4	-0.1	3.0
Zn	89.8	84.4	106.5	106.8	116.5	125.9	110.2	95.2	123.9	128.9	103.2
Cu	176.5	204.8	82.5	99.1	107.0	100.8	99.1	95.2	111.4	109.4	65.0
Ni	27.8	9.9	37.0	60.9	73.3	76.4	401.9	83.6	82.2	75.3	100.0
Cr	51.3	24.5	45.7	131.3	150.9	139.5	610.3	178.7	167.9	156.8	258.6
Ce	45.6	44.7	28.0	30.5	12.1	13.7	51.2	8.7	13.4	14.3	42.5
Nd	20.7	17.5	15.8	18.2	6.7	10.0	26.3	4.3	12.4	15.6	21.6
La	17.8	15.6	13.2	8.8	5.7	4.0	18.6	2.8	0.0	3.9	17.6
V	385.8	415.6	358.1	399.8	401.4	426.7	261.0	375.5	486.1	487.4	376.1
Ba	342.8	189.6	93.4	77.1	17.9	41.3	94.1	92.0	73.1	76.1	236.9
Sc	33.0	24.1	49.0	48.1	54.3	48.0	32.8	54.1	63.9	60.3	44.5

Basalts from the Ortaoba Unit (road east of Karakaya Tepe; site A on Figure 3.1) (cont.)

	72B/90	77A/90	80A/90	107B/90	107C/90	36a/90	90c/90	120a/90	22/10/91-12
SiO2	47.04	45.32	47.73	46.15	47.63	42.95	46.57	42.70	46.18
Al2O3	15.14	13.84	13.85	16.37	13.09	13.92	14.43	21.28	16.55
Fe2O3	12.07	15.82	14.47	11.91	12.76	17.47	13.86	13.18	13.36
MgO	6.54	5.64	7.33	6.29	5.76	8.54	5.41	4.72	5.45
CaO	9.06	5.51	7.40	4.76	9.83	6.21	7.73	9.79	9.17
Na2O	2.60	3.32	3.94	5.20	3.49	0.88	4.99	2.50	3.41
K2O	0.067	0.206	0.055	0.045	0.034	0.348	0.034	1.072	0.497
TiO2	1.786	2.032	1.789	1.452	1.827	2.124	1.857	1.062	2.072
MnO	0.201	0.162	0.167	0.289	0.233	0.193	0.237	0.239	0.222
P2O5	0.209	0.166	0.169	0.160	0.194	0.150	0.165	0.378	0.326
LOI	4.91	7.98	3.19	8.00	5.64	7.68	5.35	3.65	3.00
Total	99.62	100.01	100.10	100.10	100.48	100.48	100.63	100.57	100.24
Nb	14.8	2.9	2.5	11.2	11.0	2.8	3.0	3.2	32.6
Zr	116.3	117.4	125.7	91.4	121.0	112.8	101.9	87.9	170.1
Y	28.6	45.8	44.3	26.5	38.4	47.1	42.7	22.0	39.1
Sr	209.3	246.3	136.7	156.1	332.2	119.0	124.4	608.6	419.8
Rb	1.5	7.9	1.0	0.6	0.8	13.1	0.9	31.4	11.3
Th	0.5	-1.8	1.1	-0.2	0.3	2.2	0.8	4.3	2.2
Pb	2.3	0.8	0.1	4.5	0.8	-1.5	0.0	6.2	0.5
Zn	108.4	136.9	116.0	104.8	104.7	125.9	129.2	114.9	105.2
Cu	87.5	83.9	112.7	99.3	94.3	121.7	100.9	308.4	38.3
Ni	55.9	56.8	57.1	62.7	65.2	81.4	79.4	12.7	26.9
Cr	183.9	93.0	94.7	104.4	145.9	170.4	155.3	34.5	37.7
Ce	23.4	10.4	18.3	18.1	31.1	16.9	16.5	47.5	39.1
Nd	14.5	4.7	13.4	7.1	14.0	13.8	11.8	25.2	22.1
La	7.6	-5.1	1.9	-0.9	6.3	5.5	2.5	17.2	17.5
V	409.6	478.8	401.4	342.8	389.4	549.6	444.5	422.2	359.5
Ba	166.5	20.8	10.5	37.1	57.7	78.7	16.9	480.0	376.5
Sc	48.9	54.4	50.1	57.7	48.6	68.0	54.5	31.2	41.6

	Mudstones of the Ortaoba Unit (site 91/90)						Mudstones of the Ortaoba Unit (site 111/90)		
	91A/90	91B/90	91C/90	91D/90	91E/90	91F/90	111A/90	111B/90	111C/90
SiO2	49.83	45.90	62.28	56.93	53.26	50.48	38.55	51.61	52.00
Al2O3	19.82	18.33	21.82	21.28	26.03	26.82	16.83	21.32	24.74
Fe2O3	13.62	18.74	1.71	4.31	4.14	5.60	27.24	10.47	5.15
MgO	3.31	4.85	2.43	4.02	1.34	1.31	7.21	4.38	3.47
CaO	0.28	0.42	0.20	0.25	0.15	0.14	0.28	0.36	0.23
Na2O	1.13	0.80	1.70	0.59	1.02	0.54	0.28	0.74	0.43
K2O	4.979	3.653	6.094	5.482	7.599	7.734	1.440	5.114	7.580
TiO2	0.266	0.220	0.257	0.754	0.798	0.849	0.198	0.380	0.250
MnO	0.121	0.378	0.099	0.336	0.033	0.027	0.118	0.118	0.100
P2O5	0.064	0.057	0.080	0.073	0.066	0.086	0.064	0.070	0.051
LOI	6.45	6.97	4.12	6.13	5.30	6.35	8.56	6.36	6.30
Total	99.87	100.33	100.78	100.16	99.72	99.93	100.77	100.92	100.30
Nb	13.1	13.8	14.2	18.1	22.7	25.7	14.9	9.8	14.3
Zr	263.8	121.3	161.9	391.1	271.2	282.5	242.4	259.7	229.4
Y	42.1	42.4	36.8	73.4	57.8	53.8	37.3	70.0	48.9
Sr	23.6	28.3	27.3	17.0	22.9	17.0	10.3	24.0	13.3
Rb	230.1	166.8	227.3	210.9	291.8	304.4	69.8	212.3	305.0
Th	20.4	18.9	35.8	25.1	30.5	33.5	24.1	16.7	42.7
Pb	33.2	5.2	8.7	9.7	11.7	34.7	134.2	17.8	69.3
Zn	132.1	183.8	36.8	133.3	67.6	70.9	198.9	172.2	114.4
Cu	149.9	266.0	9.0	15.6	26.4	29.9	159.4	124.6	79.9
Ni	68.0	98.2	8.5	26.5	13.1	9.4	67.5	85.0	45.7
Cr	4.5	8.4	-0.2	1.2	68.3	75.9	4.0	9.5	6.1
Ce	114.2	45.2	116.5	134.8	123.3	127.9	119.8	107.0	121.2
Nd	39.2	9.2	45.5	55.7	48.2	50.6	49.0	45.7	46.5
La	46.8	30.7	64.5	62.9	57.6	52.8	65.4	56.3	65.6
V	18.5	20.1	8.5	16.0	138.2	143.0	14.9	49.4	64.2
Ba	429.8	234.9	855.5	839.1	1182.5	1225.0	193.8	585.6	762.8
Sc	16.2	9.8	7.2	18.5	25.1	27.1	8.6	12.9	8.9

Granodiorites from the Camlik (CAM), Beyoba (BEY) and Eybek plutons

	CAM1	CAM2	CAM4	CAM7	CAM8	CAM9	CAM11	BEY3	BEY10	Eybek
SiO2	51.25	63.85	65.39	70.75	65.58	63.78	63.67	69.92	59.32	60.56
Al2O3	14.65	14.83	15.42	15.11	15.13	14.66	15.74	15.48	15.92	17.07
Fe2O3	7.29	5.53	5.15	2.88	5.71	5.47	5.09	2.91	6.19	6.42
MgO	5.21	4.65	4.16	0.92	3.67	4.60	5.02	0.90	2.62	2.70
CaO	7.52	1.92	0.33	1.16	0.39	2.06	1.16	1.80	4.11	5.93
Na2O	2.63	2.43	3.04	4.42	2.24	2.47	2.63	4.23	4.96	3.61
K2O	1.197	3.127	3.338	2.913	3.121	2.862	2.194	2.680	1.760	1.224
TiO2	0.671	0.578	0.557	0.347	0.495	0.558	0.593	0.342	0.671	0.644
MnO	0.212	0.121	0.103	0.072	0.122	0.115	0.090	0.070	0.098	0.129
P2O5	0.176	0.140	0.138	0.101	0.123	0.140	0.149	0.107	0.192	0.167
LOI	9.04	2.84	3.01	1.16	3.11	2.76	3.58	1.10	3.68	1.13
Total	99.85	100.02	100.65	99.83	99.70	99.48	99.93	99.55	99.53	99.59
Nb	9.6	11.3	11.5	9.1	10.6	10.7	11.1	7.9	7.9	6.4
Zr	111.2	135.2	133.9	153.9	115.0	133.6	132.3	152.9	158.9	151.8
Y	17.8	23.0	29.6	16.9	14.7	24.0	26.2	21.2	22.9	24.9
Sr	307.3	393.7	154.2	297.9	138.3	392.6	325.8	320.1	443.9	504.3
Rb	66.8	121.1	131.4	71.3	149.7	109.9	104.8	62.8	48.5	35.7
Th	5.7	15.2	14.3	14.2	14.5	15.0	12.9	14.1	8.5	7.2
Pb	10.2	27.6	10.9	13.2	8.3	33.1	15.5	15.7	14.6	14.2
Zn	101.5	88.5	112.2	34.3	75.7	87.5	70.0	33.6	70.8	77.6
Cu	12.0	26.7	42.2	4.3	22.1	38.5	29.2	3.6	6.6	11.7
Ni	51.2	52.0	64.6	3.9	43.6	53.0	55.5	3.2	6.6	7.5
Cr	312.6	252.7	265.2	4.2	236.6	246.2	261.5	3.5	12.7	11.4
Ce	41.3	70.9	73.7	68.2	69.0	84.4	78.1	65.6	60.9	41.7
Nd	18.1	31.0	21.9	17.9	22.7	27.4	28.9	21.9	23.7	15.9
La	24.3	36.9	26.3	33.4	34.9	29.6	36.6	30.3	16.4	20.1
V	180.5	136.6	128.5	45.0	111.0	134.0	138.0	40.9	120.7	141.1
Ba	104.5	576.2	990.1	685.2	359.2	526.0	480.9	741.7	1262.4	672.4
Sc	27.7	21.9	23.7	4.1	20.3	20.8	22.6	4.3	13.3	22.1

Basalt blocks from the Cal Unit near Calkoy

	22/08/92-5	22/08/92-21	22/08/92-42	22/08/92-47	22/08/92-6	22/08/92-16	22/08/92-22	22/08/92-31	22/08/92-34	21/10/92-2	22/08/92-18	22/08/92-43
SiO2	38.45	45.58	46.67	47.49	44.34	40.21	58.99	42.05	46.68	40.27	43.48	36.07
Al2O3	11.39	9.25	11.26	9.22	13.24	14.33	8.25	11.04	13.79	8.89	14.31	10.39
Fe2O3	11.38	11.48	10.60	11.72	13.37	14.15	10.43	13.43	11.00	10.03	12.13	11.98
MgO	6.15	6.06	7.96	6.78	6.40	1.28	6.39	7.39	8.77	3.24	1.10	7.12
CaO	13.52	12.40	11.01	11.54	6.77	9.84	6.43	8.95	7.08	19.67	9.37	14.95
Na2O	2.78	3.05	3.71	2.50	2.39	3.48	1.71	3.59	3.52	4.14	6.09	3.00
K2O	1.517	0.627	0.649	1.365	3.055	3.148	0.701	0.519	1.312	0.121	2.005	0.600
TiO2	2.528	2.033	2.223	2.069	2.998	3.362	1.850	2.342	3.105	2.400	3.106	2.343
MnO	0.107	0.092	0.128	0.123	0.123	0.092	0.059	0.115	0.103	0.111	0.100	0.095
P2O5	0.413	0.391	0.378	0.358	0.500	0.590	0.907	0.371	0.541	0.275	0.469	0.437
LOI	11.43	8.76	5.62	6.34	6.25	8.72	3.28	9.57	4.88	10.90	7.43	12.02
Total	99.67	99.72	100.20	99.51	99.43	99.20	99.00	99.37	100.77	100.05	99.58	98.99
Nb	38.0	29.4	31.8	31.6	44.5	53.9	27.2	32.4	48.5	27.1	39.4	39.2
Zr	192.6	152.3	173.2	153.0	244.7	287.2	139.5	168.6	235.1	185.4	250.7	199.2
Y	23.7	21.4	20.2	19.1	31.7	38.1	32.3	23.4	27.0	20.3	32.7	29.8
Sr	309.6	239.6	230.1	265.1	245.0	338.3	162.8	200.3	185.3	234.0	208.1	173.0
Rb	25.4	13.0	9.2	21.1	48.9	64.0	12.8	6.9	19.4	3.0	24.2	9.5
Th	3.6	1.6	0.9	2.1	4.7	6.9	1.3	2.4	2.7	3.6	5.5	4.8
Pb	2.3	3.3	0.3	2.3	1.1	3.5	2.6	1.8	2.9	2.5	0.8	24.7
Zn	91.4	85.0	75.1	72.7	104.1	101.9	112.1	85.0	106.6	87.4	84.3	81.5
Cu	92.3	95.9	82.7	68.0	62.7	68.2	64.0	67.9	142.9	71.4	41.7	63.2
Ni	152.9	344.7	86.8	129.4	54.0	58.0	296.8	207.1	218.1	346.2	39.4	144.7
Cr	175.8	607.1	108.9	320.5	43.2	73.4	416.1	498.2	391.7	805.8	20.2	50.3
Ce	88.9	77.5	68.8	61.6	98.0	111.9	83.2	83.3	94.5	44.4	71.3	76.5
Nd	44.9	37.3	31.1	31.6	48.3	55.3	39.7	40.1	46.7	28.7	39.8	41.3
La	38.1	31.4	24.7	20.4	30.1	43.0	33.2	30.9	34.2	21.7	29.6	33.0
V	249.6	263.3	226.5	255.2	200.3	361.8	212.6	294.5	288.3	313.6	161.9	295.1
Ba	126.4	70.8	111.4	271.5	153.5	169.9	75.8	52.9	139.5	134.3	178.6	56.2
Sc	29.2	27.5	23.6	22.9	24.2	29.4	21.0	32.2	34.1	16.5	21.7	11.4

Basalt blocks from the Cal Unit along the Karaasik road

	23/08/92-2	23/08/92-24	23/08/92-4	23/08/92-19
SiO2	34.97	40.89	42.51	43.36
Al2O3	8.97	12.38	12.71	14.89
Fe2O3	7.70	8.43	8.74	9.02
MgO	8.23	10.41	11.65	3.95
CaO	20.44	11.93	10.46	13.33
Na2O	2.35	2.76	2.37	3.74
K2O	0.776	0.987	0.837	0.287
TiO2	1.915	3.025	2.877	0.958
MnO	0.119	0.123	0.141	0.260
P2O5	0.317	0.701	0.683	0.092
LOI	14.01	8.08	6.60	9.41
Total	99.80	99.70	99.58	99.30
Nb	27.8	52.2	49.8	1.2
Zr	149.5	264.0	237.4	53.0
Y	21.4	31.3	34.7	29.2
Sr	205.8	177.9	170.1	120.9
Rb	14.1	18.7	15.8	6.4
Th	3.3	5.4	2.3	-0.7
Pb	0.7	3.2	1.3	8.4
Zn	77.7	88.3	96.6	68.3
Cu	19.5	90.0	83.9	168.5
Ni	208.5	186.3	194.9	72.4
Cr	430.1	132.9	165.0	374.3
Ce	64.9	90.6	99.8	24.2
Nd	35.1	53.5	50.2	6.8
La	20.5	38.3	39.6	1.4
V	210.1	232.0	262.9	317.6
Ba	37.5	122.3	140.0	40.4
Sc	22.2	12.8	18.1	41.1

	Cal Unit sediments near Edremit			Orhanlar Greywacke
	78B/90	78C/90	79B/90	ORH3
SiO2	72.75	59.06	59.20	69.43
Al2O3	11.19	18.08	17.97	10.20
Fe2O3	3.97	8.54	7.63	5.66
MgO	1.91	2.63	3.64	2.95
CaO	2.09	0.40	0.43	2.92
Na2O	2.15	1.45	1.44	1.59
K2O	1.408	4.096	3.598	1.341
TiO2	0.559	0.850	0.796	0.668
MnO	0.059	0.188	0.087	0.149
P2O5	0.145	0.101	0.134	0.148
LOI	3.87	4.09	4.70	4.69
Total	100.10	99.49	99.61	99.75
Nb	12.3	19.1	13.1	10.3
Zr	162.4	195.4	146.0	159.3
Y	19.9	28.6	24.9	17.4
Sr	99.7	39.0	64.3	64.2
Rb	54.6	165.7	145.5	51.0
Th	10.9	19.2	11.2	6.3
Pb	13.0	36.7	19.6	15.8
Zn	68.5	131.2	98.6	76.7
Cu	14.3	66.0	41.7	24.8
Ni	72.5	101.8	105.3	93.1
Cr	160.0	139.7	209.8	202.3
Ce	69.5	96.8	90.8	38.6
Nd	28.0	29.2	31.8	14.0
La	37.7	37.4	32.4	9.4
V	82.4	193.9	192.3	119.6
Ba	172.7	346.2	424.7	235.2
Sc	8.7	21.1	30.0	13.8

	Amphibolites from Kazdag "core"					Amphibolites from Kazdag "cover"			
	10/10/92-a1	10/10/92-a2	10/10/92-a3	10/10/92-a4	10/10/92-a5	10/10/92-b1	10/10/92-b2	10/10/92-b3	10/10/92-b4
SiO2	45.70	46.05	45.67	46.15	43.33	48.62	45.54	44.83	49.36
Al2O3	17.03	16.82	17.84	17.06	17.53	17.23	15.57	13.06	16.55
Fe2O3	8.33	8.03	7.60	7.40	11.12	9.57	13.95	18.51	9.51
MgO	10.94	11.48	10.76	11.86	8.27	7.89	8.40	4.96	8.47
CaO	14.38	13.92	14.86	14.09	15.13	10.33	10.63	8.72	10.10
Na2O	1.76	1.85	1.56	1.72	1.61	3.13	2.18	3.71	3.25
K2O	0.085	0.091	0.098	0.090	0.161	0.260	0.365	0.279	0.280
TiO2	0.757	0.569	0.534	0.432	1.960	1.095	1.337	4.672	1.188
MnO	0.165	0.139	0.152	0.140	0.187	0.143	0.167	0.316	0.100
P2O5	0.004	0.002	0.002	0.005	0.061	0.142	0.118	0.368	0.143
LOI	1.07	1.13	0.01	1.28	0.88	1.49	1.71	0.40	1.11
Total	100.23	100.08	99.08	100.23	100.24	99.89	99.97	99.82	100.06
Nb	2.1	2.2	1.6	1.2	10.9	3.9	4.3	19.0	4.8
Zr	25.3	20.7	25.8	35.9	157.3	76.8	89.4	239.5	96.4
Y	18.2	12.8	15.0	13.3	39.2	25.1	30.1	69.2	28.1
Sr	155.4	136.1	224.0	152.4	330.4	177.6	143.0	142.8	220.6
Rb	0.8	0.7	0.7	0.6	0.8	7.1	11.1	9.1	4.7
Th	-0.6	-0.7	-0.7	-1.1	0.9	0.2	1.0	3.4	-0.4
Pb	7.7	4.6	7.4	5.4	10.1	3.0	2.6	2.9	6.2
Zn	63.3	66.0	58.9	56.7	79.0	54.7	72.8	108.2	37.5
Cu	36.4	14.1	15.7	19.5	62.0	11.0	24.7	191.3	10.3
Ni	140.9	228.0	191.5	255.4	91.4	281.3	222.2	11.7	190.0
Cr	353.1	700.1	518.6	650.4	255.2	362.1	389.9	31.5	323.7
Ce	7.9	8.1	4.7	1.6	35.2	16.5	20.5	39.4	20.9
Nd	4.3	4.8	2.9	4.3	18.2	7.7	13.7	26.0	12.7
La	2.7	3.5	-0.9	1.5	9.7	4.5	9.6	8.1	6.2
V	251.8	241.6	237.7	208.8	358.9	224.6	345.8	514.1	229.6
Ba	5.6	12.2	-1.0	9.2	-1.8	22.2	33.2	16.3	22.8
Sc	57.9	49.5	54.5	43.5	59.3	36.2	44.5	44.7	36.0

Peridotites from the Denizgoren Ophiolite

	DEN1	DEN7	10/10/01	10/10/02	10/10/17	DENa
SiO2	41.54	41.39	39.10	38.81	41.52	39.13
Al2O3	1.46	1.34	1.20	1.13	1.63	1.10
Fe2O3	5.80	7.35	7.65	7.31	8.24	7.44
MgO	37.37	38.71	37.05	37.96	38.82	38.14
CaO	1.63	1.45	1.74	1.19	1.87	0.49
Na2O	0.04	0.08	0.05	0.03	0.15	0.06
K2O	-0.002	0.002	-0.002	0.000	0.022	0.000
TiO2	0.023	0.029	0.034	0.028	0.029	0.030
MnO	0.098	0.116	0.143	0.132	0.118	0.121
P2O5	0.013	0.011	0.010	0.014	0.011	0.012
LOI	11.37	9.29	12.74	13.25	7.39	13.15
Total	99.34	99.76	99.71	99.85	99.79	99.67
Nb	1.5	1.8	2.2	2.0	1.8	2.0
Zr	1.7	1.5	1.2	1.5	2.2	1.9
Y	0.5	0.1	1.0	-0.1	0.8	0.8
Sr	2.4	1.5	3.2	4.3	1.1	2.4
Rb	0.3	0.6	-0.3	0.6	0.6	0.3
Th	0.1	-0.9	-0.7	-2.3	-1.4	-1.6
Pb	0.7	0.3	0.7	-0.1	0.0	1.8
Zn	36.8	38.5	35.2	38.2	44.1	41.5
Cu	4.2	9.8	6.6	5.6	17.8	7.5
Ni	2242.4	2209.1	2111.5	2214.9	1978.9	2349.0
Cr	2798.2	2490.3	2651.4	2284.2	2639.6	2826.7
Ce	-14.2	-0.8	-3.3	-3.2	-8.4	-7.1
Nd	-10.3	-5.6	-9.2	-11.5	-12.2	-13.3
La	1.8	-0.5	7.4	2.5	4.3	3.3
V	51.3	54.5	57.5	46.0	65.5	45.9
Ba	5.4	-6.6	-10.0	-3.6	-2.7	7.6
Sc	10.2	10.9	12.2	7.6	11.8	12.2

Amphibolites from the metamorphic sole of the Denizgoren Ophiolite

	DS1	DS2	DS3	DS4	DS5	DS6	DS7	DS8	DS9	DS10	DS11	DS12	DS13	DS14
SiO2	46.24	48.85	47.02	46.79	44.83	48.84	47.91	47.29	49.05	47.59	44.53	46.26	46.10	45.84
Al2O3	15.03	17.91	16.23	17.33	16.58	17.88	10.46	16.31	16.72	16.01	15.97	15.00	16.07	18.79
Fe2O3	11.02	8.05	10.04	6.53	7.03	7.85	7.74	9.24	9.20	9.47	11.52	7.74	7.50	4.84
MgO	10.66	8.21	9.81	11.16	12.66	8.01	18.77	10.04	8.65	9.59	9.07	13.53	12.65	11.79
CaO	11.04	10.00	11.06	12.88	14.01	10.47	10.41	11.26	9.13	11.19	13.99	12.82	12.66	14.50
Na2O	2.23	3.00	2.56	2.05	1.21	2.89	1.48	2.56	3.51	2.67	1.49	1.61	1.40	1.04
K2O	0.311	0.998	0.387	0.070	0.211	0.946	0.042	0.331	0.684	0.286	0.136	0.311	0.161	0.339
TiO2	0.957	0.686	0.843	0.292	0.314	0.690	0.410	0.823	0.851	1.055	0.975	0.362	0.331	0.162
MnO	0.166	0.129	0.151	0.102	0.117	0.124	0.140	0.146	0.157	0.156	0.168	0.128	0.122	0.090
P2O5	0.050	0.055	0.067	0.007	-0.001	0.042	0.009	0.055	0.059	0.088	0.072	-0.001	0.028	-0.002
LOI	2.28	2.11	2.02	2.78	2.60	1.98	2.62	1.91	1.84	2.06	2.05	2.39	2.91	2.66
Total	99.98	100.00	100.20	99.99	99.55	99.72	100.00	99.96	99.85	100.17	99.97	100.16	99.94	100.04
Nb	2.5	2.0	2.4	0.7	0.2	1.9	1.4	2.1	2.5	4.3	2.6	0.8	0.6	0.8
Zr	39.2	31.7	33.2	12.0	10.8	30.2	30.8	46.1	43.4	50.2	41.3	11.4	8.5	9.1
Y	21.8	15.0	17.0	10.9	8.4	14.2	9.4	19.9	20.1	24.2	30.1	8.6	9.7	4.0
Sr	74.8	109.6	91.5	80.7	70.1	125.9	68.6	99.1	98.9	102.9	122.5	44.4	75.3	85.6
Rb	7.6	26.2	9.5	1.1	3.5	24.3	0.9	7.5	14.2	5.3	3.0	6.7	4.0	8.6
Th	0.7	0.4	0.4	-1.0	-0.9	0.8	-0.6	-0.4	-0.1	-1.0	0.9	-0.6	-0.2	-1.2
Pb	-0.3	-0.1	-0.7	-0.9	-0.6	0.2	0.8	0.4	0.7	-0.6	1.0	0.5	0.6	-1.2
Zn	47.7	38.7	40.1	38.3	44.3	39.7	44.3	42.1	52.7	55.1	56.0	51.3	48.5	29.2
Cu	61.6	57.7	35.4	55.1	74.9	37.8	13.8	53.9	53.2	50.1	29.6	81.9	47.2	34.6
Ni	156.9	159.0	193.1	290.8	329.7	149.3	1091.3	206.8	146.2	158.1	147.6	386.9	323.2	318.1
Cr	441.0	466.7	540.5	1162.2	1251.9	461.9	1486.4	665.8	385.9	455.2	415.2	1199.6	1033.4	921.7
Ce	0.6	7.0	5.9	5.8	-1.7	7.9	5.1	7.5	11.6	17.3	14.7	-0.3	0.2	1.3
Nd	2.7	5.3	3.1	3.3	-1.7	1.6	4.4	6.1	8.3	9.1	4.7	3.1	1.6	4.3
La	-1.5	0.0	2.1	2.2	0.8	3.0	4.8	4.2	2.3	4.1	0.8	0.6	1.1	2.9
V	314.8	198.7	254.8	161.1	167.8	199.2	154.9	238.9	222.4	265.5	334.6	186.0	197.3	114.2
Ba	5.5	44.5	19.1	21.7	13.9	39.8	16.4	14.7	96.8	16.1	8.5	5.7	25.1	24.5
Sc	56.1	36.5	44.4	40.1	41.9	32.5	22.0	40.3	42.7	48.3	58.9	42.6	46.7	30.0

Amphibolites from the metamorphic sole of the Lesbos Ophiolite

	LS1	LS2	LS3	LS4	LS5	LS6	LS7	LS8	LS9	LS10	LS11
SiO2	47.09	47.07	47.22	46.15	45.31	45.36	48.58	51.11	48.36	46.29	45.36
Al2O3	19.32	17.16	15.53	14.76	14.70	14.95	14.75	15.38	14.60	15.77	15.34
Fe2O3	4.47	4.39	10.29	11.89	12.18	11.81	10.03	7.79	9.29	10.40	11.74
MgO	8.66	10.41	8.92	9.27	9.67	9.72	8.60	8.87	9.70	9.09	9.78
CaO	14.57	14.61	10.83	12.25	12.62	13.37	11.66	10.35	13.57	11.85	10.91
Na2O	1.65	1.49	2.34	1.96	1.74	1.63	2.57	2.99	1.67	2.04	2.05
K2O	0.305	0.498	0.849	0.149	0.171	0.076	0.475	0.964	0.415	0.453	0.336
TiO2	0.152	0.199	1.340	1.147	1.260	1.310	1.085	0.553	0.599	1.391	1.691
MnO	0.081	0.090	0.161	0.162	0.166	0.150	0.158	0.099	0.145	0.143	0.154
P2O5	-0.001	-0.006	0.133	0.101	0.107	0.112	0.087	0.038	0.025	0.130	0.158
LOI	3.01	3.75	2.25	1.98	2.05	1.82	1.91	1.88	1.89	2.42	2.66
Total	99.31	99.66	99.86	99.82	99.97	100.30	99.90	100.01	100.26	99.96	100.19
Nb	0.7	0.8	6.0	5.1	5.7	5.5	4.8	2.6	2.6	8.2	8.8
Zr	7.1	6.7	88.2	55.6	57.8	47.5	56.2	41.7	39.8	59.6	66.5
Y	4.0	5.6	27.5	26.4	29.8	28.6	27.1	12.9	15.2	31.2	38.7
Sr	208.9	114.8	90.1	120.2	133.7	197.6	129.1	139.8	171.1	138.3	113.5
Rb	7.5	10.7	17.1	1.6	2.2	0.3	10.0	19.8	8.0	8.3	6.2
Th	-1.3	-1.5	0.9	-0.4	0.4	0.0	0.8	0.5	0.2	-0.1	0.7
Pb	1.0	-0.2	-1.6	-1.7	0.4	1.3	0.1	1.0	-0.3	-0.7	-0.9
Zn	23.8	27.4	38.3	56.1	56.2	39.2	32.7	27.1	43.1	45.1	51.0
Cu	45.8	122.7	15.6	57.2	39.8	37.3	11.9	15.3	20.0	34.2	61.5
Ni	173.4	186.6	150.1	130.9	132.2	136.2	122.9	124.4	115.7	116.2	105.6
Cr	913.9	939.0	359.4	394.5	315.7	423.4	368.4	204.9	393.5	283.3	269.8
Ce	3.4	4.5	22.9	3.5	12.3	13.1	11.4	6.3	-0.6	9.1	23.6
Nd	1.8	3.1	13.9	2.9	8.2	11.5	7.5	3.6	3.9	7.2	12.4
La	2.2	2.7	4.0	-0.1	2.0	4.6	5.5	2.8	4.1	1.7	4.9
V	117.9	161.7	245.8	329.3	355.1	350.5	292.9	215.2	251.3	328.2	380.6
Ba	21.4	55.1	89.0	19.6	20.3	-4.2	53.6	71.5	31.6	39.6	24.0
Sc	38.8	51.8	45.0	49.4	54.3	58.9	49.4	37.6	47.8	49.6	55.7

Cherts from the Karaburun Peninsula

	6/10/92-1	6/10/92-2	6/10/92-3	6/10/92-4	6/10/92-5
SiO2	26.5	85.55	87.10	43.26	88.14
Al2O3	0.69	0.48	5.77	0.21	1.08
Fe2O3	1.73	1.08	2.00	2.63	1.32
MgO	1.09	0.02	0.36	0.33	0.08
CaO	1.66	0.21	0.10	0.49	0.19
Na2O	0.56	-0.09	-0.05	0.01	-0.17
K2O	1.038	0.05	1.469	0.386	0.185
TiO2	0.029	0.027	0.247	0.025	0.024
MnO	51.606	9.484	0.891	40.79	9.825
P2O5	0.093	0.016	0.054	0.02	0.03
LOI	12.81	2.59	1.89	8.69	2.68
Total	97.8	99.41	99.83	96.83	103.38
Nb	2.9	3.4	7.8	2.4	2.7
Zr	17.5	6.5	53.8	14.1	5.5
Y	10.3	2.1	13.3	4.3	4.5
Sr	472.1	38.8	49.8	423.0	92.8
Rb	29.9	2.8	65.0	7.3	5.4
Th	-5.1	-0.4	5.7	-4.6	0.9
Pb	3.8	4.0	9.1	2.9	14.9
Zn	7.8	42.5	44.2	9.5	124.4
Cu	-16.8	49.4	43.0	7.5	16.8
Ni	50.7	29.3	36.0	38.6	113.4
Cr	-1.3	1.5	32.6	2.8	2.6
Ce	-7.3	0.5	66.8	6.1	1.7
Nd	-36.9	-15.7	12.8	-34.4	-12.9
La	3.6	2.7	21.6	-1.1	2.6
V	17.3	25.0	45.5	13.6	21.2
Ba	26.3	16.5	329.3	68.3	117.1
Sc	-1.3	-1.2	8.9	-2.3	0.3

Laterites from Chios

	Ch-lat1	Ch-lat2	Ch-lat3	Ch-lat4	Ch-lat5
SiO2	14.79	3.71	4.57	1.88	7.49
Al2O3	2.63	0.73	0.21	0.32	0.68
Fe2O3	14.00	18.68	18.9	23.77	21.12
MgO	0.91	6.25	0.68	1.89	1.88
CaO	31.14	28.91	36.46	35.12	33.56
Na2O	0.10	-0.07	-0.15	-0.16	-0.17
K2O	0.663	0.172	0.016	0.052	0.15
TiO2	0.101	0.037	0.008	0.019	0.031
MnO	1.815	2.15	2.28	2.727	2.746
P2O5	0.05	0.031	0.024	0.014	0.024
LOI	29.27	38.04	33.48	33.93	31.68
Total	95.47	98.64	96.46	98.93	99.68
Nb	3.1	2.1	0.8	1.9	2.4
Zr	55.4	10.0	35.9	6.8	10.7
Y	37.4	4.9	33.8	13.5	13.1
Sr	76.7	148.1	37.1	109.5	169.0
Rb	20.7	8.6	-11.1	2.5	7.7
Th	-397.0	-4.1	-424.5	-9.5	-5.4
Pb	22683.6	90.9	24383.0	355.1	210.2
Zn	6894.1	32.2	39.2	17.6	121.6
Cu	287.5	27.0	76.5	41.2	35.7
Ni	21.2	10.6	8.3	10.6	14.8
Cr	20.7	6.9	6.1	6.5	6.8
Ce	154.0	25.7	134.2	8.7	26.8
Nd	3.6	-2.6	-12.8	-11.1	-6.3
La	15.8	6.4	-5.6	6.9	6.9
V	33.8	9.2	13.5	11.1	18.5
Ba	79.4	14.0	12.5	17.8	4.4
Sc	2.8	1.7	2.9	-2.1	0.2

Volcanics from blocks in Chios melange

	C37	C38	C39	C40A	C40B	C40C	C40D	C40E	C45A	C45C	C45D
SiO2	52.58	51.39	41.73	44.87	57.81	59.51	58.70	66.41	45.94	53.58	52.85
Al2O3	14.04	11.78	13.57	17.52	12.51	15.60	12.74	13.84	12.39	15.43	15.05
Fe2O3	8.15	9.13	10.24	12.20	8.69	7.11	8.83	5.89	12.01	8.26	10.71
MgO	9.05	9.54	11.06	6.51	4.73	3.43	4.70	3.04	10.28	5.51	6.35
CaO	6.35	8.14	9.24	7.25	5.01	3.99	4.33	2.23	6.94	3.30	2.69
Na2O	4.15	2.51	3.29	4.30	3.35	4.40	3.34	5.01	1.89	5.02	5.75
K2O	0.160	0.421	0.420	0.054	0.282	0.963	0.297	0.433	2.337	2.478	0.810
TiO2	0.659	0.404	0.750	0.912	0.644	0.731	0.650	0.630	2.293	2.698	2.405
MnO	0.161	0.185	0.200	0.196	0.134	0.116	0.135	0.090	0.155	0.098	0.148
P2O5	0.137	0.065	0.148	0.196	0.132	0.179	0.136	0.168	0.366	0.491	0.334
LOI	4.97	9.30	9.84	5.70	7.18	4.40	6.47	2.55	5.96	3.62	3.92
Total	100.42	102.87	100.49	99.70	100.48	100.44	100.33	100.30	100.55	100.48	101.03
Nb	7.3	3.5	6.9	7.9	4.6	5.0	4.3	36.5	32.3	19.5	20.1
Zr	72.9	43.9	79.7	85.0	54.8	66.7	54.7	408.9	503.3	751.3	241.3
Y	19.5	11.0	18.7	24.5	12.9	15.1	14.7	218.1	250.9	195.2	211.2
Sr	85.3	129.8	147.8	177.9	258.7	451.4	253.7	13.9	26.1	49.3	23.9
Rb	8.5	28.9	25.2	0.9	14.4	27.4	15.2	26.8	72.3	93.8	64.9
Th	2.7	2.1	3.6	1.5	0.7	2.1	0.6	11.3	31.5	42.4	26.1
Pb	9.9	8.3	10.9	4.2	2.8	2.8	4.8	57.3	559.6	29.4	73.3
Zn	75.2	75.5	92.1	114.0	75.4	72.1	78.3	12.8	317.7	31.6	85.6
Cu	61.7	50.1	52.3	298.0	64.6	83.0	41.7	93.7	54.1	58.5	41.8
Ni	220.2	141.8	194.6	19.0	15.8	14.4	16.1	50.7	108.2	78.8	102.3
Cr	795.6	562.6	858.6	63.9	57.1	47.5	60.4	2.8	5.3	1.5	3.6
Nd	16.9	11.3	16.3	20.6	8.5	12.2	8.5	-0.1	5.4	7.3	6.4
Ce	36.1	21.2	43.5	46.4	18.7	35.4	22.4	10.9	52.0	65.5	47.9
La	17.5	6.9	21.3	15.8	12.3	15.0	13.1	331.7	278.3	372.3	133.5
V	218.3	170.1	243.1	379.5	278.7	286.5	313.1	13.8	25.0	32.5	26.9
Ba	115.1	104.8	87.0	236.8	148.2	470.5	185.1	60.5	202.3	284.2	237.6
Sc	35.4	26.1	47.9	49.5	46.3	45.1	46.4	6.2	28.5	39.4	31.9

Volcanics from the Karaburun Peninsula

	6/10/92-2a	6/10/92-2b	6/10/92-2c	6/10/92-2d	6/10/92-2e	6/10/92-2f
SiO2	61.14	64.82	63.92	73.46	62.93	73.07
AlO2	14.62	14.46	13.31	13.44	13.82	13.54
Fe2O3	6.10	5.82	7.46	2.72	7.67	2.81
MgO	0.98	0.84	0.82	0.64	0.85	0.69
CaO	5.27	4.08	4.65	2.19	4.58	2.14
Na2O	2.59	3.01	0.53	2.97	1.42	3.12
K2O	2.746	2.385	2.677	2.180	2.828	2.149
TiO2	0.786	0.777	0.697	0.711	0.743	0.718
MnO	0.085	0.045	0.110	0.016	0.106	0.016
P2O5	0.165	0.156	0.131	0.148	0.143	0.147
LOI	5.68	3.72	6.23	2.07	4.86	2.05
Total	100.15	100.11	100.54	100.55	99.94	100.45
Nb	10.5	10.0	9.4	9.4	9.3	9.4
Zr	131.8	119.1	115.0	115.7	119.7	114.1
Y	24.3	23.0	22.1	21.2	22.5	21.0
Sr	164.3	134.4	97.5	300.4	171.3	298.5
Rb	87.3	79.0	92.0	67.1	94.3	65.5
Th	7.3	6.7	7.1	5.5	7.6	5.3
Pb	10.8	8.7	9.7	8.9	10.2	9.5
Zn	82.2	124.4	124.9	85.0	88.5	80.5
Cu	14.9	10.5	14.1	5.2	16.1	6.5
Ni	7.4	5.1	8.4	3.3	6.8	4.2
Cr	15.7	12.9	14.2	12.8	15.8	13.8
Ce	61.4	52.6	54.7	55.9	50.4	51.4
Nd	29.6	24.3	25.0	23.4	22.6	23.9
La	22.9	21.8	23.5	22.6	22.4	25.4
V	207.3	206.3	220.3	196.4	224.9	180.8
Ba	400.9	275.7	470.0	413.5	538.7	416.8
Sc	28.2	24.4	45.4	26.8	32.0	17.3

APPENDIX 3: ELECTRON MICROPROBE ANALYSES

Clinopyroxene analyses: sample 102c/90 from the Nilufer Unit

	core	rim	core	rim	core	rim	rim	core	rim
SI	52.18	51.87	51.83	52.15	51.24	51.28	51.64	51.76	52.30
TI	0.61	0.77	0.59	0.64	0.97	0.88	0.63	0.80	0.68
AL	2.54	2.71	3.39	2.97	3.59	2.83	3.20	2.70	2.53
CR	0.17	0.26	0.61	0.64	0.77	0.27	0.46	0.12	0.15
FE	6.16	6.91	5.13	5.94	7.34	7.48	5.33	7.13	6.87
MN	0.16	0.17	0.13	0.16	0.20	0.18	0.14	0.19	0.17
MG	16.95	16.80	16.98	16.67	15.93	16.23	17.00	16.40	16.47
CA	20.71	20.50	21.07	21.01	20.17	20.03	21.47	20.38	20.46
NA	0.24	0.27	0.23	0.29	0.32	0.29	0.28	0.30	0.34
TOTAL	99.72	100.26	99.96	100.47	100.53	99.47	100.15	99.78	99.97
	O= 6	O= 6	O= 6	O= 6	O= 6	O= 6	O= 6	O= 6	O= 6
SI	1.92	1.91	1.90	1.91	1.88	1.90	1.89	1.91	1.93
TI	0.02	0.02	0.02	0.02	0.03	0.02	0.02	0.02	0.02
AL	0.11	0.12	0.15	0.13	0.16	0.12	0.14	0.12	0.11
CR	0.00	0.01	0.02	0.02	0.02	0.01	0.01	0.00	0.00
FE	0.19	0.21	0.16	0.18	0.23	0.23	0.16	0.22	0.21
MN	0.00	0.01	0.00	0.00	0.01	0.01	0.00	0.01	0.01
MG	0.93	0.92	0.93	0.91	0.87	0.90	0.93	0.90	0.90
CA	0.82	0.81	0.83	0.82	0.79	0.80	0.84	0.81	0.81
NA	0.02	0.02	0.02	0.02	0.02	0.02	0.02	0.02	0.02
SUM	4.01	4.02	4.01	4.01	4.01	4.02	4.02	4.01	4.01

Clinopyroxene analyses: sample 48a/90 from the Nilufer Unit

	core	rim	core	rim	core	rim	core	core	rim
SI	49.89	51.09	52.33	52.26	51.06	50.82	49.41	49.34	49.65
TI	1.53	1.39	1.10	0.93	1.01	1.20	1.46	1.45	1.45
AL	3.46	3.05	2.33	1.92	2.58	2.89	3.47	3.29	3.35
CR	0.00	0.00	0.03	0.00	0.00	0.00	0.00	0.00	0.00
FE	10.55	10.35	8.80	10.27	11.64	11.28	11.29	10.71	10.80
MN	0.25	0.28	0.22	0.31	0.35	0.32	0.26	0.26	0.26
MG	14.72	14.40	15.86	15.86	13.67	13.82	14.53	13.98	14.11
CA	19.30	20.08	19.84	19.06	20.10	20.08	19.34	20.11	19.89
NA	0.36	0.35	0.30	0.34	0.42	0.40	0.45	0.38	0.34
TOTAL	100.06	100.99	100.81	100.95	100.83	100.29	100.21	99.52	99.85
	O= 6	O= 6	O= 6	O= 6	O=6	O=6	O=6	O=6	O=6
SI	1.87	1.89	1.92	1.93	1.91	1.89	1.86	1.87	1.87
TI	0.04	0.04	0.03	0.03	0.03	0.03	0.04	0.04	0.04
AL	0.15	0.13	0.10	0.08	0.11	0.13	0.15	0.15	0.15
CR	0.00	0.00	0.00	0.00	0.00	0.00	0.00	0.00	0.00
FE	0.33	0.32	0.27	0.32	0.36	0.35	0.35	0.34	0.34
MN	0.01	0.01	0.01	0.01	0.01	0.01	0.01	0.01	0.01
MG	0.82	0.80	0.87	0.87	0.76	0.77	0.81	0.79	0.79
CA	0.77	0.80	0.78	0.75	0.80	0.81	0.78	0.82	0.80
NA	0.03	0.03	0.02	0.02	0.03	0.03	0.03	0.03	0.02
SUM	4.03	4.01	4.01	4.02	4.02	4.03	4.04	4.03	4.03

Clinopyroxene analyses: sample 49c/90 from the Nilufer Unit

	core	core	rim	core	rim	core	rim	core	rim
SI	50.49	50.85	51.19	51.47	51.79	51.44	51.05	49.24	51.14
TI	1.02	1.10	1.05	0.95	0.78	1.05	1.09	1.20	1.13
AL	3.28	3.33	3.06	3.65	1.86	3.09	3.70	3.90	2.36
CR	0.54	0.45	0.36	1.05	0.01	0.31	0.64	0.79	0.02
FE	7.28	7.18	7.03	4.77	10.09	7.63	7.18	6.70	9.22
MN	0.15	0.17	0.17	0.09	0.29	0.16	0.16	0.15	0.27
MG	15.53	15.16	15.37	16.14	14.66	15.36	15.61	15.17	15.05
CA	21.08	21.38	21.46	21.75	20.08	20.57	20.53	21.48	20.50
NA	0.41	0.32	0.32	0.32	0.31	0.30	0.30	0.39	0.37
TOTAL	99.78	99.94	100.01	100.19	99.87	99.91	100.26	99.02	100.06
	O= 6	O= 6	O= 6	O= 6	O= 6	O= 6	O= 6	O= 6	O= 6
SI	1.88	1.89	1.90	1.89	1.94	1.90	1.88	1.85	1.91
TI	0.03	0.03	0.03	0.03	0.02	0.03	0.03	0.03	0.03
AL	0.14	0.15	0.13	0.16	0.08	0.13	0.16	0.17	0.10
CR	0.02	0.01	0.01	0.03	0.00	0.01	0.02	0.02	0.00
FE	0.23	0.22	0.22	0.15	0.32	0.24	0.22	0.21	0.29
MN	0.00	0.01	0.01	0.00	0.01	0.01	0.00	0.00	0.01
MG	0.86	0.84	0.85	0.88	0.82	0.85	0.86	0.85	0.84
CA	0.84	0.85	0.85	0.85	0.80	0.82	0.81	0.86	0.82
NA	0.03	0.02	0.02	0.02	0.02	0.02	0.02	0.03	0.03
SUM	4.03	4.01	4.01	4.01	4.01	4.00	4.01	4.03	4.02

Clinopyroxene analyses: sample 58b/90 from the Nilufer Unit

	core	rim	core	rim	core	rim	core	rim	core	rim
SI	50.70	51.12	51.63	50.31	50.63	51.43	50.51	51.22	50.00	50.83
TI	1.25	1.25	0.84	1.36	1.07	0.98	1.08	1.12	1.29	1.07
AL	3.46	2.58	2.38	2.94	3.37	2.90	3.39	3.36	3.98	3.17
CR	0.25	0.02	0.48	0.03	0.51	0.55	0.52	0.59	0.56	0.50
FE	7.71	9.31	7.03	8.64	6.93	7.09	7.31	7.02	7.20	7.27
MN	0.16	0.23	0.18	0.18	0.18	0.17	0.15	0.16	0.16	0.14
MG	15.22	14.83	16.59	14.88	15.44	15.78	15.18	15.64	14.95	15.45
CA	21.30	20.67	20.16	20.87	21.25	20.99	21.03	21.13	21.47	21.10
NA	0.30	0.32	0.29	0.36	0.30	0.31	0.37	0.30	0.30	0.32
TOTAL	100.35	100.33	99.58	99.57	99.68	100.20	99.54	100.54	99.91	99.85
	O= 6	O= 6	O= 6	O= 6	O= 6	O= 6	O= 6	O= 6	O= 6	O= 6
SI	1.88	1.90	1.91	1.88	1.88	1.90	1.88	1.89	1.86	1.89
TI	0.03	0.03	0.02	0.04	0.03	0.03	0.03	0.03	0.04	0.03
AL	0.15	0.11	0.10	0.13	0.15	0.13	0.15	0.15	0.17	0.14
CR	0.01	0.00	0.01	0.00	0.01	0.02	0.02	0.02	0.02	0.01
FE	0.24	0.29	0.22	0.27	0.22	0.22	0.23	0.22	0.22	0.23
MN	0.01	0.01	0.01	0.01	0.01	0.01	0.00	0.00	0.01	0.00
MG	0.84	0.82	0.92	0.83	0.86	0.87	0.84	0.86	0.83	0.85
CA	0.84	0.82	0.80	0.84	0.85	0.83	0.84	0.83	0.86	0.84
NA	0.02	0.02	0.02	0.03	0.02	0.02	0.03	0.02	0.02	0.02
SUM	4.02	4.02	4.02	4.02	4.02	4.01	4.02	4.01	4.02	4.02

Clinopyroxene analyses: sample 56b/90 from the Nilufer Unit

	core	rim	core	rim	core	rim	core	rim	core	rim	core
SI	49.44	49.54	50.04	48.68	49.07	53.03	49.49	49.56	48.19	52.51	50.12
TI	1.01	0.91	1.24	1.00	0.95	0.44	1.08	1.23	0.87	0.61	0.94
AL	4.43	4.52	3.77	3.30	4.78	1.72	4.12	4.35	5.25	2.71	4.13
CR	0.20	0.05	0.02	0.02	0.09	0.06	0.03	0.10	0.14	0.19	0.29
FE	9.50	11.23	11.53	17.49	11.26	9.97	10.93	9.48	12.24	9.16	8.34
MN	0.25	0.27	0.29	0.46	0.27	0.33	0.28	0.25	0.27	0.27	0.21
MG	15.58	14.83	14.53	12.78	14.84	18.54	15.41	15.36	15.63	17.63	15.82
CA	18.71	18.09	18.37	15.63	17.75	15.93	17.55	18.76	16.20	17.11	19.17
NA	0.29	0.31	0.28	0.31	0.28	0.15	0.26	0.27	0.22	0.21	0.28
TOTAL	99.41	99.75	100.07	99.67	99.29	100.17	99.15	99.36	99.01	100.40	99.30
	O= 6	O= 6	O= 6	O= 6	O= 6	O= 6	O= 6	O= 6	O= 6	O= 6	O= 6
SI	1.85	1.86	1.87	1.87	1.85	1.95	1.86	1.86	1.82	1.93	1.87
TI	0.03	0.03	0.03	0.03	0.03	0.01	0.03	0.03	0.02	0.02	0.03
AL	0.20	0.20	0.17	0.15	0.21	0.07	0.18	0.19	0.23	0.12	0.18
CR	0.01	0.00	0.00	0.00	0.00	0.00	0.00	0.00	0.00	0.01	0.01
FE	0.30	0.35	0.36	0.56	0.35	0.31	0.34	0.30	0.39	0.28	0.26
MN	0.01	0.01	0.01	0.02	0.01	0.01	0.01	0.01	0.01	0.01	0.01
MG	0.87	0.83	0.81	0.73	0.83	1.02	0.86	0.86	0.88	0.96	0.88
CA	0.75	0.73	0.74	0.64	0.72	0.63	0.71	0.75	0.66	0.67	0.77
NA	0.02	0.02	0.02	0.02	0.02	0.01	0.02	0.02	0.02	0.01	0.02
SUM	4.03	4.03	4.02	4.03	4.03	4.01	4.02	4.02	4.04	4.00	4.02

Clinopyroxene analyses: sample LOG2/90 from the Ortaoba Unit

	core	core	core	core	core	core	core	core	core	core	core
SI	49.94	49.28	50.02	50.47	50.48	52.12	50.53	50.67	49.96	49.25	49.91
TI	1.22	1.27	1.15	0.95	1.13	0.61	1.15	1.09	1.16	1.29	1.22
AL	3.41	2.87	3.56	3.31	3.74	1.67	3.06	3.50	3.69	3.21	3.49
CR	0.04	0.03	0.09	0.06	0.15	0.02	0.03	0.07	0.16	0.02	0.02
FE	10.55	13.96	9.75	10.01	10.27	12.03	11.38	10.11	9.70	13.52	11.57
MN	0.28	0.36	0.26	0.25	0.26	0.35	0.31	0.27	0.25	0.34	0.31
MG	14.24	12.93	14.68	14.36	15.01	15.91	13.97	14.68	15.01	13.23	13.82
CA	19.06	17.98	19.36	19.63	18.25	17.00	19.06	19.15	19.03	17.77	18.72
NA	0.34	0.35	0.31	0.31	0.30	0.24	0.30	0.32	0.29	0.38	0.34
TOTAL	99.08	99.03	99.18	99.35	99.59	99.95	99.79	99.86	99.25	99.01	99.40
	O= 6	O= 6	O= 6	O= 6	O= 6	O= 6	O= 6	O= 6	O= 6	O= 6	O= 6
SI	1.89	1.89	1.88	1.90	1.89	1.95	1.90	1.89	1.88	1.88	1.89
TI	0.03	0.04	0.03	0.03	0.03	0.02	0.03	0.03	0.03	0.04	0.03
AL	0.15	0.13	0.16	0.15	0.16	0.07	0.14	0.15	0.16	0.14	0.16
CR	0.00	0.00	0.00	0.00	0.00	0.00	0.00	0.00	0.00	0.00	0.00
FE	0.33	0.45	0.31	0.31	0.32	0.38	0.36	0.32	0.30	0.43	0.37
MN	0.01	0.01	0.01	0.01	0.01	0.01	0.01	0.01	0.01	0.01	0.01
MG	0.80	0.74	0.82	0.80	0.84	0.89	0.78	0.82	0.84	0.75	0.78
CA	0.77	0.74	0.78	0.79	0.73	0.68	0.77	0.77	0.77	0.73	0.76
NA	0.02	0.03	0.02	0.02	0.02	0.02	0.02	0.02	0.02	0.03	0.02
SUM	4.01	4.02	4.02	4.01	4.01	4.01	4.01	4.01	4.02	4.02	4.01

Clinopyroxene analyses: sample 91d/90 from the Ortaoba Unit

	core	rim	core	rim	core	rim	core	core	rim	core	rim	core
SI	49.61	46.55	49.40	49.99	50.37	50.67	49.32	50.19	49.12	49.69	49.49	49.96
TI	1.06	0.81	0.89	1.02	0.87	0.88	1.35	0.96	1.17	0.82	0.99	0.94
AL	4.92	5.15	3.82	3.35	3.82	3.80	3.16	3.74	2.20	3.82	3.46	4.41
CR	0.11	0.04	0.04	0.02	0.28	0.11	0.02	0.04	0.01	0.12	0.02	0.39
FE	10.39	15.50	9.86	12.32	8.24	8.98	15.04	11.19	20.81	9.96	11.02	8.73
MN	0.27	0.35	0.25	0.32	0.21	0.23	0.37	0.29	0.54	0.30	0.31	0.24
MG	15.38	14.09	14.91	14.34	16.09	15.30	12.80	15.02	8.49	14.97	14.66	16.55
CA	17.36	17.16	19.57	18.11	19.45	19.78	17.55	18.07	17.63	19.60	19.11	18.37
NA	0.23	0.32	0.30	0.30	0.25	0.28	0.36	0.31	0.34	0.30	0.35	0.32
TOTAL	99.33	99.97	99.04	99.77	99.58	100.03	99.97	99.81	100.31	99.58	99.41	99.91
	O= 6	O= 6	O= 6	O= 6	O= 6	O= 6	O= 6	O= 6	O= 6	O= 6	O= 6	O= 6
SI	1.86	1.79	1.87	1.89	1.87	1.88	1.88	1.88	1.92	1.87	1.87	1.85
TI	0.03	0.02	0.03	0.03	0.02	0.02	0.04	0.03	0.03	0.02	0.03	0.03
AL	0.22	0.23	0.17	0.15	0.17	0.17	0.14	0.17	0.10	0.17	0.15	0.19
CR	0.00	0.00	0.00	0.00	0.01	0.00	0.00	0.00	0.00	0.00	0.00	0.01
FE	0.33	0.50	0.31	0.39	0.26	0.28	0.48	0.35	0.68	0.31	0.35	0.27
MN	0.01	0.01	0.01	0.01	0.01	0.01	0.01	0.01	0.02	0.01	0.01	0.01
MG	0.86	0.81	0.84	0.81	0.89	0.85	0.73	0.84	0.49	0.84	0.83	0.91
CA	0.70	0.71	0.79	0.73	0.78	0.79	0.72	0.73	0.74	0.79	0.77	0.73
NA	0.02	0.02	0.02	0.02	0.02	0.02	0.03	0.02	0.03	0.02	0.03	0.02
SUM	4.01	4.09	4.03	4.02	4.02	4.02	4.02	4.02	4.01	4.03	4.04	4.03

Clinopyroxene analyses: samples 22/10/91-13 and 18/10/91-15 from the Ortaoba Unit

	22/10/91-13								18/10/91-15						
	core	core	core	core	core	core	core	core	core	core	core	core	core	core	core
SI	50.45	50.24	49.96	50.07	50.14	50.02	49.84	50.57	50.15	51.18	50.96	52.16	52.10	52.65	51.96
TI	1.05	1.10	1.20	1.21	1.01	1.10	1.24	1.07	1.07	0.60	0.84	0.74	0.66	0.55	0.62
AL	4.00	3.90	3.44	3.34	3.56	3.80	3.67	3.62	3.85	3.70	3.09	3.07	3.28	0.05	2.42
CR	0.22	0.10	0.03	0.01	0.05	0.09	0.06	0.13	0.24	0.06	0.02	0.03	0.06	0.05	0.01
FE	9.12	9.13	11.78	11.92	10.43	9.55	11.34	9.12	8.80	8.61	10.70	8.59	7.55	8.20	8.45
MN	0.22	0.21	0.28	0.31	0.26	0.23	0.29	0.23	0.23	0.23	0.31	0.25	0.22	0.24	0.27
MG	15.13	14.59	13.52	13.74	14.34	14.13	14.17	14.68	15.41	16.27	15.74	16.81	16.55	17.55	17.06
CA	19.07	19.94	19.11	18.62	19.12	19.89	18.37	19.97	19.00	18.76	18.22	18.90	19.86	18.08	18.85
NA	0.30	0.32	0.37	0.37	0.33	0.32	0.36	0.31	0.29	0.24	0.28	0.23	0.26	0.21	0.24
TOTAL	99.56	99.53	99.69	99.59	99.24	99.13	99.34	99.70	99.04	99.65	100.16	100.78	100.54	100.09	99.88
	O= 6	O= 6	O= 6	O= 6	O= 6	O= 6	O= 6	O= 6	O= 6	O= 6	O= 6	O= 6	O= 6	O= 6	O= 6
SI	1.88	1.88	1.89	1.89	1.89	1.88	1.88	1.89	1.88	1.90	1.90	1.91	1.91	1.93	1.92
TI	0.03	0.03	0.03	0.03	0.03	0.03	0.04	0.03	0.03	0.02	0.02	0.02	0.02	0.02	0.02
AL	0.18	0.17	0.15	0.15	0.16	0.17	0.16	0.16	0.17	0.16	0.14	0.13	0.14	0.11	0.11
CR	0.01	0.00	0.00	0.00	0.00	0.00	0.00	0.00	0.01	0.00	0.00	0.00	0.00	0.00	0.00
FE	0.28	0.29	0.37	0.38	0.33	0.30	0.36	0.28	0.28	0.16	0.33	0.26	0.23	0.25	0.26
MN	0.01	0.01	0.01	0.01	0.01	0.01	0.01	0.01	0.01	0.01	0.01	0.01	0.01	0.01	0.01
MG	0.84	0.81	0.76	0.77	0.81	0.79	0.80	0.82	0.86	0.09	0.87	0.92	0.90	0.96	0.94
CA	0.76	0.80	0.77	0.75	0.77	0.80	0.74	0.80	0.76	0.75	0.73	0.74	0.78	0.71	0.75
NA	0.02	0.02	0.03	0.03	0.02	0.02	0.03	0.02	0.02	0.02	0.02	0.02	0.02	0.01	0.02
SUM	4.01	4.01	4.02	4.01	4.01	4.01	4.01	4.01	4.01	4.01	4.02	4.01	4.01	4.00	4.02

Clinopyroxene analyses: sample 91d/90 from the Ortaoba Unit (cont.)

	rim	core	rim	core	rim	core	rim	core	rim	core
SI	50.09	50.15	50.26	51.01	50.27	50.76	49.93	50.39	50.96	44.84
TI	0.96	0.81	0.97	0.78	1.05	0.83	1.04	0.82	1.17	1.24
AL	3.63	3.92	3.71	3.93	3.77	3.10	3.47	2.53	5.67	6.51
CR	0.04	0.45	0.07	0.36	0.06	0.03	0.06	0.01	0.03	0.04
FE	10.59	7.71	10.53	8.77	10.80	9.44	9.30	13.99	15.78	19.16
MN	0.29	0.24	0.32	0.25	0.32	0.28	0.26	0.38	0.41	0.42
MG	15.43	16.11	15.79	16.65	15.54	16.31	14.97	15.54	10.42	11.72
CA	18.80	20.14	18.29	18.25	18.19	18.56	19.85	15.93	14.36	15.42
NA	0.33	0.33	0.28	0.28	0.34	0.30	0.31	0.30	1.57	0.47
TOTAL	100.16	99.86	100.22	100.28	100.34	99.61	99.19	99.89	100.37	99.82
	O= 6	O= 6	O= 6	O= 6	O= 6	O= 6	O= 6	O= 6	O= 6	O= 6
SI	1.87	1.86	1.87	1.88	1.87	1.89	1.88	1.90	1.91	1.75
TI	0.03	0.02	0.03	0.02	0.03	0.02	0.03	0.02	0.03	0.04
AL	0.16	0.17	0.16	0.17	0.17	0.14	0.15	0.11	0.25	0.30
CR	0.00	0.01	0.00	0.01	0.00	0.00	0.00	0.00	0.00	0.00
FE	0.33	0.24	0.33	0.27	0.34	0.29	0.29	0.44	0.50	0.62
MN	0.01	0.01	0.01	0.01	0.01	0.01	0.01	0.01	0.01	0.01
MG	0.86	0.89	0.88	0.91	0.86	0.91	0.84	0.87	0.58	0.68
CA	0.75	0.80	0.73	0.72	0.73	0.74	0.80	0.64	0.58	0.64
NA	0.02	0.02	0.02	0.02	0.02	0.02	0.02	0.02	0.11	0.04
SUM	4.03	4.03	4.03	4.02	4.03	4.03	4.03	4.03	3.98	4.08

Clinopyroxene analyses: sample 22/8/92-34 from the Cal Unit

	core	rim	core	rim	core	core	core	core	core
SI	48.56	50.51	48.66	47.96	47.10	49.25	51.70	51.79	49.92
TI	1.83	1.14	1.83	2.36	2.46	1.67	1.21	0.99	1.08
AL	5.07	3.33	4.62	5.31	5.74	4.37	2.55	2.38	3.83
CR	0.43	0.84	0.91	0.55	0.81	0.71	0.18	0.55	0.39
FE	7.18	5.47	6.69	7.05	7.00	6.58	6.93	5.98	7.89
MN	0.18	0.14	0.16	0.16	0.17	0.15	0.21	0.16	0.22
MG	14.59	15.57	14.80	13.99	14.04	15.45	16.16	16.61	17.33
CA	21.07	22.01	20.94	21.06	21.31	20.53	20.58	21.09	17.68
NA	0.34	0.33	0.37	0.38	0.41	0.33	0.27	0.26	0.28
TOTAL	99.25	99.34	98.98	98.82	99.04	99.04	99.79	99.81	98.62
	O= 6	O= 6	O= 6	O= 6	O= 6	O= 6	O= 6	O= 6	O= 6
SI	1.82	1.88	1.83	1.81	1.78	1.84	1.91	1.91	1.87
TI	0.05	0.03	0.05	0.07	0.07	0.05	0.03	0.03	0.03
AL	0.22	0.15	0.20	0.24	0.26	0.19	0.11	0.10	0.17
CR	0.01	0.02	0.03	0.02	0.02	0.02	0.01	0.02	0.01
FE	0.22	0.17	0.21	0.22	0.22	0.21	0.21	0.18	0.25
MN	0.01	0.00	0.01	0.01	0.01	0.00	0.01	0.00	0.01
MG	0.81	0.86	0.83	0.79	0.79	0.86	0.89	0.91	0.97
CA	0.85	0.88	0.84	0.85	0.86	0.82	0.82	0.83	0.71
NA	0.02	0.02	0.03	0.03	0.03	0.02	0.02	0.02	0.02
SUM	4.02	4.02	4.02	4.01	4.03	4.02	4.01	4.01	4.02

Clinopyroxene analyses: sample 22/8/92-42 from the Cal Unit

	rim	core	rim	core	rim	core	core	rim	core	rim
SI	50.13	51.30	49.85	51.40	50.71	50.71	50.45	51.54	51.28	49.26
TI	1.46	1.07	1.57	0.81	0.93	1.18	1.19	1.05	1.24	1.58
AL	3.95	2.81	4.12	2.61	3.36	3.14	3.16	2.10	3.02	4.10
CR	0.35	0.33	0.33	0.57	1.08	0.32	0.31	0.22	0.25	0.38
FE	5.75	5.51	6.13	5.82	4.67	5.74	5.94	6.01	5.69	5.90
MN	0.10	0.11	0.12	0.13	0.08	0.11	0.12	0.14	0.10	0.11
MG	15.14	15.81	14.93	15.52	15.96	15.60	15.45	16.17	15.66	15.10
CA	22.13	22.01	21.69	21.80	22.06	21.70	21.96	21.64	21.92	22.10
NA	0.28	0.29	0.32	0.72	0.28	0.27	0.41	0.21	0.25	0.29
TOTAL	99.29	99.24	99.06	99.38	99.13	98.77	98.99	99.08	99.41	98.82
	O= 6	O= 6	O= 6	O= 6	O= 6	O= 6	O= 6	O= 6	O= 6	O= 6
SI	1.86	1.90	1.86	1.91	1.88	1.89	1.88	1.92	1.90	1.85
TI	0.04	0.03	0.04	0.02	0.03	0.03	0.03	0.03	0.03	0.04
AL	0.17	0.12	0.18	0.11	0.15	0.14	0.14	0.09	0.13	0.18
CR	0.01	0.01	0.01	0.02	0.03	0.01	0.01	0.01	0.01	0.01
FE	0.18	0.17	0.19	0.18	0.14	0.18	0.19	0.19	0.18	0.18
MN	0.00	0.00	0.00	0.00	0.00	0.00	0.00	0.00	0.00	0.00
MG	0.84	0.87	0.83	0.86	0.88	0.87	0.86	0.90	0.86	0.84
CA	0.88	0.88	0.87	0.87	0.88	0.87	0.88	0.86	0.87	0.89
NA	0.02	0.02	0.02	0.05	0.02	0.02	0.03	0.02	0.02	0.02
SUM	4.01	4.01	4.01	4.03	4.01	4.01	4.02	4.01	4.01	4.02

Clinopyroxene analyses: sample 22/8/92-21 from the Cal Unit

	rim	core	rim	core	rim	core
SI	51.00	49.15	49.80	51.13	51.55	50.93
TI	1.07	1.68	1.52	1.17	1.07	1.06
AL	3.08	4.61	4.26	3.31	2.77	3.15
CR	0.29	0.37	0.38	0.64	0.40	0.80
FE	5.93	6.73	6.32	5.87	5.80	5.41
MN	0.13	0.15	0.15	0.15	0.14	0.12
MG	15.53	14.68	14.79	15.35	15.92	15.48
CA	21.88	21.44	21.70	21.81	21.56	21.78
NA	0.28	0.36	0.32	0.34	0.28	0.31
TOTAL	99.19	99.17	99.24	99.77	99.49	99.04
	O= 6	O= 6	O= 6	O= 6	O= 6	O= 6
SI	1.90	1.84	1.86	1.89	1.91	1.89
TI	0.03	0.05	0.04	0.03	0.03	0.03
AL	0.14	0.20	0.19	0.14	0.12	0.14
CR	0.01	0.01	0.01	0.02	0.01	0.02
FE	0.18	0.21	0.20	0.18	0.18	0.17
MN	0.00	0.00	0.00	0.00	0.00	0.00
MG	0.86	0.82	0.82	0.85	0.88	0.86
CA	0.87	0.86	0.87	0.86	0.85	0.87
NA	0.02	0.03	0.02	0.02	0.02	0.02
SUM	4.01	4.02	4.01	4.01	4.01	4.01

Garnet analyses from the Kazdag Massif (sample KAZ6A)

	1 (core)	1 (rim)	2 (core)	2 (rim)	3 (core)	3 (rim)	4 (core)	4 (rim)	5 (core)	5 (rim)	6 (core)	6 (rim)
SI	37.48	37.53	37.44	38.28	37.71	38.01	37.63	37.80	37.60	37.84	37.70	37.98
TI	0.13	0.12	0.13	0.24	0.13	0.12	0.17	0.07	0.09	0.09	0.11	0.28
AL	20.67	20.58	20.72	20.51	20.49	20.44	20.82	20.91	20.88	20.81	20.68	20.64
CR	0.01	0.03	0.02	0.02	0.04	0.02	0.01	0.02	0.01	0.02	0.02	0.01
FE	27.28	26.89	27.88	25.58	27.35	26.59	27.83	27.99	25.82	26.44	27.26	25.95
MN	1.29	0.74	2.70	1.20	1.12	0.66	0.49	0.52	2.86	2.71	1.35	0.74
MG	1.82	1.98	1.78	2.82	1.81	2.41	2.55	2.84	2.15	2.16	2.53	2.95
CA	11.34	11.85	9.58	11.46	11.50	11.96	10.52	10.29	10.65	10.35	10.48	11.40
TOTAL	100.02	99.72	100.25	100.11	100.15	100.21	100.02	100.44	100.06	100.42	100.13	99.95
	O=24	O=24	O=24	O=24	O=24	O=24	O=24	O=24	O=24	O=24	O=24	O=24
SI	5.98	5.99	5.98	6.04	6.00	6.02	5.98	5.98	5.98	6.00	5.99	6.00
TI	0.02	0.01	0.02	0.03	0.02	0.01	0.02	0.01	0.01	0.01	0.01	0.03
AL	3.89	3.87	3.90	3.82	3.85	3.82	3.90	3.90	3.91	3.89	3.87	3.85
CR	0.00	0.00	0.00	0.00	0.01	0.00	0.00	0.00	0.00	0.00	0.00	0.00
FE	3.64	3.59	3.72	3.38	3.64	3.52	3.70	3.70	3.43	3.51	3.62	3.43
MN	0.17	0.10	0.37	0.16	0.15	0.09	0.07	0.07	0.39	0.36	0.18	0.10
MG	0.43	0.47	0.42	0.66	0.43	0.57	0.60	0.67	0.51	0.51	0.60	0.69
CA	1.94	2.03	1.64	1.94	1.96	2.03	1.79	1.74	1.81	1.76	1.78	1.93
SUM	16.06	16.06	16.05	16.02	16.05	16.06	16.05	16.07	16.05	16.04	16.06	16.04

Chromian spinel analyses from the Denizgoren Ophiolite (sample DEN1)

	1 (core)	2 (core)	3 (core)	4 (core)	5 (core)	6 (core)	8 (core)	9 (core)	10 (core)	11 (core)	11 (rim)	12 (core)
SI	0.01	0.07	0.00	0.07	0.03	0.15	0.00	0.00	0.00	0.04	0.05	0.04
TI	0.19	0.20	0.19	0.16	0.22	0.18	0.17	0.20	0.17	0.18	0.18	0.19
AL	25.64	25.47	25.91	25.39	24.69	25.32	25.74	25.05	25.17	25.14	24.44	25.71
CR	39.22	39.71	39.88	39.69	39.88	39.30	39.22	40.23	39.61	38.22	39.33	39.57
FE	22.24	20.76	18.81	21.37	22.58	21.73	21.82	20.66	23.71	25.29	25.49	20.53
MN	0.64	0.63	0.60	0.65	0.68	0.63	0.66	0.64	0.69	0.70	0.72	0.62
MG	11.30	12.31	13.64	11.87	11.03	11.74	11.46	12.48	10.09	9.53	8.86	12.46
TOTAL	99.24	99.15	99.03	99.20	99.11	99.05	99.07	99.26	99.44	99.10	99.07	99.12
	O=32	O=32	O=32	O=32	O=32	O=32	O=32	O=32	O=32	O=32	O=32	O=32
SI	0.00	0.02	0.00	0.02	0.01	0.04	0.00	0.00	0.00	0.01	0.01	0.01
TI	0.04	0.04	0.04	0.03	0.04	0.03	0.03	0.04	0.03	0.03	0.03	0.04
AL	7.55	7.46	7.52	7.46	7.32	7.45	7.58	7.34	7.47	7.52	7.35	7.52
CR	7.74	7.80	7.76	7.82	7.93	7.76	7.74	7.91	7.88	7.67	7.94	7.76
FE	4.64	4.31	3.87	4.45	4.75	4.54	4.56	4.30	4.99	5.37	5.44	4.26
MN	0.14	0.13	0.13	0.14	0.14	0.13	0.14	0.13	0.15	0.15	0.16	0.13
MG	4.21	4.56	5.01	4.41	4.13	4.37	4.26	4.62	3.78	3.60	3.37	4.61
SUM	24.31	24.31	24.32	24.31	24.32	24.32	24.31	24.34	24.29	24.36	24.31	24.31

APPENDIX 4: NORMALIZING VALUES

Mid Ocean Ridge Basalt (MORB) normalizing values

Sr	120ppm	P_2O_5	0.12%
K_2O	0.15%	Zr	90ppm
Rb	2ppm	TiO_2	1.5%
Ba	20ppm	Y	30ppm
Th	0.2ppm	Sc	40ppm
Nb	3.5ppm	Cr	250ppm
Ce	10ppm		

(from Pearce, 1983; Sc and Cr from Pearce, 1982)

North American Shale Composite (NASC) normalizing values

Sc	14.90ppm	Y	35ppm
Ti	4676ppm	Zr	200ppm
V	124.5ppm	Nb	13ppm
Cr	124.5ppm	Ba	636ppm
Ni	58ppm	Ce	66.7ppm
Rb	125ppm	Nd	27.4ppm
Sr	142ppm		

(from Gromet *et al.*, 1984)

Ocean Ridge Granite (ORG) normalizing values

K_2O	0.4%
Rb	4ppm
Ba	50ppm
Th	0.8ppm
Nb	10ppm
Ce	35ppm
Zr	340ppm
Y	70ppm

(from Pearce *et al.*, 1984)

APPENDIX 5: PALAEOMAGNETIC TECHNIQUES

Collection and preparation of samples

Sites BJ01 to BJ04 were sampled by drilling cores *in situ* with an adapted petrol driven chain saw motor. The diamond-tipped stainless steel drill bit was cooled and lubricated by water pumped from a portable canister. At each site approximately 10-14 cores between 4 and 10cm long were drilled. Before their removal from the outcrop the drilled cores were accurately orientated using an orientation device attached to a hollow non-magnetic tube which was fitted around the core. A fiducial line was marked on each core through a slit in the tube. The direction of the core relative to true north (trend) and the angle of drilling relative to the horizontal (plunge) were measured. The orientated cores were then broken off at the base, removed and labelled. Broken samples were reconstructed using superglue. Sites BJ05 and BJ06 were sampled by hand. Block samples were obtained by breaking off suitable pieces of outcrop, and then replacing them in their original positions for orientation. The orientation was recorded by drawing a strike and dip line on a flat surface (generally a bedding surface).

On returning from the field, cores were drilled from the hand samples using a pedestal drill with its bit aligned perpendicularly to the orientated surface. These cores, together with those drilled directly in the field were then cut into 2.5cm long cylinders. The fiducial line along the margin of the samples was extended across the top surface of each cylinder. All remanence directions were measured with respect to this line.

Measurement of natural remanent magnetization (NRM)

NRM is generally measured on cryogenic or spinner magnetometers depending on the strength of magnetization of the rock. Spinner magnetometers utilise the alternating voltage induced when a sample is spun near a detecting coil, and about an axis in the plane of the coil. They are used for measuring the NRM of strongly magnetized rocks such as volcanics. The NRM of weakly magnetized rocks such as many limestones is measured using cryogenic magnetometers which are based on the properties of a superconducting ring. Cryogenic magnetometers use a magnetic field sensor called a SQUID (superconducting quantum interference device) magnetometer which is superconducting at liquid helium temperatures (4°K).

The NRM of the Bilecik Limestone samples was measured using the two-axis CCL cryogenic magnetometer in the palaeomagnetic laboratory at the Department of Earth Sciences, Oxford University. Measurements were made of the components (M_x, M_y, M_z) of magnetic moment of the samples. Data were fed into a computer that contained orientation data for the samples and which calculated the intensity of the NRM as well as its declination and inclination in core (i.e. sample) coordinates. Field and bedding corrections (relating the the NRM direction to present day geographical coordinates and then correcting for tectonic tilt) were then applied to the raw data.

Demagnetization techniques

a) Thermal demagnetization

Samples were progressively heated in three main batches up to maximum temperatures of 525°C, 550°C and 680°C respectively, and their remanent magnetization measured after each heating step. Samples were put in holders and placed within one of two large ovens which take approximately 18 and 44 samples respectively. Each heating step involved programming the oven to reach a certain maximum temperature and to hold it at that temperature for a required amount of time until equilibrium was reached. Large temperature steps were followed by smaller increases at higher temperatures. The samples were then cooled to 40°C or less before being removed and their NRM measured. During the entire treatment the samples were placed in the same holder positions within the oven and their directions were reversed for each heating step. The samples were kept in a zero magnetic field after each step and during their measurement, to avoid the acquisition of new spurious magnetizations.

b) AF demagnetization

Six samples were demagnetized using a tumbling alternating field (AF) demagnetizer. The tumbling AF demagnetizer allows demagnetization of all axes of the specimen during one demagnetization treatment. This technique involved placing a sample in a small drum which was then rapidly rotated within several nested gears in an alternating magnetic field. Small increments in AF peak field were followed by larger increases at higher levels.

Measurement of isothermal remanent magnetization (IRM)

To investigate the magnetic aquisition properties, and hence the magnetic phases of the Bilecik Limestone, the IRM of six samples was measured using a pulse

magnetizer. The samples were placed in a steady magnetic field whose strength was progressively increased in steps up to 800mT and their behaviour expressed as IRM acquisition curves. IRM acquisition was followed by stepwise thermal demagnetization up to a maximum temperature of 680°C.

Measurement of bulk susceptibility

Bulk susceptibility measurements were made after each measurement of NRM during the thermal demagnetization process. The measurements were made on two batches of samples (36 samples in total) using a minisep bulk susceptibility measuring device.

Data analysis

Analysis of palaeomagnetic data was carried out using computers and software from the palaeomagnetic laboratory at the Department of Earth Sciences, Oxford University. Data analysis principally involved creating Zijderveld plots and choosing vectors from them, using the Oxford "IAPD" programme (Torsvik, 1992). IAPD was also used to calculate tectonic coordinates, Fisher statistics and to plot stereoplots of the corrected data. Other programmes used for this study include the McFadden (1990) fold test programme ("McFadden"), great-circle programmes ("newcirc" and "newfit") and a programme for calculating VGPs and magnetic directions ("VGP").

APPENDIX 6: FOLD TEST CONFIDENCE LIMITS

95% and 99% confidence limits for the application of the McElhinny (1964) fold test.

N	k_2/k_1 at 95% limit	k_2/k_1 at 99% limit
2	19.0	99.0
3	6.39	16.0
4	4.28	8.47
5	3.44	6.03
6	2.97	4.85
7	2.69	4.16
8	2.48	3.70
9	2.33	3.37
10	2.22	3.13
11	2.12	2.94
12	2.05	2.79
13	1.98	2.66
14	1.93	2.55
15	1.88	2.47
16	1.84	2.38
17	1.81	2.32
18	1.78	2.26
19	1.75	2.20
20	1.72	2.15

(from McElhinny, 1964)